Experimental Evidence of Nuclear Reactions Generated in a Polarized Pd/D Lattice

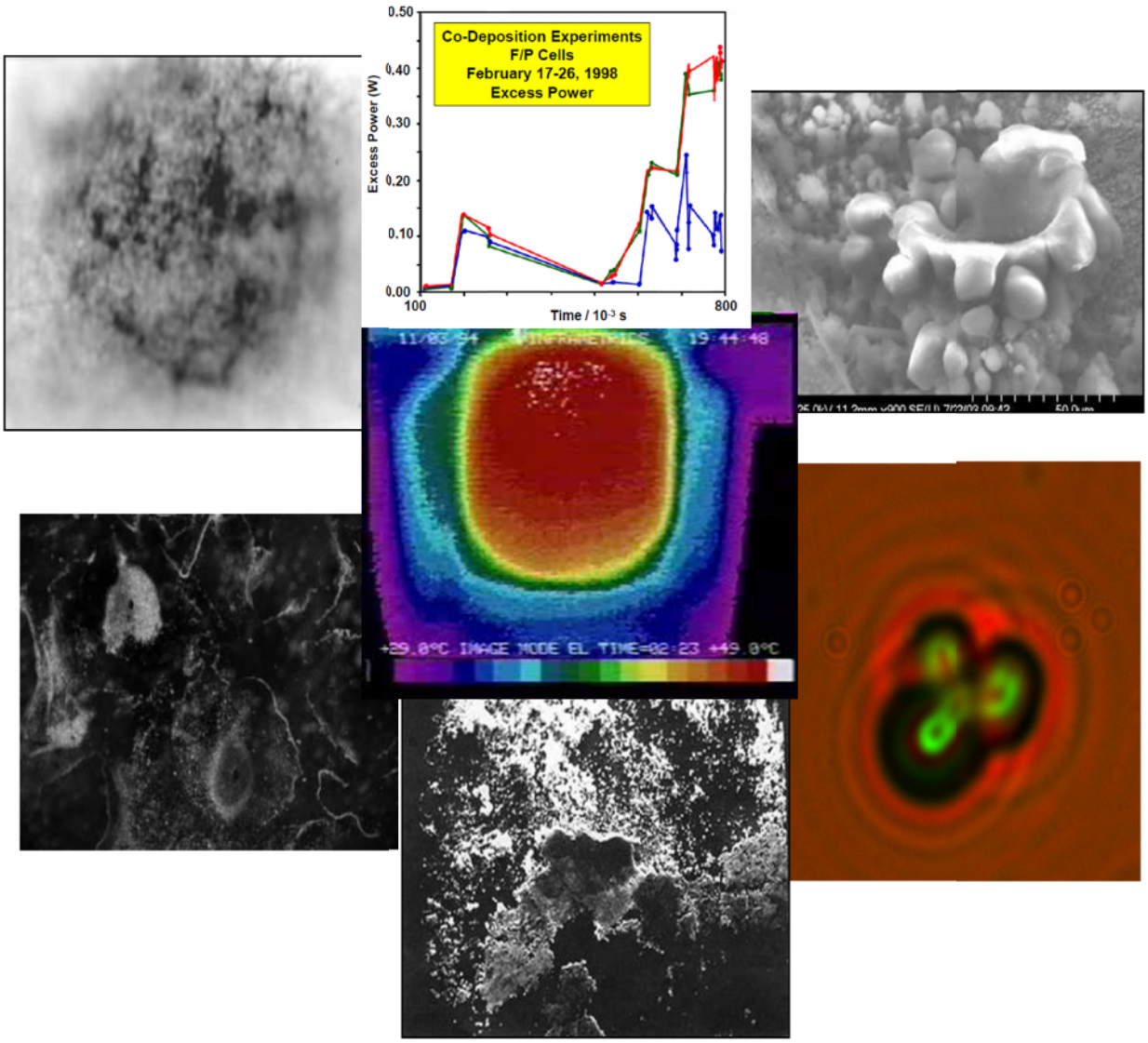

CONTRIBUTORS

Dr. Martin Fleischmann
Bury Lodge, Duck Street
Tisbury, Salisbury, Wilts, SP36LJ, UK

Dr. Stanislau Szpak
Retired
San Diego, CA USA

Dr. Pamela A. Mosier-Boss
Research Laboratory of Electronics
Massachusetts Institute of Technology
Cambridge, MA USA

Dr. Frank E. Gordon
Navy Senior Executive Service (retired)
San Diego, CA USA

Dr. Jack Dea
Collaborator
San Diego, CA USA

Dr. Melvin H. Miles
University of LaVerne,
LaVerne, CA USA

Dr. Scott R. Chubb
Remote Sensing Division
Naval Research Laboratory
Washington, DC USA

Table of Contents

PREFACE

This report reviews research activities on the polarized Pd/D_2O system. In contrast to the pioneering work of Fleischmann and his collaborators, we consider only events at, and/or, within Pd electrodes prepared by the co-deposition technique developed in this laboratory. Our effort proceeded along two paths: (i) investigation of thermal and nuclear events in the Pd host lattice and (ii) examination of the role of the interphase region. These paths were undertaken to assess the intensity of events and to provide some information on the factors controlling the initiation and maintenance of excess enthalpy generation, i.e., the "performance envelope".

The results of subsequent research were reported in a number of publications and in the Technical Report 1696 (Sept. 1995). The latter was devoted almost exclusively to the thermal behavior of the polarized Pd/D-D_2O system with emphasis on the detailed analysis of the calorimetry of electrochemical cells written by Prof. Fleischmann.

The present report contains papers which have been published, are in the course of publication, prepared for publication and those that have been rejected. In the latter case, comments of reviewers and the editor's decision are included to show the inherent bias of some editors. The contributions of Mel Miles of the University of LaVerne and Scott Chubb (deceased) from NRL are included.

It should be noted that the results of Fleischmann and his collaborators were questioned because they did not fit into the accepted views of the $d^+ + d^+$ fusion path. Indeed, because of the confusion that resulted from this assumption, at an early stages, nonsensical arguments were used in opposition to "cold fusion", *eg.*, the number of negative results is greater than positive, *ergo* "cold fusion should be rejected on statistical grounds". Most distressing was the attitude of editors of scientific journals where papers submitted for publication were rejected, often with inappropriate comments.

Chapter I: Emergence of Cold Fusion

I.1 Introductory Remarks

More than a decade ago, Professors Fleischmann and Pons announced that at low temperatures and pressures, nuclear reactions can be initiated by compressing deuterium into the palladium lattice and that these events manifest themselves in the form of excess enthalpy production. This could be demonstrated by a simple experiment which does not require the use of specialized equipment; only a cell/calorimeter, a palladium rod, a platinum counter electrode and a galvanostat are needed. What was not clearly stated was (i) that the experiment is difficult in the sense that long incubation times are required - far in excess of those needed to completely saturate the Pd lattice with deuterium - (ii) that more than a rudimentary knowledge of electrochemistry is essential.

The chronology of events leading to the discovery of cold fusion is not clear. Early reports show that low energy nuclear events were observed in the 1930s and 1940s and reported, not only in scientific journals, but also in textbooks on inorganic chemistry. There were no reported activities until the 23 March 1989 press conference. The timing and mode of the announcement was forced upon Fleischmann and Pons to preserve priority of the discovery - Fleischmann and Pons *versus* Jones (Bringham Young University). We do not know what led Jones to his work on this subject. But we do know why Fleischmann has undertaken this research. The thought processes and events preceding the announcement are presented in papers “Background of cold fusion: the genesis of a concept” and “Searching for the consequences of many-body effects in condensed phase systems” written by Prof. Fleischmann. These papers are included to demonstrate that the F-P discovery was not an accident but rather the result of years of research.

Background to Cold Fusion: the Genesis of a Concept

M. Fleischmann

Bury Lodge, Duck Street, Tisbury, Salisbury, Wilts., SP3 6LJ, U.K.

The scheme of research which led to the start-up of the project now known as "Cold Fusion" is illustrated by Fig. 1. We note that it is commonly believed that there is absolutely no way of influencing Nuclear Processes by Chemical means: therefore, any results that demonstrate that this might be possible must be due to faulty experimentation, delusion, fraud etc. However, any enquiry as to the *experimental* foundation of the first statement in Fig. 1 is normally met by the response: *"because quantum mechanics, Q.M., shows that this is so"* [1] (see further below). We are driven to the conclusion that this first statement is just part of the belief-system of Natural Scientists and we naturally also have to ask the question; "what conclusion would we draw if we subject the statement to the dictates of Field Theory ?"[2] [3],

In the 1960's we started a series of research projects aimed at answering the Question; "can we find illustrations in Chemistry (especially Electrochemistry) of the need to invoke the Q.E.D. paradigm to explain the results obtained ?" The opposition we encountered in applying this line of reasoning to the first of these projects, (i) the kinetics of fast reactions in solution at short space-times ($2x10^{-22}$cm.s to $3x10^{-12}$cm.s), see Fig.1, convinced us that such research had to be carried out using "hidden agendas", see Fig. 2

---

[1] Which coincidentally explains why I did not start this project at any time during the period 1947-1983

[2] It is well known that the Quantum Mechanical Paradigm is incomplete and that the inconsistencies produced by this paradigm are removed by Quantum Field Theory, Q.F.T., (or Quantum Electrodynamics, Q.E.D., for applications to ordinary matter).

[3] Critiques based on the application Q.M. to dilute plasmas are usually extended to cover fusion in condensed matter. The statement "no neutrons, no fusion" is a typical example of this reasoning. We note that an excellent text book covering the application of Q.E.D. to condensed matter is available (1).

Because Q.M. says so
But what about Q.E.D.?

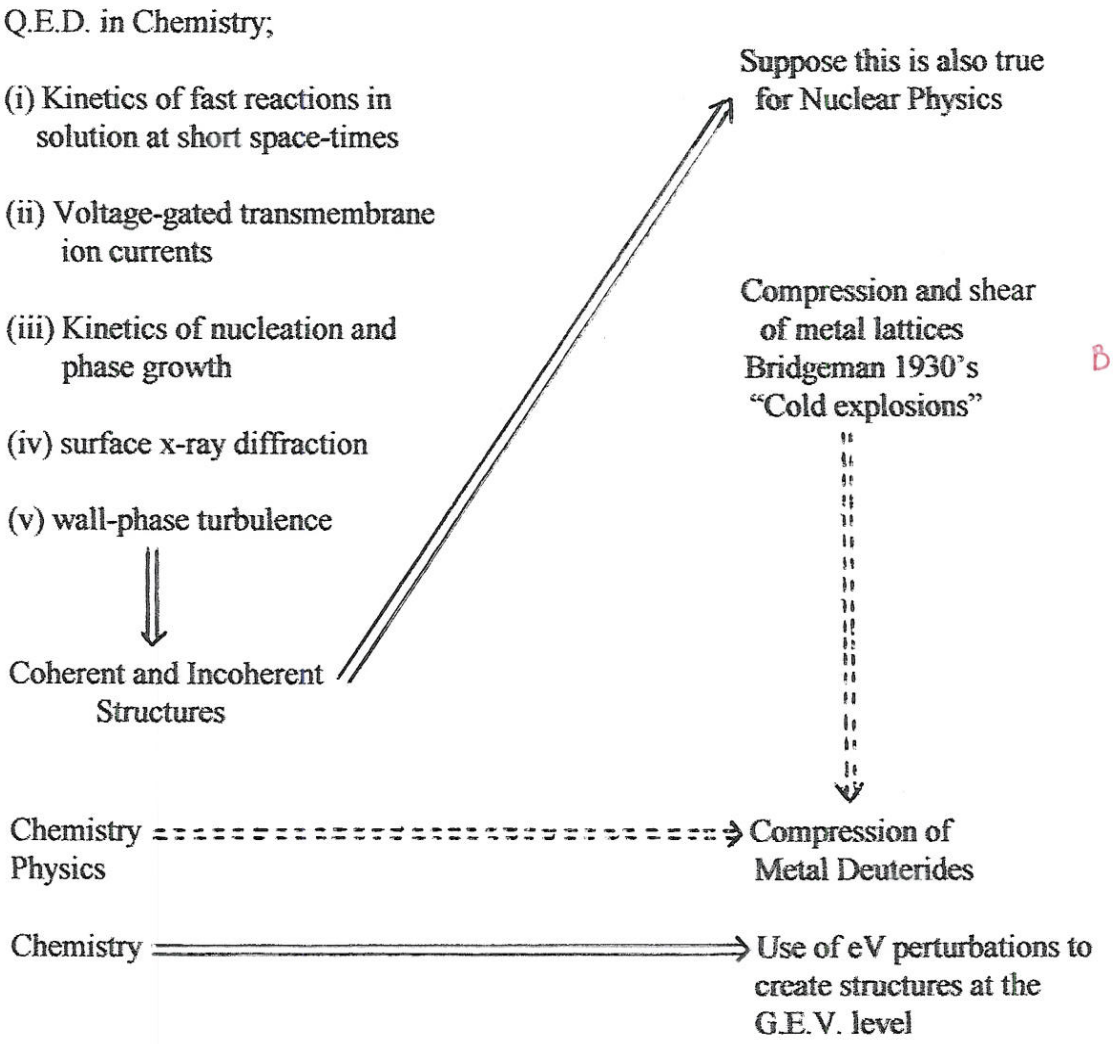

Fig. 1 The scheme of research which led to the start-up of the "Cold Fusion" project.

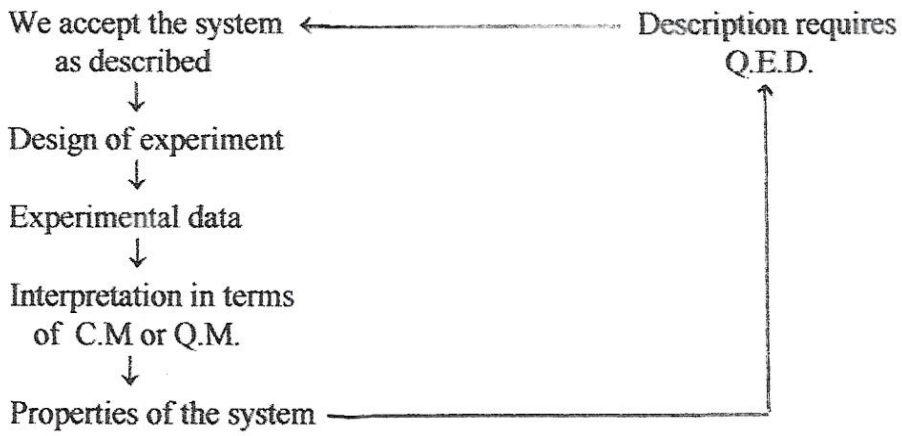

Fig. 2 The "hidden agendas" of the research projects.

Thus, using such agendas, the systems are investigated within the accepted models of C.M. or Q.M.: the influence of many-body effects and of Q.E.D. had to emerge from the interpretation of the results. It will be evident that this particular strategy had the advantage of avoiding the presupposition of the importance of Q.E.D.; for example, it might well have turned out that such effects were unimportant and/or not measurable. The strategy also had the advantage of avoiding the premature criticisms of the multitude of scientists opposed to the application of Q.E.D. to condensed phase systems ! The overall aim was the illustration of the developments of inconsistencies arising from the purely atomistic view of Quantum Physics: we need to answer the question whether the description of Nature requires collective dynamics (*field* dynamics in the physical jargon) for the analysis of the seemingly individual phenomena.

One conclusion which followed from these investigations of (i)-(v) was that condensed phase systems developed structures having dimensions lying between ~100-1000Å , structures that played a crucial rôle in the behaviour of the systems.[4] At a later date, we adopted the terminology of Q.E.D. Coherence (1) by describing the separation of the bulk material into Coherent and Incoherent Domains. We will confine attention here to just one of these topics (i)-(v) namely, surface X-ray diffraction, (iv), as this methodology gives direct information about the structure of electrolyte solutions (topics (i) and (ii) were described briefly in the Proceedings of the Ninth International Conference on "Cold Fusion",(2)). Two factors made such a seemingly impossible project feasible, (3), The first was the advent of position sensitive single photon counting, Figs. 3A and B, the second was the use of modulation techniques to enhance the selectivity towards surface diffraction, Figs. 4A and B. Fig. 3A illustrates the details of the methodology originally proposed, the use of a multi-wire proportional counter in combination with a bright rotating anode source. However, in view of restrictions in the funding, the project was eventually carried out with a linear position sensitive detector in combination with a fixed anode source. We estimated that this caused a degradation in the performance by a factor in the range 100 to 1000. Fig. 4A illustrates the diffractogram obtained when using a thin layer cell containing an electrode consisting of a thin film of silver. We observe

Figs 3A, 3B hereabouts

Figs 4A, 4B hereabouts

[4] It follows, therefore, that the effects of these structures are most readily investigated by carrying out experiments on systems having such small dimensions.

the (111) and (200) diffractions of silver superimposed on a broad background due to diffraction from the aqueous solution in the cell. Clearly, such diffractograms do not give any useful information. However, modulation of the potential between the values for the observation of the silver surface alone and that for underpotential deposition of a single layer of lead (4) coupled to long data acquisition and the use of a 15-point triangular smoothing window, gave the difference diffractogram illustrated in Fig. 4B.[5] The main features seen in Fig. 4B are a loss of order around $2\theta = 17^{\circ}$ and 44°, a differential shaped feature centred around $2\theta = 26^{\circ}$ and, associated with this a differentiation of the peak at $2\theta = 38^{\circ}$ due to the Ag (111) reflection. The loss of structure at 44° is particularly interesting as this corresponds to the Ag (200) peak which is reduced in magnitude as the lead monolayer is formed. From optical and voltametric studies it has been concluded (4) that deposition of lead on Ag (100) surfaces corresponds to an higher order phase transformation which would lead to a marked change in the structure factor but no clearly defined diffraction peak. By contrast deposition on Ag (111) surfaces has been assigned to a first order phase transformation. It is logical therefore to assign the differential peak to the formation of an incommensurate monolayer on the (111) facets of the polycrystalline silver film electrode. However, the most surprising results of the investigation were the observation of the differential peak centred around $2\theta = 26^{\circ}$ and the loss of structure around $2\theta = 17^{\circ}$. The first is most logically attributed to a lengthening of the O-O distance in the water near the electrode surface as the lead monolayer is formed (the large peak centred around $2\theta = 26^{\circ}$ is generally attributed to hydrogen bonded water). We can judge this change in structure to involve the equivalent of 20-50 monolayers of water. The second, corresponding to a nearest neighbour distance of 6-8A^{0} is most likely due to a change in the ion distribution ; we can see that the distribution of ions is much more highly ordered than that predicted by present day models of electrolyte solutions.

The main conclusion which follows from the investigation is that we cannot achieve a complete description of the system in terms of the left-hand-side of the "hidden agendas" of Fig. 2. Such a description must clearly involve strong interactions between all the species in the interfacial regions i.e. we have to consider the many-body problem within the context of field theory. We note that the application of Q.E.D. to the solvent and electrolyte solutions shows that the solvent (water) must be divided into two domains, one in which the solvent is highly structured (the coherent regions) and the second (the incoherent regions) in which the solvent is disordered; electrolyte is expelled from the coherent into the incoherent regions where it in turn forms ordered domains (1), (2), (5), (6). This line of reasoning prompts us to attribute the changes in the diffractogram, Fig. 4B, at $2\theta < 26^{\circ}$ to the selection of coherent domains by the underpotential monolayer of lead on the silver substrate coupled to an enhancement of the scattering from the incoherent regions.

By 1983 we had reached a position where it seemed logical to ask the next question posed in Fig. 1: suppose the division of solid phases into coherent and incoherent structures was also true for Nuclear Physics. If that was so, then would we be able to use the perturbations at the leV level (characteristic of chemical changes) to create coherent structures at the GEV level ? Furthermore, would we be able to

---

[5] We note that it is possible to observe such difference diffractograms notwithstanding the degradation of the performance implied by using the instrumentation illustrated in Fig. 3B rather than that originally envisaged, Fig. 3A.

observe nuclear processes in such structures ? Of course, in posing these questions we were also influenced by other relevant work such as the interpretation of Mössbauer spectra, see (1) and, especially, the observations of "Cold Explosions" by Bridgeman in the 1930's (7).[6] Furthermore, we knew that the absorption of hydrogen isotopes can lead to a similar fragmentation. This then was the background which led to the specification of the first system for our investigations; the highly forced electrolytic charging of palladium cathodes with deuterons.[7] It is appropriate here to comment also on the chosen methodology, the measurement of the thermal balances using calorimetry (8), (9). It was clear at that time that the favoured methods of Nuclear Physics could only be applied to the systems we had in mind following many modifications and with numerous restrictions. Furthermore, there were ambiguities in the interpretation of some of the results which had been obtained.[8] On the other hand, the measurement of thermal balances would be straightforward and inexpensive (an important factor as we were carrying out the initial investigation at our own expense) and such methods could achieve an high sensitivity and be reasonably free from ambiguities (however, see further below).

Bridgman

We therefore embarked on this project but without any expectation that we would obtain definitive results. The Pd/D system was investigated (coupled to the use of the Pt/D system as a suitable "blank"). However, the outcome was radically different to our expectations: the generation of excess enthalpy without any significant formation of the fusion products produced in dilute high temperature plasmas.[9] When the project reached the public domain, (8), (9), it became clear that our expectations with regard to the use of calorimetric methods could not be realised and it is important at this stage to ask why this might have been so ?

One of the causes is undoubtedly the inherent irreproducibility of the phenomenon. We believe that the process which we have observed takes place in the bulk of the electrode, (8), (9), as mediated by the surface reactions. We can see that this immediately builds in inherent irreproducibilities into the system. Moreover, it has not generally been appreciated that although it is relatively straightforward to produce palladium electrodes, the metallurgy of palladium is difficult leading to the use of unsatisfactory (and inadequately specified) electrode materials.

However, the major reason is undoubtedly the fact that the calorimetry of electrode reactions has not emerged as a viable methodology (it remains confined to a number of sub fields such as the measurement of self-discharge in batteries). Papers dealing with the precision and accuracy of calorimetric methods and comparisons of

---

[6] Intense compression and shear of lattices can lead to their fragmentation into small particles in which the high energy of the initial system is converted into kinetic energy of the fragments. We believed (and still believe) that this is a process which can only be explained by Q.E.D.

[7] Although we could see that the results obtained opened the way for very wide-ranging investigations, our own work never progressed beyond this initial concept. We described the resources required for the much wider investigations as equivalent to a Manhattan II project; this was true even for the much more limited scope of a project which remained restricted to the charging with deuterium of palladium based host lattices.

[8] See, for example, the interpretation of the tracks due to $^{3}T^{+}$ and $^{1}H^{+}$ in a Wilson Cloud Chamber (10), (11), an experiment carried out following the discovery of the first hot fusion reaction (12).

[9] The formation of ^{3}T could be shown to be far above that which could be attributed to isotopic separation with any reasonable choice of separation factors; the formation of neutrons appeared to be confined to the non-steady state of operation of the cells; the formation of ^{4}He could be detected but could not be related to the magnitude of the excess enthalpy generation.

various studies[10] are rejected outright by Journal Editors and referees[11],[12] so that the study of calorimetry does not advance. The rather wild statements which have been made in the literature about the precision and accuracy of calorimetry as applied to the Pd-D system have undoubtedly also been due to the complexities of excess enthalpy generation in this system. Thus, it does not appear to have been realised that it is impossible to calibrate any calorimetric system if this is subject to fluctuating sources of enthalpy generation. Such calibrations require at the very least a constancy of the rate of excess enthalpy generation but, better, a zero value of this rate. It follows, therefore, that such calibrations must be carried out when using suitable "blank" systems. The intervention of "positive feedback" in the Pd-D system is especially troublesome in this regard. (14) We illustrate this point by two calibrations carried out by the New Hydrogen Energy Group in Japan, Figs. 5A and B. The onset of "positive feedback" leads to a delayed approach to the steady state following the application of the calibration pulse and a delayed decay to the base-line following the termination of this pulse, Fig. 5B. Not surprisingly, attempts to derive the true heat transfer coefficient from calibrations subject to such effects lead to the impossible result that the true heat transfer coefficient is smaller than the lower-bound value e.g. see (15). As we have already noted, exact evaluations of the precision and accuracy of the instrumentation require experiments using "blank systems" (e.g. see (13)).

Figs 5A, 5B hereabouts

We must also acknowledge the fact that in the presence of excess enthalpy generation a part of this excess enthalpy may be generated outside certain designs of calorimetric cells (e.g. by the intervention of soft x-rays). This is a further factor which could lead to invalid estimates of the accuracy and precision of calorimeters investigated solely by using the Pd-based systems in D_2O-based electrolytes.

Our Conference Chairman has suggested that it would be useful if I were to give an indication of the papers on the general area of "Cold Fusion" which I have found especially interesting. I have found this to be an invidious task because, having Catholic tastes in science, I have found all the papers interesting even when I have approached these with some scepticism. Moreover, the field of publications is now very wide. However, Table 1 gives some indication of those which have aroused my special interest.

Table 1 hereabouts

I note in the first place, the papers which attempt to find a theoretical basis for the subject, Chapter 8 in (1), (16)-(19). Clearly, it will prove to be impossible to advance the research in the absence of such a theoretical foundation (or, at any rate, progress would be greatly impeded). As my interest in the subject area was part of a general investigation of the rôle of Q.E.D. in the Natural Sciences,, I have naturally been strongly drawn to the approach of Giuliano Preparata.

It will be seen that I have separated from this section (dealing with theoretical aspects) the paper by Del Giudice, De Ninno and Frattolillo covering a possible consequence of Q.E.D. Coherence namely, the question of whether we can explain transmutations at low energies (20). This subject area (21) (and see also (22)) originally seemed quite unreasonable. It also remains to be established how the generation of ^4He (23) (24) is related to the wider area of low energy transmutations. The contributions of Miles and McKubre are noteworthy in that they establish a

---

[10] Admittedly with regard to studies in "Cold Fusion"

[11] However, the usual outcome is that such papers are simply returned to the authors without comment.

[12] For one such study see (13).

correlation between excess heat production and the formation of ^4He; that of Bockris and his co-workers in that they establish the formation of ^4He in the lattice of Pd. I note also that Miles has reported the first measurements using fluidized beds of Pd particles (26). The work of McKubre et al using flow calorimetry has established that excess heat production is not an artefact of isoperibolic calorimetry !

The listing in Table 1 has also singled out a number of other contributions including that on charged particle emissions (27) and laser stimulation of excess heat production (28).Measurements at much lower incident energies of the deuteron beam than those used hitherto in the investigation of "Hot Fusion" have shown that more complicated collision processes come into play at such lower energies (such as the channel (D) (29) than the channels (A) - (C) which have been observed in "Hot Fusion" :

$$D^+ + D^+ \rightarrow H^+ (3MeV) + T^+ (1MeV) \sim 50\% \qquad (A)$$

$$D^+ + D^+ \rightarrow n (2.5MeV) + {}^3He^{+4} (0.81MeV) \sim 50\% \qquad (B)$$

$$D^+ + D^+ \rightarrow {}^4He + \gamma (24MeV) \sim 50\% \qquad (C)$$

$$D^+ + D^+ + D^+ \rightarrow T^+ (4.75MeV) + 3He^{++} (4.75MeV) \sim 10^{-2}\% \qquad (D)$$

One can therefore speculate whether channel (C) which has a very low cross-section for fusion at low pressures, may not have a much higher cross-section for fusion in a lattice where the production of ^4He is evidently not accompanied by the generation of a γ-ray (1)

The development of the theoretical studies (1), (16) has led to a recognition that one can use the electric potential developed along a thin strip (a component of the vector potential) to enhance the generation of excess enthalpy (30), (31). This is in fact the Quantum Mechanical consequence of coherence in the electrodiffusion of deuterium in palladium.[13] The formation of ^4He commensurate with excess enthalpy generation has been observed. Under extreme conditions the thin strips melt (boil ?) in the most negatively polarised region.[14] In this context, I also note the work of Arata (36) on the generation of excess enthalpy in nanoparticles of palladium. A plausible interpretation of these experiments is that these particles are destroyed by a single step (or, at any rate, by a small number of steps).[15] Our own consideration of such limiting patterns of behaviour (37) led us to the consideration of the compound Na_2ReD_9. At the time of our discussions, this compound did not exist whereas Na_2ReH_9 was known. Moreover, two research groups expert in the Chemistry of relevant syntheses, failed to make the deuterated species. Although it is possible to devise numerous arguments to explain the non-existence of Na_2ReD_9, the simplest of these is that this compound disintegrates on the typical time-scales of chemical

---

[13] The electrodiffusion of hydrogen in palladium was first observed by A. Coehn in 1929 (32). The propagation of the γ-phase of Pd-H along a wire is discussed in (33).

[14] The importance of this observation is that we can estimate the specific rate of excess enthalpy generation required to achieve this condition. These estimates lie in the range 0.5-50MWcm^{-3} depending on the nature of the assumptions. Such high rates must be contrasted with the prolonged generation of excess enthalpy at the boiling points of the electrolyte in a "conventional" electrochemical system where the specific excess rate remained restricted to ~ 2KWcm^{-3} (34), (35).

[15] Which will explain our choice of "massive" electrodes for our investigations.

syntheses. It is evident that we need to develop "calorimetric syntheses" to study the production of such potentially high energy materials.

In this context, we should also note the direct thermal imaging of "hot spots" on the surfaces of electrodes using infra-red imaging (38). Developments of this methodology (e.g. by using scanning laser-thermometry) should allow the direct determination of the space-time distributions of the fusion steps as well as of the Q-values of these steps. Two of the authors have also introduced a new variant of the electrochemical method of generating excess enthalpy the electrolytic codeposition of palladium and deuterium (39). It has been shown that this method leads to enhanced rates of excess enthalpy generation as compared to the standard method of electrolytic charging of massive electrodes with deuterium (40).

I note finally an extreme example of enthalpy generation but at zero enthalpy input at temperatures close to the boiling point of the electrolyte, a phenomenon which has been variously called "After-Effect" (41), "Heat-after-Death" and "Heat-after-Life". Such enthalpy production has been maintained for durations of up to 8 days.

I believe that the work carried out thus far amply illustrates that there is a new and richly varied field of research waiting to be explored. Moreover, it seems likely that it will be possible to develop new sources of energy which will be able to operate over a wide range of conditions. Most of the work to date has been carried out at temperatures below the boiling point of the electrolyte but we note that more than 50% of the worlds energy is consumed at temperatures below 70°C. We also note that it would be relatively straightforward to raise the Quality of the heat by using well-established methods.

TABLE 1 SOME MILESTONES IN COLD FUSION RESEARCH

G. Preparata et al	Theory of the Subject, Chapter 8 in (1), (16).
P. Hagelstein	Theories of the Subject, (17).
Scott R. Chubb	Theories of the Subject, (18)
Y. Kim	Theories of the Subject, (19)
E. Del Giudice et al	Theory of transmutations at lower energies, (20).
Y. Imamura	Low energy transmutations, (21).
G.H. Miley	Low energy Transmutations, (22).
M.H. Miles	Correlation of excess heat with production of ^{4}He (23); fluidized beds (26).
M. McKubre	Correlation of excess heat with production of ^{4}He; flow calorimetry. (24)
J.O'M Bockris	Generation of ^{4}He in the lattice; transmutations (25)
E. Del Giudice F. De Ninno et al	The importance of the vector potential; generation of ^{4}He; melting of electrodes, (29), (30).
F.E. Cecil et al and others	Charged particle emissions, (27)
D. Letts E. Takahashi	Laser stimulation (28). "Hot Fusion" processes at low incident Deuteron beam energies.
Y. Arata	Generation of heat in small particles (35); see also comments in main text (37)
S. Szpak	Hot spots and mini explosions (38); codeposition of Pd and D, (39), (40).
G. Mengoli	Heat after Death (after effect), (41).
Dispersed authorship	isotopic abundances; evidence for photofission; transmutations.

Iwamura

References

1) Giuliano Preparata, "QED Coherence in Matter," World Scientific, Singapore, New Jersey, London, Hong Kong, QC 173.454.P74 (1995), ISBN 9810 222 491.

2) M. Fleischmann in Editor Xing Z. Li, Proceedings of the 9th International Conference on Cold Fusion, Beijing, 19-24th May 2002, page lll; Tsinghua University Press, ISBN 7-302-06489-X.

3) M. Fleischmann, A. Oliver and J. Robinson, Electrochimica Acta, 31 (1986) 899.

4) A. Bewick and B. Thomas, J. Electroanal. Chem., 70 (1976) 329; 84 (1977) 127; 85 (1977) 329.

5) A. Arani, I. Bono, E. Del Giudice and G. Preparata, Int. J. Mod. Phys., B9 (1995) 1813.

6) E. Del Giudice, G. Preparata and M. Fleischmann, J. Electroanal. Chem.,482 (2000) 110.

7) Percy Williams Bridgeman, "The Physics of High Pressure," International Textbooks of Exact Science, London (1947).

8) M. Fleischmann, S. Pons and M. Hawkins, J. Electroanal. Chem., 261 (1989) 301; 263 (1989) 187.

9) M. Fleischmann, S. Pons, M.W. Anderson, L.J. Li and M. Hawkins, J. Electroanal. Chem., 287 (1990) 293.

10) P.I. Dee, Nature, 113 (1934) 564.

11) P.I. Dee, Proc. Roy. Soc., 148A (1935) 623.

12) M.C. Oliphant, P. Harteck and Lord Rutherford, Nature, 113 (1934) 413.

13) M. Fleischmann and M.H. Miles, "The Instrument Function" of Isoperibolic Calorimeters: Excess Enthalpy Generation due to the Parasitic Reduction of Oxygen", paper presented at this Meeting.

14) M. Fleischmann, S. Pons, Monique Le Roux and Jeanne Roulette, Trans. Fusion Technology, 261 (1994) 323.

15) M. Fleischmann, Proceedings of the 5th International Conference on Cold Fusion Monte Carlo (1995) 140.

16) T. Bressani, E. Del Giudice and G. Preparata, Nuovo Cimento, 105A (1989) 845.

G. Preparata, Proceedings of the 5th International Conference on Cold Fusion,

Monte Carlo, (1995) 265.

17) P. Hagelstein, see this meeting and references cited in the papers.

18) Scott R. Chubb, see this meeting and references cited in the papers.

19) Y. Kim, see this meeting and references cited in the paper.

20) E. Del Giudice, A.De Ninno and A. Fratolillo, this meeting.

21) Y. Iwamura, T. Itoh and M. Sakano in Editor F. Scaramuzzi, Proceedings of the 8th International Conference on Cold Fusion, Bologna, Conference Proceedings of the Italian Physical Society 70 (2000) 141. ISBN 88-7794-256-8.
Y. Iwamura, T. Itoh, M. Sakano and S. Sakai in Editor Xing Z. Li, Proceedings of the 9th International Conference on Cold Fusion, Tsinghua University Press, Beijing, (2002) 141, ISBN 7-302-06489-X.

22) G.H. Miley, see this meeting and references cited in the papers.

23) B.F. Bush, J.J. Lagowski, M.H. Miles and G.S. Ostrom, J. Electroanal. Chem., 304 (1991) 271

24) For a survey see Michael McKubre, Francis Tanzella, Poalo Tripodi and Peter Hagelstein, Proceedings of the 8th International Conference on Cold Fusion, Editor : F. Scaramuzzi.
Conference Proceedings of the Italian Physical Society 70 (2000) 141. ISBN 88-7794-256-8.

25) Chun-Ching Chien, Dalibor Hodko, Zoran Minevski and John O'M. Bockris, J. Electroanal. Chem., 338 (1992) 189.

26) M.H. Miles, see this meeting

27) F.E. Cecil, H. Lin and C.S. Galovich, see this meeting.

28) D. Letts, see this meeting.

29) Yuji Isobe, Shigeo Uneme, Kahou Yabuta, Hiroki Mori, Takayuki Omote,Satoshi Ueda, Kentaro Ochiai, Hiroyuki Miyamaru and Akito Takahashi, Proceedings of the 8th International Conference on Cold Fusion, Editor : F. Scaramuzzi.
Conference Proceedings of the Italian Physical Society 70 (2000) 17. ISBN 88-7794-256-8.

30) E. Del Giudice, A. De Ninno, A. Fratolillo, G. Preparata, F. Scaramuzzi, A. Bulfone, M. Cola and C. Giaunetti in Editor: F. Scaramuzzi, Proceedings of the 8th International Conference on Cold Fusion, Bologna, Conference Proceedings of the Italian Physical Society 70 (2000) 47. ISBN 88-7794-256-8.

31) A. De Ninno, A. Fratolillo, A. Rizzo and E. Del Giudice, see this meeting.

32) A. Coehn, Z. Electrochem., 35 (1929) 676.

33) C. Bartolomeo, M. Fleischmann, G. Laramona, S. Pons J. Roulette, H. Sugiura and G. Preparata, Trans, Fusion Technol; 26 (1994) 23.

34) J. Roulette, J. Roulette and S. Pons, Editor M. Okamoto, Proceedings of the 6th International Conference on Cold Fusion, Hokkaido, 1 (1996) 85.

35) M. Fleischmann, Editor F. Jaeger, Proceedings of the 7th International Conference on Cold Fusion, Vancouver, (1998) 119.

36) Y. Arata and Y.C. Zhang in Editor Xing Z. Li, Proceedings of the 9th International Conference on Cold Fusion , Beijing, Tsinghua University Press, (2002) 5, ISBN 7-302-06489-X.

37) S. Pons and M. Fleischmann, unpublished work.

38) S. Szpak, P.A. Mosier-Boss, J. Dea and F. Gordon, see this meeting.

39) P.A. Mosier-Boss and S. Szpak, Nuovo Cimento, 112A (1999) 577.

40) M. Fleischmann, M.H. Miles, S. Szpak and P.A. Mosier-Boss, submitted for publication.

41) G. Mengoli, M. Bernadini, C. Manduchi and G. Zannoni, J. Electroanal. Chem., 444 (1998) 55.

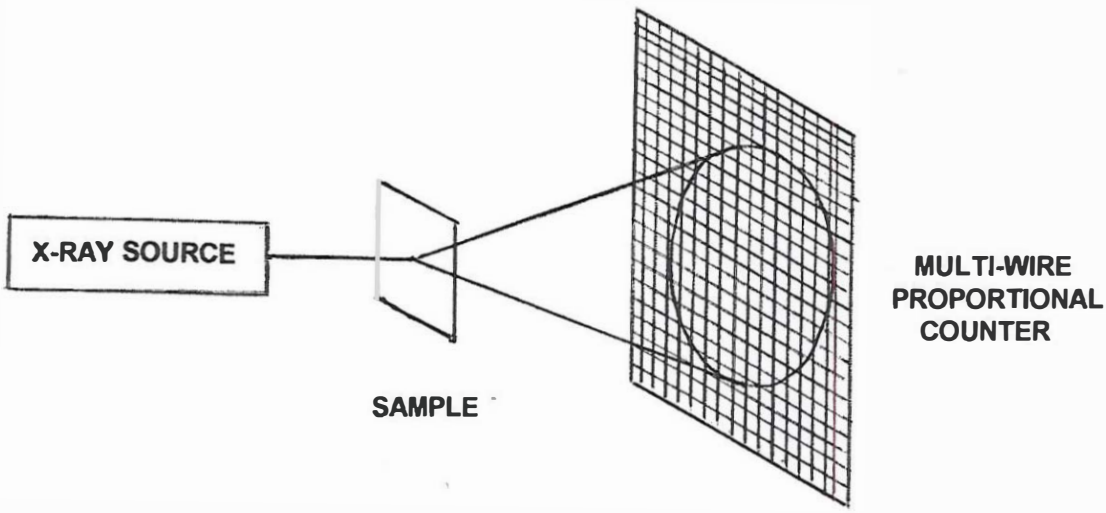

Fig.3A Proposed experiment for measuring surface X-ray diffraction.

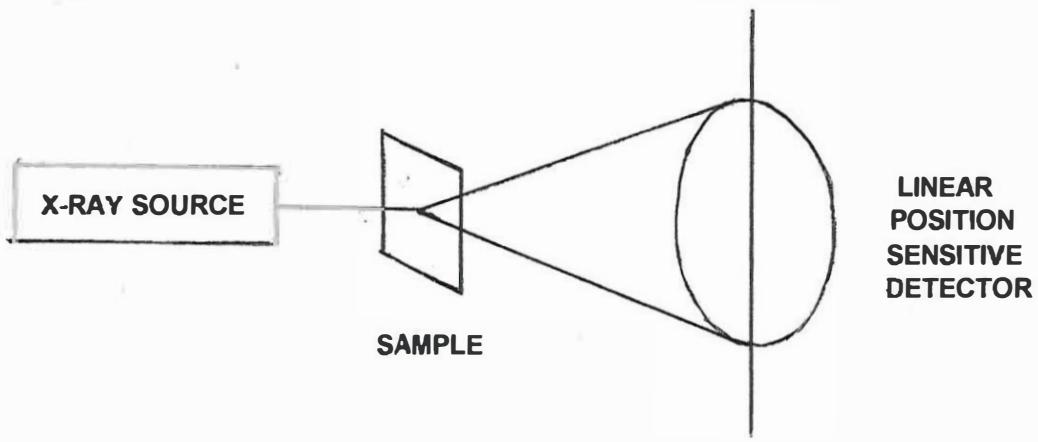

Fig.3B Execution of the experiment on surface X-ray diffraction.

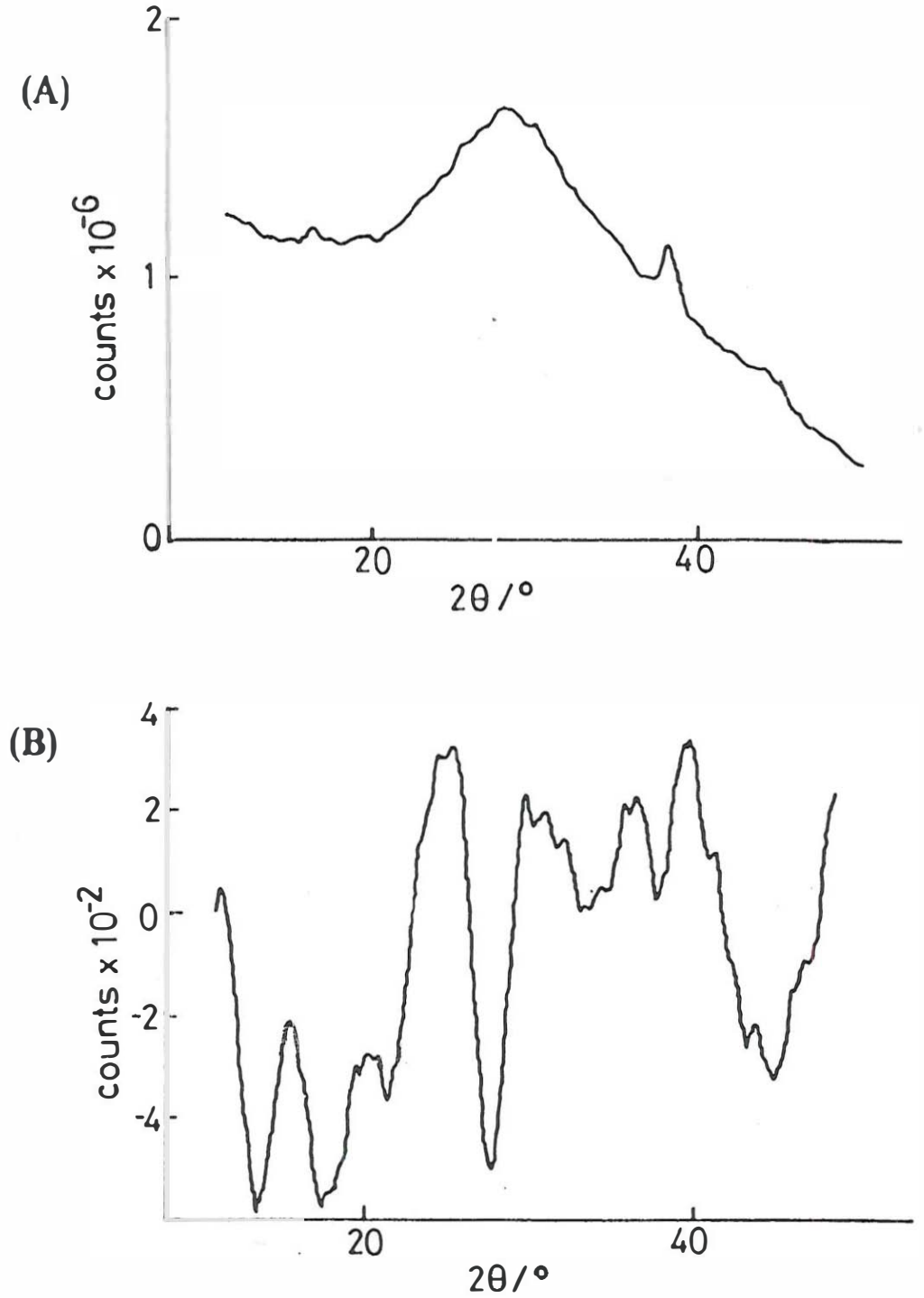

Fig.4 In-situ X-ray diffractograms for a thin silver electrode in 100mM $Pb(ClO_4)_2$ +0.5M $NaClO_4$ + 1mM $HclO_4$.
A) diffractogram obtained after 50h at - 400mV
B) difference diffractogram (diffractogram at - 400mV minus that at -100mV) after 100h modulation at 10^{-2}Hz.

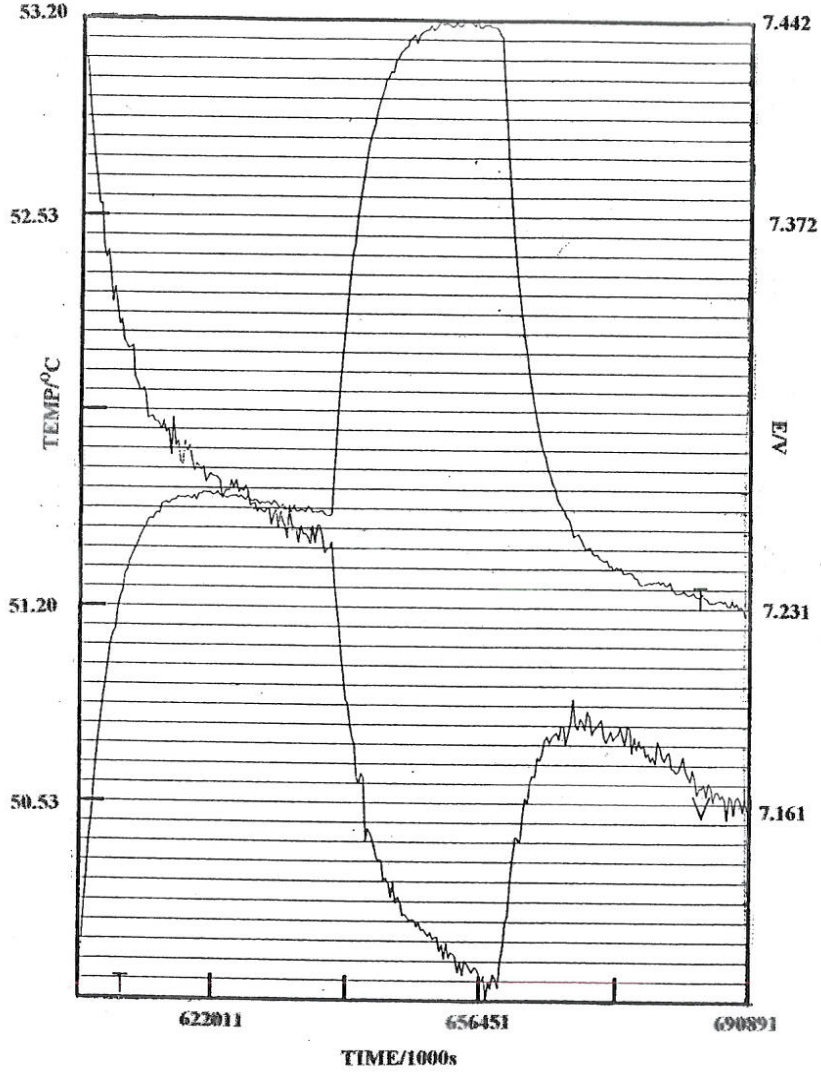

Fig.5A Calibration of an ICARUS -1 cell during the early stages of experiment 4661 conducted by N.H.E. Cathode; 0.4cm diameter by 1.25cm length polarised in 0.1M LiOD/D_2O; cell current 0.5A; calibration pulse ΔQ = 0.2504W

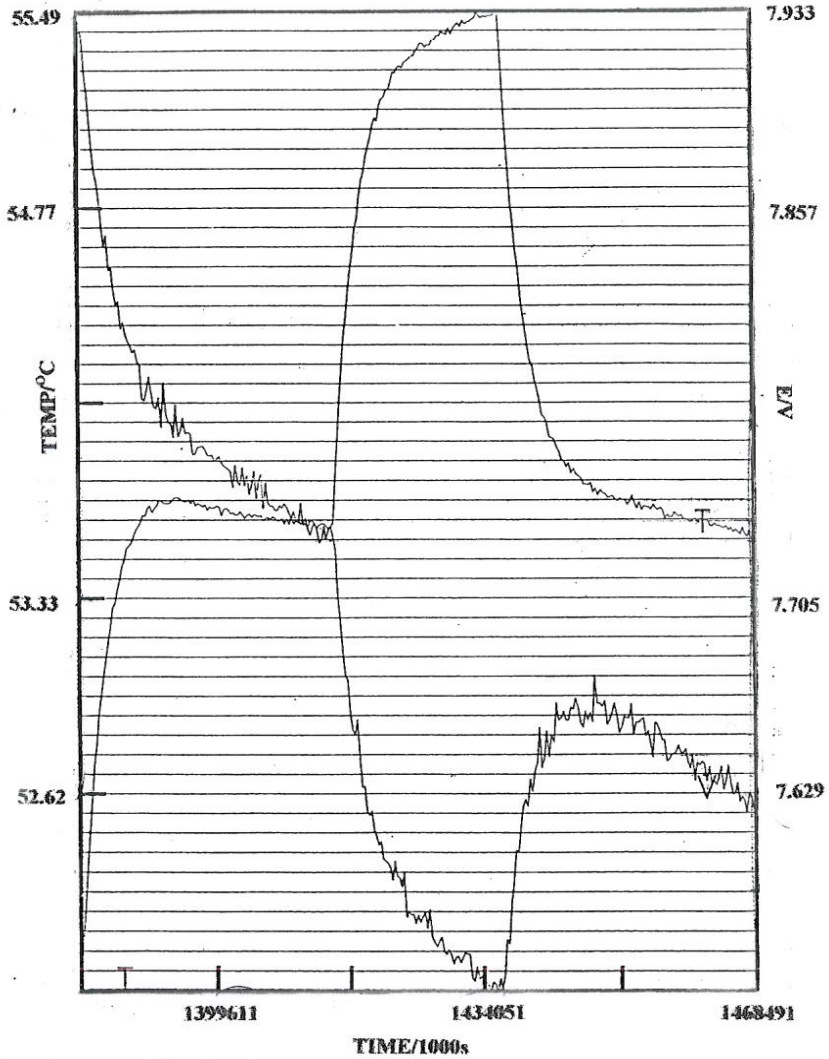

Fig.5B A calibration during the later stages of experiment 4661

SEARCHING FOR THE CONSEQUENCES OF MANY-BODY EFFECTS IN CONDENSED PHASE SYSTEMS

Martin Fleischmann
Bury Lodge, Duck Street, Tisbury, Salisbury, Wilts., SP3 6LJ, U.K.

ABSTRACT

Some of the background work which led to the decision to investigate the behaviour of D_+ electrochemically compressed into Pd host lattices is outlined. The key features of such "Cold Fusion" systems are described.

1. BACKGROUND TO THE RESEARCH ON COLD FUSION

It appears to me that most scientists have the impression that my colleague Stanley Pons and I decided one day in late 1983 to go into the laboratory and to carry out the experiment best described by the statement

"Gee-whiz, let's go in the lab and charge some Pd cathodes with D_+ and see what happens".

It is, of course, perfectly true that this is what happened. However, the conclusion that this was an isolated example is incorrect as has been realised by a relatively small number of research workers(among whom I would number pre-eminently the late Giuliano Preparata and his colleague Emilio Del Giudice). In fact, the decision to investigate the Pd/D system was preceded by a long period during which I asked the question: "is it possible to develop electrochemical experiments which demonstrate the need to interpret the behaviour of condensed matter in terms of the Q.E.D. paradigm?"

Questions which we posed prior to the development of work on "Cold Fusion";
the special position of the work initiated in

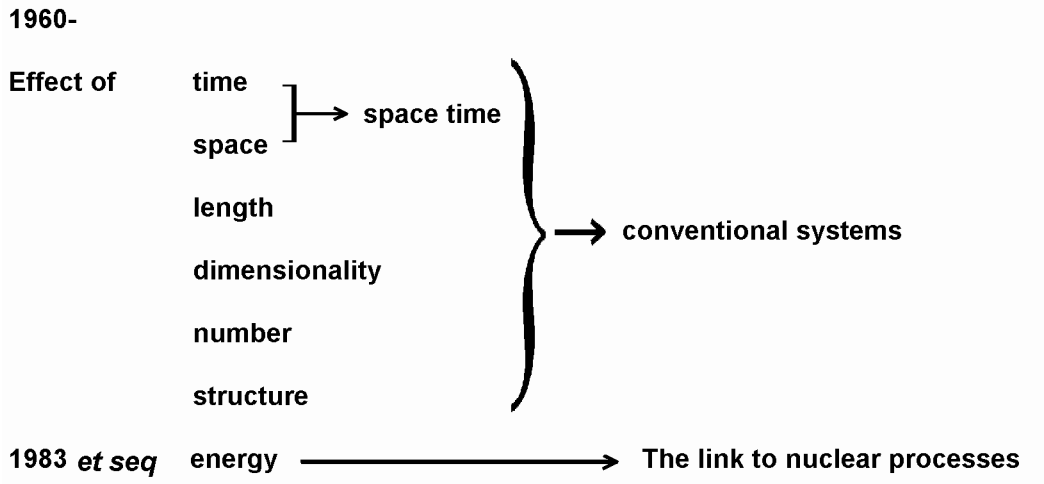

Fig. 1 Background to the work carried out in the period 1960-83

The work on "Cold Fusion" is now reaching the stage where we have a clear demonstration of the presence of the D_+ in the lattice in an extended system with an unique wave-function[1,2,3] and it is therefore opportune to return to the earlier questions.

Of course, we should realise that there are other systems subject to Q.E.D. Coherence [4] and many more examples could be proposed.

In the limited time available in this lecture, I will restrict consideration to three topics illustrating the theme of space-time, Fig. 1. The starting point for this section of our work was the consideration of the

kinetics of fast reactions in solution (in the late 1950's and early 1960's). In the development of relaxation methods it had been shown by Manfred Eigen and his co-workers[5] that the fastest reactions could be interpreted satisfactorily in terms of strong randomisation of the structure (on the time scale of the experiments) coupled to the diffusion controlled recombination of the species[6], see Fig. 2. Consideration of the time scales of the temperature-jump experiments suggests that these experiments were governed by a space-time of the order of 10^{-10}cms.

Such fast reactions in solution had been investigated earlier by a variety of electrochemical methods (e.g. see [7,8,9]). The general principle is illustrated in Fig. 3: the concentration of the species HA is reduced to zero at the electrode surface which permits the probing of the protolytic reactions adjacent to the electrode surface. In this case consideration of the length scales suggests that these reactions are governed by a space-time lying in the range 10^{-16} to 10^{-13}cms. A surprising feature of many of these experiments was the conclusion that the second order recombination rates could exceed those governed by the diffusion controlled constant, k_D. The advent of the results from the relaxation methods persuaded most (all?) scientists that the electrochemical methods gave erroneous results notwithstanding the fact that this methodology was very simple. The possibility that both sets results might, in fact, be correct does not appear to have been considered. Looking at this problem from the point of view of a Physical Chemist, the conclusion that the recombination was limited by the fastest ***observable*** rate given by any particular experimental technique appeared beset with difficulties.

In this vein we also investigated at that time protolytic reactions close to equilibrium using hydrogen ions generated at the surface of a Pd/H electrode[9], Fig. 4. This phase discontinuity and the high diffusion coefficient of hydrogen in palladium allows one to reach recombination rates some 6 orders of magnitude higher than is the case for relaxation methods. The protolytic reactions are now so fast that the "reaction layer" has a thickness given by the dimensions of the anions (here the OH^- ions: the model originally proposed by Brdicka and Wiesner[10]). It was perhaps not very surprising that the rate of recombination was limited by the hydrogen bond frequency, Fig. 4; the space-time of these experiments was therefore of order $2x10^{-22}$cms.

At that time my colleague, Alan Bewick, also constructed a temperature-jump instrument out of the residues of the Harwell Zeta Project.* This instrument allowed measurements at space-times of the order $3x10^{-12}$cms. Coupled reactions in solution were investigated, and we found the expected double relaxation due to these coupled reactions. However, deconvolution of the data showed that the individual rate constants were phase related. We concluded that there had to be a memory propagator in the system which in some unaccountable way was associated with a structure of size ~ 10^{-6}cm (so as to account for the change in behaviour from that shown by relaxation experiments with a restricted frequency response. Fig. 5 summarises the key observations in this series of experiments.

Relaxation measurements

$x = 10^{-5}$cm	$t = 10^{-5}$s	$xt = 10^{-10}$cms	$k2 = kD$

Enhanced relaxation measurements

$x = 10^{-6}$cm	$t = 3x10^{-6}$s	$xt = 3x10^{-12}$cms	$k2 \neq kD$

Electrochemical measurements

$x = 10^{-7}$cm	$t = 2.5x10^{-8}$s	$xt = 2.5x10^{-15}$cms	$k2 \neq kD$

Special Electrochemical measurements

$x = 2x10^{-8}$cm	$t = 10^{-14}$s	$xt = 2x10^{-22}$cms	$k2 >> kD$

There is a memory propagator associated with a structure of order

$x = 10^{-6}$cm

Fig. 5 The key observations for the kinetics of the reactions of ions in solution

*Footnote: This was the earliest attempt to initiate "Hot Fusion" in a plasma. The conclusion that this had been achieved was later found to be incorrect.

Furthermore, we became concerned about the nature of the model used to interpret the behaviour of electrolyte solutions. Fig. 6 illustrates this Debye-Huckel model based on the electrostatic interactions of the ions. However, the ions are not at rest and, if we accept the model of Brownian motion of the ions, Fig. 7, we can see that this model is not consistent with microscopic reversibility because the ions will radiate energy both during acceleration and de-acceleration (the Maxwell equations). Such models therefore violate the Second Law of Thermodynamics and are inadmissible.

I presented these results to a colleague whose principal interest lay in Q.C.D. His comment was immediate: "you must model these systems in terms of Q.E.D." As I recall my response was ; "just so, but how?" In the intervening years I could never find a reason for the development of a structure of order ~ 10^{-6}cm so I put the whole matter aside until 1995. In that year Giuliano Preparata and his colleagues showed that the application of Q.E.D. to water led to the conclusion that the system would be divided into coherent and incoherent regions [11]. Ions will be confined in the incoherent regions where they will themselves form a coherent system. The application of such a model to electrolyte solutions, Fig. 8, has been discussed [12].

The development of this model therefore gives a basis for the interpretation of the reactions of ions in solution but this will certainly prove to be an intractable problem. On the other hand, the interpretation of other systems may be more straightforward. At I.C.C.F. 8 I drew attention [13] to the interesting work of Zhadin et al [14] : the application of a weak static magnetic field and an even weaker alternating weak magnetic field leads to a low frequency resonance of the electrolytic conductivity, Fig. 9. My Italian colleagues do not wish to talk about this topic at the present Conference. However, I believe that the interpretation of the topic [15] is instructive, Fig. 10 : the application of the alternating field can lead to the extraction of ions from the boundary between the coherent and incoherent regions and, thereby, a transient increase in the electrolytic conductivity. This example is instructive for two principal reasons: in the first place the effects of Q.E.D. on the structure of the system take place with low or zero changes of entropy so that they are difficult to observe; secondly, the application of Q.E.D. normally leads to unexpected and unusual consequences (here the development of a "battery" induced by magnetic fields) so that the consequences are consigned to the field of "Pathological Science".

Before considering the third example of the effects of space-time on physical processes, let us return to the position in the early 1960's. Apart from the single example of discussions of the outcome of our measurements of the kinetics of fast reactions in solution, the reactions to our proposal that such systems were subject to the twin effects of memory propagators coupled to the development of a structural element were uniformly negative (frequently, quite violently so). I therefore decided that any investigation of the possible effects of Q.E.D. had to be carried out within an hidden agenda: the systems had to be investigated within the accepted frameworks of Classical and Quantum Mechanics while the possible influence of many-body effects and of Q.E.D. would have to emerge from the interpretation of the results:

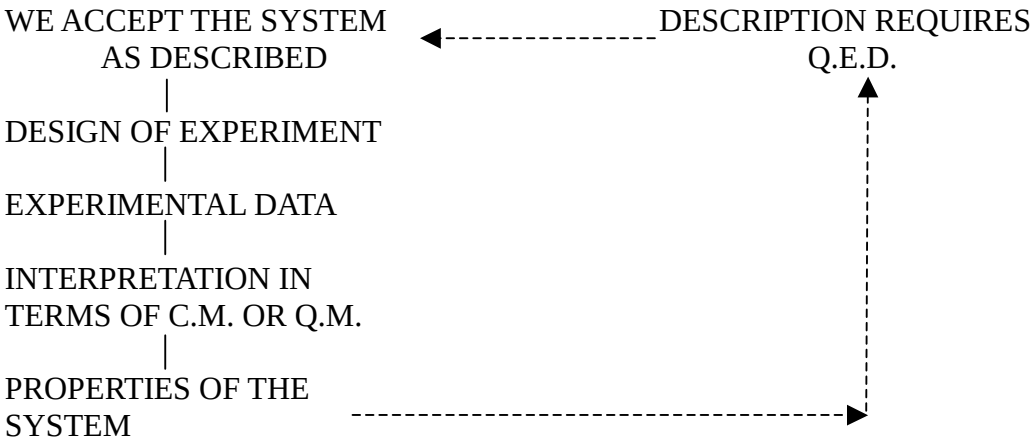

Fig.11 The hidden agenda

This process also had the advantage of avoiding the presupposition of the reality of the importance of the effects we were seeking to illustrate: after all, it might well have turned out that the effects were unimportant or not measurable! These "hidden agendas" had an important influence on the

development of the work on "Cold Fusion".

Our preoccupation with ionic processes at small space-times led to the examination of transport phenomena and chemical reactions in short pores of narrow diameter. After a number of false starts we focused eventually on transmembrane ion conduction across pores in lipid bilayers, Fig. 12. (modelling in terms of classical mechanics indicates space-times of the order $5x10^{-16}$cms). It is of interest that the very existence of such membranes (perhaps the most directly observable result for this system) is not consistent with the Second Law of Thermodynamics! A possible explanation is in terms of Q.E.D.[16].

It has been known for some time [17,18,19], that the insertion of pore forming molecules such as the polypeptide alamethicin, leads to steps in the transmembrane ion current such as those seen in Fig. 13 (taken from our own data [19]). Systems of this kind are ideal for investigation by electrochemical methods because we can determine the kinetics of transition between adjacent states (due to the insertion / removal of successive molecules of the pore former) and the energetics of each state (from the probability of the occupation of that state) [19]. Such measurements lead to the model shown in Fig. 14.

The measurements of the energetics led to the surprising result shown in Fig. 15. We can only explain such a result if the edge energy of the pore is negative whereas the bulk energy is positive so that we reach an upper reflecting state. In contrast, the kinetics of conventional 2-dimensional nucleation are governed by a positive edge and negative bulk energy, so that we reach an upper absorbing state, Fig. 15. We should note that the signs of these free energy terms could have been predicted from the very fact that the membranes are stable! However, we need to ask : how can it be that the bulk free energy is positive with regard to the macroscopic electrolyte? This explanation requires us to invoke the Q.E.D. of water [11], see Fig. 8: the "pore" is filled by an incoherent domain of the electrolyte solution which, of course, has a positive free energy with respect to the macroscopic electrolyte.

The measurement of the kinetics of transition between adjacent states leads to a further surprising result. It has been found that these transitions conform strictly to a birth-and-death process i.e. the transitions only take place between adjacent states [19]. At the same time, elementary considerations based on the size of the pores, show that these pores are empty (free of ions) for an appreciable fraction of time so that the current-time transients should follow the pattern shown in the lower half of Fig. 16. This is a simple demonstration of the fact that the "noise" levels in the experimentally observed transmembrane ion currents are too small. We conclude that the pores and their adjacent liquid volumes are parts of a single quantum system, Fig. 17 (quantum systems are only subject to quantum noise). The operation of the "hidden agenda" will be apparent.

Fig. 17 also shows the ways in which we can judge the necessity of carrying out a paradigm shift to Q.E.D. The conventional view is that this has to be judged in terms of the achievement of a mathematically complete theory. However, it appears to me that this can lead to rather sterile debates and we have therefore relied on a more empirical approach: the need to avoid violation of the Second Law of Thermodynamics in the modelling and the need to develop internally consistent interpretations. As far as this second aspect is concerned, we find all too frequently that different aspects of behaviour of a given system can be interpreted quite adequately in terms of Quantum or Classical Mechanics but that these interpretations are then not internally self-consistent (the Pd/H and Pd/D systems abound with such examples). It seems to me, therefore, that we should explore the consequences of using Q.E.D. as the paradigm of necessity at least at this stage of development of research in the Natural Sciences.

RESEARCH IN "COLD FUSION"

By the beginning of the 1970's (and, certainly, by the beginning of the 1980's) we had reached a stage which demonstrated the need to invoke Q.E.D. in the modelling of numerous systems (however, I note that we had certainly not reached a complete understanding of many of these systems). The time was therefore opportune to take the next step in the development of the research programme: the addition of small amounts of energy per species to an extended quantum system and the investigation whether this could, in the limit, lead to nuclear reactions, Fig. 1. We judged the likelihood of any clear demonstrations of such effects to be very small! (I recall saying to Stan Pons at the time: "there is a chance in a billion that we will see anything". Nevertheless, we also judged the consequences of any positive observations to be quite incalculable and we therefore decided to go ahead with this topic. A positive result in this field of research would have given us the necessary impetus to reinvestigate other systems such as those described in the previous section)

Although the winter of 1983 was the time at which we started systematic work on this topic, this was not the first time at which I had considered carrying out research in this field. I had found the papers of Alfred Coehn [20,21] at the end of 1947. Coehn had found that hydrogen deposited at the apex of a zig-zag configuration of Pd wire, Fig. 18, could be made to move more rapidly towards a negatively polarised end

of the wire than by diffusion alone, see Fig. 19, and less rapidly towards the positively polarised end (the dotted line shows a reversal of the polarity applied to the wire). There was at that time one of the periodic phases of interest in "exploding wires" and it appeared to me that the observations of Coehn might open up a slim chance of inducing nuclear processes if his methodology were combined with such explosions (which one would now describe under the heading of inertial confinement). However, at that time judged from the available perspectives of Quantum Mechanics, this was a very slim chance indeed.

This topic became better defined at the beginning of the 1970's by which time we had realised that the behaviour of D^+ in Pd could only be explained if it were in a many-body system [22] We therefore investigated the Raman Spectroscopy of β-Pd H with the intention of carrying out the experiment described by Fig. 20. The results we obtained were confusing and the topic developed rapidly into Surface Enhanced Raman Spectroscopy, SERS. We decided that the topic of using laser excitation of D^+ confined in the Palladium lattice was hardly consistent research in the University Sector!

The experiments of Coehn were not the only additional factor influencing our decision to start work on the topic of "Cold Fusion". The discovery of the "Hot Fusion" channels (A) and (B) by Oliphant, Harteck and Rutherford[23] had been followed rapidly by measurements of the first channel by Dee[24,25] using a Willson Cloud chamber.

$$D^+ + D^+ \rightarrow H^+ (3MeV) + T^+ (1MeV)\ 50\% \qquad (A)$$

$$D^+ + D^+ \rightarrow n\ (2.45\ MeV) + He\ (0.81MeV) \quad 50\% \qquad (B)$$

$$D^+ + D^+ \rightarrow He + \gamma\ (24\ MeV)\ 10^{-5}\% \qquad (C)$$

$$D^+ + D^+ + D^+ \rightarrow T^+ (4.75MeV) + {}^3He^{++} (4.75MeV)\ 10^{-2}\% \qquad (D)$$

A surprising feature of these measurements was that a significant proportion of the tracks were at 180^0 rather that the expected ~160^0 (corresponding to the incident energy of 200kV of the deuterons). As Phillip Dee observed, the tracks at 180^0 had to be attributed to the fusion of deuterons which had lost their incident energy in the target!

It is appropriate here to "fast forward" to the present day. It has been found that the cross-sections of the fusion channels observed at high incident energy are not a good guide to the behaviour at much lower energies and that more complicated collision processes come into play at these lower energies e.g. channel (D)[26]. One can therefore speculate whether channel (C) which has a very low cross-section for fusion ~ *in vacuo*, may not have a much higher cross-section for fusion in a lattice where the production of ^4He would not necessarily be accompanied by the generation of a γ -ray.

This early work in the 1930's developed rapidly into the production of self-gettering neutron tubes. It is difficult now to obtain specifications for these tubes but such information about the neutron flux as is available suggests that the excess energy produced in these tubes would be a measurable fraction of the breakeven value. Needless to say, this fraction would be much higher if there were additional outgoing channels. However, it proved to be impossible to initiate a programme on the thermal balances in theses tubes as they had been withdrawn.

As is well-known we initiated a programme on thermal balances within the Pd-D system using isoperibolic calorimeters of the type illustrated in Fig. 21: it seemed to us to be reasonably straightforward to pose the question "is the electrolysis of D_2O using Pd cathodes in thermal balance or is there any evidence for excess enthalpy generation?" While we still believe that this is the case, such calorimetric measurements have proved to be somewhat complicated. Thus, for example, it does not appear to have been appreciated that it is not possible to calibrate any calorimetric device if the system contained in the device generates fluctuating excess enthalpy. If that is the case, we will simply conclude that the measurement system is inaccurate and/or obtain an invalid calibration. In fact, it is necessary to carry out an extensive series of "blank" experiments to obtain the "instrument function" and to validate the behaviour of the system. We have found that the electrolysis of D_2O using Pt cathodes provides a suitable "blank" but we note also that such "blank" measurements have only rarely been carried out.

Let us consider the precision and accuracy of the instrumentation shown in Fig. 21. (using the analogy of shooting at a target, Fig.22). Our objective will always be to produce an instrument which is both accurate and precise; the worst case scenario will be if this instrument is both inaccurate and imprecise. However, all too often, instruments are either accurate but imprecise or else inaccurate but precise. Initially we believed that the behaviour of the calorimeters was given by this last description. We therefore laid great stress on the determination of the differential lower bound heat transfer coefficient which describes the local behaviour of the calorimeter with the assumption that there is no excess enthalpy

generation. An example for a "blank" experiment is shown in Fig. 23. We can see that the heat transfer coefficients show a small systematic decrease with time (due to the progressive lowering of the electrolyte level caused by the electrolysis) superimposed on the natural errors of the system (due to the "noise" in the thermal measurements). Use of the central value of the heat transfer coefficient to evaluate the rates of excess enthalpy generation gives results such as those illustrated in Fig. 24 where we make a comparison to the results predicted by a normal distribution (see further below).

By contrast, in the presence of variable rates of excess enthalpy generation, the lower bound heat transfer coefficient shows much more marked variations with time than those shown in Fig. 23. We can then use the maximum value of this coefficient as a measure of the true heat transfer coefficient and evaluate the rates at other times throughout the measurement cycle. Fig.25 illustrates this methodology for an experiment carried out at the New Hydrogen Energy Centre in Japan. We can distinguish clearly the initial excess enthalpy due to the exothermic absorption of deuterium in the lattice; this excess enthalpy decreases with time and is followed by a slow build up due to the phenomena we are studying. The results for this experiment are in close accord with those for a closely similar experiment previously published [27].

Although the standard deviation of the point-by-point measurements of the rates of excess enthalpy generation are quite high (5.87 mW, see Fig. 24.) the predicted mean rate is very small (0.079 mW, see Fig. 24). This low mean rate therefore sets a limit on the measurement of excess enthalpy generation in experiments on the Pd/D system, say 10^{-4}x rate of enthalpy input. The high standard deviation is due to the need to differentiate the inherently noisy temperature-time series when calculating the point-by-point values of the lower bound heat transfer coefficients. A better procedure is therefore the evaluation of the integral lower bound heat transfer coefficients based on the backward or forward integration of the time series, Fig. 26 see [29]. It is of some interest that such data can be reduced to a single, time-independent, heat transfer coefficient having a relative standard deviation <0.01%, Fig. 27. It has also been found that the values of the true heat transfer coefficient (based on the injection of known levels of enthalpy using the resistance heater shown in Fig. 21) are very close to the lower bound values which shows that the instrumentation is both accurate and precise (cf Fig. 22).[30].

It has frequently been asserted that our wish to evaluate experimental data sets at high precision and accuracy was part of some kind of abstract exercise. Here I would wish to make three comments on such assertions. In the first place, I can see little point in reducing the precision and accuracy of such evaluations because we will always wish to have the highest achievable levels of statistical significance. Thus we can see that the rates of excess enthalpy generation shown in Fig. 25 reach 300σ! Secondly, such assertions ignore one of the principal objectives of our work which was to measure excess enthalpy generation using microelectrodes (or else assemblies of such microelectrodes), see insert on Fig. 21. The use of such microelectrodes would lead to a marked improvement in the energy efficiency because the Ohmic losses in solution would be markedly reduced. However, this particular development would require calorimetric measurements at much lower power inputs than is the case when using electrodes of conventional size i.e. it requires the development of precise and accurate calorimetry. Thirdly, elementary considerations show that the combination of such microelectrodes with the concepts of electrodiffusion might well give devices in which every discharged deuterium species would undergo fusion and thereby lead to a direct determination of the Q value(s) of the reaction(s).

In this connection we should also note the direct measurement of the temperature excursions at "hot spots" by using infrared imaging [31], a topic which will be covered in a further contribution to this Conference [32]. It is evident that the further development of this methodology (or else the development of alternative methods for localised temperature measurements such as of laser thermometry) should allow the determination of the Q values of all such "hot spots" distributed over the surface of thin film electrodes.

It also appears to me that the need to make repeated calibrations of the calorimetric systems, e.g. see Fig. 28, has not been appreciated. It is found that with increasing time the systems pass through a phase of "positive feedback" i.e. an increase of temperature as caused, for example, by the calibration pulses, leads to an increased thermal output e.g. compare Figs. 29 and 30 given by a data set collected by N.H.E. This onset of "positive feedback" leads to a delayed approach to the steady state following the application of the calibration pulse and a delayed decay to the base-line following the termination of this pulse, Fig.30. Not surprisingly, attempts to derive the true heat transfer coefficient from calibrations subject to such effects lead to the impossible result that the true heat transfer coefficient is smaller than the lower bound value! e.g. see [33].

Transitions through the region of positive feedback lead to the onset of oscillations, Fig.31, which we attributed initially to a transition from an exo to an endothermic regime for the absorption of deuterium [28] but which could probably be attributed more correctly to a transition from a β-to a γ-phase. [34]. We have found it to be desirable to "drive" the systems through such regions (so as to reach the boiling point of the electrolyte, Fig. 28) as prolonged operation in the region of the onset of positive feedback can destroy

the phenomenon of excess enthalpy generation. It is then found that the cells can remain at elevated temperatures but at zero enthalpy input, a phenomenon which has been variously called "Heat-after-Death"[35], "Heat-after-Life" and "After-Effect". The clearest demonstration of this phenomenon is to be found in the publications of Mengoli et al e.g. see Fig. 32 [36].

This phenomenon clearly requires further investigation as it points the way towards the construction of energy efficient systems and as it must be related to other observations of excess enthalpy generation with zero enthalpy input. Equally excess enthalpy generation at the boiling points of the electrolytes require further investigation as the operation of the systems under these conditions would provide sources of low grade heat (however, we should note that steam compression could be used to raise the quality of the heat). Measurements of this kind require the use of some form of dual calorimeter such as those illustrated in Fig. 33 [37,38] where the system can be driven to the boiling point in the lower section while boiling conditions can be maintained in the upper section. It is necessary to use some form of dual calorimetry as the dynamic range of any given instrument is too small to span the whole range of thermal outputs.

Fig. 34 illustrates a measurement made in l994 with an ICARUS-9 calorimeter where boiling conditions were maintained for ~ 50 days at ~ 100% excess enthalpy and specific excess enthalpy outputs > l kW cm^{-3}. However, we should note that the energy efficiency of this system was restricted by the low concentration of electrolyte in the lower section of the calorimeter.

I believe that we need to ask: do the experiments carried out so far (as well as the experiments which could be performed as logical extensions) not indicate that useful and practicable sources of heat could be developed on reasonable time scales? However, we also need to ask: how do we now stand with regard to our understanding of this topic and does this understanding have any wider implications for the development of the Natural Sciences? Here I would recall that a major factor in the initiation of this work was the realisation that hydrogen and deuterium in the palladium lattice could be part of an extended Quantum System. Work presented at this Conference [2] (see also [1]) shows that this idea is indeed correct and that the deuterons can be described by an unique wave function. I believe that this "proof-of-concept" should give an impetus to the search for the wider implications of the Q.E.D. paradigm in the Natural Sciences. Needless to say, the integration of the "Preparata Effect"[2] into the research on "Cold Fusion" should also lead to clearer demonstrations of the phenomena and the implementation of such devices for energy generation.

REFERENCES

[1] M.Cola, A. De Ninno, E. Del Giudice and G. Preparata, Proceedings of the 8th International Conference on Cold Fusion, Conference the Italian Physical Society, Volume 70, ISBN 88-7794-256-8, Editor F. Scaramuzzi, Bologna (2000), 349.

[2] E. Del Guidice, A. De Ninno, A. Frattolillo, M. Porcu and A. Rizzo, this Conference.

[3] E. Del Guidice, A. De Ninno, M. Fleischmann, A. Frattolillo and G. Mengoli, this Conference.

[4] see G.Preparata "Q.E.D. Coherence in Matter" World Scientific Publishing Co. Pte. Ltd. Singapore 1995, QC 173. 454. P74, ISBN 9810 222 491.

[5] M. Eigen and P. De Maeyer, Chapter 18 in Techniques of Organic Chemistry, Editor A. Weissberger, Interscience, New York and London (1963)

[6] P. Debye, Trans. Electrochem. Soc., 82,265 (1942).

[7] W. Vielstich and D. Jahn, Z. Elektrochem., 64,43 (1960).
J.Alberry and R.P. Bell, Proc. Chem. Soc.,169 (1963).
P.Ruetschi, Z. phys. Chem., 5, 323 (1955)
J.Giner and W. Vielstich, Z. Elektrochem., 64, 128 (1960).
H.W. Nurnberg, G. von Riesenbeck and M. von Stackelberg, Z. Elektrochem., 64, 130 (1960).

[8] K. Wiesner, Z. Electrochem., 49, 164 (1943).
R. Brdicka and K. Wiesner, Coll. Czech. Chem. Comm., 12, 39, 138 (1947).

[9] A. Bewick, M. Fleischmann, J.N. Hiddleston and Lord Wynne-Jones, Discussion of the Faraday Society, 39, 149 (1965).

[10] R. Brdicka and K. Wiesner, Naturwiss. 31, 247, 391 (1943).

[11] R. Arani, I. Bono, E. Del Giudice and G. Preparata, Int. J. Mod. Phys, B9, 1813 (1995).

[12] E. Del Giudice, G. Preparata and M. Fleischmann, J. Electroanal. Chem.,482, 110 (2000).

[13] M. Fleischmann, "Giuliano Preparata : An Appreciation" Conference Proceedings of the Italian Physical Society, Volume 70, ISBN 88-7794-256-8 Editor F. Scaramuzzi, Bologna, (2000), xxiii.

[14] M.N. Zhadin, V.V. Novikov, F.S. Barnes and N.F. Pergola, Bioelectromagnetics 19, 41 (1998).

[15] E. Del Giudice, M. Fleischmann, G. Preparata and G. Talpo, accepted for publication in Bioelectromagnetics.

[16] E. Del Giudice and G. Preparata, I. of Biological Physics, 20, 105 (1994).
[17] P. Mueller and D.O. Rudin, Nature, 217, 713 (1967).
[18] L.G.M. Gordon and D.A. Haydon, Biochim. Biophys. Acta, 436, 541 (1976).
[19] M. Fleischmann, C. Gabrielli, M.T. Labram, A.I. McMullen and T.H. Wilmshurst, J. Membrane Biol., 55, 9 (1980).
[20] A. Coehn, Z. Electrochem., 35, 676 (1929).
[21] A. Coehn and W. Specht, Z. fur Physik, 62 1 (1930).
[22] B. Dandapani and M. Fleischmann, J. Electroanal chem., 39, 323 (1972).
[23] M.L. Oliphant, P. Harteck and Lord Rutherford, Nature, 413, (1934).
[24] P.I. Dee, Nature, 113, 564 (1934).
[25] P.I. Dee, Proc. Roy. Soc., 148A, 623 (1935).
[26] Masaguki Ohta and Akito Takahashi, Proceedings of the 8th International Conference on Cold Fusion, Conference Proceedings of the Italian Physical Society, Volume 70, ISBN 88-7794-256-8, Editor F. Scaramuzzi, Bologna. (200) 403.
[27] M. Fleischmann and S. Pons, Proceedings of the 3rd International Conference on Cold Fusion, Frontiers of Science Series No 4, Universal Academy Press Inc., ISBN 4-946443-12-6, Editor H. Ikegami, Tokyo, (1992) 47.
[28] M. Fleischmann, S. Pons, Monique Le Roux and Jeanne Roulette, Trans Fusion Technology 26, 323 (1994).
[29] e.g. see M.H. Miles, M. Fleischmann and M.A. Imam, Naval Research Laboratory Report NRL/MR/6320-01-8526 (2001), Washington D.C. 20375-5320.
[30] Internal Report,
[31] S. Szpak and P. A. Mosier Boss, Il Nuovo Guiento 112A, 577 (1999).
[32] M. Miles, this Conference.
[33] M. Fleischmann, Proceedings of the 5th International Conference on Cold Fusion, Monte Carlo, (1995) 140.
[34] T. Bressani, E. Del Giudice and G. Preparata, Nuovo Cim, 101A, 845 (1989).
[35] S. Pons and M. Fleischmann, Trans. Fusion Technology 26, 87 (1994).
[36] G. Megoli, M. Bernadini, C. Manduchi and G. Zannoni, J. Electroanal. Chem., 444, 55 (1998).
[37] T. Roulette, J. Roulette and S. Pons, Proceedings of the 6th International Conference on Cold Fusion, Editor M. Okamoto, Hokkaido (1996) Volume 1 85
[38] M. Fleischmann, Proceedings of the 7th International Conference on Cold Fusion, Editor F. Jaeger, Vancouver, (1998) 119.

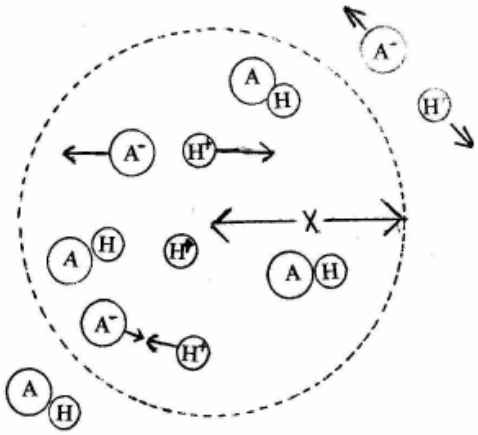

Fig.2 1960's: The fast reactions of ions in solution

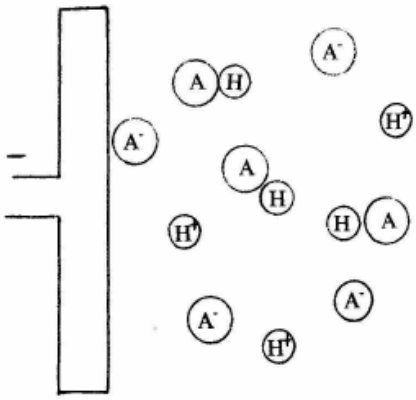

Fig.3 The principle of electrochemical measurements of fast reactions of ions in solution

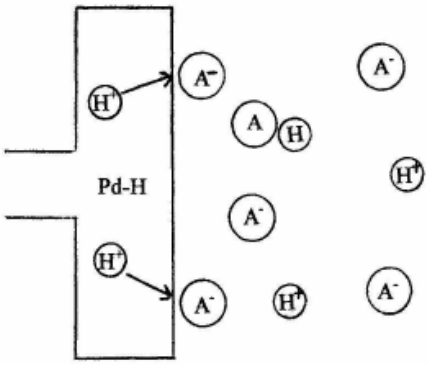

Fig.4 Special electrochemical experiments on the kinetics of fast ionic reactions in solution

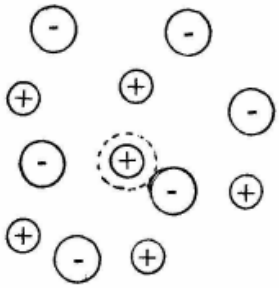

Fig.6 The space charge formed by the electrostatic interaction of ions

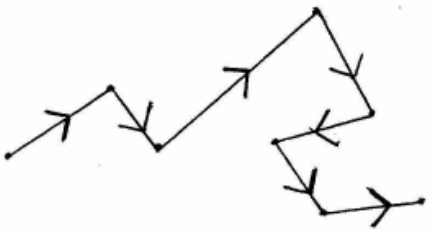

Fig.7 The Brownian movements of ions; the ions are at rest at these points

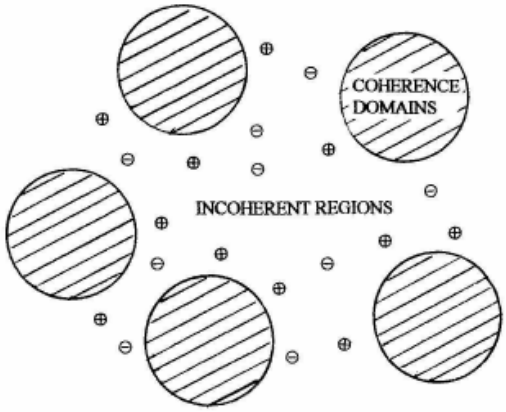

Fig.8 The model of electrolyte solutions based on the principle of Q.E.D. Coherence (12)

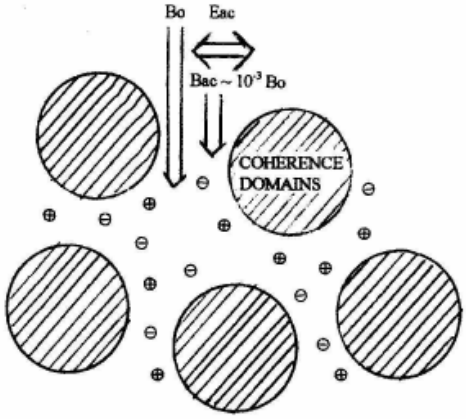

Fig.9 The action of weak static and alternating magnetic fields (14) on electrolyte solutions

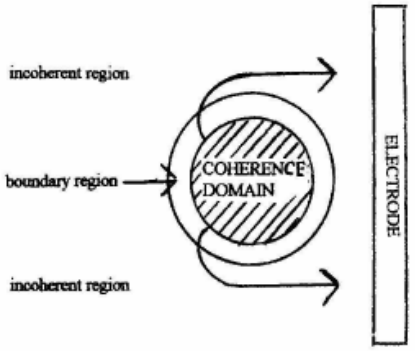

Fig.10 Interpretation (15) of the resonance of the electrolytic conductivity based on the Q.E.D. Coherence of water (11)

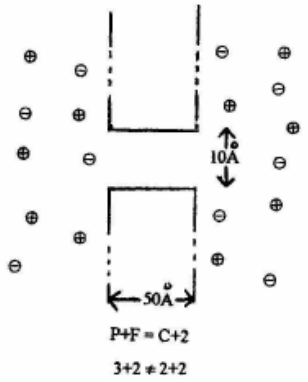

Fig.12 The transmembrane ion conduction across pores in black lipid bilayers; violation of the Second Law of Thermodynamics.

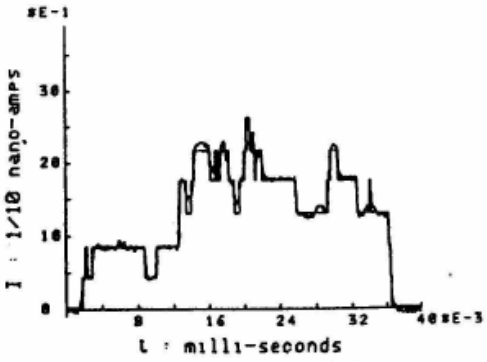

Fig.13 Section of a current (I) - time (t) record of the voltage gated transmembrane ion current induced by alimethicin in a black lipid membrane

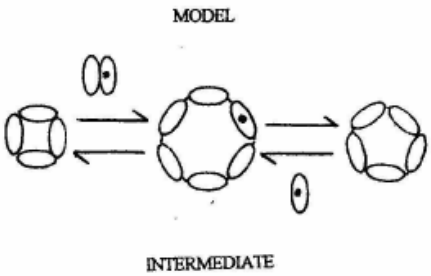

Fig.14 The model for the formation / removal of a pore in the black lipid bilayers

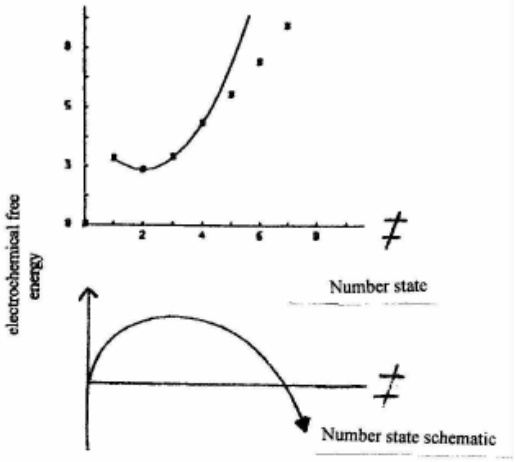

Fig.15 Comparison of the energetics of pore formation with the usual behaviour for two-dimensional nucleation

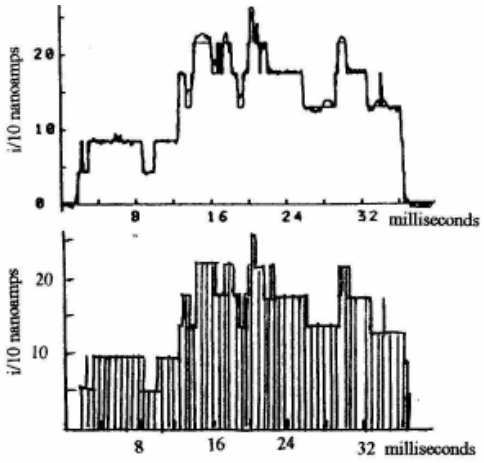

Fig.16 Comparison of the experimentally observed current-time series with that predicted from elementary considerations of the ion transduction process

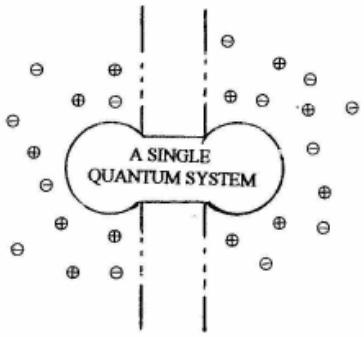

Fig.17 The model of the pore revealed by the hidden agenda.

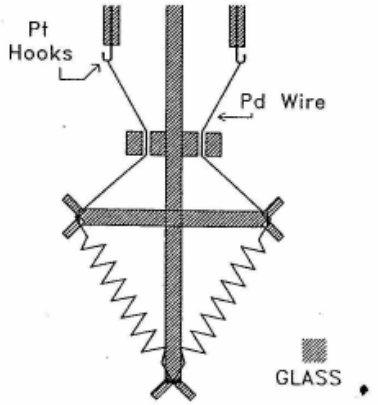

Fig.18 Schematic of Coehn's original experiment (20), (21) for measuring the electrodiffusion of hydrogen along a palladium wire

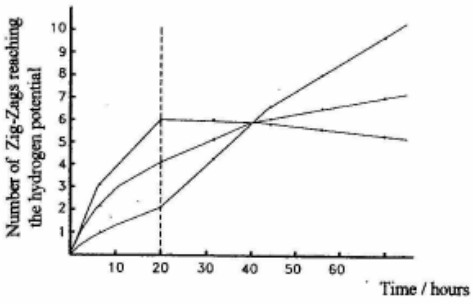

Fig.19 An example of Coehn's measurement (20) (distance between zig-zags = 1.85mm)

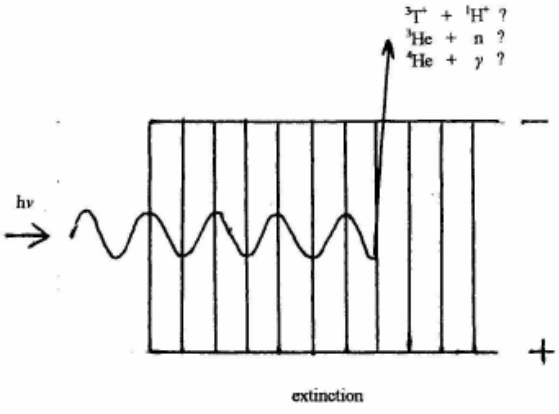

Fig.20 an experiment proposed for the combination of laser excitation with the electrodiffusion of D^+ in a palladium diffraction grating

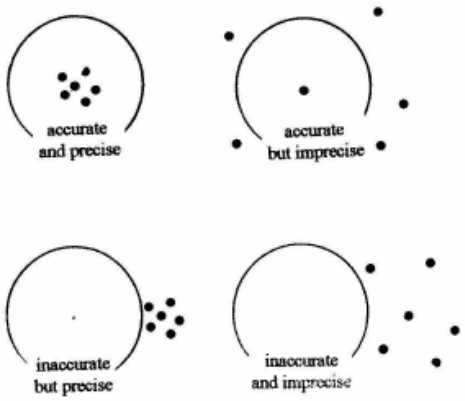

Fig.22 Comparison of "precision" and "accuracy"

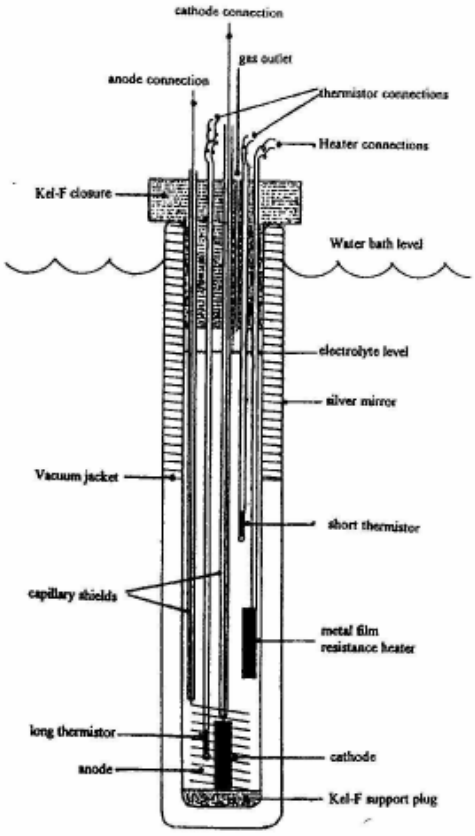

Fig.21 An example of the isoperibolic calorimeters used in our investigations of Cold Fusion Systems

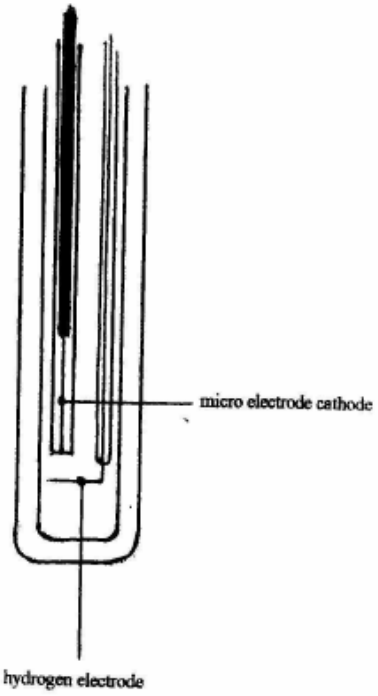

Fig.21 insert: Microelectrode cathode

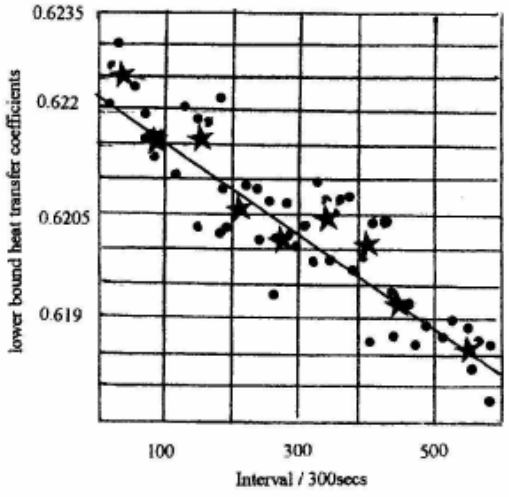

Fig.23 The 11-point means and further 6-point means of the 11-point means of the differential lower bound heat transfer coefficients

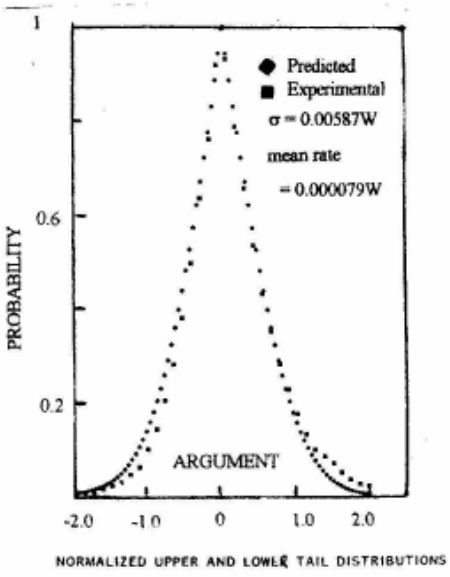

Fig.24 Pt electrode polarised in 0.1Mli0D / D_2O

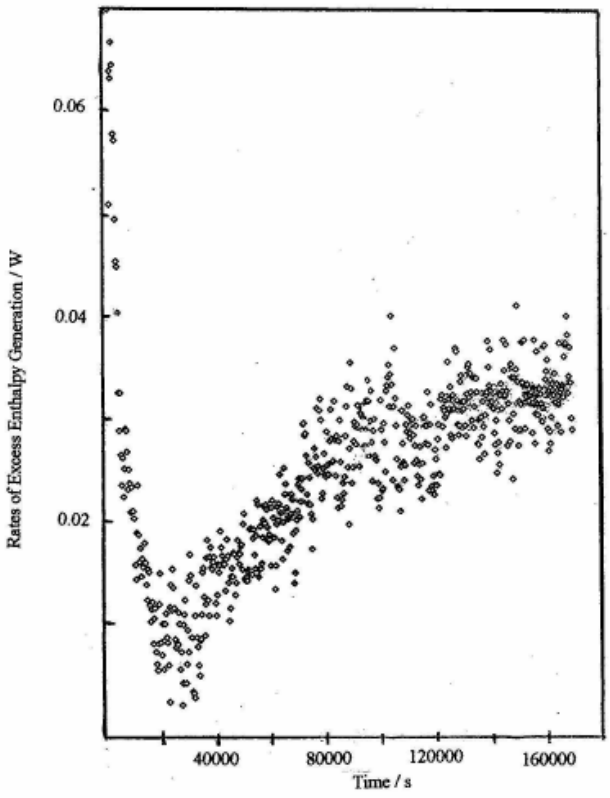

Fig. 25 Variation of the rate of excess enthalpy generation with time for cell 4241 during the first two days of operation of the experiment carried out by N.H.E. Pd electrode polarised in 0.1M LiOD/D_2O.

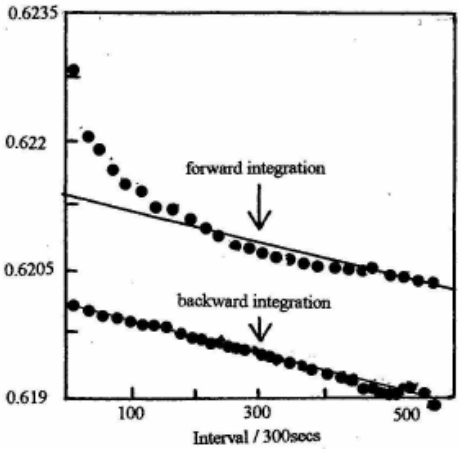

Fig.26 The integral heat transfer coefficients $(k_R')_{21}$ and $(k_R')_{31}$ based on the backward and forward integration of the experimental data

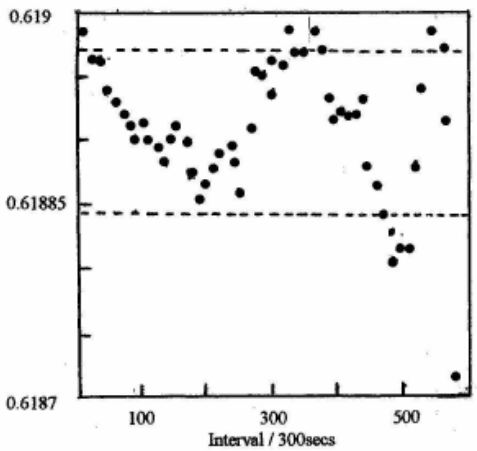

Fig.27 The reduction of the data in Fig.24 to a single time-independent value of the heat transfer coefficient. The dotted lines show ± σ of the data

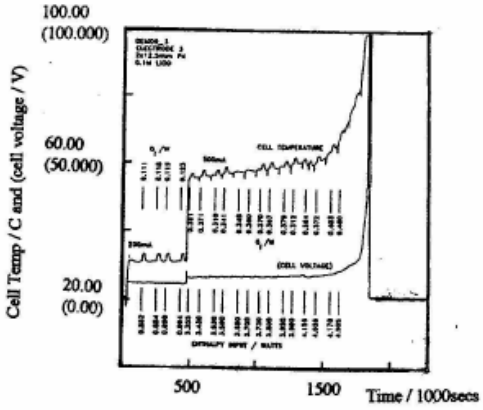

Fig.28 The repeated calibration of an isoperibolic calorimeter

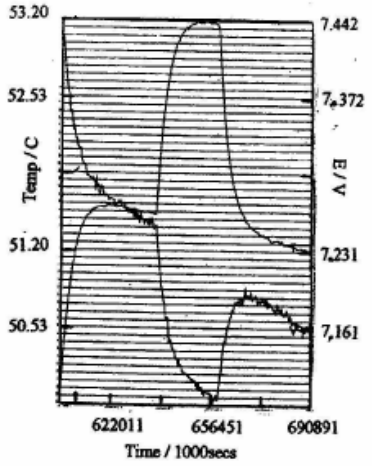

Fig.29 A calibration of an ICARUS-1 cell during the early stages of experiment 4661 conducted by N.H.E. Pd A 10 cathode, 0.4cm diameter, 1.25cm length, 0.1MliODD/D_2O; cell current 0.5A; calibration pulse DQ = 0.2504W.

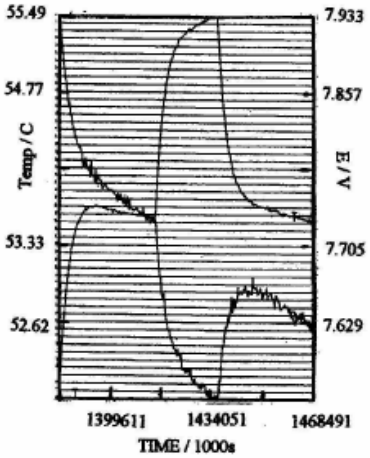

Fig.30 A calibration during the later stages of experiment 4661

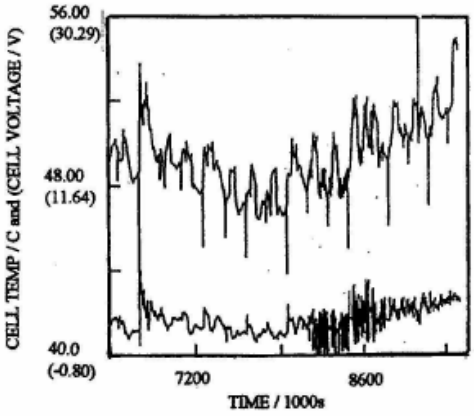

Fig.31 Oscillations in the cell voltage and cell temperature induced by the onset of "positive feedback"

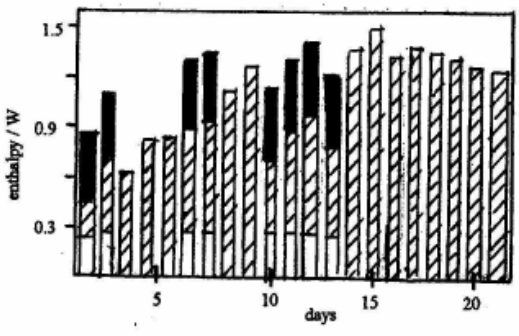

Fig. 32 Generation of excess enthalpy in the temperature region of the boiling point (lightly shaded bars) following the termination of Polarization on Day 14 (36)

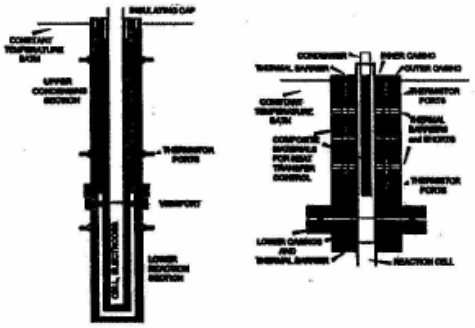

Fig.33 The ICARUS-9 calorimeter

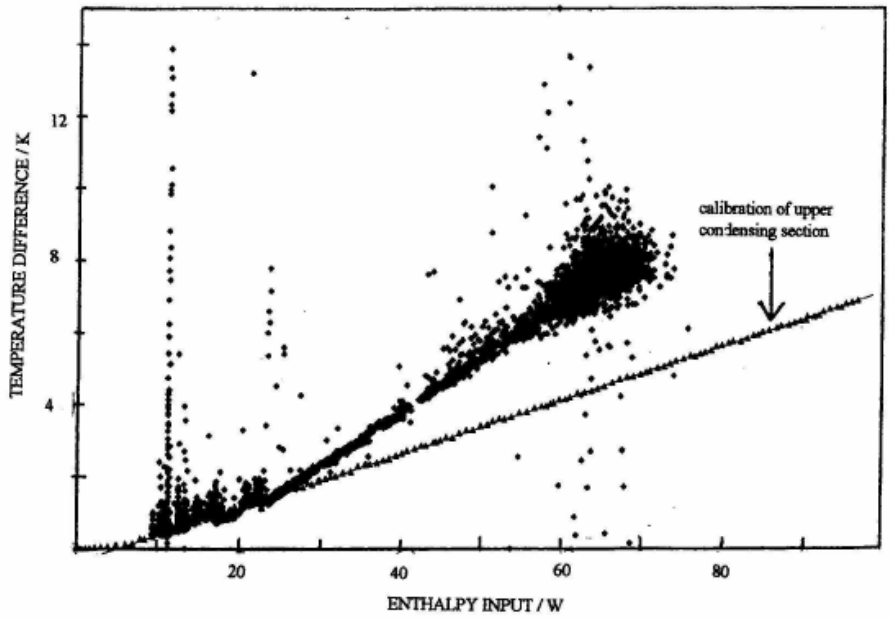

Fig. 34 Comparison of thermal output in the upper section of the ICARUS-9 calorimeter (Fig.33) with the calibration line for this section

Chapter II: Research Topics at SPAWAR Systems Center San Diego (SSC-San Diego)

II.1 Introductory Remarks

The involvement of SSC-San Diego scientists in the research of the F-P effect dates back to May 1989 when they proposed a variant of the usually employed "massive" electrodes, *viz* electrodes prepared by the co-deposition technique, a process in which the Pd^{2+} ions are electrodeposited onto a non-deuterium absorbing metallic substrate (*eg*., Au, Cu, etc.) in the presence of evolving deuterium. Preliminary data, reported in 1991, indicated that electrodes prepared by co-deposition represent an ideal research tool to investigate the F-P effect because: (i) they retain all of the features of "massive" electrodes (*eg,*. positive feed-back, life-after -death), (ii) there is no incubation time, (iii) the D/Pd atomic ratio exceeding unity is obtained within seconds, (iv) the intensity of the F-P effect is higher than using conventional electrodes, and (v) the reproducibility is close to 100%.

In the early days, the reaction responsible for the F-P effect was thought to be $d + d \rightarrow products$. There were difficulties in accepting this model due to a complete lack of the expected reaction product, more specifically, the absence of neutrons. Not having access to the advice of theoretical physicist(s), The approach of SSC-San Diego scientists was as follows: They started with the proposition that any process, chemical or nuclear, can be expressed by a simple statement: $R \rightarrow \sum P + Q$. This statement identifies a process in which specie R (a reactant) is transformed into species $\sum P$ (reaction products) and where Q represents anenergy component of the process(es). This notation provides no information about the mechanism(s) that is associated with the transition process. However, it is obvious that the state of the reactant R is constrained by experimental protocol while that of $\sum P$ is determined by energy considerations as well as the mechanism of the transition from R to $\sum P$. It follows therefore that from an analysis of the reaction products together with energy output, one can arrive at the most probable set of events leading to the initiation of the F-P effect as well as other manifestations of nuclear activities.

II.2 List of Publications

The list of research topics investigated by SSC- San Diego over a decade and the conclusions reached are presented in the reproduced papers published in scientific journals, papers submitted for publication and papers that have been rejected - in some instances without peer review.

II.2.1 Publications in Scientific (Refereed) Journals

1. "On the Behavior of Pd Deposited in the Presence of Evolving Deuterium," S. Szpak, P.A. Mosier-Boss, and J.J. Smith, *J. Electroanal. Chem*., **301**, 255 (1990).

2. "Electrochemical charging of Pd rods," S. Szpak, C.J. Gabriel, J.J. Smith and R.J. Nowak, *J. Electroanal. Chem*., **309**, 273 (1991).

3. “Charging of the Pd^{n}H System: Role of the Interphase,” S. Szpak, P.A. Mosier-Boss, S.R. Scharber, and J.J. Smith, *J. Electroanal. Chem*., **337**, 147 (1992).

4. “Absorption of Deuterium in Palladium Rods: Model vs. Experiment.” S. Szpak, P.A. Mosier-Boss, C.J. Gabriel, and J.J. Smith, *J. Electroanal. Chem*., **365**, 275 (1994).

5. “Comments on the Analysis of Tritium Content in Electrochemical Cells,” S. Szpak, P.A. Mosier-Boss, R.D. Boss, and J.J. Smith, *J. Electroanal. Chem*., **373**, 1 (1994).

6. “Deuterium Uptake During Pd-D Codeposition,” S. Szpak, P.A. Mosier-Boss, and J.J. Smith, *J. Electroanal. Chem*., **379**, 121 (1994).

7. “Cyclic Voltammetry of Pd/D Co-deposition,” S. Szpak, P.A. Mosier-Boss, S.R. Scharber, and J.J. Smith, *J. Electroanal. Chem.*, **380**, 1 (1995).

8. “On the Behavior of the Cathodically Polarized Pd/D System: Search for Emanating Radiation,” S. Szpak, P.A. Mosier-Boss, and J.J. Smith, *Physics Letters A*, **210**, 382 (1996).

9. “On the Behavior of the Cathodically Polarized Pd/D System: A Response to Vigier's Comments,” S. Szpak and P.A. Mosier-Boss, *Physics Letters A*, **211**, 141 (1996).

10. “On the Behavior of the Pd/D System: Evidence for Tritium Production,” S. Szpak, P.A. Mosier-Boss, R.D. Boss, and J.J. Smith, *Fusion Technology*, **33**, 38 (1998).

11. “On the Release of ^{n}H from Cathodically Polarized Palladium Electrodes,” S. Szpak and P.A. Mosier-Boss, *Fusion Technology*, **34**, 273 (1998).

12. “Calorimetry of the Pd + D Codeposition,” P.A. Mosier-Boss, S. Szpak and M.H. Miles, *Fusion Technology*, **36**, 234 (1999).

13. “The Pd/^{n}H System: Transport Processes and Development of Thermal Instabilities,” P.A. Mosier-Boss and S. Szpak, *Il Nuovo Cimento*, **112**, 577 (1999).

14. “Thermal Behavior of Polarized Pd/D Electrodes Prepared by Co-Deposition,” S. Szpak, P.A. Mosier-Boss, M.H. Miles, and M. Fleischmann, *Thermochimica Acta*, **410**, 101 (2004).

15. “The Effect of an External Electric Field on Surface Morphology of Co-Deposited Pd/D Films,” S Szpak, P.A. Mosier-Boss, C. Young, and F.E. Gordon, *J. Electroanal. Chem*., **580**, 284 (2005).

16. “Evidence of Nuclear Reactions in the Pd Lattice,” S. Szpak, P.A. Mosier-Boss, C. Young, and F.E. Gordon, *Naturwissenschaften*, **92**, 394 (2005).

Reprints of the journal articles from 1996 to 2005 are included in this volume of the technical report. Earlier journal articles can be found in volume I of this technical report.

II.2.2 Conference Presentations/Proceedings/Posters

1. "Reliable Procedure for the Initiation of the Fleischmann-Pons Effect," S. Szpak, P.A. Mosier-Boss, and J.J. Smith, in *The Science Of Cold Fusion*, T. Bressani, E. Del Giudice, and G. Preparata, eds., *Proceedings of the II Annual Conference on Cold Fusion*, Como, Italy, June 1991.

2. "Comments on Methodology of Excess Tritium Determination," S. Szpak. P.A. Mosier-Boss, and J.J. Smith, *Proceedings ICCF-3*, H. Ikegami, ed., Third International Conference on Cold Fusion, Nagoya, Japan, Oct. 1992.

3. "Thermal and Pressure Gradients in Polarized Pd/D System," P.A. Mosier-Boss, J. Dea, and S. Szpak, Amer. Phys. Soc., Indianapolis, IN, March 2002.

4. "The Dynamics of the Pd/D-D_2O-Li^+ System as a Precursor to the Fleischmann-Pons Effect," S. Szpak and P.A. Mosier-Boss, 2003 ANS Annual Meeting, San Diego, CA, June 2003.

5. "Polarized D^+/Pd-D_2O System: Hot-Spots and Mini-Explosions," S. Szpak, P.A. Mosier-Boss, J. Dea, and F. Gordon. ICCF-10, Cambridge, MA, Aug. 2003.

6. "Precursors and the Fusion Reactions in Polarized Pd/D-D_2O System: Effect of an External Electric Field," S. Szpak, P.A. Mosier-Boss, and F. Gordon. ICCF-11, Marseille, France, Nov. 2004.

7. "Experimental Evidence for LENR in a Polarized Pd/D Lattice", S. Szpak, P.A. Mosier-Boss, and F. Gordon, Amer. Phys. Soc., Los Angeles, CA, March 2005.

Reprints of the proceedings papers from ICCF-10 and ICCF-11 are included in this volume of the technical report.

II.2.3 Papers in Preparation for Publication

1. "The dynamics of the Pd/D-D_2O-Li^+ system as a precursor to the Fleischmann-Pons effect," S. Szpak, P.A. Mosier-Boss and J. Dea

2. "A note on the development of temperature and pressure gradients in a polarized Pd/D system," J. Dea, P.A. Mosier-Boss and S. Szpak.

Copies of these manuscripts are included in this volume of the technical report.

II.2.4 Papers Rejected

1. “Thermal behavior of the Pd/D system: Transition from exothermic to endothermic absorption,” S.Szpak and P.A. Mosier-Boss, submitted to and rejected by *Thermochimica Acta.*

2.”Nuclear reactions in the Pd lattice,” S. Szpak, P.A. Mosier-Boss, C. Young and F.E. Gordon, submitted to and rejected without comments by *Nature.*

Copies of these manuscripts and the reviewer comments are included in this volume of the technical report.

II.2.5 Patents

1. “Electrochemical Cell Having a Beryllium Compound Coated Electrode,” S. Szpak and P.A. Boss, Navy Case 76707. U.S. Patent No. 5,928,483 issued 7/27/99.

A copy of the patent is included in this volume of the technical report.

II.2.6 Technical Reports

1. “Metal/Hydrogen Energy Storage: Selected Technical Issues,” S. Szpak and P.A. Mosier-Boss, Technical Report 1657, June 1994, Naval Command Control and Ocean Surveillance Center RDT&E Division, San Diego, CA 92152-5000.

2. “Anomalous Behavior of the Pd/D System,” S. Szpak and P.A. Mosier-Boss, Technical Report 1696, September 1995, Naval Command Control and Ocean Surveillance Center RDT&E Division, San Diego, CA 92152-5000.

3. “Thermal and Nuclear Aspects of the Pd/D_2O Systems. Vol. 1: A Decade of Research of Navy Laboratories,” S. Szpak and P.A. Mosier-Boss, Technical Report 1862 vol. 1, Feb. 2002, Space and Naval Warfare Systems Center San Diego, San Diego CA 92152-5001.

4. “Thermal and Nuclear Aspects of the Pd/D_2O Systems. vol. 2: Simulation of the Electrochemical Cell (ICARUS) Calorimetry,” S. Szpak and P.A. Mosier-Boss, Technical Report 1862 vol. 2, Feb. 2002, Space and Naval Warfare Systems Center San Diego, San Diego CA 92152-5001.

II.3 Research Topics - Relevant Publications

The selected research topics emphasize (i) the state of the reactant, R, *i.e.*, the state of the last step preceding the nuclear event, (ii) the analysis of reaction product(s) and (iii) the energetics associated with the reaction itself, *eg.*, thermal, mechanical, nuclear. The topics are discussed in papers designated by the number and section (*eg*., 1, II.2.1 means the first paper in the section II.2.1).

II.3.1 The State of Reactant R

The state of the reactant-precursor, R, is determined by the experimental protocol. The topics that deal with these aspects include:
(i) processes associated with co-deposition (including rate and the degree of charging), 1, 2, 3, 6, 7, (II.2.1)
(ii) processes associated with D_2 evolution (including formation of an interphase region), 4, 7 (II.2.1)
(iii) effect of cell current/overpotential (including emphasis on the effect of the system deviation from equilibrium), 13 (II.2.1)
(iv) properties of the interphase region, 3 (II.2.1)
(v) effect of external electrostatic ffield, 15 (II.2.1)

II.3.2 The $\Sigma P + Q$ *Term.*

Topics involving the state of reaction products and the energy output that are examined include:
(i) nuclear (tritium production and X-ray emanation), 5, 8, 9, 10, 11 (II.2.1); 2 (II.2.2); 2 (II.2.4)
(ii) thermal (excess enthalpy, temperature distribution, catastrophic event), 12, 14 (II.2.1);3 (II.2.2); 2 (II.2.3); 1 (II.2.1)
(iii) mechano-chemical manifestation (mini-explosions); 5 (II.2.2); 2 (II.2.3)

ELSEVIER

22 January 1996

PHYSICS LETTERS A

Physics Letters A 210 (1996) 382–390

On the behavior of the cathodically polarized Pd/D system: Search for emanating radiation

S. Szpak [a], P.A. Mosier-Boss [a,*,1], J.J. Smith [b]

[a] *Naval Command, Control and Ocean Surveillence Center RDT & E Division, San Diego, CA 92152-5000, USA*

[b] *Department of Energy, Washington, DC 20585, USA*

Received 14 November 1994; revised manuscript received 12 September 1995; accepted for publication 12 November 1995

Communicated by J.P. Vigier

Abstract

Evidence for the emission of low intensity X-rays during cathodic polarization of the Pd/D system(s) is presented. The Pd/D system was prepared by charging with electrochemically generated deuterium either palladium foil or palladium electrodeposited from D_2O electrolytes. Experimental and analytical procedures are described in detail.

1. Introduction

Production of excess energy in a cathodically polarized Pd/D system has been reported by Fleischmann and Pons [1]. In particular, they claimed that the rate of excess enthalpy generation could only be explained by a nuclear process since the magnitude of this excess was at least 100 times that of any known chemical reaction. However, the difficulty in accepting this view has been the lack of correlation between the excess energy produced and the quantity of nuclear debris generated by classical nuclear paths. Alternative models have been proposed which predict, irrespective of the origin of the source of excess heat production, that the requisite energy deposited within the Pd lattice should result in emanation of X-rays arising from the disturbance of the electronic structure of the Pd/D system [2–5].

In this Letter, we present data collected during an investigation of the emanation of soft X- and γ-rays in the course of the Pd/D codeposition and during the period of deuterium evolution on such electrodes reported by us previously [6]. In support of our conclusions, we provide detailed information on cell design, data collection and examine the statistics of background radiation measured for a period of months. In the interpretation of the X-ray data we include computer synthesis of events that tend to reproduce the experimentally observed spectra. Because of the lack of theoretical guidance, we present the experimental evidence and avoid interpretation of the mechanism(s) giving rise to the radiation.

2. Experimental

In developing the experimental procedure we have concentrated on the importance of shielding, sensitivity of detectors, and cell design.

* Corresponding author.

[1] E-mail: bossp@nosc.mil.

0375-9601/96/$12.00

SSDI 0375-9601(95)00915-9

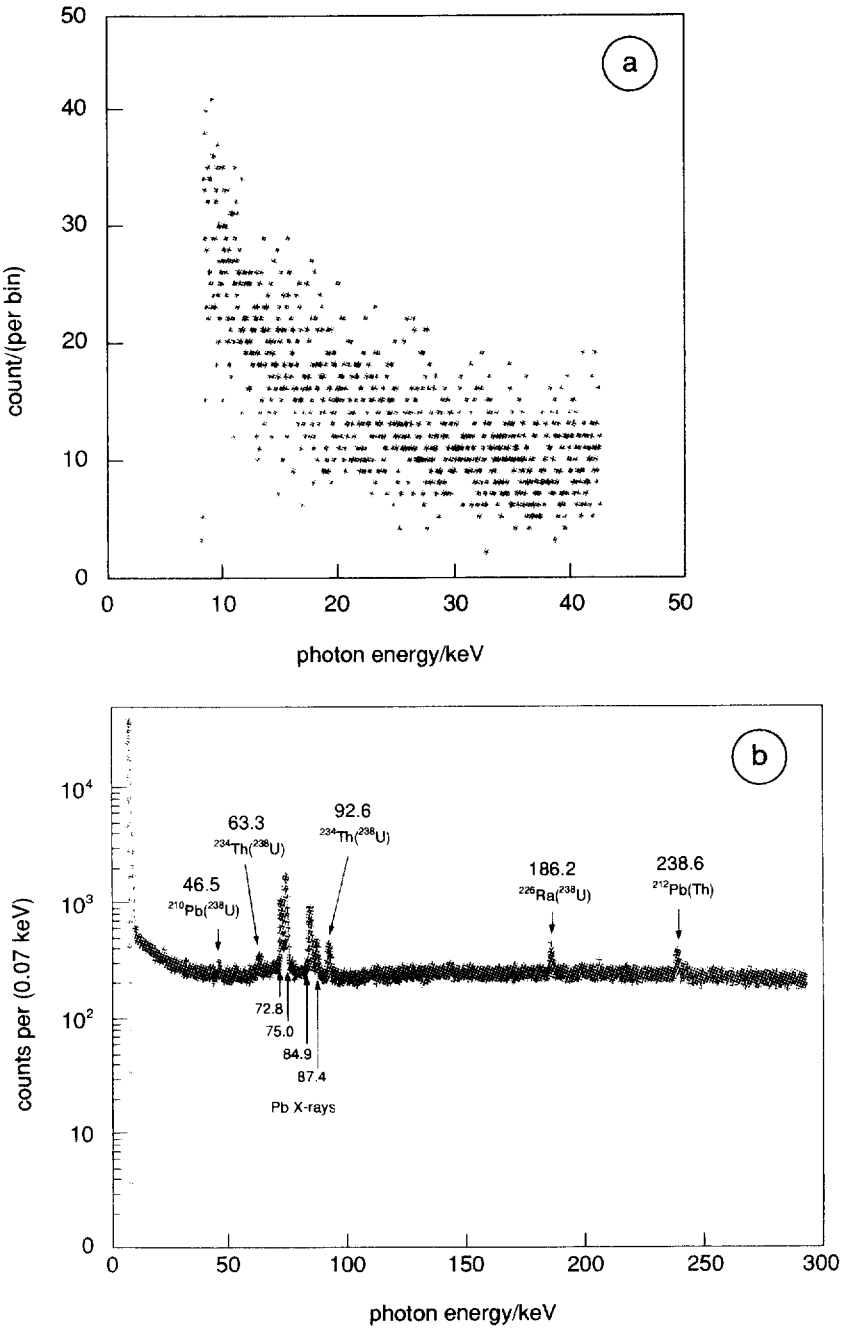

Fig. 1. Background spectra in the Pb cave. (a) Featureless region from 7 to 45 keV, for the Si(Li) X-ray detector; total count of 1.2×10^4; counting time of 361.2 h. (b) 0 to 300 keV region, with spectral peaks identified, for the HPGe detector; total count of 1.06×10^6; counting time of 275.6 h.

2.1. Background radiation-shielding

Background radiation was monitored continuously by a NaI(Tl) detector placed in a lead-shielded cave and intermittently by Ge and Si(Li) detectors in a separate lead-shielded cave when the electrolytic cell was not in operation. The two caves, located approximately 2.0 m from each other, were shielded by ca. 5 cm thick lead bricks. The Pb shielding reduced the background radiation, defined here as the spectrum recorded with the electrolytic cell in place but with no cell current, by a factor of twenty. Both detectors showed constant background over a period of several months. The γ- and X-ray detectors and the electrolytic cell remained in a fixed position during experimental runs. Examples of the background spectrum, recorded in the cave and covering regions from 7 to 40 keV and 15 to 300 keV are illustrated in Figs. 1a and 1b, respectively. It is seen that the region from 7 to 40 keV is featureless; in contrast, the region between 15 and 300 keV exhibits well defined peaks.

2.2. Radiation detection; X-, γ-rays

The procedure and data reduction are as follows: Signals from the p-type high purity Ge detector (HPGe-EG & G Ortec), with crystal dimensions of 5.8 cm diameter and 6.8 cm length, are amplified and analyzed by a Davidson portable multichannel analyzer using 4096 channels with a gain of either 30 or 300. Other features: the crystal has an absorbing layer of Al (1 mm) and inactive Ge (0.7 mm); the number of equivalent attenuation lengths equals 13, 1.9 and 0.6 at 20, 40 and 60 keV, respectively. The relative efficiency of the crystal is 37% at 1.33 MeV (defined as Ge efficiency/3 in. $\times$ 3 in. NaI(Tl) at 25 cm). The spectral data are recorded on minicassette tape and transferred to a work station for processing. Cell spectra which have equivalent calibration parameters are compared with the background spectrum on a bin-by-bin basis using the standard χ-square distributed test statistics. The signed square root of the test statistics for each bin is plotted in units of standard deviation as a function of bin energy. The procedures and data reduction for the continuous monitoring of background radiation by the NaI(Tl) detector (2 in. $\times$ 8 in. crystal coupled to RCA 8575 PMT) are as follows: PMT signals are amplified and analyzed with a Nuclear Data Portable MCA using 512 channels. Spectral data (50–1500 keV) are recorded on minicassette tape for further processing. Each data accumulation period count rate for the 75–1500 keV range is calculated and plotted. The intensity of the X-rays flux was measured with a Si(Li) detector, (Kevex model PSI-amplifier model 4561), placed in close proximity to the operating electrochemical cell.

2.3. Cell design

Three types of electrochemical cells were employed. The first type, shown in Fig. 2a, was designed to provide overall information on spectra up to ca. 3000 keV and to monitor the temperature of cell elements in order to observe, in a crude fashion, time dependent heat generation in the course of Pd/D codeposition and electrolysis of D_2O, respectively. For this purpose, the working electrode and the spirally wound Pt counter electrode were centrally located and the thermocouples attached accordingly.

In the second design, Fig. 2b, the working and counter electrode assembly was modified to provide an open structure of the counter electrode. A flat Pd foil, instead of a cylinder (cf. Fig. 2a) was used as the working electrode. The uniformity of the charging current was realized by maintaining a uniform distance between the electrodes. This design allowed us to record lower energy levels of the emitted X-rays by placing the whole electrode assembly within 0.5 to 0.7 cm of the X-ray detector's beryllium window. However, the increase in sensitivity was at the expense of temperature measurements; the latter was monitored in the electrolyte phase only.

Finally, to extend the detection capabilities to still lower intensities of the radiation flux and lower energy levels, the third design employing a cathode in the form of an open wire Ni mesh, onto which Pd is deposited, and placed in close proximity to a thin, ca. 0.03 mm wall cell made of Mylar, Fig. 2c, was introduced. The cell design differs from that used by Bennington et al. [2] or Ziegler et al. [7] in two ways: it assures a more uniform distribution of the charging current density and, because of the open structure of the working electrode and the close proximity to the detector, it substantially reduces the attenuation of X-rays while maintaining uniform current density.

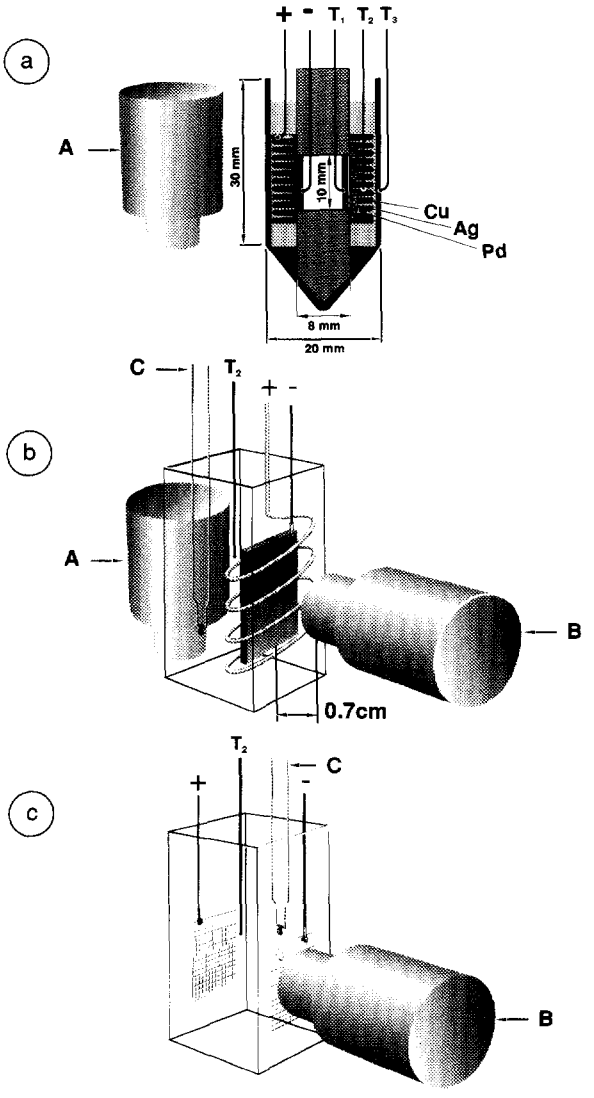

Fig. 2. Electrolytic cells. (A) γ-ray detector; (B) X-ray detector; (C) reference electrode; thermocouples: T_1 attached to the interior of the working electrode; T_2 immersed in the electrolyte; T_3 to measure the cell wall temperature. (a) Centrally located electrodes assembly; cell designed for examination of the spectral region 15–3000 keV. (b) Movable electrode assembly: closest approach of the working electrode to the detector window of 0.5 cm; cell designed for the spectral region 15–300 keV and provided with dual detection system. (c) Cell designed for detection of soft X-rays. The detector window is separated from the working electrode by the thickness of the Mylar sheet.

The cells were connected to a power source and operated under either potentiostatic or galvanostatic control (EG & G model 362). Only a limited set of calorimetric data could be secured in the cells designed for the detection of electromagnetic radiation. Of these designs, Figs. 2a–2c, the calorimetric data recorded for the cylindrical electrodes, Fig. 2a, are deemed to be more reliable than the designs employing mesh electrodes. The cell current, potential and temperature were recorded every 10 min.

3. Results

In what follows, we consider observations made on Pd electrodes prepared by (i) electrodeposition from an aqueous solution of $Pd(NH_3)_4Cl_2$ at low current densities (e.g., 200 μA cm^{-2}) for a period of ca. 20 h followed by codeposition from the D_2O-electrolyte for the spectral region 15–3000 keV; (ii) using commercially available Pd foil for the spectral region 15–300 keV; and (iii) codeposition of Pd/D from the $PdCl_2$–LiCl–D_2O solution for the spectral region 7–40 keV.

3.1. Spectral region: 15–3000 keV

The first set of experiments was designed to provide an overview of the electromagnetic spectrum associated with events occurring during the cathodic polarization of the Pd/D system. The effect of two charging techniques was examined, viz., charging by a codeposition process and by absorption of electrochemically generated deuterium. It is noted that these two techniques produce vastly different surface morphologies: in the first case, a dendritic surface is created [6] and in the second case, prolonged charging promotes the formation of surface fissures [8]. In both cases, the spectral region 15–3000 keV, after subtraction of background, was featureless. Examining the data in terms of counts per second, we note an overall $1.8 \pm 0.1\%$ increase in the count rate during cell operation, Figs. 3a and 3b. To determine that the observed increase in count rate is statistically significant and not due to random events, we employ the t-test [9] where t is given by

$$t = \frac{\bar{x}_1 - \bar{x}_2}{\sqrt{\sigma_1^2/n_1 + \sigma_2^2/n_2}}, \qquad (1)$$

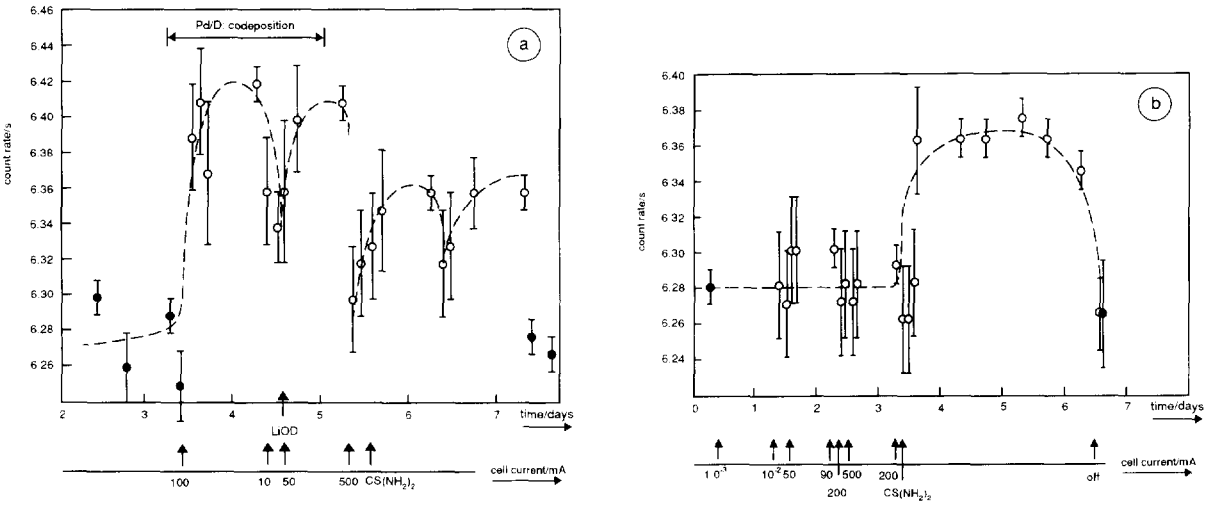

Fig. 3. Electromagnetic flux emitted during cathodic polarization of the Pd/D system; spectral region 15–3000 keV recorded by the Ge detector. Cell design as in Fig. 2a; electrode area of 2.51 cm^2 Ag deposited from a cyanide solution at 2 mA cm^{-2} for 10 min; the Pd layer is deposited from a $Pd(NH_3)_4Cl_2$–H_2O–LiCl solution at 200 μA cm^{-2} for 48 h; the cell current profile under galvanostatic control and electrolyte modifications is indicated; background – solid circles; operating cell – open circles. (a) Electrolyte: 0.003 M $PdCl_2$–0.3 M LiCl–D_2O LiOD added after depletion of Pd^{2+} ions (indicated by an arrow); addition of $CS(NH_2)_2$ is indicated by an arrow. Statistical information: background: $n = 6$, $\bar{x} = 6.272$, $\sigma = 0.019$; codeposition: $n = 9$ (the first 9 data points of cell operation); $\bar{x} = 6.383$, $\sigma = 0.027$, $t = 9.2$, $P(9.2) = 3.57 \times 10^{-20}$; $n = 9$ (the last 9 data points of cell operation); $\bar{x} = 6.336$, $\sigma = 0.023$, $t = 5.7$, $P(5.7) = 2.143 \times 10^{-8}$. (b) Electrolyte: 0.1 M LiOD; addition of $CS(NH_2)_2$ indicated. Statistical information: background and inactive period, first 9 data points of cell operation: $n = 11$; $\bar{x} = 6.285$, $\sigma = 0.016$; active period: $n = 11$, $\bar{x} = 6.322$, $\sigma = 0.048$, $t = 2.45$, $P(2.45) = 1.429 \times 10^{-2}$.

where $\bar{x}_1$ and $\bar{x}_2$ are the mean values for data sets consisting of n_1 and n_2 measurements, respectively, and σ_1 and σ_2 are the standard deviations of the means. The probability, $P(t)$, that increases with the count rate for n measurements are due to random events is very high for low values of t. However, that probability decreases rapidly with increasing t values (see Ref. [9], Table A VI.2). Here, we consider a t value greater than or equal to 3 ($P(3) = 2.699 \times 10^{-3}$) indicative that the difference between the means of the n_1 and n_2 data sets are statistically significant. The results of the statistical analyses are summarized in the figure captions.

While an increase in the count rate (ca. 4%) occurred shortly after the initiation of the Pd/D codeposition process on a dendritic surface, Fig. 3a, several days of charging were required to observe the same effect on a smooth surface, Fig. 3b. The common features for the two surface morphologies are: low level radiation as evidenced by the increase of the count rate and the effect of surface active agents, e.g., thiourea, on the initiation and/or re-activation of the X-ray producing process(es), Figs. 3b and 3a, respectively. As shown in Fig. 3a, the ca. 4% increase in the count rate terminated after the completion of the codeposition process (ca. 50 h). During the Pd/D codeposition, the count rate was not affected by the cell current profile and the emitted radiation, with $t = 9.2$, $P(9.2) = 3.57 \times 10^{-20}$, is accompanied by excess enthalpy production, as inferred from the higher temperature of the working electrode than that of the electrolyte phase. After completion of the codeposition process, a decrease in the count rate is observed. The addition of thiourea resulted in a statistically significant, $t = 5.6$, $P(5.6) = 2.143 \times 10^{-8}$, increase in count rate and the temperature of the bulk electrode exceeded the temperature of the electrolyte, clearly indicating the excess enthalpy production. Similarly, in Fig. 3b, an increase in count rate is observed with the addition of thiourea. Here, however, the statistics are weaker since $t = 2.45$, $P(2.45) = 1.429 \times 10^{-2}$. Nevertheless for $t = 2.45$, the probability that the increase in count rate is the result of random events is 1.4%.

3.2. Spectral region: 15–300 keV

Analyses of the 15–3000 keV spectral region indicate that the increase of the count rate occurs at low energy. Consequently, we redesigned the cell to reduce the attenuation of the radiation flux, Fig. 2b, and, additionally, we employed two independently operating detectors capable of viewing overlapping regions, viz., one for the X-ray and one for the γ-ray regions. Four experiments, each of ca. one month duration, showed the same characteristic features, namely a simultaneous increase of the count rate as observed by both detectors. In this set of experiments, a Pd foil was charged under controlled overpotential in the sulfate electrolyte with $BeSO_4$ as the additive. The results, summarized in Fig. 4, are as follows: No radiation above background is noted during the initial period of charging (ca. first eight days). The flux intensity varies with time as illustrated in the γ-ray count rate by the two periods of time I and II. Within these periods a statistically significant increase in the radiant flux, with $t = 8.69$, $P(8.69) = 3.31 \times 10^{-18}$ and $t = 14.89$, $P(14.89) < 10^{-23}$, respectively, has occurred. Examining the same periods of time for the X-ray component we note no increase in the count rate within the first region ($t = 0.44$, $P(0.44) = 3.3 \times 10^{-1}$). In contrast, region II reveals a statistically significant increase in the count rate, as evidenced by $t = 5.0$, $P(5.0) = 5.73 \times 10^{-7}$. The flux intensity exhibits a weak dependence on the overpotential (also cell current). Parenthetically, we observe upon subtraction of the background, no clearly discernible peaks within this spectral region.

3.3. Spectral region: 7–40 keV

The electrolytic cell shown in Fig. 2c was employed to examine the low energy spectral region, e.g., 7–40 keV. In all runs we observed an increase in the count rate especially in the low energy end. In some instances, as illustrated in Fig. 5, it appears that weak peaks are emerging, one at ca. 11 keV, point A, the other at ca. 20 keV, point B. The position of point B is unchanged while that of peak A tends to shift to lower energies without clearly defined changes in experimental conditions.

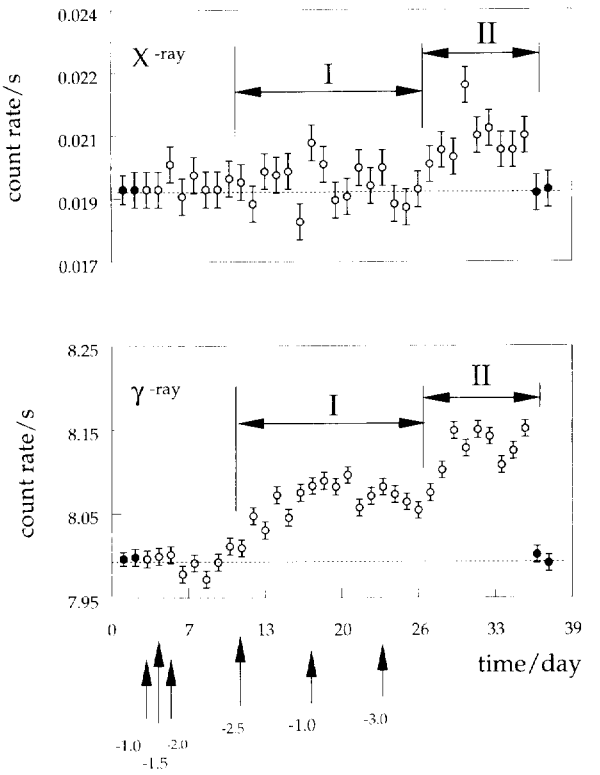

Fig. 4. Electromagnetic flux emitted during cathodic polarization of the Pd/D system; spectral region 0–300 keV: upper segment: spectral region 7–40 keV; lower segment: spectral region 40–300 keV. The arrows indicate the applied overpotential, in V, versus the Ag/AgCl reference electrode; background – solid circles; operating cell – open circles. The dashed line in both plots indicates background count rate. Cell design as in Fig. 2b; electrode: Pd foil, area 2 cm^2; electrolyte: 0.3 M Li_2SO_4–D_2O–Be (100 ppm added as $BeSO_4$). Statistical information of the 7–40 keV region: background: $n = 12$ (four background data points plus the first eight data points during cell operation), $\bar{x} = 0.0191$, $\sigma = 0.00026$; region I: $n = 16$, $\bar{x} = 0.01917$, $\sigma = 0.00057$, $t = 0.44$, $P(0.44) = 3.3 \times 10^{-1}$; region II: $n = 9$, $\bar{x} = 0.0204$, $\sigma = 0.00068$, $t = 5.00$, $P(5.00) = 5.73 \times 10^{-7}$. Statistical information of the 40–300 keV region: background: $n = 12$ (four background data points plus the first eight data points during cell operation), $\bar{x} = 7.994$, $\sigma = 0.006$; region I: $n = 16$, $\bar{x} = 8.057$, $\sigma = 0.030$, $t = 8.69$, $P(8.69) = 3.31 \times 10^{-18}$; region II: $n = 9$, $\bar{x} = 8.126$, $\sigma = 0.026$, $t = 14.89$, $P(14.89) < 10^{-23}$.

4. Discussion

The cell design employed in this research was selected to optimize the probability of detecting X-emissions during electrochemical loading of Pd. Si-

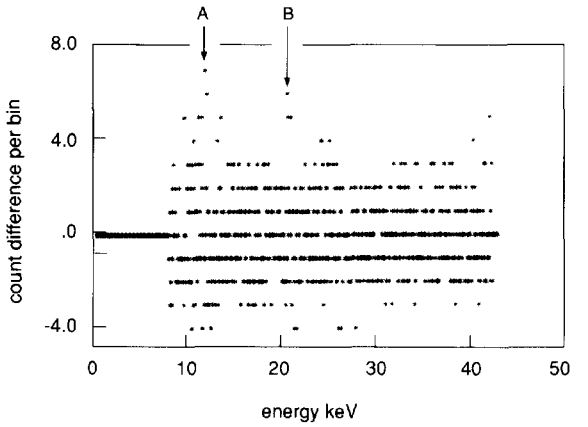

Fig. 5. X-ray spectrum emitted during cathodic polarization of the Pd/D system; spectral region 7–40 keV; background spectrum subtracted. Cell design as in Fig. 2c.

multaneous measurement of other possible markers, e.g., excess heat was not possible without disturbing the integrity of the experimental procedure. The results presented here represent a condensation of data collected over the course of two years and include experiments run under a variety of electrochemical conditions.

4.1. Methodology of measurements

Reliable analysis of low level radiation fluxes requires that the detectors and cell be shielded. However, even with shielding background radiation arises from cosmic rays interacting with the heavy atoms of the shielding material, e.g., Pb, cf. Fig. 1b. To insure an acceptable interpretation of weak signals, a continuous and independent monitoring of the background is needed, preferably by an instrument having higher sensitivity. For this purpose we selected the NaI(Tl) detector. In our experimental arrangement the background radiation, in identically shielded caves, was five times higher than when measured by the Ge detector. As indicated, vide Section 2.1, the background radiation was constant throughout the course of our experiments. To illustrate, the mean value of the background count rate from the NaI(Tl) detector for a six week period was 10.17 ± 0.04 cps while the values for each of the individual weeks was 10.144 ± 0.056, 10.147 ± 0.036, 10.185 ± 0.038, 10.174 ± 0.025, 10.134 ± 0.028, and 10.112 ± 0.030.

The argument usually offered for the rejection of the reported behavior of the polarized Pd/D system is that the low intensity of the radiant flux is, in reality, due to electrical noise. This argument is less compelling if a dual detection system is employed. Here, the dual system, consisting of the Si(Li) and Ge detectors, viewing simultaneously the electrochemical cell and operating independently from each other, exhibited the same behavior, i.e., a simultaneous increase of the count rate as illustrated in Fig. 4. While there is a general correspondence in the count rates between the X-ray and γ-ray detectors, i.e., the peak count rates for both detectors vary in the same manner, they exhibit different slopes. The γ-ray data in Fig. 4b appears to have two components: one which correlates with the X-ray data and another which corresponds to a monotonic increase in count rate. It is noteworthy that with termination of cell operation, the count rates observed by both detectors were as typical as that observed for background. Such behavior suggests a complex mechanism(s) responsible for the generation of the radiation.

4.2. Analysis

Several factors support the argument that the observed increases of the count rates can be attributed to electromagnetic emanation from the cell. First, as shown in Fig. 4, there is definite correspondence in count rates versus time between the X-ray and γ-ray detectors. Second, the additives, e.g., thiourea and Be^{2+} ions as well as the surface morphology, affect the intensity of the radiation flux, cf. Figs. 3 and 4. Third, the codeposition method of loading exhibited a shorter initiation time before the appearance of positive count rate deviations than the electrochemically charged electrodes; and finally, the increased count rates are observed sporadically, similar to other reported activities in these systems.

The low energy spectral distribution, cf. Fig. 5, reveals two features, viz., an increase of the count rate and the presence of rather weak peaks, one at ca. 20 keV and another at ca. 8–12 keV. This behavior is in general agreement with statements presented by other researchers. For example, Bennington et al. [2] stated: "any nuclear event depositing its energy within the Pd lattice will, in theory, produce X-rays by refilling of the K_α-shell of the excited Pd atoms". Buehler et

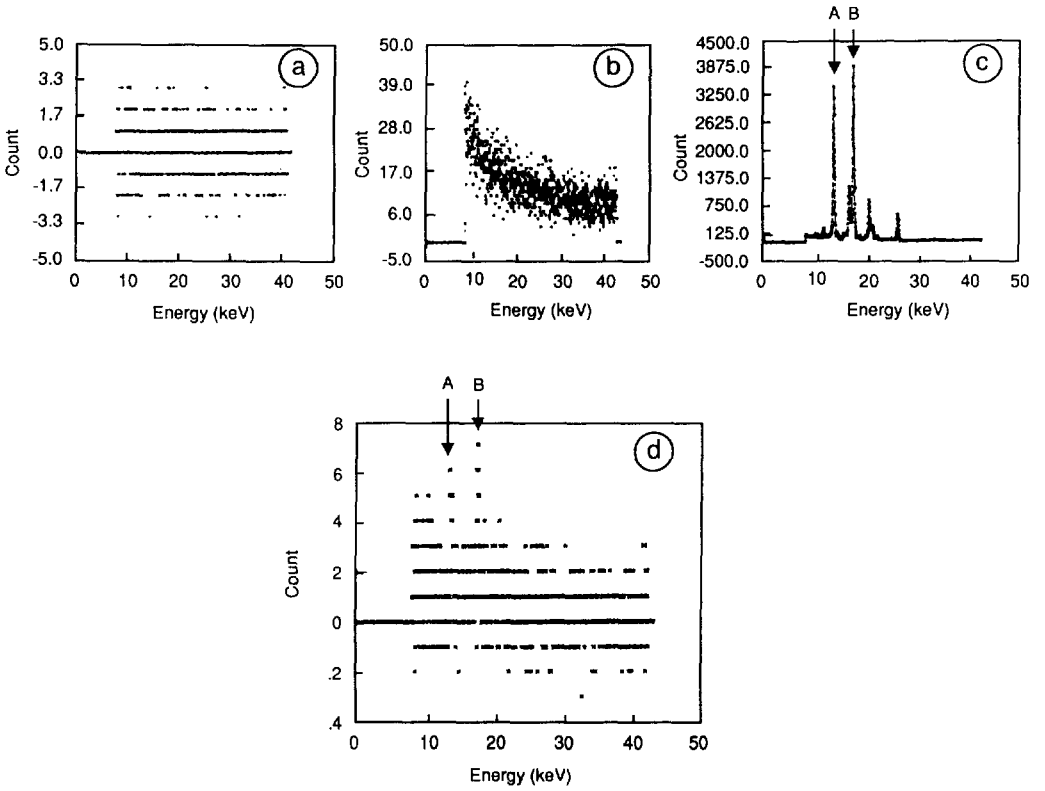

Fig. 6. Computer simulation of the addition (superposition) of weak spectral lines to the broad energy distribution (bremsstrahlung). (a) The difference of two background files illustrating a symmetric distribution about zero. (b) Energy distribution of the X-ray emanating from thorium oxide. (c) X-ray spectrum of Am: peak A: 13.76 keV L_{α_2}: $L_{III}M_{IV}$; peak B: 17.71 keV L_{β_1}: $L_{II}M_{IV}$. (d) Computer simulated energy distribution for a sum of: 0.0015 Am spectrum (cf. Fig. 6c); 0.02 ThO_2 spectrum (cf. Fig. 6b) and a difference of two separate backgrounds, all normalized to a 24 h period. Note: (i) asymmetry about zero due to bremsstrahlung; (ii) the emergence of weak Am peaks A and B.

al. [3] noted that charged particles, generated in the course of a nuclear event, e.g., p^+, t^+, α^{2+} particles, would ionize the Pd atoms to produce the K_α or K_β X-rays. On the other hand, because of the high density of oscillating plasma, a broad energy spectrum is expected [4,5,10].

We interpret the spectrum illustrated in Fig. 5, as resulting from the superposition of a weak peak upon a featureless background, e.g., the sharp peak of Pd K_α superimposed upon the bremsstrahlung arising from the oscillating plasma of the cathodically polarized Pd/D system. To demonstrate this we proceed as follows: First, as expected, the subtraction of two backgrounds recorded by the same arrangement within two time periods, is symmetrical around zero, Fig. 6a. Second, we constructed a model spectrum which contained a simulated bremsstrahlung component and a discreet line source component to determine the appearance of the resulting composite. To simulate the bremsstrahlung, we recorded the thorium oxide spectrum, Fig. 6b, while the americium spectrum was selected to represent the contribution of a line source, i.e. sharp peak(s), Fig. 6c. Addition of these spectra and the subtraction of the background resulted in the spectrum in Fig. 6d. The spectrum in Fig. 6d exhibits a structure very much like the experimental spectrum presented in Fig. 5. While this is not definitive evidence that Fig. 5 is a composite, it at least demonstrates that a spectrum consisting of a few energy peaks superimposed on a bremsstrahlung background is a con-

sistent interpretation of the observed spectrum shown in Fig. 5. Based on this interpretation, the emerging point B, Fig. 5, is most likely the Pd K_α peak. The assignment of peak A is less certain. Employing the approximate formula relating the energy of the K series to the number of protons, Z, viz., $Ry(Z-1)^2$; Ry = 13.5 eV gives for the 11–12 keV energy range the value of Z = 28–30. One of the elements having the required number of protons is nickel, used here as the substrate onto which the Pd/D system was deposited. However, the known energy of the Ni K series is substantially less than that observed here. We cannot rule out the possibility that peak A is due to Pt, which is a cell component (our anode) and has L line emissions in the 10–13 keV range. It is possible that during prolonged electrolysis in Cl^- solutions, small amounts of Pt could be transported from the anode to the cathode.

With respect to the effect of additives on radiation emission processes, both Be^{+2} and thiourea are known to increase the rate and degree of deuterium uptake. Similarly, radiation emissions are observed with extended surfaces, such as the globular or dendritic growths associated with Pd/D codeposition, which increase deuterium uptake. Collectively, these observations provide evidence for a coupling between deuterium uptake and radiation emissions.

5. Conclusions

Accepting the conclusion that weak electromagnetic radiation is responsible for the observed results, we make the following statements:

(i) While attempting to monitor the emanation of X-rays from the cathodically polarized Pd/D system, an adequate shielding must be provided and the working electrode must be placed close to the detector window.

(ii) The cathodically polarized Pd/D system emits X-rays with a broad energy distribution and with an occasional emergence of recognizable peaks. Because of the low intensity of the electromagnetic flux, its detection requires that cells be constructed accordingly.

(iii) The emission of X-rays appears to be sporadic and of limited duration.

(iv) Surface morphology influences radiation emissions – codeposited Pd/D electrodes exhibit shorter initiation times prior to the observation of radiation emissions. In the cases when either Be^{2+} ions or thiourea were added to the electrolyte, similar positive effects were observed.

Acknowledgement

The authors would like to thank Dr. Frank Gordon for his enthusiastic support. We would also like to thank the referees for suggesting that the line between 10 and 13 keV may be attributed to the Pt L lines.

References

[1] M. Fleischmann and S. Pons, J. Electroanal. Chem. 261 (1989) 301.
[2] S.M. Bennington, R.S. Sokhi, P.R. Stonadge, D.K. Ross, M.J. Benham, T.D. Beynon, P. Whithey, I.R. Harris and J.P.G. Farr, Electrochim. Acta 34 (1989) 1323.
[3] D.B. Buehler, L.D. Hansen, S.E. Jones and L.B. Rees, Is reported "excess heat" due to nuclear reactions?, in: Frontiers of cold fusion (Universal Academy Press, Tokyo, 1993) p. 245.
[4] Y. Kucherov, A. Karabut and I. Savvatimova, Heat release and product yield of nuclear reactions in Pd–D systems, in: Fourth ICCF, December 1993, Lahaina, Hawaii.
[5] J.P. Vigier, New hydrogen energies in specially structured dense media: Capillary chemistry and capillary fusion, in: Frontiers of cold fusion (Universal Academy Press, Tokyo, 1993) p. 409.
[6] S. Szpak, P.A. Mosier-Boss and J.J. Smith, J. Electroanal. Chem. 302 (1991) 255.
[7] J.F. Ziegler, T.H. Zabel, J.J. Cuomo, V.A. Brusic, G.S. Cargill, E.J. O'Sullivan and A.D. Marwick, Phys. Rev. Lett. 62 (1989) 2929.
[8] D.R. Rolison, W.E. O'Grady, R.J. Doyle and P.P. Trzaskoma, Anomalies in the surface analysis of deuterated palladium, in: Proc. First Annual Conf. on Cold fusion, Salt Lake City, UT, p. 272.
[9] S.L. Meyer, Data analysis for scientists and engineers (Wiley, New York, 1975).
[10] R. Antanasijevic, I. Lakicevic, Z. Maric, D. Zevic, A. Zaric and J.P. Vigier, Phys. Lett. A 180 (1993) 25.

ELSEVIER

23 September 1996

PHYSICS LETTERS A

Physics Letters A 221 (1996) 141–143

On the behavior of the cathodically polarized Pd/D system: a response to Vigier's comments

S. Szpak, P.A. Mosier-Boss [1]

Naval Command, Control and Ocean Surveillance Center RDT & E Division, San Diego, CA 92152-5000, USA

Received 23 May 1996; accepted for publication 24 May 1996
Communicated by P.R. Holland

Abstract

Electrodes prepared by Pd/D codeposition exhibit highly expanded surfaces which achieve high degrees of D/Pd loading within seconds. In this communication, morphology of the Pd electrode, the structure of the interphase, and selected thermal effects are discussed.

In response to Professor Vigier's comments, we assemble in this Letter other observations of the behavior of the Pd/D system when under cathodic polarization. This material is provided with the hope that such data may contribute to unraveling the mysteries of the Fleischmann–Pons effect announced on 23 March 1989. Here, we address: (1) morphology of the Pd electrode, (2) structure of the interphase, and (3) selected thermal effects. Only electrodes prepared by the codeposition technique, i.e., by palladium electrodeposited in the presence of evolving deuterium, are considered [1].

(1) *Electrode morphology.* Electrodes prepared by codeposition exhibit highly expanded surfaces consisting of small spherical nodules, Fig. 1a. A high degree of deuterium loading, with the atomic ratio D/Pd > 1, is obtained within seconds [2]. This behavior appears to be similar to that observed by Celani et al. (cited in Ref. [3]).

(2) *Structure of the interphase.* The metal side of the electrode/electrolyte interphase comprises, at least, two layers of vastly different deuterium content [4]. The presence of D_2^+ species in the interphase, at moderate cathodic overpotentials, has been suggested [4], supporting the tight orbit model. Moreover, the interphase is an active participant in the rate of charging, the intensity of emanating X-rays [5] as well as other manifestations, e.g., tritium production and its distribution between the electrolyte and vapor phases [6].

(3) *Thermal effects.* Observed thermal effects cover a wide range: from electrolyte cooling to the melting of the Pd electrode [7]. Electrolyte cooling in the initial stages of codeposition has been observed [1]. With further charging, the electrode temperature (measured by a thermocouple) exceeds that of the electrolyte by a few degrees. However, when viewed

[1] Corresponding author. E-mail: bossp@nosc.mil.

PII S0375-9601(96)00450-1

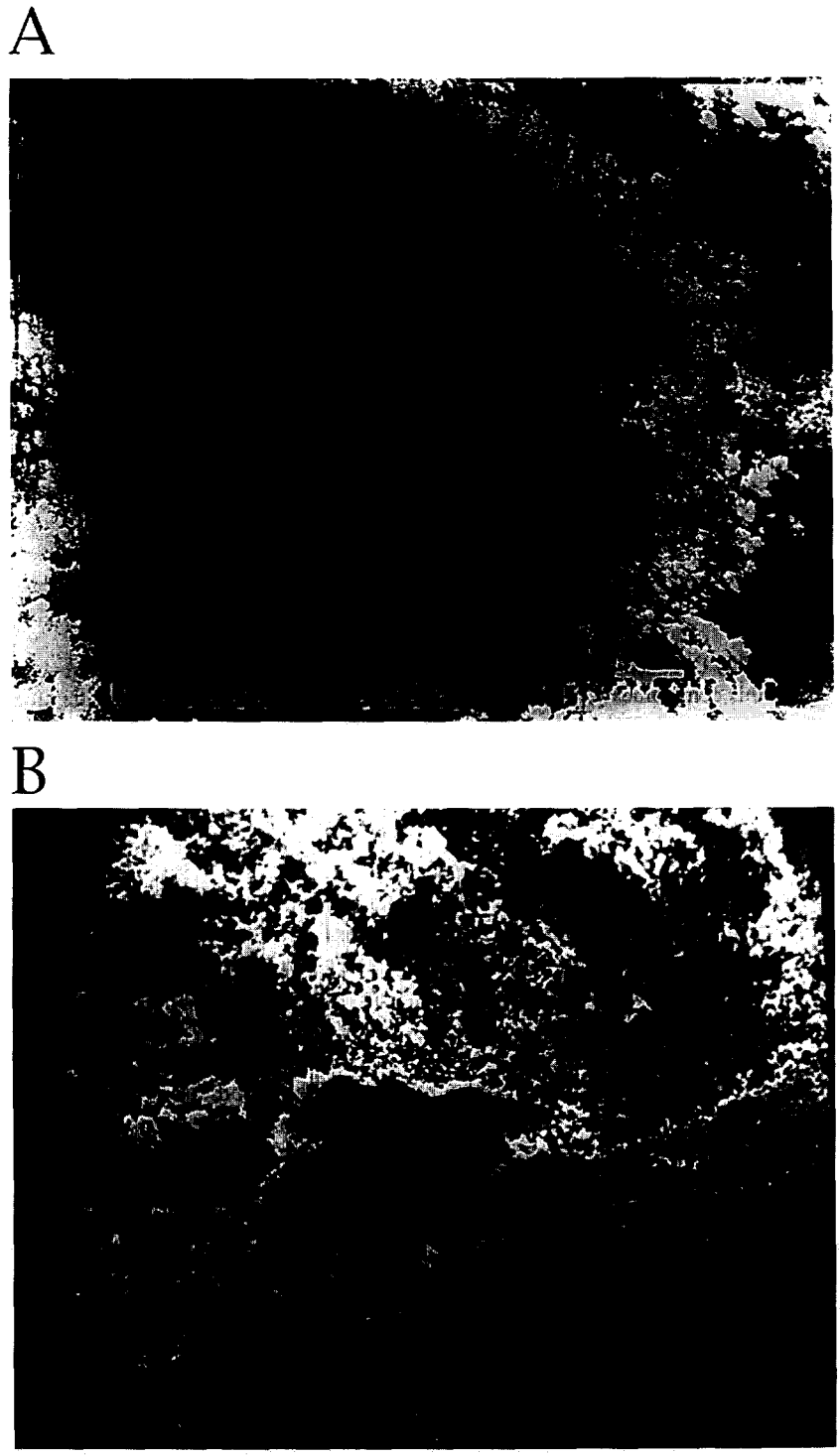

Fig. 1. SEM photographs of (a) a Pd electrode freshly prepared by co-deposition and (b) Pd film deposited on cell wall following melting of the Pd electrode during D_2O electrolysis.

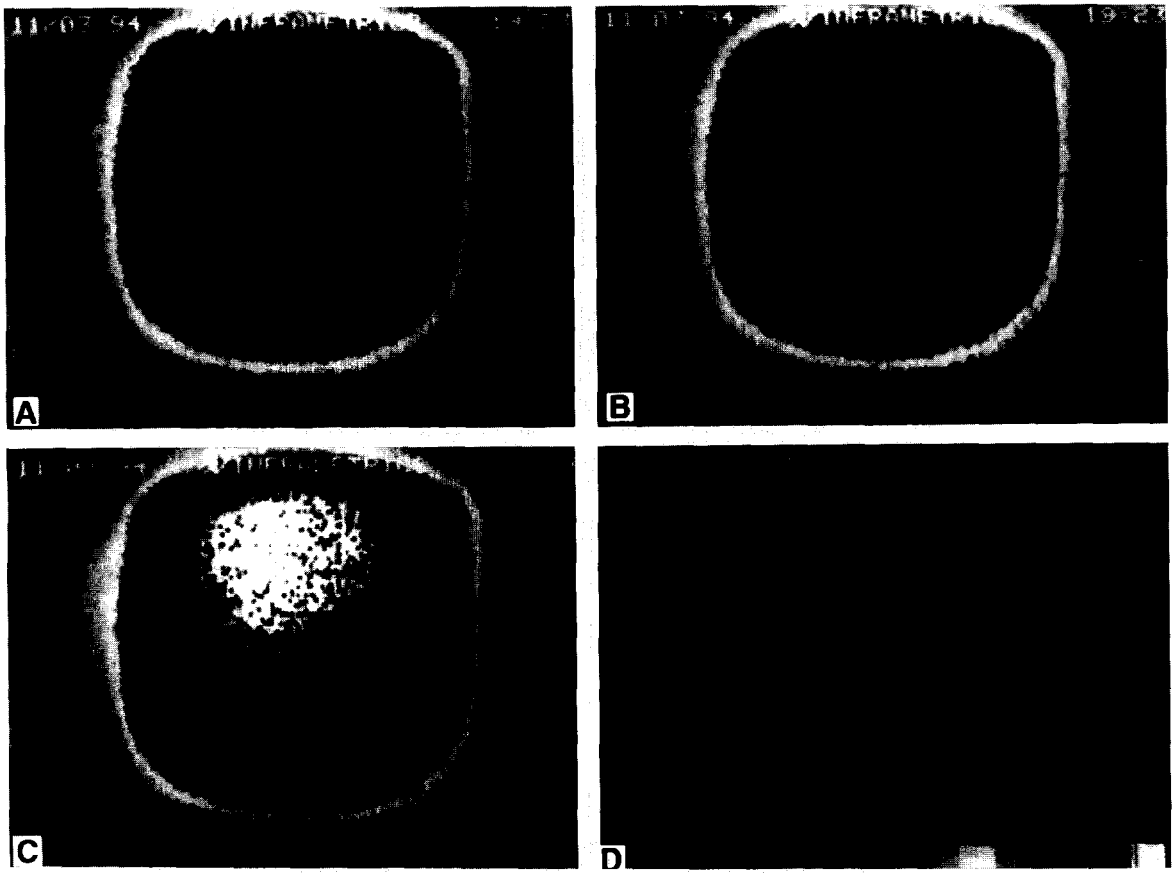

Fig. 2. Temperature distribution of the Pd electrode, prepared by co-deposition on a Ni screen, during cathodic polarization as recorded by an infrared camera. (a) Appearance of "hot spots"; (b), (c) merging of hot spots to form larger temperature zones; (d) graphical representation of temperature distribution.

with an infrared camera, the chaotic appearance/disappearance of hot spots is observed, followed by merging in larger islands that often exhibit oscillations in size, Figs. 2a and 2b. The most extreme temperature rise, exceeding the melting point of Pd, was observed once. In this case, molten Pd was deposited on the wall of the electrolytic cell in the form of a thin film, Fig. 1b.

In selecting the topics for inquiries into the Fleischmann–Pons effect, we kept in mind the closing sentence in Born's 1943 address to the Durham Philosophical Society [8]: "My advice to those who wish to learn the art of scientific prophecy is not to rely on abstract reason, but to decipher the secret language of Nature from Nature's documents, the facts of experience."

References

[1] S. Szpak, P.A. Mosier-Boss and J.J. Smith, J. Electroanal. Chem. 302 (1991) 121.
[2] S. Szpak, P.A. Mosier-Boss and J.J. Smith, J. Electroanal. Chem. 379 (1994) 121.
[3] J.P. Vigier, Phys. Lett. A 221 (1996) 138.
[4] S. Szpak, P.A. Mosier-Boss, S.R. Scharber and J.J. Smith, J. Electroanal. Chem. 380 (1995) 1; 337 (1992) 147.
[5] S. Szpak, P.A. Mosier-Boss and J.J. Smith, Phys. Lett. A 210 (1996) 382.
[6] S. Szpak, P.A. Mosier-Boss and J.J. Smith, submitted to Phys. Lett. A.
[7] S. Szpak and P.A. Mosier-Boss, unpublished data (1993).
[8] M. Born, Experiment and theory in physics (Dover, New York, 1953).

NUCLEAR REACTIONS IN SOLIDS

KEYWORDS: *Pd/D system, tritium production*

ON THE BEHAVIOR OF THE Pd/D SYSTEM: EVIDENCE FOR TRITIUM PRODUCTION

STANISLAW SZPAK, PAMELA A. MOSIER-BOSS, and ROGER D. BOSS
Naval Command, Control and Ocean Surveillance Center RDT&E Division
San Diego, California 92152-5000

JERRY J. SMITH *U.S. Department of Energy, Washington, D.C. 20585*

Received November 22, 1996
Accepted for Publication August 3, 1997

Evidence for tritium production in the Pd/D system under cathodic polarization is presented. A comparison of the observed distribution and that calculated, based on the conservation of mass, leads to the conclusion that tritium is produced sporadically at an estimated rate of ~10^3 to 10^4 atom/s. The results of several runs are interpreted by employing the concept of an electrode/electrolyte interphase and the accepted kinetics of hydrogen evolution. Burstlike events followed by longer periods of inactivity yield poor reproducibility when distributions are averaged over the total time of electrolysis.

I. INTRODUCTION

An early report on the behavior of the Pd/D system, with atomic ratio [D]/[Pd] > 0.8, suggested that fusion of deuterons occurs within the palladium lattice when the system is under prolonged cathodic polarization.[1] Apart from the reported enormous excess enthalpy, supporting evidence for nuclear activities are emanating radiation (X and/or gamma rays) and the production of new nuclei. Indeed, weak radiation was demonstrated recently.[2] Among the expected new nuclei to be produced is tritium. For a number of reasons, tritium production appears to be an appropriate topic for investigation:

1. A half century ago Oliphant et al.[3] reported that transmutation of deuterium into tritium and hydrogen occurs when a perdeutero inorganic compound, e.g., $(ND_4)_2SO_4$, is bombarded with low-energy deuterons.

2. A theoretical treatment concerning the occurrence of nuclear events when deuterium is electrochemically compressed in condensed matter indicates that tritium production can arise from a *d-d* reaction in which the excited state of ^{4}He decays into $t + p$ (Ref. 4).

3. By mass balance arguments, low-rate production of tritium has been reported by (among others[5,6]) Will et al.,[7] whose closed cell measurements make a compelling argument for excess tritium as a product of electrolysis.

4. The analytical methods for the determination of tritium content are now well developed.

In this paper we describe in detail the experimental procedures (Secs. II.A and II.B) and present data on tritium content and its distribution recorded during the electrolysis of heavy water (Sec. II.C). Specifically, in the course of charging the palladium lattice with electrochemically generated deuterium, we observed periods of detectable production of tritium. These periods occur sporadically and appear to be controlled, to a degree, by the structure of the interphase (Sec. III).

II. EXPERIMENTAL

The experimental procedure employed follows closely that described previously.[8] Here, we report data obtained from two sets of experiments: (a) an electrolyte-gas phase tritium distribution recorded at ~24-h intervals with intermittent electrolyte additions using an arbitrarily selected cell current profile and (b) a three-phase distribution occurring within the time period required to reduce the initial volume of electrolyte by half at a priori selected constant cell current.

II.A. Electrolytic Cell—Current Profile

The electrochemical cell and recombiner are shown in Fig. 1. Each cell, with graduated wall to provide an

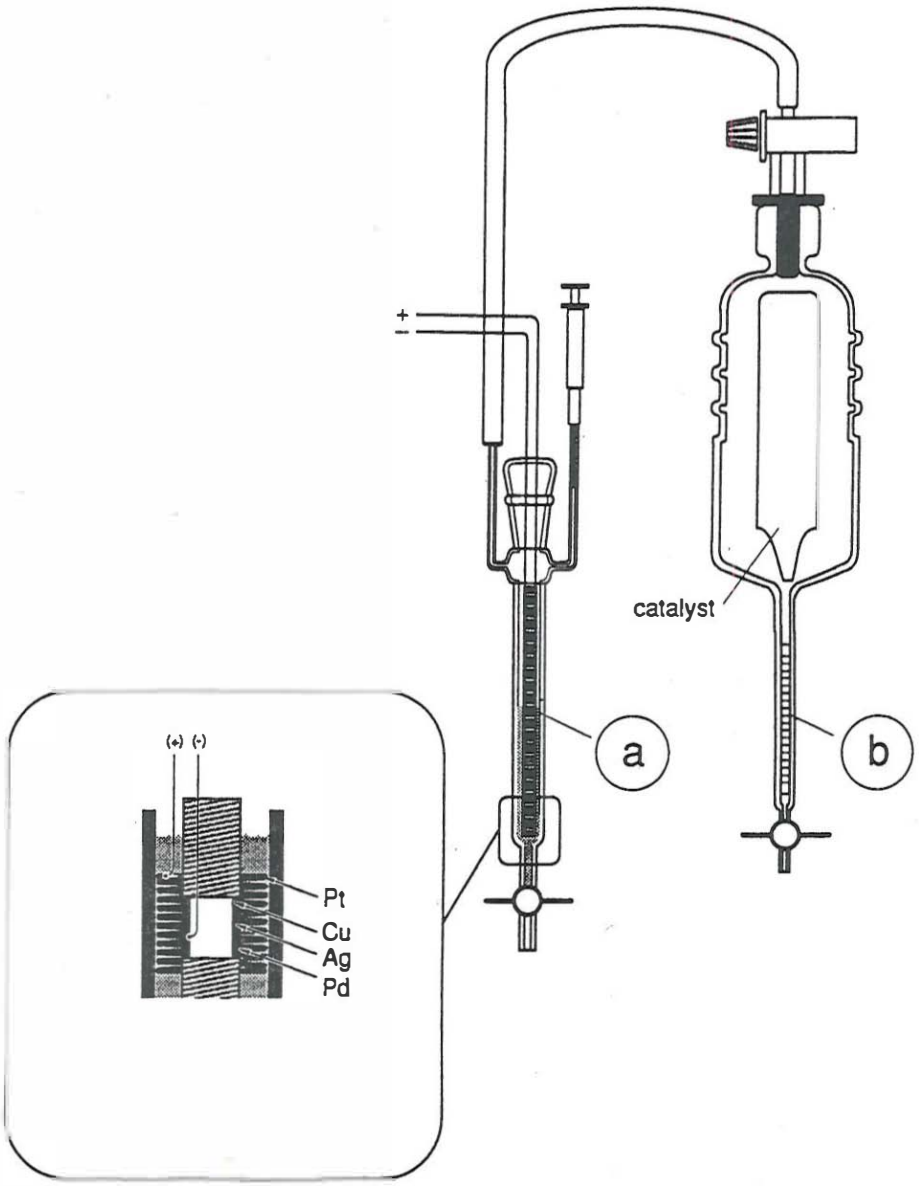

Fig. 1. Experimental cell and recombiner assembly (schematic): (a) electrolytic cell, (b) recombiner; inset shows detail of cell assembly.

additional check on the volume of electrolyte, was connected to a recombiner containing a catalyst (supplied by Giner, Inc.) of sufficiently large surface area (~100 cm^2) to ensure nearly complete recombination of evolving gases. The working palladium electrode was prepared as follows: an ~3.0-cm^2 copper foil was wrapped around a glass rod (Fig. 1 inset). Onto this foil a thin film of silver was deposited from a cyanide bath to provide a better lattice match with the electrodeposited palladium layer. The palladium electrodes of two vastly different surface morphologies were prepared: one with a smooth surface by deposition from a $Pd(NH_3)_2Cl_2$-H_2O solution at low-current densities and the second with a mossy (dendritic) surface by electrodeposition from a $PdCl_2$-LiCl-D_2O solution in the presence of evolving deuterium. The placement of the counterelectrode, made of a tightly coiled platinum wire, ensured uniform current distribution on the working electrode.

The electrochemical charging of the palladium electrodes was under galvanostatic control by a power source delivering constant current with a 0.1% ripple (EG&G Par model 363 potentiostat/galvanostat). The composition of electrolyte employed during charging is given as cited in this paper. To increase the detection sensitivity, only heavy water with a low tritium content, ~19 dpm/ml (supplied by Isotec, Inc.), was used.

II.B. Sampling Procedure—Tritium Analysis

The sampling procedure is illustrated in Fig. 2. A known volume of electrolyte and tritium content $V(t_1)$ is electrolyzed at a constant cell current i for a period of $\Delta t = t_2 - t_1$. During this time period the electrolyte volume is reduced by $V_e(t_2) = iM_w\Delta t/2\mathcal{F}\rho$. At time t_2, a sample is withdrawn, further reducing the electrolyte volume by V_s. Immediately after sampling, the electrolyte volume is restored by addition of the electrolyte in the amount of $V_a(t_3) = 2V_s + V_e$. After a few minutes to allow for mixing, a second sample V_s (t_4) is removed for tritium analysis. Removal of a second sample, following the electrolyte addition, ensures that the electrolyte volume and tritium content are accurately known at the beginning of the next time interval. The sampling and addition procedures were carried out without the interruption of the cell current flow.

Tritium content of the samples was measured by a liquid scintillation technique. In particular, 1 ml of sample is added to 10 ml of Fischer Scientific ScintiVerse E Universal LSC cocktail in a borosilicate vial. The prepared solutions were counted for 600 min in a Beckman LS 6000 LL scintillation counter. This instrument reports counts per minute (count/min) and disintegration per minute (dpm) with a 2σ error. To eliminate interference from chemiluminescence, all electrolyte samples were distilled to dryness and the distillate was analyzed for tritium content. Samples collected in the recombiner required no pretreatment.

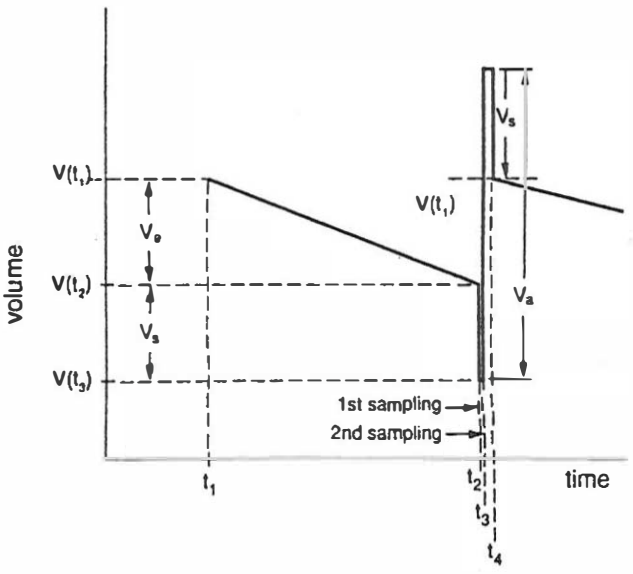

Fig. 2. Sampling profile for constant cell current density: $V(t_1)$ = initial volume (also, initial volume for any charging period); $V(t_2)$ = volume after the passage of charge $i\Delta t$; V_s = sample volume; V_a = volume added; t_2 = time of first sampling; t_3 = electrolyte addition time; t_4 = time of second sampling.

The determination of the tritium content in the working palladium electrode is a two-step procedure, namely, the transfer of sorbed tritium into a liquid phase followed by scintillation counting. Two methods were employed to accomplish this transfer: the anodic oxidation of sorbed tritium and the method described by Will et al.[7] In the first case, the working electrode, while under cathodic overpotential, was rinsed by flushing the cell with NaCl-H_2O solution to remove all D_2O containing tritium and placing it under the anodic overpotential of +0.5 V compared with the Ag/AgCl reference. In the second case, the palladium electrode was dissolved in aqua regia and neutralized with $CaCO_3$. As with the electrolyte samples, the resultant solutions from both treatments were distilled to dryness, followed by scintillation counting of the distillate.

Error analysis included the assessment of the precision of measurements in

1. electrolyte volume
2. sampling/addition time intervals
3. constancy of cell current
4. tritium analysis.

On the basis of an extensive investigation,[8] we concluded that the largest error, as indicated by the instrument readout and determined by standard procedures, is in the tritium analysis. The typical error of ±1.2 dpm is not the statistical error of counting but the cumulative uncertainty due to the propagation of error determined by a procedure commonly employed in the presentation of experimental data.

II.C. Data Presentation

A qualitative assessment of tritium distribution between the electrolyte and gas phases resulting from a prolonged evolution of deuterium generated by the electrolysis of D_2O is given in Figs. 3 through 6. The electrolyses were carried out under varying cell current profiles and composition of additives. Changes in cell current, times of sampling, and recombiner efficiency are indicated in the figures (axes i, V_a, and ϵ_r), while actual experimental data are provided in Appendices A through D.

Three distinct cases can be seen from the data:

1. prolonged electrolysis without tritium production (Fig. 3)
2. sporadic tritium production with periods of inactivity wherein the isotopic separation factor is at or near the normal value for T/D systems throughout (Figs. 4 and 5)
3. sporadic tritium production in which selective enhancement of the gas phase tritium level occurs (Fig. 6).

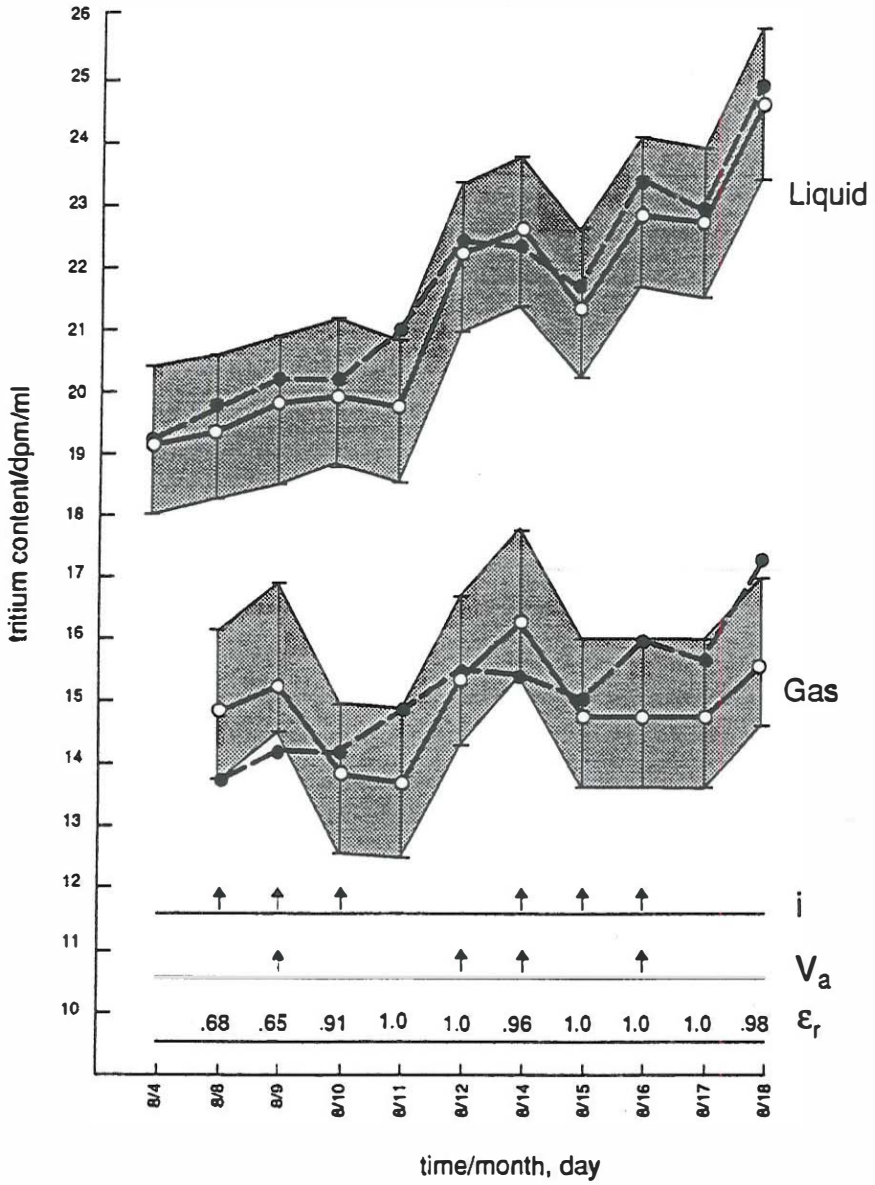

Fig. 3. Two-phase tritium distribution (s = 0.71): computed (dashed) and experimental (solid line). Electrode: area = 3 cm^2; Cu-Ag-Pd [deposited from $Pd(NH_3)_2Cl_2$]; electrolyte: 0.3 M LiOD; additive: 113 ppm B_2O_3; cell current, electrolyte addition, and recombining efficiency indicated by arrows along the time coordinate (i, V_a, and ϵ_r, respectively). Additional data are given in Appendix A.

In all cases, there is good agreement between the calculated and observed tritium distribution; namely, the experimental (open circles) and calculated (solid circles) fall within the cumulative uncertainty of ±1.2 dpm (shaded area). Those instances where significant deviation between the observed and expected concentration of tritium in both phases occurs indicates the periods of tritium production, as indicated by arrows.

Case 1: The tritium distribution summarized in Fig. 3 serves as an example of the absence of tritium production over the ~3-week duration of the electrolyses, thereby serving as a blank test of the model calculation for a different charging profile. It is seen that the observed and calculated values are in good agreement, allowing the determination of the separation factor s (see Sec. III.B).

Case 2: In contrast, Figs. 4 and 5 show active periods of type 2 mentioned earlier. In Fig. 4, one active period of ~3-days' duration (June 21, 22, 23), occurs 30 days after the initiation of charging. Figure 5 shows two active periods (April 21 to May 3 and May 19, 20, 21), separated by 14 days of inactivity. In these instances

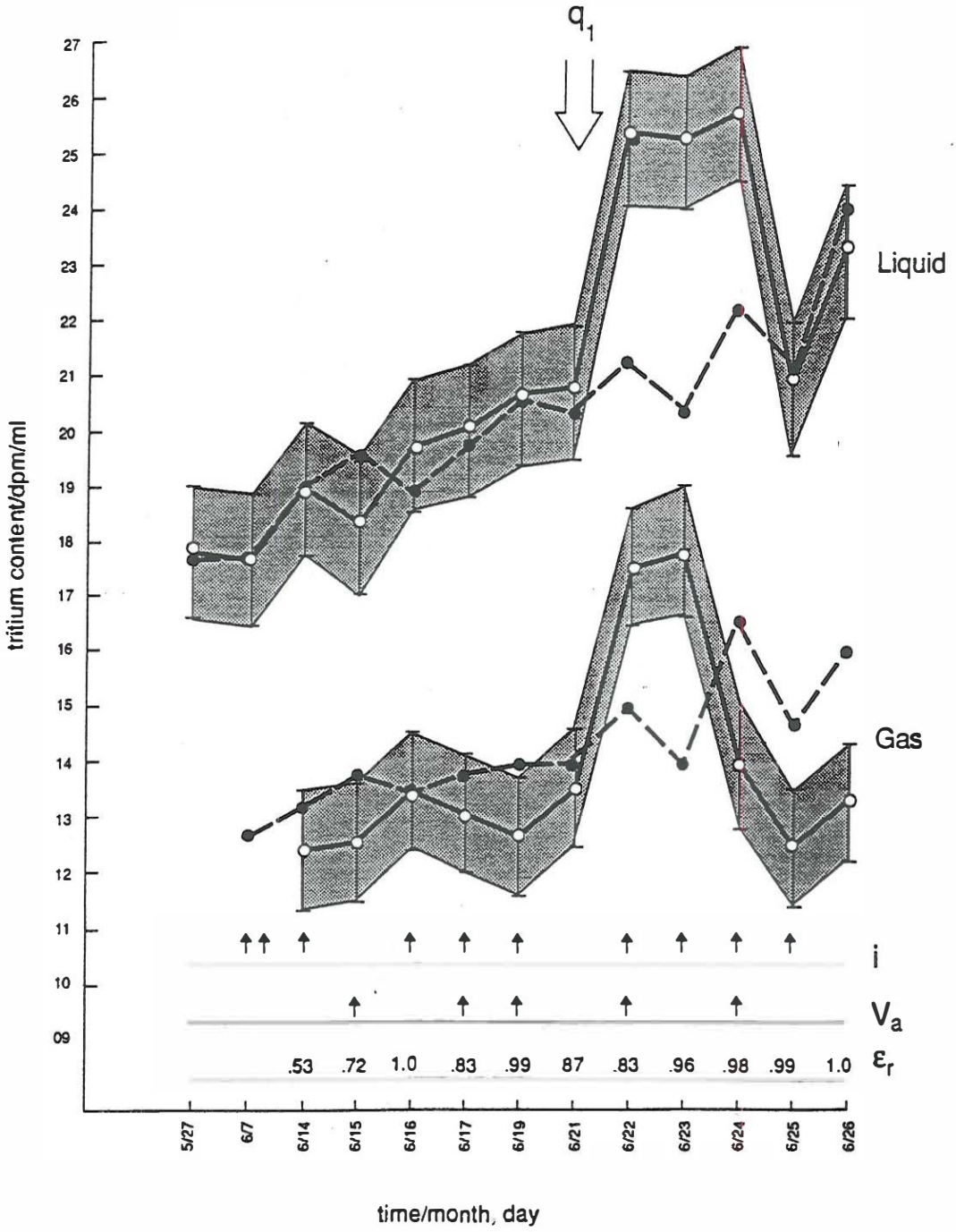

Fig. 4. Two-phase tritium distribution ($s = 0.71$): computed (dashed) and experimental (solid lines). Electrode area = 2.5 cm^2; Cu-Ag-Pd deposited from $Pd(NH_3)_2Cl_2$; electrolyte: 2.6×10^{-3} *M* $PdCl_2$ − 0.31 *M* LiCl; additive: 200 ppm $MgCl_2$; cell current (mA), electrolyte addition, recombiner efficiencies indicated. Additional data are given in Appendix B.

the isotopic separation factor does not change, and the enrichment occurs in both the electrolyte and gas phases. The constancy of the isotopic separation factor, $s = 0.68 \pm 0.04$, indicates that the reaction path for the cathodic charge transfer did not change either in the course of prolonged electrolysis or between runs and that tritium generated during the active periods first entered the electrolyte phase resulting in the isotopic distribution controlled by the electrodic reaction.

Case 3: The data summarized in Fig. 6 show an active period in which tritium enrichment is limited to the

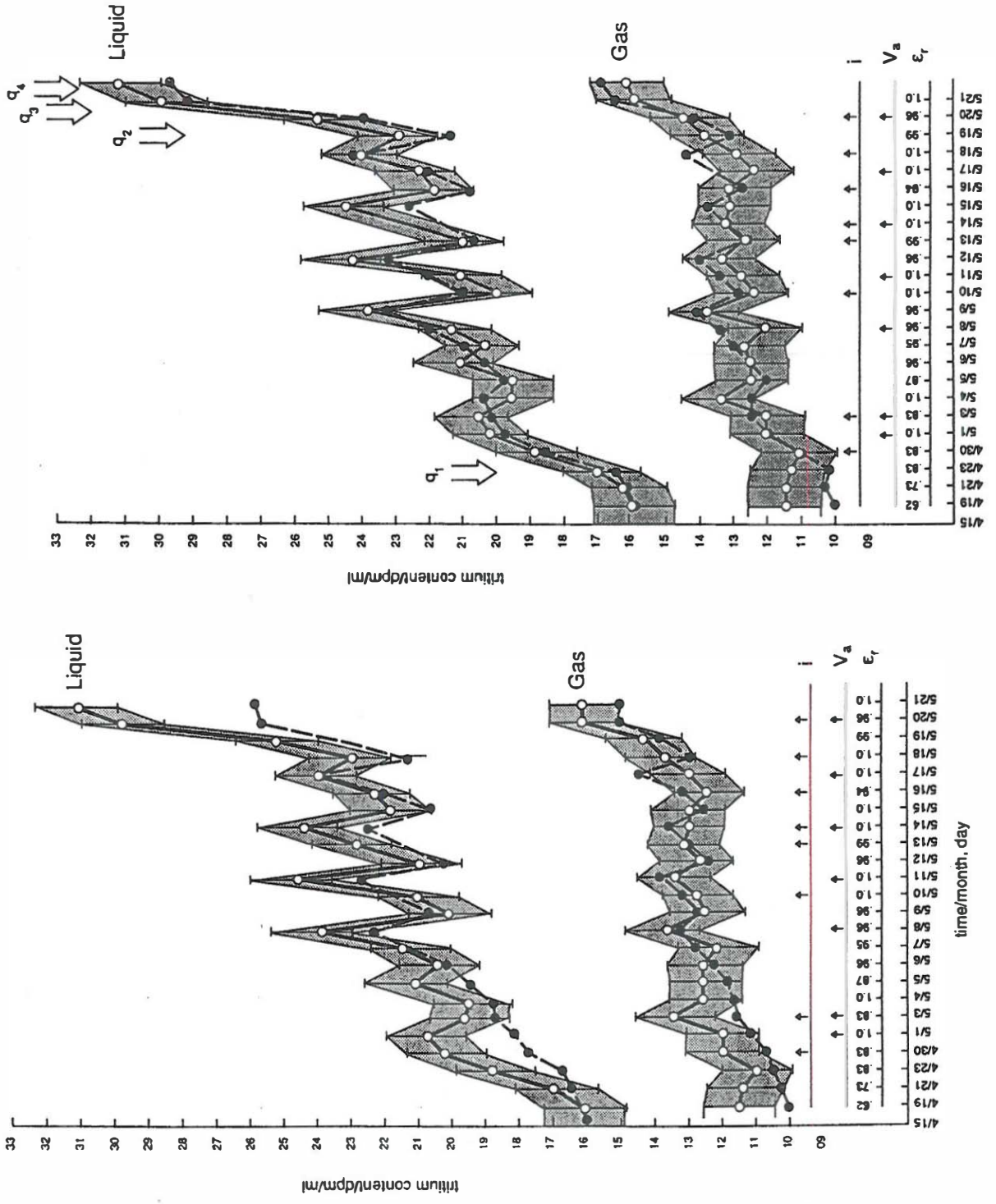

Fig. 5. Two-phase tritium distribution ($s = 0.63$). Electrode area = 2.7 cm^2; Cu-Ag-Pd deposited from $Pd(NH_3)_2Cl_2$; electrolyte: 0.33 *M* Li_2SO_4 (50 ml); additive: 100 ppm $BeSO_4$; cell current, recombining efficiency, electrolyte additions indicated. Additional data are given in Appendix C.

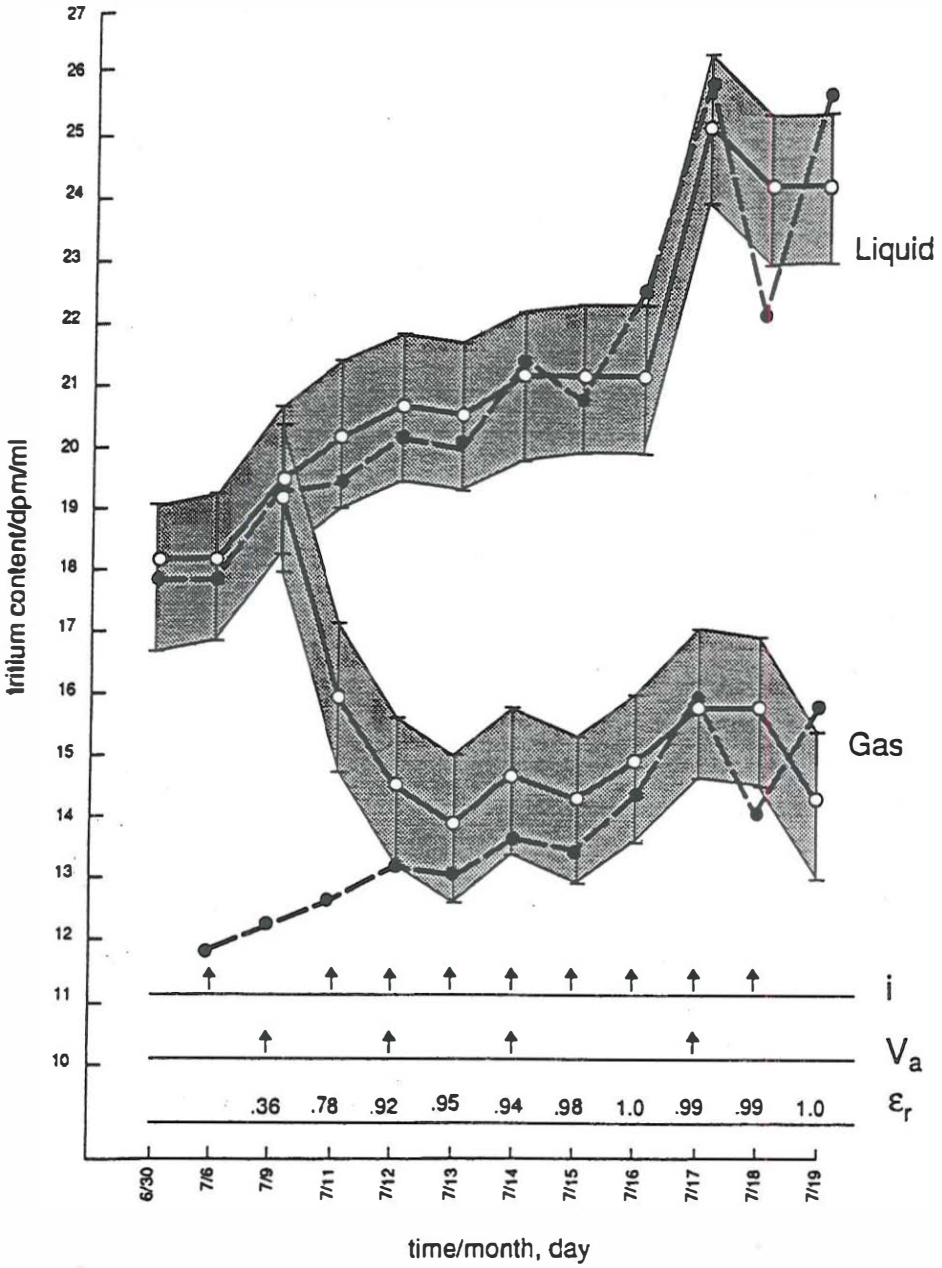

Fig. 6. Two-phase tritium distribution ($s = 0.67$). Note that the s value was computed using data of the last 7 days. Electrode: prepared by codeposition; electrolyte: 0.05 M $PdCl_2$ + 0.6 M LiCl; cell current, recombiner efficiency, D_2O addition indicated. Additional data are given in Appendix D.

gaseous phase only. This enrichment occurs shortly after the completion of the codeposition process and is subsequently followed by a period of inactivity. The time-dependent tritium concentration in the electrolyte agrees at all times with the computed values when $s = 0.67$.

We wish to remark that the absence of tritium production (Fig. 3) means only that within the investigated time interval no activities were observed. It does not mean that they could not occur at some later date, a position expressed earlier by Bennington et al.[9]

III. DISCUSSION

In what follows, we examine the structure of the interphase and the origin and constancy of the isotopic separation factor and provide an interpretation of experimental data.

III.A. Structure of the Interphase—Transport Paths

The kinetic aspects of the hydrogen/deuterium evolution reaction are presented in numerous textbooks, of

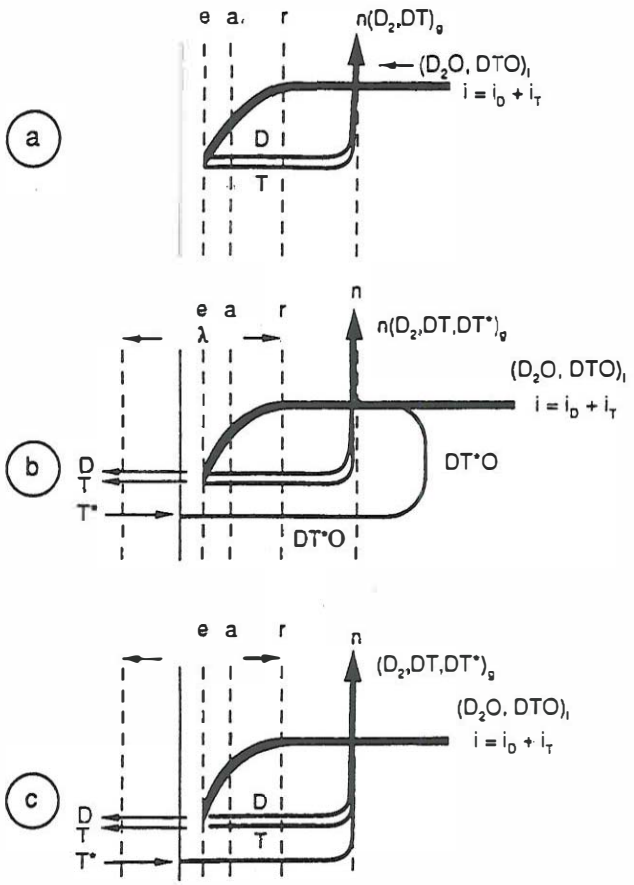

Fig. 7. Structure of the interphase; tritium distribution paths, where r = reaction site, a = adsorption site, e = charge transfer site, n = nucleation and gas evolution plane. (a) Fluxes on nonabsorbing electrode: $i = i_D + i_T$ denotes cell current and currents producing gaseous deuterium and tritium; (b) fluxes on absorbing electrode—path A; (c) fluxes on absorbing electrode—path B.

which the most thorough is the Bockris and Reddy treatise.[10] Here, we limit our discussion to the thermodynamic structure of the electrode/electrolyte interphase formulated by van Rysselberghe.[11] For our purpose, we include the metal side and indicate only the relevant processes that influence the magnitude as well as the constancy of the isotopic separation factor (Fig. 7). Irrespective of the operating rate determining step, species undergoing electroreduction $c_m^{(r)}$ (m = D_2O, DTO) are in equilibrium with those in the bulk (b) electrolyte, i.e., $c_m^{(r)} \leftrightarrow c_m^{(b)}$. Superscript ($r$) refers to the location where the reactive species affect the rate through their electrochemical potentials, the r plane (Fig. 7a). The reaction product, in an adsorbed state $c_m^{(a)}$ is in equilibrium with those dissolved in the electrolyte $c_m^{(b)}$, and when its solubility limit is exceeded, gas bubbles, which also are in equilibrium with the bulk electrolyte, are formed. The set of restrictive conditions that ensures the constancy of the separation factor is as follows:

1. Evolution reaction of hydrogen isotopes is independent of each other; i.e., $i = i_D + i_T$.
2. Sufficiently high overpotentials are applied so that the reverse reactions may be neglected.
3. The system operates in a stationary state; i.e., equilibria between various species are established, resulting in $d\theta_m/dt = 0$ (Ref. 12).

Under these conditions, the tritium distribution occurs via path A, whereby the cell current i is divided into i_T and i_D and the hydrogen evolves from the electrolyte phase at the n plane. This is manifested by an increase in tritium concentration in both phases (Fig. 3).

For the deuterium-absorbing electrode material, the concept of the interphase must be extended to include the metal side, as indicated in Figs. 7b and 7c by λ. If tritium is produced within the bulk electrode and transferred to the electrolyte phase, it must be first brought to the adsorption plane (a plane). The constancy of the s factor requires an equilibrium condition between species located within the interphase and demands that all tritium-bearing species first enter the electrolyte phase, i.e., follow path A (Fig. 7b). The data summarized in Figs. 4 and 5 support transport via path A. The latter condition requires the presence of a charged ^nH (n = 1,2,3) species in the λ layer that interacts with the OD^- ion. The existence of such species, e.g., $[T\cdots T]^+$, $[D\cdots T]^+$, $[D\cdots D]^+$, was postulated in our recent publication.[13] If, however, the conditions are such that transport to the electrolyte phase is prevented, path B becomes operative, resulting in substantial enrichment of the gas phase (Fig. 7c).

The data summarized in Fig. 6 show selective enrichment of the gaseous phase, suggesting that path B is the method of transport. The return to a normal distribution indicates a transition from path B to A. This behavior suggests that tritium production occurs shortly after completion of the codeposition process and is affected by the morphology (mossy, dendritic) of the palladium surface. The transition from path B to A implies an active participation of the interphase region that, most likely, is attributed to the restructuring of the electrode surface as well as to the enhanced concentration of hydrogen isotopes within the interphase region during the codeposition process. A detailed presentation of the restructuring processes can be found in Ref. 14.

III.B. Tritium Distribution—Governing Equations

In the presentation of data and the subsequent analysis, we assume the constancy of the isotopic separation factor. As shown in Ref. 8, the time dependence of tritium content in an open cell, operating galvanostatically with intermittent sampling, is given by Eq. (1):

$$f(t) = [m(0) - r(i)t]^{s-1} \times \left[\frac{f(0)}{m(0)^{s-1}} + \int_0^t \frac{q(t)}{[m(0) - r(i)t]^s} dt \right] , \quad (1)$$

which, for $q(t) = q \neq 0$, we have Eq. (2):

$$f(t) = f(0)\left[\frac{m(0) - r(i)t}{m(0)}\right]^{s-1} + \frac{q}{(s-1)r(i)} \times \left\{1 - \left[\frac{m(0) - r(i)t}{m(0)}\right]^{s-1}\right\}, \quad (2)$$

while, for $q(t) = 0$ it reduces to Eq. (3):

$$f(t) = f(0)\left[\frac{m(0) - r(i)t}{m(0)}\right]^{s-1}, \quad (3)$$

where

f = tritium mass fraction

m = mass of the electrolyte phase

$r(i) = iM_w/2\mathcal{F}$ = the rate of change associated with the passage of cell current i

q = rate at which tritium is added/removed from the solution phase by whatever process including transport of tritium generated in the bulk electrode

s = isotopic separation factor.

The isotopic separation factor is defined here as $s = (c_T/c_D)_g/(c_T/c_D)_l$ and should be inverted to conform to values usually cited in the literature.

III.C. Data Analysis—Quantitative Aspects

The essential difference between the method employed here and elsewhere[5] concerns selection of the numerical value of the isotopic separation factor. This number is usually taken from the literature and may or may not represent the kinetic and thermodynamic properties of the interphase pertinent to the experimental conditions. Here, the value of the s factor is determined individually for each experimental run by selecting that value that best fits the recorded data (see Fig. 3).

In principle, the rate of tritium production is calculated by subtracting Eq. (3) from either Eq. (1) or (2). Taking as an example results plotted in Fig. 4, the difference between the observed and calculated tritium concentration in the electrolyte phase, on June 22, is ~4.0 dpm/ml. Tritium generation rates are estimated by a curve fitting technique[8] or by computer modeling in which an arbitrarily selected q value is inserted into the experimental data and computer matched to obtain agreement with the observed distribution throughout the duration of the experiment. A good agreement was recorded for rate of tritium generation when $q = 6 \times 10^3$ atom/s during the period of June 21, 22. This would indicate a total production of 5.2×10^8 tritium atoms. An unexpected phenomenon of the apparent change in the s factor observed after the burst of tritium production is currently under investigation.

An estimate of tritium production rate by a computer modeling technique is illustrated in Figs. 5a and 5b. In particular, the computed tritium distribution, with $q(t) = 0$ and data tabulated in Appendix C, is shown in Fig. 5a (solid circles), while the actual experimental distribution is shown by the open circles. Using the previous argument, we identify two periods of tritium production, the first occurring between April 21 and May 1 and the second starting on May 18. The experiment was terminated on May 21. The results of computer modeling based on tritium production: on April 21, 22, 23 with $q_1 = 4 \times 10^3$ atom/s for $\Delta t = 3.016 \times 10^3$ min; on May 18 with $q_2 = 3 \times 10^3$ atom/s for $\Delta t = 1.442 \times 10^3$ min; on May 19 with $q_3 = 7 \times 10^3$ atom/s for $\Delta t = 1.421 \times 10^3$ min; and on May 20 with $q_4 = 3 \times 10^3$ atom/s for $\Delta t = 1.489 \times 10^3$ min are shown in Fig. 5b. An excellent agreement with experimental distribution is evident with the total tritium production of 1.8×10^9 atoms.

The data shown in Fig. 6 provide the evidence for tritium production through the enrichment of the gas phase while retaining agreement between the computed and experimental point in the liquid phase. Unfortunately no estimate of the total amount of tritium production can be reliably made because of poor recombination efficiency. The poor efficiency means that the tritium content was, in reality, substantially higher than indicated (due to the faster rate of $D_2 + \frac{1}{2}O_2 \rightarrow D_2O$ compared with that of $DT + \frac{1}{2}O_2 \rightarrow DTO$).

III.D. Tritium Generation Sites

The question of the location of the generation site for tritium production during the electrolysis of D_2O on a palladium electrode cannot be resolved by the method just described. Data in Figs. 4, 5, and 6 were interpreted in terms of Eqs. (1), (2), and (3). As written, these equations ignore the tritium absorption by the palladium lattice and, consequently, cannot provide any information concerning the location of the generating sites. However, this omission does not invalidate conclusions reached as long as $c_T \ll c_D$ and s is constant.

As in the earlier work of Will et al.,[7] the resolution of this problem is sought by employing a total mass balance that, in addition, requires the determination of tritium content in the bulk of the palladium electrode. The amount of tritium generated during several runs and its three-phase distribution is tabulated in Table I. This table lists the experimental conditions (columns 1 through 5) and the distribution of tritium among the liquid, gas, and bulk electrode (columns 6, 7, and 8). A net increase in tritium content is indicated in columns 9 and 10 as either gain in disintegrations per minute or in the number of tritium atoms produced in the course of an experiment.

Data assembled in Table I are in general agreement with results obtained under conditions of intermittent sampling (Figs. 3 through 6). Three conclusions can be made:

TABLE I

Three-Phase Tritium Distribution (by Mass Balance)

Systems	Volume (ml) $t = 0$	Volume (ml) $t = t_f$	$T(l)/(dpm/ml)$ at $t = 0$	ϵ_r	Tritium (dpm/ml) Liquid	Tritium (dpm/ml) Gas	Tritium (dpm/ml) Electrode	$T = T(t_f) - T(t_0)$ dpm	$T = T(t_f) - T(t_0)$ Atoms
Ag/0.3 *M* LiCl	49.71	23.55	18.9 ± 1.2	0.97	22.4 ± 1.2	15.2 ± 1.1	---	−14 ± 50	
(Cu)Pd/0.1 *M* LiOD	49.7	23.66	18.9 ± 1.2	0.998	24.1 ± 1.2	13.1 ± 1.1	ND[a]	−28 ± 50	
(Ag)Pd/0.1 *M* LiOD + 80 ppm Al	49.72	29.49	18.0 ± 1.2	1.00	25.4 ± 1.2	13.3 ± 1.1	2.3 ± 1.3	123 ± 50	5.1×10^{11}
(Ag)Pd/0.3 *M* LiOD + 231 ppm Al	49.69	19.79	16.5 ± 1.2	0.97	20.3 ± 1.2	13.1 ± 1.1	0.9 ± 1.3	−27 ± 50	
(Au)Pd/0.3 *M* LiCl[b] (codeposition)	46.72	11.8	14.5 ± 1.9	0.56 (1.00)	25.4 ± 2.1	13.4 ± 1.8 (29.1)	ND[a,c]	90 ± 80 (637) ± 80	2.6×10^{12}
(Au)Pd/0.3 *M* LiCl[b] (codeposition)	37.1	16.1	17.0 ± 1.9	0.50 (1.00)	25.1 ± 2.1	13.4 ± 1.8	ND[a,c]	60 ± 60 (336) ± 60	1.3×10^{12}

[a]ND = not detectable.
[b]Samples were counted for 240 min instead of 600 min.
[c]Determined by method of Will et al.

1. The long time between samplings obliterates the fine details of the behavior of the Pd/D system. For example, on the basis of the mass balance (rows 1, 2, and 4), no statement can be made concerning production of tritium or lack thereof since the apparent change is much less than the analytical error and is, therefore, not significantly different from no change.

2. Tritium production, if any, takes place within, or in the close proximity of the interphase. Only when Al^{3+} ions were added to the electrolyte was tritium detected in the bulk electrode.

3. Electrolysis on dendritic surfaces (following the codeposition) favors transport of tritium to the gas phase via path B.

IV. CONCLUDING REMARKS

Because of the controversial nature of the palladium lattice–assisted nuclear events, we have refrained from speculations and concentrated on presentation and interpretation of experimental data. Every effort was made to minimize analytical errors. Although closed cells can be considered superior to closed-system arrangements for the detection of tritium generation in electrolytic cells, closed cells, by design, represents an integrating system that may not be desirable for ascertaining the intermittent tritium generation. In this communication, we have shown that the cell/recombiner assembly and our experimental protocols yield results identical with those obtained using closed cells. This is because the greatest source of error in both experimental approaches is in the tritium content measurement itself and not in the electrolyte volume. In conclusion, we emphasize the following points:

1. The evidence for tritium production is based on the difference between the computed and observed concentration of tritium, the nonequilibrium distribution of tritium, and the total mass balance.

2. One of the characteristic features of the behavior of the Pd/D system is the sporadic nature of burstlike tritium generation. Short times between samplings are necessary to facilitate the display of the burstlike behavior. Such behavior would not be detectable using a closed-cell system.

3. Current data indicate that tritium production takes place within the interphase with the distribution governed primarily by path A. A speculative argument can be presented to indicate that the generated tritium is forced into the bulk electrode by conditions at the solution side of the interphase, e.g., addition of Al^{3+} ions, and that electrode surface morphology tends to affect the two-phase distribution; e.g., dendritic surfaces tend to promote transport via path B.

APPENDIXES

Experimental data relevant to the computation of tritium distribution, using Eq. (3), are tabulated in Appendices A through D. They are assembled to supplement the information provided in the respective figure captions.

APPENDIX A

INVENTORY OF INPUT PARAMETERS FOR FIG. 3

Run: 4 Aug 1993 to 18 Aug 1993

Electrolyte
Volume: 24.80 ± 0.01 ml
Composition: 0.3 *M* LiOD + 133 ppm B (as B_2O_3) in D_2O with T = 19.3 ± 1.2 dpm/ml
Additions: 0.1 *M* LiOD + 50 ppm B in D_2O with T = 19.0 ± 1.2 dpm/ml
Separation factor, s = 0.71
Sampling volume, V_s = 1.60 ± 0.01 ml

Sampling Date	i (mA)	Δt (min)	ϵ_r	V_a (ml)	Tritium Electrolyte	Gas (dpm/ml)
8-8	−50	1421	0.68		19.4 ± 1.2	15.0 ± 1.2
	−100	4270				
8-9	−200	1738	0.65	12.11 ± 0.02	19.8 ± 1.2	15.7 ± 1.2
8-10	−300	1315	0.91		20.0 ± 1.2	13.8 ± 1.2
8-11	−400	1442	1.00		19.7 ± 1.2	13.6 ± 1.2
8-12	−400	1593	1.00	12.11 ± 0.02	22.2 ± 1.2	15.5 ± 1.2
8-14	−400	2460	0.96	18.17 ± 0.02	22.6 ± 1.2	16.6 ± 1.2
8-15	−600	1498	1.00		21.4 ± 1.2	14.6 ± 1.2
8-16	−800	1458	1.00	18.98 ± 0.03	22.9 ± 1.2	14.8 ± 1.2
8-17	−1000	1668	1.00		20.3 ± 1.2	14.8 ± 1.2
8-18	−1000	1249	0.98		24.6 ± 1.2	15.8 ± 1.2

APPENDIX B

INVENTORY OF INPUT PARAMETERS FOR FIG. 4

Run: 27 May 1993 to 26 June 1993

Electrolyte
Volume: 24.84 ± 0.01 ml
Composition: 0.01 *M* $PdCl_2$ + 0.314 *M* LiCl in D_2O with T = 17.8 ± 1.2 dpm/ml
Additions: 0.1 *M* LiCl + 200 ppm $MgCl_2$ in D_2O with T = 17.0 ± 1.2 dpm/ml
Separation factor, s = 0.71
Sampling volume, V_s = 1.58 ± 0.01 ml

Sampling Date	i (mA)	Δt (min)	ϵ_r	V_a (ml)	Tritium Electrolyte	Gas (dpm/ml)
6-7	−1	8612			17.7 ± 1.2	
	−2	1645				
	−3	5546				
6-14	−50	2947	0.53		18.9 ± 1.2	12.4 ± 1.1
	−100	7281				
6-15	−200	1496	0.72	8.93 ± 0.03	18.7 ± 1.2	12.6 ± 1.1
6-16	−200	1217	1.00		19.7 ± 1.2	13.5 ± 1.1
6-17	−300	1430	0.83	8.93 ± 0.03	20.0 ± 1.2	13.1 ± 1.1
6-19	−400	2801	0.99	11.90 ± 0.03	20.5 ± 1.2	12.7 ± 1.1
6-21	−300	3282	0.87		20.7 ± 1.2	13.6 ± 1.1
6-22	−300	1435	0.83	11.90 ± 0.03	25.3 ± 1.2	17.6 ± 1.1
6-23	−500	1411	0.96		25.2 ± 1.2	17.8 ± 1.1
6-24	−600	1366	0.98	17.87 ± 0.03	25.7 ± 1.2	13.9 ± 1.1
6-25	−800	1211	0.99		20.8 ± 1.2	12.5 ± 1.1
6-26	−1000	1363	1.00		23.3 ± 1.2	13.3 ± 1.1

APPENDIX C

INVENTORY FOR INPUT PARAMETERS FOR FIGS. 5a AND 5b

Run: 15 Apr 1993 to 21 May 1993

Electrolyte
Volume: 48.89 ± 0.01 ml
Composition: 0.333 *M* Li_2SO_4 + 100 ppm Be (as $BeSO_4$) in D_2O with T = 15.9 ± 1.2 dpm/ml
Additions
(a) 0.1 *M* Li_2SO_4 in D_2O with T = 15.9 ± 1.2 dpm/ml
(b) 0.1 *M* Li_2SO_4 = 100 ppm Be (as $BeSO_4$) in D_2O with T = 15.9 ± 1.2 dpm/ml
(c) D_2O with T = 16.0 ± 1.2 dpm/ml
Separation factor, s = 0.63
Sampling volume, V_s = 2.06 ± 0.01 ml

Sampling Date	i (mA)	Δt (min)	ϵ_r	V_a (ml)	Tritium Electrolyte	Gas (dpm/ml)
4-19	−50	1212	0.62		16.1 ± 1.2	11.5 ± 1.1
	−100	4286				
4-21	−100	2950	0.73		16.9 ± 1.2	11.4 ± 1.1
4-23	−100	3016	0.83		18.7 ± 1.2	11.0 ± 1.1
4-30	−100	9845	0.83		20.2 ± 1.2	12.0 ± 1.1
5-1	−200	1424	1.00	8.94 ± 0.01	20.8 ± 1.2	12.0 ± 1.1
5-3	−200	2977	0.93	20.85 ± 0.02	19.4 ± 1.2	13.5 ± 1.1
5-4	−400	1470	1.00		19.4 ± 1.2	12.5 ± 1.1
5-5	−400	1325	0.87		21.4 ± 1.2	12.5 ± 1.1
5-6	−400	1487	0.96		20.4 ± 1.2	12.6 ± 1.1
5-7	−400	1524	0.95		21.2 ± 1.2	12.1 ± 1.1
5-8	−400	1734	0.98	19.88 ± 0.02	24.2 ± 1.2	13.9 ± 1.1
5-9	−400	1090	0.98		20.1 ± 1.2	12.5 ± 1.1
5-10	−400	1667	1.00		21.0 ± 1.2	12.8 ± 1.1
5-11	−500	1396	1.00	23.83 ± 0.02	24.8 ± 1.2	13.5 ± 1.1
5-12	−500	1305	0.96		20.9 ± 1.2	12.8 ± 1.1
5-13	−500	1551	0.99		23.0 ± 1.2	13.2 ± 1.1
5-14	−600	1194	1.00	25.34 ± 0.02	24.6 ± 1.2	13.0 ± 1.1
5-15	−700	1450	1.00		21.8 ± 1.2	13.0 ± 1.1
5-16	−700	1543	0.94		22.4 ± 1.2	12.4 ± 1.1
5-17	−800	1622	1.00	26.81 ± 0.02	24.1 ± 1.2	12.9 ± 1.1
5-18	−800	1355	1.00		23.0 ± 1.2	13.8 ± 1.1
5-19	−900	1442	0.99		25.2 ± 1.2	14.3 ± 1.1
5-20	−900	1421	0.96	10.45 ± 0.01	29.6 ± 1.2	16.1 ± 1.1
5-21	−1000	1489	1.00		31.2 ± 1.2	16.1 ± 1.1

APPENDIX D

INVENTORY OF INPUT PARAMETERS FOR FIG. 6

Run: 30 June 1993 to 19 July 1993

Electrolyte
Volume: 24.71 ± 0.01 ml
Composition: 0.053 *M* $PdCl_2$ + 0.602 *M* LiCl in D_2O with T = 17.9 ± 1.2 dpm/ml
Additions: D_2O with 17.9 ± 1.2 dpm/ml
Separation factor, s = 0.67
Sampling volume, V_s = 1.58 ± 0.01 ml

Sampling Date	i (mA)	Δt (min)	ϵ_r	V_a (ml)	Tritium Electrolyte	Gas (dpm/ml)
7-6	−0.5	1392			18.1 ± 1.2	
	−1	1432				
	−2	5862				
7-9	−200	4227	0.36	11.90 ± 0.03	19.5 ± 1.2	19.2 ± 1.2
7-11	−200	2848	0.78		20.4 ± 1.2	15.9 ± 1.2
7-12	−300	1476	0.92	11.90 ± 0.03	20.8 ± 1.2	14.4 ± 1.2
7-13	−400	1406	0.95		20.6 ± 1.2	13.8 ± 1.1
7-14	−500	1515	0.94	14.88 ±-0.03	21.2 ± 1.2	14.8 ± 1.2
7-15	−600	1361	0.98		21.3 ± 1.2	14.2 ± 1.2
7-16	−700	1421	1.00		21.3 ± 1.2	14.9 ± 1.2
7-17	−800	1329	0.99	23.81 ± 0.04	25.3 ± 1.2	16.1 ± 1.2
7-18	−900	1561	0.99		24.4 ± 1.2	15.9 ± 1.2
7-19	−1000	1471	1.00		24.3 ± 1.2	14.4 ± 1.2

ACKNOWLEDGMENT

The authors acknowledge the interest and support received from F. Gordon of the Naval Command, Control and Ocean Surveillance Center (NISE West).

REFERENCES

1. M. FLEISCHMANN and S. PONS, "Electrochemically Induced Nuclear Fusion of Deuterium," *J. Electroanal. Chem.*, **261**, 301 (1989).

2. S. SZPAK, P. A. MOSIER-BOSS, and J. J. SMITH, "On the Behavior of the Cathodically Polarized Pd/D System; Search for Emanating Radiation," *Phys. Lett. A*, **210**, 382 (1996).

3. M. L. OLIPHANT, P. HARTECK, and LORD RUTHERFORD, "Transmutation Effects Observed with Heavy Water," *Nature*, **133**, 413 (1934).

4. J. SCHWINGER, "Nuclear Energy in Atomic Lattice," presented at 1st Ann. Conf. Cold Fusion, Salt Lake City, Utah, 1990.

5. E. STORMS, "Review of Experimental Observations About the Cold Fusion Effect," *Fusion Technol.*, **20**, 433 (1991).

6. C.-C. CHIEN, D. HODKO, Z. MINEVSKI, and J. O'M. BOCKRIS, "On an Electrode Producing Massive Quantities of Tritium and Helium," *J. Electroanal. Chem.*, **338**, 189 (1992).

7. F. G. WILL et al., "Studies of Electrolytic and Gas Phase Loading of Palladium with Deuterium," *The Science of Cold Fusion, Proc. 2nd Ann. Conf. Cold Fusion*, Como, Italy, 1991.

8. S. SZPAK, P. A. MOSIER-BOSS, R. D. BOSS, and J. J. SMITH, "Comments on the Analysis of Tritium Content in Electrochemical Cells," *J. Electroanal. Chem.*, **373**, 1 (1994).

9. S. M. BENNINGTON et al., "Search for the Emission of X-Rays from Electrolytically Charged Palladium-Deuterium," *Electrochim. Acta*, **34**, 1323 (1989).

10. J. O'M. BOCKRIS and A. K. N. REDDY, *Modern Electrochemistry*, Plenum Press, New York (1974).

11. P. VAN RYSSELBERGHE, "Some Aspects of the Thermodynamic Structure of Electrochemistry," *Modern Aspects of Electrochemistry*, Vol. 4, J. O'M. BOCKRIS, Ed., Plenum Press, New York (1966).

12. J. O'M. BOCKRIS and S. SRINIVASAN, "Theoretical Calculations of the Separation Factors in the Hydrogen Evolution Reaction for the Slow Discharge Mechanism," *J. Electrochem. Soc.*, **111**, 844 (1964).

13. S. SZPAK, P. A. MOSIER-BOSS, S. R. SCHARBER, and J. J. SMITH, "Charging of the Pd/H System: Role of the Interphase," *J. Electroanal. Chem.*, **337**, 147 (1992).

14. L. SCHLAPBACH, "Surface Properties and Activation," *Topics in Applied Physics*, Vol. II, Chap. 2, Springer-Verlag, Berlin (1978).

Stanislaw Szpak (PhD, University of Pennsylvania, 1961) is a scientist (emeritus) at Naval Command, Control and Ocean Surveillance Center (NRaD), San Diego, California. His research interests include electrochemistry and energy conversion.

Pamela A. Mosier-Boss (PhD, Michigan State University, 1985) is a scientist at NRaD. Her research interests include sensor development, Raman spectroscopy, and electrochemistry.

Roger D. Boss (PhD, Michigan State University, 1985) is a scientist at NRaD. His research interests include superconductivity and modeling of large systems.

Jerry J. Smith (PhD, University of California, Berkeley, 1965) is a program manager in the Division of Materials Sciences, for the U.S. Department of Energy. His research interests include surface sciences and energy conversion.

Reprinted from Fusion Technology, vol. 33, pp 38–51 , January 1998, "On the Behavior of the Pd/D system: Evidence for Tritium Production by S. Szpak P.A. Mosier-Boss and R.D. Boss.

NUCLEAR REACTIONS IN SOLIDS

KEYWORDS: *tritium transport across the interface*

ON THE RELEASE OF $^{3}_{1}H$ FROM CATHODICALLY POLARIZED PALLADIUM ELECTRODES

STANISLAW SZPAK and PAMELA A. MOSIER-BOSS
Space and Naval Warfare Systems Center, San Diego
Code D364, San Diego, California 92152-5001

Received January 12, 1998
Accepted for Publication June 2, 1998

Release paths for tritium produced during electrochemical compression of deuterium in a Pd lattice are examined. Arguments in support of the reversal of diffusion caused by gas evolution on the electrode surface are presented.

I. INTRODUCTION

Tritium production via electrochemically generated deuterium in the Pd lattice was observed by, among others, Chien et al.,[1] Storms and Talcott,[2] Will et al.,[3] and Szpak et al.[4] Except for the massive production reported by Chien et al., the observed rates were low ($\sim 10^4$ atoms/s averaged over a 24-h period[4]). In this paper, we examine transport of the absorbed hydrogen and its isotopes out of the cathodically polarized Pd electrode. The model presented here differs from that proposed by Storms[5] and Storms and Talcott-Storms,[6] who concluded that the mode of transport out of the electrode interior is through capillaries produced by stresses associated with volume expansion. Here, we discuss an alternate transport route, namely, that resulting from the surface inhomogeneities associated with gas evolution.

II. ELECTRODE/ELECTROLYTE INTERPHASE

As reported earlier,[4] tritium produced during prolonged electrolysis was transported out of the electrode interior by two distinct paths: the first resulting in the enrichment of both the electrolyte and gas phases, the second producing enhancement only in the gas phase. It was noted that transport out of the electrode interior was retarded by the addition of, for example, Al^{3+} ions to the electrolyte. These observations and the emanation of weak X rays[7] suggest that the nuclear events leading to the tritium production are located in close proximity to the electrode surface.

Transport of hydrogen (or its isotopes) out of the electrode interior, when under cathodic polarization, is possible by (a) convective flow of the hydrogen gas via interconnected voids forming, in effect, open channels and (b) hydrogen flux reversal generated by nonuniform primary current density distribution associated with gas evolution. Random distribution of gas bubbles results in local changes in current density (and overpotential), which, in turn, produce changes within the interphase. The discussion that follows is based on the model of the interphase structure with the following features:

1. The electrode/electrolyte interphase is an assembly of nonautonomous layers with its structure determined by the operating processes,[8] while the interface is the contact surface (surface of discontinuity).

2. The absorbed hydrogen causes lattice distortion accompanied by volume changes and has high mobility.

3. At the relevant current densities, bubbles of gaseous hydrogen are formed and rapidly removed from the electrode/electrolyte contact surface.

4. Reaction sites are located in close proximity to the contact surface.

This model does not include (see Sec. IV) the following:

1. transport assisted by a random distribution of interconnected voids[9]
2. presence of a random distribution of nuclear reaction sites[10]
3. ionization of absorbed deuterium at high D/Pd atomic ratios[11]
4. the effect of local volume changes on transport.[12]

III. FLOW REVERSAL ASSOCIATED WITH GAS EVOLUTION

The time rate of change of the absorbed deuterium in the electrode interior is governed by particle flux through the contact surface and transport in the bulk. In our model, we specify the electrode interior as consisting of N layers ($N = 1,2,\ldots,10$) and initially assume a uniformly distributed particle flux (uniform current density). However, such an assumption is not valid for electrodes charged in the presence of gas evolution. To a first approximation, the effect that evolved gas has on the redistribution of absorbed hydrogen and its isotopes can be observed by setting the cell current to zero and watching how the system relaxes at the surface and in close proximity to the surface.

The progress in electrode loading, as well as other pertinent information, is obtained by numerically solving the following set of equations[13]:

$$\frac{d\eta}{dt} = \frac{1}{C_{dl}}(I - j_1 - j_2) \ , \tag{1}$$

$$\frac{d\theta}{dt} = \frac{1}{\Gamma_m \mathrm{F}}(-j_1 + j_2 + j_3 + j_4) \ , \tag{2}$$

$$\frac{d\zeta_1}{dt} = -\frac{1}{\delta}\left[\frac{j_4}{Z_m \mathrm{F}} + k_d Z_m(\zeta_1 - \zeta_2)\right] \ , \tag{3}$$

and

$$\frac{d\zeta_i}{dt} = \frac{k_d Z_m}{\delta}(\zeta_{i-1} - 2\zeta_i + \zeta_{i+1}) \ , \tag{4}$$

where

j_1 = charge transfer current for Volmer path

j_2 = charge transfer current for Heyrovsky-Horiuti path

j_3 = equivalent current for Tafel path

j_4 = equivalent current for the absorption step

Γ_m = maximum number of sites per unit area

Z_m = maximum number of sites per volume

θ, ζ = fractional occupation sites

δ = layer thickness

C_{dl} = capacitance of the double layer

F = Faraday constant.

Equations (1), (2), and (3) state that deuterium is deposited onto the electrode surface by the Volmer path and removed by the Heyrovsky-Horiuti path, the Tafel path, and absorption.

Changes in the surface concentration $\Gamma_m\theta(t)$, overpotential $\eta(t)$, and absorbed deuterium within the layers $Z_m\zeta(t)$ during the electrode loading (at $I = 40$ mA/cm², $t = 100$ s) followed by complete unloading are shown in Figs. 1a and 1b for two diffusion coefficients $D = 10^{-10}$ and $D = 10^{-8}$ cm²/s (rate constants: $k_d = 2.0 \times 10^{-4}$ and $k_d = 2.0 \times 10^{-2}$). It is seen that on loading, the time-dependent surface coverage and electrode overpotential are identical, but the distribution of the absorbed hydrogen differs. For the selected set of rate constants, the transport is diffusion controlled in Fig. 1a, while Fig. 1b illustrates the surface control. The situation is quite different immediately after cell current termination; i.e., the direction of deuterium transport is reversed. In particular, during the first 900 s, the surface coverage is transport controlled [note: as indicated, $\theta(t)$ is less for $D = 10^{-10}$ than for $D = 10^{-8}$ cm²/s]. After this time period, a complete overlap of $\theta(t)$ curves indicates surface-controlled events.

The formation, growth, and detachment of electrogenerated hydrogen gas bubbles have a profound effect on the overall process(es) in both the solution and metal side of the interphase. The effect of gas bubbles on the outflow of absorbed hydrogen by the exchange between the absorbed and adsorbed atoms is simulated by tracing its distribution in close proximity to the contact surface, here limited to the first three layers (Figs. 2a and 2b). In modeling tritium outflow, two factors are important: the residence time and the change in chemical potential of adsorbed hydrogen at the bubble formation site. Here, we arbitrarily assumed the nuclear reaction sites to be in the second layer (i.e., in close proximity to the contact surface) and calculated the change in the distribution of absorbed hydrogen as a function of time resulting from setting the cell current to zero. The rate at which this change occurs is governed by bulk transport. This difference is illustrated in Figs. 2a and 2b for $D = 10^{-8}$ and $D = 10^{-10}$ cm²/s. In highly concentrated systems,[11] where the diffusion coefficient may be as high as 10^{-5} cm²/s, rapid exchange between the absorbed and adsorbed species favors tritium release as suggested in Ref. 4 rather than by the convective flow in channels.

IV. DISCUSSION

The evolution of gas bubbles on the electrode surface precludes uniform distribution of the current density and, therefore, overpotential. This, in turn, results in the removal of an external force acting on interphase of the hydrogen-loaded electrode and ensures local formation of gradients. How deep into the electrode interior these gradients extend depends on the residence time of the gas bubbles and the relaxation time of the process(es) under consideration. In addition to the electric potential gradients operating within the interphase, gradients arising from the volume changes and their effect on the transport should be considered. Moreover, if a nuclear event takes place, its net energy must be added. The

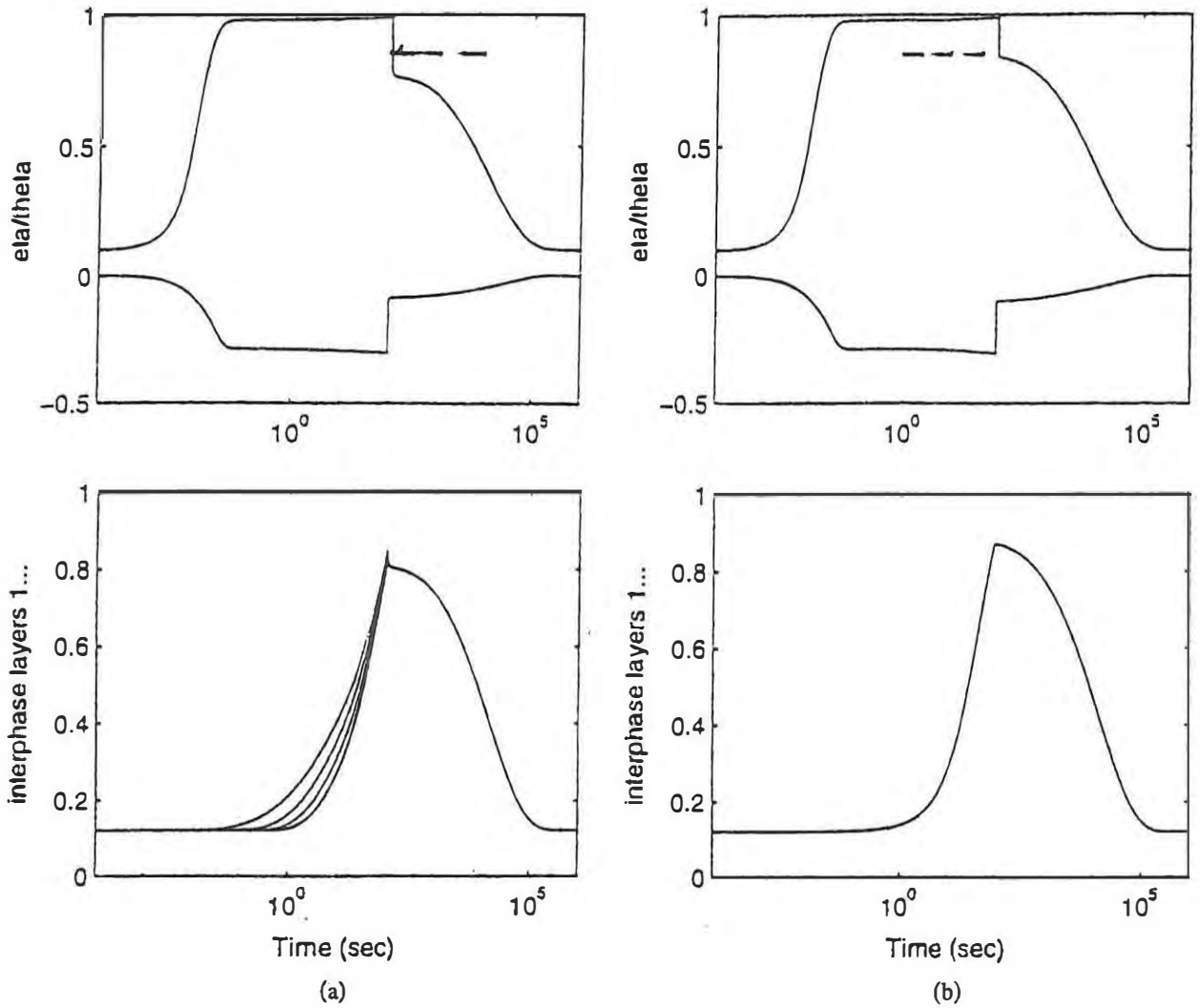

Fig. 1. Time-dependent characteristics of absorption and desorption. Modeling parameters: $N = 10$, $\theta_0 = 0.1$, $\zeta_0 = 0.12$; $\Gamma_m = 10^{-11}$ mol/cm^2; $Z_m = 10^{-1}$ mol/cm^3; $\delta = 10^{-5}$ cm; rate constants: $k_1 = 10^5$ cm^3/mol·s; $k_2 = 10^2$ cm^3/mol·s; $k_3 = 10$ cm^2/mol·s; $I = 40$ mA/cm^2, loading time $t = 100$ s. Upper: deuterium distribution as a function of time: (a)—for D = 10^{-10} cm^2/s and (b)—for D = 10^{-8} cm^2/s. Lower: surface coverage and overpotential as a function of time: (a)—for D = 10^{-10} cm^2/s and (b)—for D = 10^{-8} cm^2/s.

resultant question is, Do these events affect transport properties, and, if so, could they promote flow reversal without first creating capillaries? In particular, we address the question of whether or not the formation of capillaries is the only condition that promotes the removal of tritium produced during cathodic polarization out of the electrode interior.

We note that the transport of absorbed hydrogen through a Pd lattice, and particularly within the interphase at high D/Pd ratios, is described by the flux density of the Einstein-Smoluchowski equation

$$j = \beta c f(x) - D\frac{\partial c}{\partial x} - c\frac{\partial D}{\partial x} \quad , \qquad (5)$$

where function $f(x)$ arises from the interaction of ³H atoms with external strain[14] and electric[15] fields and where β is the mobility (defined here as the ratio of average velocity to applied force). Since concentration and temperature gradients are expected at the nuclear reaction sites and, at high D/Pd ratios, the diffusion coefficient is a function of concentration,[11] Eq. (5) is preferred for the examination of transport in close proximity to the contact surface. Depending on conditions, some of the terms in Eq. (5) can be omitted; thus,

1. For dilute solutions, where D is a constant, only the $D\partial c/\partial x$ term is retained.[16]

2. In the presence of voids, two cases can be differentiated: (a) discrete voids exhibiting distribution in size and position and (b) interconnected voids with channels extending to the contact surface. If the former applies, D is a function of position, and term $\partial D/\partial x$ is retained. If

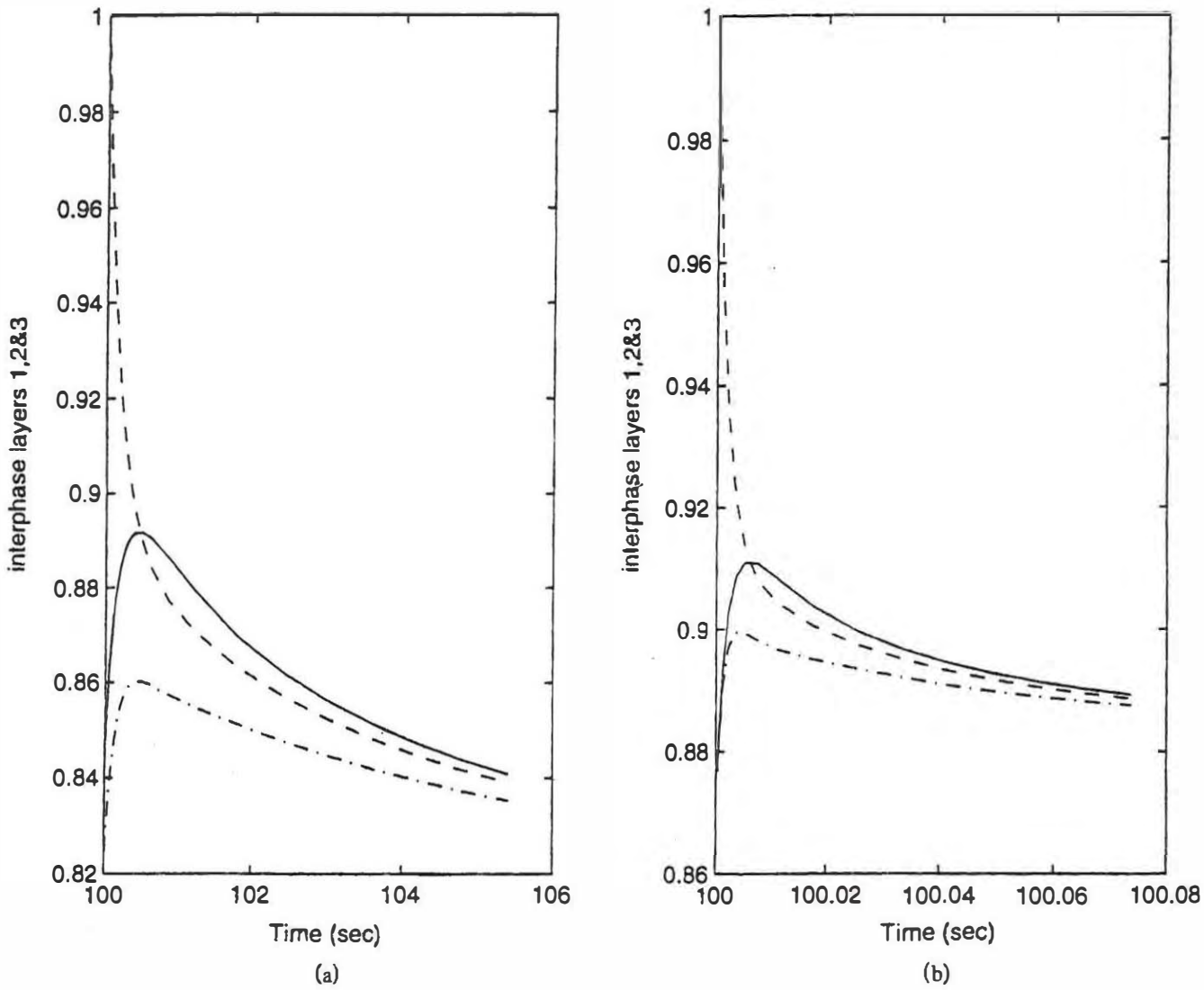

Fig. 2. The ¦H distribution in the first three layers with $\zeta_2 = 1$. Modeling parameters as in Fig. 1. Solid line, first layer; dashed line, second layer; dashed-dotted line, third layer. (a)—for $D = 10^{-10}$ cm²/s and (b)—for $D = 10^{-8}$ cm²/s. Note difference in timescale.

the latter applies, $\partial D/\partial x$ is dropped and $f(x)$ represents the pressure gradient, i.e., we have a case of diffusion assisted by a convective component.

3. If a nuclear reaction (e.g., production of tritium) occurs, not only are all terms retained but a source term must be added, resulting in the temperature gradient $\partial T/\partial x$.

As the hydrogen concentration increases, voids containing molecular hydrogen are formed. When their internal pressure exceeds the strength of the electrode material, channels extending in all directions are created, as illustrated in Fig. 3. Some of them reach the contact surface and allow a rapid outflow of hydrogen, thus preventing the initiation of nuclear events such as tritium production, alternatively, their termination. Consequently, it is important to determine conditions that promote channeling. This has been discussed by Bockris and Subramanyan[17] and Flitt and Bockris.[18] Briefly, conditions that promote channeling are related to the mechanism of the hydrogen evolution reaction[17] (HER) and the energetics of adsorbed hydrogen atoms.[18] In particular, fast j_1 slow j_3 favors channeling, while slow j_1 fast j_3 and slow j_1 fast j_2 do not. In other cases, such as fast j_1 slow j_2, coupled j_1 slow j_3 and coupled fast j_1 slow j_2 may promote channeling, depending on rate constants of the participating paths.

Because the chemical potential gradient $\nabla\mu$ is the generalized force for the flow of matter, it is instructive to transform Eq. (5) into

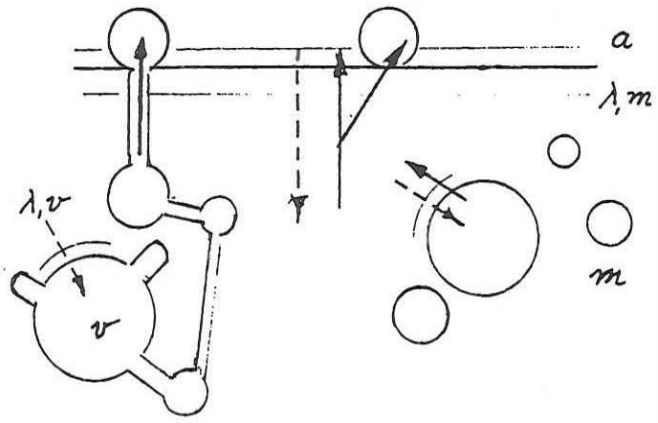

Fig. 3. Schematic representation of interconnected (left) and discrete (right) voids. Arrows indicate flux direction: dashed line, during loading; solid line, during unloading. Values λ, a, v, and m are defined in text.

$$v = -\frac{D}{RT}\frac{\partial \mu}{\partial x} + \left[\beta f(x) - \frac{\partial D}{\partial x}\right], \qquad (6)$$

where $v = j/c$ is the average particle flux velocity, and to use this equation to discuss the transport of tritium from the reaction site to the bulk of contacting phases.

Consider a fully charged Pd electrode containing discrete and interconnected voids of varying size distributed throughout the electrode interior, shown in Fig. 3. In the absence of mass flow, the polarized electrode represents a closed system subject to the action of an external force η. Underthese conditions, equality of chemical potential can be assumed, i.e., $\mu^{(a)} = \mu^{(\lambda,m)} = \mu^{(m)} = \mu^{(\lambda,v)} = \mu^{(v)}$, where superscripts denote the respective locations:

λ, m = subsurface layer

m = bulk metal

λ, v = subsurface/void gas layer

v = gas in the void.

Qualitatively, the effect of formation and growth of the gas bubble reduces and, for a brief period of time, eliminates the external force acting at the point of contact. Since $\mu^{(a)} = f(\theta,\eta)$ (Ref. 17), it follows that upon the reduction of η, a condition $\mu^{(v)} > \mu^{(\lambda,v)} > \mu^{(m)} > \mu^{(\lambda,m)} > \mu^{(a)}$ exists, resulting in production of localized gradients, $\nabla\mu$, and exit of deuterium, and, respectively, tritium from the electrode interior into either the electrolyte or the gas bubble [paths A and B (see Ref. 4)]. Quantitative assessment would involve the relaxation times of the individual steps. There is some experimental evidence suggesting the importance of the $(\lambda, m) \rightarrow (a)$ step in the course of unloading.[19]

V. CONCLUDING REMARKS

In summary, we note the following:

1. Tritium production requires high D/Pd atomic ratios. This requirement is met if there are no channels reaching the contact surface. The electrogenerated tritium is distributed among voids and bulk material. Should new conditions arise that create channels, e.g., a change in the HER mechanism, a short time release of tritium would take place. In our experimental work,[4] there is no clear evidence for this to occur.

2. Conditions believed to affect the initiation of the Fleischmann-Pons effect is the existence of gradients and other "hidden variables."[12] Such conditions do exist in the vicinity of the contact surface and are, in part, due to evolving gas bubbles. The thickness of the active region depends on the residence time of gas bubbles and the dominant transport step. The estimated thickness for diffusion control is in the micron range.

3. Gas evolution promotes a continuous exchange between the ³H atoms residing in the subsurface layer with those in the adsorbed state. Atoms in the adsorbed state exchange with the molecules of the contacting electrolyte phase or gaseous phase, leading to two distinct transfer paths.

ACKNOWLEDGMENTS

The authors acknowledge the interest and support received from F. Gordon, Code D30, Space and Naval Warfare Systems Center, San Diego. Numerical computations were performed by D. Evans.

REFERENCES

1. C. C. CHIEN, D. HODKO, Z. MINEVSKI, and J. O'M. BOCKRIS, "On an Electrode Producing Massive Quantities of Tritium and Helium," *J. Electroanal. Chem.*, **338**, 189 (1992).

2. E. STORMS and C. TALCOTT, "Electrolytic Tritium Production," *Fusion Technol.*, **17**, 680 (1990).

3. F. G. WILL, K. CEDZYNSKA, and D. C. LINTON, "Tritium Generation in Palladium Cathodes with High Deuterium Loading," *Trans. Fusion Technol.*, **26**, 209 (1994).

4. S. SZPAK, P. A. MOSIER-BOSS, R. D. BOSS and J. J. SMITH, "On the Behavior of the Pd/D System: Evidence for Tritium Production," *Fusion Technol.*, **33**, 38 (1998).

5. E. STORMS, "The Nature of the Energy-Active State in Pd-D," *Infinite Energy*, **1**, 77 (1996).

6. E. STORMS and C. TALCOTT-STORMS, "The Effect of Hydriding on the Physical Structure of Palladium and on the Release of Contained Tritium," *Fusion Technol.*, **20**, 246 (1991).

7. S. SZPAK, P. A. MOSIER-BOSS, and J. J. SMITH, "On the Behavior of the Cathodically Polarized Pd/D System: Search for Emanating Radiation," *Phys. Lett.*, **A210**, 382 (1996).

8. R. DEFAY, I. PRIGOGINE, A. BELLEMANS, and D. H. EVERETT, *Surface Tension and Absorption*, Longmans, Green and Company, Ltd., London (1966).

9. W. BECK, J. O'M. BOCKRIS, J. McBREEN, and L. NANIS, "Hydrogen Permeation in Metals as a Function of Stress, Temperature and Dissolved Hydrogen Concentration," *Proc. R. Soc.*, **A290**, 220 (1966).

10. S. SZPAK and P. A. MOSIER-BOSS, "On the Behavior of the Cathodically Polarized Pd/D System: A Response to Vigier's Comments," *Phys. Lett. A*, **221**, 141 (1996).

11. C. BARTOLOMEO, M. FLEISCHMANN, G. LARRAMONA, S. PONS, J. ROULETTE, H. SIGIURA, and G. PREPARATA, "Alfred Coehn and After: The α, β, γ of the Palladium-Hydrogen System," *Trans. Fusion Technol.*, **26**, 23 (1994).

12. M. FLEISCHMANN, S. PONS, M. LeROUX, and J. ROULETTE, "Calorimetry of the Pd-D_2O system: The Search for Simplicity and Accuracy," *Trans. Fusion Technol.*, **26**, 323 (1994).

13. S. SZPAK, C. J. GABRIEL, J. J. SMITH, and R. J. NOWAK, "Electrochemical Charging of Pd Rods," *J. Electroanal. Chem.*, **309**, 273 (1991).

14. J. VOELKL, "The Gorsky Effect," *Ber. Bunsenges.*, **72**, 797 (1968).

15. G. GOMILA and J. M. RUBI, "Non-Equilibrium Thermodynamic Description of Junctions in Semiconductor Devices," *Physica A*, **234**, 851 (1997).

16. M. A. V. DEVANATHAN and Z. STACHURSKI, "The Adsorption and Diffusion of Electrolytic Hydrogen in Palladium," *Proc. R. Soc. A*, **270**, 90 (1962).

17. J. O'M. BOCKRIS and P. K. SUBRAMANYAN, "The Equivalent Pressure of Molecular Hydrogen in Cavities Within Metals in Terms of the Overpotential Developed During the Evolution of Hydrogen," *Electrochim. Acta*, **16**, 2169 (1971).

18. H. J. FLITT and J. O'M. BOCKRIS, "Concerning Adsorbed and Absorbed Hydrogen on and in Ferrous Metals," *J. Hydrogen Energy*, **7**, 411 (1982).

19. S. SZPAK, P. A. MOSIER-BOSS, C. J. GABRIEL, and J. J. SMITH, "Absorption of Deuterium in Palladium Rods: Model vs Experiment," *J. Electroanal. Chem.*, **365**, 275 (1994).

Stanislaw Szpak (PhD, University of Pennsylvania, 1961) is a scientist (emeritus) at Space and Naval Warfare Systems Center San Diego (SSC SD), San Diego, California. His research interests include electrochemistry and energy conversion.

Pamela A. Mosier-Boss (PhD, Michigan State University, 1985) is a scientist at SSC SD. Her research interests include sensor development, Raman spectroscopy, and electrochemistry.

Reprinted from Fusion Technology, vol 34, pp 273–278, November 1998, "On the Release of ?H from Cathodically Polarized Palladium Electrodes by S. Szpak and P.AS. Mosier-Boss. Copyright 1998 by the American Nuclear Society, La Grange Park, Illinois.

CALORIMETRY OF THE Pd + D CODEPOSITION

ELECTROLYTIC DEVICES

KEYWORDS: *calorimetry, Pd+D, codeposition*

STANISLAW SZPAK and PAMELA A. MOSIER-BOSS*
Spawar Systems Center San Diego, San Diego, California 92152-5000

MELVIN H. MILES *Naval Air Warfare Center Weapons Division China Lake, California 93555-6001*

Received November 2, 1998
Accepted for Publication December 2, 1998

Thermal activities associated with electrochemical compression of deuterium produced on electrodes prepared by Pd+D codeposition are discussed. Three cases are considered: activities during and shortly after commencement of current flow, those observed during runs of several days duration, and surface temperature distribution recorded by infrared scanning. Experimental results show excellent reproducibility, high-power outputs, and the development of thermal instabilities resulting in the formation of local hot spots.

I. INTRODUCTION

An alternate method for the initiation of the Fleischmann-Pons effect is to employ an electrode prepared by Pd + D codeposition. This technique involves the electrodeposition from a Pd^{2+} salt solution at cell currents (potentials) so adjusted as to deposit the Pd film in the presence of evolving deuterium.[1] The effectiveness of this approach with regard to generation of nuclear and thermal events was reported by us in the initial phase of our investigation. One advantage of the codeposition process is rapid saturation with deuterium; atomic ratios D/Pd > 1.0 were measured within minutes.[2] Thus, the condition for the initiation of the Fleischmann-Pons effect is realized after brief periods of time as demonstrated by X-ray emission[3] and tritium production.[4]

Early in the investigation of the codeposition process, we reported that cathodically polarized Pd + D electrodes are hotter by 1.5 to 2°C than the electrolyte solution when measured by a thermocouple.[1] However, when viewed with an infrared camera, the electrode surface temperature exceeded that of the electrolyte by ~6°C (Ref. 5). In what follows, we present evidence for excess enthalpy production: Sec. IV.A, shortly after completion of the codeposition process; Sec. IV.B, in the course of a long charging time; and Sec. IV.C, the development of instabilities. The appropriate experimental procedures are briefly outlined.

*E-mail: bossp@nosc.mil

II. FORMULATION OF CALORIMETRIC EQUATION

In the simplest arrangement, an electrochemical cell is a three-phase, multicomponent assembly wherein the charge transfer reactions and associated transport processes occur. Initially, this system is in thermal, mechanical, and chemical equilibrium. On initiation of current flow, significant changes in temperature and concentration take place, i.e., the development of gradients, which in turn initiate transport processes in the electrolyte phase and across the electrolyte-gas interface. The increase in temperature arises from the irreversible processes: the joule heating, the electrodic processes, and the exothermic absorption of deu-. terium by the palladium electrode as well as due to exchange with the environment.

II.A. Enthalpy Balance

In deriving the calorimetric equation, we balance the change in the enthalpy of the electrolyte phase with the enthalpy gain or loss attributed to the participating processes. In particular, applying the enthalpy balance to an open electrochemical system (not including the cell walls and electrodes), we obtain, with $dn_j < 0$,

$$\frac{\partial H}{\partial T}\cdot dT - \Sigma \frac{\partial H}{\partial n_j}\cdot dn_j = dH^* - dw + \Sigma dH^{(1\to v)} + \Sigma dH^{(1\to e)} \quad , \qquad (1)$$

where

dH^* = energy produced (e.g., heat of absorption, excess enthalpy)

dw = work done on the surroundings

$\Sigma dH^{(1\to v)}$ = enthalpy transferred between the electrolyte and the gas phase

$\Sigma dH^{(1\to e)}$ = enthalpy transferred to or from the environment.

The direction of transfer determines the sign, i.e., the quantity removed from the system is negative. By dividing each term of Eq. (1) by dt and identifying the participating processes, we obtain the governing differential equation

$$\left[\Sigma m_i c_i \frac{dT}{dt}\right] + m_o c_s \left[1 - \frac{It}{2m_o F}\right]\frac{dT}{dt} = J^* + I(E_c - E_{th}) + \Sigma J^{(1\to 2)} + \Sigma J^{(1\to e)} \quad , \qquad (2)$$

where the first term accounts for the contribution of all cell components except the electrolyte. This term must be carefully evaluated during the course of long-term experiments and, in particular, during the calibration procedure because the relaxation time is strongly affected by the physicochemical properties of walls and enclosures.

The solution of Eq. (2) requires specification of the initial conditions and evaluation of all other terms consistent with the mode of operation and the cell design. The initial conditions are the equilibrium conditions, i.e., the temperature of the whole system is that of the environment, and the composition of the gas phase is $D_2{:}O_2$ = 2:1 with vapor in equilibrium with the electrolyte. The rate of heat transfer out of the cell depends on the cell geometry, construction of the enclosure, and mode of transport. The simplest case is that of an adiabatic wall. If the enclosure is a diathermal wall, then the heat transfer may occur via radiation with some convective contributions or via convection with minor radiative contributions.

II.B. Heat Content of the Electrolyte Phase

As written, the second term on the left side in Eq. (2) represents the rate of change in the heat content of the electrolyte as a function of time, evaluated at the temperature $T(t)$. Assuming a 100% faradic efficiency, the consumption of D_2O, in a cell operating for t s at the current density, $I\ (\mathrm{A\cdot cm^{-2}})$, is $It/2F$, so that the time rate of change in the electrolyte heat content is $m_o c_s(1 - It/2Fm_o)$, where m_0 is the initial amount of D_2O.

II.C. Electrical Work *dw*

A unique feature of an operating electrochemical cell is the occurrence of charge transfer reactions whereby electrons are generated at the negative electrode and are transferred in an external circuit and consumed at the positive electrode in another charge transfer reaction. In a steady state, the number of electrons leaving and entering the cell is the same, which means that an electrochemical cell can be considered a closed system with regard to the electrical charge (note that potential difference buildup occurs at the phase boundary only). Irrespective of the direction of current flow, the product IE_C must be a positive quantity. By convention, the positive current is flowing out of the cell so that the electrical work term in Eq. (1) is positive. The enthalpy input to the cell is $I(E_c - E_{th})dt$, where E_{th} is the thermoneutral potential.

II.D. Rate of Enthalpy Transfer

The $J^{(1\to e)}$ term is, as a rule, of the form of the generalized Ohm's law, $J_q = k[T^{(1)} - T^{(2)}]$, and where k is usually taken to be constant within this temperature range. Its numerical value depends on the composition of the wall, with the applicable computation methodology described in textbooks on heat transfer.

In the system under consideration, the $J^{(1\to v)}$ term represents the sum of the enthalpy carried out by the rising bubbles saturated with D_2O vapor at the cell temperature $J_1^{(1\to v)}$ and that due to the phase change $J_2^{(1\to v)}$. The respective rates are the following:

$$\frac{I}{F}\left[0.5c_{D_2} + 0.25c_{O_2} + 3pc_s/4(p^* - p)\right]$$

and

$$0.75IpL^{(1\to v)}/F(p^* - p) \quad ,$$

where

p^* = atmospheric pressure

p = vapor pressure of D_2O

L = latent heat of evaporation.

II.E. Temperature-Dependent Parameters

Excluding the J^* term, all terms on the right side of Eq. (2) are temperature dependent in a simple way except for the $I(E_c - E_{th})$ term. The temperature dependence of the specific heat is usually taken as a linear function of temperature. The term accounting for the enthalpy transport to the vapor phase consists of two parts: $J_1(I,T)^{(1\to v)}$ and $J_2(p^*,T)^{(1\to v)}$, of which J_1 identifies the small amount of heavy water evaporating into the D_2 and O_2 gas bubbles. This term is a function of the cell current and temperature, and it is negligible except at high solution temperatures and/or cell currents. The second, J_2, denotes the loss of water due to evaporation. The rate of evaporation is proportional to the solution temperature, and as the temperature approaches the boiling point, the J_2 dominates. The J_2 dependence is calculated using the Clausius–Clapeyron formula and can be evaluated quite

easily, but not the J_1 term because of the number of factors that must be considered, among them the size of the gas bubbles, the degree of their saturation, etc. Less clear is the temperature dependence of the term $I(E_c - E_{th})$. Following Fleischmann et al.,[6] the correction factor is

$$\psi = \frac{dE_c}{dT}\Delta T + \frac{3}{4F}\cdot\frac{d}{dT}\left[\frac{p}{p^* - p}(c_s\Delta T + L^{(1\to v)})\right]\Delta T \ .$$

This procedure involves expanding the temperature dependent $(E_c - E_{th})$ term into the Taylor series, retaining the first term only on account of smallness of T, and expressing E_{th} by the change in the enthalpy function of the electrolyte due to the increase by T.

III. REMARKS CONCERNING THE OPEN CELL CALORIMETRY

A calorimeter is an apparatus designed to measure quantities of heat associated with the occurrence of specific processes (e.g., heat of reaction, heat of absorption, etc.) or the property of matter (e.g., specific heat). The basis for such measurements is the conservation of energy and requires knowledge of the processes under consideration, the sequence of events, the construction of the apparatus, and the experimental procedure employed, i.e., the development of the calorimetric equation for an operating electrochemical cell employs conservation of energy and adjusts the applicable walls and constraints in a manner consistent with the cell design and relevant experimental procedures. Procedures for the isoperibolic designs, employed for long charging times, have been described in a number of publications (Ref. 7 and references therein) and will not be discussed here. For the examination of short duration runs, an adiabatic enclosure might be appropriate. A comprehensive description is given in the following discussion.

III.A. Calorimetric Equations in Condensed Form

Consider a system consisting of an electrochemical cell containing a known amount of electrolyte and totally immersed in a water bath. Initially this system is in equilibrium and, for the duration of an experiment, the bath is in contact with an infinite heat sink (i.e., $T^{(e)}$ = const). Applying the conservation of energy, in the form of condensed Eqs. (1) and (2), the time rate of the temperature change in the cell after its activation is

$$C_1\frac{dT^{(1)}}{dt} = Q_1 - J_q^{1\to 2} - J_q^{1\to e} \qquad (3)$$

and in the water bath

$$C_2\frac{dT^{(2)}}{dt} = Q_2 + J_q^{1\to 2} - J_q^{1\to e} \ , \qquad (4)$$

where

C_1 = $m_i c_i$ = heat capacity of the electrolyte and includes all cell components

C_2 = heat capacity of the fluid bath

Q_1 = rate of heat production in the electrolyte phase

Q_2 = heat supplied to the bath to maintain $T^{(1)} = T^{(2)}$

J_q's = heat fluxes exchanged between the system elements.

III.B. Construction of an Adiabatic Wall

Equation (3) is the energy balance in terms of the rate of heat generation due to irreversibilities of the charge transfer processes, the rate of heat exchange between the cell and the water bath, and the rate of heat loss to the environment. Since the term Q_1 is always positive, it follows that $T^{(1)} > T^{(2)}$ results in an outflow of heat generated within the cell. The construction of an adiabatic wall requires that $J_q^{(1\to 2)} = J_q^{(2\to 1)}$ at all times. This requirement is fulfilled as long as $\Delta T = 0$, i.e., as long as $J_q^{(2\to e)} = Q_2 - C_2[Q_1 - J_q^{(1\to e)}]/C_1$, which for $Q_1 \gg J_q^{(1\to e)}$ is further simplified to $J_q^{(2\to e)} = Q_2 - C_2Q_1/C_2$ and provides a rough guide for the design and operation of an adiabatic wall separating the cell from the bath. Since, in practice, $\Delta T \neq 0$, the maintenance of an adiabatic wall requires that $\int J_q^{(1\to 2)}\,dt = \int J_q^{(2\to 1)}\,dt$, i.e., that ΔT oscillates about its zero value. Employing for the thermal flux an expression of the form $J_q = k\Delta T$ and introducing a new set of variables, i.e., $\Delta T = T^{(1)} - T^{(2)}$, $\theta = T^{(1)} - T^{(e)}$ with θ = const, Eq. (3) becomes Eq. (5):

$$\frac{d\theta}{dt} = q_1 - \kappa_{12}\Delta T - \kappa_{1e}\theta \ . \qquad (5)$$

Using the same variables, by subtracting Eq. (4) from Eq. (3), we obtain an expression for the change in T.

$$\frac{d\Delta T}{dt} = (q_1 - q_2) - (\kappa_{12} + \kappa_{12}^* + \kappa_{2e})\Delta T + (\kappa_{2e} - \kappa_{1e})\theta \ , \qquad (6)$$

where $q_i = Q_i/C_i$; $\kappa_i = k_i/C_i$; and $\kappa^* = k_{12}/C_2 = \kappa_{12}C_1/C_2$. Conditions forcing ΔT to oscillate about zero can be determined by solving the set of coupled differential equations.[8]

To maintain an adiabatic wall, the positive ΔT due to $q_1 > 0$ must be countered by q_2 to reverse the direction of the heat flow. One way to construct and maintain an adiabatic wall is as follows: At $t < t_0$, the system is in equilibrium. At t_0 the flow of cell current is initiated causing the system's temperature to rise as shown schematically in Fig. 1 by solid $T^{(1)}$ and dashed $T^{(2)}$ lines. At t_1

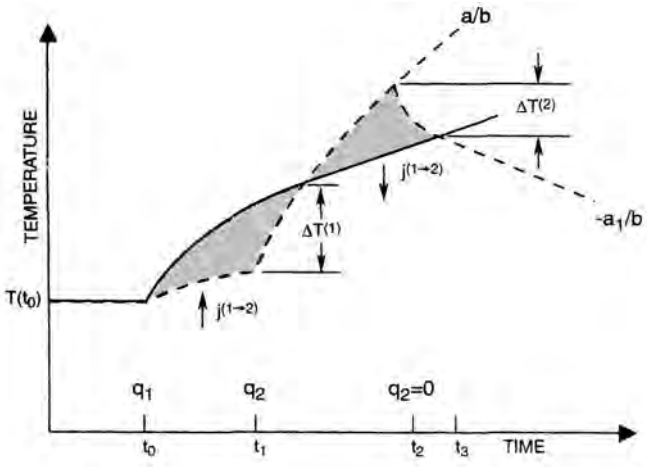

Fig. 1. Temperature tracking to maintain an adiabatic wall. The values $T^{(1)}$ and $T^{(2)}$ are the temperature differences that trigger (on/off) the heat source in the bath.

the difference T reaches an a priori specified value, and the heat source q_2 in the bath is activated. If $q_2 > q_1$, then the temperature $T^{(2)}$ rises faster than $T^{(1)}$, in time—at t_2—reducing T to zero. To maintain the adiabatic wall, it is necessary to transfer the same amount of heat in both directions $[H^{(1\to2)} = H^{(2\to1)}]$. These periods are determined by numerically solving Eqs. (5) and (6).

Some rough and yet useful information concerning the form of the $T(t)$ function can be derived if θ is considered a constant. Rewriting Eq. (6) in an equivalent form, yields

$$\frac{d\Delta T}{a - b\Delta T} = dt \ , \tag{7}$$

where

$$a = (q_1 - q_2) + (\kappa_{2e} - \kappa_{1e})\theta$$

$$b = (\kappa_{12} + \kappa^* + \kappa_{2e}).$$

Upon integration, we get for $q_2 = 0$ and for $q_2 > q_1 + (\kappa_{2e} - \kappa_{1e})\theta$, respectively,

$$\Delta T = \frac{a}{b} + \left[\frac{a}{b} - \Delta T(0)\right] e^{-b(t-t(0))} \ . \tag{8}$$

and

$$\Delta T = -\frac{a}{b} + \left[\frac{a}{b} - \Delta T(0)\right] e^{-b(t-t(0))} \ . \tag{9}$$

Evidently, the system relaxes with the characteristic time constant, $\tau = 1/(\kappa_{12} + \kappa^* + \kappa_{2e})$, i.e., the relaxation time is governed by the C_1/C_2 ratio, the cell temperature, materials of construction, and the system's contact with the environment. For any selected $\Delta T^{(1)}$, there is a corresponding $\Delta T^{(2)}$ that ensures $H^{(1\to2)} = H^{(2\to1)}$. For practical purposes, this condition is satisfied by the requirement that $T(t)$ oscillates about zero.

III.C. Temperature Tracking

In any implementation of calorimetric measurements based on Eqs. (3) and (4), a means of controlling the heat input to the bath surrounding the reaction cell must be provided to maintain the temperature difference, $T = 0$, or at least, so that it averages to zero over an experimental run. Because of the large amount of temperature data required for an experiment, digital acquisition of the data is necessary. Consequently, digital control of the experiment is a natural choice. In a digital system, the relevant temperature measurements are made in sequence in a repetitive cycle, with some dead time for writing data to a disk, and the analog values are truncated to the precision of the analog to converter being used. These two procedures should not be considered independently because often the truncation error exceeds the allowable temperature error, and appropriate averaging is required. For averaging to improve a measurement, the analog signal must be dithered, either deliberately or by noise over a range corresponding to the least significant bit of the digitized signal. For example, with a 12 bit analog to digital converter having an input of 20 to + 20 mV, the least significant bit corresponds to a 10 μ input signal change or a change of 0.25 C for a T type thermocouple where the sensitivity is about millicoulomb per microvolt. Typically, there might be present 10 μV root mean square noise referred to the input, so that averaging 100 samples would be expected to reduce the error to ~0.03 C without having to dither the input. Averaging 100 samples has other implications, however, since the averaging takes place over a range of temperature difference T that depends on both the cooling rate of the cell and the heating rate of the bath as given in Eqs. (5) and (6). On average, a temperature offset occurs that depends on whether T takes longer to recover from a positive value than from a negative value, which would increase the likelihood that the bath heater will be incorrectly turned on rather than incorrectly turned off.

IV. THERMAL EFFECTS DURING CODEPOSITION

To reiterate, the codeposition process is a process where the electroreduction of Pd^{2+} ions occurs simultaneously with the evolution of deuterium. The principal advantage of this technique is the elimination of the prolonged charging time required for, and a better reproducibility of, the initiation of the Fleischmann Pons effect. Three cases of thermal activities seen on Pd electrodes prepared by codeposition will be presented: Sec. IV.A, excess of enthalpy production during and shortly after completion of codeposition; Sec. IV.B, excess enthalpy production monitored over a period of several days; and

Sec. IV.C, the development of thermal instabilities recorded by an infrared scanning.

IV.A. Short-Duration Experiment

An example of thermal behavior during the codeposition process is illustrated in Fig. 2 where excess enthalpy $0.239C^{(1)}\Delta T^{(1)} - \int I(E_c - E_{th})\,dt$ (y axis) is plotted against the energy supplied to the cell from an external source, $\int IE_c\,dt$ (x axis). During data collection, the cell was isolated from the environment by an adiabatic wall in the manner described earlier. The electrolytic cell was a thin walled glass vessel with the cathode/anode assembly located at the bottom. (Details of the electrode assembly are given in Ref. 4, Fig. 1). The electrode charging was under potentiostatic control and relevant data, e.g., cell voltage, cell current, electrolyte temperature, and the maintenance of the adiabatic enclosure were recorded, and the excess enthalpy production was plotted. A program taking into account corrections indicated in Sees. II.A through II.E was devised and employed.

Inspection of Fig. 2 reveals two time periods—the first showing a negative while the second a positive gain in enthalpy production. The negative gain indicates that endothermic processes occur shortly after the commencement of codeposition. These reactions cannot be identified at this time except to suggest that they might indicate some form of entropic cooling or, perhaps, the formation of the gamma phase as indicated by Fleischmann et al.,[9] where by extrapolation of experimental data a reversal from exothermic to endothermic hydrogen absorption occurs at D/Pd equals —0.85, becoming substantial at D/Pd = 1.0 (for comparison see Ref. 9, Fig. 4). Such high concentrations are obtained in seconds during co deposition[2] and might form the gamma phase, thus explaining the rise in the electrode temperature observed on termination of the cell current flow (for comparison see Ref. 1, Fig. 3 insert).

In contrast to the burst like production of tritium[4] or emanation of soft X rays,[3] excess enthalpy generation proceeds at a steady rate with occasional bursts, see points A, B, C, and D in Fig. 2. The rate of excess enthalpy production is only slightly dependent on the electrolyte temperature, at least within the range 20 to 70 C, being higher at higher temperatures.

IV.B. Long-Term Experiments

The long term experiments were carried out in three Fleischmann Pons type cells. These Dewar type electrochemical cells are silvered in their top portions so that the heat transfer is confined almost exclusively to radiation across the lower part, which is not silvered.[6,7] In each cell, the copper rod 2.5 cm in length and 0.4 cm in diameter served as the cathode. A platinum wire spirally wound to ensure uniform current density was employed. Initial composition of the electrolyte was as follows:

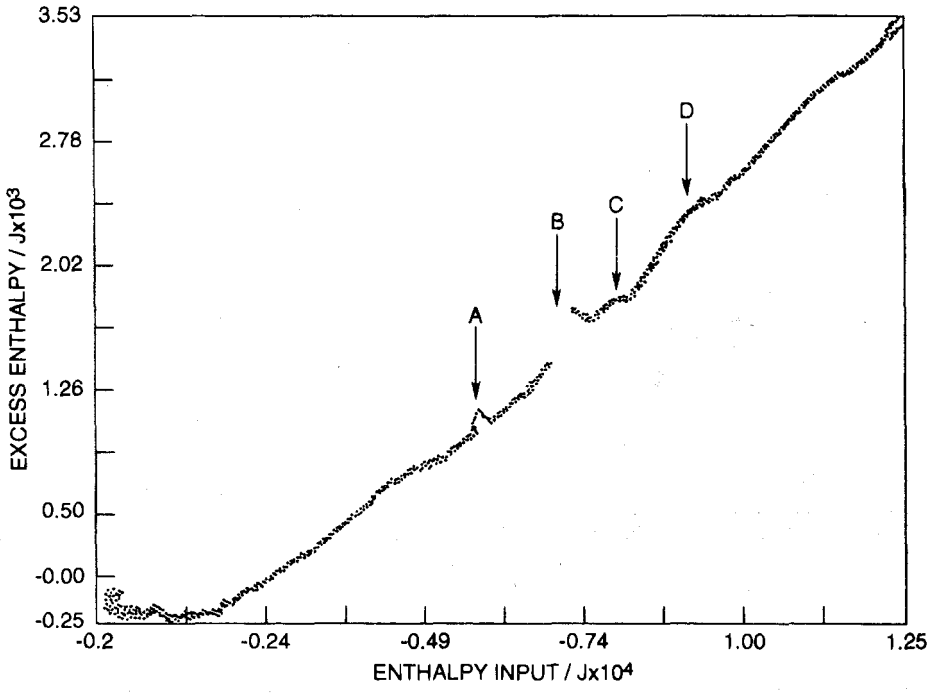

Fig. 2. Excess enthalpy generated in the course of Pd + D codeposition and shortly thereafter. Electrolyte composition: 0.03 *M* PdCl2 + 0.3 *M* LiCl in D_2O. Points A, B, C, and D indicate accelerated excess enthalpy production.

0.025 *M* $PdCl_2$ + 0.15 *M* ND_4Cl + 0.15 *M* ND_4OD in D_2O (Isotec, Inc., 99.9 at.% D).

Three cells, each containing 91 cm^3 of electrolyte, were operating simultaneously under galvanostatic control. The applied current profile and excess power generated are shown in Fig. 3. It is noted that the codeposition process was completed after 1 day of operation with a marginal excess power commencing immediately and its substantial increase upon an increase in the cell current (see point A, Fig. 3).

While examining Fig. 3, several additional points can be made:

1. Data points in Fig. 3 refer to the excess power generated at the time of measurements.

2. Production of the excess power depends on the cell current; in particular, it increases with the increase in the cell current.

3. The most striking feature is the excellent reproducibility.

4. The excess power output exceeds by far the average reported for solid Pd rods.

IV.C. Development of Thermal Instabilities

Thermal events occurring during the electrochemical compression of the Pd + D system were and are discussed in terms of excess enthalpy produced over a period of time, often several days. Thus, they represent an average value and provide no information on the distribution and nature of heat sources. However, if the surface of a polarized Pd electrode is viewed with an infrared camera, it reveals the presence of randomly distributed, in both time and space, heat sources of short duration. Figures 4a and 4b show snapshots of hot spots (white dots) and temperature gradients associated with their presence, i.e., Fig. 4a is the view perpendicular to the electrode surface, and Fig. 4b presents the three dimensional temperature distribution. Restating, Fig. 4a provides information on the location of hot spots and Fig. 4b on the temperature gradients, the latter suggesting that the hot spots are located just beneath the contact surface.

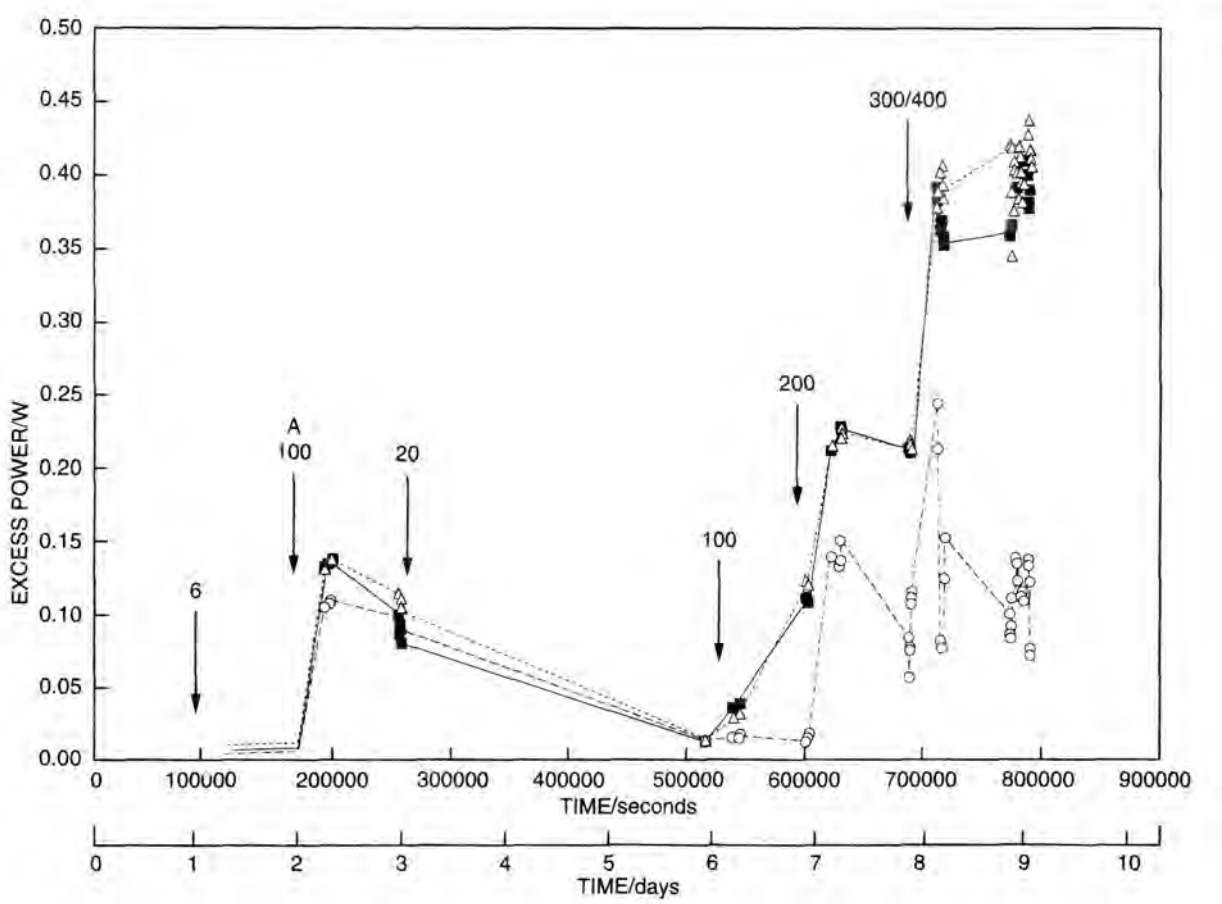

Fig. 3. Excess power generated during prolonged D_2O electrolysis on electrodes prepared by codeposition. Electrolyte composition: 0.025 *M* $PdCl_2$ + 0.15 *M* ND_4Cl + ND_4OD in D_2O. Note that for the final two days, the cell current was 400 mA in cells indicated by open circles and triangles and 300 mA in cells indicated by solid squares.

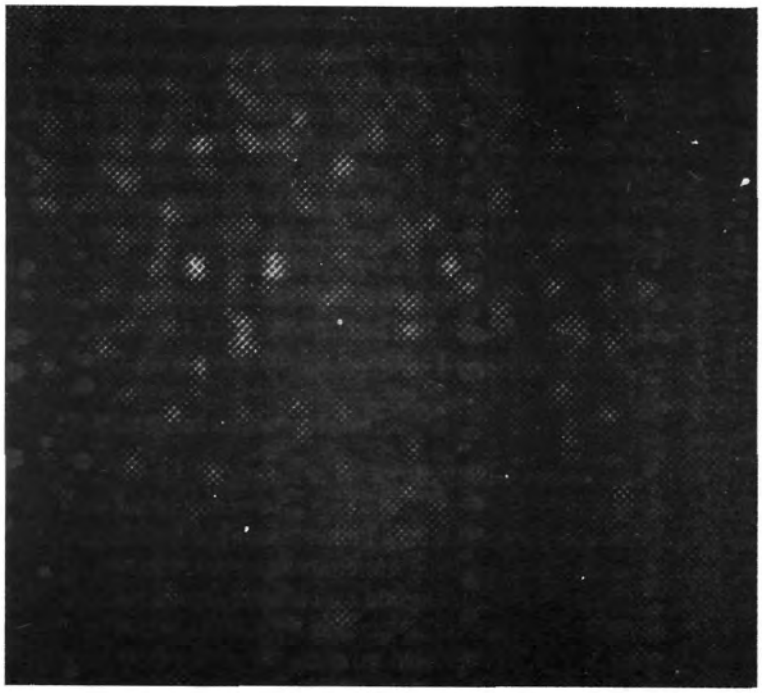

(a)

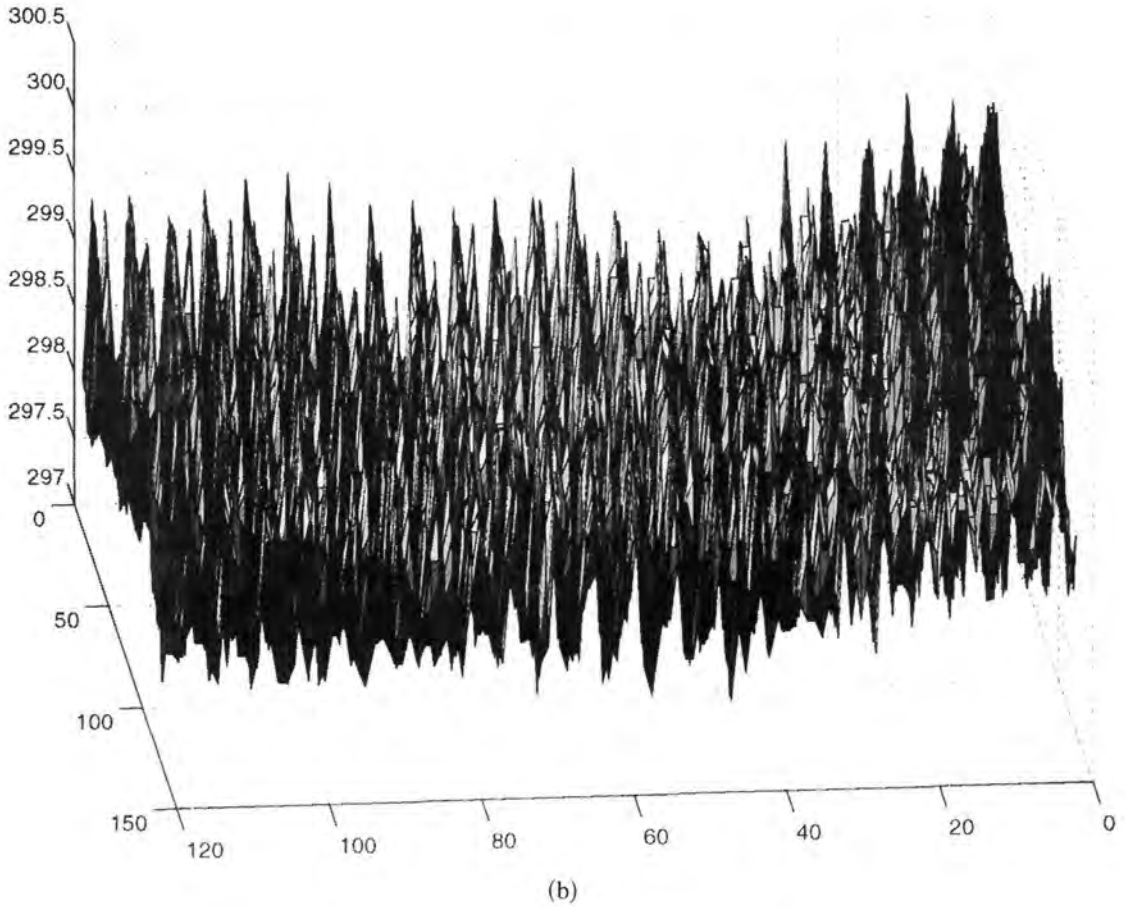

(b)

Fig. 4. Infrared photographs of the electrode surface: (a) view perpendicular to the surface showing distribution of hot spots and (b) view parallel to the electrode surface showing temperature gradients. The photographs were taken by an infrared camera manufactured by Lynx Real-Time Systems, Los Gatos, California 95030.

The development of instabilities and/or oscillatory behavior is expected in nonlinear systems, of which an operating electrochemical cell is a prime example.[8] The development of such instabilities is consistent with ideas advanced recently by Fleischmann et al.[9] They postulated that production of excess enthalpy can be expressed in terms of a number of time and space dependent variables and their differentials, $Q = f[E_c, dE_c, \eta, d\eta; \theta, d\theta, X, dX, \gamma, d\gamma]$. These variables are: cell voltage, cathodic overpotential (in particular its Volta component), surface coverage, deuterium content (expressed as D/Pd atomic ratio), and the formation of the gamma phase. Some of these variables can be controlled by an experimenter; others cannot (so called "hidden variables"). Because these variables are interconnected, they can lead to the development of instabilities of the type illustrated in Figs. 4a and 4b.

V. CLOSING COMMENTS

Experimental evidence concerning thermal activities generated by the electrochemical compression of deuterium within the Pd lattice on electrodes prepared by codeposition has led us to the following conclusions:

1. The major impediment in accepting the excess enthalpy production by electrochemical compression of deuterium generated by electrolysis of heavy water on Pd electrodes is removed, i.e., the excess enthalpy production is reproducible.

2. The excess enthalpy generated in cells where the cathode is prepared by codeposition is, on the average, higher than that produced in cells employing solid Pd rods.

3. The heat sources are highly localized, and judging from the steepness of temperature gradients, they are located in close proximity to the electrode solution contact surface.

ACKNOWLEDGMENTS

The authors acknowledge the interest and support received from F. Gordon, Spawar Systems Center, San Diego. MHM thanks N. Asami for the hospitality during his stay as a NEDO Guest Researcher at the NHE laboratory in Sapporo, Japan, where part of this work was performed.

REFERENCES

1. S. SZPAK, P. A. MOSIER BOSS, and J. J. SMITH, "On the Behavior of Pd Deposited in the Presence of Evolving Deuterium," *J. Electroanal. Chem.,* **302,** 255 (1991).

2. S. SZPAK, P. A. MOSIER BOSS, and J. J. SMITH, "Deuterium Uptake During Pd D Codeposition," *J. Electroanal. Chem.,* **379,** 121 (1994).

3. S. SZPAK and P. A. MOSIER BOSS, "On the Behavior of the Cathodically Polarized Pd/D System: Search for Emanating Radiation," *Phys. Lett. A,* **210,** 382 (1996).

4. S. SZPAK, P. A. MOSIER BOSS, R. D. BOSS, and J. J. SMITH, "On the Behavior of the Pd/D System: Evidence for Tritium Production," *Fusion Technol.,* **33,** 38 (1998).

5. S. SZPAK and P. A. MOSIER BOSS, "On the Behavior of the Cathodically Polarized Pd/D System: A Response to Vigier's Comments," *Phys. Lett. A,* **221,** 141 (1996).

6. M. FLEISCHMANN, S. PONS, M. W. ANDERSON, L. J. LI, and M. HAWKINS, "Calorimetry of Palladium Deuterium Heavy Water System," *J. Electroanal. Chem.,* **287,** 293 (1990)

7. M. H. MILES, B. F. BUSH, and D. E. STILWELL, "Calorimetric Principles and Problems in Measurements of Excess Power during Pd/D_2O Electrolysis," *J. Phys. Chem.,* **98,** 1948 (1994).

8. . . . KOPER, "Theory of Electrochemical Instabilities," *Electrochim. Acta,* **37,** 1771 (1992).

9. M. FLEISCHMANN, S. PONS, M. LeROUX, and J. ROULLETTE, "Calorimetry of the Pd D_2O System: The Search for Simplicity and Accuracy," *Fusion Technol,* 26, 323 (1994).

Stanislaw Szpak (PhD, University of Pennsylvania, 1961) is a scientist (emeritus) at the Space and Naval Warfare Systems Center San Diego (SSC SD), San Diego, California. His research interests include electrochemistry and energy conversion.

Pamela A. Mosier Boss (PhD, Michigan State University, 1985) is a scientist at SSC SD. Her research interests include sensor development, Raman spectroscopy, and electrochemistry.

Melvin H. Miles (PhD, University of Utah, 1966) is a research chemist at the Naval Air Warfare Center Weapons Division, China Lake, California. His research interests include electrochemistry and the development of energy conversion devices.

Mosier-Boss, P.A. and S. Szpak, *The Pd/(n)H system: transport processes and development of thermal instabilities.* Nuovo Cimento Soc. Ital. Fis. A, 1999. **112**: p. 577.

The Pd/^{n}H system: Transport processes and development of thermal instabilities

P. A. Mosier-Boss and S. Szpak

Spawar Systems Center San Diego-San Diego, CA 92152-5001, USA

(ricevuto il 2 Dicembre 1998; revisionato il 24 Maggio 1999; approvato il 15 Giugno 1999)

Summary. — Surface temperature distribution associated with excess enthalpy production during the codeposition process is presented. The interpretation is sought *via* the multilayer concept of the electrode/electrolyte interphase. The effect of gas evolution on activities within the interphase is considered.

PACS 28.90 - Other topics in nuclear engineering and nuclear power studies.

Recent years have witnessed renewed interest in the hydrogen economy, with emphasis on the metal/hydrogen system and its application to energy conversion efforts. Two industrially important aspects are emphasized, *viz.* the amount of hydrogen stored and the rate at which it can be transferred (absorbed/desorbed) because they are crucial factors in the design and construction of electrochemical energy conversion devices. The March 1989 announcement of excess enthalpy generation [1], the Fleischmann-Pons effect, provided an added incentive to examine in greater detail the behavior of the Pd/D system at very high electrode loadings and at high cell currents.

In an earlier modeling of transport processes, we adopted a multilayer concept of the interphase, formulated transport equations based on the conservation of charge and matter and analyzed events occurring in proximity to the electrode/solution contact surface as a function of the cell current for a set of rate constants characterizing the hydrogen evolution reaction [2]. This model is employed here in the analysis of thermal events associated with the Pd + D codeposition.

1. - Thermal events during Pd + D codeposition

Thermal events occurring during the electrochemical compression of the Pd/D system are usually discussed in terms of excess enthalpy produced over a period of time, often several days. Thus, they represent an average value and provide no information on the distribution of heat sources. However, when the surface of the electrode producing excess enthalpy is viewed with an infra-red camera, the presence of randomly distributed (in time and space) heat sources of short duration is revealed which subsequently merge to form larger oscillating islands. An example of hot spots recorded in the early stages of

codeposition is illustrated in figs, la and b. In this example, a Ni screen, placed close to the very thin cell wall (Mylar film), served as the negative electrode, upon which a deuterium-saturated Pd film was formed by the codeposition process [3,4]. Such electrodes exhibit a "carpet-like" appearance, *i.e.*, the structure that assures locally a non-uniform distribution of current density and/or overpotentials as well as very rapid absorption of deuterium. Simultaneous evolution of gas bubbles introduces an added component, *viz.* a source of random distribution of localized gradients (electrical, mechanical and chemical).

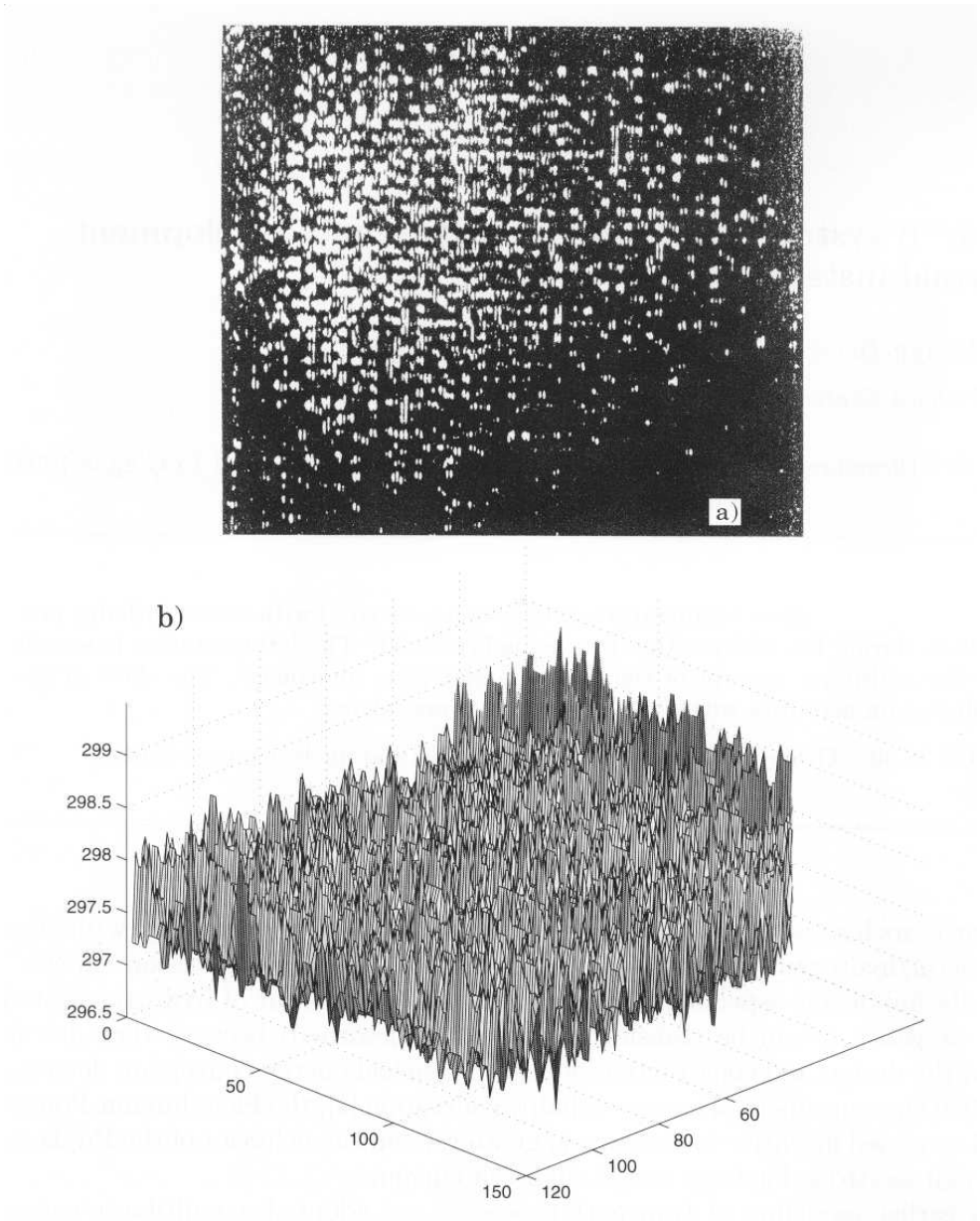

Fig. 1. - Infra-red photographs of the electrode surface, a) View perpendicular to the electrode surface showing distribution of hot spots, b) View parallel to the electrode surface showing temperature gradients. Photographs taken by infra-red camera manufactured by Lynx Real-Time Systems, Los Gatos, CA 95030.

Qualitatively, judging from the steep temperature gradients, fig. 1b, heat sources are of high intensity and located very close to the contact surface. Evidently, the subsurface region of the active Pd/D system consists of domains of high deuterium concentration (activity). Once formed; these domains are unstable. During current flow they are the source of excess enthalpy generation—in the absence of current flow they generate an outflow of deuterium.

2. — Development of thermal instabilities

It is known that processes which are stable in contacting bulk phases may become unstable in the interphase region and *vice versa*. The development of instabilities and/or oscillatory behavior is expected in highly nonlinear systems, of which an operating electrochemical cell is a prime example [5,6]. The development of such instabilities was discussed by Fleischmann *et al.* [7,8]. They postulated that production of enthalpy in an operating Pd/D_2O cell can be expressed as a function of a set of time/space-dependent variables and their differentials,

(1) $$Q = \Phi(E, \mathrm{d}E, \eta, \mathrm{d}\eta, \theta, X, \mathrm{d}X, \gamma, \mathrm{d}\gamma).$$

These variables are: cell voltage, E, cathodic overpotential, η (in particular its Volta component) on the solution side of the interphase, surface coverage θ, deuterium content, X (expressed as the D/Pd atomic ratio), and the formation of the γ-phase. They noted that this functional dependence may lead to a number of features, among them the development of local instabilities. Indeed, the development of such instabilities, resulting in localized hot spots, was reported by us previously [9].

3. — Discussion

Some of the variables in eq. (1) can be controlled by the experimenter, others cannot. Because these variables are interconnected, they can lead to the development of instabilities. To get a clearer picture of the events leading to the development of instabilities, we examine the following: i) the structure of the interphase, ii) the nature of adsorbed species, iii) the development of an active interphase and iv) interphase relaxation.

3.1. *Structure of electrode/electrolyte interphase.* — The electrode/electrolyte interphase is an assembly of non-autonomous layers whose structure is determined by operating processes [10]. The interface is defined as the contact surface (surface of discontinuity). This view is adopted because otherwise the interphase would have to be considered a single element, *i.e.*, the heterogeneous nature of the real interphase would have to be disregarded.

Transport of electrochemically generated hydrogen across the interphase is due to the coupling of interfacial processes: $(b) \rightarrow (r_1) \rightarrow (ad) \rightarrow (\lambda_2)$ and the transport of interstitials: $(\lambda_2) \rightarrow (m)$ in the electrode interior [3]. The processes of interest during charging are: reduction of H^+, D^+ ions/H_2O, D_2O molecules occurring within the charge transfer layer, (r_1), reactions (i) and (ii):

(i) $$H^+_{(r1)} + e^-_{(r1)} \leftrightarrow H_{(ad)};\ j_1,$$

(ii) $H^{+}_{(r1)}+H_{(ad)}+e^{-}_{(r1)} \leftrightarrow H_{2,(g)}$; j_2.

The adsorbed hydrogen restructures the electrode surface and either leaves the electrode surface by forming gas bubbles, reaction (iii), or enters the subsurface region. (λ_2), reaction iv):

(iii) $H_{(ad)}+H_{(ad)} \leftrightarrow H_{2,(g)}$; j_3,

(iv) $H_{(ad)} \leftrightarrow H_{(ab)}$; j_4.

Reaction paths (i)-(iv) state that hydrogen is deposited onto the electrode surface by the first process, the Volmer path, j_1, and removed by the Heyrovsky-Horiuti, j_2, the Tafel path, j_3, and by absorption, j_4. The absorbed hydrogen is present in the form of protons which at high concentrations may form clusters [4], reactions (v) and (vi), respectively.

(v) $H_{(ab)} \leftrightarrow H^{+}_{(r2)}+ e^{-}_{(r2)}$,

(vi) $H_{(\lambda 2)}+H^{+}_{(\lambda 2)} \leftrightarrow H^{+}_{2,(ab)}$.

The ionization, (v), and cluster formation, (vi), are considered chemical reactions. However, processes leading to desorption, *i.e.*, the reduction of protons in the reaction layer, (r_2), reactions (vii) and (viii), respectively, are viewed as the solid state analogs of the Volmer and Heyrovsky-Horiuti paths

(vii) $H^{+}_{(r2)}+e^{-}_{(r2)} \leftrightarrow H_{(ab)}$,

(viii) $H^{+}_{(r2)}+H_{(\lambda 2)}+e^{-}_{(r2)} \leftrightarrow 2H_{(ab)}$.

Consequently, while rates of i) and ii) are governed by the Galvani potential, those in the solid-state, (vii) and (viii), depend on the surface potentials [7,8] followed by fast exchange, reaction (iv). We note that in this context an electron is considered either a reactant or product and expressions $e^{-}_{(\lambda 2)} \rightarrow e^{-}_{(r1)}$; $e^{-}_{(\lambda 2)} \rightarrow e^{-}_{(r2)}$, represent the same, but energetically different, entities. (Note: Symbols H and D are used interchangeably.)

Transport paths and the resulting structure of the interphase are illustrated in fig. 2—upper for absorption, lower for desorption. To reiterate, the cell current, I, is split into two streams, j_1 and j_2 (*cf.* (i) and (ii)) yielding H in the adsorbed state that enters the subsurface layer (λ_2) at the rate j_4. The absorbed hydrogen undergoes ionization to H^+, (v), followed by diffusion. On desorption, the H^+ species are transported to the (λ_2) layer where they acquire electrons through a chemical recombination reaction, j_{ch} and an electrochemical step, j_{el}. Subsequently, the neutral species are transferred to the (λ_1) layer at the rate j_{-4} followed by oxidation, j_{-1}; and reduction and removal, j_{-2}, from the electrode surface. This chain of events is not affected by the amount of absorbed hydrogen. However, kinetic parameters reflecting their mechanistic aspects may substantially vary with the hydrogen content.

3.2. *Nature of adsorbed species.* - The adsorbed hydrogen, deposited on polarized Pd surfaces, exists in two forms: the underpotentially adsorbed hydrogen, H_{up}, with $\Delta G < 0$ and the overpotentially adsorbed, H_{op} with $\Delta G > 0$. The H_{up} forms a multicoordinated covalent bond with the Pd and occupies a 3-fold site while the H_{op} is singly coordinated with a much weaker bond [11]. Consequently, binding of an atom to a surface involves two subsystems, electronic and ionic, where the contribution of the electronic subsystem to the binding is given by the work function difference.

One of the, as yet, unresolved problems concerns the species that are transported across the contact surface. Jerkiewicz *et al.* [12] suggest that H_{op} undergoes interfacial transfer. A similar view was expressed by Flitt and Bockris [13], who stated that the low bond energy sites favor absorption. This view is also shared by Chevillot *et al.* [14]. In their view, the adsorption/absorption can be regarded as, to quote, "the proton passes from one screened system to another, *i.e.*, from the electron screening in the metal to ionic screening of the solvated ion in solution". The strongly adsorbed hydrogen is bound by a quasi-covalence while the weakly adsorbed H displays a metallic character which favors the equilibrium with the configuration of a proton in solution.

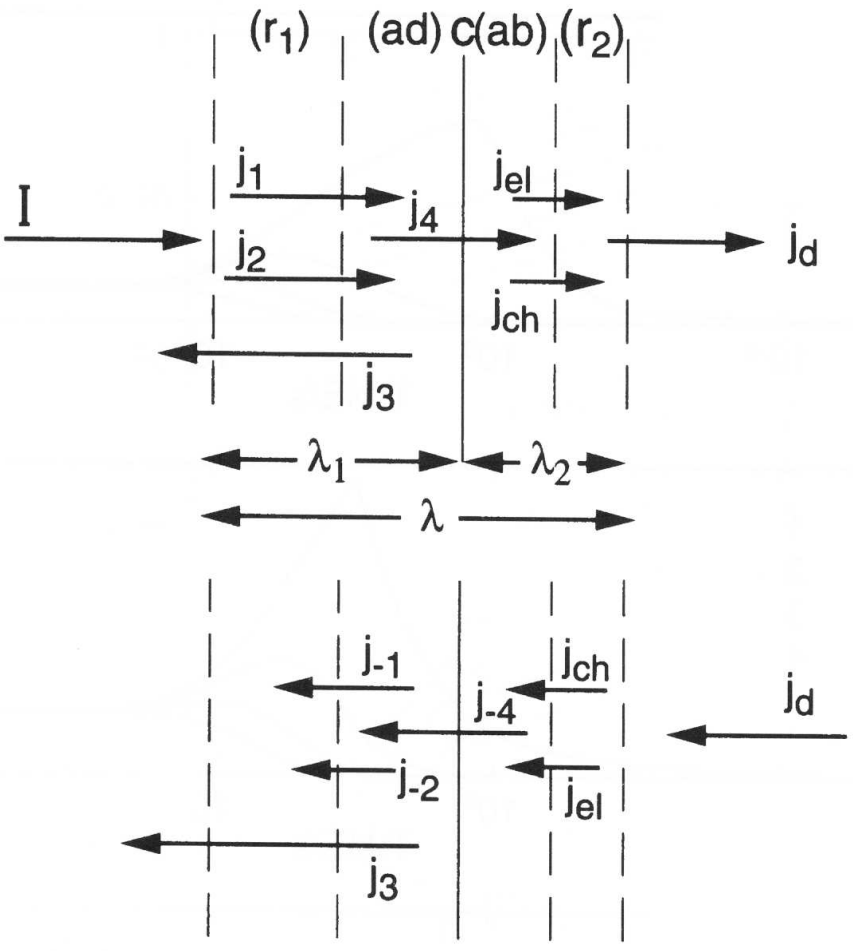

Fig. 2. - Concept of the Pd/D_2O interphase: (ad) adsorption layer, (c) contact surface, (ab) absorption layer, r_1 and r_2 reaction layers, *b* and *m* homogeneous solution and metal phases, respectively. *I* total current, j_1 Volmer path, j_2 Heyrovsky-Horiuti path, j_3 Tafel path (equivalent), j_4 and j_{-4} are adsorbed-absorbed exchange equivalent currents. j_{ch} and j_{el} are the H^+ fluxes generated within the subsurface layer, (λ_2), by dissociation and oxidation, respectively. (λ) is an interphase region consisting of a set of non-autonomous layers (λ_1) = (ad)+(r_1), (λ_2) = (ab)+(r_2).

Recent work of Jerkiewicz *et al.* [12] discussed the structure of the interphase in terms of participating processes. Using our notations, they assumed that the step $H_{(ad)} \leftrightarrow H_{(ab)}$ is fast and that the $H_{(ab)}$ species may be partially ionized. They argued that the surface coverage determines the operating driving force for diffusion and that, because of the fast phase transfer step, the diffusional flux depends on overpotential through $H_{(ad)} \leftrightarrow H_{(ab)}$ being in quasi-equilibrium. Jerkiewicz and Zolfaghari [11] added another step in which the $H^+ \cdot 4H_2O$ species "encounters the region close to the electrode surface where H^+ discharge takes place with the formation of absorbed H". In our terminology, this region is defined as the reaction layer, r_1.

3.3. *Development of an active interphase*. - The formation, growth and detachment of electrogenerated hydrogen gas bubbles have a profound effect on the overall processes in both the solution and the metal side of the interphase. The evolution of gas bubbles on the electrode surface precludes uniform distribution of the cd and, therefore, overpotential. This, in turn, results in the removal of an external force acting upon the interphase of the hydrogen-loaded electrode and promotes formation of local gradients, *i.e.*, the formation of conditions believed to initiate the Fleischmann-Pons effect. How deep into the electrode interior these gradients extend depends on the residence time of the gas bubbles and the relaxation time of the processes under consideration.

To illustrate the effect of gas evolution on the redistribution of hydrogen by the exchange between absorbed and adsorbed atoms, one sets the cell current to zero and observes how the system relaxes at, and in the vicinity of, the surface. Using reasonable values for the rate constants of the participating processes [2], the distribution of absorbed deuterium in the first four layers immediately after cell current termination is illustrated in figs. 3a, b and c for diffusion coefficients $D = 10^{-6}$, 10^{-8} and $10^{-10} cm^2 s^{-1}$ and a charging current of $40 mA cm^{-2}$ for t = 1, 10 and 1000 seconds. Inspection of the $\zeta_i(t)$ (i = 1,2,3 and 4) curves (fraction of absorbed deuterium) shows that the diffusion coefficient controls the rate and efficiency of absorption, *viz.*, at high diffusion coefficients, *e.g.*, $D < 10^{-8}$, surface processes determine the rate of absorption and the fraction of desorbed hydrogen.

Because of the random distribution of gas bubbles on the electrode surface and the in and out transport of deuterium, situations may arise causing the concentration of absorbed deuterium to be higher in the second layer than in the first layer. The redistribution of deuterium following current termination, fig. 4. indicates the formation of concentration gradients in close proximity to the contact surface. Evidently, the gas evolution contributes to the formation of a zone with time- and space-dependent concentration of deuterium which, in turn, must be considered in the analysis of transport in the bulk material.

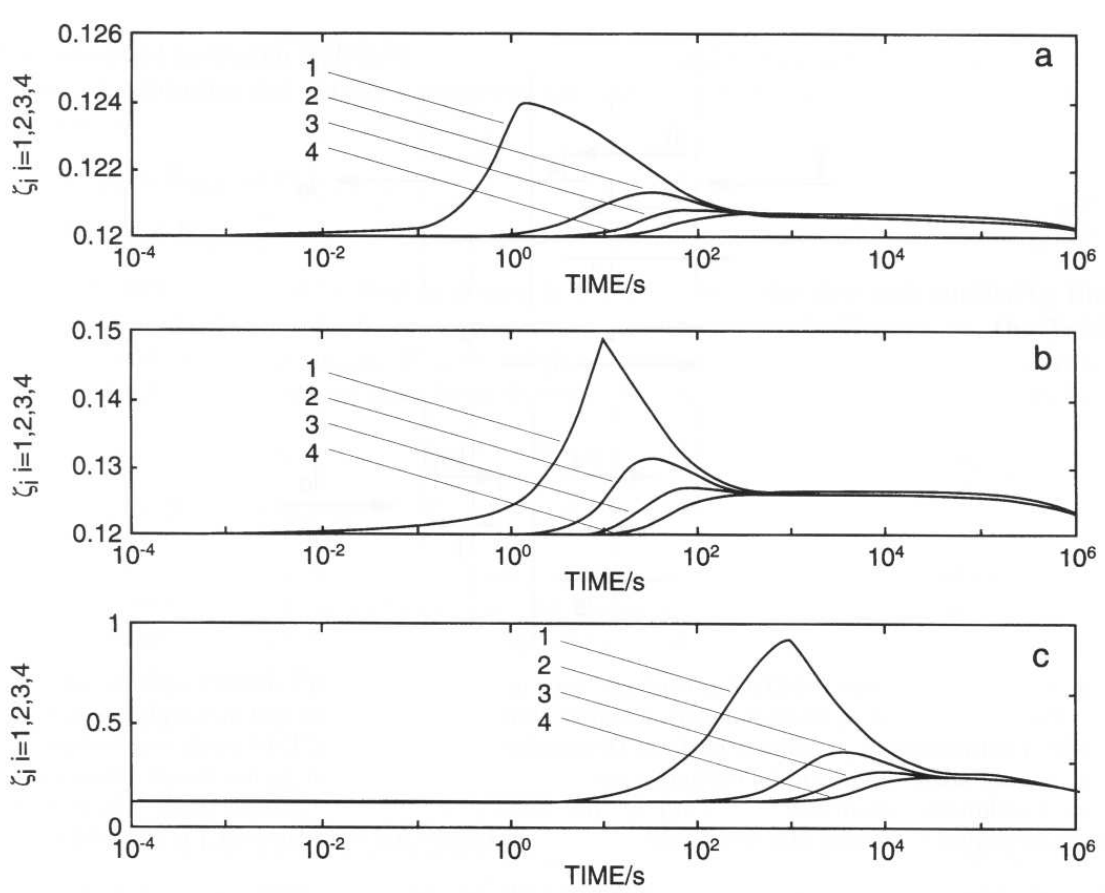

Fig. 3. - Time-dependent distribution of absorbed hydrogen during loading at I = 40 mAcm^{-2} and unloading for: a) $D = 10^{-6}$cm^{2}s^{-1}; b) 10^{-8}cm^{2}s^{-1} and $D = 10^{-10}$ cm^{2}s^{-1}. Cell current terminated at 1, 10 and 1000 seconds, respectively. Rate constants: $k_1 = 10^3$ cm^{3}mol^{-1}, $k_2 = 10^2$ cm^{3}mol^{-1}, $k_3 = 10^3$ cm^{2}mol^{-1}, $k_4 = 2 \times 10^5$ cm^{3}mol^{-1}s^{-1} and $k_d = 2 \times 10^{-2}$ cm^{4}mol^{-1}s^{-1}.

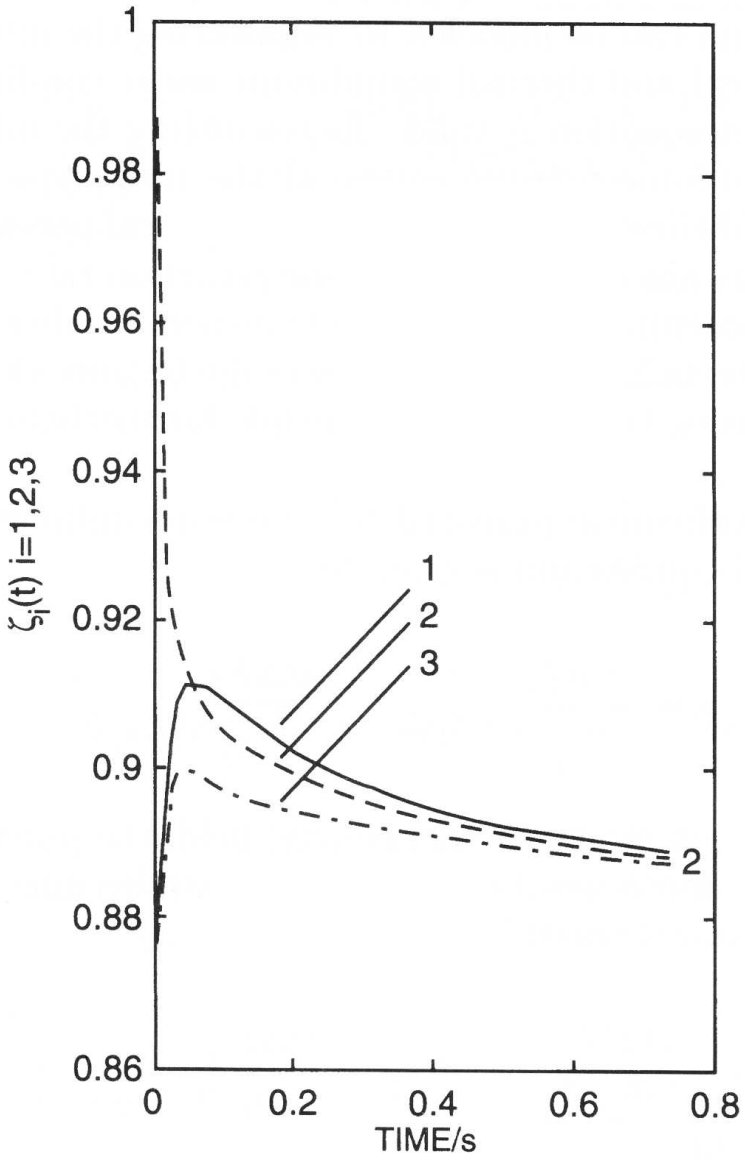

Fig. 4. - Time-dependent distribution of absorbed hydrogen following cell current termination. Rate constants as in fig. 3. Assumed highest concentration in the second layer.

3.4. *Interphase relaxation.* - The electrode/electrolyte interphase is a non-electroneutral entity. The application of an external field further magnifies the non-electroneutral character. In particular, any change in the applied external field will greatly affect events occurring in the interphase region. It is within this environment that the effect of gas evolution on the interphase events should be discussed. The consequence of gas evolution is a localized change in the electrode potential which, in turn, changes the magnitude of the operating driving forces, *i.e.*, chemical/electrochemical potentials.

The use of the chemical potential as the driving force for the transport of species between two phases is subject to the application of the Gibbs-Duhem equation, *i.e.*, the requirenment that the temperature and concentration can be defined, or that local equilibrium can be assumed, which means that "local extensive property is the same

function of the local macroscopic variables as at equilibrium" [15]. But the use of the electrochemical potential as the driving force for, *e.g.*, transport across the interphase or other processes, puts the system in a non-equilibrium state. A non-equilibrium interphase in local equilibrium can be modeled by segmenting the interphase into individual layers, each in mechanical and thermal equilibrium under conditions of transport, *i.e.*, where the Gibbs-Duhem equation is valid. Reassembling the interphase and assuming local equilibria, the non-homogeneous nature of the interphase is restored. While in each layer the Gibbs-Duhem equation is valid, the chemical potentials of the *i*-th species in the neighboring layers are different. Transport/reaction rates are determined by the difference in chemical potentials or, in the "no transport condition", by the acting fictitious forces. Thus, the term Σn_i, $\mathrm{d}\mu_i = 0$ expresses the balance of thermodynamic forces, *i.e.*, it represents an analog to d'Alembert principle for mechanical system and not the Gibbs-Duhem equation.

The chemical/electrochemical potential in a system containing charged particles in mechanical and thermal equilibrium is given by

$$\mu = \frac{\partial \Delta G}{\partial n_i}\bigg|_{p,T,n_i \neq n_j} = \frac{\partial \Delta F}{\partial n_i}\bigg|_{V,T,n_j \neq n_i} . \tag{2}$$

When this system is placed in an external electric field, the potential energy of charged particles becomes a function of position, *i.e.*, the system becomes non-electroneutral. In this case, the electrochemical potential is given by

$$\mu = \frac{\partial \Delta G}{\partial n_i}\bigg|_{p,T,n_i \neq n_j,\psi} = \frac{\partial \Delta F}{\partial n_i}\bigg|_{V,T,n_j \cdot \psi \neq n_i} , \tag{3}$$

where ψ is the external potential arising from uniform distribution of charges on the contact surface. The electrochemical potential of any charged species present in a thin layer can be evaluated by taking the derivative of the Gibbs (Helmholtz) free energy while keeping the temperature, pressure (volume), mole number and the externally applied potential constant [16].

A change in the electrochemical potential affects the species present at the contact surface as well as charged species in the absorbed state in close proximity to the contact surface. To assess qualitatively the ensuing changes, it is convenient to consider the structure of the interphase and the processes that occur as it transits from one "stopped condition" to another, the relaxation of the interphase. The complex nature of the interphase arises not only from the processes (i)-(viii) but also from changing volume and/or pressure. Thus, we can visualize a relaxation spectrum which leads to the development of gradients. Furthermore, a rapid change in the chemical potential may affect the kinetics of transformation, *e.g.*, diffusional transport from that described by the usual parabolic equation to hyperbolic one [17].

4. — Concluding remarks

1) Unlike joule heating, excess enthalpy generation occurs in the form of localized events in close proximity to the contact surface.

2) The higher the electrolyte temperature, the more frequent the events. In the limit, these events overlap to produce oscillating islands.

3) Although gas evolution is not the primary reason for the initiation of the thermal events, it substantially modifies the structure of the interphase.

* * *

The authors wish to express their gratitude to Dr. F. Gordon, Spawar Systems Center San Diego, Code D30 for his interest, encouragement and support.

REFERENCES

[1] Fleischmann M., Pons S. and Hawkins M., *J. Electroanal. Chem.*, **261** (1989) 301.
[2] Szpak S., Gabriel C. J., Smith J. J. and Nowak R. J., *J. Electroanal. Chem.*, **309** (1991) 273.
[3] Szpak S., Mosier-Boss P. A., Gabriel C. J. and Smith J. J., *J. Electroanal. Chem.*, **365** (1994) 275.
[4] Szpak S., Mosier-Boss P. A., Scharber S. R. and Smith J. J., *J. Electroanal. Chem.*, **337** (1992) 147.
[5] Kopper M. T. M., *Electrochim. Acta*, **37** (1992) 1771.
[6] Kopper M. T. M. and Sluyters J. H., *Electrochim. Acta*, **38** (1993) 1535.
[7] Fleischmann M., Pons S., LeRous M. and Roulette J., *Trans. Fusion Technol.*, **26** (1994) 323.
[8] Pons S. and Fleischmann M., *J. Chim. Phys.*, **93** (1996) 711.
[9] Szpak S. and Mosier-Boss P. A., *Phys. Lett. A*, **221** (1996) 141.
[10] Van Rysselberghe P., *Some Aspects Of The Thermodynamic Structure Of Electrochemistry*, in *Modern Aspects Of Electrochemistry*, Vol. 4 (Plenum Press, New York) 1966.
[11] Jerkiewicz G. and Zolfaghari A., J. Electrochem. Soc., 143 (1996) 1240.
[12] Jerkiewicz G., Borodzinski J. J., Chrzanowski W. and Conway B. E., *J. Electrochem. Soc.*, **142** (1995) 3755.
[13] Flitt H. J. and Bockris J. O'M., *J. Hydrogen Energy*, **7** (1982) 411.
[14] Chevillot J.-P., Farcy J., Hinnen C. and Roussau A., *J. Electroanal. Chem.*, **64** (1975) 39.
[15] Defay R., Prigogine I. and Bellemans A., *Surface Tension and Adsorption* (Longmans, Green and Co, Ltd, London W1) 1951.
[16] Sorensen T. B. and Compan V., *Electrochim. Acta*, **42** (1997) 639.
[17] Sobolev S. L., *Technical Physics*, **43** (1998) 307.

Available online at www.sciencedirect.com
SCIENCE DIRECT®
Thermochimica Acta 410 (2004) 101–107
thermochimica acta
www.elsevier.com/locate/tca

Thermal behavior of polarized Pd/D electrodes prepared by co-deposition

S. Szpak [a], P.A. Mosier-Boss [a,*], M.H. Miles [b], M. Fleischmann [c]

[a] *SPAWAR Systems Center San Diego, Code 2636, 53560 Hull Street, San Diego, CA 92152-5001, USA*
[b] *Department of Chemistry, Bates College, Lewiston, ME 04240, USA*
[c] *Ente Nazionale Energie Alternative, Frascati, Italy*

Received 16 December 2002; received in revised form 24 June 2003; accepted 16 July 2003

Abstract

Thermal behavior of polarized Pd/D electrode, prepared by the co-deposition technique, serving as a cathode in the Dewar-type electrochemical cell/calorimeter is examined. It is shown that: (i) excess enthalpy is generated during and after the completion of the co-deposition process; (ii) rates of excess enthalpy generation are somewhat higher than when Pd wires or other forms of Pd electrodes are used; (iii) positive feedback and heat-after-death effects were observed; and (iv) rates of excess power generation were found to increase with an increase in both cell current and cell temperature, the latter being higher.

Keywords: Excess enthalpy generation; Positive feedback; Heat-after-death

1. Introduction

Calorimetry is the preferred method of analysis of the thermal behavior of electrochemical cells. It is noted that such studies provide the basis for the investigation of the thermal behavior of a wide range of reactions, especially irreversible processes, in particular, an excess enthalpy generation in the negatively polarized Pd/D electrodes, the Fleischmann–Pons (F–P) effect. In an attempt to confirm/reject the Fleischmann–Pons claims, a number of cells/calorimeters were used: isoperibolic, differential, flowing fluid and zero gradient of which isoperibolic calorimetry was introduced in three designs, viz. open cell with radiative heat transfer [1–5], open cell with conductive heat transfer and closed cell with conductive heat transfer.

The basis for calorimetric measurements is the conservation of mass and energy and thus it requires the knowledge of processes under consideration, the sequence of events, the construction of the apparatus as well as the experimental procedure employed. Consequently, the formulation of an accurate model of an experiment is essential in the study of electrochemical calorimetry, in general, and the F–P effect, in particular.

In examining the thermal behavior of the Pd/D system prepared by the co-deposition technique [6], we considered not only excess enthalpy generation but also other aspects such as positive feedback and heat-after-death. It is clear that calorimetry can provide more information than just whether or not excess enthalpy is generated.

2. Background information

The reported excess enthalpy production, the F–P effect, was challenged on various grounds. In order to answer some of them and show that they do not apply to the present work, we provided the relevant background information.

2.1. The Pd/D co-deposition technique

The Pd/D co-deposition is a process where palladium and deuterium are simultaneously deposited onto non-absorbing metallic substrates, e.g. Au and Cu, at sufficiently negative potentials from electrolytes containing palladium salts dissolved in heavy water. Once the solution composition is specified, the surface morphology and bulk structure can be

* Corresponding author. Fax: +1-619-767-4339.
E-mail address: bossp@spawar.navy.mil (P.A. Mosier-Boss).

0040-6031/$ – see front matter © 2003 Elsevier B.V. All rights reserved.
doi:10.1016/S0040-6031(03)00401-5

Nomenclature

C_p	heat capacitance ($J\,g^{-1}\,mol^{-1}\,K^{-1}$)
$E_c(t)$	cell voltage at time t (V)
E_{th}	thermoneutral potential at bath temperature (V)
F	Faraday constant ($C\,g^{-1}\,mol^{-1}$)
ΔH_{ev}	rate of evaporative cooling (W)
i	iteration number
I	cell current (A)
J	thermal flux (W)
k_R	effective heat transfer coefficient ($W\,K^{-4}$)
L	latent heat of evaporation ($J\,g^{-1}\,mol^{-1}$)
M	number of moles of D_2O at $t = 0$
p	vapor pressure at the cell temperature (Pa)
p^*	atmospheric pressure (Pa)
$Q_f(t)$	rate of excess enthalpy generation (W)
t	time (s)
ΔT	temperature difference between the cell and the water bath (K)
V	volume (m^3)

Greek letters

β	dimensionless term in Eq. (A.1)
γ	current efficiency toward a given reaction

controlled by the cell current, thus ensuring reproducibility since both the metallurgical and surface chemistry aspects, are repeatable.

Incidentally, the co-deposition technique is not the only method for charging the Pd lattice to high D/Pd atomic ratios. These high ratios can be obtained by charging from the gaseous phase at extremely high pressures. The advantages/disadvantages of the electrochemically and pressure driven charging has been discussed, among others, by Conway and Jerkiewicz [7].

2.2. Structure of, and the processes within, the electrolyte/electrode interphase

The complex structure of the Pd/D_2O interphase and the operating forces acting upon it during loading/unloading can be best visualized by considering the sequence of events taking place. Briefly, the relevant points are: (i) transport and reduction of D^+ ions; (ii) deuterium is deposited onto the electrode surface by the Volmer path, and removed by the Heyrovsky–Horiuti and Tafel paths, and by absorption; and (iii) the absorbed deuterium undergoes ionization followed by transport (diffusion) into the bulk metal.

The layer separating the electrolyte and the metal bulk phases contains particles that interact with particles in neighboring phases. If the number of interacting particles is large comparing to the total number of particles, then this layer is defined as non-autonomous. Hence, the electrode/electrolyte interphase can be viewed as an assembly of non-autonomous layers whose structure is determined by operating processes [8].

2.3. The $D_2 + O_2$ recombination reaction

Except for Joule heating, the exothermic absorption of deuterium and the F–P effect, no other heat sources are activated during the co-deposition process. The frequently cited $D_2 + O_2$ recombination reaction, as being responsible for excess enthalpy generation, is not supported by experiment (recombination of evolving gases yielded volumes that were better than 1.0% of those calculated assuming 100.0% Faradaic efficiency [9], or theoretical considerations [10]). And yet the notion that recombination is responsible for the excess enthalpy generation persists. For example, Shanahan [11] observed that the short-lived hot spots [12,13] support the recombination theory. In his view, to quote: "The infrared photography of Szpak et al. is supportive evidence of this, if one considers the oxidation in subsurface bubbles to be rapid, which should be true of $D_2 + O_2$ flames". Such interpretation is, indeed, difficult to understand and therefore accept. As pointed out by Fleischmann and Pons [14], such "hot spots" would have an intensity of ca. 6 nW—hence, impossible to detect by IR camera.

2.4. The D^+ in the Pd lattice

While the processes in the electrolyte phase up to and including adsorption are well known, those occurring on and after crossing the contact surface remain unclear, especially at high concentrations of absorbed deuterium. With this in mind, Fleischmann and co-workers [15] posed a number of questions among them: (i) what is the nature of species at high X ($X = [D]/[Pd]$); (ii) what is the dynamics of D while in the Pd lattice; and (iii) what is the structure of the system under conditions of high X? These questions were reformulated and partially answered by Preparata [16] using quantum electrodynamics coherence in condensed matter reasoning. His conclusions, pertinent to the present work, at high X ($X > 0.7$) are: (i) the D^+ species are highly mobile (diffusion coefficient as high as $10^{-3}\,cm^2\,s^{-1}$ has been reported [17]); and (ii) the chemical potential of D^+ in tetrahedral sites is more negative that that in octahedral sites. The consequence of the latter is the formation of the γ-phase.

2.5. Dewar-type calorimetry

An independent evaluation of the Dewar-type cells, used by Fleischmann and Pons (and also in this research), by Hansen and Melich [18] states that these cells are "easily capable of 1.0% accuracy".

A Dewar-type electrochemical cell, shown in Fig. 1, exhibits the following characteristics:

(i) at low to intermediate cell temperatures (20–60 °C), heat transfer from the cell is dominated by radiation

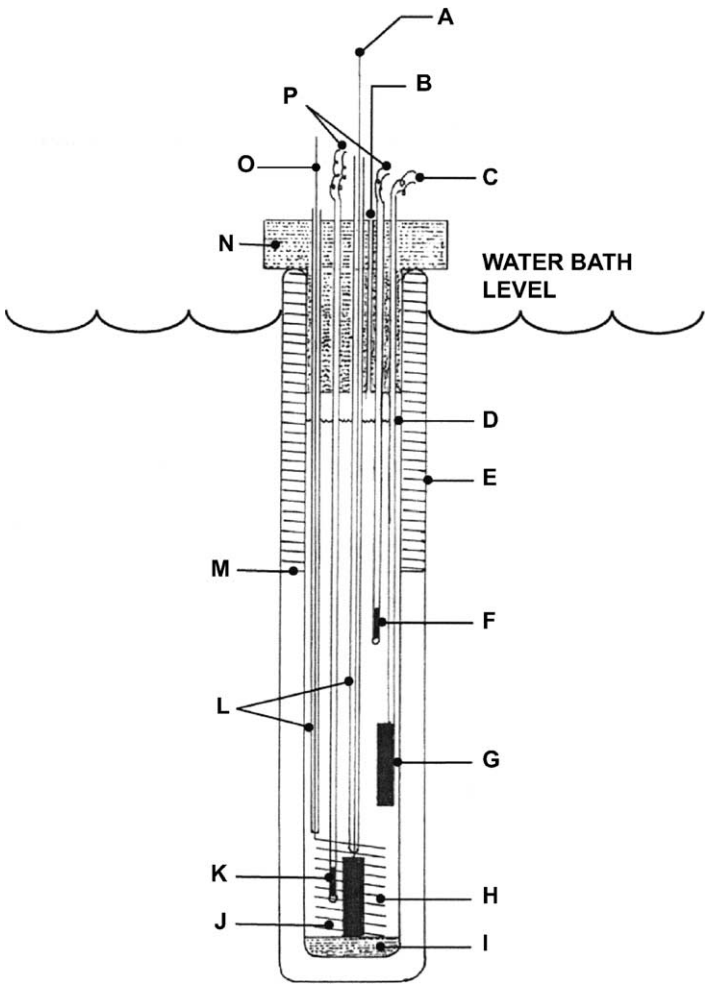

Fig. 1. The Dewar-type calorimeter used in this work: (A) cathode connection; (B) gas outlet; (C) heater connections; (D) electrolyte level; (E) silver mirror; (F) short termistor; (G) metal film resistor heater; (H) cathode; (I) Kel-F support plug; (J) anode; (K) long termistor; (L) capillary shields; (M) vacuum jacket; (N) Kel-F closure; (O) anode connection; (P) termistor connection.

across the vacuum gap of the lower portion of Dewar vessel;

(ii) the values of the heat transfer coefficient are close to those given by the product of the Stefan–Boltzmann coefficient and the radiant surface areas of the cells ($0.7 < 10^9 k_R < 0.76\,W\,K^{-4}$);

(iii) the variation of the heat transfer coefficient with time (due to the progressive decrease in the level of electrolyte) may be neglected as long as the liquid level remains in the silvered portion (heat balance within 99.0%);

(iv) at $I = 0.5$ A and $p = 101{,}325$ Pa, the cooling due to evaporation is ca. 10% of that due to radiation;

(v) measured uniformity of temperature of the electrolyte during cell operation is 0.02–0.3 s and somewhat more when resistive heater is employed;

(vi) contribution of conduction is ca. 6.9%;

(vii) relaxation time $\tau = C_p M^0 / 4k_R = 3600$ s;

(viii) mixing: radial, 3 s; axial, 20 s [19], i.e. cell behaves as a well-stirred tank;

(ix) electrolyte volume (cell dimensions) selected so that the rate of change of the electrolyte temperature with enthalpy input is of $10\,K\,W^{-1}$.

3. Experimental

3.1. Experimental set-up

The experiment was carried out using an electrochemical system consisting of an Hi-Tek DT 2101 potentiostat/galvanostat. A separate potentiostat/galvanostat was used to deliver constant currents to the resistive heater used to calibrate the cells. The system was controlled by a 486 data acquisition computer which also controlled an Hewlett-Packard 44705A multiplexer and data acquisition system. This data acquisition system was on an IEEE–GPLB bus so that it would be anticipated that there would not have been any timing errors introduced into the measurements. Data were taken every 300 s.

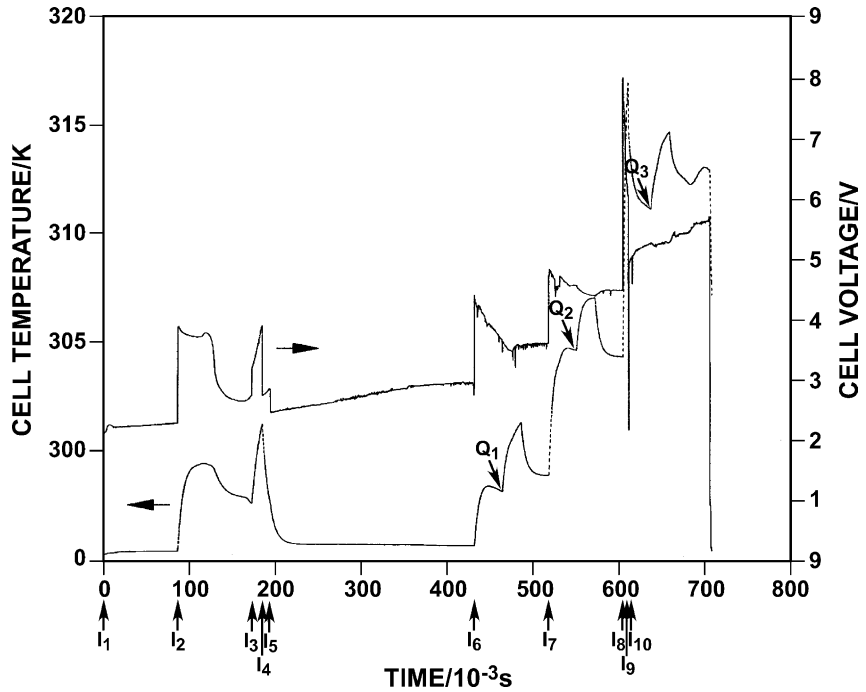

Fig. 2. Cell temperature, $T(t)$, and cell voltage, $E_c(t)$, as a function of time. Changes in the cell current at times indicated by arrows facing up. Resistive heater employed at times indicated by arrows facing down. Charging currents: $I_1 = 0.006$ A, $I_2 = 0.1$ A, $I_3 = 0.2$ A, $I_4 = 0.05$ A, $I_6 = 0.1$ A, $I_7 = 0.2$ A, $I_8 = 0.4$ A, $I_9 = 0.02$ A, $I_{10} = 0.3$ A. Calibration pulse: $Q_1 = Q_2 = Q_3 = 0.2500$ W.

The Dewar-type electrochemical cell was employed for the examination of the thermal behavior of the Pd/D system. A copper rod ($l = 2.5$ cm, $r = 0.2$ cm), upon which palladium and deuterium were co-deposited from a solution containing 0.025 M $PdCl_2$ + 0.15 M ND_4Cl + 0.15 M ND_4OD in D_2O (Isotec Inc., 99.9 at.% D) served as the negative electrode. Briefly, the co-deposition process (at $I = 0.006$ A) was completed in the first 24 h.

3.2. Data evaluation

Because the calorimetric equation is both non-linear and inhomogeneous, a number of simplifications must be made to provide a correct interpretation of thermal data and reach meaningful conclusions of a practical nature. Experience has shown that at low to intermediate temperatures, e.g. 20–60 °C, the behavior of a Dewar-type calorimeter is modeled adequately by the differential equation (cf. Appendix A

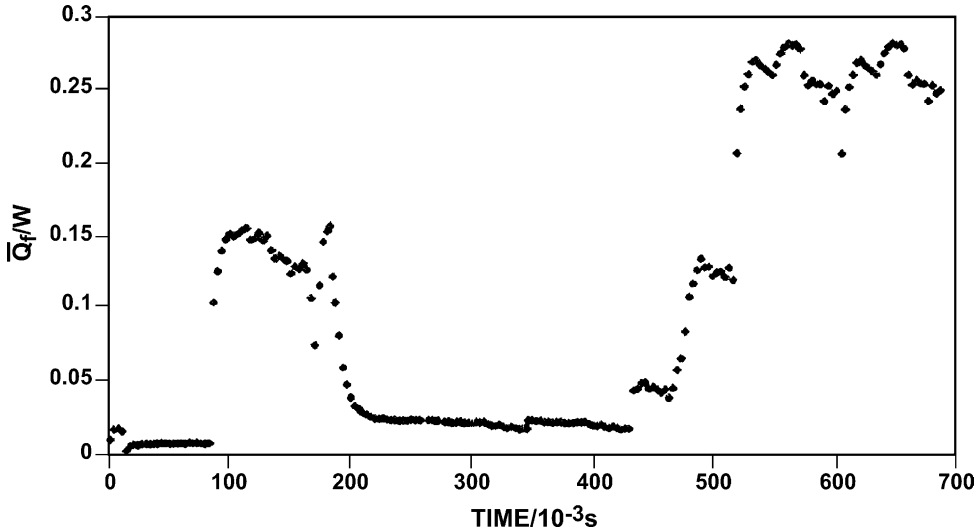

Fig. 3. Excess enthalpy generation, $\bar{Q}_f(t)$, as a function of time. Parameters used: $C_pM = 450$ J K^{-1}; $k_R = 0.85065$ W K^{-4}.

for a complete calorimetric equation):

$$C_pM\frac{dT}{dt} = (E_c - E_{th})I + Q_f(t) + Q_3 - \frac{3I}{4F}\left[\frac{p(t)}{p^* - p(t)}(C_{p,g} - C_{p,l})\Delta T(t) + L\right] - k_R[(T_b + \Delta T(t))^4 - T_b^4]. \quad (1)$$

To measure the excess enthalpy generation, as indicated in Eq. (1), two parameters must be known, viz. the heat transfer coefficient, k_R and the water equivalent, C_pM. These parameters are inherently connected with the cell construction and experimental protocol, i.e. once determined for a given cell, they can be used for subsequent runs of the same cell. For the cell used in this research, the parameters are: $k_R = 0.85065 \times 10^{-9}\,W\,K^{-4}$ and $C_pM = 450\,J\,K^{-1}$.

3.3. The $E_c(t)$ and $T(t)$ data

Since the evaluation is based on the examination of the cell voltage–time, $E_c(t)$, and cell temperature–time, $T(t)$, data in response to input enthalpies, $I(E_c - E_{th})$ and Q_3, it was necessary to prescribe their time profiles in a manner yielding maximum information. Fig. 2 shows the $E_c(t)$ and $T(t)$ data due to the enthalpy inputs, $(E_c(t) - E_{th})I$, at times indicated by arrows facing upwards and by a resistive heater with $Q_3 = 0.2500\,W$ by arrows facing down. Briefly, three distinctly different time periods can be identified. The first period includes the co-deposition at 0.006 A, and charging at 0.1 A increased to 0.2 A and followed by a stepwise reduction to $I = 0.05$ and 0.02 A. The second time interval is the period of low charging rate ($I = 0.02$ A) for ca. 72 h. The third time interval is characterized by drastic changes in cell operation—the cell current was increased/decreased in larger steps and, in addition, resistive heater was engaged at times indicated.

The $T(t)$ data are the normal, i.e. in the sense that an increase in the enthalpy input causes an increase in the cell temperature and vice versa. However, the examination of the $E_c(t)$ data reveals that there exist time periods when the cell temperature increases with decreases in the input enthalpy. As in the case of cells employing conventional electrodes, in this instance energy conservation requires the presence of additional (unidentified) heat sources.

4. Thermal effects

In an earlier communication [20], we have reported that in cells employing electrodes prepared by the co-deposition technique, excess enthalpy is generated reproducibly, at somewhat higher rates than on solid Pd electrodes and without the usual incubation period. Here, by examining the $T(t)$ data in conjunction with known enthalpy inputs, we extend the analysis to include the "positive feedback" and the "heat-after-death".

4.1. Excess enthalpy generation

Whether or not a particular cell generates excess enthalpy is determined by the energy and mass balance. Fig. 3 shows the 11-point average of the excess enthalpy generated, $\bar{Q}_f(t)$ whose integrated amount over the duration of this experiment was 75 kJ.

The comment has often been made that excess enthalpy generation can be explained by recombination of the electrically evolved gases. In this experiment, the total consumption of D_2O was 7.7 cm^3 instead of 7.2 cm^3, assuming 100% Faradaic efficiency, which is within experimental error.

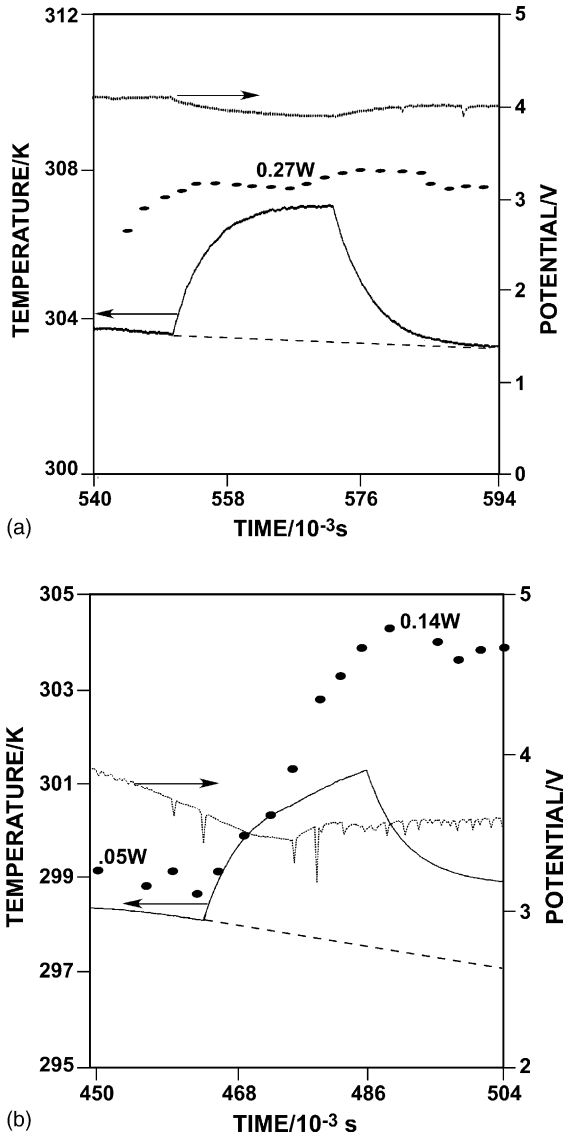

Fig. 4. The $E_c(t)$ and $T(t)$ curves following the application of calibration pulse: (a) at constant rate of excess enthalpy generation; (b) illustrating positive feedback.

Of special interest is the excess enthalpy generation during the co-deposition, i.e. at low current densities (e.g. as low as 6 mA cm^{-2}). Whether or not the excess heat observed in the course of co-deposition is due solely to exothermic absorption is difficult to ascertain because not much is known about the current efficiencies of the various operating reaction paths. More detailed calorimetry, beyond what was done in this experiment, would be required to assess the rate of excess enthalpy generation, if any. If, in fact, excess enthalpy is generated during the co-deposition period, it would have a profound influence on the understanding of its origin. However, making reasonable kinetic and thermodynamic assumptions together with high D/Pd atomic ratios of >1.0 within the Pd/D co-deposited films [21], one could conclude that an excess enthalpy generation cannot be excluded during the co-deposition process.

4.2. Effect of thermal perturbations—positive feedback

It is known that a perturbation of a system yields kinetic information through the examination of the $T(t)$ curves. Following the application of a calibration pulse, the $T(t)$ can be obtained by integration of Eq. (1). With constant E_c and Q_f, cell temperature, $T(t)$, increases exponentially and asymptotically approaches a new value. Upon cessation of the calibration pulse, cell temperature relaxes to a value that would have attained in the absence of the calibration pulse. A different behavior is expected for time-dependent cell voltage, $E_c(t)$, or variable rate of excess enthalpy generation, $Q_f(t)$.

During the experimental run, calibration pulses, Q_1, Q_2 and Q_3, were applied as indicated in Fig. 2. We selected for further discussion calibration pulses Q_1 and Q_2 representing different cell response to heat input. In one case, Fig. 4a, application of calibration pulse causes an exponential increase in cell temperature which, upon termination of calibration pulse, relaxes to the sloping temperature line. Inspection of Fig. 2 shows that within the time period of temperature perturbation, the cell voltage remained constant (at $E_c = 4.0$ V) indicating either no excess enthalpy generation or generation at a constant rate. Inspection of Fig. 3 shows the latter, i.e. generation at a constant rate of $Q_f = 0.24$ W.

The cell response to the thermal input Q_1, Fig. 4b, is different. Here, upon cessation of the thermal input, cell temperature does not relax to the expected value. Inspection of Figs. 2 and 3 reveals a time-dependent $E_c(t)$ and $Q_f(t)$, viz. decreasing E_c and increasing Q_f from 0.05 to 0.14 W. A positive feedback is apparent.

4.3. Effect of cell current perturbation—heat-after-death

A perturbation in cell current yields another characteristics of the Pd/D system, namely heat-after-death. At the beginning of the third day the charging current was increased to 0.2 A for a brief period of time, followed by a stepwise decrease to 0.05 A and finally to 0.02 A, which was maintained for the next ca. 72 h. The most important single result of this time period, viz. heat-after-death, is found in the analysis of the excess enthalpy decay following the stepwise reduction in the cell current. The decay of the six-point average, $\bar{\bar{Q}}_f$, of $\bar{Q}_f$ is shown in Fig. 5. In constructing this figure, it was assumed that the upper bound of any parasitic excess enthalpy generation due to the recombination is 0.009 W given by the last value of $\bar{Q}_f$ at $t = 24$ h, i.e. the values of $\bar{Q}_f$ are the lower bound values. The detailed interpretation of the data requires the knowledge, at the very least, of the current efficiencies for the various reaction paths and the thermodynamics of the co-deposition process(es). However, it appears to us that if we make various plausible assumptions, then we must conclude that the Pd/D co-deposition is accompanied by excess enthalpy generation. Incidentally, some activity within the Pd/D films persisted long after termination of cell current [22].

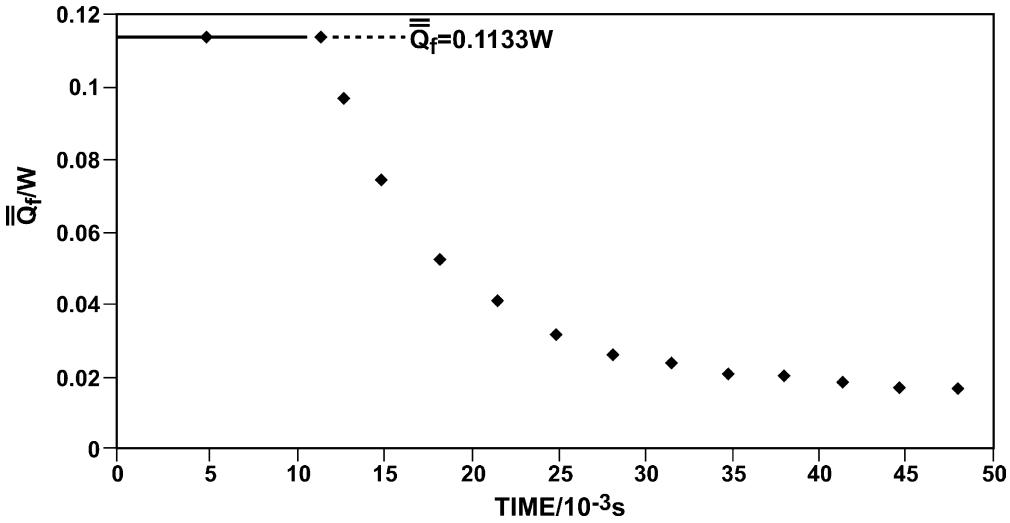

Fig. 5. The decay of $\bar{Q}_f(t)$ following the reduction in cell current (cf. Fig. 4) indicating the heat-after-death phenomenon.

5. Concluding remarks

In closing, we remark that results and conclusions of calorimetric measurement of the polarized Pd/D system are not limited to the excess enthalpy generation. Through the analysis of the effect of system's perturbation, both thermal and electrical, other characteristics can be displayed, e.g. positive feedback and heat-after-death.

Acknowledgements

The authors would like to thank Dr. F. Gordon for his interest and support.

Appendix A. Complete calorimetric equation

The complete calorimetric equation for the Dewar-type calorimeter is:

$$C_p M^0 \left[1 - \frac{(1+\beta)\gamma I t}{2FM^0}\right] \frac{\mathrm{d}\Delta T}{\mathrm{d}t} - C_p \frac{(1+\beta) I \Delta T}{2F} = \sum J_i, \quad i = 1, \ldots, 6, \tag{A.1}$$

where β is dimensionless term allowing for more rapid time-dependent decrease of water equivalent of cell than that expected from electrolysis alone and/or carried away in H_2, O_2 gas bubbles; γ is the current efficiency and can be taken to be unity. The term $[1 - ((1+\beta)It/2FM^0)]$ allows for change in the water equivalent, $C_p M^0$, with time.

The rates of enthalpy transfers are:

- $J_1 = (E_c(t) - E_{th})I$ is the enthalpy flow into the cell.
- $J_2 = Q_f(t)$ is the rate of excess heat generation within the Pd electrode and transferred into the electrolyte.
- J_3 is the known calibration heat source.
- $J_4 = -(\gamma I/F)[0.5C_{p,D_2} + 0.25C_{p,O_2} + 0.75(p/(p^* - p))C_{p,v}] + 0.75(\gamma IpL)/(p^* - p)$ is the enthalpy content of the gas stream.
- $J_5 = -k_R[1 - ((1+\gamma)It/2FM^0)][(T_b + \Delta T)^4 - T_b^4]$ is a product of the time-dependent heat transfer coefficient and the effect of radiation. The parameter $\gamma = 1$ for cells operating at $0 < 60\,^\circ$C.
- $J_6 = (\gamma I/F)\int_0^t [0.5 + 0.75p/(p^* - p)]C_{p,l}\Delta T\,\mathrm{d}t$ is the enthalpy input due to the addition of water to make up for the losses due to the electrolysis, $\gamma I/F$ and evaporation, $0.75p/(p^* - p)$.

The flow of cell current, I, produces changes in both the temperature and composition. Restricting our attention to the electrolyte subsystem, there is an enthalpy gain within the Δt time period in the amount of $\int_{\Delta t}(E_c - E_{th})I\mathrm{d}t$ (Joule heating) and the change in the mole numbers, n_k, due to the charge transfer reactions and evaporation, J_6. The effect of β on $Q_f(t)$ can be neglected if the cells operate at $T < 60\,^\circ$C.

References

[1] S. Pons, M. Fleischmann, Calorimetry of the Pd–D system, in: Proceedings of the First International Conference on Cold Fusion (ICCF-1), 1990, p. 1.
[2] S. Pons, M. Fleischmann, The calorimetry of electrode reactions and measurements of excess enthalpy generation in the electrolysis of D_2O using Pd based cathodes, in: Proceedings of the Second International Conference on Cold Fusion (ICCF-2), 1991, p. 349.
[3] M. Fleischmann, S. Pons, Calorimetry of the Pd/D system: from simplicity via complications to simplicity, in: Proceedings of the Third International Conference on Cold Fusion (ICCF-3), 1992, p. 47.
[4] M. Fleischmann, S. Pons, M. LeRoux, J. Roulette, Calorimetry of the Pd/D_2O system: the search for simplicity and accuracy, in: Proceedings of the Fourth International Conference on Cold Fusion (ICCF-4), 1993, p. 323.
[5] M. Fleischmann, Simulation of the electrochemical cell (ICARUS) calorimetry, in: Thermal and Nuclear Aspects of the Pd/D_2O system, vol. 2, Technical Report 1862, February 2002.
[6] S. Szpak, P.A. Mosier-Boss, J.J. Smith, J. Electroanal. Chem. 302 (1991) 255.
[7] B.E. Conway, G. Jerkiewicz, Z. Phys. Chem. 183 (1994) 1319.
[8] R. Defay, I. Prigogine, A. Bellemans, Surface Tension and Adsorption, Longmans & Green, London, 1951.
[9] S. Szpak, P.A. Mosier-Boss, R.D. Boss, J.J. Smith, Fusion Technol. 33 (1998) 38.
[10] F. Will, J. Electroanal. Chem. 426 (1997) 177.
[11] K.L. Shanahan, e-mail to M.A. Imam, 20 June 2002.
[12] P.A. Mosier-Boss, S. Szpak, Nuovo Cimento 112A (1999) 577.
[13] S. Szpak, P.A. Mosier-Boss, Phys. Lett. A 221 (1996) 141.
[14] M. Fleischmann, S. Pons, Phys. Lett. A 187 (1994) 276.
[15] C. Bartolomeo, M. Fleischmann, G. Larramone, S. Pons, J. Roulette, H. Sugiura, G. Preparata, Trans. Fusion Technol. 26 (1994) 23.
[16] G. Preparata, Trans. Fusion Technol. 26 (1994) 397.
[17] F. Celani, A. Spallone, P. Tripodi, D. Di Gioacchino, S. Pace, G. Salvaggi, P. Marini, V. DiStefano, M. Nakamura, A. Mancini, The effect of β–γ phase on H(D)/Pd overloading, in: Proceedings of the Seventh International Conference on Cold Fusion (ICCF-7), 1996, p. 62.
[18] W.N. Hansen, M.E. Melich, Trans. Fusion Technol. 26 (1994) 355.
[19] M. Fleischmann, S. Pons, M. LeRoux, J. Roulette, Trans. Fusion Technol. 26 (1994) 323.
[20] S. Szpak, P.A. Mosier-Boss, M.H. Miles, Fusion Technol. 36 (1999) 234.
[21] S. Szpak, P.A. Mosier-Boss, J.J. Smith, J. Electroanal. Chem. 379 (1994) 121.
[22] J. Dea, P.A. Mosier-Boss, S. Szpak, Thermal and pressure gradients in polarized Pd/D systems, in: Proceedings of the Spring Meeting of the American Physical Society, Indianapolis, IN, 2002.

Available online at www.sciencedirect.com
SCIENCE DIRECT®
Journal of Electroanalytical Chemistry 580 (2005) 284–290
Journal of Electroanalytical Chemistry
www.elsevier.com/locate/jelechem

The effect of an external electric field on surface morphology of co-deposited Pd/D films

S. Szpak, P.A. Mosier-Boss*, C. Young, F.E. Gordon

Spawar Systems Center San Diego, San Diego, CA 92152-5001, United States

Received 1 June 2004; received in revised form 15 February 2005; accepted 22 March 2005
Available online 23 May 2005

Abstract

The polarized PdD electrode undergoes significant morphological changes when exposed to an external electric field. These changes range from minor, e.g. re-orientation and/or separation of weakly connected globules, through forms that result from a combined action of the field as well as that connected with the evolution of gaseous deuterium, to shapes that require substantial energy expenditure.

Keywords: Co-deposition; Morphology; PdD–D_2O system; Electrostatic field

1. Introduction

A prolonged electrolysis of H_2O/D_2O, with the H_2/D_2 evolution taking place on solid Pd electrodes, produces substantial morphological changes in their surfaces [1]. They reported the following characteristic features: (i) the starting etch morphology affects the development of specific surface morphologies, e.g. the formation of ''parallel rows of sharply edged ridges'', (ii) an intergranular uplifting of ''structured'' relative to ''unstructured'' grains and (iii) the PdD_x–D_2O system is more reactive than the PdH_x–H_2O system. Features (i) and (ii) indicate that, near the surface, a permanent deformation of the electrode material has occured. The origin of change in surface morphology was not discussed in detail.

The starting point in our discussion is an observation that any solid undergoes permanent shape change when the internal forces exceed the elastic limits. In general, three types of forces can be identified as acting during the deformation of a solid, viz. (i) internal forces, i.e. those forces that obey Newton's law, (ii) applied (or external) forces, and (iii) capillary forces. The capillary forces (forces that act between the internal and surface molecules, or between solid boundary and the molecules of surrounding fluid) can be classified as either internal or external forces. When surface forces are non-uniformly distributed, they act as external forces [2].

If, in fact, capillary forces are involved in producing shape changes, then they can be magnified by placing the operating cell in an electrostatic field. In what follows, we examine the response of the Pd/D film, prepared by co-deposition [3], i.e. by simultaneous reduction of Pd^{2+} and D^+/D_2O ions/molecules to an external electric field. The discussion is qualitative, because a complete determination of the deformation involves the solution of equations of the theory of elasticity with well defined boundary conditions. Because of the very complex nature of this system, this cannot be done even if drastic simplifications are invoked. In agreement with Rolison and Trzaskoma [1] observation, we found also that the Pd/D_2O system is more reactive than the Pd/H_2O system and, for this reason, only the behavior of the former is presented.

* Corresponding author. Tel.: +1 619 553 1603; fax: +1 619 767 4339.
E-mail address: pam.boss@navy.mil (P.A. Mosier-Boss).

0022-0728/$ - see front matter © 2005 Elsevier B.V. All rights reserved.
doi:10.1016/j.jelechem.2005.03.039

2. Experimental

In an attempt to confirm the premise that surface forces initiate and, to a degree, govern the evolution of new structures during the electrolysis of D_2O, we followed the experimental protocol as described in Section 2.1.

2.1. Experimental protocol

An operating PdD//D_2O, 0.3 M LiCl//Pt cell was placed in an electrostatic field generated by a parallel plate capacitor where the field strength was maintained and controlled by setting the potential difference at a specified level. The cell geometry is shown in Fig. 1. The PdD electrode was prepared by the Pd electrodeposition onto an Au foil from a solution of 0.03 M $PdCl_2$ + 0.3 M LiCl dissolved in D_2O. The electrodeposition was under galvanostatic control with the current density profile as follows: 1.0 mA cm^{-2} for 8 h, 3 mA cm^{-2} for 8 h and at 5.0 mA cm^{-2} until all Pd^{2+} ions were reduced, i.e. when, by visual inspection, the solution becomes colorless. Upon completion of the Pd deposition, the cell current was increased to a value needed to maintain a visible gas evolution (usually 30–50 mA cm^{-2}) for the next 2–3 h followed by the cell placement in an electric field (2500–3000 V cm^{-1}) with the cell current increased to about 100 mA cm^{-2} for the next 48 h or longer. It is noteworthy that, after the co-deposition is completed, the cauliflower structure [4] is not affected by the applied current density. However, during the co-deposition low current densities are required to prevent the formation of powdery deposits.

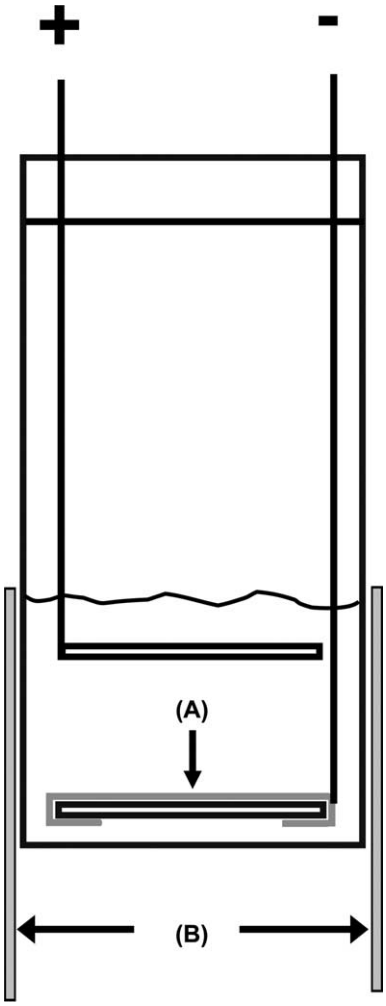

Fig. 1. Electrochemical cell. A – Au foil, B – copper plate (volume of electric field grater than volume of electrolyte).

3. Effect of an electric field

The variety of forms/structures resulting from the exposure to an electrostatic field (vide infra) strongly suggest that they arise from the co-operative and/or competitive interaction between cell components, relevant processes and their driving forces. Thus, to provide a rational interpretation one must: (i) consider the interaction of the field with the system and, in particular, with a conductor, liquid dielectric and the relationship between the surface forces and the bulk response (background information), (ii) define the system and its initial conditions (i.e. conditions just before the cell placement in an electric field), (iii) examine the effect of the field on the operation of individual components of the electrochemical cell.

3.1. Background information

To facilitate the identification of the dominant processes responsible for the change in both the surface morphology and the bulk structure, we review the interactions between the electrostatic field and the elements of an operating electrochemical cell. In particular, we include thermodynamic considerations, interactions with conductors, liquid dielectrics and the laws governing the bulk response to the surface forces.

3.1.1. Thermodynamic considerations

The energy transferred into molecules by stationary electric fields of less than 10^4 V cm^{-1} is small compared with the energies of chemical bonds. Consequently, from a thermodynamic point of view, the electric field is regarded as a new variable [5,6]. Its effect is included in the $\Sigma_i l_i \delta L_i$ term of the infinitesimal change in the internal energy

$$\delta U = T\delta S + \Sigma_i l_i \delta L_i + \Sigma_j \mu_j \delta n_j \quad (1)$$

where l_i and L_i are the work coefficients and work coordinates (other symbols have their usual meaning). In

the electrolyte phase, this term reads: $-p\delta V + \mathbf{E}\delta(\mathbf{P}V)$, where the work coefficient is the electric field strength **E**, and the conjugate work co-ordinate, $\mathbf{P}V$, is the product of the electric polarization, **P**, and volume V, while for the electrified interphase additional terms must be added. An extensive treatment of the thermodynamics of electrified interfaces can be found in [7] and references therein.

The thermodynamics of a solid system is analogous to that of a liquid with 6 quantities, $V_0\epsilon_i$, replacing volume, V (the quantity, $V_0\epsilon_i$ is a product of reference volume and the strain component; the associate intensive parameter is the stress component). Thus, the fundamental equation of a solid system is $U = U(S, V_0\epsilon_1, \ldots, V_0\epsilon_6, n_j)$. In particular, internal forces are associated with the strain just as the pressure is associated with the volume in a liquid system [5].

3.1.2. Conductors

Of interest here are the following effects: (a) introduction of an uncharged conductor into the field reduces the total energy of the field, (b) an uncharged conductor located outside the field is attracted towards the field, (c) a conductor, charged or uncharged, when placed in an electric field, cannot remain in stable equilibrium and (d) a "negative force" acts on the surface of a conductor [2, pp. 7, 31]. Consequently, if this conductor is constrained then it will suffer shape change, either reversible or permanent, depending upon the conditions at the surface and the time interval involved.

3.1.3. Liquid dielectric

While a conductor, when placed in an electric field always suffers "negative pressure", a dielectric may either expand or contract, i.e. it may experience either negative or positive pressure. For the detailed discussion consult [2, p. 54].

3.1.4. Forces acting on the contact surface: shape change

The relationship between the surface forces and the bulk response (the Gauss theorem) is given by

$$\int \operatorname{div}\mathbf{A}\,\mathrm{d}\tau = \oint A_n\,\mathrm{d}\sigma, \tag{2}$$

where the div operator derives a vector from tensor. The left side term is the algebraic sum of all sources/sinks continuously distributed over the volume element. The right side defines the outflow, if positive and the inflow, if negative. Eq. (2) indicates that forces acting on any finite volume in a body can be reduced to forces applied to the surface of that volume and vice versa [8]. Consequently, it follows that the shape change at constant volume is associated with material motion due to internal forces acting on the surface. Thus, the deformation will be determined by the distribution of surface forces, while the rate of deformation by their magnitude.

However, internal stresses can be present without the presence of external loads, e.g. due to inhomogeneities, imperfections, etc, a likely situation in co-deposited films and the continuous evolution of deuterium. Thus, the change in shape and the degree of deformation depends on the distribution of the surface forces and indirectly through structural changes caused by these forces or other reactions.

3.2. The Pd/D–D_2O system: initial conditions

An operating cell is viewed as a system consisting of three subsystems, viz. the electrolyte, the interphase and the bulk Pd/D. The interphase itself is an assembly of non-autonomous layers defined by van Rysselberghe [9]. The electrolyte, an ionic conductor, is treated as a dielectric with added extraneous charges (positive and negative ions). The Pd/D system is considered a conductor containing, in addition to free electrons also mobile positive particles, the D^+ species.

Just before the application of an external electric field all intensive state variables were constant in time, i.e. all irreversible processes inside the system occur continuously (there is a continuous exchange between the system and surroundings). The processes involved are: reduction of D^+/D_2O ions/molecules and evolution of D_2. The mechanism of these reactions is not important except to say that all operating driving forces remain constant in time.

3.3. Effect of electric field

By placing an operating electrochemical cell, a part of the field energy is transferred to the cell. In particular, the electrostatic field affects each individual subsystems, viz. electrolyte, interphase and bulk electrode, in a different way. Moreover, the action may be either direct or indirect; in the latter case, it affects a process which is not directly connected with the presence of the electrical charge.

3.3.1. The electrolyte phase

The electrolyte phase contains mobile positive and negative ions distributed in a manner that assures charge neutrality (except at boundaries). It is known that an ion in contact with water is solvated, which means that the central ion is surrounded by an oppositively charged ionic cloud. When subjected to an external electric field, each ion is acted upon with a net force representing the difference between the accelerating force arising from the applied field and the opposing forces, viz. (i) the electrophoretic contribution associated with the structure of the moving entity (i.e. the central ion is accelerated in one direction while its ionic cloud in another), and (ii) the force connected with the relaxation of the ionic cloud [10].

3.3.2. Interphase

To reiterate, the interphase is an assembly of non-autonomous layers defined by the set of processes: $D^+_{(r)} + e^-_{(r)} \rightarrow D_{(ad)} \rightarrow D_{(ab)} \rightarrow D^+_{(l)} + e^-_{(l)} \rightarrow D^+_{(m)}$. The positive and negative charges present in the interphase (the $D^+_{(r)}$, $D^+_{(l)}$, $e^-_{(r)}$, $e^-_{(l)}$ species) are mobile with the degree of mobility depending upon local conditions. When subjected to the applied field, the response is similar to that of the electrolyte phase, i.e. separation and drift of charged particles and an analog to mixing by time/space dependent adsorption of deuterium.

Evidently, the interaction between the applied field and the forces acting at the surface during the reduction of D^+ ions (D_2O molecules) is primarily responsible for the observed changes in surface morphology illustrated in Figs. 3–7. The basis for this conclusion is the Gauss theorem, Eq. (2), and the structure of the interphase arising from the participating processes, inclusive of transport processes [9]. The bulk response arising from the Gauss theorem depends on the degree of change in the internal energy which, in turn, depends on the work of deformation, i.e. on the product of the strain component, $V_0\epsilon$, and its conjugate stress component, σ.

3.3.3. Bulk Pd/D

Any charges on a conductor must be located at its surface. Charged mobile species, viz. D^+, are also present in the bulk Pd/D material. In general, they will not be affected by an external field, since no field can exist there. However, in the present case, they might be affected by the field generated by the flow of cell current, i.e. the electrodiffusion of D^+ might occur.

4. Results and interpretation

The application of an external electrostatic field substantially changes the structure of the PdD deposits. This is illustrated in a series of SEM photographs taken from a number of runs. We selected examples of various structures to emphasize the complexity of the system as well as to indicate the impossibility of a quantitative analysis. The selected examples include minor deformation of the original structure shown in Fig. 2, definitive shape change, unusual structures, to a deformation associated with, what appears to be, a catastrophic event.

4.1. Reference morphology

In the absence of an external field, the structure of the deposits consists of globules, 3–7 μm in diameter, arranged in short columns, Fig. 2. Each of the individual globules is an aggregate of much smaller, almost spherical units, having diameters in a sub-micron range (micro-globules). The structure is uniform throughout the electrode and does not change with time or with the current density after the completion of co-deposition.

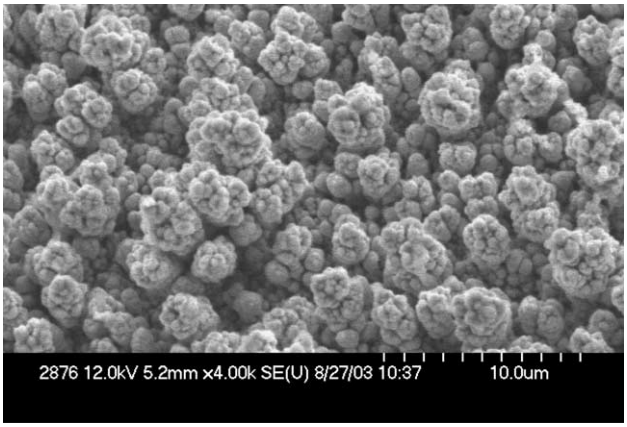

Fig. 2. SEM of co-deposited PdD film.

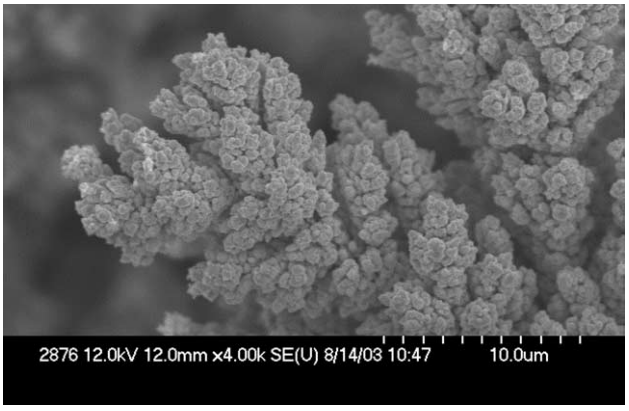

Fig. 3. SEM of the PdD film shortly after exposure to electric field.

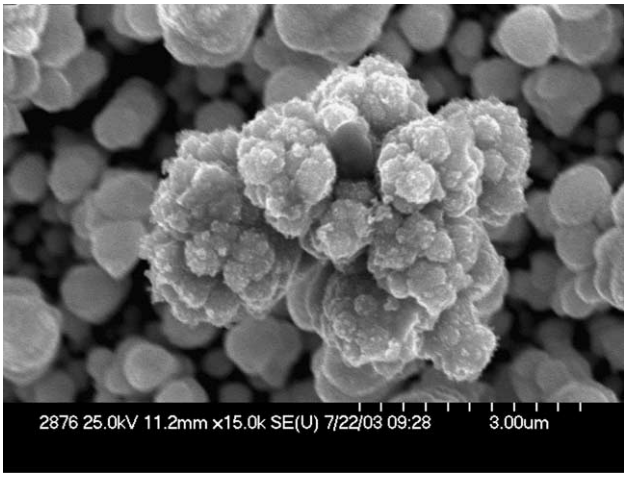

Fig. 4. SEM of the PdD film showing separation of globules and "smoothing" of their surface.

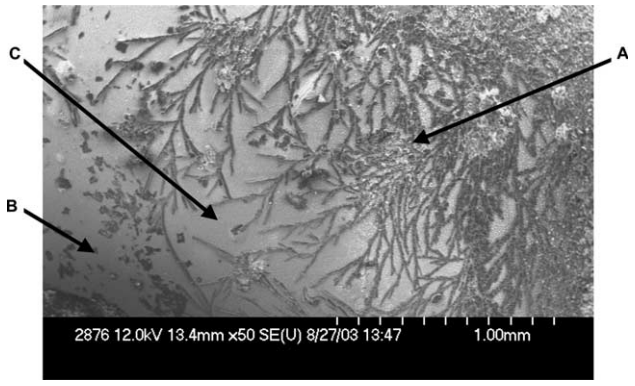

Fig. 5. Formation of branches (fractals) by the free floating micro-globules guided by local field.

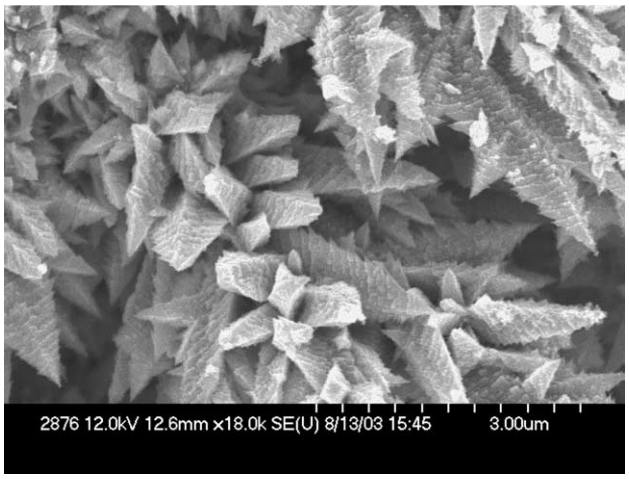

Fig. 6. Dendritic growth due to the action of the cell current on micro-globules immobilized in tight pores.

4.2. Re-orientation: globules separation

The first noticeable effect, after placing the cell in an electric field, is the ''swelling'' of the co-deposited PdD material followed by a displacement toward the negative plate of the capacitor. These visual observations suggest that (i) the swelling arises from an interaction of the constrained porous structure with an external field, (ii) the displacement toward the negative plate indicates weakening of the mechanical constraints and assigns a positive charge to the structural elements of the porous structure of the PdD material. The re-orientation of globules position without substantial change in their size or appearance is shown in Fig. 3. We note that such re-orientation is associated with an increase in volume thus it would appear as ''swelling'' of the original structure. Indeed, this swelling is observed within minutes after engaging the electrostatic field.

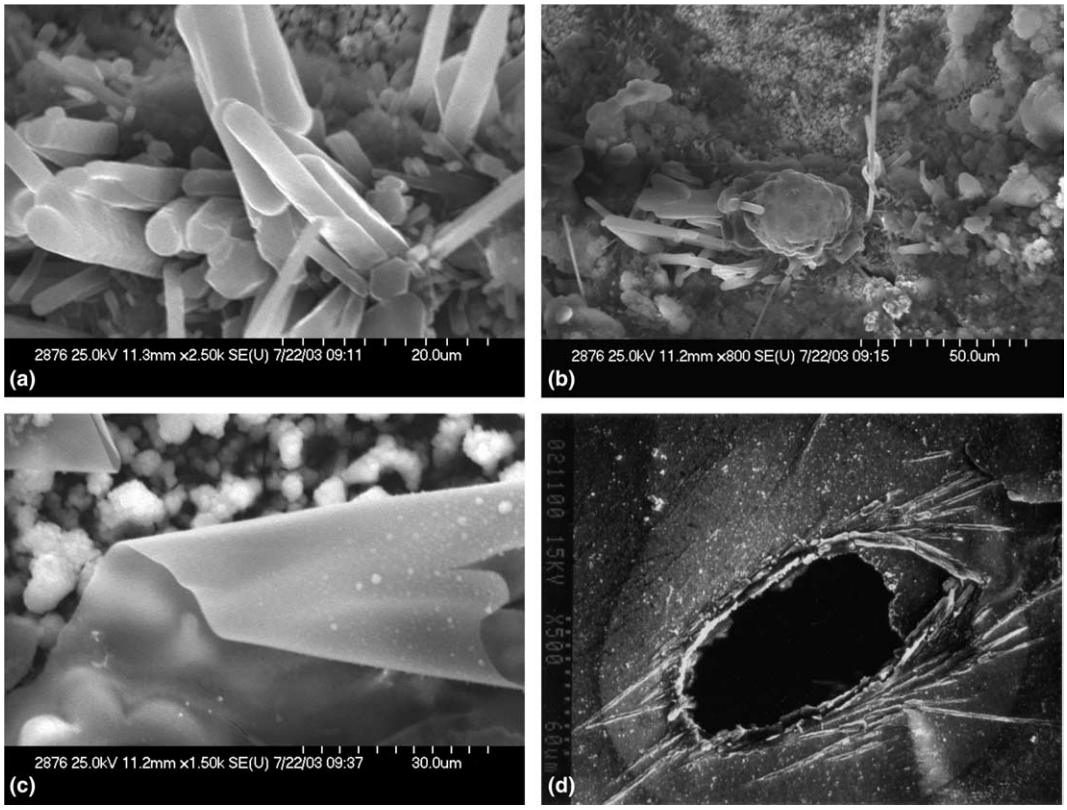

Fig. 7. Examples of the shape change requiring substantial energy expenditure. (a) Formation of circular and square rods, (b) a boulder with an extended wire, (c) a folded thin film, (d) a crater.

Another example of the disintegration of the PdD structure is shown in Fig. 4. This figure illustrates the breaking of the bonds holding together individual globules. The breaking of bonding and the separation of globules may be due to action of electrical forces alone or may be due to combined action of electric and mechanical forces arising from the bulk material response to the changing magnitude of surface forces (cf the Gauss theorem).

4.3. Effect of current distribution

A different set of processes appears to be responsible for the structural changes, viz. (i) the formation of branches (fractals), Fig. 5, and (ii) the production of dendritic growth, Fig. 6. In what follows, we argue that these two very different forms may have a common origin, namely that they are the result of a combined action of the current flow through a porous structure, the presence of evolving deuterium and the electric field on the separated micro-globules suspended in the electrolyte and restricted by the porous structure.

The observed morphological and structural changes occur during the reduction of D^+/D_2O ions/molecules at porous electrode. Thus, at least three factors should be considered: (i) the external field, (ii) the distribution of the cell current and (iii) the presence of gaseous deuterium within the confines of the structure. Since the depth of current penetration (for a given electrode kinetics, current density, etc) into the electrode depends on pore size and assuming that all factors are involved, a different response to the field are expected at different sites of the PdD material.

At sites of a relatively large pore size, the micro-globules are acted upon by two factors, the electric field and the convective flow due to mixing by the evolving deuterium. The electric field redistributes the surface charges while the evolving gas brings micro-globules in contact with each other. Viewing Fig. 5, we identify three areas having distinct features: area A with high density of branches and un-attached micro-globules, a sparsely populated by micro-globules, area B, and area C where un-attached micro-globules are absent and where branches (fractals) are well defined. The latter indicates that the growth of branches is by addition of micro-globules leading to an apparent reversal of the action of an electric field (cf. Section 4.2 and Fig. 4).

Entirely different situation exists in small pore sizes; the pore wall my be covered by gaseous deuterium and thus shifting the cell current deeper into the porous structure. If a micro-globule is placed in the current path, and, if the potential drop over the length of the micro-globule in the electrolyte is greater than the sum of the anodic and cathodic overpotentials needed to dissolve Pd and deposit the Pd^{2+} ions, then dendritic growth is possible, as demonstrated in [11].

4.4. Unexplained shapes

While the morphologies shown in Fig. 3–6 can be accounted for on the basis of information assembled in Section 3.1, those in Fig. 7 suggest that additional factors are involved in producing the observed shape changes. Of the great variety of forms, we selected those illustrating the re-shaping of the spherical globules into (i) rods (circular and square), Fig. 7(a), (ii) long wire, Fig. 7(b), (iii) folded thin film, Fig. 7(c), and (iv) a crater, Fig. 7(d), the latter suggesting the presence of a violent event.

5. Closing remarks

In order to change the shape of a solid (at constant volume) energy must be supplied. This requirement raises a number of questions, among them: (i) how much energy is needed to produce the observed changes in both, original surface morphology and/or structure; (ii) is there enough energy available; (iii) what is the energy transfer path; (iv) at what rate the energy should be transferred to the solid to account for the observed changes.

(i) *Energy requirement*. A minimum of the energy expenditure is required to produce changes illustrated in Figs. 3–6. However, the changes shown in Figs. 7(a)–(d), cannot be produced by the action of electric forces alone. Considerable work is needed to account for the variety of shapes. It appears that the process of shape change is driven by energy transferred from the electrostatic field and directed by the field.

(ii) *Energy of the electrostatic field*. Total energy of an electrostatic field is proportional to the field strength which, in turn, is proportional to the voltage difference between the plates of the condenser. Consequently, as long as the voltage between plates is maintained at the same level, the energy supply is unlimited.

(iii) *Energy transfer path*. Two energy transfer paths operate during the experimental run, viz. transfer from the field and that associated with the electrochemical process, principally due to absorption of deuterium. Work in progress is directed to the assessment of their contribution.

Parenthetically, nothing substantial can be gained (in terms of understanding) by conducting a set of parallel experiments involving "light" water. In contrast, a comparison with "light" water is essential when evaluating excess enthalpy generation (the Fleischmann–Pons effect) [12]. Here, a cursory examination of the response of the $PdH–H_2O$ system showed essentially the same

behavior as the PdD–D_2O system, i.e. the swelling of the cathode material as well as its leaning toward the negative capacitor plate. Qualitatively, under the same conditions, the PdH–H_2 system shows fewer shape changes and the absence of the distinct features such as those illustrated in Fig. 7.

In conclusion, we recall a quote by Rolison et al. [13] "...the surface and near–surface characterization of electrolytically prepared PdD_x system requires great care and attention, but with the reward of unusual results."

References

[1] D.R. Rolison, P.P. Trzaskoma, J. Electroanal. Chem. 287 (1990) 375.
[2] L.D. Landau, E.M. Lifshitz, Electrodynamics of Continuous Media, Pergamon Press, 1960.
[3] S. Szpak, P.A. Mosier-Boss, J.J. Smith, J. Electroanal. Chem. 302 (1991) 255.
[4] S. Szpak, P.A. Mosier-Boss, S.R. Scharber, J.J. Smith, J. Electroanal. Chem. 380 (1995) 1.
[5] R. Haase, Thermodynamics of Irreversible Processes, Adison-Wesley Publishing Co, Inc., 1969.
[6] H.B. Callen, Thermodynamics, John Wiley & Sons, New York, London, Sydney, 1960.
[7] P. Nikitas, J. Electroanal. Chem. 316 (1991) 23.
[8] A. Sommerfeld, Lectures on theoretical physics, Mechanics of Deformable Bodies, vol. II, Academic Press, New York, 1950.
[9] P. van Rysselberghe, in: J.O'M. Bockris (Ed.), Modern Aspects of Electrochemistry, 4, Plenum Press, New York, 1966.
[10] J.O'.M. Bockris, A.K.N. Reddy, Modern Electrochemistry, Plenum Press, New York, 1974.
[11] S. Szpak, T. Katan, P.J. Carlen, J. Electrochem. Soc. 133 (1986) 1340.
[12] H. Gerischer, in: The Science of Cold Fusion, Proc. of the II Annual Conference on Cold Fusion, Como, Italy, 1991.
[13] D.R. Rolison, W.E. O'Grady, R.J. Doyle, P.P. Trzaskoma, in: Proc. First Annual Conference on Cold Fusion, Salt Lake City, 1990.

Naturwissenschaften (2005) 92: 394–397
DOI 10.1007/s00114-005-0008-7

SHORT COMMUNICATION

Stanislaw Szpak · Pamela A. Mosier Boss · Charles Young · Frank E. Gordon

Evidence of nuclear reactions in the Pd lattice

Received: 8 September 2004 / Accepted: 12 May 2005 / Published online: 29 July 2005

Abstract An operating Pd//D_2O, Li^+, Cl^-//Pt cell, placed in an external electrostatic field, yielded unexpected results, viz. (i) Morphological changes in the form of discrete sites exhibiting molten-like features, i.e. features that require substantial energy expenditure. (ii) Presence of elements (Al, Mg, Ca, Si, Zn, . . .) that could not be extracted from cell components and deposited on discrete sites. The cell design and the experimental protocol assuring reproducibility is described in detail.

Introduction

Low temperature nuclear reactions were first reported nearly a century ago. In a brief communication, Oliphant et al. (1934) disclosed that by bombardment of perdeutero inorganic compounds, e.g. $(ND_4)_2SO_4$, by deuterons produced tritium and hydrogen. One year later, commenting on the Oliphant et al. communication, Dee (1935) stated: "... this no doubt being the result of transmutations effected by slower diplons which have lost energy by collision in the target." This view was not challenged for the next 50 years. The situation has changed dramatically with the Fleischmann and Pons announcement (23 March 1989) that an operating cell Pd//D_2O, LiOD//Pt produced excess enthalpy in the amount that could not be accounted by any known chemical or electrochemical process.

The presence of light elements (e.g. He, T) was expected in view of the suggested D + D reaction path. The lack of direct correspondence between the amount of nuclear ash and the excess power suggested that other, as yet, unidentified nuclear process(es) could be responsible. To test this suggestion, a search for heavier elements was initiated. The first attempt was by Rolison and O'Grady (1991) who through surface analysis, done after a prolonged electrolysis of Pd electrodes, showed the surface to contain a number of heavy elements. The search for the low temperature transmutations continued. A review of this effort was provided, among others, by Miley and Patterson (1996), Bockris and Mallove (1999) and Miley and Shrostra (2003). In most cases, the experimental methodology was different from that associated with the Fleischmann and Pons experimental protocol. The closest, in approach, is the work of Klopfenstein and Dash (1998) who found a number of new elements when heavy water was electrolysed on Ti electrodes. However, their work differed from the finding of this communication in that here: (i) co-deposited Pd/D electrodes were used and (ii) the cell was placed in an external electrostatic field.

S. Szpak · P. A. Mosier Boss (✉) · C. Young · F. E. Gordon
SPAWAR Systems Center San Diego,
San Diego, CA 92152, USA
e-mail: pam.boss@navy.mil

Materials and methods

Cell construction

An electrochemical cell, Fig. 1a, consisted of (i) a rectangular vessel (2 cm × 2 cm × 8 cm) made of clear plastic (acrylic) with copper plates attached to parallel walls; (ii) negative electrode (cathode) – an Au foil 1.5 cm in length 0.5 cm wide and a Pt wire, all anchored to a polyethylene base, as illustrated in Fig. 1b; (iii) positive electrode (anode) – a Pt screen to allow for the escape of gaseous reaction products; (iv) an electrolyte −20 mL of the solution having composition 0.03 M $PdCl_2$ + 0.3 M LiCl in D_2O. The cell assembly was connected to a galvanostat, the copper plates to a regulated high voltage source. The cathode assembly is placed parallel to the electric field.

Cell operation

The experimental protocol covers three time periods: (i) preparation of the Pd electrode, (ii) "stabilization" of the system and (iii) exposure to an external field after increasing the current to put the system in far from equilibrium condition.

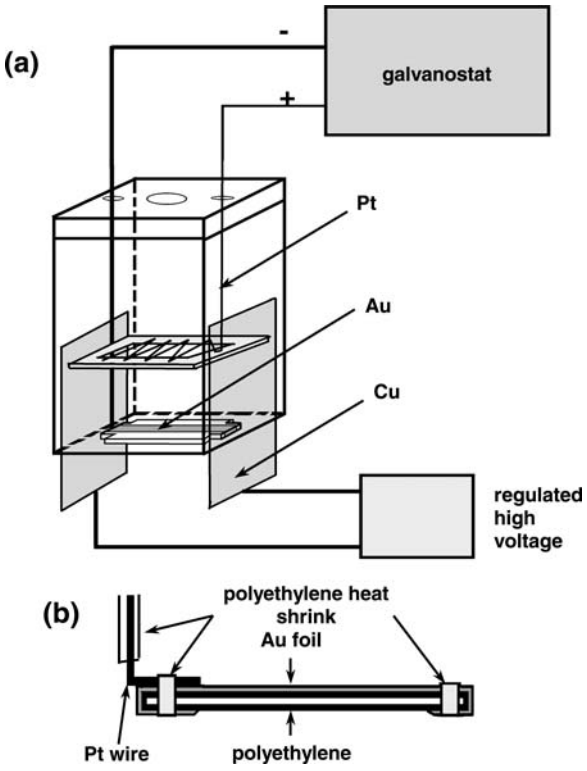

Fig. 1 (**a**) Electrochemical cell (**b**) Assembly of the Au cathode

1. The Pd/D films are prepared by the co-deposition process in which palladium and deuterium are simultaneously deposited onto substrates that do not absorb deuterium, e.g., Au, Cu, at sufficiently high-negative potentials from an electrolyte containing Pd salt dissolved in D_2O (Szpak et al. 1994). The appropriate cell current profile depends on the surface area and the composition and amount of electrolyte in the cell. For the present case, the cell current profile was as follows: 1 mA for the first 24 h followed by 3.0 mA for a period necessary to reduce all Pd^{2+} ions (i.e., when the solution becomes colorless).
2. The "stabilization" period refers to the time needed to assure uniform distribution of the D/Pd atomic ratio throughout the electrode volume. This is done by raising the cell current to a value yielding a visible D_2 gas evolution, for the present case 30–50 mA, and maintaining it for 2–3 h.
3. The activation of an external electric field is done by connecting the copper plates to the regulated high-voltage source. In the present experiment, the potential difference of 6000 V was maintained for at least 48 h. The far from equilibrium condition is realized by increasing the cell current to 100 mA or higher.
4. The Pd/D structure is examined by scanning electron microscopy (SEM) using an instrument equipped with an energy-dispersive X-ray analysis system (EDX).

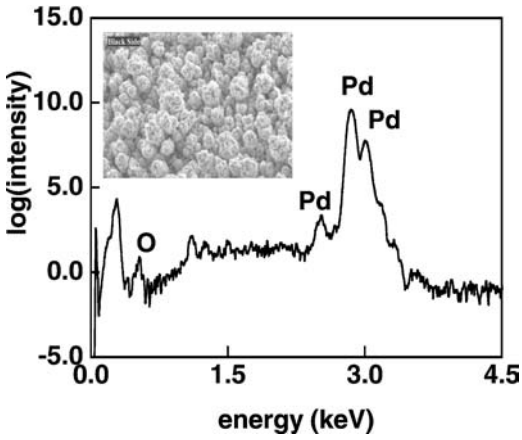

Fig. 2 The EDX of the Pd/D film deposited in the absence of an electric field. Insert: SEM of the film

Results

The structure of the co-deposited Pd/D material, after electrolysis of D_2O in the absence of an external field, including the EDX analysis of its surface, is illustrated in Fig. 2. The electrode structure consists of globules 3–7 μm in diameter arranged in short columns. Each of the individual globule is an aggregate of much smaller, almost spherical units, having a diameter in the sub-micron range. This "cauliflower-like" structure is uniform throughout the electrode. The analysis by EDX results in Pd −95.17, O −4.83 wt%, i.e. it shows only elements originally present in the cell.

If, upon the completion of the co-deposition, an external field is activated, then morphological changes occur. Among the various structural forms, we find morphologies with molten-like features, Figs. 3a–c, the development of which requires high-energy expenditure. The question that arises is: Are these structural changes due to the action of the electrostatic field alone or is additional energy required to produce the features? One such energy source is that of a nuclear origin. If the distinct features are the result of a nuclear reaction, then their chemical composition should reflect it. Indeed, compelling evidence is provided by the EDX analysis of selected spots from various runs illustrated in Figs. 3a–c. The analysis of the boulder-like form, Fig. 3a(ii), shows the presence of Al-21.72, O-71.48, Pd-6.80 wt% while the area adjacent to it Pd-95.17, O-4.83 wt%, Fig. 3a(iii). In the second example, Fig. 3b (i), the "crater-like" form, we find in the center Al-21.87, Mg-0.46, O-71.11 and Pd-6.75 wt%, Fig. 3b (ii), and in the periphery Al-21.27, Mg-4.33, O-68.19 and Pd-6.21 wt%, Fig. 3b (iii). In the third example, Fig. 3c, the results are: O-45.49, Mg-0.43, Al-0.50, Si-1.71, Cl-1.54, Ca-19.80, Zn-1.57 Pd-9.10, Au-19.86 wt%.

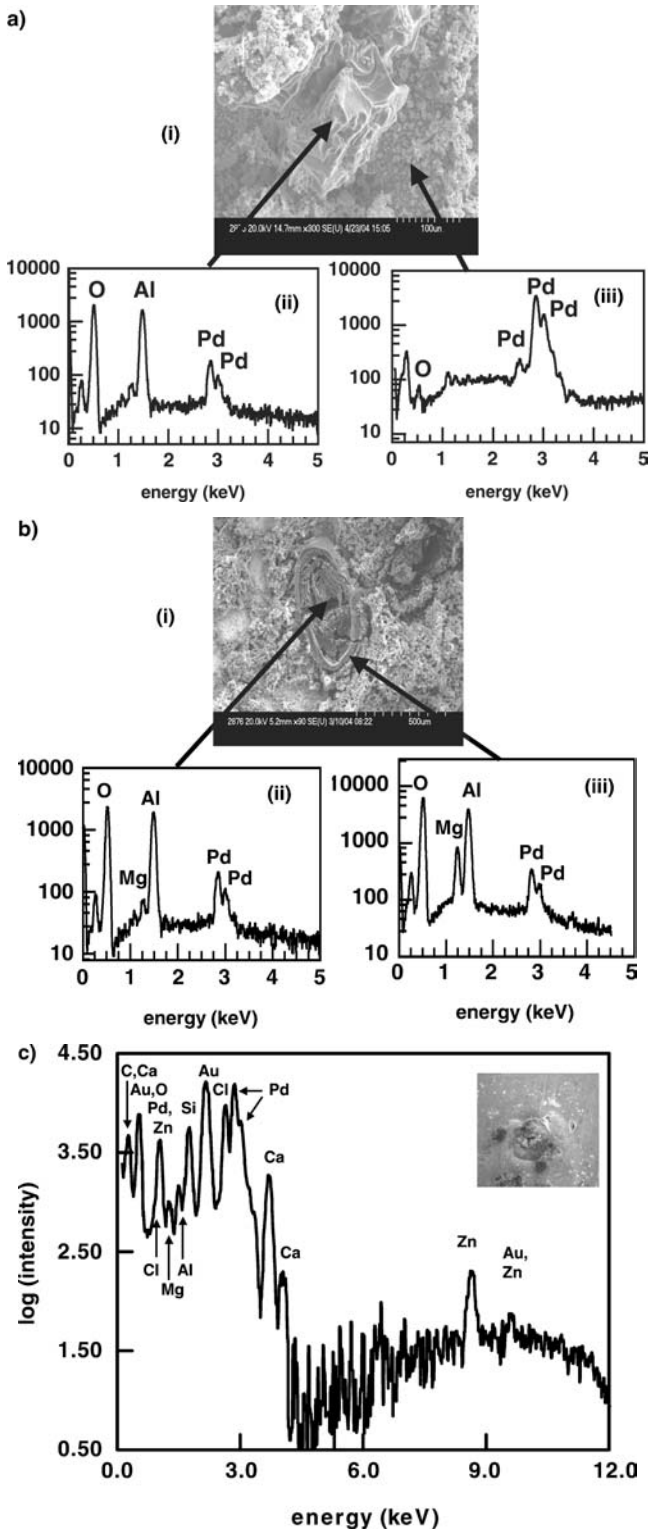

Fig. 3 (**a**) (i) SEM of "boulder-like" structure; (ii) EDX of "boulder-like" structure; (iii) EDX of area adjacent to it (**b**).(i) SEM showing a "crater-like" structure (ii) EDX of center of crater (iii) EDX of periphery of crater. (**c**) EDX of blister-like (insert) structure

The source of "new elements" (Al, Ca, Mg, Si, ...) could be either transmutation or contamination. Arguments against the latter are: (i) Total amount of impurities in 20 mL of electrolyte is about 0.5 mg (based on 95.5% pure reactants with Al, Ca, Mg below detectable limits by standard analytical procedures), i.e. too small to account for the observed concentrations of e.g., Al 21.27%, Fig. 3b(ii), or Ca 19.80%, Fig. 3c.(ii) Elements Al, Ca, Mg cannot be co-deposited under the experimental conditions. However, if they could be co-deposited they would be uniformly distributed throughout the electrode volume and not localized. (iii) The segregation effects associated with the surface transport processes are not likely to occur in the "cauliflower-like" structures. (iv) All cell components were analyzed for the presence of "new elements". None was found. Oxygen, chlorine cannot be associated with a nuclear reaction, rather they arise from reaction with components of the electrolyte immediately after the cessation of cell current flow, i.e. when reducing conditions are removed. The gold peaks in Fig. 3c are due to the substrate onto which the Pd/D was co-deposited. In areas in which the gold peaks were observed, the Pd/D film had separated from the underlying gold substrate.

Discussion

An operating cell is viewed as a system consisting of three subsystems: The electrolyte, the interphase and the bulk Pd/D. The region separating the bulk phases, here, the electrolyte and bulk Pd metal, constitute the interphase. In general, the interphase is an assembly of non-autonomous layers (segments) (Defay et al. 1996). In practice, different representations can be employed. In one representation, the interphase includes the electrical double layer on the solution side of the contact surface and the corresponding feature on the metal side. In another representation, thermodynamic considerations dictate its structure (van Rysselberghe 1996). In the present case, the first representation was used to discuss the shape change and the second in the search for precursors.

Shape change

It is known that (i) a conductor, charged or not, placed in an electric field, cannot remain in a stable equilibrium and a "negative" pressure acts on the surface (Landau and Lifshitz 1960) and (ii) the relation between the surface forces and the bulk response is given by the Gauss' theorem which states that the forces acting on any finite volume in a body can be reduced to forces applied to the surface of that body and vice versa. Consequently, the shape change is associated with the motion due to internal forces derived from the surface forces. The shape change is determined by surface forces whereas the rate of deformation by their magnitude (Szpak et al. 2005).

A system far from equilibrium tends to promote cluster formation which, in turn, produces hot spots that can be

displayed by infra–red (IR) imaging of the electrode surface (Mosier-Boss and Szpak 1999). The presence of "hot spots" indicates that (i) there are regions of specific interactions involving absorbed deuterium and the Pd lattice and (ii) these interactions produce intense heat sources capable of melting palladium. Thus, a model for the transition from a "cauliflower-like" morphology to shapes illustrated in Figs. 3a–c is as follows: (i) a small volume of the Pd is melted by an intense localized heat source, (ii) a blob of molten metal takes on the shape determined by the distribution the surface forces (iii) solidification, due to the heat dissipation, which produces a new and permanent shape. These distinctly different morphologies are the areas where the "new elements" are found.

Precursors

In the reaction $A \rightarrow B + C$, whether chemical or nuclear, the reactant is constrained by the imposed experimental condition while the products by energy considerations. Here, the experimental protocol, by putting the system in far from equilibrium condition, assures (i) domain/cluster formation and (ii) "self-organization", the latter occurs when the system is open and capable of exchanging parts of its energy with environment (Glandsdorff and Prigogine 1966). Both, formation of active domains and the "self-organization" is supported by experiment (hot spots). The applicable reaction path, for the present case, is: $\ldots..R_{-} \rightarrow A \rightarrow \sum P_i + \sum Q_i$ where dots represent reduction of D^+ and/or D_2O, adsorption, absorption, ionization and cluster formation. $\sum P_i$ refers to the reaction products – the "new elements" and $\sum Q_i$ is the energy produced/consumed. The "self-organization" refers to the production of precursor(s). Just how the external electric field interacts with the system is not quite clear. What is clear is that the interphase is involved and that, through its non-autonomous character, the events at the contact surface are transferred to sub-surface region where they promote the formation of precursors (reactant A) leading to the nuclear events.

The results presented in this communication should be regarded as preliminary since they are limited to one cell current profile and one value for the strength of the external field. We wish to emphasize that the interpretation offered is the first attempt to explain the anomalous behavior.

As more facts are obtained then, in all probability, a clearer picture will emerge.

References

Bockris JO'M, Mallove EF (1999) The occurrence of cold nuclear reactions widespread throughout Nature? Infinite Energy, 27:29–38

Dee PI (1935) Some experiments upon Artificial Transmutation using the Cloud-track Method. Proc Roy Soc A 148:623–637

Defay R, Prigogine I, Bellemans A (1966) Surface tension and adsorption. Longmans Green, London, pp 369–389

Glandsdorff P, Prigogine I (1971) Thermodynamic theory of structure, stability and fluctuations. Wiley-Interscience, London New York Sydney Toronto, pp xxi– xxiii 290

Klopfenstein MF, Dash J (1998) Thermal imaging during electroysis of heavy water with a Ti cathode. Proceedings of the Seventh International Conference on Cold Fusion (ICCF-7), pp 98–102

Landau LD, Lifshitz EM (1960) Electrodynamics of continuous media. Pergamon Press Oxford, London New York, pp 3, 312–334

Miley GH, Patterson JA (1996) Nuclear transmutations in thin film nickel coatings undergoing electrolysis. J New Energy 1:5–30

Miley GH, Shrostra PJ (2003) On transmutations in solids. Trans Am Nucl Soc 88:627–635

Mosier-Boss PA, Szpak S (1999) The Pd/^{n}H system: Transport processes and development of thermal instabilities. Il Nuovo Cimento 112A:577–585

Oliphant ML, Hartreck P Lord Rutherford (1934) Transmutation effect observed with heavy hydrogen. Nature 133:413

Rolison DR, O'Grady WE (1991) Observation of elemental anomalies at the surface of palladium after electrochemical loading of deuterium or hydrogen. Anal Chem 63:1697–1702

van Rysselberghe P (1966) Some aspects of the thermodynamic structure of electrochemistry. In: Bockris JO'M (ed) Modern aspects of electrochemistry No 4. Plenum Press, New York, pp 1–46

Szpak S, Mosier-Boss PA, Smith JJ (1994) Deuterium uptake during Pd-D co-deposition. J Electroanal Chem 379:121–127

Szpak S, Mosier-Boss PA, Young C, Gordon FE (2005) The effect of an external electric field on surface morphologyof co-deposited Pd/D films. J Electroanal Chem (in press)

POLARIZED D^+/Pd–D_2O SYSTEM: HOT SPOTS AND MINI-EXPLOSIONS

S. SZPAK, P.A. MOSIER-BOSS, J. DEA AND F. GORDON
Spawar Systems Center San Diego, San Diego, CA 92152-5001, USA

Two types of activities occurring within the polarized D^+/Pd–D_2O system, viz. the presence of localized heat sources (hot spots) and associated with them mini-explosions, are described. The "birth and death" of hot spots is monitored by IR imaging while the mini-explosions are displayed by the voltage spikes exhibited by a piezoelectric substrate onto which a Pd/D film was co-deposited. Processes leading to the formation of unstable domains as a precursor to the observed behavior is examined.

1. Introduction

The characteristic feature of the polarized Pd/D–D_2O system is the generation of excess enthalpy measured by calorimetry. However, calorimetry alone cannot provide an answer to a number of questions, among them (i) continuous or discrete heat sources, (ii) their location and (iii) the sequence of events leading to the initiation of thermal events.

In an earlier communication,[1] we presented an example of discrete heat sources. Here, we discuss the evolution of the electrode surface temperature in greater detail, provide supporting evidence for the presence of discrete heat sources by displaying the associated pressure gradients, and discuss the conditions leading to the formation of unstable domains, i.e. conditions preceding the initiation of the Fleischmann–Pons (F–P) effect.

2. Thermal behavior

The evolution of thermal activities in the negatively polarized Pd/D_2O system was examined using an experimental arrangement shown in Fig. 1 and (b). Figure 1(a) illustrates the position of an infrared camera facing the negative electrode. To record the evolution of thermal behavior it is necessary to place the negative electrode upon which a deuterium saturated Pd film is being deposited very close to the thin cell wall (Mylar film). The infrared camera was operated in two modes: (i) to measure the cell temperature across the cell (along the X–X line), Fig. 2, and (ii) to display the presence of hot spots.

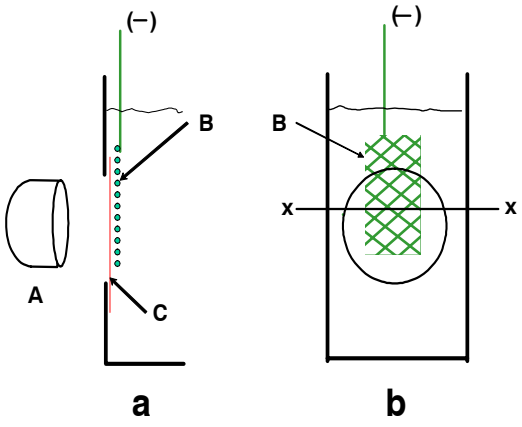

Figure 1. Experimental arrangement for infrared imaging: (a) side view—position of the IR camera; (b) front view—placement of the negative electrode (Ni screen): (A) infrared camera; (B) Ni screen; (C) Mylar film.

2.1. *Temperature profile*

The cell temperature profile, plotted in Fig. 3, was taken periodically during the electrolysis. The difference between the electrode surface temperature and that in solution, ΔT, increases with time, being initially at ca. 2 °C and reaching a value as high as ca. 17 °C 2 h later. The increase in the surface temperature, curve a, is irregular indicating bursts in excess enthalpy generation. In contrast, the solution

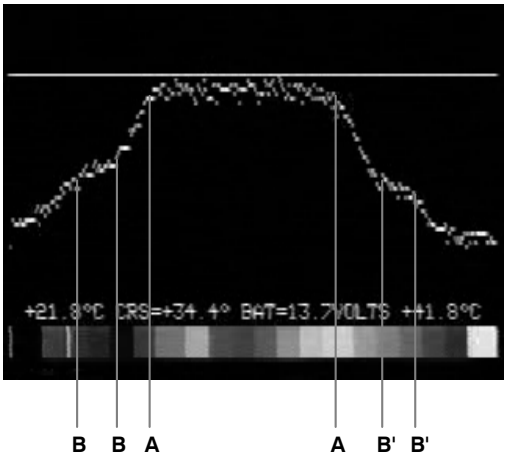

Figure 2. Cell temperature profiles. A–A electrode surface temperature; B–B solution temperature.

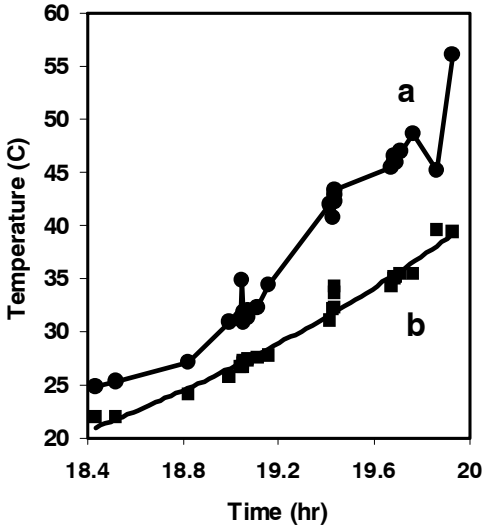

Figure 3. Evolution of the temperature difference, ΔT, as a function of time: (a) electrode surface temperature; (b) solution temperature.

temperature, curve b, increases smoothly which is an expected behavior because the weight (volume) of solution exceeds that of the Pd/D electrode assembly.

2.2. *Development of hot spots*

Thermal activity in the form of "hot spots," Fig. 4(a)–(d), was detected early during the Pd/D co-deposition process. We note that (i) the rate of heat generation is not uniform, (ii) thermal activities occur at low cell temperature and at low cell currents and (iii) the intensity of thermal activity increases with an increase in both cell temperature and cell current, Fig. 5. Here, the temperature of hot spots cannot be estimated because it exceeded the camera range.

3. Lattice distortion

An expected consequence of localized heat sources is lattice distortion and the development and propagation of stresses within the Pd/D lattice. The display of mechanical distortion can be followed by co-depositing the Pd/D films onto pressure sensitive substrates, e.g. piezoelectric ceramic material.[2] To eliminate external factors that might interfere with the interpretation of the sensor's response the electrochemical cell was shielded (Faraday cage) and the whole assembly placed on a shock absorbing material, as illustrated in Fig. 6.

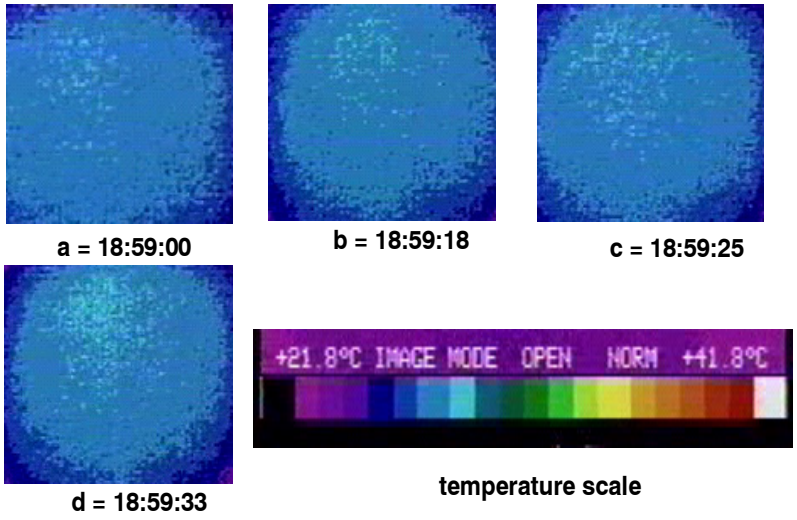

Figure 4. Time/space dependency of "hot spots," their intensity and frequency during co–deposition. Temperature scale included. "Hot spots" images at times indicated.

3.1. *Single events*

An ideal response of a piezoelectric sensing device to thermal mini-explosion is illustrated in Fig. 7. A single isolated event is shown in Fig. 8(a). Here, we see clearly a single voltage spike which, in the negative direction, corresponds to the pressure pulse. After a brief period of time, $\Delta t = 0.06\,\mathrm{s}$, we note the arrival of

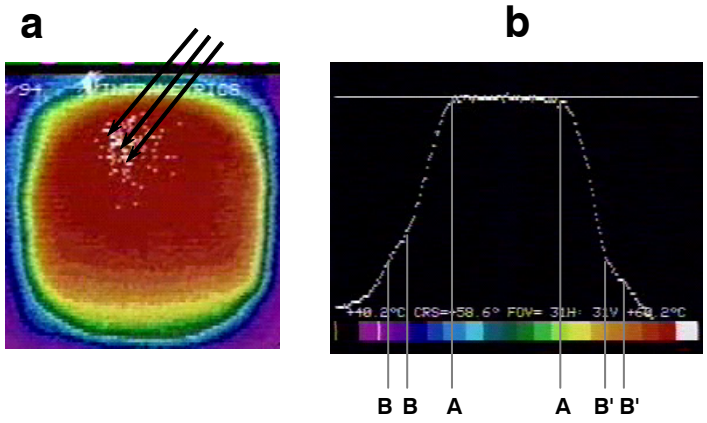

Figure 5. Time/space dependency of "hot spots." (a) At elevated temperature; arrows indicated spots whose temperature was outside of the camera range; (b) distribution of cell temperature. A–A electrode surface temperature; B–B solution temperature.

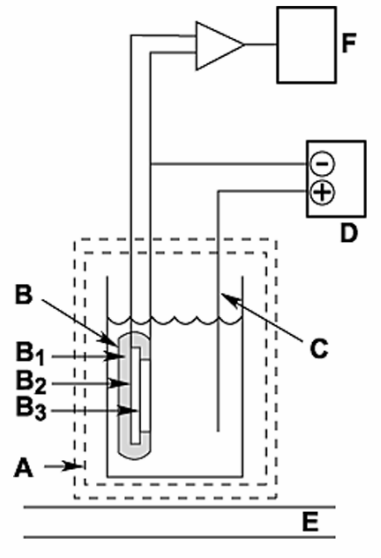

Figure 6. Experimental arrangement for recording mini-explosions. A: Faraday cage; B: negative electrode assembly (B_1: insulating material; B_2: piezoelectric substrate; B_3: Pd/D film); C: positive electrode; D: potentiostat/galvanostat; E: shock absorbing material; F: oscilloscope (LeCroy digital); E: laboratory bench.

the temperature front (voltage spike in the opposite direction), followed by the system relaxation. Using a simple model, e.g. that of a spherical reaction site, one could, from the magnitude of the voltage spikes and the Δt, reach some conclusion concerning the position and strength of the heat source. Such singular events are seen in the early periods of the co-deposition. Interestingly, these voltage bursts persisted for hours following the termination of current flow.

3.2. *Bursts*

A typical voltage–time behavior indicating a burst of events within the Pd/D film is shown in Fig. 8(b). These bursts were observed at constant current densities as low as ca. $4.0\,\mu\mathrm{A\,cm^{-2}}$. An expanded trace of such bursts shows a series of of voltage spikes, indicated by arrows. Their frequency and intensity increased with an increase in the cell current and cell temperature. At temperature near the boiling point, thermal activities were very intense as indicated by the magnitude of the voltage spikes, illustrated in Fig. 9.

4. Discussion

The appearance of discrete reaction sites implies the transition from a stable to an unstable regime, alternatively a transition from non-reactive to reactive sites. We

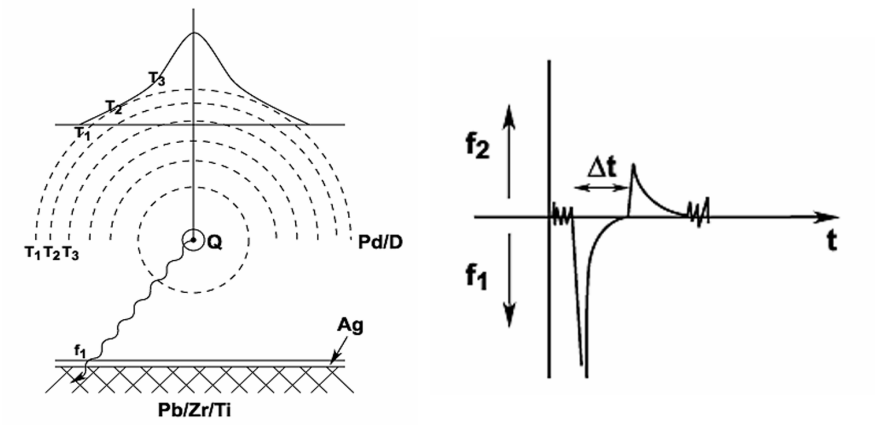

Figure 7. Ideal representation of a mini-explosion: left: location of the instantaneous heat source and associated effects; right: a response of a piezoelectric sensor (f_1: compression; f_2: expansion).

regard the formation of these domains as being the last step prior to the initiation of the F–P effect. Furthermore, we define a reference state in which all flow of matter is stopped but the flow of energy is permitted. The reference state is maintained by an overpotential, alternatively, by the cell current. In the reference state in which all octahedral sites are occupied, the overpotential acts as an external potential, i.e. it determines the distribution of all mobile charges (both D^+ and e^-). The

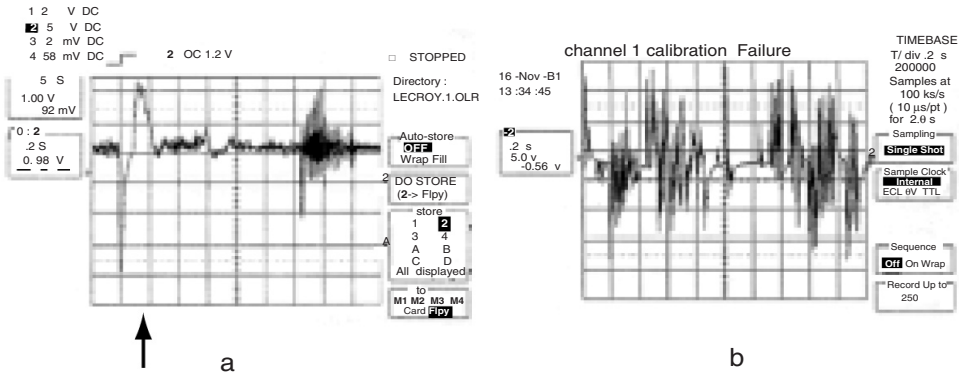

Figure 8. Typical response of a piezoelectric sensor. Left (A): an isolated event; right (B): an expanded set of events, arrows indicate recognizable pattern.

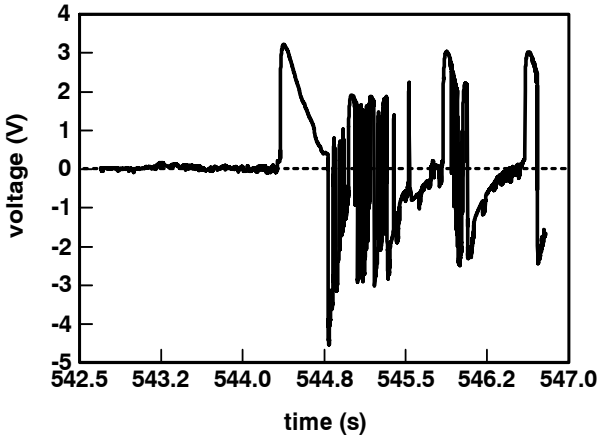

Figure 9. Response of a piezoelectric sensor to events occurring at the boiling point. The high voltage spikes (no amplification) indicate very strong pressure and temperature gradients activating the sensor's response.

vanishing of all mass fluxes demands that all chemical potentials within the Pd/D system be equal.

We examine the associated dynamics leading to the instabilities of what should otherwise be stable behavior, via (i) the construction of an interphase across which deuterium transport occurs, and (ii) the system's response to perturbations in the cell current/potential.

4.1. *Construction of the Pd/D_2O interphase*

Here, as in an earlier communication,[1] we follow closely the procedure outlined by van Rysselberghe.[3] Briefly, the interphase region consists of a set of non-autonomous layers where the overall overpotential can be broken into parts pertaining to the various layers and where these layers are determined by the sequence of processes/reactions. Each layer of the set of non-autonomous layers is homogeneous and of sufficiently large volume so that the concentration and temperature are well defined and their location is given by the driving forces, the chemical potentials. The structure of the Pd/D–D_2O interphase arises from the set of steps involved in the electrochemical charging viz electroreduction of D^+ ions in the reaction layer, followed by adsorption, absorption, placement in the Pd lattice, ionization (dissociation), and transport into the bulk metal (Fig. 10).

Restricting our attention to the relevant part of the structure of the interphase and the processes therein, we examine the dynamics of the Pd/D–D_2O system under the following set of assumptions: (i) the e^-'s are treated as a component as are the $D^{(\theta)}$, $D^{(a)}$, $D^{(\lambda)}$, D^+ species,[4] (ii) the transition from D_{ad} to D_{ab} is fast so that during charging they remain in quasi-equilibrium, (iii) ionization, $D_l \rightleftharpoons D^+ + e^-$, is considered a chemical reaction occurring in a s- electron rich environment.

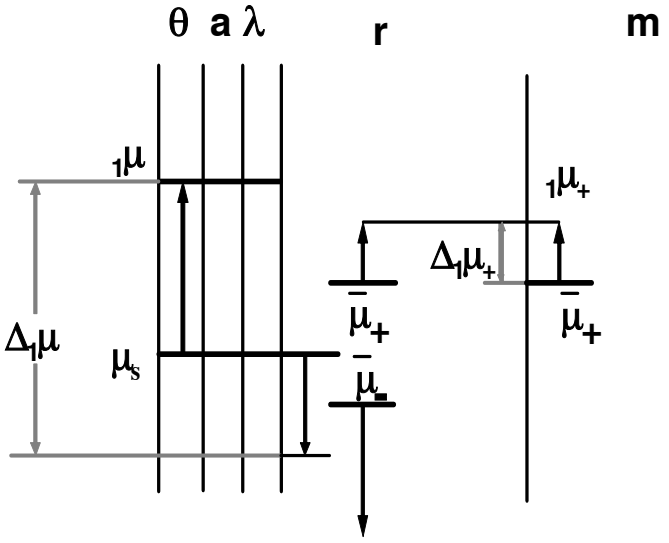

Figure 10. Structure of the interphase. Layers: $\theta-$ adsorption, a: adsorption, $\lambda-$ lattice placement, r: reaction (dissociation), m: bulk metal; μ_s- chemical/electrochemical potentials at the reference state (equality $\mu_s = \mu^{(\theta)} = \mu^{(a)} = \mu^{(\lambda)} = \mu^{(r)}$ and $\bar{\mu}_+^{(r)} = \bar{\mu}_+^{(m)}$ refer to the stationary state). Chemical potentials ${}_1\mu^{(\theta)} = \cdots$ are potentials associated with the change in the electrode overpotential. The equality ${}_1\mu^{(\theta)} =_1 \mu^{(a)} =_1 \mu^{(\lambda)}$ indicates fast adsorption $\rightarrow$ absorption $\rightarrow$ lattice placement. $\Delta_1\mu$ and $\Delta_1\bar{\mu}_+$ are the driving forces arising from the change in the electrode overpotential.

4.2. *Stability with respect to overpotential variation*

The negatively polarized Pd/D electrode of an operating electrochemical cell is a complex system. Its behavior with respect to perturbation in the overpotential, η, will be first examined by considering a set of thought experiments in which a closed system containing D, D^+ and e^- at equilibrium will be subjected to (i) action of an external potential, η, (ii) the addition of electrons in the absence of η, and (iii) addition of electrons in the presence of η.

(i) The external potential affects only charged species via the internal potential, χ. If the system contains an equal number of positively and negatively charged particles, then the action of an external potential is canceled.

(ii) If the number of negatively charged particles is greater than the number of positively charged (e.g. by addition of electrons) then the addition of negatively charged particles increases the chemical potential, $\mu^{(r)}$, due to an increase in the second term of Eq. (2). The net result is the decrease in the concentration of positively charged particles.

(iii) The action of the external potential on the system with unequal number of charged particles is more complex. In the system where the negative charges exceed the

positive, the net result is the decrease of the $\mu^{(r)}$ (note—logarithmic term in Eq. (2) changes slower than the linear term). The composition of the quasi-equilibrium is determined by both the excess of negative particles and the magnitude of the applied potential, i.e. $\mu^{(r)} = f[q_-, \chi]$. As the external potential is increased, the $\mu_+^{(r)}$ also increases.

In assessing the response to the variation in overpotential we take note of condition (iii). In addition, we assume that the surface coverage remains constant, i.e. that the extra cell current is used exclusively for the deuterium evolution reaction. Thus, condition (iii) yields

$$\mu^{(r)} = \bar{\mu}_+^{(r)} + \bar{\mu}_-^{(r)} \tag{1}$$

with

$$\bar{\mu}_{(+,-)} = \bar{\mu}^0_{(+,-)} + RT \ln c_{(+,-)} + z q_{(+,-)} |\chi|, \tag{2}$$

where $c_{(+,-)}$ are the volume concentrations, $q_{(+,-)}$, is the charge density and χ is the internal potential. The subscripts +,– refer to deuterons and s–electrons, respectively, and the superscripts identify the layer under consideration.

Even a small deviation from the reference state results in instability. By definition, $\mu = \partial U/\partial n|_{S,V,n,\ldots}$ Consequently, the stability/instability of the Pd/D system with respect to varying overpotential is determined by taking the derivative of the chemical potential. The chemical potential of the adsorption layer depends linearly on over potential,[5] i.e. $\mu^{(\theta)}(\eta) = \mu^{(\theta)} + |\eta|F$ and $\mu^{(r)} = \bar{\mu}_+^{(r)} + \bar{\mu}_-^{(r)}$. Substitution of (2) into (1), followed by differentiation, yields

$$\frac{\partial \mu^{(r)}}{\partial \chi} = q_+ - q_-. \tag{3}$$

Since $\partial \mu^{(r)}/\partial \chi < 0$, so is also $\delta U < 0$, i.e. the system is unstable with respect to the variation in overpotential.

4.3. *Formation of active domains*

The review of the thermal behavior suggests the following:

(i) The discrete heat sources were noted shortly after the initiation of current flow. Thus, they are located near the contact surface and the supercharged layer, in which [D]/[Pd] > 1, is formed instantaneously.[6]

(ii) The nuclear active site must contain a large number of single events to produce a visible image. Unfortunately, our experimental set-up could not yield quantitative assessment. However, based on other considerations the estimated the number of single events to be between ca. 10^4–10^9.

(iii) The random time/space distribution of hot spots as well as their varying intensity with time, Fig. 4(a)–(d), exclude the existence of fixed location of the nuclear-active-sites. The random distribution and the varying intensity arises from the coupling of the various processes occurring on both sides of the contact surface in response to fluctuations.

(iv) Both, the frequency and intensity are a strong function of temperature. In particular, both increase with an increase in temperature, exhibiting the so-called positive feedback, cf. Figs. 3 and 5. This is, perhaps, the most direct indication of the influence of the chemical environment.

To reiterate, active domains containing several thousands of particles are formed in the close proximity to the contact surface. The random distribution suggests that the beginnings of the new phase are generated as a result of fluctuations, while the strong temperature dependency attests to the action of forces of a chemical nature. In earlier communications,[1,7] we pointed out that changes in an external force, e.g. the overpotential, substantially affects the dynamic behavior as well as the structure of the interphase which contains complexes of the form $[D...D]^+$. In a system containing high D^+/Pd ratio in a s-electron rich atmosphere (according to Preparata,[8] ca. 40% of the metal volume is occupied by the s-electrons) and assisted by a high external potential, the high value of the $\mu_+^{(r)}$ promotes the formation of deuteron clusters, possibly of the form $[D_n^+ e_m^-]$. Evidently, the s- electrons play a dominant role in the formation of an assembly of complexes, $[D_n^+ e_m^-]$.

5. Concluding remarks

The last step in the series of consecutive events leading to the F–P effect is the formation of active domains, the seats of the reaction(s), yielding an excess enthalpy. The arguments presented here arise from the following statements:

(i) The electrode/electrolyte interphase is viewed as an assembly of a set of homogeneous layers identified by the processes occurring therein or with the associate chemical/electrochemical potentials.

(ii) The ionization (dissociation) of D in the Pd lattice is a chemical reaction (mass action law is obeyed, the chemical potential is the sum of the electrochemical potentials of constituents, etc.)

(iii) the s-electrons play a dominant role in both, the high values of $\overline{\mu}_+$ as well as in the forming of $[D_m^- e_n^-]$ complexes.

References

1. P.A. Mosier-Boss and S. Szpak, *Nouvo Cim.* **112A**, 577 (1999).
2. J. Dea, P.A. Mosier-Boss, and S. Szpak, in *Proceedings of the American Physical Society Spring meeting, Indianapolis, IN, 2002.*
3. P. van Rysselberghe, in *Modernn Aspects of Electrochemistry, Vol. 4*, ed. J.O'M. Bockris (Plenum Press, New York, 1966).
4. R. Defay, I. Prigogine and A. Bellamans, *Surface Tension and Adsorption* (Longmans, Green & Co. Ltd., London, 1966).
5. B.E. Conway and G.Z. Jerkiewicz, *Phys. Chem.* **183**, 281 (1994).
6. S. Szpak, P.A. Mosier-Boss and C.J. Gabriel, *J. Electroanal. Chem.* **365**, 275 (1994).
7. S. Szpak, P.A. Mosier-Boss, S.R. Scharber and J.J. Smith, *J. Electroanal. Chem.* **337**, 147 (1992).
8. G. Preparata, *Trans. Fusion Technol.* **26**, 397 (1994).

PRECURSORS AND THE FUSION REACTIONS IN POLARISED Pd/D-D_2O SYSTEM: EFFECT OF AN EXTERNAL ELECTRIC FIELD

S. Szpak, P. A. Mosier-Boss, F. E. Gordon
SPAWAR Systems Center San Diego, San Diego CA 92152-5001, USA

The effect of an external electric field on the physical appearance of the Pd/D electrode in an operating cell is discussed. It is shown that the individual globules of the "cauliflower – like" structure undergo a shape change exhibiting two distinct features, *viz* those that require energy expenditure that can be extracted from the applied external field (*eg* re-orientation, separation of individual globules, dendrite formation) and those that require energy expenditure far in excess of one that can be supplied by the electric field alone (*eg* exhibiting features usually associated with the solidification of a molten metal under liquid or the presence of localized catastrophic events leading to the formation of craters). It is shown, by energy-dispersive X-ray method, that the needed energy is provided by nuclear events occurring in the region close to the electrode surface. The nuclear events are of the type: precursor $\rightarrow$ unstable nucleus $\rightarrow$ stable nucleus.

1.0 Introductory remarks

Apart from an excess enthalpy generation, there are other reported manifestations of unusual activities in the negatively polarised Pd/D-D_2O system[1]. Among them (i) changes in surface morphology far greater than those associated with the lattice expansion[2] and (ii) accumulation of impurities in the surface (sub-surface) region that exceeds the amounts that can be transferred from the cell components during prolonged cell operation[3]. In what follows, we shall demonstrate that both these features are magnified if an operating cell is placed in an external electrostatic field. Furthermore, we shall show that the accumulation of "impurities" is, in fact, the result of nuclear activities yielding elements not originally present.

To provide rational interpretation, one must (i) define the system and its initial conditions, (*ie* the conditions just before the cell placement in an electric field), (ii) consider the interaction of the field with the system and, in particular, with a conductor, liquid dielectric and the relationship between the surface forces and the bulk response, (iii) examine the effect of the field on the operation of individual components of the electrochemical cell.

1.1 System and its behavior

An operating cell is viewed as a system consisting of three subsystems, *viz* the electrolyte, the interphase and the bulk Pd/D. The interphase itself is an assembly of non-autonomous layers as defined by van Rysselberghe[4]. The electrolyte, an ionic conductor, is treated as a dielectric with added extraneous charges (positive and negative ions). The Pd/D material is a conductor containing, in addition to free electrons, mobile positive particles, the D^+ complexes. Just before the application of an external field, all intensive state variables are constant in time, *ie* all irreversible processes inside the system occur continuously (there is continuous exchange between the system and surroundings). The processes involved are: reduction of D^+/D_2O ions/molecules and the evolution of deuterium. The mechanism of these reactions is not important except to say that all operating driving forces remain constant in time.

The system's reference state is maintained by an overpotential, η. The vanishing of all mass fluxes (at the reference state) demands that all chemical potentials be equal. The overpotential acts as an external potential, *ie* it determines the distribution of all mobile charges as well as their electrochemical potentials. The ionization $D^{(l)} \rightarrow D^{+}$, complex and precursor formation occur in an s-electron rich environment, *ie* where $q^{+} << q^{-}$.

The IR imaging of the electrode surface shows that excess heat is generated at discrete locations which, in turn, implies the formation of domains. The existence of hot spots indicates the presence of highly energetic fast reactions which, in turn, produce pressure and temperature waves traveling through the electrode. Indeed, such waves were observed by the response of a pressure sensitive material onto which the Pd/D films were deposited[5].

1.2 System far from equilibrium

The characteristics of systems far from equilibrium are: (i) the formation of new structures is always the result of an instability which may be due to either internal or external fluctuations to the system, (ii) fluctuation is always followed by the response which may bring the system to its original conditions or may produce a new structure, (iii) the system's stability is determined by a complex interplay of kinetic and thermodynamic quantities (*ie* no statement can be made that is independent of kinetic considerations), (iv) chemical instabilities lead to spontaneous "self-organization" if the system is able to exchange part of the energy or matter with the outside world in order to establish a microscopic internal order (an open system must be maintained, if self-organization is to occur), (v) as the overpotential is increased, the probability of cluster formation increases (increase in the rate of formation of hot spots).

Parenthetically, in systems far from equilibrium the complexes can be viewed as "supermolecules" where the physical laws, as formulated for systems at or near equilibrium, may not apply. To quote: "....there exist new dynamic states of matter induced by a flow of free energy far from equilibrium. Such states are governed by a new physical chemistry on a supermolecular level, while all laws referring to the molecular level, remain essentially unchanged. In all cases considered, the coherent behaviour on the supermolecular level corresponds in fact to an amplification of specific molecular properties (such as kinetic constants) in far from thermodynamic equilibrium conditions" [6, p. 290].

1.3 Field interactions with cell components

(i) Conductors. Introduction of an uncharged conductor into the field reduces the total energy of the field. An uncharged conductor located outside the field is attracted towards the field. A conductor, charged or not, when placed in an electric field cannot remain in stable equilibrium. Consequently, if a conductor is constrained then it will suffer shape change, either reversible or permanent, depending upon conditions at the surface and the time involved.

(ii) Electrolyte. The electrolyte phase contains mobile positive and negative ions distributed in a manner that assures charge neutrality (except at boundaries). It is known that an ion in contact with water is solvated, which means that the central ion is surrounded by an oppositely charged ionic

cloud. When subjected to an electric field, each ion is acted upon with a net force representing the difference between the accelerating force arising from the applied field and the opposing forces, *viz* (i) the electrophoretic contribution associated with the structure of the moving entity and (ii) the force connected with the relaxation of the ionic cloud[7].

(iii) Interphase. Charging of the Pd lattice with hydrogen isotopes by electrochemical means occurs through a number of consecutive processes, *ie* charge transfer, adsorption, absorption *etc*. These processes define the thermodynamic structure of the interphase (as opposed to its physical structure). The set of processes involved is as follows: $D^{+(b}{}_1{}^{)} \rightarrow D^{+(r}{}_1{}^{)} \rightarrow D^{\theta} \rightarrow D^{(b}{}_2{}^{)} \rightarrow D^{(l)} \rightarrow D^{(r}{}_2{}^{)} \rightarrow [(D^{+} \cdot e^{-})_n - D^{+}]$ denoting charge transfer, adsorption, absorption, placement in Pd lattice, ionization, complex formation[8].

(iv) The bulk Pd/D. Any charge on a conductor must be located at its surface. Charged mobile species (D^+ complexes) are also present in the bulk Pd/D material. In general, they will not be affected by an external field, since no field can exist there. However, in the present case, they might be affected by the field generated by the flow of the cell current, *ie* the electro-diffusion might occur.

(v) Internal stresses - shape change. The relationship between the surface forces and the bulk response is given by

$$\int div A d\tau = \oint A_n d\sigma \qquad (1)$$

where the *div* operator derives a vector from tensor. The left side term is the algebraic sum of all sources/sinks continuously distributed over the volume element. The right side defines the outflow, if positive and the inflow, if negative. Equation (1) indicates that forces acting on any finite volume in a body can be reduced to forces applied to the surface of that volume and *vice versa.* Consequently, it follows that the shape change at constant volume is associated with motion due to internal forces acting on the surface. Thus, the deformation will be determined by the distribution of surface forces, while the rate of deformation by their magnitude.

Internal stresses can be present without the presence of external loads, *eg* due to inhomogeneities, imperfections, *etc* a likely situation in the co-deposited film and the continuous evolution of deuterium.

(vi) Location/size. The presence of discrete, randomly distributed sites (hot spots, craters, boulders, *etc*) implies the existence of volumes within the electrode material where conditions promoting the highly energetic reactions exist. In estimating their magnitude, one must make a certain number of assumptions, *eg* (i) energy per single event is that of the reaction $D + D \rightarrow He$, (ii) the number of single events to produce a crater is on the order of 10^4 or higher, depending upon its radius[9], (iii) the number of single events needed to generate the "hot spot" displayed by IR imaging is on the order of 10^4 or higher, depending upon its size and brightness. Under these conditions and assuming the loading ratio greater than unity, one can calculate the radius of this volume to be on the order of 100 Å or higher. The events take place within the bulk material in the close vicinity to the contact surface.

2.0 Experimental/Results

An operating PdD//D_2O, 0.3 M LiCl//Pt cell was placed in an electrostatic field generated by a parallel plate capacitor where the field strength was maintained and controlled by setting the potential difference at a specified level. The cell geometry is shown in Fig. 1. The Pd/D electrode was prepared by the Pd deposition onto an Au foil from a solution of 0.03M $PdCl_2$ + 0.3M LiCl dissolved in D_2O. The electrodeposition was under galvanostatic control with the current profile as follows: 1.0 mA cm^{-2} for 8 hrs, 3mA cm^{-2} for 8 hrs and at 5.0 mA cm^{-2} until all Pd^{2+} ions were reduced. Upon completion of the Pd deposition, the cell current was increased to a value needed to maintain a visible gas evolution (usually 30 - 50 mA cm^{-2}) for the next 2 - 3 hrs followed by placement in an external electric field (1000 - 3000 V cm^{-1}) with the cell current increased to about 100 mA cm^{-2} for the next 48 hrs or longer.

Figure 1. An electrochemical cell. 1 - clear plastic (acrylic) wall. 2 - Pt screen. 3 - Co--deposited PdD layer. 4 - Au foil. 5 - Cu foil. Cell connected to a galvanostat; electric field maintained by a regulated high voltage source (not shown).

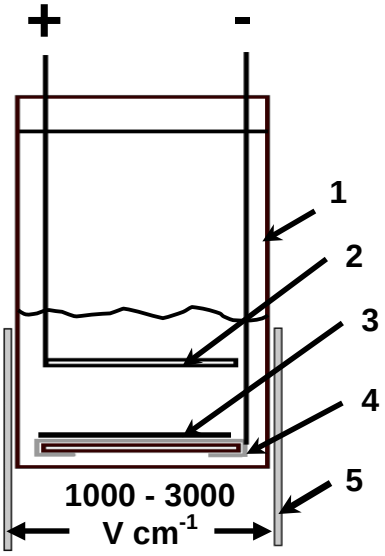

The surface morphology and the bulk structure of the co-deposited Pd/D film, shown in Fig. 2a, undergoes substantial changes when the operating cell is placed in an external electrostatic field. This is illustrated in a series of SEM photographs taken from various runs. In the absence of an electric field, the electrode structure consists of globules, 3 - 7 μm in diameter, arranged in short columns. Each of the individual globules is an aggregate of much smaller, almost spherical units, having a diameter in a sub-micron range. This structure is uniform throughout the electrode.

2.1 Morphological changes - minor deformations

The first noticeable effect, seen shortly after placing the cell in an electric field, is swelling of the co-deposited material followed by displacement toward the negative capacitor plate. The re-orientation without substantial change in their size is shown in Fig. 2b. We selected examples of various structures to emphasize the complexity of the system as well as to indicate the impossibility of a quantitative analysis. The selected examples include minor deformation of the original structure, definitive shape change, unusual structures to a deformation associated with, what appears to be, a localized catastrophic event.

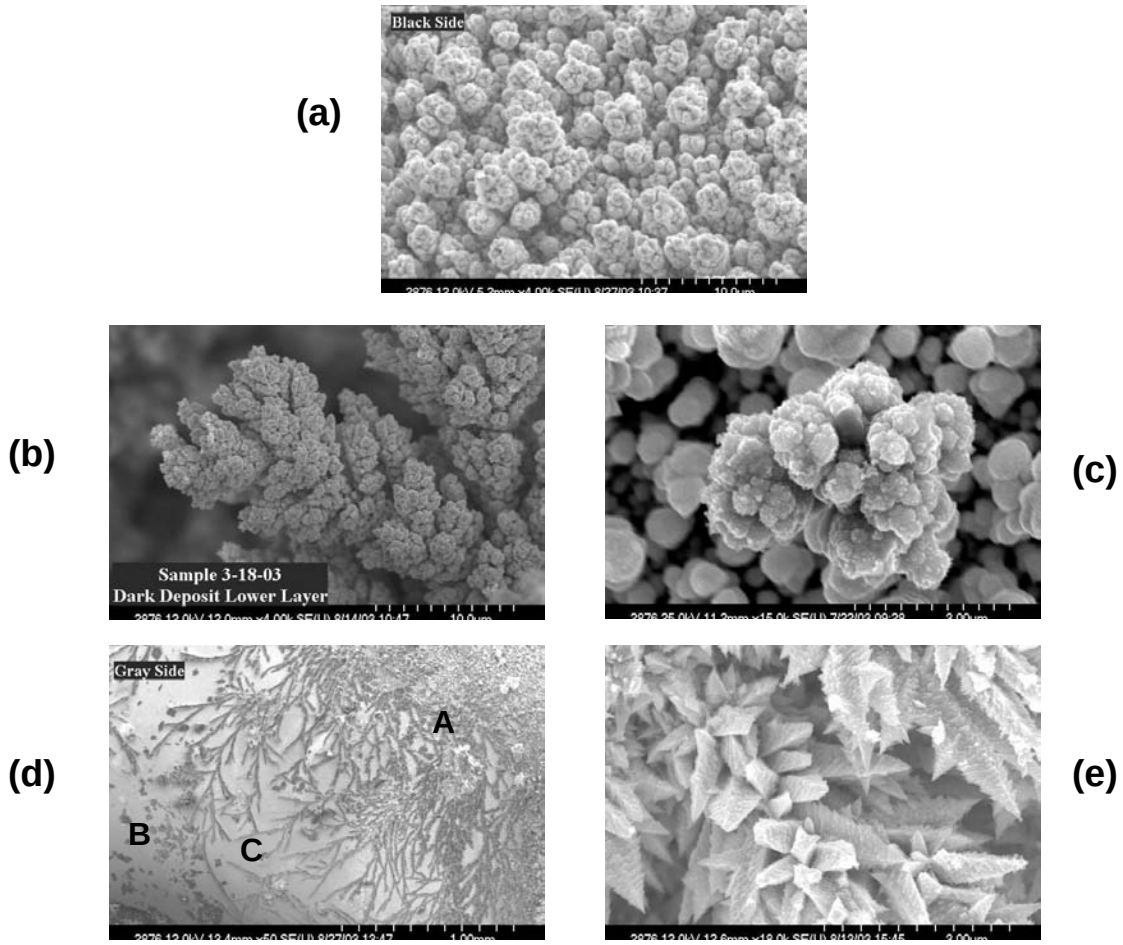

Figure 2. An illustration of minor morphological changes. a - reference morphology (no field). b - re-orientation. c - disintegration. d - branches (fractals). e - dendritic growth.

Another example of the disintegration of the Pd/D structure is shown in Fig. 2c. This figure illustrates the breaking of the bonds holding together the individual globules. The breaking of the bonding and the separation of globules may be due to action of the electric field alone or may be due to combined action of electrical and mechanical forces arising from the bulk material response to the changing magnitude of the surface forces.

A different set of processes appears to be responsible for the structural changes, *viz* (i) formation of branches (fractals), Fig. 2d and (ii) the production of dendritic growth, Fig. 2e. In what follows, we argue that these two very different forms may have a common origin, namely that they are the result of a combined action of the current flow through a porous structure, the presence of evolving deuterium, and the electric field on the separated micro-globules suspended in the electrolyte and restricted by the porous structure.

The observed morphological and structural changes occur during the reduction of D^+/D_2O ions/molecules at the porous electrode. Thus, at least three factors should be considered: (i) the external field, (ii) the distribution of the cell current and (iii) the presence of gaseous deuterium

within the confines of the structure. Since the depth of current penetration (for a given electrode kinetics, current density, *etc*) into electrode depends on pore size and assuming that all factors are involved, a different response to the field is expected at different sites of the Pd/D material. At sites of a relatively large pore size, the micro-globules are acted upon by two factors, the electric field and the convective flow due to mixing by the evolving deuterium. The electric field redistributes the surface charges while the evolving gas brings micro-globules in contact with each other. Viewing Fig. 2d we identify three areas having distinct features: area A with high density of branches and un-attached micro-globules, area B which is sparsely populated by micro-globules and area C where the un-attached micro-globules are absent and where branches are well defined. The latter indicates that the growth of branches by addition of micro-globules leading to an apparent reversal of the action of an electric field.

Entirely different situations exist in small pore sizes; the pore wall may be covered by gaseous deuterium, thus shifting the cell current deeper into the porous structure. If a micro-globule is placed into the current path, and if the potential drop over the length of the micro-globule in the electrolyte is greater than the sum of cathodic and anodic overpotentials needed to dissolve Pd and deposit the Pd^{2+} ions, then the dendritic growth is possible[11].

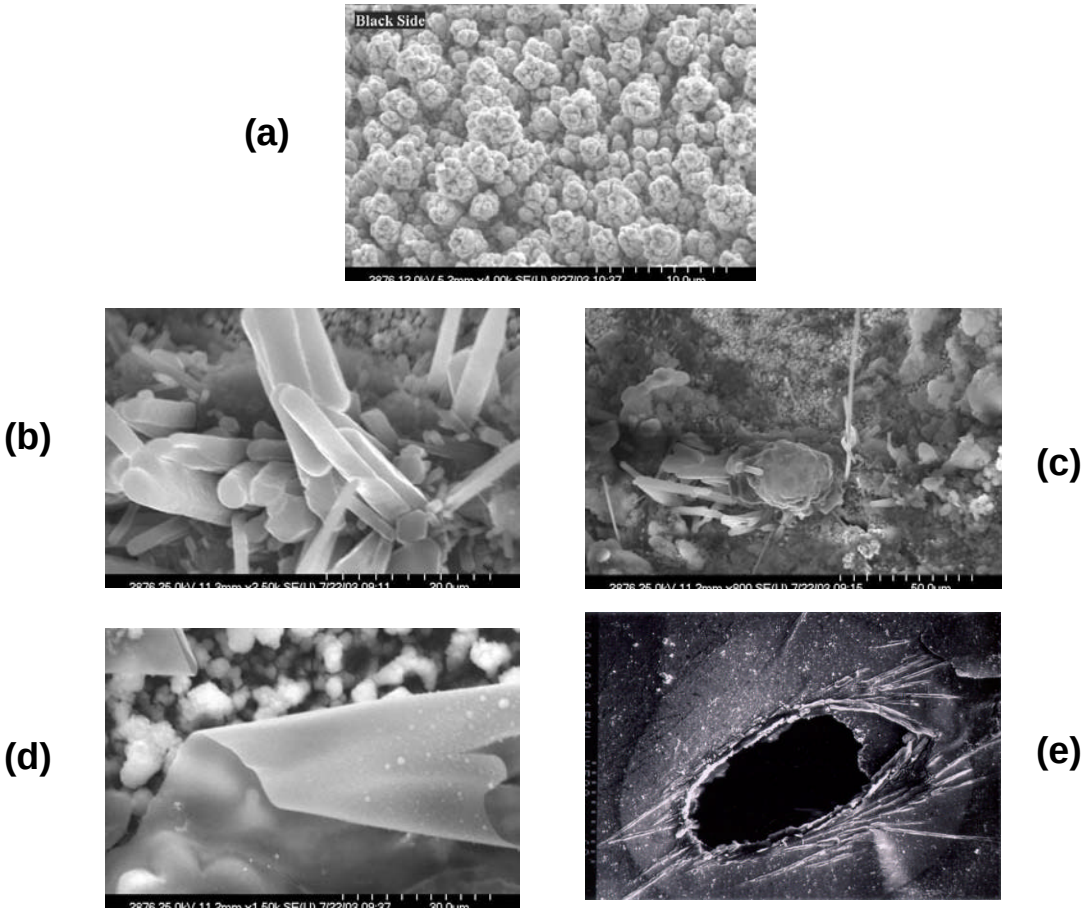

Figure 3. An illustrattion of significant morphological changes. a - reference morphology (no field). b - circular and square rods. c - boulder and long wire. d - folded thin layer. e - crater.

2.2 Morphological changes - shape changes

The transition from the "cauliflower-like" morphology to other forms is expected due to an interaction of the electric field and the response of a solid to the action of surface forces. While the morphologies shown in Figs. 2b - 2e can be accounted for, those in Figs. 3b - 3e suggest that additional factors are involved in producing the observed shape changes. Of the great variety of forms, we selected those illustrating the re-shaping of the spherical globules into (i) rods (circular and square), (ii) long wire, (iii) folded thin film and (iv) a crater, the latter suggesting the presence of a violent event. These structural changes require substantial energy expenditure, far in excess of that that can be extracted from the electric field. One such source is of nuclear origin as first suggested by Fleischmann *et al* [12]. and supported by the emission of soft X-rays[13], charged particles[14] and tritium[15] and helium[16] production.

The SEM photographs, Figs. 3b-3e, show well defined areas that seem to represent solidification of molten metal occurring under a liquid. If, as suggested earlier (*vide supra*) that the energy needed to melt a metal is of nuclear origin, then the chemical analysis of these distinctly different areas should reflect it. To illustrate, we selected three morphologically different cases, *viz* (i) a thin layer detached from the Au substrate, Fig. 4, (ii) boulder-like region, Fig. 5, and (iii) a place where, most likely, a catastrophic event has occurred, Fig. 6.

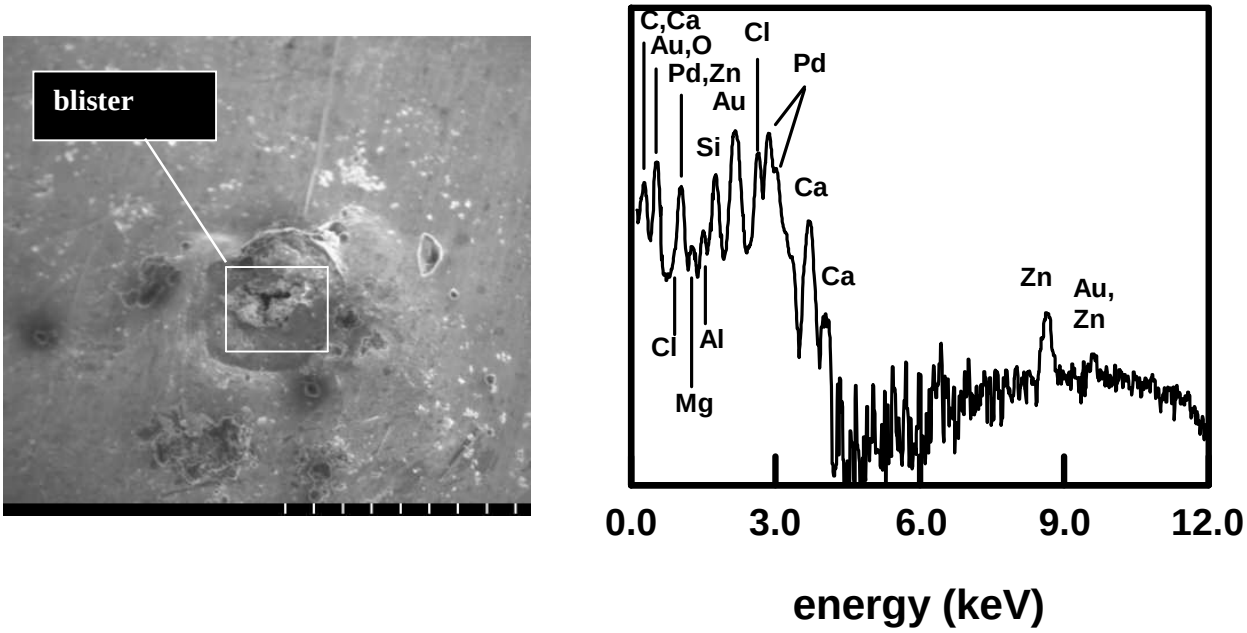

Figure 4. SEM of Pd/D electrode, after being placed in an external electrostatic field, showing a "blister-like" deformation. XRF spectra showing the chemical composition of the blister.

Analysis of the detached thin film, Fig. 4, showed the presence of Ca, Al, Si, Mg, Zn and Au, O and Cl. Since the latter three elements are present in the cell components, they cannot be attributed to nuclear events (futher experiments are needed for verification). The presence of these new elements on the electrode surface, after a long term polarization, was claimed to be due to the concentration of impurities[2,3]. While we cannot express an opinion as to the validity of such statement, we can show unambiguously that in our experiments this is not the case. The impurities,

whether originating from solution or from cell components should be uniformly distributed over the electrode surface and not concentrated in clearly recognizable spots. In addition, to minimize the notion that they are the result of contamination, initiated in either solution or cell components, we selected two cases: the boulder-like, Fig. 5 , and the crater-like segments of the electrode surface, Fig. 6. Analysis of the boulder-like segment showed the presence of a single element, Al, and that resembling a crater, the presence of two elements, namely Mg and Al. Without the aid of a Maxwell demon, it would be difficult to argue that such directed motion of impurities can take place. The only sensible answer is that they were produced in the course of electrolysis of D_2O in a cell placed in an external electric field by nuclear events.

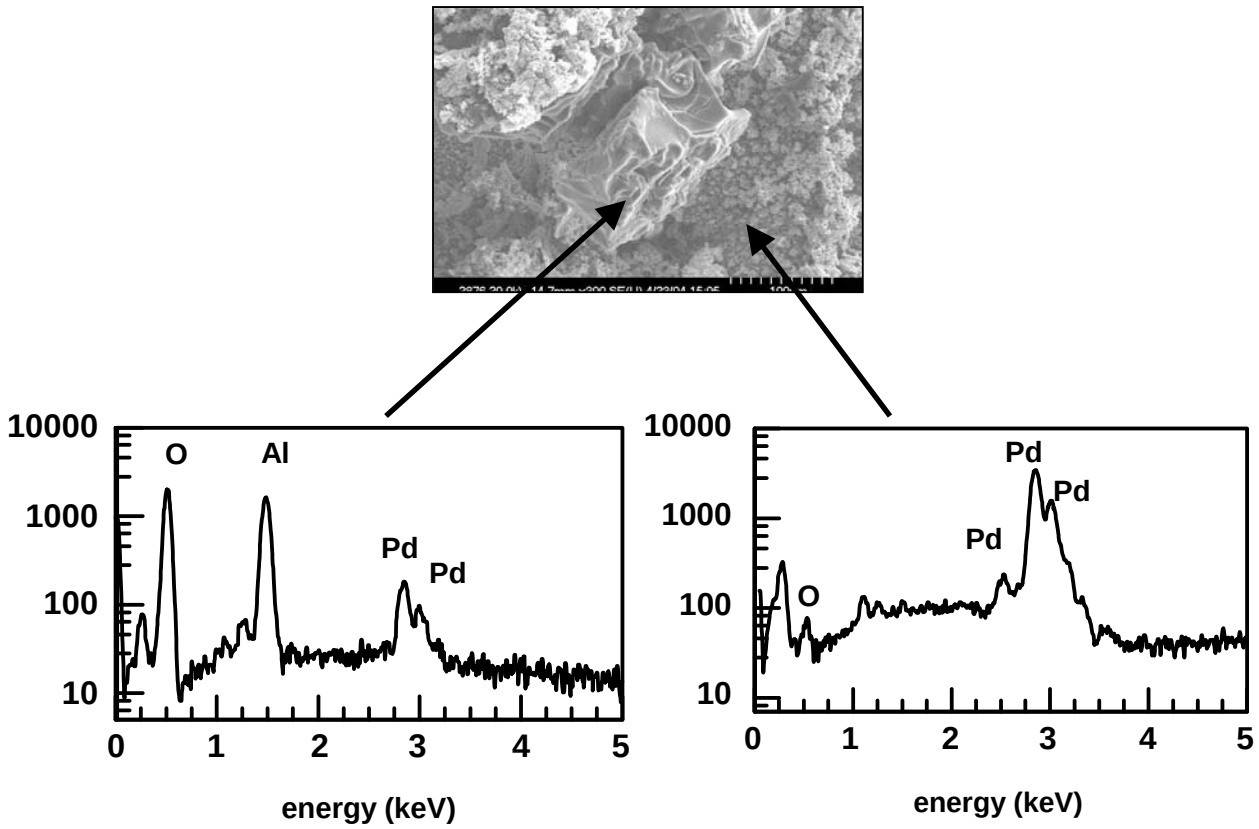

Figure 5. SEM of Pd/D electrode, after being placed in an external electrostatic field, showing a "boulder-like" deformation. XRF spectra showing the chemical composition of the boulder and the area adjacent to the boulder.

2.3 More about reaction sites

The progression of an experimental research, *experiment → interpretation of results → conclusions → new experiment → etc*, is illustrated in Figs. 7a - 7c. In a separate study[10], we showed that the excess heat is not produced continuously over the entire electrode volume but at isolated, randomly distributed in time and space, reaction sites. The short lived "hot spots", Fig. 7a, are, in fact, "mini—explosions" arising from fast and highly energetic reactions. Such "mini—explosions" can be displayed by bringing an excess heat generating electrode in contact with an appropriate sensor.

Indeed, by co-depositing the Pd/D film onto a piezoelectric substrate, one can display the pressure and temperature waves, originating within the bulk electrode, as they arrive at the sensor's surface, Fig. 7b.

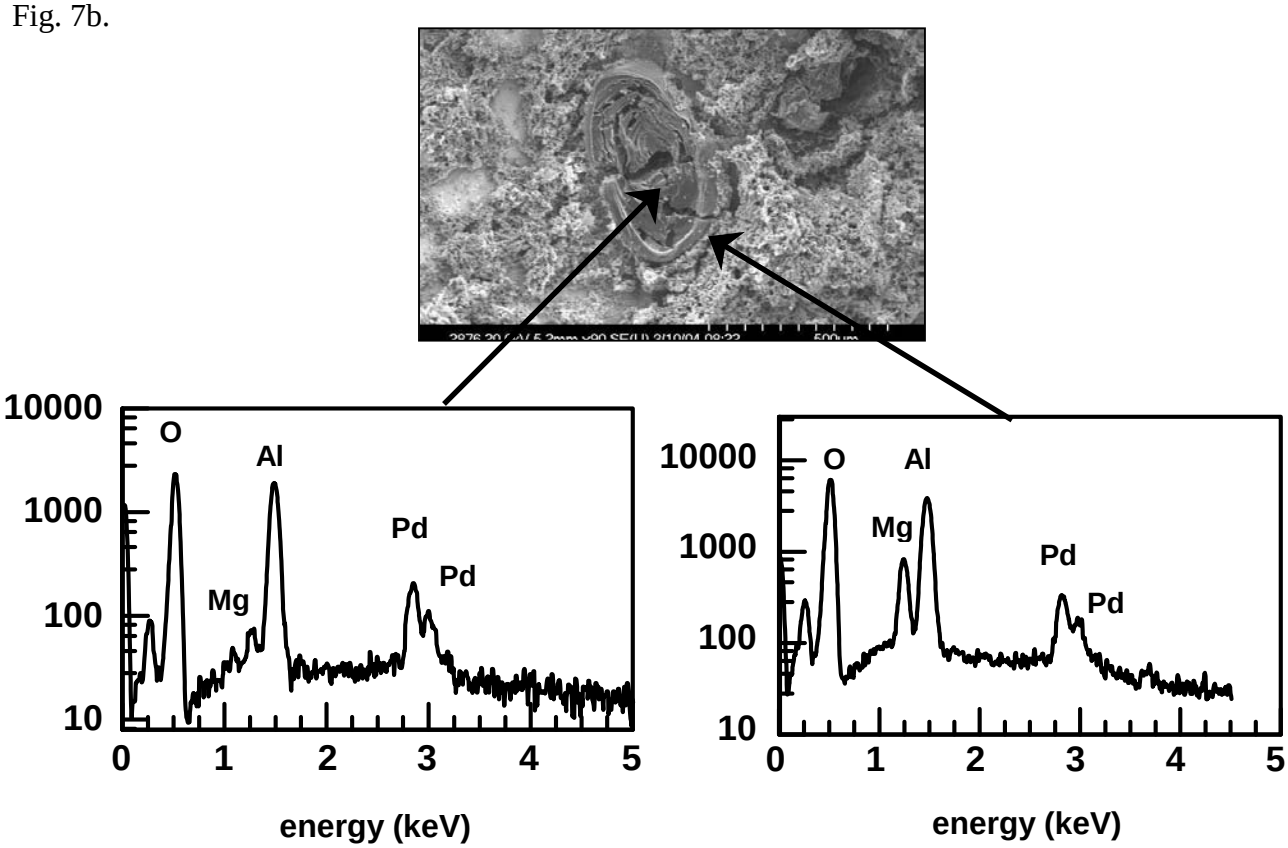

Figure 6. SEM of Pd/D electrode, after being placed in an external electrostatic field, showing a "crater -like" deformation. XRF spectra showing the chemical composition of the inside and outer rim of the crater.

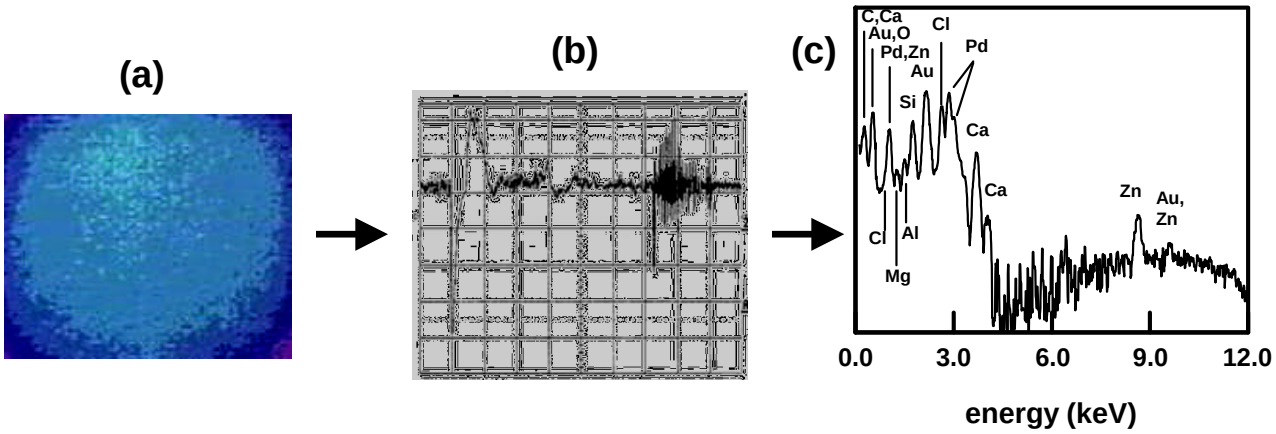

Figure 7. Sites and energetics of events. a - discrete hot spots. b- mini-explosion(s). c - chemical composition indicating nuclear origin.

In accordance with the concept that one experiment leads to another we noted the following: An analysis of experimental results suggests that events occurring at the contact surface of the interphase region influence the events in the bulk, *ie* influence the intensity and type of the nuclear events through the interactions between the D^+ complexes and the Pd lattice assisted by the stress fields at the reaction sites. Consequently, by placing an operating cell in an external electric field one would expect to see effects quite different from those observed in the absence of field. This is illustrated in Fig.7c.

3.0 Discussion

The variety of forms/structures resulting from the exposure to an electric field can be divided in two groups *viz* those that arise from the co-operative and/or competitive interaction between cell components, relevant processes and their driving forces and those that require substantial energy expenditure.

3.1 Search for precursors.

In a previous communication[17] we examined the the behavior of the Pd/D-D_2O system using cyclic voltammetry. An analysis of voltammograms indicated the presence of what we have interpreted as D_2^+ species in analogy to the existing H_2^+ molecule-ion. The H_2^+ molecule-ion was first considered in electrochemical systems by Horiuti[18] and was modeled by Gryzinski[19]. Basically, it involves injection of an s-electron into an orbit in a manner so that $[(H^+ \cdot e^-)\text{-}H^+]$ molecule-ion is formed. Here, the s-electron effectively shields one of the H^+ ions. The s-electron injection can be written as follows: $H^+ + H^+ + e^- \rightarrow [(H^+ \cdot e^-)\text{-}H^+]$ indicating that (1) the reaction is of the electron-ion recombination type and that (2) shielding of one of the originally close H^+ ions removes the Coulomb barrier and creates chemical bond.

(i) Formation of $[(D^+ \cdot e^-)_n\text{-}D^+]$ molecule-ion. Using the same arguments, we have

$$D^+ + D^+ + e^- \rightarrow [(D^+ \cdot e^-)\text{-}D^+]$$

and, by addition of another D^+ ion

$$[(D^+ \cdot e^-)\text{-}D^+] + D^+ + e^- \rightarrow [(D^+ \cdot e^-)_2\text{-}D^+]$$

or, in general

$$[(D^+ \cdot e^-)_n\text{-}D^+] + D^+ + e^- \rightarrow [(D^+ \cdot e^-)_{n+1}\text{-}D^+]$$

Similarily, an addition of two complex molecule-ions can occur yielding

$$[(D^+ \cdot e^-)_m\text{-}D^+] + [(D^+ \cdot e^-)_n\text{-}D^+] + e^- \rightarrow [(D^+ \cdot e^-)_{m+n}\text{-}D^+]$$

These complexes interact with the Pd lattice – this is symbolically indicated as $Pd\cdots[(D^+ \cdot e^-)_n\text{-}D^+]$. Each of these reactions occurs with the rate constant that is affected by an electric field.

(ii) Complex distribution. The multiple reaction paths result in a distribution of complexes of varying number of $(D^+ \cdot e^-)$ units. Two factors would have to be considered when assessing the distribution pattern: the reaction rate constants and the stability (mechanical) of the complex $[(D^+ \cdot e^-)_n\text{-}D^+]$.

(a) Reaction rate. The reaction path can be viewed as an electron-ion recombination occurring in an external electric field. The effect of an electric field on the rate constant of such reactions was examined by Wojcik and Tachiya[20]. Evidently, the rate constant is affected by an external field in a way that depends on the conditions outside the molecule-ion boundary. In particular, the action of an external field may either accelerate or slow down the electron-ion recombination reaction.

(b) Mechanical stability. The mechanical stability of the $[(D^+ \cdot e^-)_n\text{-}D^+]$ as well as the stability of a domain (of complexes) $Pd\cdots[(D^+ \cdot e^-)_n\text{-}D^+]_N$ can be examined using the liquid drop analogy, *ie via* the energy considerations and, in particular, by the change in the potential energy associated with the deformation of the spherical drop. The energy of the complex molecule-ion (represented as a liquid drop) consists of two parts:(i) binding energy (energy needed to take the complex apart) and (ii) surface (capillary) energy while that of a domain includes also the electrostatic energy. To evaluate, one can employ the liquid drop model and carry out calculations in a manner similar to that used in assessing the stability of a nucleus.

(c) Distribution. Two distributions are considered (i) that of a $[(D^+ \cdot e^-)_n\text{-}D^+]$ complex and (ii) that of a $Pd\cdots[(D^+ \cdot e^-)_n\text{-}D^+]_N$ domain. In both cases, the stability conditions are derived from energy considerations associated with the shape change resulting from the motion of components (charged or not) that occur within the molecule-ion or the domain. In both cases, capillary energy plays an important role. The shape changes arise from fluctuations which, in turn, modify the magnitudes of the potential and kinetic energies of the molecule-ion, respectively the $Pd\cdots[(D^+ \cdot e^-)_n\text{-}D^+]_N$ domain. The interaction with an environment (the Pd lattice and/or s-electrons) occurs in a coherent way.

3.2 Fusion reactions

(i) Fusion of light elements, T, He. The production of light elements (T and He) occurs *via* the following set of events:

(i) An s-electron is captured by the molecule-ion, $[(D^+ \cdot e^-)\text{-}D^+]$, so that the precursor $[(D^+ \cdot e^-)\text{-}D^*]$ is formed, $([(D^+ \cdot e^-)\text{-}D^+] + e_s^- \rightarrow [(D^+ \cdot e^-)\text{-}D^*])$. The electron capture (K-capture) is favored at the "heavy end" of the periodic table where the K-orbits are small and the probability of an electron to be at nucleus is large. In our case, the high probability is assured by high concentration of energetic s-electrons within the domains. The rate of transmutation of the molecule-ion to a precursor increases with an increase in the chemical potential of s-electrons. This can be demonstrated as follows: for the reaction $_ZM^A + e_s^- \rightarrow {}_{Z-1}X^A + \nu$ at equilibrium, the chemical potentials must be equal. The chemical potential of a single molecule (here, the precursor) is just its internal energy, $-\varepsilon$. Consequently, $-\varepsilon_M + \mu(e^-) = -\varepsilon_X$. Now, since the neutrino leaves the system, its chemical potential does not appear and furthermore, an increase in the s-electron concentration or their energies, tends to increase the e_s^- capture. Following the s-electron capture the electrostatic energy of the complex molecule-ion is reduced causing its collapse to the precursor.

(ii) The electron capture effectively changes the nature of the force acting between the shielded deuterons, *ie* change from chemical bonding to nuclear forces, to form $[(D^+ \cdot e^-) \cdots D^*]$ or $_1(X)^4$, a highly excited nucleus.
(iii) The excited nucleus can decay *via* the β emission to He: $_1(X)^4 - e^- \rightarrow {}_2He^4$
and *via* the proton emission followed by β emission to T: $_1(X)^4 - p^+ \rightarrow {}_0(X)^3 - e^- \rightarrow {}_1X^3 = T$
(emission of charged particles was observed).

(ii) Fusion of heavier elements, qualitative observations. Fusion of heavier elements, *eg* Al, Mg, Si, Ca, Zn, *etc*. occurs (in our system) when an operating cell is placed in an external electric field. Qualitatively, the newly fused elements are found to be randomly distributed over the electrode surface area indicating highly localized reaction sites. The analysis of the reaction sites show either a single element, *eg* Al, or more than one element, *eg* Al and Mg. There appears to be some correlation between the structure of the reaction site, as displayed by SEM, and the number of fused elements present. A common feature exhibited in both cases (presence or absence of field) is the presence of highly localized reaction sites (Note the hot spots displayed by IR imaging in the absence of field).

(iii) Proposed fusion mechanism for heavier elements. In formulating the fusion mechanism, we note the following:
(a) Fusion must be a single event in the sense that it follows the reaction scheme:
precursor + trigger $\rightarrow$ unstable "nucleus" $\rightarrow$ stable nucleus.
One triggering mechanism might be due to e_s^- -capture assisted by local conditions, *eg* stress field, electric field, *etc*.
(b) Fusion must involve events within the precursor as well as to provide the balancing charge of electrons in the K,L,M,N,.. orbits.
(c) Fusion to heavier elements (in our system) requires the presence of an external electrostatic field. The fields used in our experiments were on the order of 10^3 V cm^{-1}, *ie* too small to affect chemical bonding within the precursor. Consequently, there are a number of questions that need to be answered, *viz* how the field interacts with the system as a whole to produce precursors containing a large number of $(D^+ \cdot e^-)_n$ elements within the $[(D^+ \cdot e^-)_n - D^+]$ complex. Is the fusion reaction leading to multiple elements due to a single large precursor which disintegrates when in an excited state to yield multiple elements, or is a number of precursors present within the domain?

4.0 Concluding remarks

1. The most obvious effect of an external electric field is the shape change of the individual globules of the "cauliflower" structure of the co-deposited material. With the shape change there is a change in the defects density as well as in the stress field intensity. Both these factors affect the interaction between the D^+-complexes and the Pd lattice, *ie* they contribute to the formation of the $Pd \cdots [(D^+ \cdot e^-)_n - D^+]_N$ domains.

2. The concentration of the D^+-complexes is determined by the overpotential. The effect of an external electric field is minimal.

3. Excess enthalpy is generated by highly energetic fast reactions that resemble "mini-explosions".

This view is supported by IR imaging (hot spots), by the response of the pressure/temperature sensitive substrates (piezoelectric material) onto which the Pd/D films are co-deposited and by SEM examination and analysis of selected isolated spots showing elements not originally present.

4. The formation of precursors as well as the fusion reactions is of the type: A + B $\rightarrow$C + D. As written, this statement implies conservation of matter - otherwise, both the reactants and products are not constrained. In practice however, the initial conditions of the reactants are specified by the experimental protocol while those of products by energy considerations and the rate constants. If such reaction occurs in, *eg* the Pd lattice, additional constraints are operative. Consequently, in the reaction: ${}_{Z}M^{A} + e_{s}^{-} \rightarrow {}_{Z-1}X^{A} + \nu$, the particles are constrained by an interaction with the Pd lattice. This, we indicate by writing $Pd\cdots {}_{Z}M^{A}$, *etc*. It is with this in mind that we examine the effects of placing an operating cell in an external electrostatic field.

5. The triggering activities (to initiate fusion reactions) are located within the first few atomic layers and, most likely, involve changes in the electronic structure of this region. These changes are transferred deeper into the Pd lattice where the nuclear events occur.

References

1. S. Pons and M. Fleischmann, *Calorimetry of the palladium--deuterium system,* Proc. ICCF-1, p.1 (1990).
2. D.R. Rolison and P.P. Trzaskoma, J. Electroanal. Chem., **287**, 375 (1990).
3. D.R. Rolison, W.E. O'Grady, R.F. Doyle and P.P. Trzaskoma, *Anomalies in the surface analysis of deuterated palladium,* Proc. ICCF-1, p. 272 (1990).
4. P. van Rysselberghe, *Some Aspects of the Thermodynamic Structure of Electrochemistry* in *Modern Aspects of Electrochemistry* vol. 4, J. O'M. Bockris, ed., Plenum Press, New York, 1966.
5. S. Szpak, P.A. Mosier-Boss, J. Dea and F.E Gordon, *Polarised D^{+}/Pd-D_2O system: Hot spots and mini-explosion,* Proc. ICCF - 10, p. 113 (2003).
6. P. Glansdorff and I. Prigogine, *Thermodynamic Theory of Structure, Stability and Fluctuations*, Wiley-Interscience.
7. J. O'M. Bockris and A.K.N. Reddy, *Modern Electrochemistry*, Plenum Press, New York, 1974.
8. S. Szpak and P.A. Mosier-Boss, Nuovo Cimento, submitted.
9. George Russ, http://d2fusion.com/volcanoes.html.
10. P.A. Mosier-Boss and S. Szpak, Nouvo Cimento, **112A**, 577 (1999).
11. S. Szpak, T. Katan and P.J. Carlen, J. Electrochem. Soc., **133**, 1340 (1986).
12. M. Fleischmann, S. Pons and M. Hawkins, J. Electroanal. Chem., **201**, 301 (1989).
13. S. Szpak, P.A. Mosier-Boss and J.J. Smith, Physics Letters A, **210**, 382 (1996).
14. A.G. Lipson, A.S. Roussetski, G.M. Miley and E.I. Saunin, *Phenomenon of an energetic charged particle emission from hydrogen/deuterium loaded metals,* Proc. ICCF - 10 (2003).
15. S. Szpak, P.A. Mosier-Boss, R.D. Boss and J.J. Smith, Fusion Technol., **33**, 38 (1998).
16. B.F. Bush, J.J. Lagowski, M.H. Miles and G.S. Ostrom, J. Electroanal. Chem., **304**, 271 (1991).
17. S. Szpak, P.A. Mosier-Boss and R.S. Scharber, J. Electroanal. Chem., **337**, 147 (1992).
18. J. Horiuti, *The mechanism of the hydrogen electrode reaction* in *Transactions of the symposium on electrode processes*, E. Yeager, ed., J. Wiley & Sons, New York, 1961.
19. M. Gryzinski, Physics Letters A, **123**, 170 (1987).
20. M. Wojcik and M. Tachiya, J. Chem. Physics, **109**, 3999 (1998).

(blank page)

(blank page)

THE DYNAMICS OF THE Pd/D-D_2O-Li^+ SYSTEM AS A PRECURSOR TO THE FLEISCHMANN-PONS EFFECT

S. Szpak, P.A. Mosier-Boss and J. Dea

Spawar Systems Center San Diego, San Diego, CA 92152-5001

Summary – The dynamics of excess heat generation is discussed in terms of the electrode/electrolyte interphase, processes in the reaction space and the effect of overpotential acting as an external force. The origin and properties of the active regions, derived from the IR imaging and piezoelectric sensing, is discussed. The importance of free electrons on the initiation of the F-P effect is noted.

1.0 Introduction

The characteristic feature of the polarized Pd/D_2O-Li^+ system, as demonstrated by calorimetry, is the generation of excess enthalpy, the F-P effect[1]. However, because a calorimeter is an integrating device, it cannot provide an answer to a number of questions, *viz*. (i) where are the excess enthalpy producing reactions located? (ii) are these continuous or discrete heat sources? (iii) if discrete then what is the sequence of processes that lead to instabilities?

In an attempt to seek an answer, we selected a set of experimental facts from which some conclusions can be drawn. For example, the poor reproducibility and the variable conditions initiating the F-P effect, indicate the existence of thresholds while the bursts in eg tritium production[2], suggest the presence of non-equilibrium states that favor the formation of active domains. Such domains, if they are the seat of the heat generating reaction sites, could be displayed by infrared imaging. Indeed, active sites have been observed on surfaces of electrodes prepared by the co-deposition process[3].

Facts lead to deductions which, in turn, suggest new experiments. The observed “hot spots”, with the steep temperature gradients and of short duration, indicate that these high intensity heat sources can be viewed as mini-explosions. Such events have been displayed by the Pd/D films co-deposited on pressure sensitive surfaces of a piezoelectric material[4].

In an earlier communication[5], we presented an example of discrete heat sources. Here, we discuss the evolution of the electrode surface temperature in a greater detail, provide supporting evidence for the presence of discrete heat sources by displaying the associated pressure gradients and discuss the conditions leading to the formation of unstable domains.

2.0 Experimental

The Pd/D electrode was prepared by the co-deposition technique, a process involving simultaneous reduction of Pd^{2+} ions and heavy water. The electrolyte composition was as follows: 0.03 M $PdCl_2$, + 0.3 M LiCI + D_2O. The co-deposition was carried out at a very low cell current, on the order of $\mu A/cm^2$ during the first hour followed by a gradual increase to cell currents corresponding to several hundred mA/cm^2 for the next two hours.

2.1 Evolution of thermal activities

The evolution of thermal activities in the negatively polarized Pd/D_2O system was examined using an experimental arrangement shown in Figs. la and lb. Figure 1a illustrates the position of an infrared camera facing the negative electrode. To record the evolution of thermal behavior it is necessary to place the negative electrode, a Ni screen, upon which a deuterium saturated Pd film was deposited, very close to the thin cell wall (Mylar film). The infrared camera was operated in two modes: the first, to measure the cell temperature across the cell (along the X-X line), Fig. 1b and the second, to record the temperature distribution on the electrode surface to display the presence of hot spots).

(i) Cell temperature profile

A typical cell temperature profile is shown in Fig. 2, where the A-B section indicates the electrode surface temperature while sections C-D and E-F the solution temperature. The cell temperature profile, plotted in Fig. 3, was taken periodically during the electrolysis. Evidently, the difference between the electrode surface temperature and that in solution, ΔT, increases with time, being initially at *ca* 2 ° C and reaching a value as high as *ca* 17 ° two hours later. It is noteworthy that the increase in the surface temperature, curve a, is irregular indicating bursts in excess enthalpy generation. In contrast, the solution temperature, curve b, increases smoothly which is an expected behavior because the weight (volume) of solution substantially exceeds that of the Pd/D electrode assembly.

Incidently, Bedeaux and Ratkje[6] provided a rationale for the temperature difference arising from coupling of interfacial processes. There is no doubt that dissipative processes contribute to the observed ΔT. However, this contribution is negligible for a system operating at conditions of this experiment.

(ii) Development of hot spots

Thermal activity in the form of “hot spots,” Figs. 4a - 4d, were detected early during the Pd/D co-deposition process. Judging from the number of hot spots, we note that (i) the rate of heat generation is not uniform, (ii) thermal activities occur at low cell temperature and at low cell currents. These observations seem to contradict the commonly held view that long incubation

times are required and current densities in excess of 100 mA/cm^2 are always needed to initiate and maintain the F-P effect.

The intensity of thermal activity increases with an increase in both cell temperature and cell current. An example is shown in Fig. 5. Here, the temperature of hot spots cannot be estimated because it exceeded the camera range. This conclusion is supported by the temperature profile across the electrode surface shown in Fig. 5b. Note that the location of hot spots coincides with the temperature distribution in Fig. 5b.

(iii) Propagation of pressure gradients

An expected consequence of localized heat sources is lattice distortion and the development and propagation of stresses within the Pd/D lattice. The display of mechanical distortion can be followed by co-depositing the Pd/D films onto a pressure sensitive substrate, eg piezoelectric ceramic material[4]. Now, piezoelectricity is characterized by a one-to-one correspondence of direct and inverse effects, ie the internal stresses resulting from the electric field are proportional to the field itself and the deformation is accompanied by the appearance of a field proportional to the deformation. Because of high sensitivity, its use as a sensing device must be done under strictly controlled conditions. To eliminate external factors that might interfere with the interpretation of the sensor's response, the electrochemical cell was shielded (Faraday cage) and the whole assembly placed on a shock absorbing material, as illustrated in Fig. 6. An ideal response of a piezoelectric sensing device to thermal mini-explosion is illustrated in Fig. 7. In general, there are two types of forces that interact with the piezoelectric material, *viz.* those that cause the contraction of the piezoelectric material and those that result in its expansion. An example of the first kind is the pressure change due to eg appearance of localized heat source within the Pd/D film; of the second kind – the change in temperature of the piezoelectric material.

A single isolated event is shown in Fig. 8. Here, we see clearly a single voltage spike which, in the negative direction, corresponds to the pressure pulse. After a brief period of time, Δt = 0.06 sec., we note the arrival of the temperature front (voltage spike in the positive direction), followed by the system relaxation. Using a simple model, eg that of a spherical reaction site, one could, from the magnitude of the voltage spikes and the Δt reach some conclusion concerning the position and strength of the heat source. Such singular events are seen in the early periods of the co-deposition. Interestingly, these voltage bursts persisted for hours following the termination of current flow.

A typical voltage-time behavior indicating a burst of events within the Pd/D film is shown in Fig. 9. These bursts were observed at constant current densities as low as *ca* 4.0 μA cm^{-2}. An expanded trace of such bursts shows a series of voltage spikes, indicated by arrows. Their frequency and intensity increased with an increase in the cell current and cell temperature. At temperature near the boiling point, thermal activities were very intense as indicated by the magnitude of the voltage spikes, illustrated in Fig. 10.

3.0 Discussion

The appearance of discrete reaction sites implies the transition from a stable to an unstable situation, alternatively a transition from non-reactive to reactive sites. We regard the formation of these domains as being the last step prior to the initiation of the F-P effect. The lack of kinetic data does not permit us to carry any quantitative assessment. However, the thermodynamic reasoning can offer, in a qualitative way, some useful information needed to formulate a phenomenological model consistent with the observed instabilities.

In what follows, we examine the associated dynamics leading to the instabilities of what should be otherwise a stable behavior, *via* (i) the construction of an interphase across which deuterium transport occurs, and (ii) the system's response to perturbations in the cell current/potential. Finally, we demonstrate the correctness of the model *via* the selected experimental observations.

3.1 Construction of the Pd/D_2O interphase

The equilibrium state of an electrified interphase may be defined either through the boundary conditions or by imposing given values to the selected variables. On the other hand, in non-equilibrium situations, the system can only be defined through the boundary conditions. Here, as in an earlier communication[5], we follow closely the procedure outlined by van Rysselberghe[7] and Defay et al.[8]. Briefly, the interphase region consists of a set of non-autonomous layers where the overall overpotential can be broken into parts pertaining to the various layers and where these layers are determined by the sequence of processes/reactions. Each layer of the set of non-autonomous layers is homogeneous and of sufficiently large volume so that the concentration and temperature are well defined and their location is given by the driving forces, the chemical potentials. The structure of the Pd/D-D_2O interphase arises from the set of steps involved in the electrochemical charging *viz.* electroreduction of D^+ ions in the reaction layer, followed by adsorption, absorption, placement in the Pd lattice, ionization (dissociation), and transport into the bulk metal.

Restricting our attention to the relevant, part of the structure of the interphase and the processes therein, Fig. 11, we examine the dynamics of the Pd/D-D_2O system under the following set of assumptions: (i) the e^-'s are treated as component as are the D_{ad}, D_{ab}, D_l D_l^+ species[9] (ii) only the weakly bound D_{ad}'s are absorbed[10,11], (iii) the transition from D_{ad} to D_{ab} is fast so that during charging they remain in quasi-equilibrium[11]; (iv) ionization, $D_l \leftrightarrow D_l^+ + e_l^-$ is considered a chemical reaction.

3.2 Response of the Pd/D system to perturbations

The energy of the Pd/D system, subject to action of an external potential, η, is a function of state variables, $U = U(S, V, n, .. , \eta)$. Here, the discussion is limited to the response to the variation in overpotential and includes: identification of the reference system, the stability with respect to $\delta\eta$, the evolution of the supercharged layer and the formation of active domains.

3.2.1 Reference state

The Pd/D electrode charged to the β- phase is characterized as follows: (i) All octahedral sites are occupied (ii) the overpotential, η, acts as an external potential, ie it determines the distribution of all mobile charges (both D^+ and e^-), (iii) the homogeneous bulk phases (electrode and electrolyte) are separated by an inhomogeneous interphase region consisting of a set of homogeneous segments (layers) defined by the individual steps of the charging/discharging process, (iv) ionization occurs in a s-electron rich environment, ie $q_- >> q_+$ (v) in the reference state all flow of matter is stopped – however, the flow of energy is permitted, ie the reference state is maintained by an overpotential, η, alternatively, by the cell current, I. The vanishing of all mass fluxes demands that all chemical potentials be equal. In the present case, it requires that $\mu^{(\theta)} = \mu^{(\alpha)} = \mu^{(\lambda)}$. In assessing the response of the variation in overpotential, $\delta\eta$, we take note of conditions (ii), (iv) and (v). In addition, we assume that the surface coverage, θ, remains constant, ie that the extra cell current, δI, is used exclusively for the deuterium evolution reaction. Thus, condition (iv) yields

$$\mu^{(r)} = \overline{\mu}_+^{(r)} + \overline{\mu}_-^{(r)} \tag{1}$$

With

$$\overline{\mu}_{(+,-)} = \overline{\mu}_{(+,-)}^0 + RTlnc_{(+,-)} + zq_{(+,-)}|\chi| \tag{2}$$

where $c_{(+,-)}$ are the volume concentrations, $q_{(+,-)}$ are the charge, χ is the potential. The subscripts +,- refer to deuterons and s-electrons, respectively and the superscripts identify the layer under consideration.

3.2.2 Stability with respect to $\delta\eta$

The negatively polarized Pd/D electrode of an operating electrochemical cell is a complex system. Its behavior with respect to perturbation in overpotential will be first examined by considering a set of thought experiments in which a closed system containing D, D^+ and e^- at equilibrium will be subjected to (i) action of an external potential, η, (ii) the addition of electrons in the absence of η and (iii) addition of electrons in the presence of η.

The action of an external potential on the system behavior enters through the effect on the respective chemical/electrochemical potentials as indicated by Eqs. (1) and (2). Thus,

(i) The external potential affects only charged species *via* the χ potential, Fig. 10. If the system contains an equal number of positively and negatively charged particles, then the action of an external potential cancels out.

(ii) If the number of negatively charged particles is greater than the number of positively charged (eg by addition of electrons) then the addition of negatively charged particles increases the

chemical potential, $\mu^{(r)}$ due to an increase in the second term of Eq. (2). The net result is the decrease in the concentration of positively charged particles.

(iii) The action of the external potential on the system with unequal number of charged particles is more complex. In the system where the negative charges exceed positive, the net result is the decrease of the $\mu^{(r)}$ (Note – logarithmic term in Eq. (2) changes slower than the linear term). The composition of the *quasi-equilibrium* is determined by both the excess of negative particles and the magnitude of the applied potential, ie $\mu^{(r)} = f[q_-, x]$. As the external potential is increased, the $\mu_+^{(r)}$ also increases. This fact will play an important role in the F-P effect (cf section 4.0).

3.2.3 Charging and the evolution of a supercharged layer

Even a small deviation from the reference state results in instability. By definition, $\mu = \partial U/\partial n|_{S,V,n,..}$. Consequently, the stability/instability of the Pd/D system with respect to varying overpotential is determined by taking the derivative of the chemical potential. The chemical potential of the adsorption layer depends linearly on overpotential, ie $\mu^{(\theta)}(\eta) = \mu^{(\theta)} + |\eta|F$[12] and $\mu_l = \overline{\mu}_+ + \overline{\mu}_-$. Substitution of (2) into (1), followed by differentiation, yields

$$\frac{\partial \mu^{(r)}}{\partial \chi} = -q_- \tag{3}$$

Since $\frac{\partial \mu^{(r)}}{\partial \chi} < 0$, so is also $\delta U < 0$, ie the system is unstable with respect to the variation in overpotential. The time rate of change of $n_+^{(r)}$ and $n^{(r)}$ is given by (4) and (5), respectively.

$$\frac{dn_+^{(r)}}{dt} = l_r A_r^{(r)} - l_m A_r^{(r\to m)} \tag{4}$$

$$\frac{dn^{(r)}}{dt} = l_\lambda A^{(\lambda\to r)} - l_r A^{(r)} \tag{5}$$

Combining (4) an (5) and noting that within the reaction space $dn_+^{(r)} = -dn^{(r)}$, we have

$$\frac{dn_+^{(r)}}{dt} = l_r A_r^{(r)} - \frac{1}{2}\left[l_\lambda A^{(\lambda\to r)} + l_r A_r^{(r\to m)}\right] \tag{6}$$

where A is the affinity [$A_r^{(r)} = \mu^{(r)} - \left(\overline{\mu}_+^{(r)} + \overline{\mu}_-^{(r)}\right)$, etc.] and *l*'s are the respective proportionality coefficients

The affinities are function of the state variables and the external potential, $\eta = \eta(\theta) + \psi$ where ψ is the potential in excess of that needed the maintenance of the reference state. Equation (6) shows in a qualitative way, the effect of ψ on the system behavior (see section 4.0).

3.2.4 Formation of active domains

CANR, the chemically assisted nuclear reactions is the acronym for the F-P effect, coined by Storms[12] who suggested that other than purely physical considerations should enter into the discussion of factors affecting the excess enthalpy generation, as well as manifestations of other nuclear activities. To quote "nuclear reactions can only occur when the required chemical environment is created." Unfortunately, no further elaboration was provided.

Some insight into the environment can be obtained from thermal analysis of the surface of electrodes prepared by the co-deposition technique. We refer to Figs. 4, 5, 8, 9 and 10, ie we refer to the activities recorded by the IR camera and the piezoelectric sensing device, namely incubation time, size, distribution and the effect of temperature.

(i) Incubation time – the discrete heat sources, were noted shortly after the initiation of current flow. Thus, they are located near the contact surface and the supercharged layer is formed instantaneously [13].

(ii) Size – the nuclear active site must contain a large number of single events to produce a visible image. Unfortunately, our experimental set-up could not yield quantitative assessment. However, based on other considerations, Chubb[14] estimated the number of single events to be between *ca* $10^4 - 10^9$.

(iii) Distribution - the random time/space distribution of hot spots as well as their varying intensity with time, Figs. 4a-4d, exclude the existence of fixed location of the nuclear-active-sites. Thus, the direct influence of structural aspects of the electrode material is doubtful. Rather, the random distribution and the varying intensity arises from the coupling of the various processes occurring on both sides of the contact surface in response to fluctuations, a point stressed by Fleischmann et al.[15].

(iv) Effect of temperature – both, the frequency and intensity are a strong function of temperature. In particular, both increase with an increase in temperature, exhibiting the so-called positive feedback, cf Figs. 3, 5 and 10. This is, perhaps, the most direct indication of the influence of the chemical environment.

To reiterate, active domains containing several thousands of particles are formed in the close proximity to the contact surface. The random distribution suggests that embryos of the new phase are generated as a result of fluctuations while the strong temperature dependency points out to the action of forces of the chemical nature. In earlier communications[5,16], we pointed out that changes in an external force, eg the overpotential substantially affect the dynamic behavior as well as the structure of the interphase which contains complexes of the form $[D...D]^+$. In a system containing high D^+/Pd ratio in an s-electron rich atmosphere (according to Preparata[17] *ca* 40 % of the metal volume is occupied by the s-electrons) and assisted by high external potential, the high value of the $\mu_+^{(r)}$ promotes the formation of deuteron clusters,

possibly of the form $[D_n^+ . e_m^-]$. Evidently, the s-electrons play a dominant role in the formation of assembly of complexes, $[D_n^+ e_m^-]$. An additional supporting evidence for the active participation of free electrons in the initiation of the F-P effect is the reproducible generation of excess enthalpy in Pd/B alloys[18] (each B atom donates three electrons) .

4.0 Predictive capabilities of the model

Fleischmann et al.[15] postulated that the excess enthalpy generation in the polarized Pd/D system can be adequately represented by a product of two functions – the first, containing the operational variables, the second – the state variables. McKubre et al.[19] noted that a model, that is consistent with the observed initiation of the F-P effect, must involve three factors: (i) average D/Pd loading ratio of, at least, 0.9, (ii) incubation time on the order of several hundred hours in excess of that needed for a complete saturation of the electrode with deuterium and (iii) changes in the power input. In their view, the long incubation time suggests that the d+d reaction may require one or more additional partners transferred from the electrolyte, (*eg* Li, B, Si) while the varying power input indicates a complex interplay of processes occurring on both sides of the contact surface.

The adsorbed deuterium is in an atomic state while it is in a nuclear state when involved in excess heat generation. The transition occurs within the reaction layer. Consequently, the events in the reaction layer are responsible for the system's behavior. To examine the predictive capabilities of the present model, we consider first a Pd rod (wire) immersed in the D_2O saturated with deuterium. The set of consecutive participating processes leading to the rest potential, is: adsorption → absorption → placement in the lattice → dissociation → transport by diffusion. It represents an open system with driving potential arising from the presence of the electric double layer. In the course of time, system comes to an equilibrium resulting in a rest potential, η_0.

The rest potential, η_0, is due to cooperation between the processes on both sides of the contact surface. A change in this potential affects the chemical potential of the adsorbed deuterium and initiates the processes described in Fig. 10 and expressed by Eq. (6).

The evaluation of Eq. (6) requires the knowledge of the effect of η on the individual chemical/electrochemical potentials and processes. The potential distribution, shown in Fig. 10, consists of two branches, the external potential, η and the internal potential, χ. Bearing in mind that the $\mu^{(\theta)}$ is a linear function of η[20], it follows that both, $\mu^{(\alpha)}$ and $\mu^{(\lambda)}$ are also linear functions of η while $\mu^{(r)} = \overline{\mu}_+^{(r)} + \overline{\mu}_-^{(r)}$ is a function of η and χ.

Equation (6) states that for a given value of q_- in the reaction space there is only one stationary state possible for each external potential. It occurs when $dn_+/dt = 0$. Futhermore, Eq. (6) states the following:

(i) The incubation time is defined as time required for the transition from one stationary state to another of higher D^+/Pd ratio. It can vary from sample to sample.

(ii) The high loading ratio is facilitated by high overpotentials and, therefore, at high power inputs and favored for high $q_{..}$. It can also vary from sample to sample.

The observation by DeNinno and Violante[21] that a pulsing regime consisting of short high potential/current pulse followed by longer low potential/current pulses greatly enhances the electrode loading. The present model accounts rather well for such behavior. An increase in the external potential increases also the internal potential which, in turn, increases the $\overline{\mu}_{+}^{(r)}$ and decreases the $\mu^{(r)}$ thus promoting an influx of D from the λ- layer. Upon lowering the potential (period of low current), the $\mu^{(r)}$ increases, thus preventing or substantially reducing the transfer back to the λ- layer but allowing an enhanced diffusion into the bulk metal. The action is analogous to a pumping action: at high potentials there is an accumulation of deuterium within the reaction space and during the low period there is an expulsion into the bulk metal. An effective low/high regime may vary from sample to sample.

The present model would also predict the behavior of the Pd/D co-deposited films. The generation of excess enthalpy is due to the loading ratio of D/Pd > 1.0. At such high ratios, the formation of clusters (reactive domains) is expected even at low overpotentials.

References

1. M. Fleischmann and S. Pons, J. Electroanal. Chem., **261**, 301 (1989)
2. S. Szpak, P.A. Mosier-Boss, R.D. Boss and J.J. Smith, Fusion Technology, **33**, 38 (1998)
3. S. Szpak, P.A. Mosier-Boss and J.J. Smith, ibid., **302**, 255 (1991)
4. J. Dea, P.A. Mosier-Boss and S. Szpak, *Thermal and pressure gradients in polarized Pd/D system*, American Physical Society Spring meeting, Indianapolis, IN April 2002
5. P.A. Mosier-Boss and S. Szpak, Nouvo Cim., **112A**, 577 (1999)
6. D. Bedeaux and S.l{. Ratkje, J. Electrochem. Soc., **143**,767 (1996)
7. P. van Rysselbrghe, *Some Aspects of the Thermdynamic Structure of Electrochemistry, in Modern Aspects of Electrochemistry*, J O'M. Bockris ed., vol. 4, Plenum Press, New York 1966
8. R. Defay, N. Ibl, E. Levart, G. Milazzo, G. Valensi and P. van Rysselberghe, J. Electroanal. Chem., **7**, 417 (1964)
9. G. Jerkiewicz and A. Zolfaghari, J. Electrochem. Soc., **143**, 1240 (1996)
10. H. J. Flitt and J. O'M. Bockris, J. Hydrogen Energy, **7**, 411 (1982)
11. B.E. Conway and G. Jerkiewicz, Z. phys. Chem., **183**, 281 (1994)
12. E. Storms, Proc. ICCF - 7, p. 356, Vancouver (Canada),
13. S. Szpak, P.A. Mosier-Boss and C.J. Gabriel, J. Electroanal. Chem., **365**, 275 (1994)
14. S. R. Chubb, private communication, April 2003
15. M. Fleischmann, S, Pons, M. LeRoux and J. Roulette, Trans. Fusion Technol., **26**, 323 (1994)
16. S. Szpak, P. A. Mosier-Boss, S. R. Scharber and J. J. Smith, J. Electroanal. Chem., **337**, 147 (1992)

17. G. Preparata, Trans. Fusion Technology, **26**, 397 (1994)
18. M.H. Miles, K.B. Johnson and M.A. Imam, *Electrochemical loading of hydrogen and deuterium into palladium and palladium-boron alloys*, ICCF-6.
19. M.C.H. McKubre, S. Crouch-Baker, A.M. Riley, 5.1. Smedley and F.L. Tanzanella, Frontiers of Cold Fusion, Universal Academy Press, Tokyo (Japan), 1993
20. P. van Rysselberghe, Bull. Ac. Roy. Belg., **22**, 1330 (1936); **23**, 416 (1937).
21. A. DeNinno and V. Violante, *Quasi-plasma transport model in deuterium overloaded palladium cathodes*, lCCF-3, p. 107

(blank page)

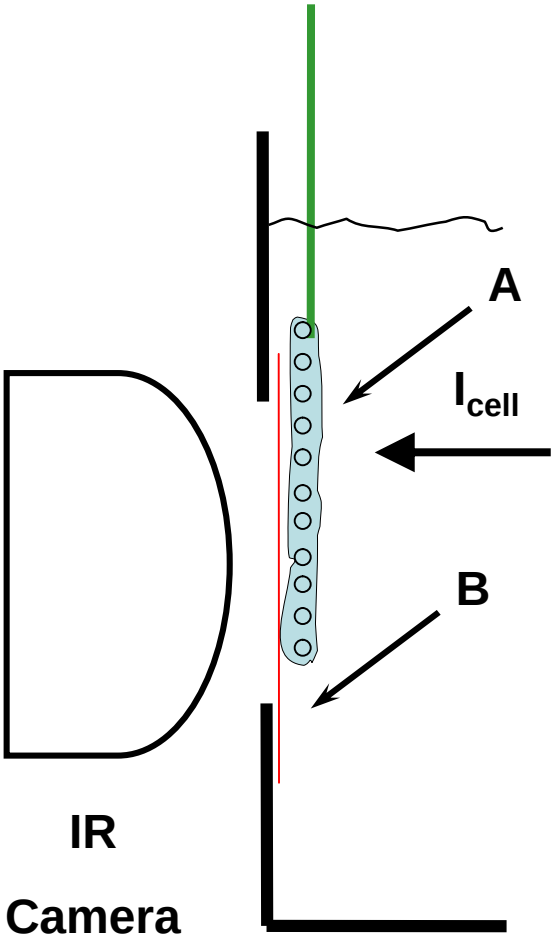

Fig. 1a

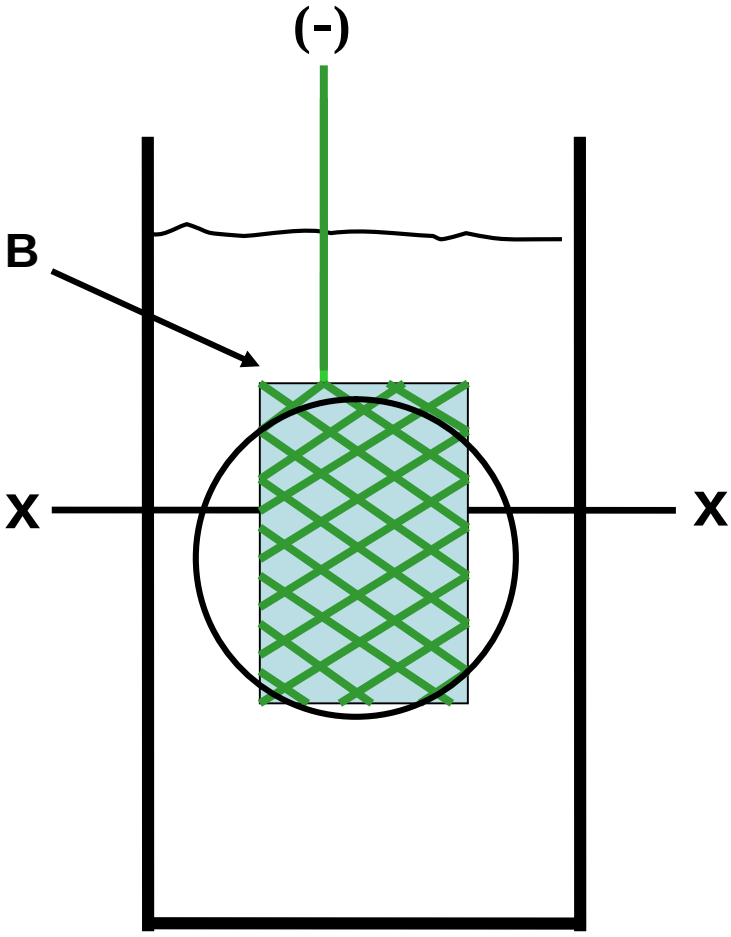

Fig. 1b

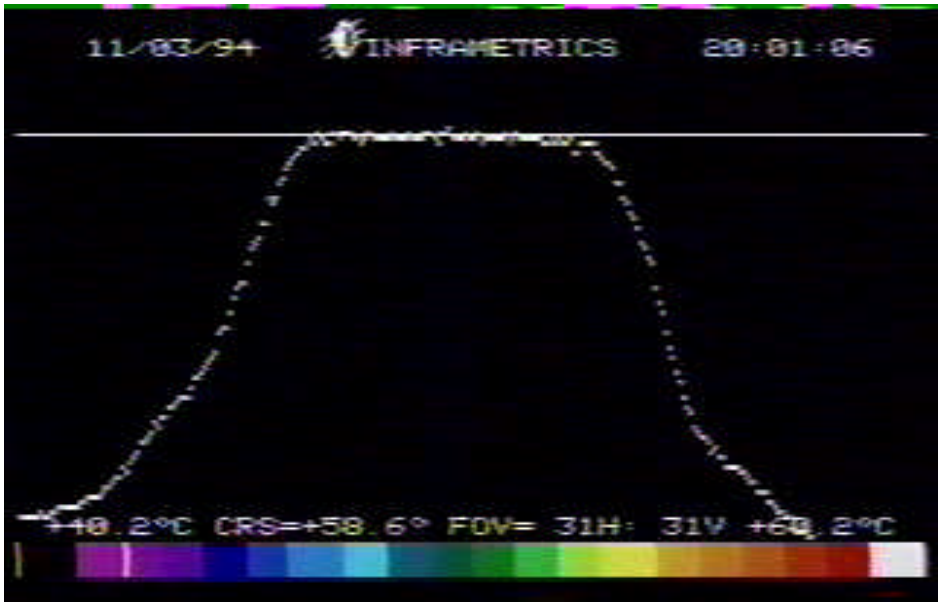

Fig. 2

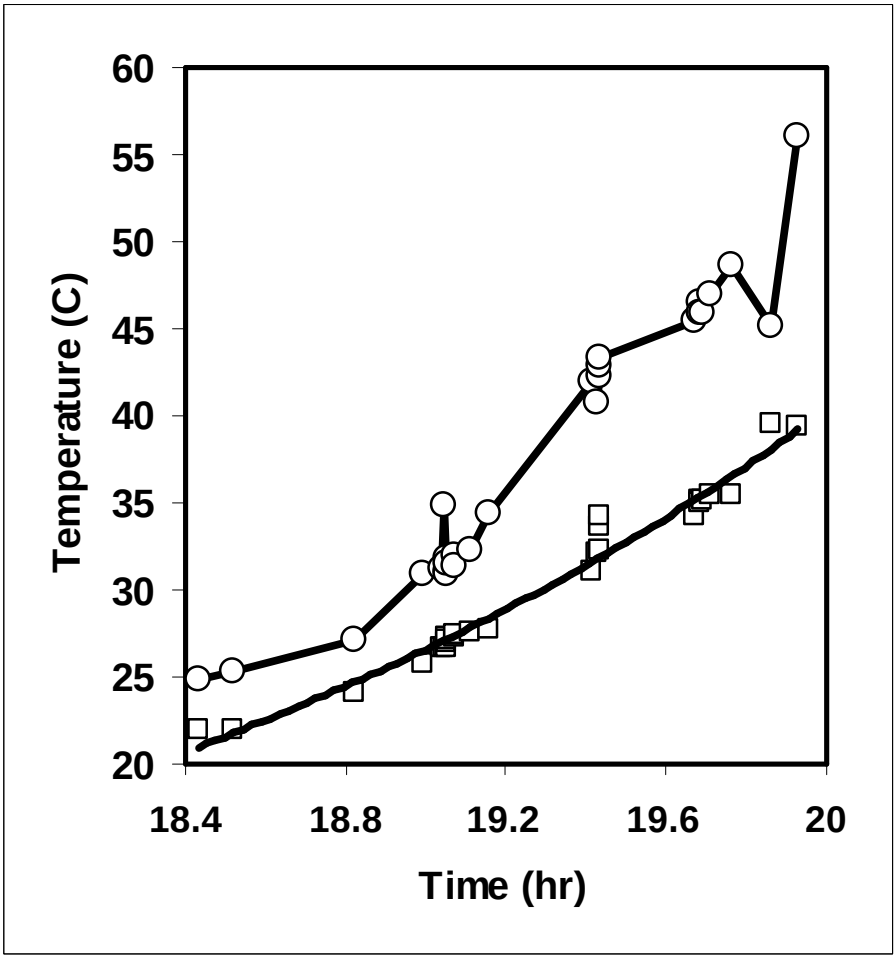
60
55
50
45
40
35
30
25
20
Temperature (C)
18.4
18.8
19.2
19.6
20
Time (hr)

Fig. 3

Fig. 4

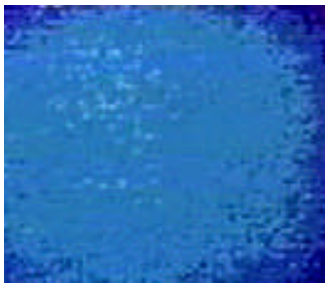

a = 18:59:00

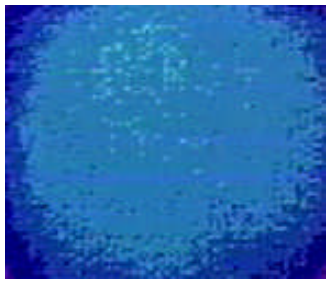

b = 18:59:18

c = 18:59:25

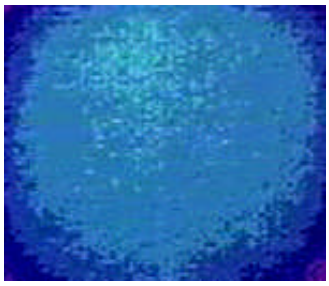

d = 18:59:33

temperature scale

Fig. 5

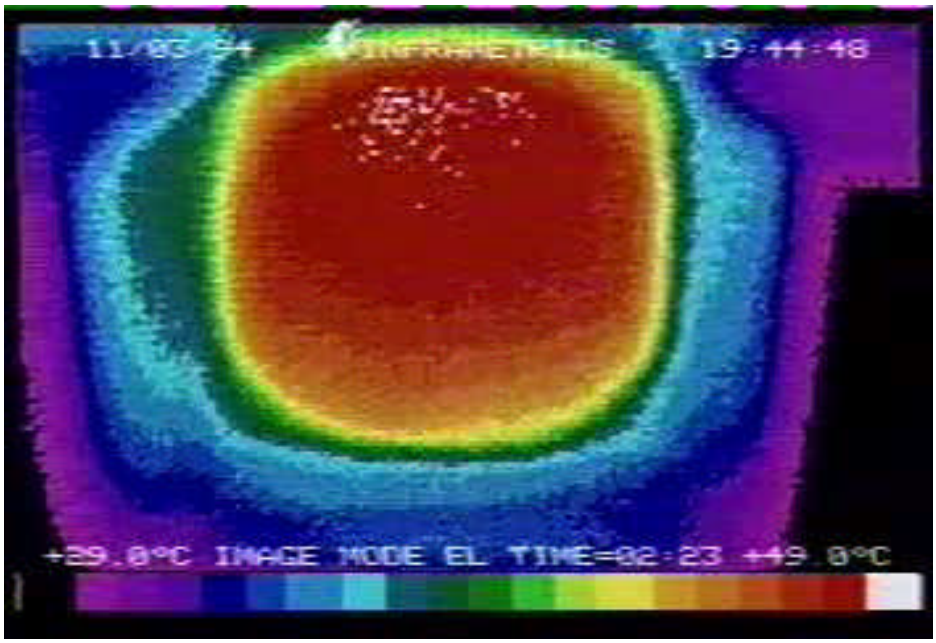

Experimental Arrangement

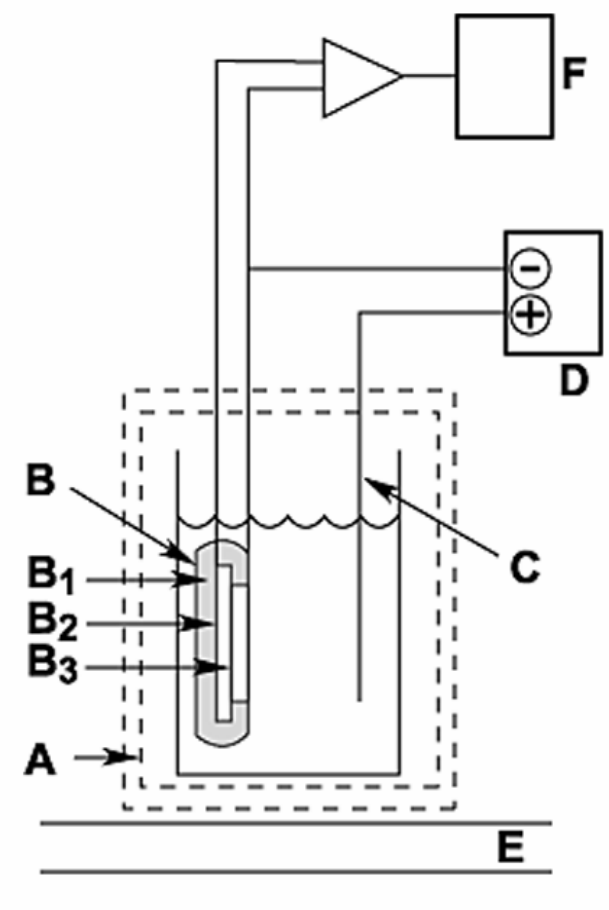

A – Faraday cage
B – negative electrode assembly (B1 – insulating material; B2 – piezoelectric substrate; B3 Pd/D film)
C – positive electrode
D – potentiostat/galvanostat
E – shock absorbing material
F – oscilloscope (LeCroy digital)
E – laboratory bench

Fig. 6

Methodology

Natural consequence of discrete heat sources is the distortion of the crystal lattice creating propagating stresses.

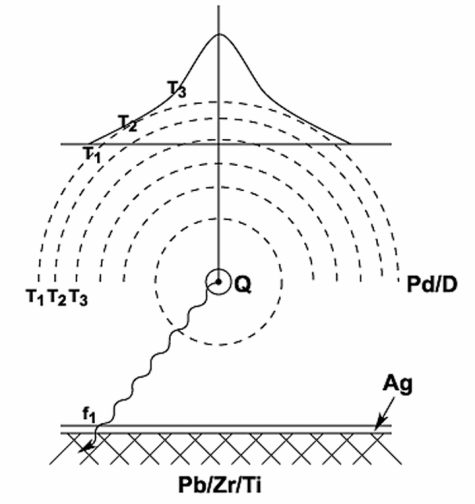

Construction of a pressure sensitive device. Co-deposition on piezoelectric substrate (lead-zirconium-titanate; r = 1.143 x 10^{-2} m; λ = 2.0x 10^{-3} m; Source: Piezokinetics, Bellefonte, PA).

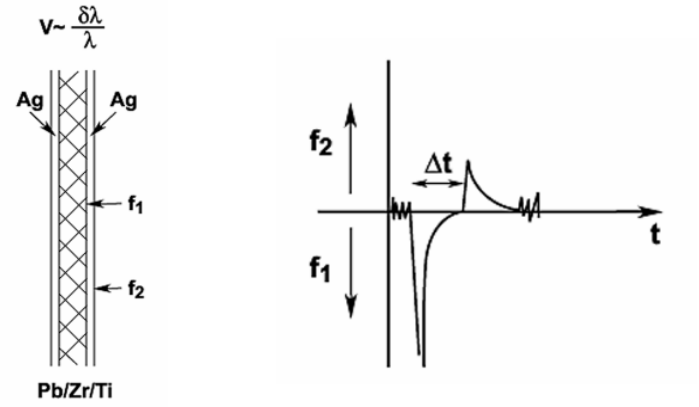

Piezoelectricity is characterized by a one-to-one correspondence of direct and inverse effects. Thus, internal stresses resulting from electric field are proportional to the field itself and the deformation is accompanied by the appearance of a field proportional to the deformation

Fig. 7

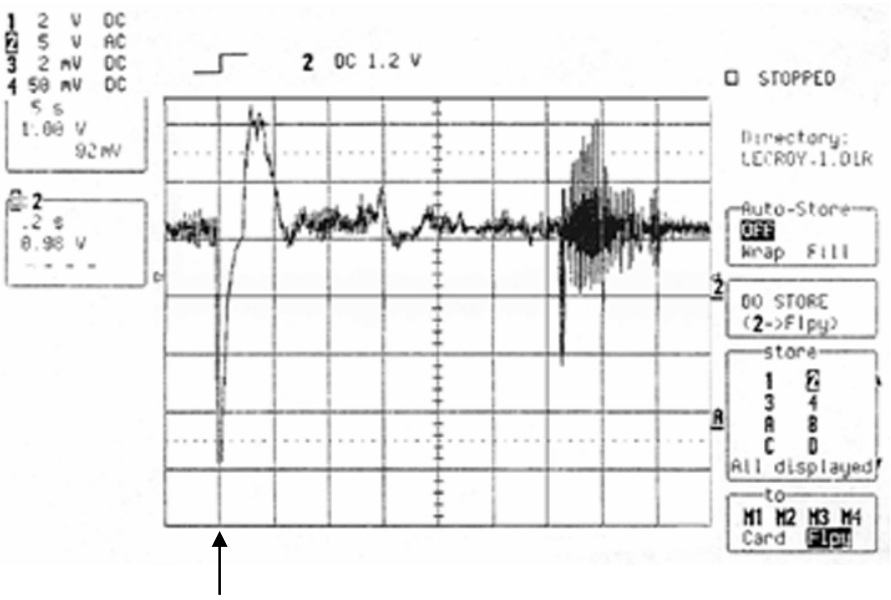
1 2 V DC
2 5 V AC
3 2 mV DC
4 50 mV DC
5 s
1.00 V
92 mV
2
.2 s
0.98 V
2 DC 1.2 V
STOPPED
Directory:
LECROY.1.DLR
Auto-Store
OFF
Wrap Fill
00 STORE
(2->Flpy)
Store
1 2
3 4
A B
C D
All displayed
to
M1 M2 M3 M4
Card Flpy

Fig. 8a

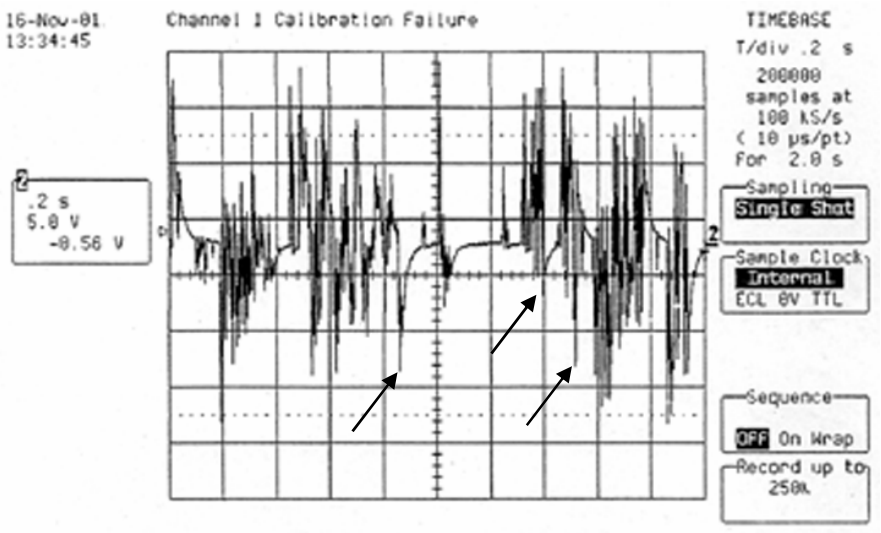
16-Nov-01
13:34:45
Channel 1 Calibration Failure
TIMEBASE
T/div .2 s
200000
samples at
100 kS/s
(10 µs/pt)
For 2.0 s
2
.2 s
5.0 V
-0.56 V
Sampling
Single Shot
Sample Clock
Internal
ECL 0V TTL
Sequence
OFF On Wrap
Record up to
250k

Fig. 8b

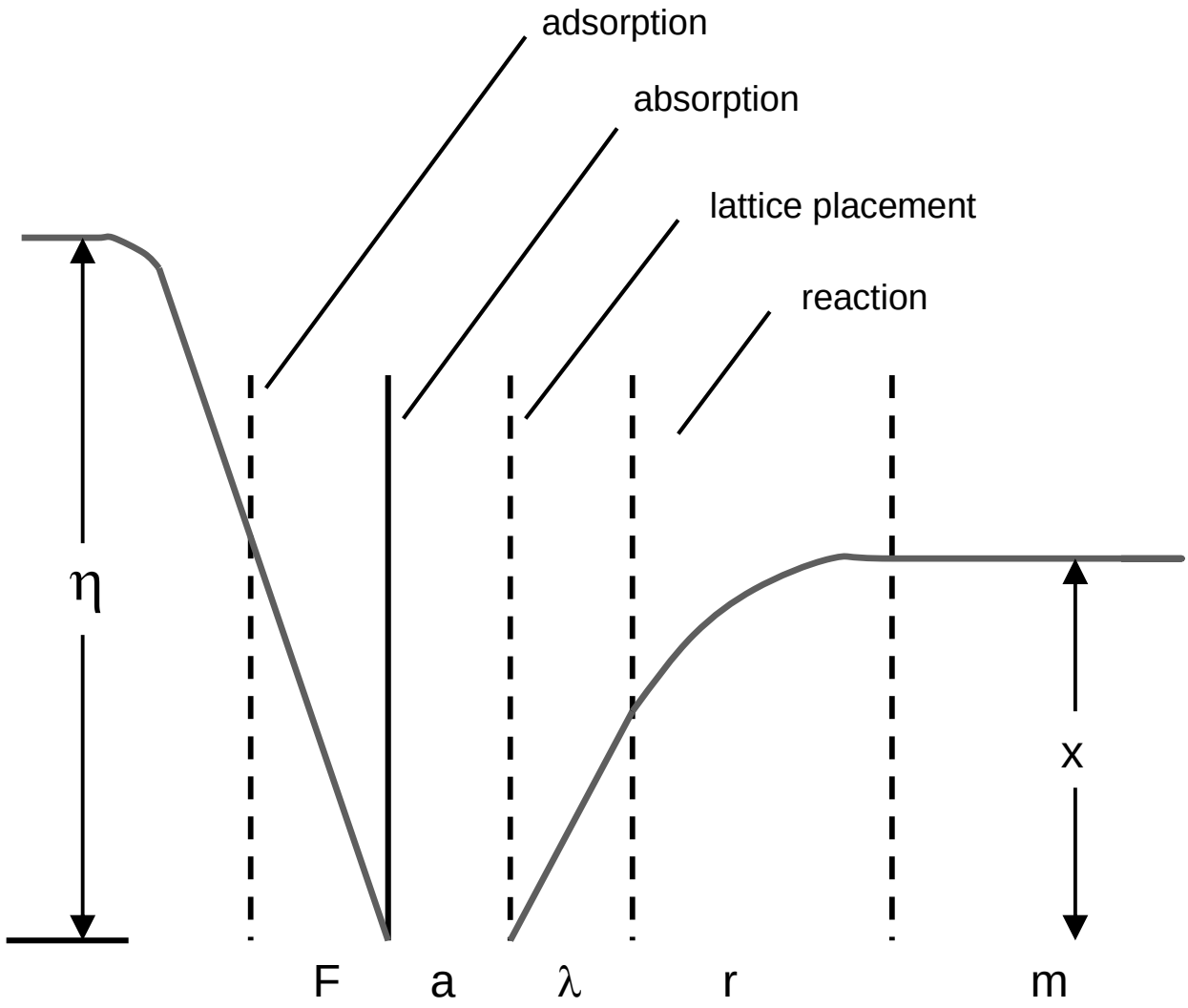
adsorption
absorption
lattice placement
reaction
η
x
F a λ r m

Fig. 10

A note on the development of temperature and pressure pulses in a polarized Pd/D system

J. Dea, P.A. Mosier-Boss and S. Szpak

Spawar Systems Center San Diego-San Diego, CA 92152-5001

Negatively polarized Pd/D electrodes, prepared by the co-deposition technique, and immersed in heavy water, generate excess enthalpy at well-defined spots randomly distributed in time and space[1-3]. An expected consequence of localized heat sources is lattice distortion and the development and propagation of stresses within the Pd/D film. While the presence of hot spots can be monitored by the IR imaging of the surface temperature[2,3], the display of mechanical distortions can be followed by co-depositing the Pd/D films onto a pressure sensitive substrate, eg piezoelectric ceramic material. Indeed, in the course of the Pd/D co-deposition on such substrates, we have observed voltage spikes that can be attributed to pressure and temperature pulses, occurring shortly after the initiation of current flow, as well as upon its termination.

Experimental

The experimental arrangement is shown in Fig. 1. The Pd/D co-deposition was carried out at constant cell current from a solution containing 0.03M $PdCl_2$, and 0.3M LiCl dissolved in D_2O. The Pd/D film was deposited onto a piezoelectric substrate (lead-zirconium-titanate; source: Piezokinetics, Bellefonte, PA) in the form of a disk, $r = 1.143 \times 10^{-2}$ m, $l = 2.0 \times 10^{-3}$ m with a deposited Ag film on both sides.

Results and interpretation

The interpretation is aided by consideration of the characteristic features of the co-deposition process and the cathode assembly. These are as follows:

(i) Co-deposition: The Pd/D co-deposition process involves simultaneous reduction of Pd^{2+} ions and heavy water. As the Pd^{2+} ions are depleted, especially at high cell currents, vigorous gas evolution takes place. The formation, growth and detachment of gas bubbles from the electrode surface are the sources of various forces acting on the electrode surface. Electrodes prepared by the co-deposition technique exhibit a "carpet-like" appearance, ie the structure that assures locally a non-uniform distribution of current density.

(ii) Piezoelectricity: Piezoelectricity is characterized by a one-to-one correspondence of direct and inverse effects[4]. Internal stresses resulting from the electric field are proportional to the field itself and the deformation is accompanied by the appearance of a field proportional to the deformation.

Voltage spikes

A typical voltage-time behavior indicating a burst of events within the Pd/D film, is shown in Fig. 2. These bursts were observed as early as a few minutes after the initiation of current flow and at current densities as low as *ca* 4 μA cm^{-2}, Fig. 2. Their frequency and intensity increased with an increase in the cell current. Interestingly, these voltage bursts persisted for hours/days upon termination of current flow.

An expanded trace of such bursts, Fig. 3 , shows a series of voltage spikes (indicated by arrows). These spikes represent a change in the forces acting on the surface. In general, there are two types of forces, *viz.* those that (i) cause contraction of the piezoelectric material and those that (ii) result in its expansion. An example of the first kind is a pressure change due to eg appearance of a localized heat source within the Pd/D film; of the second kind – detachment of gas bubbles and/or the change in temperature of the piezoelectric material. In addition, any local change in the current density would produce voltage spikes in the direction that depends on the change in the electric charge on surface, arising from eg changes in the cell current.

A single event isolated from a burst is shown Figs. 4 and 5. Here, we see clearly a single spike which, in the negative direction, corresponds to pressure pulse. After a brief period of time, Δt = 0.06 sec., we note the arrival of the temperature front (voltage in the positive direction), followed by the system relaxation. Using a simple model, eg that of a spherical reaction space one could from the magnitude of the voltage spikes and the Δt reach some information concerning the position and strength of the heat source. Other examples of measured piezoelectric responses of an operating cell as a function of time are shown in Figure 6. A more accurate assessment would require a calibration of the piezoelectric substrate – work currently in progress.

Concluding remarks

Co-deposition at high negative potentials results in the formation of an electrode structure that is not in equilibrium and that, in turn, is subject to of various gradients (eg chemical, mechanical and electrical). Simultaneous evolution of gas bubbles introduces an added component *viz.* a random distribution of localized gradients, ie it produces a number of forces that affect the piezoelectric material. Thus, it is the ambiguity that must be resolved for an accurate interpretation of the voltage spikes. However, because the voltage spikes are seen also at zero cell current, ie when the electrode is free from the evolving gases or changes in the surface charges, we can follow the progress in the behavior with confidence.

The significance of these points is as follows: the presence of pressure spikes during the co-deposition is consistent with the excess enthalpy generation reported by us earlier[3,5]. The occurrence of pressure gradients upon termination of current flow is expected in view of the heat-after-death effect, discussed by Pons and Fleischmann[6]. A connection between excess heat generation, the presence of pressure gradients and the initiation of the Fleischmann-Pons effect is considered.

The presence of voltage spikes indicate that within the Pd/D film small "explosions" associated with the excess enthalpy generation do occur. Furthermore, it would appear that, within the Pd/D system, there are active domains (high D concentration, γ– phase formation). Once formed, these domains become the source of the heat producing reactions.

References

1. S. Szpak, P.A. Mosier-Boss and J.J. Smith, J. Electroanal. Chem., **302**, 255 (1991)
2. S. Szpak and P.A. Mosier-Boss, Physics Letters A **221**, 141 (1996)
3. P.A. Mosier-Boss and S. Szpak, Nuovo Cimento, **112 A**, 577 (1999)
4. A. von Hippel, *Dielectrics*, in *Handbook of Physics*, E. U. Condon and H. Odishaw, eds., p.4-103, McGraw-Hill Book Co, Inc., New York – Toronto – London, 1958
5. S. Szpak, P.A. Mosier-Boss and M.H. Miles, Fusion Technoloigy, **36**, 234 (1999)
6. S. Pons and M. Fleischmann, Trans. Fusion Technology, (ICCF-4), p. 87 1994

Figure captions

Figure 1 - Experimental set-up. A – Faraday cage, B – negative electrode assembly (B_1 – insulating material, B_2 – piezoelectric substrate, B_3 – Pd/D film), C – positive electrode, D – potentiostat/galvanostat, E – shock absorbing material, F – oscilloscope (Le Croy digital), E – laboratory bench.

Figure 2 – Burst of events observed at current density *ca* 4 μA cm^{-2}.

Figure 3 – Expanded view of a burst of events. Arrows indicate pressure pulses.

Figure 4 – Example of a single event. Point A – pressure spike, point B temperature spike

Figure 5 – A single event observed at zero cell current.

Figure 6. Recorded responses of an operating cell as a function of time.

Figure 1

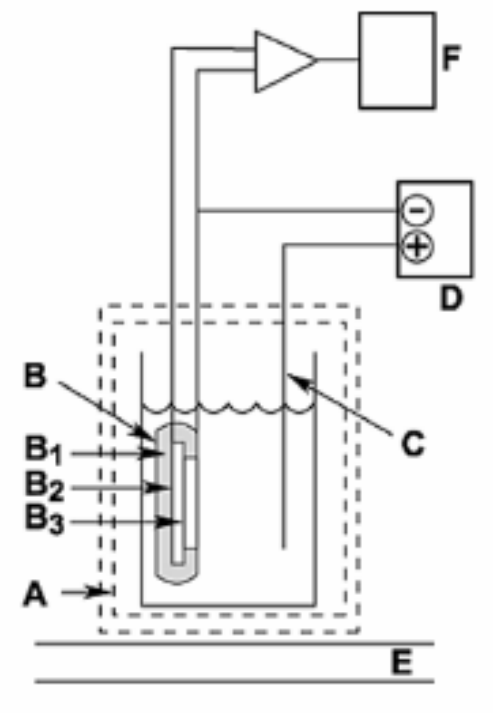

Figure 2

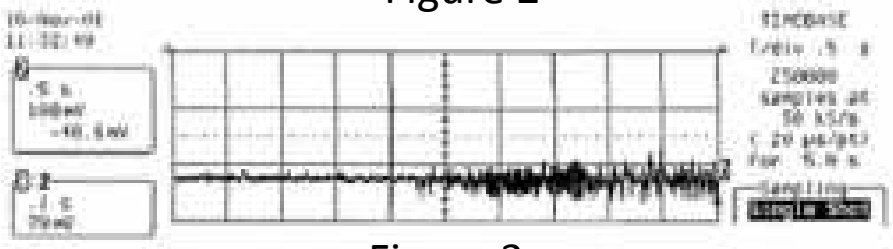

Figure 3

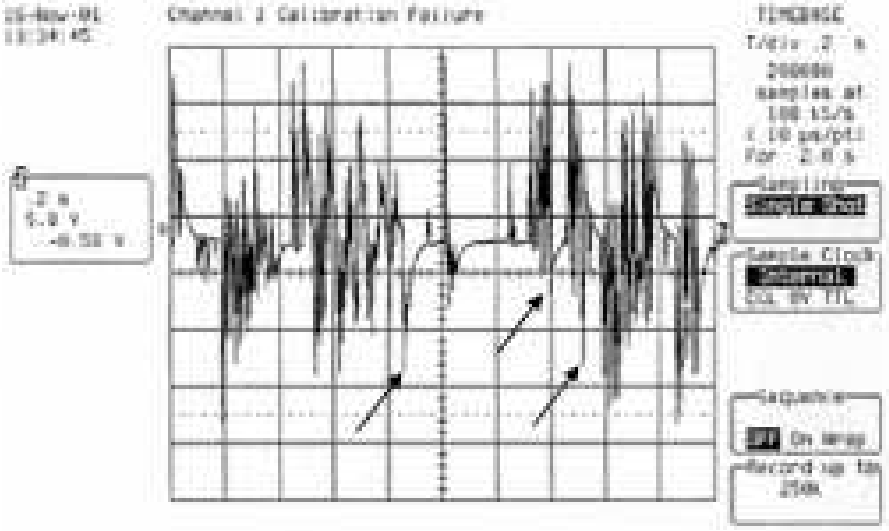

Figure 4

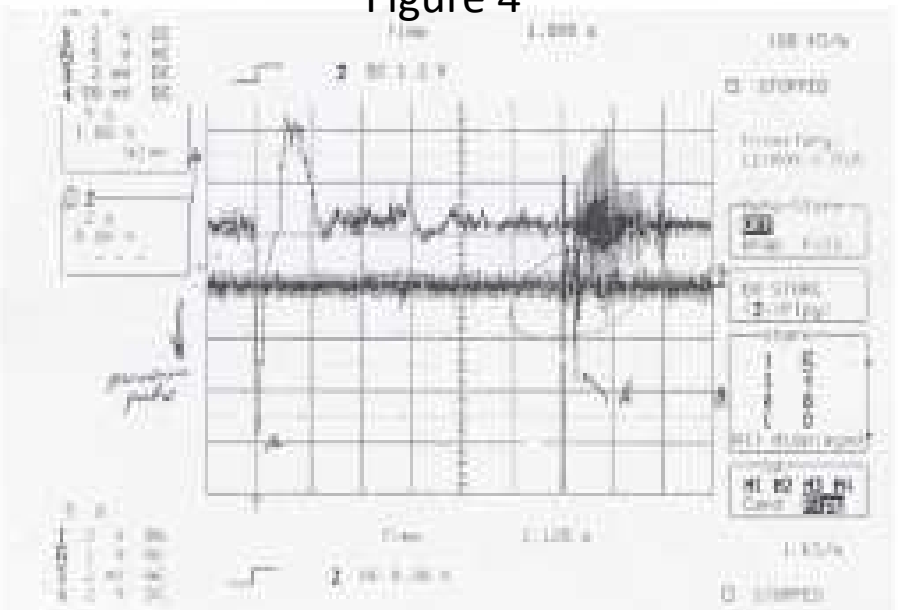

Figure 5

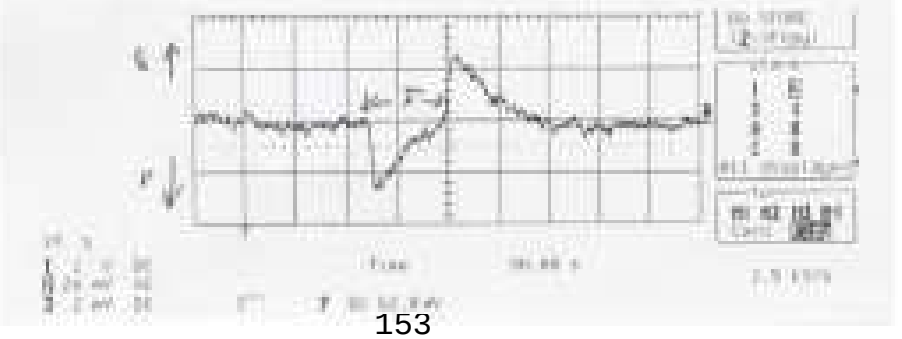

Figure 6

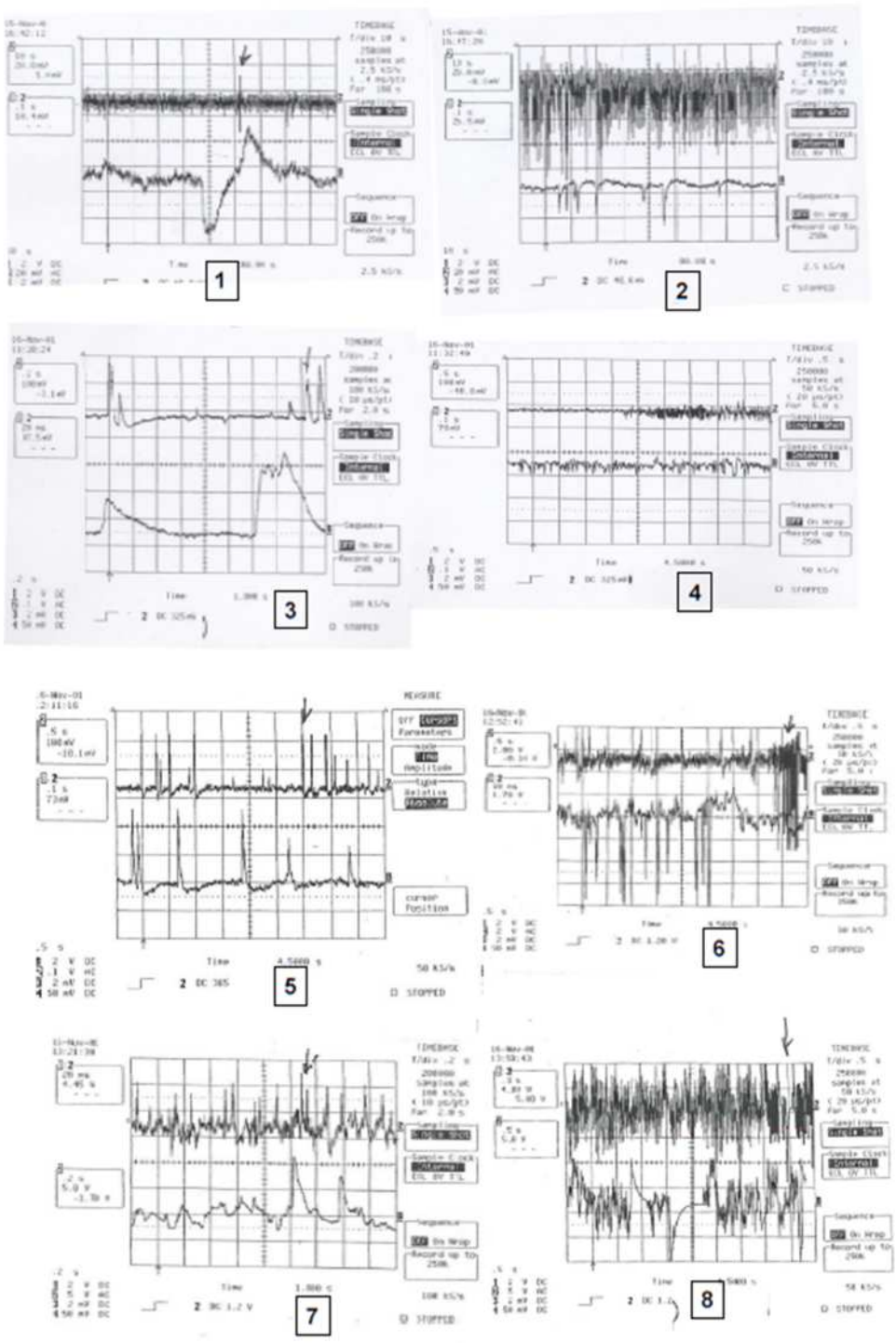

Figure 6 (cont.)

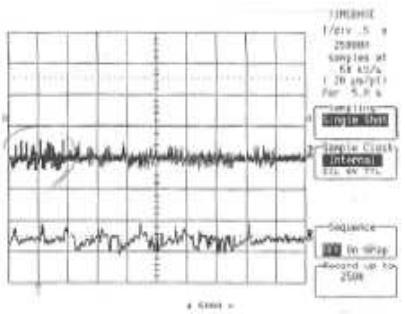

9

(blank page)

THERMAL BEHAVIOR OF THE Pd/D SYSTEM: TRANSITION FROM EXOTHERMIC TO ENDOTHERMIC ABSORPTION

S. Szpak and P.A. Mosier-Boss

SPAWAR Systems Center San Diego, San Diego, CA 92152.-5001

Abstract

Thermal behavior of the early stages of the Pd/D co-deposition process is examined. Calorimetric measurements indicate that (i) absorption of deuterium at high [D]/[Pd] atomic. ratios is endothermic, (ii) the exothermic Fleischmann-Pons (F-P) effect occurs almost immediately and (iii) the cause of the F-P effect are the localized, high intensity heat sources of very short duration.

1.0 Introduction

Prior to the 23rd March 1989, the date of the announcement of the Fleischman-Pons (F-P) effect, there was no interest in the thermal behavior of the Pd/D system, in general, and in its polarized version, in particular. Following that date, there was an explosion of activities too numerous to list (references can be found in the Proceedings of International Conference on Cold Fusion, ICCF - 1 through ICCF - 10). Briefly, the F-P effect refers to excess enthalpy generation during electrolysis of heavy water using a “massive” Pd as the negative electrode.

It has been generally accepted that one of the conditions necessary to initiate the F-P effect, is high [D]/[Pd] atomic ratio. Furthermore, it has been suggested, on theoretical grounds[1], that such high ratios are associated with the formation of the β– phase and that, the transition from the β– to the γ– phase should be accompanied by the transition from exothermic to endothermic absorption of deuterium[2].

In what follows, we shall demonstrate, via calorimetric measurements, that at high [D]/[Pd] atomic ratios there occurs a transition from an exothermic to endothermic absorption of deuterium by the palladium lattice. Furthermore, a correct interpretation of the thermal behavior of electrolytic cells requires both the knowledge and consideration of all of the participating processes, especially (i) the kinetics of electrode reactions and (ii) the realization that calorimetric measurements, when coupled with other observations, may lead to a better understanding of the co-deposition process.

2.0 Background information

In assembling the background information we considered the following: (i) elements of the electrochemical cell. (ii) thermodynamic constraints through the use of Pourbaix diagrams, (iii) the co-deposition process and (iv) the partial molar absorption as a function of the [D]/[Pd] atomic ratio.

2.1 Electrochemical cell

An electrochemical cell, in its simplest arrangement, is an open system consisting of subsystems representing the cell working elements: an electrolyte, positive and negative electrodes and the associated auxiliary elements, eg thermistors, calibration heater etc. It can operate: (i) as an energy source or (ii) as a mass convertor. Within an infinitesimal time interval, *dt*, during which a. stationary current passes through the cell, a positive charge, *Idt*, is transported through the cell from the positive to the negative electrode while the negative charge, *–Idt*, passes through the external circuit. The effect of the passage of cell current can be summarized by examining the thermodynamic and kinetic aspects.

2.2 Pourbaix diagrams

A convenient way to examine the often very complex processes associated with the cell operation, is to construct the relevant Pourbaix diagrams[3]. Briefly, the Pourbaix (or the potential- pH) diagrams represent a summary of electron and proton transfer reactions that are prevented/favored on thermodynamic grounds. Thus, (i) reactions of the type $M \rightarrow M^{n+} + ne^-$ being independent of the pH, are represented by straight lines parallel to the *pH*-axis with displacement, proportional to the $log(c_{Mn+})$, (ii) reactions of the type $M + nH_2O \rightarrow M(OH)_n + 2nH^+ + ne^-$, ie where the potential is a linear function of the pH are drawn with a slope of $-2.3RT/F$ (= 0.06V at 25°C), (iii) regions to the left from the point at which the $E_{M/M^{n+}} - pH$ intersects the $E_{H/H+} - pH$ line identify instability while those to the right of the point of intersection are regions whose stability is assured by the protective layer of $M(OH)_n$. Although originally prepared for studies in corrosion, they can be useful in the examination of electrochemical cells irrespective of their intended use.

2.3 The co-deposition process

In 1991 we proposed an alternate method to prepare the Pd/D working electrode, namely by the co-deposition technique[4]. As we have shown recently[5], these electrodes exhibit common features with “massive” electrodes, *viz.* (i) excess enthalpy generation, (ii) positive feed-back and (iii) “heat-after-death”. The system differs, however, in that. (i) the excess enthalpy generation occurs within minutes and with somewhat greater efficiency, (ii) the heat sources are randomly distributed in time and space, a feature that has not been reported to occur on “massive” electrodes.

The co-deposition refers to a simultaneous electro-reduction of Pd^{2+} ions and D_2O/D^+ molecules/ions. Thus, it requires that the cell current, *I*, be split into two partial currents i_1 and i_2 accounting for the reduction of the Pd^{2+} ions and D_2O molecules, respectively. It is further assumed that the charge transfer reactions are independent of each other so that $I = i_1 + i_2$. To prevent the formation of powdery deposits, the rate of D_2 evolution should only slightly exceed the rate of Pd deposition. The maximum rate of an acceptable Pd/D deposit is controlled by

diffusion, ie at cell currents approximately twice that of the limiting current given by $i_{1,lim} = 2FADc/\delta$, where F is the Faraday constant, A is the surface area, D is the diffusion coefficient, c is the concentration of Pd^{2+} ions and δ is the thickness of the diffusion layer.

It is instructive to examine the Pd/D co-deposition using, as background, the simplified Pourbaix diagram. Relevant parts of such diagram together with the superimposed potential/current relationship for the reduction of Pd^{2+} ions as well as the H_2O/D_2O molecules, are shown in Fig. 1. As indicated, the electro-reduction of the Pd^{2+} ions from simple Pd salts, eg $PdCl_2$, requires highly acidic solutions, ie to the left of point A, Fig. 1. Thus, due to the very low concentration of Pd^{2+} ions ($Pd(OH)_2$ will precipitate at pH 1.5 for $c_{Pd^{2+}} = 10^{-6}$ mol/cm^3) only hydrogen/deuterium evolution reaction would occur. The Pourbaix diagram indicates that for an effective co-deposition, point A must be shifted in the direction of higher pH values. This can be done by eg complexing[1,5].

2.4 Absorption of deuterium

The partial molar enthalpy of absorption, Δ*H/R*, as a function of the [D]/[Pd] atomic ratio, is plotted in Fig. 2. Evidently, as the [D]/[Pd] ratio increases, the negative Δ*H/R* also increases. It reaches a maximum at [D]/[Pd] = 0.4 and decreases with the further increase in the [D]/[Pd] atomic ratio. No data are available for [D]/[Pd] >0.8. However, if the trend continues, then one would expect a transition from an exothermic to endothermic behavior to occur at [D]/[Pd] = 0.85.

3.0 Electrochemical calorimetry

The characteristic feature of the electrochemical calorimetry is the need for long time observations. That requires a detailed analysis of the heat transfer coefficients and the calibration procedure. For short time measurements, a more convenient design is that employing an adiabatic enclosure since it eliminates the need for calibration. However, it introduces difficulty connected with the maintenance of the adiabatic enclosure.

3.1 Electrochemical cell in an adiabatic enclosure

An electrochemical cell/calorimeter is modeled adequately by the non-linear and inhomogeneous differential equation (cf Appendix in [2]). However, for a cell/calorimeter, provided with an adiabatic enclosure[6], operating at low cell currents and temperatures, all enthalpy fluxes (ie calibration heat source, enthalpy content of the gas stream enthalpy transfer to the environment) can be neglected. Consequently, for cells with an adiabatic enclosure an adequate description is given by Eq. (1)

$$c_p m \frac{dT}{dt} = I[E_c - E_{th}] + q(t) \qquad (1)$$

where $c_p m \left(= \sum c_{p,i} m_i\right)$ is the "water equivalent" [2], I is the cell current, E_c is the

cell potential, E_{th} is the thermoneutral potential and $q(t) = \sum q_i(t)$ represents the sum of rates of heat produced/consumed (intensity of sources/sinks) due to any number of processes. An adiabatic enclosure separating two systems, A and B, is maintained by assuring that, at all times, $J_q^{A\to B} = J_q^{B\to A}$, ie that the heat outflow is balanced by heat inflow. In practice, we require that within the time period $\Delta t = t_2 - t_0$, $\int_{t_0}^{t_1} J_q^{A\to B} dt = \int_{t_1}^{t_2} J_q^{B\to A} dt$ or, at least, oscillates about zero. During the co-deposition, all relevant data (eg cell potential, cell current, electrolyte temperature as well as the maintenance of the adiabatic enclosure) are to be recorded.

3.2 Evaluation of the $Q(t) = \sum_i \int_{\Delta t} q_i(t)dt$ term

The excess enthalpy produced/consumed within time interval Δ*t*, ie the *Q*(*t*) term can be evaluated from the plot of $0.239c_p m\Delta T - \int_{\Delta t} I[E_c - E_{th}]dt$ vs $\int_{\Delta t} IE_c dt$. A plot for a typical run is shown in Fig. 3. Evidently, at first *Q*(*t*) is negative and becomes less with an increase in the co-deposition time. The negative value of *Q*(*t*) indicates that, at the beginning of the run, the cell acts as refrigerator, ie in an apparent violation of the second law of thermodynamics. Since the second law cannot be violated, it follows that an endothermic process has occurred at the beginning of the co-deposition process.

The co-deposition is a simultaneous electro-reduction of the Pd^{2+} ions and D^+/D_2O molecules as well as absorption of deuterium. Of these processes only absorption of deuterium could be endothermic. This view confirms an earlier suggestion made by Fleischmann et al.[2] that at high [D]/[Pd] atomic ratios the absorption of hydrogen might be endothermic (cf. Fig. 2). In this connection, we recall that the co-deposition is accompanied by high [D]/[Pd] atomic ratios[7].

4.0 Interpretation of the Q(t) vs $\int_{\Delta t} IE_c dt$ curve

Equation (1), as written, represents the enthalpy balance for the case where the only reaction is the deuterium evolution. Thus, it applies for "massive" electrodes where the enthalpy of the evolved deuterium can be recovered by the recombination reaction, $D_2 + \frac{1}{2}O_2 \rightarrow D_2O$. In the case of electrodes prepared by the co-deposition technique, Eq. (1) applies only after the completion of Pd/D co-deposition. In the present case, Eq. (1) must be modified to reflect the existing situation. During Pd/D co-deposition, a part of the electrochemically generated deuterium is absorbed, $i_{2.1}$, and part, $i_{2.2}$, appears as evolving gas. In the balance equation, the first is connected with the presence of heat source/sink while only the second can be recovered by the recombination reaction. Consequently, the term $\int_{\Delta t} I[E_c - E_{th}]_c dt$ should read $\int_{\Delta t}\left[IE_c - i_{2,2}E_{th}\right]dt$ so that the *Q*(*t*) term is evaluated by plotting $0.239c_p m - \int_{\Delta t}\left[IE_c - i_{2,2}E_{th}\right]dt$ vs $\int_{\Delta t} IE_c dt$.

4.1 The shapes of the Q(t) vs $\int_{\Delta t} IE_c dt$ *curve*

The points of the *Q*(*t*) vs $\int_{\Delta t} IE_c dt$ curve (the dotted line, Fig. 3) were calculated under the assumption of complete depletion of the Pd^{2+} ions. But, at the beginning of the co-deposition there is practically no gas evolution so that the calculated values are less than those shown in Fig. 3. In particular, for a constant cell current, the corrected values are $Q(t)_{corr} = Q(t)(1 - E_{th}/E_c)^{-1}$ curve in Fig. 3.

We consider two cases, *viz.* (i) the shape in the absence of the F-P effect and (ii) in its presence.

(i) in the absence of the F-P effect, for a constant cell current, the negative *Q*(*t*) increases at a rate proportional to the volume of the Pd/D film as well as the concentration of the Pd^{2+} ions in solution. Thus, with the passage of time, the rate becomes less and approaches asymptotically zero, ie the *Q*(*t*) curve approaches a constant value.

(ii) The shape of both, the experimental and the corrected *Q*(*t*) vs $\int_{\Delta t} IE_c dt$ represents a sum of, at least, two terms, $q_1(t)$ and $q_2(t)$, the first denoting the endothermic absorption (acting as a sink) and the second the exothermic F-P effect (acting as a heat source). Initially, the increase in the *Q*(*t*) suggests that the principal process is the endothermic absorption. The development of the shallow minimum means that shortly after the initiation of the current flow, a positive term (excess enthalpy production. the F-P effect) became active. At first, its contribution was small. However, with the passage of time, it appears that the rates of both processes were in constant, ratio. With the further passage of time, the exothermic F-P effect became dominant.

4.2 Supporting evidence

Supporting evidence corroborating the occurrence of processes that results in the observed behavior is provided by (i) the infrared imaging of the electrode surface and (ii) the voltage spikes seen when the substrate, upon which the co-deposition takes place, is made of a pressure sensitive material (piezoelectric).

(i) The infrared imaging of the electrode surface showed that, the co-deposition is accompanied by the formation of hot spots[8]. An example is shown in Fig. 4. The presence of hot spots not only supports the existence of the F-P effect but characterizes it as having the form of localized, short duration and high intensity heat sources.

(ii) Natural consequence of discrete heat sources is the distortion of the crystal lattice creating propagating stresses. An immediate consequence of high intensity discrete heat sources is the possibility that response would be similar to that caused by “mini-explosions”. The accompanied mechanical distortion can be displayed by co-depositing the Pd/D films onto pressure sensitive substrate, eg piezoelectric ceramic material[9]. To eliminate external factors that might interfere

with the interpretation of the sensor's response, the electrochemical cell was shielded (Faraday cage) and the whole assembly was placed on a shock absorbing material.

In general, there are two types of forces that interact with the piezoelectric material, *viz.* those that cause the contraction of the piezoelectric material and those that result in its expansion. An example of the first kind is the pressure change due to eg appearance of a localized heat source within the Pd/D film; that of the second kind – due to arrival of the temperature front.

A single isolated event of a "mini-explosion" is shown in Fig 5a where the voltage spike in the negative direction corresponds to a pressure pulse while that in the positive direction indicates an arrival of the temperature front. Singular events are seen in the early periods of the co-deposition. Often a singular event is followed by a voltage-time behavior which is consistent with the occurrence of a burst of events (Fig. 5a). An expanded trace of such burst is shown in Fig. 5b. It is noteworthy that such activities were observed at current densities as low as 40 mA cm^{-2}. The frequency of bursts and their intensity increased with an increase in cell current and cell temperature. It is noteworthy that at temperatures close to the boiling point, thermal activities are very intense.

5.0 Concluding remarks

To reiterate:

1. The Pd/D co-deposition system provides an interesting variant of the original methodology employed by Fleischmann and Pons. Its characteristic feature: high rates of excess enthalpy generation.

2. Calorimetric measurements support, in a qualitative way, the transition from exothermic to endothermic absorption of deuterium at high [D]/[Pd] atomic ratios.

References

1. G. Preparata, Trans. Fusion Technology. **26**(1994)397
2. M. Fleischmann, S, Pons, M. LeRoux and J. Roulette, Trans. Fusion Technology, **26**(1994) 323
3. M. Pourbaix, *Atlas of Electrochemical Equilibria in Aqueous Solutions*. Pergamon Press, Ltd., London, 1966
4. S. Szpak, P.A. Mosier-Boss and J.J. Smith, Electroanal. Chem., **302** (1991) 255
5. S. Szpak, P.A. Mosier-Boss, M.H. Miles and M. Fleischmann, Thermochim. Acta, **410** (2004) 101
6. S. Szpak, P.A. Mosier-Boss and M.H. Miles, Fusion Technology, **36** (1999) 234
7. S. Szpak, P.A. Mosier-Boss, and J.J. Smith, J. Electroanal. Chem., **379** (1994) 121
8. P. A. Mosier-Boss and S. Szpak, Nuovo Cimento, **112A** (1999) 577

9. S. Szpak, P.A. Mosier-Boss, J. Dea and F. Gordon, Proc. ICCF-10, Cambridge, MA, 2003.

Figure captions

Fig. 1 Light lines – Potential-pH equilibrium diagram for the Pd/H_2O system at 25°C.
(a): $2H_2O \rightarrow O_2 + 4H$(b): $H_2 \rightarrow 2H^+ + 2e^-$
(1): $Pd \rightarrow Pd^{2+} + 2e^-$
(2): $Pd + 2H_2O \rightarrow PdO_2 + 2H^+ + 2e^-$
(3): $Pd + H_2O \rightarrow PdO + 2H^+ + 2e^-$
(4): $Pd^{2+} + H_2O \rightarrow PdO + 2H^+$
(5): $Pd + H \rightarrow Pd/H$

Heavy lines – The potential/current relation for cathodic reactions; i_1 for Pd^{2+} reduction, i_2 for D_2 evolution: effective co-deposition at overpotential $\eta_1 < \eta < \eta_2$.

Fig. 2 The relative partial molar enthalpy of hydrogen in palladium as a function of [D]/[Pd] atomic ratio. Notes: Data from ref. [2]; Assumption Pd/D systems exhibits the same dependence.

Fig. 3 The shape of the $Q(t)[= q_1(t) + q_2(t)]$ vs $\int_{\Delta t} IE_c dt$ curve curves.
Initial period $-q_2(t) = 0$; period A – B – q_1(t) approx equal q_2(t) period B – C – $-q_2(t) > q - 1(t)$. Curve a corrected Q(t) vs $\int_{\Delta t} IE_c dt$

Fig. 4 Hot spots (localized heat sources) by IR imaging

Fig. 5 Response of piezoelectric sensor to arriving pressure and temperature fronts. Fig. 5a an isolated event; Fig. 5b – expanded series of events.

(blank page)

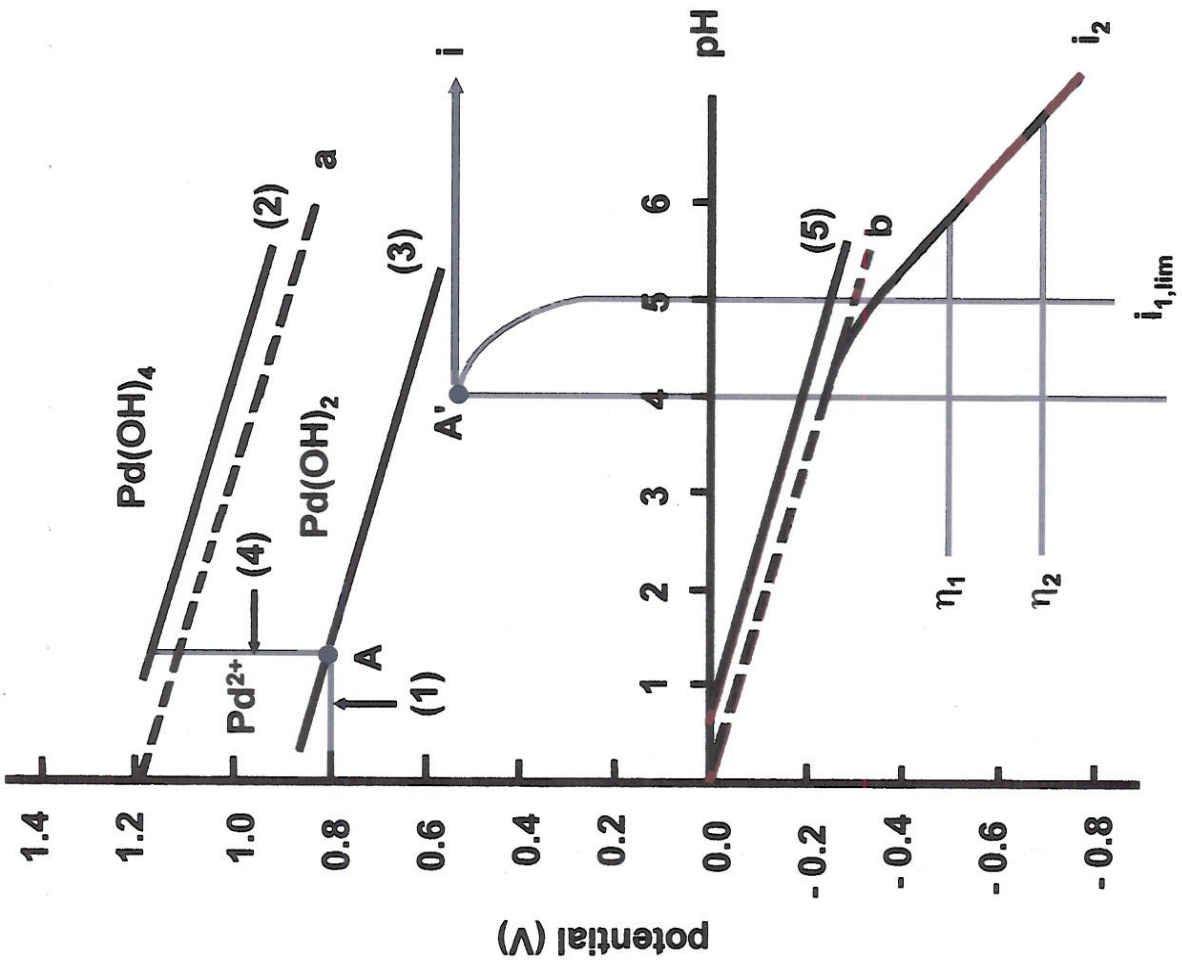
potential (V)
1.4
1.2
1.0
0.8
0.6
0.4
0.2
0.0
-0.2
-0.4
-0.6
-0.8
pH
1
2
3
4
5
6
i
A'
A
(1)
(2)
(3)
(4)
(5)
a
b
Pd(OH)4
Pd(OH)2
Pd2+
i2
i1,lim
η1
η2

Figure 1

Figure 2

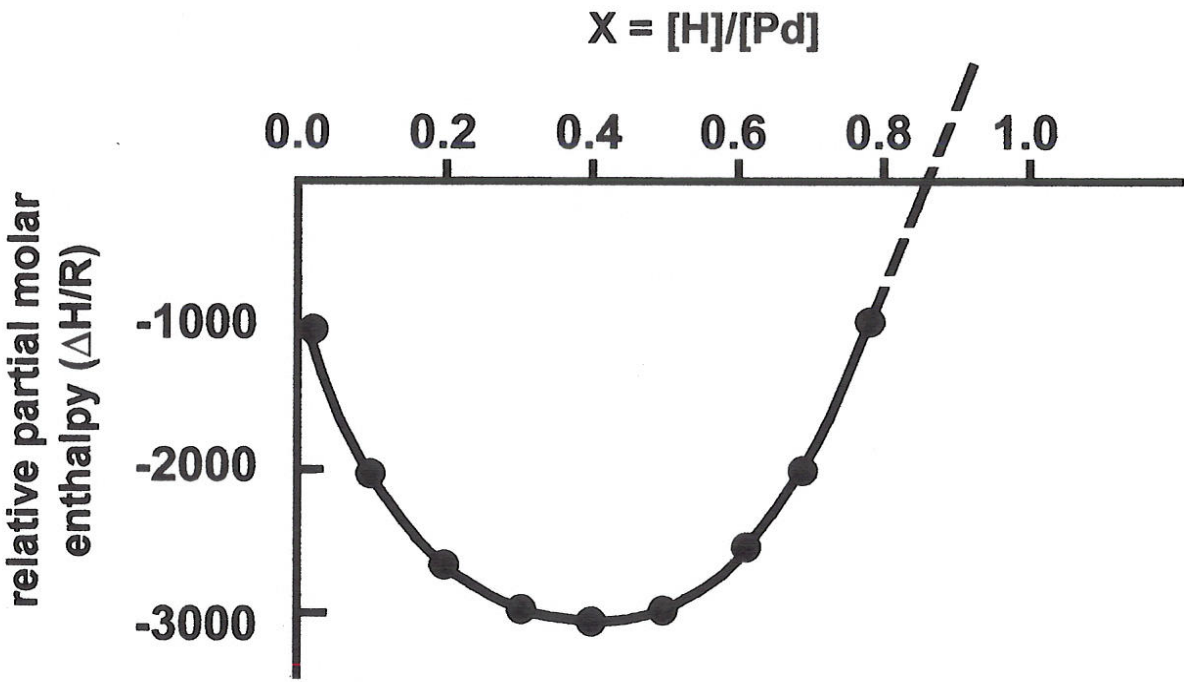
X = [H]/[Pd]
0.0
0.2
0.4
0.6
0.8
1.0
relative partial molar enthalpy (ΔH/R)
-1000
-2000
-3000

Figure 3

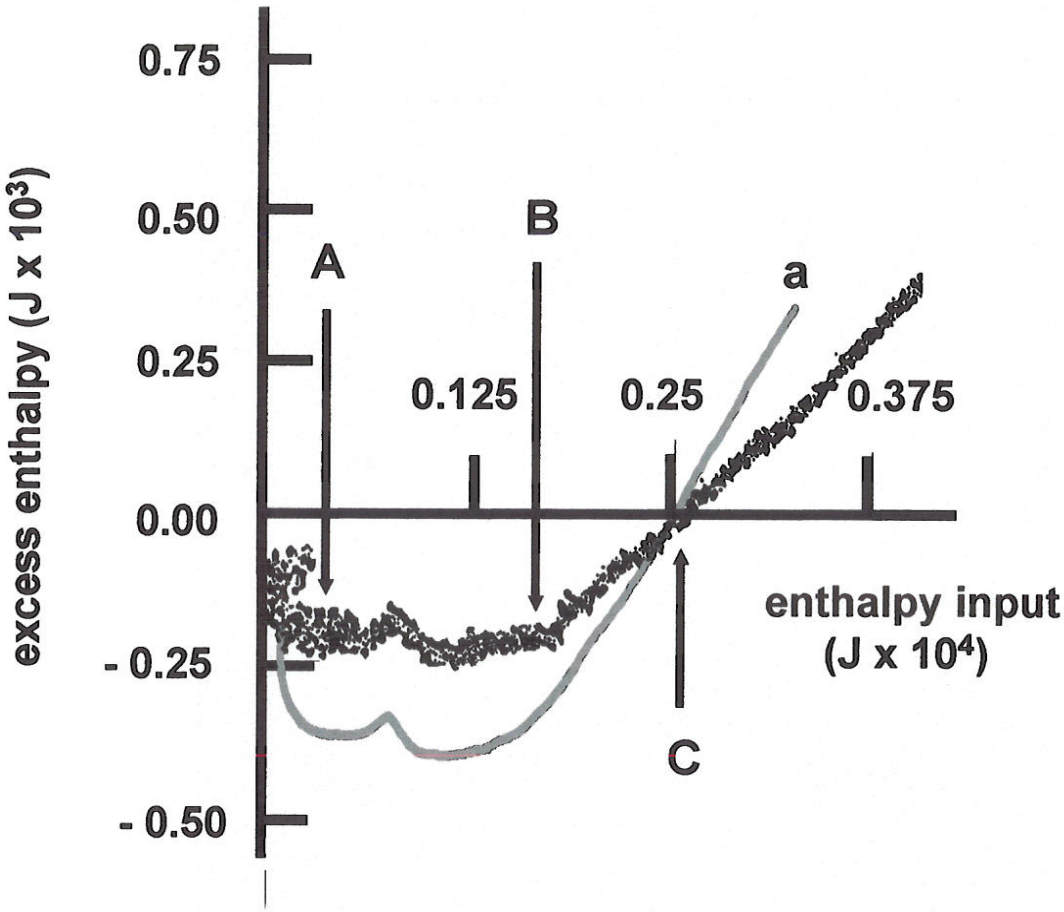
0.75
0.50
0.25
0.00
- 0.25
- 0.50
excess enthalpy (J x 10³)
A
B
a
0.125
0.25
0.375
C
enthalpy input
(J x 10⁴)

Figure 4

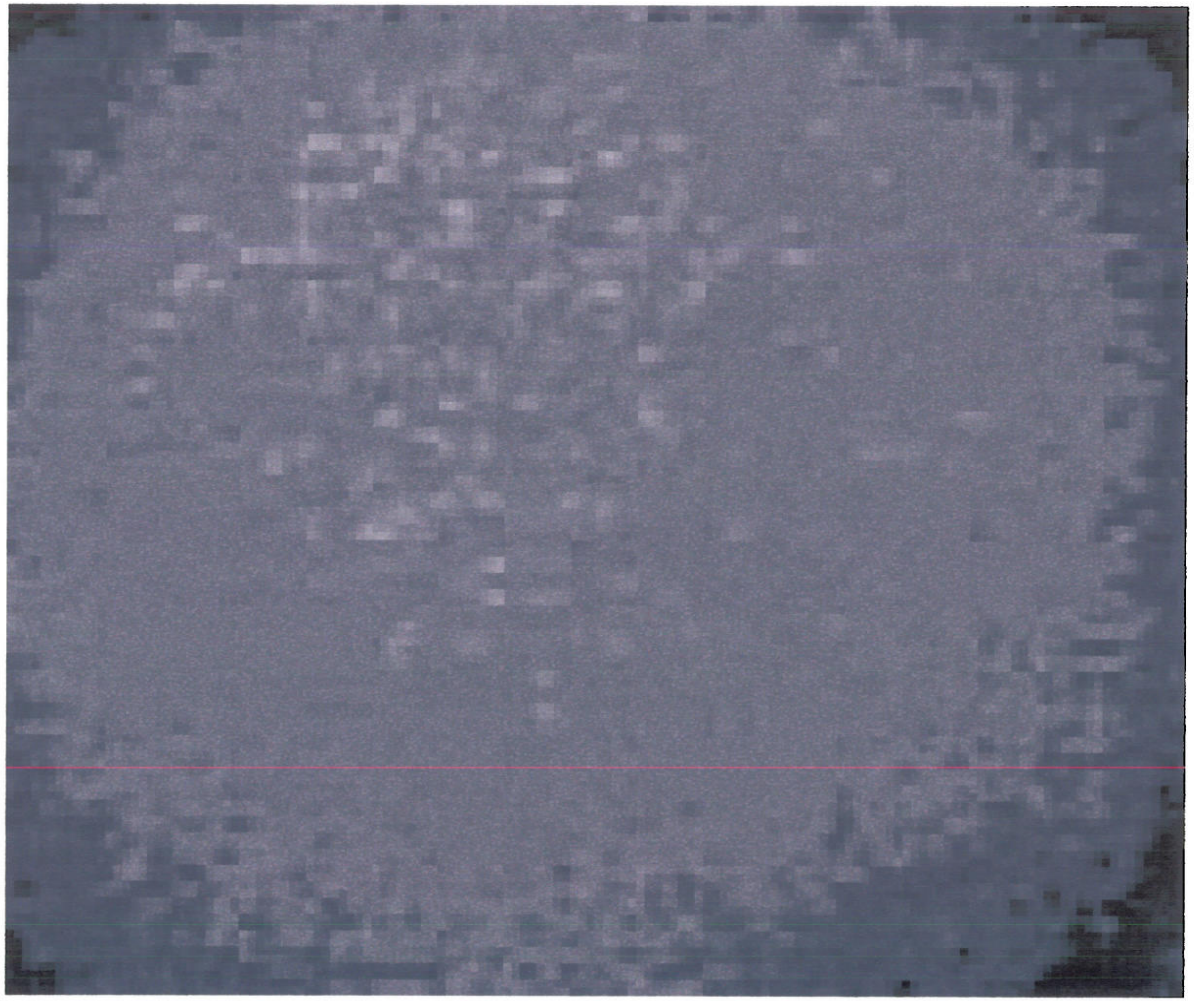

Figure 5

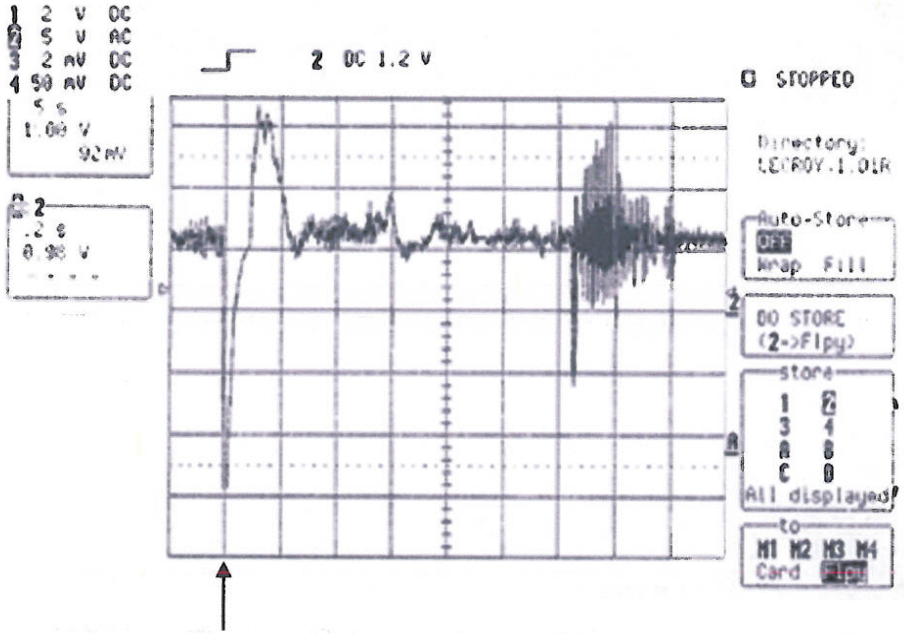
2 DC 1.2 V
STOPPED
Directory:
LECROY.I'DIR
Auto-Store
OFF
Wrap Fill
DO STORE
(2->Flpy)
Store
All displayed
to
M1 M2 M3 M4
Card Flpy

a

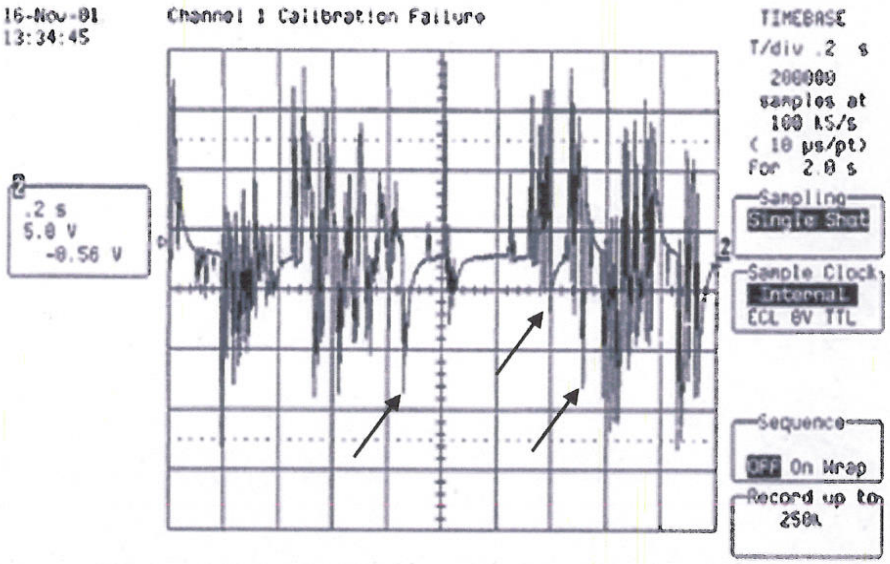
16-Nov-01
13:34:45
Channel 1 Calibration Failure
TIMEBASE
T/div .2 s
200000
samples at
100 kS/s
(10 µs/pt)
For 2.0 s
.2 s
5.0 V
-0.56 V
Sampling
Single Shot
Sample Clock
Internal
ECL 0V TTL
Sequence
OFF On Wrap
Record up to
2500

b

Boss, Pam SPAWAR

From: [redacted]
Sent: Friday, June 25, 2004 11:19 AM
To: pam boss
Subject: LDH791

Dr. Boss
One review of this paper has finally been obtained, unfortunately it is quite negative. The reviewer questions the quality of the experimental work and comments on the inadequacy of the literature review. Based on this review I have decided to reject the paper. Because only hard copy is available, I will mail the review to you. Thank you for submitting your work to Thermochimica Acta.

[redacted]

Referee comments (retyped from original).

This is a review for the paper LDH791, "Thermal Behavior of the Pd/D System: Transition from Exothermic to Endothermic Absorption", by Szpak, and Mosier-Boss. This is a "cold fusion" paper with many of their characteristics, e. g.,every reference except of the general ref. 3, is to another "cold fusion" paper.

There is the statement on line 2 of the abstract "Calorimetric measurements indicate that...", i. e., their results are all based on calorimetric measurements but there is little, if any, description of a calorimeter and the experimental details of the calorimetric measurements are not given.

There is no mention of the temperature of their experiments. The abscissa in Figure 1 are not labelled.

Figure 2 gives a plot of the relative partial molar enthalpy (it is not specified whetcher this is per mol D or D_2) against H/Pd, presumably the authors mean D/Pd. This plot is attributed to reference [2], M. Fleischmann, s. Pons,.. To my knowledge, Fleischmann and Pons never made such measurements, at least in a non-electrochemical calorimeter. The authors should give the original reference for the source of this data. In any case, these data are erroneous at moderate temperatures because there is a two-phase plateau region from about D/Pd = 0.02 to 0.60 at 298 K where the enthalpy is an integral value not a relative partial molar value. This integral value ie equal to -17.3 kJ/mol D for absorption across the two phase region. The authors should refer to Sakamoto, et al., *J. Phys.: Condens. Matter,* **8** *(1996) 3229* where data are obtained up to D/Pd = 0.85.

The fact that according to their Fighure 2 (which may be OK for D contents outside the two phase region, e.g., above D/Pd = 0.6), the relative partial molar enthalpy may become endothermic for D_2 solution at high D contents, does not mean that co-deposition of D^+ and Pd^{+2} will be endothermic. If the partial molar value is endothermic at a certain D/Pd value, does not mean that an integral value will be endothermic. When D enters the Pd, the heat will be an integral heat, $\int_0^b \Delta H_D dr$ where r = (D/Pd) and b is some high value where the molar value is endothermic. However most of the ΔH_D values in the integral will be exothermic and the integral will be exothermic znd the integral heat will be also exothermic. (The authors should consider the sign of the area under the curve in their Figure 2 from (D/Pd) = 0 to 1.0).

In my opinion, this paper should be rejected and not because it deals with "cold fusion", but because the experiments are poorly described, there is inadequate references to the literature and the calorimetric aspects are confused.

San Diego, 12 July 2004

We have no interest in challenging your decision concerning our recent paper "Thermal behavior .. etc". However, we must bring to your attention that the reviewer comments are both factually incorrect and irrelevant. Also, it might be of interest to you why we have submitted this paper to your journal. The preparation of this paper was prompted by the suggestion of Prof. Craig (at that time chief editor of Thermochimica Acta.) following the acceptance of our earlier paper that future contributions from our laboratory would be welcome.

Contrary to the view expressed by the reviewer, this is not a "cold fusion" paper. It deals with the thermal behavior of a polarized Pd/D-D_2O system and, in particular, it presents some unique features, not previously described. In retrospect, perhaps the more descriptive title would be "...selected features" rather than "...transition...".

We do not know what guidelines and/or instructions are given to reviewers. However, we expect the review to be unbiased, factual and, above all, relevant to the content of the submitted communication. With this in mind, we cite the closing sentence of the review. It reads: *In my opinion, this paper should be rejected and not because it deals with "cold fusion "but because the experiments are poorly described, there is inadequate references to the literature and the calorimetric aspects are confused.* To take it apart: (i) Was the statement .. *not because it deals with cold* fusion necessary? One would expect an unbiased review as a matter of principle; (ii) .. *experiments poorly described.* It is too general to respond. (iii) . .. *inadequate references*. In the first paragraph, *we wrote references can be found in Proceedings of... etc.;* (iv) ... *calorimetric aspects are confused.* The analysis of data presented in Fig. 3 is based on the premise *that* the Second Law of thermodynamics *cannot* be violated. This alone should remove any confusion.

In addition:

(i) We agree with the reviewer, cell calorimetry is not described in detail. Details can be found in reference [6] (Fusion Technology, **36**, 234 (1999)

(ii) Factually incorrect, the pH-axis (abscissa) in Fig. 1 is labeled.

(iii) Figure 2 is redrawn from Fleischmann and Pons paper. We emphasize that, for the purpose of this paper, only the trend was important and that, by extrapolation, the change from exothermic to endothermic absorption should occur at D/Pd = 0.85.

(iv) The reviewer devoted a whole paragraph to explain the meaning of the definitive integral. His discussion is logical and totally irrelevant. The electrochemistry of the Pd/D co-deposition is discussed in reference [7 and references therein] (J. Electroanal. Chem., **379**, 121 (1994) where we have shown that the D/Pd atomic ratio approaching and exceeding unity is obtained within seconds. Consequently, there is no two-phase region associated with the co-deposition process.

In closing, it appears to us that the reviewer did not read the relevant material prior to commenting on the content of our paper. In this communication we described, what we believe to be an interesting behavior thus far not reported. What surprises us is the fact that you have rejected this paper on the basis of one reviewer's advice which, as we have shown, represents an uninformed opinion.

Dr P. A Boss

Dr S. Szpak

Nuclear reactions in the Pd lattice.

S. Szpak, P.A. Mosier-Boss, C. Young, J. Dea, F.E. Gordon
SPAWAR Systems Center San Diego

This note describes an experimental procedure that initiates and promotes the occurrence of low energy nuclear reactions. Briefly, this procedure involves the placing of an operating electrochemical cell, (Pd/D//D_2O, Li^+, Cl^-//Pt), in a stationary electrostatic field, followed by scanning electron microscopy (SEM) examination using an instrument equipped with an energy dispersive x-ray analysis system.

The SEM photograph of the Pd/D electrode prepared by the reduction of Pd^{2+} ions at current densities that assure high [D]/[Pd] atomic ratios[1], is shown in Fig. 1. If, upon completion of the Pd deposition, the cell is placed into an external electrostatic field, then morphological changes occur. The transition from the "cauliflower-like" morphology to other forms, such as the formation of fractals, craters, dendrites, etc.[2], is expected due to an interaction of an external electric field with the cell components *viz.* the liquid dielectric (D_2O) with extraneous charges (Li^+, Cl^- ions)[3] and the response of a solid to the action of surface forces.[4] Among the various structural forms we find morphologies with molten-like features, the development of which requires high energy expenditure, Figs. 2 and 3.

The question that arises is: Are the structural changes due to the action of the external electrostatic field alone, or is additional energy required to produce the distinct features shown in Figs. 2 and 3. One such source is that of a nuclear origin, as proposed by Fleischmann *et al.*[5], i.e. by nuclear reactions that occur within the negatively polarized Pd/D-D_2O system. If the structures shown in Figs. 2 and 3 are the result of a nuclear event, then their chemical composition should reflect it. Indeed, an analysis by the energy-dispersive x-ray method showed elements not originally present. In particular, the analysis of the "boulder-like" form, Fig. 2, shows the presence of Al, Fig. 2a, while the area adjacent to it, Fig. 2b, contains Pd only. In the second example, Fig. 3, the "crater-like" form, we find Al in the center, Fig. 3a, and Al and Mg on the periphery, Fig. 3b.

In conclusion we note the following characteristic features: (i) Events are highly localized (ii) In addition to Al and Mg, other elements are produced e.g. Ca, Si, Zn and Pb (iii) Oxygen peak is not associated with a nuclear reaction, rather it arises from reactions with components of the electrolyte immediately after the cessation of cell current flow, i.e. when reducing conditions are removed, (iv) The events described are reproducible in the sense that they are seen in every experimental run. What is not reproducible, is their distribution which is spatially nonuniform and the number of "new" elements found.

The occurrence of low energy nuclear reactions at room temperature is questioned on theoretical grounds and is rejected by most theorists. But, as the noted Japanese theoretical physicist, H.

Yukawa , stressed: “When new facts appear, the true theoretician should adapt his theories to these facts, not the reverse.”[6] Here, we presented the facts.

Experimental procedure in outline

(i) Cell – clear plastic, 2 cm × 2 cm × 5cm

(ii) Electrodes – negative: An Au foil, 1.5 cm in length, 0.5 cm wide; positive: a Pt screen

(iii) Electrolyte – 20 mL of 0.03 M $PdCl_2$ + 0.3 M LiCl in D_2O

(iv) Operating conditions – Cell current at 1.5 mA (at cd 1 mA^{-2}) for the first 24 hours; current increased to 3.0 mA for the period necessary to reduce all Pd^{2+} ions. Cell current increased to *ca* 30 – 50 mA (visible gas evolution) for 2 – 3 hours followed by the placement of the cell in an external electrostatic field in the manner that the Pd/D electrode will be parallel to the potential gradient of 2500 – 3000 Vcm^{-1} for the next 24 – 72 hours.

1. Szpak, S., Mosier-Boss, P.A. & Smith J.J., J. Electroanal. Chem., 379, 121-127 (1994)
2. Szpak, S., Mosier-Boss, P.A., Young, C., J. Electroanal. Chem., submitted
3. Landau, L. D., and Lifshitz, E. M., *Electrodynamics of Continuous Media*, Pergamon Press, Oxford-London-New York-Paris, 1960
4. Sommerfeld, A., *Lectures on theoretical physics, Vol. II* Academic Press, Inc., New York 1952
5. Fleischmann, M., Pons, S., Anderson, M. W, Li., L.J. & Hawkins, M., J. Electroanal. Chem., **287** 293 (1990)
6. Vigier, J.P., “New hydrogen energies in special he structured dense media: capillary chemistry and capillary fusion” in *Frontiers of cold fusion*, H. Ikegami, ed., Universal Academy Press Inc., Tokyo 1993

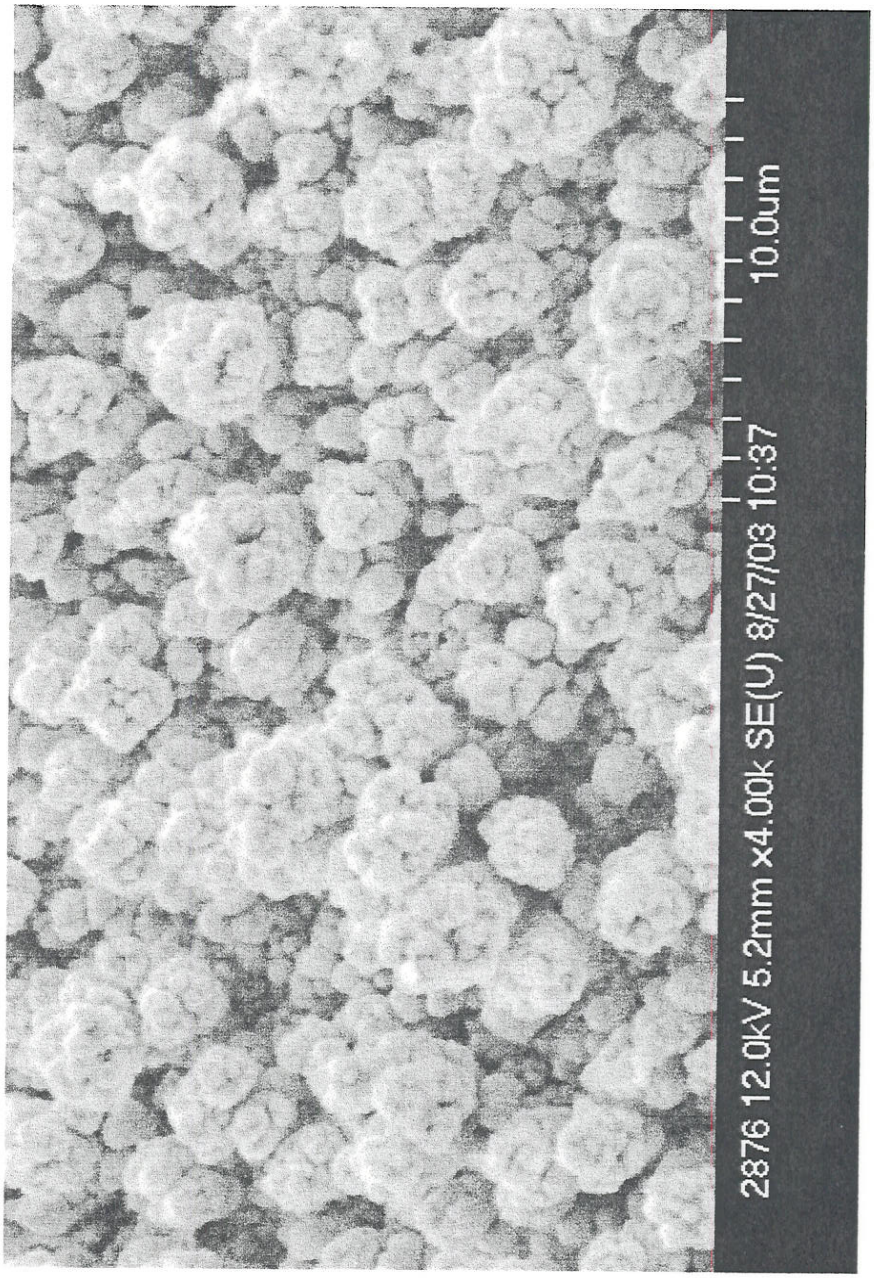

Figure 1

Figure 2

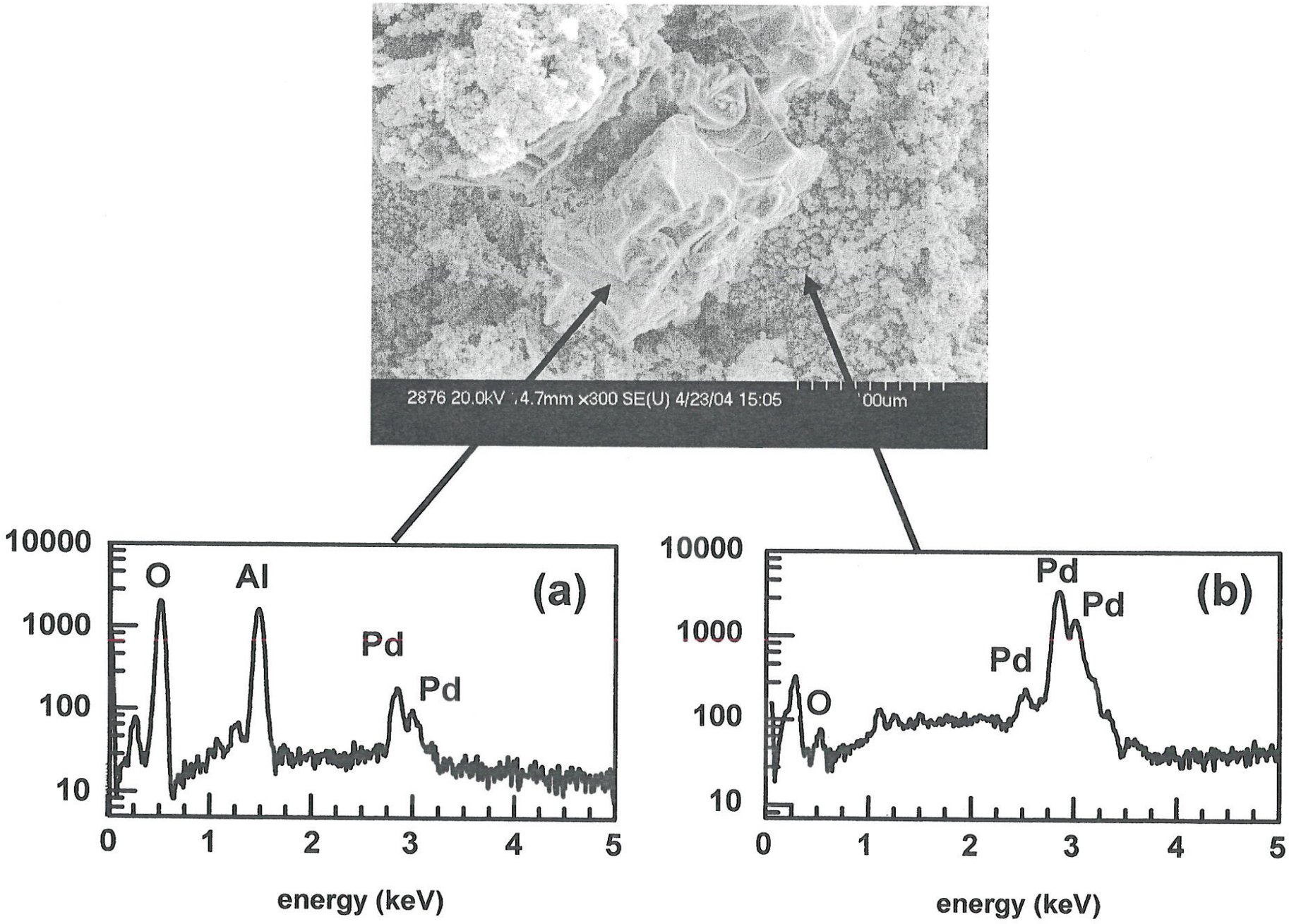
2876 20.0kV 4.7mm x300 SE(U) 4/23/04 15:05
00um
10000
1000
100
10
O
Al
Pd
Pd
(a)
0
1
2
3
4
5
energy (keV)
10000
1000
100
10
O
Pd
Pd
Pd
(b)
0
1
2
3
4
5
energy (keV)

Figure 3

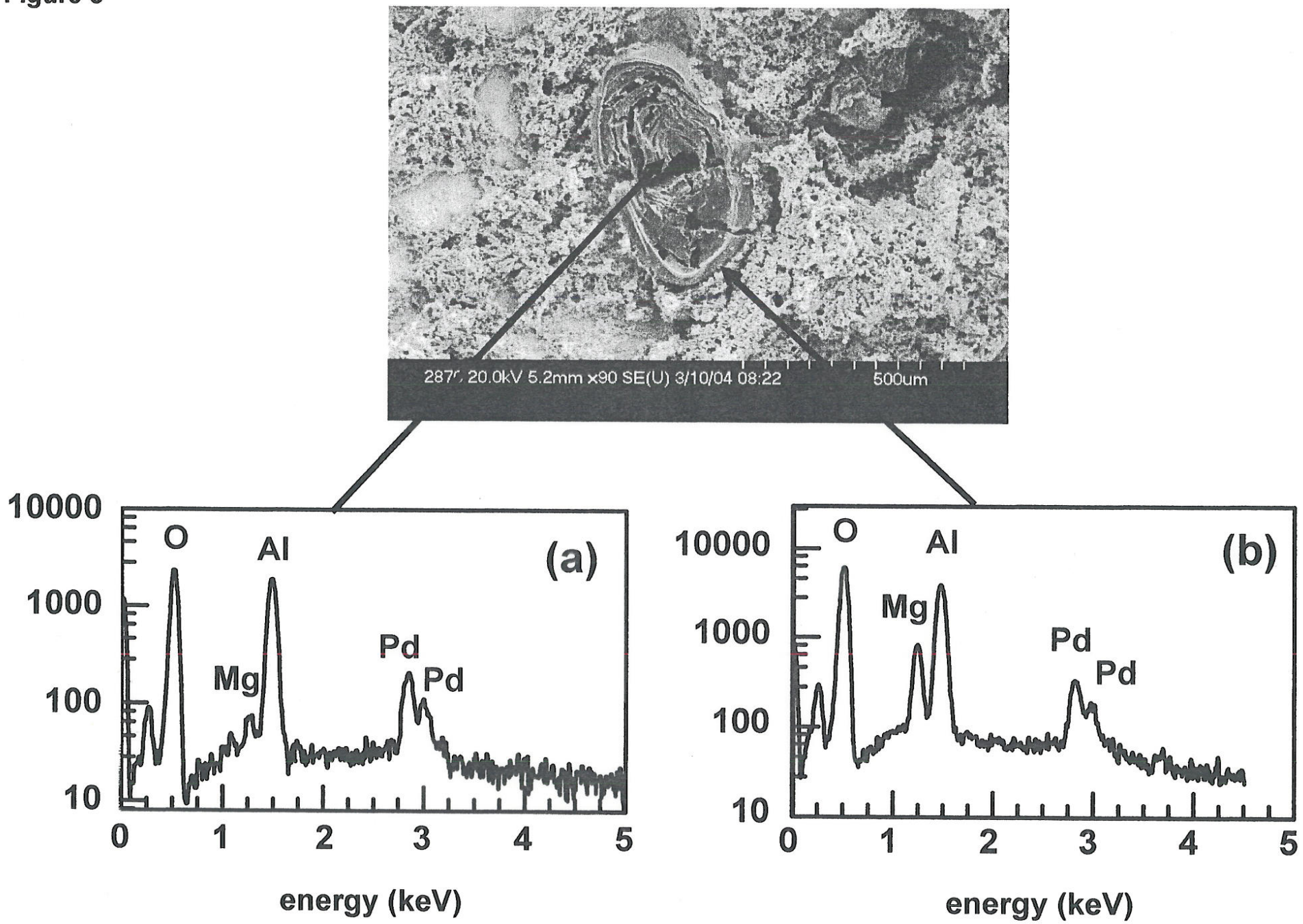
287? 20.0kV 5.2mm x90 SE(U) 3/10/04 08:22
500um
10000
1000
100
10
O
Al
Mg
Pd
Pd
(a)
0
1
2
3
4
5
energy (keV)
10000
1000
100
10
O
Al
Mg
Pd
Pd
(b)
0
1
2
3
4
5
energy (keV)

US005928483A

United States Patent [19]

Szpak et al.

[11] **Patent Number: 5,928,483**

[45] **Date of Patent: Jul. 27, 1999**

[54] **ELECTROCHEMICAL CELL HAVING A BERYLLIUM COMPOUND COATED ELECTRODE**

[75] Inventors: **Stanislaw J. Szpak**; **Pamela A. Boss**, both of San Diego, Calif.

[73] Assignee: **The United States of America as represented by the Secretary of the Navy**, Washington, D.C.

[21] Appl. No.: **08/969,175**

[22] Filed: **Nov. 12, 1997**

[51] **Int. Cl.**[6] **C25B 11/00**

[52] **U.S. Cl.** ..... **204/290 R**; 204/293; 204/272; 429/59; 429/101; 429/218.2; 429/231.6; 29/623.5; 29/746

[58] **Field of Search** ..... 204/290 R, 293, 204/243.1, 272; 429/59, 101, 218.2, 231.6; 29/746, 623.5

[56] **References Cited**

U.S. PATENT DOCUMENTS

4,393,125	7/1983	Skarstad et al. .	
4,528,084	7/1985	Beer et al. .	
4,560,444	12/1985	Polak et al. .	
4,585,579	4/1986	Bommaraju et al.	252/387
4,655,892	4/1987	Satta et al. .	
4,677,041	6/1987	Specht .	
4,795,533	1/1989	Young et al. .	
5,032,474	7/1991	Hunter .	
5,298,340	3/1994	Cocks et al. .	
5,466,543	11/1995	Ikoma et al.	429/59
5,690,799	11/1997	Tsukahara et al.	204/290 R

Primary Examiner—Bruce F. Bell

Attorney, Agent, or Firm—Harvey Fendelman; Peter A. Lipovsky; Michael A. Kagan

[57] **ABSTRACT**

An electrochemical cell comprises a container; an electrolyte held within the container, a first electrode positioned in the electrolyte; and a second electrode having a beryllium compound coating. The second electrode is positioned in the electrolyte and generally centered within the first electrode. The second electrode is made of a material selected from the group that includes palladium, AB_2 alloys, and AB_5 alloys, where A represents magnesium, zirconium, and lanthanum, and B represents vanadium, chromium, manganese, or nickel. The beryllium compound coating is formed by charging the second electrode in the presence of a beryllium salt.

10 Claims, 2 Drawing Sheets

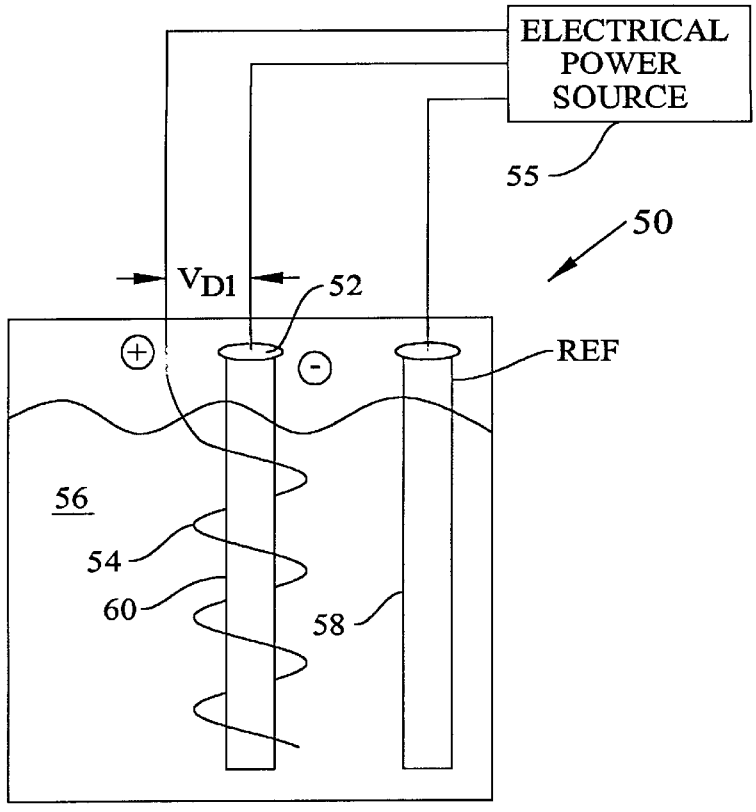

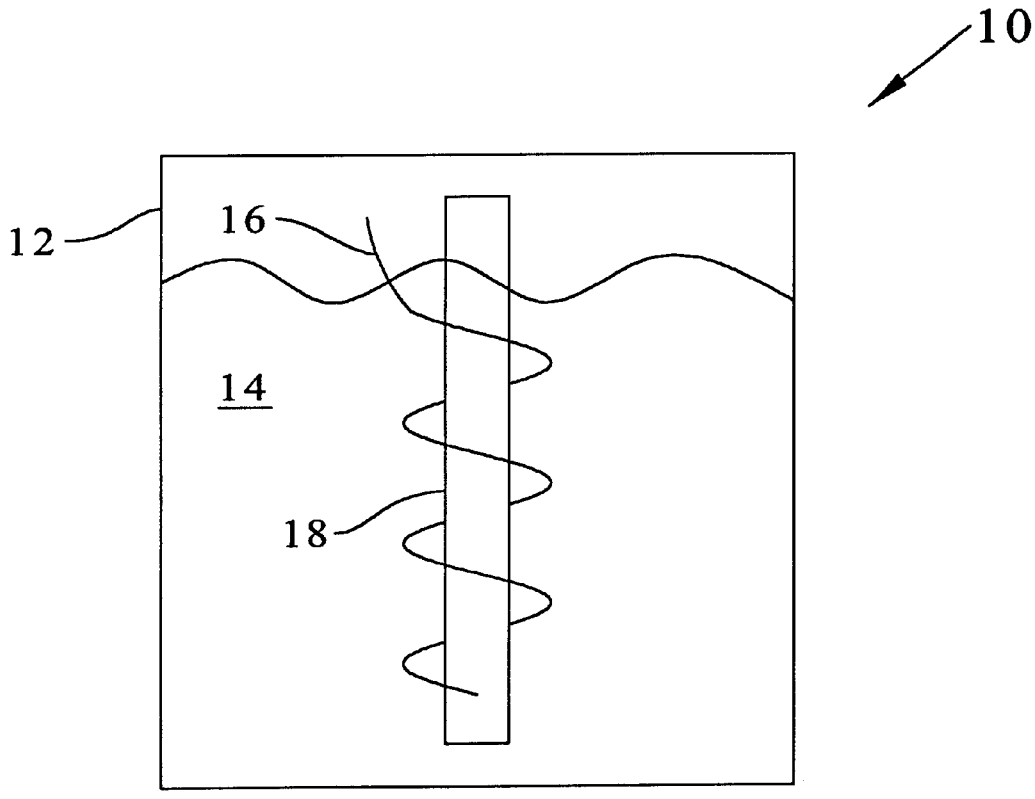

FIG. 1

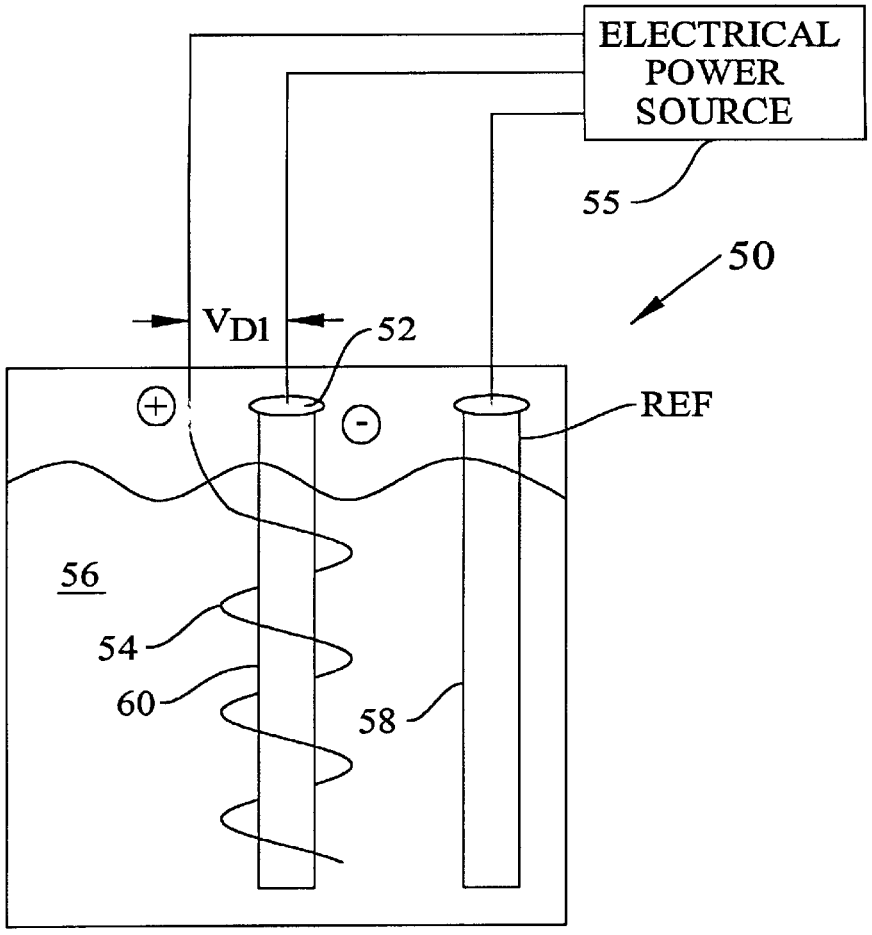

FIG. 3

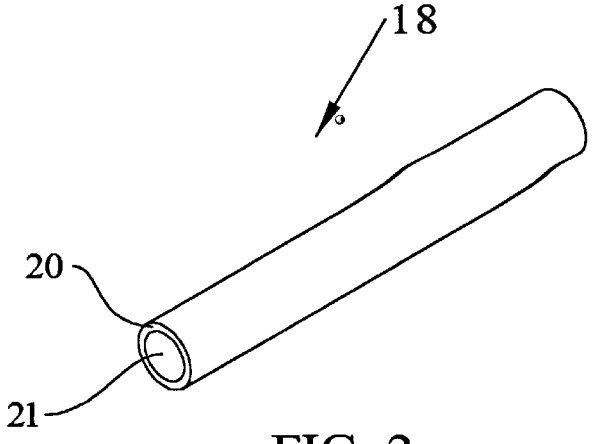

FIG. 2

ELECTROCHEMICAL CELL HAVING A BERYLLIUM COMPOUND COATED ELECTRODE

BACKGROUND OF THE INVENTION

The present invention generally relates to the field of electrochemistry, and more particularly, to an electrochemical cell having a metal hydride electrode.

Metal hydride systems show a great deal of promise as electrical energy storage devices due to their high theoretical energy and power densities, rechargeability, and potential broad range applications. Although the first intermetallic hydride was developed thirty years ago and despite construction of the first prototype metal hydrogen electrode twenty years ago, metal hydrogen electrodes still experience many shortcomings. These include high cost of alloys, poor hydrogen storage capabilities, difficult activation, pyrophoricity, problems of impurities, thermodynamic instabilities, embrittlement, and corrosion in alkaline media.

There are two classes of metal hydride alloys employed as negative electrodes. They are the AB_2 and AB_5 ($LaNi_5$) alloys, where A may be represent magnesium, zirconium, and lanthanum, and B may be substituted by nickel, vanadium, chromium, or manganese. Both classes of alloys include many additional metal components which improve performance, life, and self-discharge. The rate at which AB_2 or AB_5 alloys can absorb hydrogen generated electrochemically and the degree of loading is greatly influenced by the interphase region formed when an electrode is exposed to an electrolyte. In the simplest case, the interphase region takes the form of the electrical double layer. In the more complex cases and, in particular, during the charge transfer reaction, it consists of layers, each associated with a participating elementary process. In this representation, the interphase region is an open system in which a number of consecutive processes takes place, of which the slowest one determines the rate. These processes include transport of the reactants from the bulk to the electrode surface by diffusion, adsorption on the electrode surface, charge transfer, desorption of the reaction products, followed by transport of the reaction products away from the electrode surface. In a discharging battery, these same processes occur; however, in a battery the electrons ultimately flow into an external circuit where the electrical work is delivered. In the negative electrode, the relevant processes during charge/discharge of a metal hydride battery occurs in a multi phase environment—gas, liquid, and solid.

The central role of the interphase in transport of electrochemically generated hydrogen into the electrode interior has been discussed recently and the non-autonomous character of the interphase was stressed. It was shown that the interphase is an active element and that its properties are determined by those of the contacting phases, i.e., the electrode interior as well as the electrolyte. The interphase region may be affected in the course of battery operation, especially as a result of cycling. During charging/discharging operational modes, the electrode matrix expands and contracts. With cycling, this mechanical stress results in embrittlement and consequent loss of performance by the electrochemical cell.

Therefore, a need exists for an additive which would 1) control both electrodic reactions and transport properties; 2) allow high degrees of H/M loading, and 3) reduce the effects of mechanical stress during cycling to provide increased life of batteries and/or fuel cells.

SUMMARY OF THE INVENTION

The present invention provides an electrochemical cell which comprises a container, an electrolyte held within the container, a first electrode positioned in the electrolyte; and a second electrode having a beryllium compound coating. The second electrode is positioned in the electrolyte and generally centered within the first electrode. The second electrode preferably is made of a material selected from the group that includes palladium, AB_2 alloys, and AB_5 alloys. The beryllium compound coating is believed to prevent or at least greatly diminish embrittlement of the second electrode that would otherwise occur during charging and discharge cycling of the electrochemical cell. The beryllium compound coating may be formed by charging the second electrode in the presence of a beryllium salt.

Another aspect of the invention is directed to an electrode comprising a substrate and a beryllium compound coating formed on the substrate. The substrate preferably is made of a material selected from the group that includes palladium, AB_2 alloys, and AB_5 alloys. The electrode is formed by employing the electrode as a cathode in an electrolyte solution containing a water soluble beryllium salt. The beryllium salt disassociates which frees a beryllium cation, Be^{++}, which migrates to and is deposited on the electrode.

The beryllium compound coating on the electrode increases the hydrogen storage capacities of the electrode, as well as its discharge/charging cycling lifetime. In general, any water soluble beryllium salt can be used as a source of beryllium, which is simply added to a suitable electrolyte.

BRIEF DESCRIPTION OF THE DRAWINGS

FIG. **1** shows an electrochemical cell embodying various features of the present invention.

FIG. **2** is a perspective, end-on view of the cathode used in the electrochemical cell of FIG. **1** showing the beryllium coating.

FIG. **3** shows an electrochemical cell which may be used for manufacturing a cathode having a beryllium compound coating.

Throughout the several view, like elements are referenced using like references.

DESCRIPTION OF THE PREFERRED EMBODIMENT

Referring to FIG. **1**, there is shown an electrochemical cell **10** which comprises a container **12**, an electrolyte **14**, a first electrode, or anode **16** positioned in the electrolyte **14**, and a second electrode, or cathode **18** which includes, as shown in FIG. **2**, a substrate on which is formed a beryllium compound coating **20**. The first and second electrodes **16** and **18**, respectively are immersed in the electrolyte **14**. The second electrode **18** is generally centered within the first electrode **16**, shown by way of example to be configured as a helix. However, it is to be understood that the first electrode **16** may be configured into other three dimensional shapes as long as they assure uniform current distribution. The second electrode **18** preferably is made of a material selected from the group that includes palladium, and metal hydride alloys such as AB_2 alloys, and AB_5 alloys. The first electrode may be made of platinum or any other electrically conductive material which does not corrode in the electrolyte **14**. The second electrode **18** is preferably centered within the first electrode **16** so that there is uniform current density between the electrodes **16** and **18** both during recharging and discharging operational modes of the electrochemical cell **10**.

An example of the manufacture of electrode **18** is described with reference to FIG. **3**. An electrochemical cell **50** was created that includes a container, cathode **52**, platinum anode **54**, and electrolyte **56** in which the cathode **52** and anode **54** are immersed. Palladium (Pd) foil served as the cathode **52** and was charged for about 8 hours with hydrogen or its isotopes from electrolyte **56** consisting essentially of 0.3 M Li_2SO_4 to which 100 ppm of beryllium sulfate ($BeSO_4$) was added. Another suitable water soluble beryllium salt is beryllium chloride ($BeCl_2$). An electrical power source **55**, such as a potentiostat, was used to charge cathode **52** potentiostatically with respect to a reference electrode **58** made of Ag/AgCl which also was immersed in the electrolyte **56**. The beryllium salt dissolved in the electrolyte **56** provides Be^{+2} ions. Electrical current flow between the cathode **52** and anode **54** varied between $-10/cm^2$ mA to -1 A/cm^2. When the charging was terminated, the Pd electrode **52** had a reddish-brown beryllium compound coating **60** having a thickness estimated to be few microns formed on the surface of cathode **52**. The coating **60** is believed to have been an insoluble beryllium compound. The beryllium compound coating **60** then was scraped away, to reveal that the Pd cathode **52** had a pristine appearance. An important advantage of the invention is that the Pd cathode **52** was not black or brittle as observed in experiments which did not have beryllium added to the electrolyte. Although the electrolyte **56** contained 100 ppm of beryllium sulfate, it is to be understood that the invention may be practiced with either lesser or greater concentrations of beryllium in an electrolytic solution, so long as there is enough beryllium to coat the electrode of interest. By way of example, the voltage difference, V_{D1} between the cathode **52** and the anode, or counter electrode **54** was in the range of about −2.5 V to −2.0 V.

The hydrogen sorption of metal hydrides depends, in part, upon its metallurgy. During charging/discharging cycles of a metal hydride electrode, the lattice of the electrode expands and contracts. The resultant mechanical stresses caused by the charging/discharging cycles to which the electrode is subjected result in the formation of micro cracks of the electrode, usually along grain boundaries and metallurgical defects. Such micro cracks are believed to provide an escape route for sorbed hydrogen out of the lattice of the metal comprising the electrode. As a result, both hydrogen storage capacity of the electrode cycle lifetime are greatly reduced.

Electrode **18** may also be manufactured of particles of AB_2 or AB_5 alloys which are coated with palladium. The palladium coating may be applied by electroless plating, or by barrel plating at low current densities from a solution which may contain 0.1 to 1 M $Pd(NH_3)_4Cl_2$ salt. The coated particles then are pressure sintered to provide a rigid, porous structure having voids that expose a large surface area of the electrode on which the beryllium coating then may be formed. The particles may range in size from submicron to several microns, depending on the requirements of a particular application. An electrode **18** formed by the techniques described above has a higher density of hydrogen absorbing material and, therefore provides higher hydrogen content to an electrochemical cell compared to a cell which includes an electrode formed with an electrically conductive binding material. A pressure sintered electrode **18** offers flexibility in design because of porosity control, i.e., it may be used in low discharge rate applications, high discharge rate applications, or applications that require a broad range of discharge rates.

Obviously, many modifications and variations of the present invention are possible in light of the above teachings. For example, other effective additives to the electrolyte are magnesium salt or thiourea could be used in place of beryllium. It is therefore to be understood that within the scope of the appended claims, the invention may be practiced otherwise than as specifically described.

We claim:

1. An electrochemical cell, comprising:

a container;

an electrolyte in said container;

a first electrode positioned in said electrolyte; and

a second electrode having a beryllium compound coating positioned in said electrolyte.

2. The electrochemical cell of claim **1** wherein said second electrode is made of a material selected from the group that includes palladium, AB_2 alloys, and AB_5 alloys, where A represents magnesium, zirconium, and lanthanum, and B represents vanadium, chromium, manganese, or nickel.

3. The electrochemical cell of claim **1** wherein said second electrode is generally centered within said first electrode.

4. A method for manufacturing an electrochemical cell, comprising the steps of:

fabricating an electrochemical cell which includes:

a container;

an electrolyte solution which includes a water soluble beryllium salt contained in said container;

a first electrode positioned in said electrolyte; and

a second electrode positioned in said electrolyte;

charging said second electrode to form a beryllium compound coating on said second electrode.

5. The method of claim **4** wherein said second electrode is made of a material selected from the group that includes palladium, AB_2 alloys, and AB_5 alloys, where B represents vanadium, chromium, manganese, or nickel.

6. The method of claim **4** wherein said second electrode is generally centered within said first electrode.

7. The electrochemical cell of claim **4** wherein said beryllium salt is selected from the group that includes beryllium sulfate and beryllium chloride.

8. An electrode, comprising:

a substrate made of a material selected from the group that includes palladium, AB_2 alloys, and AB_5 alloys, where A represents magnesium, zirconium, and lanthanum, and B represents vanadium, chromium, manganese, or nickel; and

a beryllium compound coating formed on said substrate.

9. An electrochemical cell, comprising:

a first container;

a first electrolyte contained in said first container;

a first electrode positioned in sad first electrolyte; and

a second electrode positioned in said first electrolyte, where said second electrode is made of a material selected from the group that includes palladium, AB_2 alloys, and AB_5 alloys, B represents vanadium, chromium, manganese, or nickel, and said second electrode has a beryllium compound coating; and said second electrode is manufactured by contacting said second electrode and a third electrolyte to a second electrolyte solution which includes a beryllium salt and charging said second electrode to form said beryllium compound coating on said second electrode.

10. An electrochemical cell, comprising:

a first container;

a first electrolyte contained in said first container;

a first electrode positioned in said first electrolyte; and

a second electrode positioned in said first electrolyte, where said second electrode is made of a material selected from the group that includes palladium, AB_2 alloys, and AB_5 alloys, B represents vanadium, chromium, manganese, or nickel, and said second electrode has a beryllium compound coating; and said second electrode is manufactured by contacting said second electrode and a third electrolyte to a second electrolyte solution which includes a material selected from the group consisting essentially of magnesium salt and thiourea, and charging said second electrode.

* * * * *

Chapter III: Contributions from Naval Research Laboratory and the Department of Chemistry, University of La Verne.

The recent works of Dr Melvin H. Miles, formerly at the Naval Weapon Center, China Lake, currently at the University of La Verne, La Verne, CA 91750 and Dr Scott R. Chubb of the Naval Research Laboratory, Washington, DC are included in this chapter.

Dr. Miles' research into the Fleischmann-Pons effect is well known. Over the years, since the announcement on the 23rd March of 1989, he published a number of papers dealing primarily with excess enthalpy production. He was the first to establish proportionality between excess enthalpy production and He^4 content in the evolving gases generated by the electrolysis of heavy water. His second, very important contribution was, to employ PdB alloys as the electrode material to enhance the rate of excess enthalpy generation and to improve the reproducibility of massive electrodes.

Theoretical aspects of the unusual behavior of the polarized Pd/D-D_2O system are the subject examined theoretically by Dr Chubb. Dr Scott R Chubb, a noted theoretical physicist. His numerous publications have contributed much to our understanding of events occurring in solids. His recent work, "Semi-classical conduction of charged and neutral particles in finite lattices," is included in this report.

III.1 Correlation of Excess Enthalpy and Helium-4 Production: A Review, M. H. Miles

III.2 Precision and Accuracy of Cold Fusion Calorimetry, M.H. Miles and M. Fleischmann

III.3 Palladium-Boron Alloys and Methods for Making and Using Such Alloys, M. H. Miles and M. Ashraf Imam

III.4 Semi-Classical Conduction of Charged and Neutral Particles in Finite Lattices, Scott R. Chubb

CORRELATION OF EXCESS ENTHALPY AND HELIUM-4 PRODUCTION: A REVIEW

M.H. MILES
Department of Chemistry, University of La Verne
La Verne, CA 91750, USA
E-Mail: mmiles@ulv.edu or melmiles1@juno.com

Three different sets of experiments conducted in the Navy Laboratory (NAWCWD) at China Lake, California (1990-1994) clearly established that helium-4 is the main fusion product in the Pd/D_2O+LiOD electrolysis system. A correlation between excess enthalpy and excess helium-4 was measured in 18 out of 21 experiments. The observation of no excess enthalpy was correlated with no excess helium in 12 out of 12 experiments. Thus 30 out of 33 experiments agree with the hypothesis that the excess enthalpy produced in cold fusion studies is correlated with helium-4 production: $D + D \rightarrow {}^4He + 23.8$ MeV. Furthermore, the measured rate of helium-4 production was always in the appropriate range of 10^{10} to 10^{12} atoms per second per watt of excess power.

1. Introduction

At the beginning of the cold fusion controversy in 1989, critics rightfully demanded evidence of nuclear products to confirm any fusion reactions. Because of the unusual rush to judgment of this new field as well as the early introduction of ridicule, cold fusion was quickly labeled as error, incompetence and fraud.[1] Therefore, experimental results obtained in 1990 or later are largely ignored by the scientific community. Furthermore, the scientists who have continued with cold fusion research are labeled as "believers" and compared with the followers of religion.[2]

The China Lake experiments funded by the Office of Naval Research (ONR) were the first that clearly established that helium-4 is the main fusion product in palladium-heavy water electrolysis systems. Many other laboratories have now reported evidence of helium-4 in cold fusion experiments. Should these important experimental results be ignored simply because they were obtained in 1990 and later rather than in 1989? The purpose of this review is to present a summary of the evidence for helium-4 production that was obtained in three separate sets of Navy experiments conducted in the time period of 1990 to 1994.

2. First set of 15 Experiments (1990-1991)

The first set of 15 experiments conducted at China Lake (1990-1991) used glass flasks (500 mL) to collect samples of the electrolysis gases.[3] The entire system was self-flushing because of the continuous evolution of deuterium and oxygen gases. Furthermore, the gas collection system was always under positive pressure via the evolution of the effluent gases through an oil bubbler.[3,4] Experimental details of the electrochemical cell and calorimetry as well as the day-by-day excess enthalpy measurements are presented elsewhere.[3,4] The electrolysis gas samples collected in 500 mL glass flasks were sent to the University of Texas for helium analysis.[5] The excess power (P_{EX}) and helium-4 measurements for the ten Pd/D_2O+LiOD electrolysis samples are presented in Table 1.

Table 1. Excess power and helium measurements for Pd/D_2O + 0.2M LiOD experiments (1990).

Sample (Date)	P_{EX} (W)	P_{out}/P_{in} (X)	^4He (Atoms/500 mL)	$^4He/s \bullet W$
12/14/90-A	0.52[a]	1.20[a]	10^{15}	10^{12}
10/21/90-B	0.46	1.27	10^{15}	10^{12}
12/17/90-A	0.40[b]	1.19[b]	10^{14}	10^{11}
11/25/90-B	0.36	1.15	10^{15}	10^{12}
12/17/90-B	0.29[b]	1.11[b]	$<10^{13}$	$<10^{10}$
11/20/90-A	0.24	1.10	10^{14}	10^{11}
11/27/90-A	0.22	1.09	10^{15}	10^{12}
10/30/90-B	0.17	1.12	10^{13}	10^{10}
10/30/90-A	0.14	1.08	10^{13}	10^{10}
10/17/90-B	0.07	1.03	$<10^{13}$	$<10^{10}$

[a] i=250 mA/cm^2. All other experiments used i=200 mA/cm^2 (500 A).
[b] Possible calorimetric error due to low D_2O solution level. This error was more serious for the 12/17/90-B sample and likely caused the excess power measurement to be too large.

The helium-4 measurements at the University of Texas consisted of mass spectrometry observations of either no peaks or small, medium, and large helium-4 peaks.[5] There were no control samples of known helium concentrations in D_2 +O_2 mixtures for comparison. Initially, a detection limit of $8x10^{11}$ atoms of helium-4 was estimated[5], but the actual detection limits were expected to be higher.[4] In retrospect, this initial detection limit exceeds the sensitivity of the best commercial laboratory that was later used for the detection of helium-4 ($\pm 1.0x10^{12}$ atoms or ± 0.10 ppb). Additional experiments using metal flasks showed that the mean background helium concentration in our system was 4.4 ± 0.6 ppb or $5.1\pm0.7x10^{13}$ ^4He atoms/500 mL.[6,7] Therefore, in Table 1, the small, medium, and large helium-4 peaks are assigned values of 10^{13}, $10^{14,}$ and 10^{15} helium-4 atoms per 500 mL above background levels.[7] This assignment yields helium-4 production rates of 10^{10} to 10^{12} ^4He $s^{-1}W^{-1}$. The first sample (10/17/90-B) was taken early in the experiment before the excess enthalpy effect developed[4], thus this sample acts as a control. When excess enthalpy was measured, 8 out of 9 samples showed excess helium-4. The one exception (12/17/90-B) could possibly be explained as a calorimetric error due to the unusually low level of D_2O in this cell.[7]

The diffusion of atmospheric helium into the 500 mL glass flasks must be considered in this first set of experiments. Based on the measured surface area and thickness of these Pyrex flasks, the theoretical rate of atmospheric helium diffusing into the flasks is $2.6x10^{12}$ atoms/day.[6] Actual experimental measurements by two different commercial laboratories yielded mean values of $3.2x10^{12}$ atoms/day for nitrogen-filled flasks and $2.1x10^{12}$ atoms/day for flasks filled with D_2+O_2 electrolysis gases.[6] Hydrogen and deuterium gases also diffuse through glass, thus it is reasonable that the outward diffusion of deuterium could somewhat slow the rate of the inward diffusion of atmospheric helium, and this was observed experimentally.[4] Based on the experimental diffusion rate of $2.1x10^{12}$ atoms/day for glass flasks containing D_2+O_2, it would require 24 days for the diffusion of atmospheric helium into these flasks to equal the background helium level ($5.1x10^{13}$ atoms/500 mL) for our system. Therefore, the diffusion of atmospheric helium into these glass sample flasks can be ruled out as an experimental error source. This information was not available in our earlier publications.[3-5]

Five additional control samples were generated using Pd/H_2O+LiOH. No excess enthalpy was measured calorimetrically at China Lake and no helium-4 was detected in

any of these samples by the University of Texas.[3,4] This provided additional evidence that contamination by atmospheric helium could be ruled out. Including the first sample (10/17/90-B, Table 1) from the Pd/D_2O+LiOD study, there were a total of six samples that showed no excess helium-4 when the calorimetry measured no excess enthalpy.

3. Second Set of 3 Experiments (1991-1992)

Most of our experiments in 1991 failed to generate any significant anomalous effects. Late in that year, two experiments began to produce excess enthalpy. Glass flasks (500 mL) were again used to collect three electrolysis gas samples. However, these samples were sent to Rockwell International in order to obtain more accurate helium-4 measurements (±0.10 ppb). Furthermore, measurements of helium-4 for these samples were continued over a period exceeding 100 days to provide for the accurate determination of the rate of atmospheric helium diffusing into these glass flasks. The results of this study are present in Fig. 1.

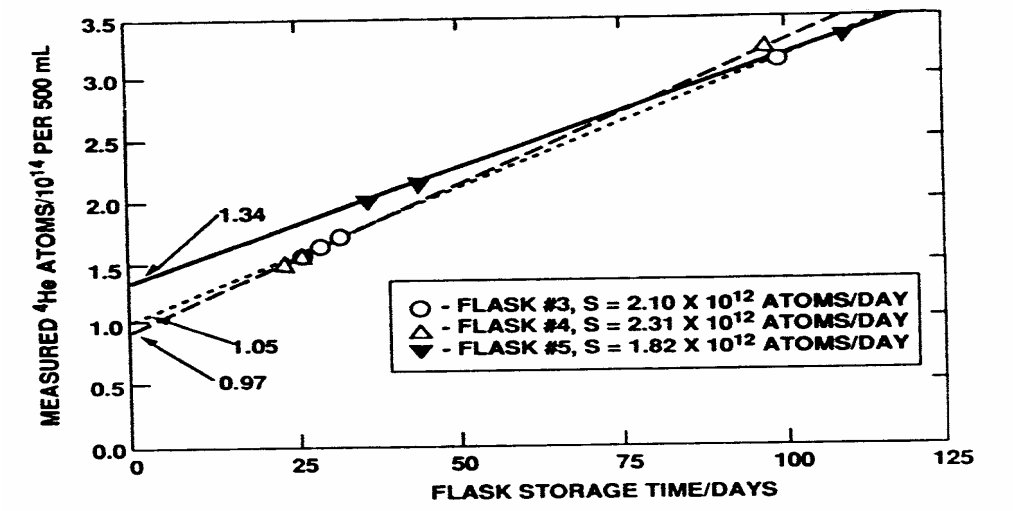

Figure 1. Measurements of helium-4 by Rockwell International for three glass flasks filled with D_2+O_2 from Pd/D_2O electrolysis involving excess enthalpy production.

It was this same set of experiments that determined a mean rate of 2.1×10^{12} atoms/day for atmospheric helium diffusing into these flasks. The three glass flasks gave individual values of 2.10×10^{12}, 2.31×10^{12}, and 1.82×10^{12} atoms/day (Figure 1). As shown in Figure 1, the three lines are extrapolated to zero time to yield 1.34×10^{14}, 1.05×10^{14} and 0.97×10^{14} ^{4}He atoms per 500 mL. These values are the concentrations of helium-4 at the time when the samples were collected. Our system background level of helium-4 (0.51×10^{14} atoms/500 mL) can now be subtracted to find the amount of helium-4 produced per second per watt (W) of excess power. The experimental results as well as the results of these calculations are given in Table 2. It is interesting to note in Table 2 that a Geiger-Mueller (GM) alpha-beta-gamma detector (Ludlum Model 44-7) positioned near the electrochemical cells recorded an anomalous high count (27 σ) during the time period when two of these samples were collected.[6]

Table 2. Second set of experiments yielding excess power and helium production during D_2O electrolysis.

Sample (Date)	P_{EX} (W)	P_{out}/P_{in} (X)	^4He[a] (Atoms/500 mL)	$^4He/sW$[b]
12/30/91-B (Flask 5)	0.100[c]	1.08	$1.34x10^{14}$	$2x10^{11}$
12/30/91-A (Flask 3)	0.050[c]	1.02	$1.05x10^{14}$	$2x10^{11}$
01/03/92-B (Flask 4)	0.020[d]	1.01	$0.97x10^{14}$	$5x10^{11}$

[a] Error range reported by Rockwell International was $\pm 0.01x10^{14}$ atoms/500 mL($\pm 1\ \sigma$).
[b] Corrected for a background level of $5.1x10^{13}$ atoms/500 mL.
[c] I=525 mA. An anomalous GM count (27 σ) was measured during this period.
[d] I=500 mA. The GM count rate was within the normal range.

It requires 4440 s to produce 500 mL of electrolysis gases (D_2, O_2) at 525 mA for normal laboratory conditions (T=296 K, P=690 Torr) at China Lake.[7] Therefore, the calculation for the first sample (12/30/91-B) in Table 2 is given in Equation 1.

$$\frac{(1.34-0.51)x10^{14}\ He\ atoms/500\ mL}{(4440\ s/500\ mL)(0.100\ W)} = 1.9x10^{11}\ He\ atoms\ s^{-1}W^{-1} \quad (1)$$

This sample likely represents the most accurate combination of excess power and excess helium measurements in these studies, and the result is close to the theoretical rate of $2.6x10^{11}$ $^4He\ s^{-1}W^{-1}$ for the $D+D \rightarrow {}^4He+23.8$ MeV fusion reaction.[6]

A closer examination of Table 2 shows that the different amounts of helium-4 reported by Rockwell International are statistically very significant. The error in these measurements of helium-4 was only $\pm 0.01x10^{14}$ atoms/500 mL ($\pm 1\ \sigma$), therefore the difference between the highest ($1.34x10^{14}$ atoms/500 mL) and the lowest ($0.97x10^{14}$ atoms/500 mL) measurements (Table 2) is a 37 σ effect. Furthermore, the background level of helium-4 in our system was later accurately measured as $0.51\pm0.06x10^{14}$ atoms/500mL.[6,7] Therefore, the highest level of helium-4 measured in Table 2 ($1.34x10^{14}$ atoms/500 mL) is statistically a 14 σ effect above the system background i.e. $(1.34\text{-}0.51)x10^{14}/0.06x10^{14}$. Except perhaps for the cold fusion field, any measurements that produce even a 5 σ effect are considered to be very significant by the scientific community. During these experiments, neither Rockwell International nor the China Lake laboratory knew results of both the excess power and helium measurement until after this study was completed and all results were reported to a third party (J.J. Lagowski of the University of Texas).[6] Moreover, the background helium-4 level for our system was not determined until several years later (see Table 3).

4. Third Set of 15 Experiments (1993-1994)

The final set of 15 China Lake experiments employed metal flasks to collect the electrolysis gas samples.[8,9] This eliminates the diffusion of any atmospheric helium into the collected gas sample sent out for analysis. For these experiments, the helium analysis was performed by the U.S. Bureau of Mines laboratory in Amarillo, Texas. A major goal of these studies was to determine the background level of helium-4 in our electrolysis system. Therefore, everything was arranged exactly as in the previous two sets of experiments except that metal flasks were used in place of the glass flasks for the collection of electrolysis gas samples. As in previous experiments, the palladium material was in the form of cylindrical rods or wires unless stated otherwise.

Table 3 presents the experimental results for six control experiments where no excess power was measured at any time over the entire duration of the study.[9] One experiment used H_2O+LiOH while the other five employed D_2O+LiOD solutions.

Table 3. Helium measurement in control experiments using metal flasks. No excess power was measured.

Electrode (Dimensions)	Flask/Cell (Date)	^4He[a] (ppb)	^4He (Atoms/500 mL)
Pd[b] (4 mm x 1.6cm)	1/C (2/24/93)	4.8 ±1.1	$5.5x10^{13}$
Pd-Ag[b] (4 mm x 1.6 cm)	2/D (2/24/93)	4.6 ±1.1	$5.2x10^{13}$
Pd[b] (4 mm x 1.6 cm)	3/C (2/28/93)	4.9 ±1.1	$5.6x10^{13}$
Pd-Ag[b] (4mm x 1.6 cm)	4/D (2/28/93)	3.4±1.1	$3.9x10^{13}$
Pd[c] (1 mm x 1.5 cm)	3/C (7/7/93)	4.5±1.5	$5.1x10^{13}$
Pd[d] (4.1 mm x 1.9 cm)	3/D 3/30/94	4.6 ±1.4	$5.2x10^{13}$
(Mean)		(4.5 ±0.5)	($5.1 \pm 0.6x10^{13}$)

[a] Helium analysis by U.S. Bureau of Mines, Amarillo, Texas.
[b] D_2O + LiOD (I=500 mA).
[c] H_2O + LiOH (I=500 mA).
[d] D_2O + LiOD (I=600 mA).

The experiments in Table 3 established that the mean background level of helium-4 in our system was $5.1\pm0.6x10^{13}$ atoms/500 mL (4.5±0.5 ppb). Theoretical calculations show that this background helium-4 is due to the diffusion of atmospheric helium through the thick rubber vacuum tubing (50 cm length) that was used to connect our electrolysis cell to the metal collection flask.[9,10] The diffusion of atmospheric helium through the glass components of our electrolysis cell is theoretically much too small to explain our measured background level of helium-4. The background level of helium can be reduced to 0±1 ppb when metal lines are used to replace the rubber vacuum tubing.[11]

Table 4 shows the results for similar experiments that produced excess power and used metal flasks to collect the electrolysis gas samples.[9] Details of the China Lake calorimetry that was used during this period are presented elsewhere.[12] The amount of helium-4 measured is higher for each study than the amount found in any of the control experiments.

Table 4. Excess power and helium measurements for experiments using metal flasks.

Electrode (Dimensions)	Flask/Cell (Date)	P_x (W)	^4He[a] (ppb)	^4He (Atoms/500 mL)	^4He s/W[b]
Pd Sheet[c] (1.0 mm x 3.2 cm x 1.6 cm)	3/A (5/21/93)	0.055	9.0±1.1	$1.02x10^{14}$	$1.6x10^{11}$
Pd[c] (1 mm x 2.0 cm)	4/B (5/21/93)	0.040	9.7±1.1	$1.09x10^{14}$	$2.5x10^{11}$
Pd[c] (1 mm x 1.5 cm)	1/C (5/30/93)	0.040	7.4±1.1	$0.84x10^{14}$	$1.4x10^{11}$
Pd[c] (2 mm x 1.2 cm)	2/D (5/30/93)	0.060	6.7±1.1	$0.75x10^{14}$	$7.0x10^{10}$
Pd[d] (4 mm x 2.3 cm)	1/A (7/7/93)	0.030	5.4±1.5	$0.61x10^{14}$	$7.5x10^{10}$
Pd[d] (6.35 mm x 2.1 cm)	2/A (9/13/94)	0.070	7.9±1.7	$0.90x10^{14}$	$1.2x10^{11}$
*Pd-B[d] (6 mm x 2.0 cm)	3/B (9/13/94)	0.120	9.4±1.8	$1.07x10^{14}$	$1.0x10^{11}$

[a] Helium analysis by U.S. Bureau of Mines, Amarillo, Texas.
[b] Corrected for background helium level of $0.51x10^{14}$ atoms/500 mL.
[c] D_2O + LiOD (I=400 mA).
[d] D_2O + LiOD (I=500 mA).
* NRL material prepared by Dr. M.A. Imam.

The rate of helium-4 production shown in Table 4 ranges from $7.0x10^{10}$ to $2.5x10^{11}$ atoms $s^{-1}W^{-1}$. As found in the previous two sets of experiments, these results are again reasonably close to the theoretical rate of $2.6x10^{11}$ ^4He $s^{-1}W^{-1}$ for the D+D fusion reaction. One of the samples in Table 4 that produced excess enthalpy and correlated helium-4 production was the novel Pd-B material made by Dr. Imam at the Naval Research Laboratory (NRL).[13] This material has produced excess enthalpy in nearly every experiment, and extensive calorimetric measurements have been reported. [14-20]

There were two measurements using metal flasks for collecting electrolysis gas samples that produced excess power but showed no excess helium-4.[9] Both measurements involved a cell that used a Pd-Ce alloy cathode. These two measurements recorded 0.17 and 0.30 W of excess power but only 4.6±1.4 and 4.7±1.3 ppb of helium-4, respectively, in the electrolysis gas samples. If experimental error is ruled out, then it may be speculated that either the Pd-Ce alloy involves a different fusion reaction or that the helium atoms produced remained trapped in the Pd-Ce electrode.[9]

In summary, the final set of China Lake experiments employed metal flasks to collect the electrolysis gas samples. When excess enthalpy was measured, 7 out of 9 samples registered excess helium-4 production (Table 4). When no excess heat was present, all 6 samples showed no excess helium-4 (Table 3).

5. Discussion

The results of these three sets of experiments established that most of the helium-4 produced in the fusion reaction is released to the electrolysis gas stream. This suggests that the D+D fusion reaction either occurs at or near the electrode surface or that the heavily deuterided palladium somehow allows the helium-4 to readily escape from the bulk material. Assuming that $^2D + {}^2D \rightarrow {}^4He$ + 23.8 MeV is the fusion reaction and that all of helium-4 produced escapes to the electrolysis gas stream, then the theoretical

relationship between the excess power and the helium concentration in the gas sample can be calculated. Results for these calculations are shown in Table 5 for a typical electrolysis current of 500 mA.

Table 5. Theoretical relationship between excess power and the helium-4 concentration in the electrolysis gases. The magnitude of experimental error is also presented.

P_x (W)	^4He[a] (ppb)	^4He (Atoms/500 mL)	^4He Error[b] %	Calorimetric Error[c] %
0.020	2.2	2.55×10^{13}	45	100
0.050	5.6	6.38×10^{13}	18	40
0.100	11.2	1.28×10^{14}	8.9	20
0.200	22.4	2.55×10^{14}	4.5	10
0.500	56.0	6.38×10^{14}	1.8	4
1.000	112.0	1.28×10^{15}	0.89	2
10.000	1112.0	1.28×10^{16}	0.089	0.2

[a] For I=500 mA assuming $^2D + {}^2D \rightarrow {}^4He + 23.8$ MeV.
[b] For ±1.0 ppb error.
[c] For ±0.020 W error.
NOTE: N. Lewis (Cal Tech) and D. Albagli (MIT) reported gas-phase helium-4 detection limits of 1000 ppb (1 ppm).

The excess power measurements in the China Lake experiments ranged from 0.52 W to 0.020 W (Tables 1, 2, 4). Larger excess power effects would be helpful, but the fact that increasing the temperature increases the excess power (positive feedback) was not known at the time of these experiments.[14-21] Furthermore, the China Lake calorimetry was not designed to operate at higher temperatures. Future studies of helium-4 production at higher temperatures are desirable that use the Fleischmann-Pons Dewar calorimetry where the calorimetric error is less than ±0.001 W.[14,15,22] It should be noted that two prominent studies in 1989 reported evidence against any helium-4 in the gas phase while using a detection limit of 1000 ppb (Table 5). An excess power of nearly 10 W would be required before such instruments would detect any helium-4 production (Table 5). Ten watts of excess power would drive many cold fusion calorimetric cells to boiling.

Combining the three different sets of China Lake experiments (Tables 1, 2, 4) shows a correlation between the measurements of excess enthalpy and excess helium-4 in 18 out of 21 experiments. The three exceptions are the two studies involving the Pd-Ce alloy and an experiment with a possible calorimetric error due to an unusually low D_2O level (Table 1, sample 12/17/90-B). There were also twelve studies where no excess enthalpy was measured by the calorimetry (Table 3 plus six control studies in the first set of experiments). When no excess enthalpy was measured, 12 out of the 12 experiments produced no excess helium-4. Thus 30 out of 33 experiments conducted in the Navy laboratory at China Lake agree with the hypothesis that the excess enthalpy in cold fusion experiments is correlated with helium-4 production. An exact statistical treatment shows that the probability is only one in 750,000 that the China Lake set of heat and helium measurements could be this well correlated due to random experimental errors.[9] Furthermore, the rate of helium-4 production was always in the appropriate range of 10^{10} to 10^{12} atoms per second per watt of excess power for all three sets of experiments. These results stand as solid evidence that the main process producing excess enthalpy in the Pd/D_2O+LiOD electrolysis system is D+D fusion with helium-4 as the major product.

Many other research groups have now reported evidence of helium-4 production in cold fusion experiments.[1] These groups include Bockris et al[23], Liaw et al[24], and

McKubre[25]. An important recent study in Italy suggests that the measurement of helium-4 can even replace the calorimetry as the most accurate measurement of the excess enthalpy.[26]

The D+D fusion reaction offers a solution to the world's energy need and the eventual shortage of oil and other chemical fuels. A simple calculation shows that there are sufficient deuterium atoms (10^{43}) in the oceans of the world to provide for the present energy needs of the world's population for more than one billion years.

6. Summary

The Navy experiments conducted in the laboratory at China Lake, California were the first to clearly establish that helium-4 is the main fusion product in the Pd/D_2O+LiOD electrolysis system. The first set of experiments was conducted in 1990. Two additional sets of Navy experiments verified the first study and provided convincing evidence that the excess enthalpy in cold fusion experiments is correlated with the $D+D \rightarrow {}^4He$ + 23.8 MeV fusion reaction. These results for helium-4 production have now been substantiated by many other research groups.

References

1. C.G. Beaudette, "Excess Heat: Why Cold Fusion Research Prevailed", 2nd Edition, Oak Grove Press (ISBN 0-9678548-3-0), South Bristol, Maine, 2002.

2. S.K. Ritter, *Chem. Eng. News*, **81**, No. 34, p. 33 (2003).

3. M.H. Miles, B.F. Bush, G.S. Ostrom, and J.J. Lagowski in "The Science of Cold Fusion", ICCF-2 Proceedings, T. Bressani, E. Del Giudice and G. Preparata, Editors, Italian Physical Society, pp. 363-372 (1991).

4. M.H. Miles, R.A. Hollins, B.F. Bush, J.J. Lagowski, and R.E. Miles, *J. Electrochem. Soc.*, **346**, 99 (1993).

5. M.H. Miles, G.S. Ostrom, B.F. Bush, and J.J. Lagowski, *J, Electrochem. Soc*., **304**, 271 (1991).

6. M.H. Miles, B.F. Bush, and J. J. Lagowski, *Fusion Technol.*, **25**, 478 (1994).

7. M.H. Miles, *J. Phys. Chem. B*, **102**, 3642 1998)

8. M.H. Miles, K.B. Johnson, and M.A. Imam in "Progress in New Hydrogen Energy", ICCF-6 Proceedings, M.Okamoto, Editor, Vol. 1, pp. 20-28 (1996).

9. M.H. Miles, B.F. Bush, and K.B. Johnson, Anomalous Effects in Deuterated Systems", NAWCWPNS TP 8302, 98 pp., September 1996.

10. M.H. Miles and B.F. Bush, *Trans. Fusion Technol.*, **26**, 156 (1994).

11. B.F. Bush, private communication. See also ICCF-7 Proceedings p. 42, 1998.

12. M.H. Miles, B.F. Bush, and D.E. Stilwell, *J. Phys. Chem.*, **98**, 1948 (1994).

13. B. Daviss, *New Scientist*, **177**, No. 2388, 36 (2003).

14. M.H. Miles, M. Fleischmann, and M.A. Imam, "Calorimetric Analysis of a Heavy Water Electrolysis Experiment Using a Pd-B Alloy Cathode", NRL/MR/6320—01-8526, 155 pp., March 26, 2001.

15. S. Szpak, P.A. Mosier-Boss, M.H. Miles, M.A. Imam, and M. Fleischmann in "Thermal and nuclear Aspects of the Pd/D_2O System", Vol. 1, S. Szpak and P.A. Mosier-Boss, Editors, Technical Report 1862, pp. 31-89, February 2002.

16. M.H. Miles in "Conference Proceedings – ICCF-8", Vol. 70, F. Scaramuzzi, Editor, Italian Physical Society (ISBN 88-7794-256-8), pp. 97-104, May 2000.

17. M.H. Miles, M.A. Imam, and M. Fleischmann in "Conference Proceedings, ICCF-8", Vol. 70, F. Scaramuzzi, Editor, Italian Physical Society (ISBN 88-7794-256-8), pp. 105-119, May 2000.

18. M.H. Miles, M.A. Imam, and M. Fleischmann in "Energy and Electrochemical Processes For a Cleaner Environment", C. Comninellis, M. Doyle, and J. Winnick, Editors, Proceedings Volume 2001-23, The Electrochemical Society (ISBN 1-56677-356-3), Pennington, NJ, 2001.

19. M.H. Miles, M.A. Imam, and M. Fleischmann in "Batteries and Supercapacitors", G.A. Nazri, E. Takeuchi, R. Koetz, and B. Scrosati, Editors, Proceedings Volume 2001-21, The Electrochemical Society (ISBN 1-56677-354-7), Pennington, NJ, 2003

20. M.H. Miles, M.A. Imam, and M. Fleischmann in "ICCF-10 Proceedings", 2003 (in press).

21. M. Fleischmann in "Condensed Matter Nuclear Science, ICCF-9 Proceedings", Xing Z. Li, Editor, Tsinghua University Press (ISBN 7-302-06489-X), Beijing, China, pp. III-XVII (2003).

22. M. Fleischmann in "ICCF-10 Proceedings", 2003 (in press).

23. C.C. Chien, D. Hodko, Z. Minevski, and J.O'M. Bockris, *J. Electroanal. Chem.*, **338**, 189 (1992).

24. B.Y. Liaw, P. Tao, P. Turner, and B.E. Liebert, *J. Electroanal. Chem*., **319**, 161 (1991).

25. M. McKubre, F. Tanzella, P. Tripodi, and P. Hagelstein in "Conference Proceedings, ICCF-8", F. Scaramuzzi, Editor, Italian Physical Society (ISBN 88-7794-256-8), pp. 3-10, May 2000.

26. A. DeNinno, A. Frattolillo, A. Rizzo, and E. Del Giudice in "ICCF-10 Proceedings", 2003 (in press).

PRECISION AND ACCURACY OF COLD FUSION CALORIMETRY

Melvin H. Miles and Martin Fleischmann*,
Department of Chemistry, University of LaVerne, LaVerne, CA 91750 (mmiles@ulv.edu)
*Bury Lodge, Duck Street, Tisbury, Salisbury, Wilts, SP36LJ, U.K.

Introduction

The cold fusion controversy centers on the precision and accuracy of the calorimetric systems used to measure excess enthalpy generation.[1-3] For open, isoperibolic calorimetric systems, there is no true steady state during D_2O+LiOD electrolysis. Exact calorimetric measurements, therefore, require modeling by a differential equation that accounts for all heat flow pathways into and out of the calorimetric systems.[1-8] The improper use and misunderstanding of this differential equation is a major source of confusion concerning cold fusion calorimetric measurements.[1,9-13]

The precision and accuracy of isoperibolic cold fusion calorimetry can be assessed by means of experiments on "blank systems" where no excess enthalpy generation due to cold fusion is expected. Therefore, a clean platinum (not palladium) cathode was polarized in D_2O+0.1M LiOD using platinum also as the anode. The only excess enthalpy generation expected would be from the recombination of the evolved D_2 and O_2 gases. Although the amount of recombination in cold fusion experiments has been a source of controversy,[2,3] various experimental studies have shown that the recombination effect is small at the large current densities used in cold fusion experiment.[2,3,9,14]

Materials and Methods

Calorimetric Cell

Long and narrow calorimetric cell designs promote rapid radial mixing of the electrolyte by the electrolysis gas evolution and minimize heat transfer through the top of the cell relative to the desired pathway through the cell wall to the water bath.[1,9] The use of Dewar cells makes the heat transfer pathway predominantly due to radiation across the vacuum gap of the Dewar cell. Therefore, the heat transfer coefficient can be calculated theoretically by the product of the Stefan-Boltzmann coefficient and the radiant surface area of the cell (109.7 cm^2 in these experiments). Multiplying by the Stefan-Boltzman coefficient, 5.6703×10^{-12} $Wcm^{-2}K^{-4}$, yields a theoretical heat transfer coefficient of 0.622×10^{-9} WK^{-4} for this cell. The Dewar cell used was approximately 2.5 cm in diameter (I.D.) and 22.0 cm in height with the upper 8.0 cm silvered to minimize the effect of the electrolyte level.[1,9]

The platinum cathode used in these experiments was 0.1 cm in diameter and 2.0 cm in length (A=0.63 cm^2). The temperature of the thermostated water bath (approximately 21°C) was precisely controlled to ±0.01°C.

Calorimetric Equations

From basic thermodynamic principles, the calorimetric cell is the system of interest, and the First Law of Thermodynamics expressed as power (J/s or W) becomes

$$P_{calor} = P_{EI} + P_H + P_X + P_{gas} + P_R + P_C + P_W \quad (1)$$

Equation 1 represents the differential equation used to model this open, isoperibolic calorimetric system.

By definition, P_{EI} is the electrochemical power, P_H is the internal heater power, P_X is any anomalous excess power, P_{gas} is the power resulting from the gas stream (D_2, O_2, D_2O vapor), P_R is the power transferred by radiation from the cell to the water bath, P_C is the power transferred by conduction and P_W represents the rate of any pressure-volume work. As usual, positive quantities represent power added to the system (calorimetric cell) and negative quantities represent power given off to the surroundings. The mathematical expressions for these terms are as follows:

$$P_{calor} = C_p M(dT_{cell}/dt) \quad (2)$$

$$P_{EI}=(E(t)-E_H)I \quad (3)$$

$$P_{gas} = -(I/F)\{[0.5\, C_{P,D2}+O.25\, C_{P,\,O2}+0.75\,(P/(P^*-P))C_{P,D2O\,(v)}]\Delta T + 0.75\,(P/(P^*-P))\,L\} \quad (4)$$

$$P_R=-k_R f(T) \text{ where } f(T)=T_{cell}^4 - T_b^4 \quad (5)$$

$$P_C= -k_C\,(T_{cell} - T_b) \quad (6)$$

$$P_W= -RT\,(dn_g/dt) = -RT(0.75I/F) \quad (7)$$

Definitions for many of the symbols used are given elsewhere.[1,9]

Assuming P_C and P_W are relatively small compared to P_R, then

$$P_R^{'} =P_R+P_C+P_W=-k_R^{'} f(T) \quad (8)$$

where $k_R^{'}$ is the pseudoradiative heat transfer coefficient. The validity of this assumption can be determined by comparing $k_R^{'}$ with the theoretical value calculated from the Stefan-Boltzmann coefficient. By assuming $P_X=0$, a lower bound heat transfer coefficient can be evaluated using Eqs. 1 and 8.

$$(k_R^{'})_1 = (P_{EI}+P_H+P_{gas} - P_{calor}) / f(T) \quad (9)$$

The presence of any excess power would increase $f(T)$, thus yielding a lower value for $(k_R^{'})_1$. For this blank experiment, P_X will be small, thus $(k_R^{'})_1$ will be close to the true value. By use of the 12 hour heating pulse, and assuming the excess power (P_X) is constant with time, the true heat transfer coefficient can also be evaluated

$$(k_R^{'})_2 = (P_{EI}+P_H+P_X+P_{gas}-P_{calor})/f(T) \quad (10)$$

Complete mathematical details are presented elsewhere.[9,11-13]

Analogous with differential equations for reaction kinetics, more accurate calorimetric results can be obtained by the integration of the data sets.[11-13] Both forward and backward integration methods were used with the calorimetric differential equations (Eq. 1). A variety of methods, therefore, can be used to evaluate the

pseudoradiative heat transfer coefficient including lower bound, true, differential, forward integration and backward integration techniques.[9-13]

Each experimental cycle lasted exactly two days over a total of 16 days. For each cycle, the internal cell heater was off for 12 hours, then turned on at $t=t_1$, for 12 hours and then off at $t=t_2$ for the final 24 hours. Addition of D_2O occurred at the beginning of each cycle. The cell current was constant at 0.2000 A.

Results and Discussion

Various methods were used to evaluate the pseudoradiative heat transfer coefficient, $k_R^{'}$, at $t=t_2$ for each two-day experimental cycle. For example, mean values were $(k_R^{'})_1=0.62013\times10^{-9}$ WK^{-4} (lower bound, Eq. 9) and $(k_R^{'})_2=0.62059\times10^{-9}$ WK^{-4} (true, Eq. 10). The most accurate method for determining $k_R^{'}$ was backward integration that yields a mean value of $(k_R^{'})_{262}^{0} = 0.62083\times10^{-9}$ WK^{-4} for this calorimetric cell. All values obtained for $k_R^{'}$ were close to the theoretical result of 0.622×10^{-9} WK^{-4} calculated from the Stefan-Boltzmann coefficient, and this result validates the assumption made in Eq. 8.

The two calorimetric experimental parameters required for Eq. 1 are $k_R^{'}$ and the water equivalent of the system, C_pM. For integration, the calorimetric equation (Eq. 1) can be written in a straight line form, y=mx+b, where the intercept yields $k_R^{'}$ and the slope is C_pM [9-13]. The various integration methods yield an over-all mean value of $C_pM = 340.1\pm0.8$ JK^{-1}. This is the least accurate calorimetric parameter, but its effect can be minimized by evaluations made at the end of the heating pulse ($t=t_2$) where $CpM\ (dT_{cell}/dt) \approx 0$. Theoretical calculations based on the mass of heavy water used and the glass and metal components in contact with the electrolyte give C_pM values in approximate agreement with the experimental values.[9]

The differential rate of excess enthalpy production due to recombination in this blank system can be estimated from the equation obtained by subtracting Eq. 9 from Eq. 10

$$P_X=[(k_R^{'})_2-(k_R^{'})_1]f(T) \qquad (11)$$

This estimate yields $P_X = 0.6$ mW. The more accurate calorimetric results using integration methods yields $P_X = 1.1\pm0.1$ mW for recombination in these experiments. Theoretical calculations using Henry's Law and Fick's Law of Diffusion yield approximately 1 mW due to the reduction of oxygen at the cathode in this electrolysis system. The electrochemical oxidation of deuterium or hydrogen does not occur at the platinum oxide surface of the anode.

The ability of this calorimetry to measure excess power within ±0.1 mW with an enthalpy input to the cell of approximately 800 mW demonstrates a precision of 99.99%. Additional evaluations show that the accuracy of this calorimetry is also close to 99.99%. The logical conclusion from the control study is that excess enthalpy measurements using this cold fusion calorimetric system cannot be scientifically dismissed as calorimetric errors.

Palladium-boron alloy materials prepared at the Naval Research Laboratory (NRL) have shown a remarkable ability to produce the excess power effect.[9,15] A calorimetric system similar to the system used in this blank study yielded excess power effects in the range of 100 to 400 mW over a 50 day period in experiments using a

Pd-B cathode.[9] The measured excess power increased to over 9 W (9000 mW) during the final boil-off phase.[9] Excess power continued for several hours after this Pd-B cell boiled dry.[9]

References

1. Miles, M.H., Bush, B.F. and Stilwell, D.E. (1994). *J.Phys. Chem.*, **98**, 1948.
2. Miles, M.H. (1998). *J. Phys. Chem. B,* **102**, 3642.
3. Miles, M.H. (2000). *J. Electroanal. Chem*., **482**, 56.
4. Fleischmann, M., Pons, S. and Hawkins, M. (1989). *J. Electroanal. Chem.*, **261**, 301 err (1989), **263**, 187.
5. Fleischmann, M, Pons, S., Anderson, M.W., Li, L.J., Hawkins, M. (1990). *J. Electroanal. Chem*., **287**, 293.
6. Fleischmann, M. and Pons, S. (1992). *J. Electroanal. Chem*., **332**, 33.
7. Szpak, S., Mosier-Boss, P.A. and Miles, M.H. (1999). *Fusion Technol*., **36**, 234.
8. Szpak, S., Mosier-Boss, P.A., Miles, M.H. and Fleischmann, M. (2004). *Thermochimica Acta*, **410**, 101.
9. Miles, M.H., Fleischmann, M. and Imam, M.A. (2001). Naval Research Laboratory Report Number NRL/MR/6320-01-8526, March 26, 2001.
10. Szpak, S. and Mosier-Boss, P.A. (2002). SPAWAR Systems Center Technical Report Number 1862, Volume 2, San Diego, CA.
11. Fleischmann, M. and Miles, M.H. (2006). In "Condensed Matter Nuclear Science", pp. 247-268, P.L. Hagelstein and S.R. Chubb, Editors, World Scientific, New Jersey, ISBN No. 981-256-564-7.
12. Fleischmann, M. and Miles M.H. (2006). Manuscript No. JP058292J submitted to *J. Phys. Chem*. Note: Editor George C. Schatz rejected this manuscript and ruled that the two reviewers did not need to respond to the detailed rebuttal by the authors to the reviewers comments.
13. Szpak, S. and Mosier-Boss, P.A. (2006). SPAWAR System Center Technical Report, San Diego, CA (in press). Note: Contains complete *J. Phys. Chem.* manuscript (Ref. 12) as well as comments of the two reviewers and the unanswered rebuttal of these comments by the authors.
14. Will, F.G. (1997). *J. Electroanal. Chem*., **426**, 177.
15. Miles, M.H. and Imam, M. Ashraf (2004). U.S. Patent Number 6,764,561 June 20, 2004.

US006764561B1

(12) **United States Patent**
Miles et al.

(10) **Patent No.: US 6,764,561 B1**
(45) **Date of Patent: Jul. 20, 2004**

(54) **PALLADIUM-BORON ALLOYS AND METHODS FOR MAKING AND USING SUCH ALLOYS**

(75) Inventors: **Melvin H. Miles**, Ridgecrest, CA (US); **M. Ashraf Imam**, Great Falls, VA (US)

(73) Assignee: **The United States of America as represented by the Secretary of the Navy**, Washington, DC (US)

(*) Notice: Subject to any disclaimer, the term of this patent is extended or adjusted under 35 U.S.C. 154(b) by 0 days.

(21) Appl. No.: **09/651,270**

(22) Filed: **Aug. 30, 2000**

Related U.S. Application Data

(60) Provisional application No. 60/205,255, filed on May 19, 2000.

(51) **Int. Cl.**[7] **C22F 1/14**
(52) **U.S. Cl.** **148/678**; 148/538; 148/557
(58) **Field of Search** 148/639, 628, 148/430, 538, 539, 557

(56) **References Cited**

U.S. PATENT DOCUMENTS

2,478,225	A	8/1949	Atkinson	75/10
3,515,542	A	6/1970	Larsen	75/122.5
3,597,194	A	8/1971	Savage	75/134 N
4,046,561	A	9/1977	Prosen	75/172
4,341,846	A	7/1982	Hough et al.	428/670
4,396,577	A	8/1983	Smith, Jr. et al.	420/580
5,518,556	A	5/1996	Weber et al.	148/430
5,942,206	A	8/1999	Uhm et al.	423/648.1

OTHER PUBLICATIONS

Sakamoto, Y.; Baba, K.; Flanagan, Ted B., The effect of alloying of palladium on the hydrogen–palladium misibility gap. Z. Phys. Chem. (Munich) (1988), 15 8(2), 223–35.*
Sakamoto, Y.; Kaneko, H.; Tsukahara, T.; Hirata, S., Diffusion of hydrogen in palladium–(cerium, yttrium, boron) alloys, Ser. Metall. (1987), 21(4), 415–20.*
Van Vlack, Elements of Material Science and Engineering, 3rd Edition, 1975, Addison–Wesley Publishing Company, Inc pp. 367–369.*

* cited by examiner

Primary Examiner—Sikyin Ip
(74) *Attorney, Agent, or Firm*—John J. Karasek; Joseph T. Grunkemeyer

(57) **ABSTRACT**

A palladium-boron composition and methods of making and using same are provided. In one aspect, the invention comprises an alloy comprising palladium and boron, the boron being in solid solution in the palladium and the alloy having a two-phase structure, wherein each phase of the two-phase structure has the same crystal structure as the other phase and has a different set of lattice parameters from the other phase such that the palladium is greatly hardened by the presence of the smaller phase crystals within the spaces between the larger phase crystals. The composition is carefully prepared by a process wherein palladium and an amount of boron sufficient to place the boron in solid solution, but insufficient to combine with the palladium, are placed together and repeatedly arc melted, cooled and turned over until sufficiently mixed. The hardened composition can be used to create thinner membranes for hydrogen purification and improved electrodes for generation of heat energy, and other electrochemical processes.

12 Claims, 4 Drawing Sheets

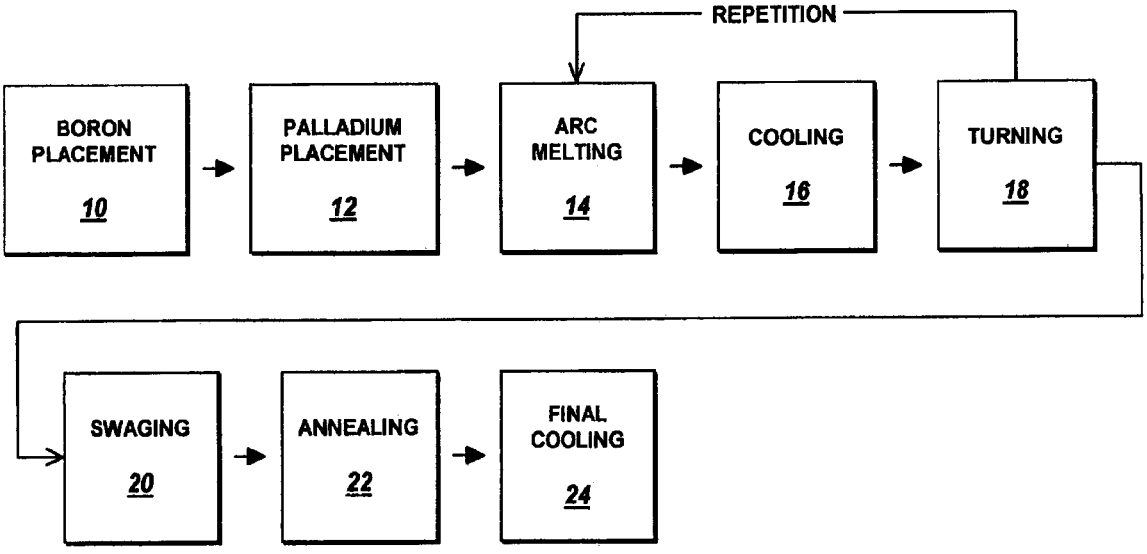

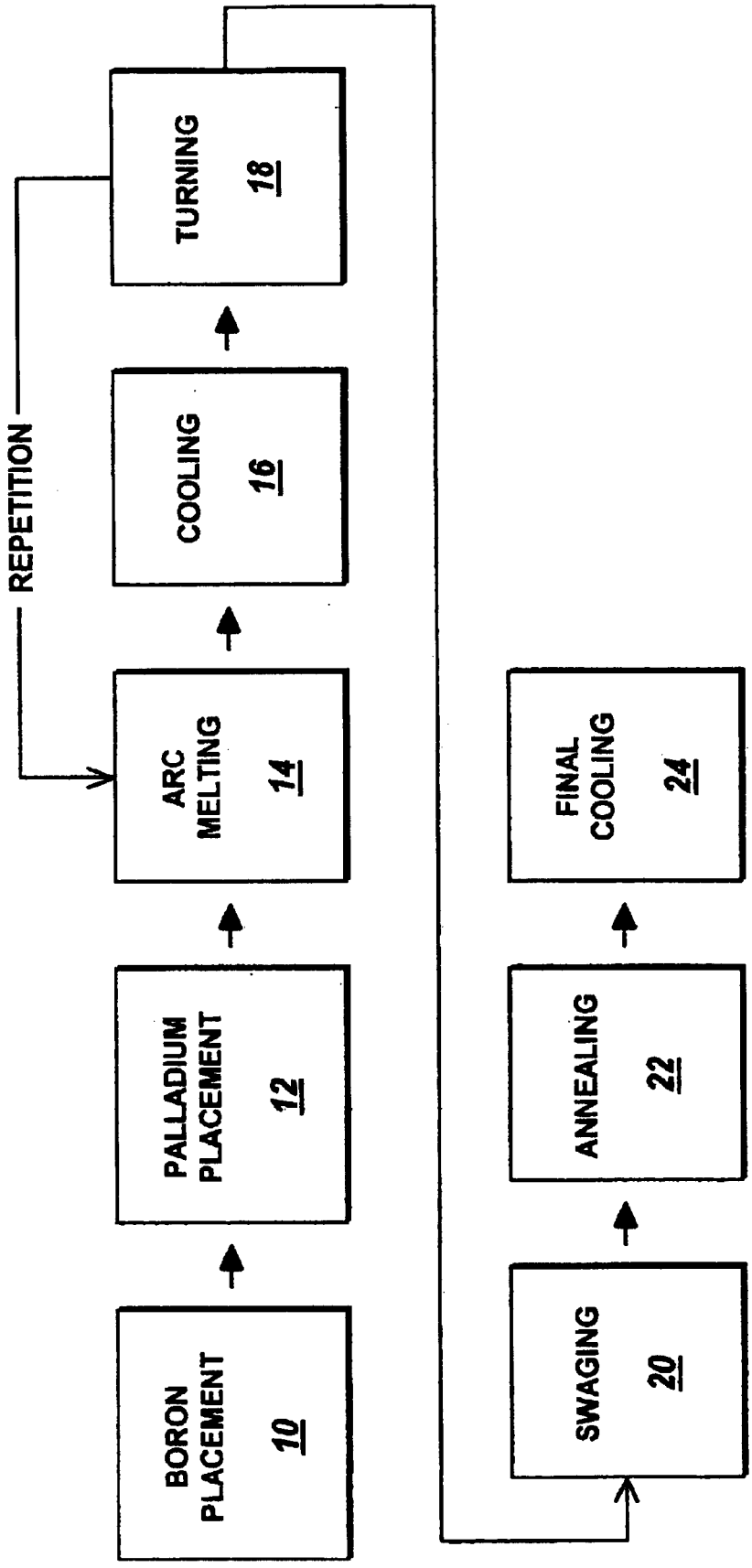
BORON PLACEMENT 10
PALLADIUM PLACEMENT 12
ARC MELTING 14
COOLING 16
TURNING 18
SWAGING 20
ANNEALING 22
FINAL COOLING 24
REPETITION

FIG. 1

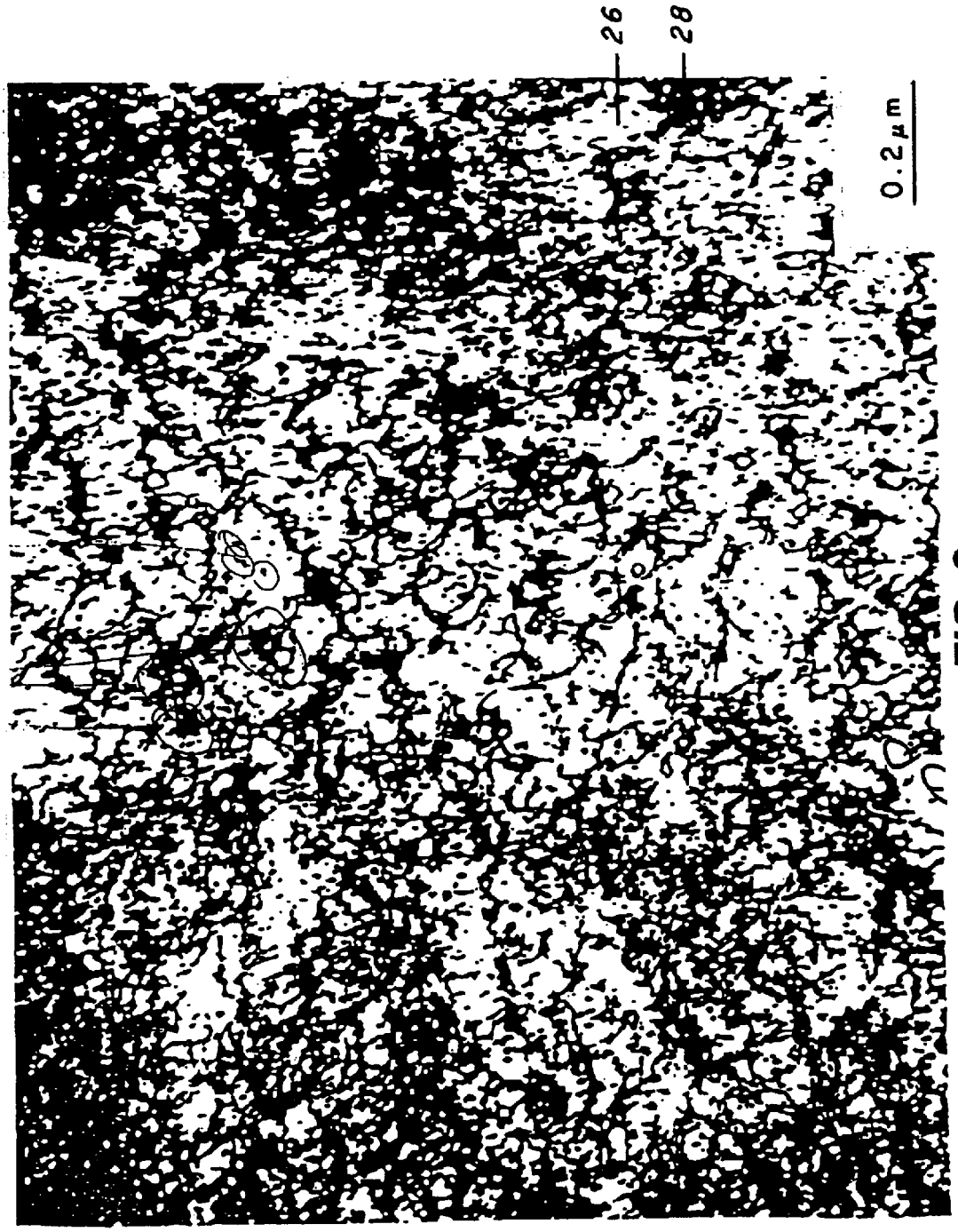

FIG. 2

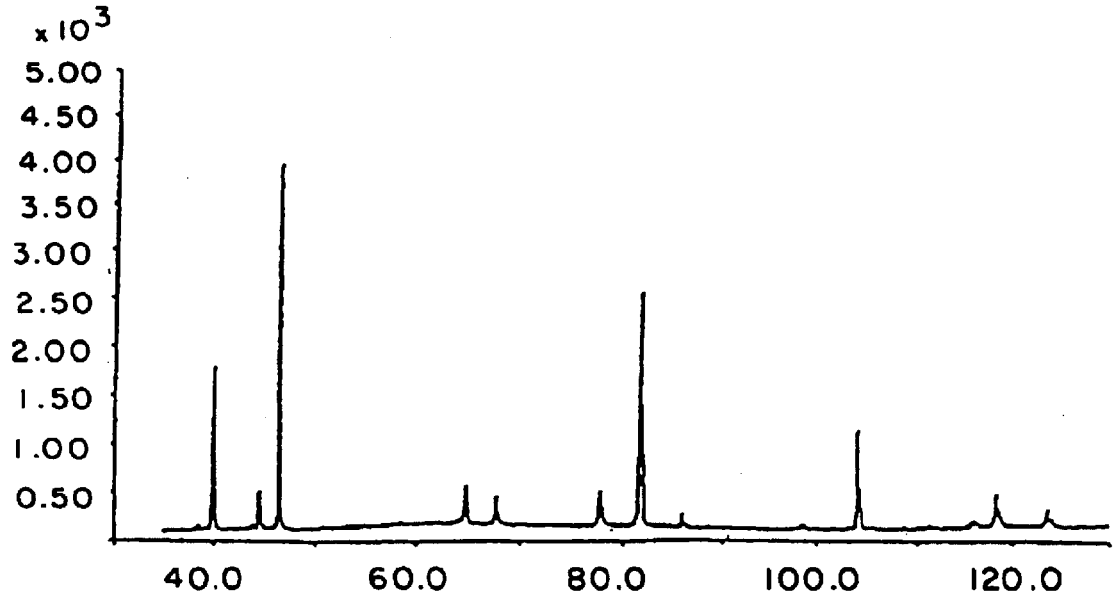
x 10^3
5.00
4.50
4.00
3.50
3.00
2.50
2.00
1.50
1.00
0.50
40.0
60.0
80.0
100.0
120.0

FIG. 3a

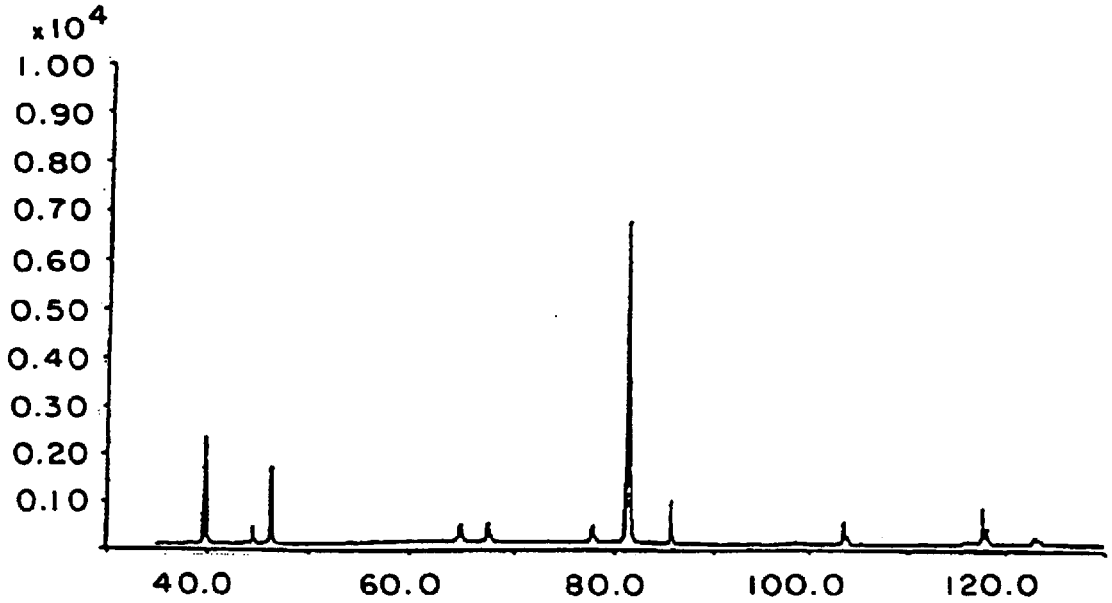
x10^4
1.00
0.90
0.80
0.70
0.60
0.50
0.40
0.30
0.20
0.10
40.0
60.0
80.0
100.0
120.0

FIG. 3b

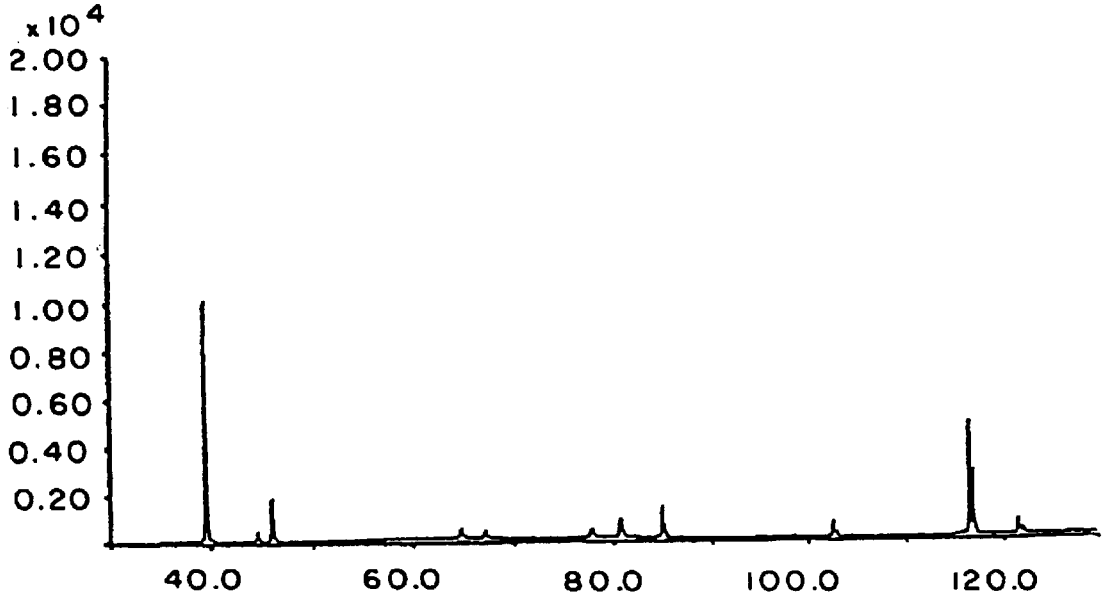
x10^4
2.00
1.80
1.60
1.40
1.20
1.00
0.80
0.60
0.40
0.20
40.0
60.0
80.0
100.0
120.0

FIG. 3c


100.0
80.0
60.0
40.0
20.0
40.0
60.0
80.0
100.0
120.0

FIG. 3d

PALLADIUM-BORON ALLOYS AND METHODS FOR MAKING AND USING SUCH ALLOYS

This application is a non-provisional application and claims priority under a provisional application Ser. No. 60/205,255, filed on May 19, 2000.

FIELD OF THE INVENTION

The present invention generally relates to processes for the production of a high-strength alloy that may be used as a gas purification membrane, as an electrode for numerous applications including the generation of heat energy or other electrochemical processes, and more particularly to the preparation and use of two-phase palladium-boron alloys which have greater strength and hardness than other palladium metals or alloys and which thus can be advantageously utilized in a variety of applications including hydrogen purification membranes or electrodes.

BACKGROUND OF THE INVENTION

With increased use of electrical processes and hardware, processes utilizing the excellent reliability and conductivity of palladium, an extremely valuable but expensive metal, have become of increasing importance, particularly when used as an electrode. However, it has long been known that the hardness of palladium is often less than optimal for many of these processes. Accordingly, there has been a distinct need in this field to develop palladium alloy electrodes that are harder and more resilient than pure palladium while still offering the superior electrical characteristics of pure palladium.

In addition, interest has increased in the quick and efficient production of hydrogen, which has, because of its many industrial and scientific applications, assumed greater importance. Hydrogen is typically purified from surrounding gas by using a membrane permeable to hydrogen, but not to the other gases. In this process, the hydrogen passes through the membrane and is collected on the other side. With respect to hydrogen production, there is much interest in methods of increasing the hardness and durability of these membranes which are again typically composed of palladium. One proposed solution to overcoming the hardness problem would be to harden the palladium metal without affecting its hydrogen purification characteristics, which would allow for thinner membranes than those of pure palladium. This would allow either the same amount of hydrogen to be purified at a great cost savings, or a larger amount of hydrogen could be purified for the same cost. However, suitable methods for developing palladium or palladium alloys with sufficient hardness have not yet been achieved.

Further, the demand for energy increases each year while the world's natural energy sources such as fossil fuels are finite and are being used up. Accordingly, the development of alternative energy sources is very important and a number of potential new energy sources are under study. Although there have been many attempts to develop a palladium compound which can be utilized in processes to generate heat, such as through the introduction of aqueous deuterium, none of these attempts have been successful or repeatable, and there is thus a distinct need to develop palladium alloys which can be utilized for the generation of heat as a potential energy source.

Previously, it has been known to prepare single-phase alloys made of palladium and other minor elements. For

example, the prior art includes various palladium alloys which include boron, such as Weber et al. U.S. Pat. No. 5,518,556 (a boron-containing surface layer), Hough et al. U.S. Pat. No. 4,341,846 (an electroless boron/palladium plating material), Smith Jr. et al.. U.S. Pat. No. 4,396,577 (a brazing alloy containing boron, palladium and other metals) and Prosen U.S. Pat. No. 4,046,561 (an alloy for porcelain applications containing boron, palladium and other metals).

However, what is lacking in the prior art is a pure boron/palladium composition of sufficient strength to be used as a reactive structure rather than a coating material, and which may be used in thin hydrogen purification membranes or as an electrode in a heat-generating process. There thus remains a distinct need to develop palladium alloys which can be utilized advantageously in a variety of applications where pure palladium is unsuitable either because of the expense or insufficient hardness.

SUMMARY OF THE INVENTION

In accordance with the invention, there is provided a two-phase alloy comprised of palladium and boron wherein the boron is in solid solution in the palladium and wherein each phase of the two-phase structure has the same crystal structure as the other phase but has a different set of lattice parameters from the other phase. In addition, a method of preparing the two-phase alloy of the invention is also provided wherein the boron in powder form is preferably placed in an airless compartment, palladium in sponge form is placed in the compartment overlying the boron, the boron and palladium are melted together to form a mixture via a heating apparatus such as an electric arc, the mixture is cooled to solidification, turned over for complete mixing, and the melting, cooling and turning process is preferably repeated until a mixture with the desired homogeneity is attained. In the preferred process, the amount of boron is such that it is insufficient to form a compound of boron in the palladium, but sufficient to remain in solid solution with the palladium.

In the particularly preferred embodiment, the composition of the present invention comprises 0.1 to 0.8 by weight percent boron, and 99.2 to 99.9 percent by weight percent palladium, and the palladium and boron comprise at least 99.9% of the composition. It is also preferred that the second phase forms crystallites which are on average at least twice as large as the crystallites of the first phase, and that the diameter of the crystallites in the first phase is in the range of 10 to 100 Angstroms.

In a particularly preferred method or preparation in accordance with the invention, the palladium and boron are placed on a copper hearth in a mixing chamber which is part of an arc melting means. The arc melting is then performed between about 2079° C. and 2200° C., for a period of between about 4 and 10 minutes. The melting, cooling and turning steps are preferably repeated roughly 3–10 times. After a complete mixture results from melting, turning, and cooling, the composition may also be swaged to reduce the diameter of the alloy. The alloy is annealed at elevated temperature to reduce the residual stress, and then undergoes a final cooling to room temperature. The annealing is performed between about 650 and 700° C., and for less than about three hours.

Preferably the alloy composition of the present invention can be formed into a membrane for use in the purification of hydrogen, or can be made into an electrode useful for numerous purposes, including the loading of the electrode with deuterium for the generation of heat energy, or other standard electrochemical purposes.

Further features and advantages of the present invention will be set forth in, or apparent from, the detailed description of preferred embodiments which follows below.

BRIEF DESCRIPTION OF THE DRAWINGS

FIG. **1** is a schematic view of the process of preparing a palladium-boron alloy in accordance with the present invention.

FIG. **2** is a transmission electron micrograph of a palladium/0.62% boron alloy composition in accordance with the present invention which shows the two phases.

FIG. **3***a* is a graphic representation of an X-ray diffraction pattern of palladium/0.18% boron.

FIG. **3***b* is a graphic representation of an X-ray diffraction pattern of palladium/0.38% boron.

FIG. **3***c* is a graphic representation of an X-ray diffraction pattern of palladium/0.62% boron.

FIG. **3***d* is a graphic representation of an X-ray diffraction pattern of pure palladium.

DETAILED DESCRIPTION OF THE PREFERRED EMBODIMENTS

In accordance with the present invention, there is provided a composition comprising a two-phase alloy of palladium and boron which has superior tensile strength and hardness when compared to pure palladium, and which can thus be used in a variety of applications, including use as a hydrogen purification membrane or as an electrode in numerous electrochemical processes.

In the preferred process of producing the palladium/boron alloy of the present invention, as shown in the flowchart of FIG. **1**, there is a series of preferred steps for making the boron-palladium composition with a two-phase crystalline structure. In this preferred process, boron in powder form is first placed within a structure capable of producing heat sufficient to melt metal alloys, such as on a copper plate, or hearth, within a compartment filled with argon, after evacuation of the compartment, suitable for arc melting and cooling. Copper is preferably used as the material for the hearth because of copper's excellent conductivity for the arc melting phase. The copper hearth is cooled with water from below to keep it from melting into the alloy as it has a lower melting point than either boron or palladium. The hearth, and the mixture resting upon it, are cooled by the transfer of heat from the composition through the hearth to the coolant water. The system is not reliant on air cooling because of its water cooling means. The entire process preferably occurs in the chamber which is filled with argon gas after evacuating the chamber. Exposure to air cannot be allowed because oxygen or air would oxidize the palladium and the boron, ruining the process. The process is usually performed in a container with a noble gas, typically argon. In this process, palladium is placed in the compartment **12** so that it is overlying the boron powder in the cavity. The palladium is preferably introduced in a pure palladium sponge form.

The palladium-boron alloy produced in accordance with the present invention preferably comprises about 0.05 to 2.0 percent by weight boron, most preferably 0.1 to 0.8 weight percent, and from about 98.0 to 99.5 percent by weight percent palladium, most preferably from about 99.2 to 99.9 weight percent. The amount of boron present in the cavity is fixed so that it is small enough not to form a compound of boron in the palladium but is sufficient to react with oxygen in the palladium while the boron is in solid solution in the palladium. Very small amounts of the composite are used herein. Typically, there will be 100 g of palladium and an amount of boron in accordance with the ranges as set forth above.

In the preferred process, after the palladium and boron are placed within the cavity, a heating source such as an electric arc is used to melt the boron and palladium together to form a mixture **14**. Although there are several other well-known forms of heating that would be suitable for the present invention, an electric arc is preferably used because it offers rapid control which prevents the Boron from vaporizing prematurely. The palladium is preferably placed on top of the boron because of the differences in density. The denser palladium prevents splatter or flying of the boron. Additionally, the lower melting point of palladium allows it to form a protective shell over the boron before the boron begins melting. A melting arc is generated between a tungsten tip just above the mixture and the conductive copper hearth upon which it rests.

The melting point of boron, the higher of the pair, is 2079° C. so the melting must be done at least at this temperature. However, the temperature preferably should not exceed about 2200° C. or the boron will begin to vaporize. The melting time should be about 5 minutes. A melting time greater than 10 minutes at the aforementioned temperature would result in vaporization of a portion of the boron.

After the palladium and boron are melted, the mixture is cooled The mixture solidifies upon cooling **16**. The mixture is preferably turned over after cooling and solidification **18** to provide a more homogeneous mixture by preventing settling of the boron and palladium into layers. The mixture is turned over with the tungsten tip of the arc mechanism.

After the initial melting and cooling to bind the loose boron powder to the palladium, the melting step **14**, cooling step **16**, and turning over step **18** (as shown in FIG. **1**) are repeated as often as necessary to eliminate any boron or palladium pockets, and for thoroughly mixing the mixture into a solution of a desired homogeneity to be attained suitable for commercial use. The steps are preferably repeated anywhere from about 3–10 times, with about 4–5 times particularly preferred, and the solution is then mixed by the use of a combination of gravity and random movement, followed by repeated melting, cooling and turning cooled solid solution over.

After a homogeneous mixture is prepared, the material preferably undergoes an additional step of swaging **20**, if so desired, for reducing the alloy to a fixed diameter. A die is preferably used and the metal is forced into a bar shape of the appropriate diameter. Swaging is particularly useful when producing an electrode from the raw alloy material.

After the material undergoes swaging **20**, the rods are cut into appropriate lengths and machined into usable electrode form. The alloy is annealed **22** to reduce the residual stress. The alloy begins at room temperature and is heated to approximately 650° C. for approximately 2 hours. The time and temperature in this step are important because too high a time or temperature would result in a larger grain size of the composition which would detract from hardness and render the composition ineffective. For example, temperatures at 700° C. and above would begin to produce undesirable results in the final alloy. Grain size would also become dangerously large after approximately 3 hours. After annealing, the solution is cooled to room temperature in a final cooling step **24**.

The composition resulting from the above process is a boron in solid solution in the palladium, with the alloy having a two-phase structure. As shown in FIG. **2**, the first

and second phase, **26** and **28**, respectively, of the two-phase structure have the same crystal structure but different sets of lattice parameters so that the crystals of the second phase are larger than the crystals of the first phase. The diameter of the crystallites in the first phase **26** is in the range of 10 to 100 Angstroms, whereas the diameter of the crystallites in the second phase **28** is much larger.

The differing sizes of the crystals of the phases creates a "miscibility gap" meaning that the miscibility of the two phases with each other is high because the crystals of the smaller first phase can easily rest in gaps between the larger crystals of the second phase. This "filling" of the gaps of the larger crystals binds the crystals of both phases together and results in a hardened composition.

The amount of boron in the mixture appears to be critical. It has been found that the amount of boron must be maintained below 2 weight percent of the mixture for solution. Anything more and it will begin to bond with the palladium, preventing formation of the two-phases.

This composition can show the same or better strength than pure palladium with much less thickness. This is advantageous in the creation of palladium hydrogen purification membranes because less palladium would be needed to create a membrane and achieve the same results using it. This is because sturdy membranes of much less thickness are enabled by the present invention than would be possible using palladium alone. The advantage herein is that because of the additional hardness of the palladium-boron alloy of the invention, a much smaller amount of expensive palladium may be used to provide a membrane of the same capacity compared to palladium alone. Palladium is one of the precious metals and is, therefore, very costly. This would allow much greater membrane capacity through reduced material costs. How much the thickness of the membrane would be able to be decreased with the present composition would depends upon such factors as design, gases to be purified, and the extent of purification desired.

Preferably, the hardened palladium-boron alloy can be made into a membrane to purify hydrogen. The openings in the palladium are sufficient to allow hydrogen to pass but not other gases. Therefore, palladium is commonly used to purify hydrogen using the membrane, and the gas to be purified is usually placed on one side and a vacuum is on the other. This pressure differential forces the hydrogen through the membrane to towards the vacuum. The larger gases cannot fit through the membrane and are left behind. Further, the material would be advantageous for purifying hydrogen because its increased strength offers increased overall membrane reliability.

The hardened electrode would also be advantageous for use in etching, polishing, electrochemical machining, semiconductor wafer manufacture and other electrochemical processes in which use of a hardened palladium cathode retaining superior palladium electrical characteristics is advantageous.

An additional application of the alloy, which has been borne out by experimental data is as an electrode in the generation of energy in the form of heat. In a preferred process using the alloy of the present invention in the form of an electrode, the electrode in connected to a platinum cathode and immersed in water containing deuterium. The immersed electrode is loaded with deuterium from the surrounding electrolyte. As a current is applied, excess energy from the loaded electrode in the form of heat is generated. Using the palladium-boron electrode manufactured in accordance with the present invention, excess enthalpy has been achieved, and this result has been far more reproducible than in past experiments of this type, which may result in a new energy source at low cost.

Although the invention has been described above in relation to preferred embodiments thereof, it will be understood by those skilled in the art that variations and modifications can be effected without departing from the scope and spirit of the invention.

EXAMPLES

Palladium-boron composition samples containing 0.18% boron, 0.38% boron and 0.62% boron were prepared in accordance with the invention. Palladium sponge was used as a palladium source for its high purity. The boron source was a powder commonly referred to as five-nine boron (99.999% pure boron).

In accordance with the present method, approximately 100 g of palladium and a corresponding amount of boron giving the concentrations set forth above were measured. The boron powder and palladium were placed on a copper hearth within a compartment. The compartment is airless, with an argon atmosphere. The samples were melted. A typical arc melting apparatus having 12v and 300 amps was used for the melting. The two elements used for the arc melting are a tungsten tip immediately above the sample and the copper hearth. The melting was performed at about 2100 c and the melting time was about 5 minutes. The mixture was then cooled for approximately 30 minutes and the mixture turned over. The melting, cooling and turning steps were repeated 4–5 times.

To make electrodes from the composition, the alloy was swaged to 0.4 cm diameter. The swaged rods were cut into 3.5 cm lengths and machined into usable electrode form. The samples were annealed at approximately 650 c for approximately 2 hours. The samples were cooled for two hours until they returned to room temperature.

Nine samples in electrode form were tested. This testing centered around the generation of heat with the electrode. Each palladium-boron electrode was connected to a platinum anode, and the palladium-boron cathode was then immersed in water containing deuterium. After immersion, the electrodes were then electrochemically "loaded" with hydrogen. It is believed extra loading was possible due to the two-phase structure brought about by the solution of boron within the palladium. Of nine samples tested, eight yielded positive results of heat. The results of these experiments are more repeatable than any experiment of this type completed thus far. Not surprisingly, amount of heat varied with, and had a positive relationship to, boron content.

X-ray diffraction studies were carried out to characterize the three compositions of the two-phase palladium/boron alloy in accordance with the present invention. The diffractions were obtained in a Phillips diffractometer with generator settings of 50 kV, 30 mA and a copper target. Two distinct phases of the same cubic structure were found in all three compositions of the alloy. Lattice parameters for the samples were measured. As can be seen in FIG. **3**, the two distinct phases have the same crystal structure but different lattice parameters. The lattice parameter in a first phase remains constant with changes in the boron content of the alloy whereas the lattice parameter of a second phase N increases with an increase in the boron content. As the boron increased, the amount of crystals in the second phase increases at the expense of the first phase, as expected.

The 0.62% boron sample was studied with a transmission electron microscope. FIG. **2** shows the Selected Area Dif-

fraction (SAD) pattern. Lattice parameters of the two phases **26**, **28** measured from x-ray diffraction and SAD are consistent, and confirmed the production of the palladium/boron alloys in accordance with the present invention.

What is claimed is:

1. A method of preparing a composition, said method comprising the steps of:

(a) placing boron in a compartment evacuated of air and filled with another gas;

(b) placing palladium in a cavity overlying the boron in said compartment, wherein the amount of boron is insufficient to form a compound of boron in the palladium and is sufficient to react with oxygen in the palladium while said boron is in solid solution with said palladium;

(c) melting the boron and palladium together to form a mixture;

(d) cooling the mixture for producing a solidified mixture;

(e) turning the mixture over for reversing the vertical locations of the top and bottom portions of the mixture; and

(f) repeating steps (c) through (e) until a mixture at the desired homogeneity is attained;

wherein the composition is a two-phase palladium-boron composition;

wherein the composition is not annealed under conditions that substantially reduce the hardness of the composition.

2. A method according to claim **1**, wherein the palladium is introduced in the form of palladium sponge and the boron is introduced in the form of a powder.

3. A method according to claim **1**, wherein the boron and palladium are melted using electric arc means to create an electric arc for melting the boron and palladium.

4. A method according to claim **3**, wherein the boron and palladium are placed on a copper hearth in a chamber, and wherein said copper hearth is part of the arc melting means.

5. A method according to claim **1**, wherein the method further comprises swaging the mixed alloy for reducing the diameter of the alloy.

6. A method according to claim **5**, wherein the method further comprises the steps of annealing the alloy for reducing residual stress, and cooling the alloy.

7. A method of preparing a palladium-boron composition according to claims **6**, wherein the annealing is performed between about 650° C. and about 700° C. for less than about three hours.

8. A method according to claim **1**, wherein steps a)–f) occur in the order specified.

9. A method according to claim **1**, wherein the melting of the boron and palladium is carried out at a temperature between about 2079° C. and about 2200° C. for a time period between about 4 and about 10 minutes.

10. A method according to claim **1**, wherein steps c) to e) are repeated about 3–10 times.

11. The method of claim **1**, wherein the composition is not annealed at or above about 700° C.

12. The method of claim **1**, wherein the composition is not annealed for more than about three hours at about 650° C.

* * * * *

Semi-Classical Conduction of Charged and Neutral Particles in Finite Lattices

Scott R. Chubb
Remote Sensing Division
Naval Research Laboratory, Washington, DC 20375, USA

Although no formal justification for theories of semi-classical dynamics and conduction in energy band systems exists, beginning from an ordered ground state, it is possible to justify when the associated treatment can apply either for ultra cold neutral atoms (“atomic matter waves”) in finite optical lattices or for charged particles in finite, periodic crystal lattices. The essential physics is the fact that when the ground state is ordered, the lowest energy forms of reaction are initiated in "bulk regions" through perfectly elastic, Umklapp processes (similar to lattice recoil in the Mossbauer effect), in which the bulk region moves rigidly. As opposed to the conventional picture in which conduction occurs through the occupation of energy band, “quasi-particle” states, the semi-classical dynamical equations can be justified, based on a rigorous model, associated with a broken gauge symmetry (invariance of neutrally-charged “bulk regions” with respect to Galilean transformations that maintain particle-particle separation). Implications of these results in areas related to transport of hydrogen and its isotopes in nano-crystalline structures of palladium (Pd) and of neutral, coherent atomic waves in finite, optical lattices are presented.

Keywords: Generalized Multiple Scattering, Atomic Bose Einstein Condensate, Optical Lattice, Periodic Order, Bloch's Theorem, Broken Gauge Symmetry

I Introduction

This paper formalizes and generalizes a number of intuitive ideas associated with electron band theory in solid state physics, in the idealized limit of infinitely-repeating, periodic lattices, to situations involving finite structures, with real boundaries. Implications of the results include: 1. The prediction of a novel variant of a known, phenomenon, Zener/Electronic Breakdown in insulators (Zener 1934), in which ions in nano-scale palladium-deuteride (PdD) crystals (as opposed to electrons in insulating crystals) that initially, effectively, are confined to particular regions of space, begin to move, spread-out, and conduct charge after they are subjected to an applied, external electric field for a sufficiently long period of time; and 2. A rigorous treatment of scattering at low temperatures that can be used to identify critical time- and length-scales for problems related to the transport of neutral atomic matter waves in finite, optical lattices (Deutsch & Jessen 1998), in the presence of gravitational fields (Anderson & Kasevich 1998).

The arguments are general: they can be applied to all ordered or partially ordered solids, in the limit of low, but finite temperature. In particular, in this paper, the terms order and periodic order are used inter-changeably. A solid that possesses partial order (or partial, periodic order) refers to the requirement that the particles in some finite volume, within the solid, occupy one or more many-body states Ψ possessing some degree of periodic symmetry, for some finite period time. This last condition is defined by the requirement that one or more Bragg diffraction peaks (Ashcroft & Mermin 1976A), beyond the zeroeth order peak, be observable in the diffraction pattern that results when particular particles (x-rays, neutrons, etc.) scatter elastically off of the solid . An ordered, periodic, or periodically ordered solid refers to the limit in which the resolution between different diffraction peaks and the number of peaks asymptotically approach the resolution and number that one would conventionally associate with a diffraction pattern involving a situation in which a macroscopic number of scattering centers can be involved with the scattering processes that are responsible for the pattern. For the purpose of determining critical time- and length- scales associated with experiments involving finite size optical lattices, a number of the arguments involving finite size effects (and the associated overlap features) in partially ordered solids can also be generalized to optical lattices. (This topic is addressed in the final section of the paper.)

The underlying logic associated with the analysis follows from a number of general results that are required in order to insure that the reaction rate be minimized (through minimal overlap with potential perturbations) for a potential process that can couple the ground state (GS) to the lowest-lying excited states, in a solid or lattice. In particular, in general, the GS of a many-body system is required to have minimal overlap with external perturbations and with the lowest-lying excited states. But in the idealized limit in which a set of measurements can be performed, in such a way that the measurement process does not affect the energy of any of a number of potential many-body states (including the GS), locally, in a particular region of space, each measurement can be viewed as a form of "symmetry operation". When each of these symmetry operations can be related to the others through one or more continuously-varying parameters (for example, through measurements of a continuously-varying angle or displacement, performed outside the particular region of space), the set of symmetry operations is referred to as a gauge symmetry.

But because no symmetry operation is perfect, residual perturbations, tied to the measurement process exist. In the presence of these perturbations, the overlap of the GS with low-lying excited states is minimized through processes that minimize the GS energy. The resulting changes in wave function overlap and energy occur through a process that is referred to as broken gauge symmetry. Provided the particular region (which will be referred to as the bulk region) occurs within the solid (or within a lattice), where the numbers of neutral and charged particles are conserved (relative to a particular, well-defined boundary or boundary region), the rate of change of any process involving the GS and its overlap with low-lying excited states (through residual perturbations) is dominated by a universal broken gauge symmetry that occurs in ordered, finite lattices (the loss of translation symmetry at the boundaries of a lattice). In this particular limit: 1. In the absence of the residual perturbations, the energy remains invariant with respect to the gauge symmetry operation associated with performing a rigid shift of the bulk region, in which the coordinate of each particle in the bulk is shifted by the same, constant amount; 2. Since, by construction, the associated coordinate transformation (which is referred to as a Galilean, coordinate transformation) preserves the separation between each particle and the remaining particles in the bulk, a large degeneracy exists, and (in the presence of broken gauge

symmetry) the lowest-lying excited states are all related to the GS through one of the possible (Galilean) transformations; and 3. In the presence of residual interactions, the lowest-lying excited states conserve particle number within the bulk region.

Since the associated transformations do not alter the relative separations between any of the particles, effectively, the resulting change in position of the particles can be viewed as occurring through a form of "perfect" rigid body motion, in which the entire collection of particles moves with a common velocity, that is similar to the nearly-perfect, lattice recoil that occurs when a gamma ray strikes a nucleus, without exciting a lattice vibration, in the Mossbauer effect. In this limit, the overlap between the GS and lowest-lying excited states can involve processes that do not alter the relative separations between particles in the bulk. The associated effects, by construction, occur as a result of a breakdown of a form of (Galilean) relativity, associated with the underlying gauge symmetry. For this reason, in the absence of residual perturbations, effectively, it is impossible to perform a measurement that preferentially distinguishes between the behavior of particles in the bulk region in one reference frame, relative to the comparable behavior of particles in a second, moving reference frame that can be related to the first reference frame through a rigid, Galilean transformation. The resulting symmetry leads to a large degeneracy associated with elastic processes that can transfer momentum, instantly, from the boundaries of the bulk region to the center of mass of the bulk. In the limit in which the resulting motion (of the bulk) involves a transfer of momentum Δp that has associated with it a DeBroglie wavelength $\lambda_d = \frac{h}{\Delta p}$ (h=Planck's constant) that is constrained by the condition that $\lambda_d = na$ (n=integer, a=lattice spacing between adjacent unit cells), a resonant process can take place, in which, effectively, a small fraction $\frac{\Delta p}{N}$ of Δp is transferred instantly to the center-of-mass of each unit cell in the lattice. (Here, N is the total number of unit cells in the lattice.)

Historically, in infinitely-repeating lattices, an alternative picture has evolved. In it, the associated resonant processes (which will be referred to as Umklapp processes [Ashcroft & Mermin 1976B, Peierls 1929]) involve interactions in which momentum is not conserved between "quasi-particles". Instead, momentum is transferred to the lattice elastically. Although momentum conservation requires that quantitative bounds exist for the amounts of momentum that can be transferred from a crystal lattice to a surface or interface (and vice-versa) through these kinds processes, traditionally, in models in which the lattice is infinitely-repeating and periodic, these bounds have been poorly defined.

In fact, in finite solids, at low, but finite temperature, precise, size-dependent bounds can be identified. In particular, although in larger crystals, collisions with phonons tend to reduce the magnitudes of the associated effects, in smaller crystals (or in optical lattices), this is not the case. In the case of PdD and PdH, the effects can be quite large and can lead to a coherent form of interaction that mimics an insulator-superconductor transition. In particular, when an electric field is applied for a sufficiently long period of time, in these systems, a form of insulating-conducting transition can take place, in which the charge carriers are H- or D- ions. The associated process is very similar to the transition, suggested by Zener (1934), that might occur when an electric field is applied to an insulator for a sufficiently long time. As opposed to the situation in which "electrical conduction" through "Zener/Electrical breakdown" can occur (which is the name that is frequently used for the kind of effect that Zener suggested), because the charge carriers in PdH and PdD can be ions, an analogous process (which will be referred to

in this paper as "ionic conduction" through "Zener/Ionic breakdown") can take place. In the case of PdD, since D- ions (deuterons) are bosons, the associated "ionic conduction" technically is a form "super-conduction," and the Zener/Ionic breakdown process refers to a form of insulator-superconductor transition However, since the amount of ionic charge involved is small, the important effects, conventionally associated with superconductivity, are so small that they probably can not be observed.

The range of time-scales (which varies between weeks and fractions of a second) for initiating this kind of effect appear to be consistent with the comparable range of incubation times that have been observed to be required before anomalous heat is initiated during the prolonged electrolysis of D_2O by PdD. The fact that the shortest time-scales required for Zener/Ionic breakdown and the observation of Excess Heat both occur in PdD crystals that have characteristic dimensions ~10's of nm suggests that Excess Heat is being triggered by Zener/Ionic breakdown.

Including the Introduction, the paper contains seven sections. In the second section, background about the underlying limit (associated with broken gauge symmetry) is presented. In the third section, rules concerning general properties of the ground state (GS) and lowest-lying excitations are presented (including a formal proof of a generalized form of Bloch's theorem). In the fourth section, these rules are extended to a situation in which external forces are applied to the lattice, and a formal, rigorous derivation of the semi-classical transport equations is given. In the fifth section, a new, general framework (which will be referred to as Generalized Multiple Scattering Theory) is presented for including the effects of collisions and finite temperature T in the underlying dynamics. In the sixth section, an analysis is given of a particular limit (involving the onset of broken gauge symmetry) associated with coherent effects that become most pronounced either at finite, but vanishing-ly small T (in larger crystals), or in situations involving smaller crystals in which an external force acts on many particles at once (as in an Umklapp process) in a nearly perfectly rigid fashion.

In this section, bounds associated with the potential forms of coherent transfer of momentum (through Umklapp processes) from interior (bulk) regions of the lattice to regions outside the bulk are presented. Also, a formal, rigorous argument is included that quantifies limitations of Zener/Electronic breakdown and related phenomena, including, Bloch oscillations, in optical (and other) lattices, and the new effect (alluded to above) of Zener/Ionic breakdown in nano-scale PdH and PdD crystals.

This section concludes by examining the implications of Generalized Multiple Scattering Theory in more general terms. In particular, an explicit, concrete example, involving the identification of critical length, and time scales, associated with finite size, in the problem of measuring the gradient of the gravitational force, is used to demonstrate the usefulness of the formalism. This last calculation has practical utility in the problem of observing variations in gravitational force, using coherent atom waves, from airborne platforms.

The final section provides a brief summary of the key results of the paper.

II Background Concerning Conduction Near Absolute Zero

Although the semi-classical theory of electron dynamics and conduction (Ashcroft & Mermin 1976C) has been widely used, it has no formal justification, based on a microscopic theory. In fact, beginning from the GS of a many-body system in which the density of all of the particles, approximately periodically repeats itself, over some finite region of space, it is possible to

formally justify when this treatment of conductivity applies for electrons, potentially for lighter ions (such as protons, deuterons and tritons), and/or, as discussed below, (in the case of optical lattices [Deutsch & Jessen 1998]) neutral atoms, based on a microscopic theory, in a finite crystal. The essential physics of the associated argument is that when the GS is ordered, the lowest energy forms of interaction are initiated in the periodically ordered (bulk) regions but induce disorder through processes that are perfectly elastic, either within the initial region (or throughout most of it), while effectively transferring the momentum of the process instantly to the center-of-mass (CM) of the bulk, as a whole (as in the response of a solid to a gamma ray in the Mossbauer effect). At higher temperatures, alternative effects, involving phonon/ion and electron band state excitations (in systems possessing charged particles), or collisionally-induced excitations of band state particles (in the case of neutral atoms in optical lattices) can occur, in which (ion and electron) charge, or (in the case of neutral atoms) a flux of atoms, again, is transported to surface and interfacial regions. (In this context, and henceforth, the term ion refers to the nucleus of hydrogen or one of its isotopes.)

These conclusions follow from two key features of an ordered solid, near T=0: 1.) The motion of bulk regions of the solid (which are regions in which charge is always conserved, and net changes in charge and total charge always vanish) or optical lattice (in which the number of atoms is conserved), relative to locations outside of the bulk region (in which charge, or atom number, is allowed to change), can never be determined without introducing some form of external perturbation; and 2.) The GS wave function of an ordered many-body system, in bulk regions, has minimal overlap with excited states that couple to outside forces and perturbations, involving non-bulk regions where charge imbalance (or, in the case of neutral atoms, in an optical lattice, a loss of particles) is allowed to take place. The first characteristic implies a form of symmetry: In a finite lattice, it is never possible to determine the constant zero of (kinetic) energy or momentum of the bulk region, relative to non-bulk regions, but, to determine the GS, in bulk regions, it can be assumed energy is conserved. Then, it is impossible to determine if bulk region particles are at rest or in motion.

This symmetry has important consequences: A.) Because rigid translations of the bulk uniformly shift the momentum of each bulk region particle, these kinds of translations do not alter the relative interactions between (or fluxes involving) different particles within the bulk region. B) The GS is defined in a preferred reference frame, in which the balance between outside forces defines the zero of energy and momentum, which, together, establish the energies and overlap of possible many-body states.

An important point is that the relationship between the velocity **v** and momentum **p**, of a charged particle, possessing charge e and mass m, is not **p**=m**v**. The precise relationship is m**v**=**p**-e/c**A**, where **A** (the vector potential) is defined by the magnetic field, **B** (through the relationship $\nabla \times \mathbf{A}=\mathbf{B}$) and Maxwell's Equations. In particular, quantum mechanically, **p** and **A** can both change instantaneously by the same amount, even discontinuously, at any location, without changing the value of v of any particular particle. The example of a Mossbauer-like, Galilean translation, in which all particles in the bulk region are rigidly shifted, relative to an observer, further illustrates subtleties associate with the effect. In particular, since no net accumulation of charge occurs, it is impossible to determine if the bulk region is in motion or at rest. This means that in the reference frame of an outside observer who moves with velocity -V_{cm}, the bulk region appears to move rigidly with total momentum $P_{cm}=MV_{cm}$ (M= mass of bulk solid), while in the frame in which both observer and bulk region are stationary, $P_{cm}=0$. Because

the transformation is rigid, the relationship between the wave functions $\Psi_{bulk}(P_{cm} = MV_{cm})$ and $\Psi_{bulk}(P_{cm} = 0)$ in the different frames involves a simple, change in phase:

$$\Psi_{bulk}(P_{cm} = MV_{cm}) = e^{\frac{iMV_{cm} \bullet R_{cm}}{\hbar}} \Psi_{bulk}(P_{cm} = 0) = \prod_{i=1,N_{total}} e^{ik_i * r_i} \Psi_{bulk}, (1)$$

where R_{cm} is the position of the CM, $\hbar k_i = m_i V_{cm}$ is the momentum that a neutral particle with mass m_i would have in the reference frame in which all particles move with velocity V_{cm}. The subtlety occurs because near T=0 it is never possible to determine whether or not the "bulk ", as envisioned, in this last example, is in motion or at rest, or whether or not its particles really are "neutral", quantum mechanically. This has important consequences. In particular, non-local forms of coherence can occur, in which it is possible to maintain a vanishing temperature T situation, with no interaction, whatsoever in bulk regions. This occurs when the entire bulk region moves all at once, but with different amounts of momentum (associated with different particles, as in Eq. 1).

III Generalization of Bloch's Theorem in Finite Lattices, Near T=0

Depending on whether the bulk is in motion or at rest, relative to non-bulk regions, wherever a particular coordinate r associated with a particle of mass m, and charge e, appears in an expression involving the total many-body wave function Ψ, the expression should be multiplied by a pre-factor of the form, exp**(ik r),** where $\hbar$**k**=mV_{cm} + <**e/cA(r)**>, and <**e/cA(r)**>= $\hbar$**k**$_o$ =**p**$_o$ is the average, minimum (zero) of the momentum of the particle. Here, degeneracy can occur because A (as well as the value of k_o) is never uniquely defined since the gradient of an arbitrary function can always be added to A, without altering the value of the magnetic field.

However, near T=0, it is also required that in the presence of a finite lattice, the associated forms of interaction between many-body states involve minimal, mutual overlap, in bulk regions. Thus, it follows that a discrete form of the degeneracy is involved in which, a priori, any one of the possible states, associated with a particular wave-vector, can couple to an alternative state associated with a different wave-vector, through an outside perturbation. As a consequence, through any of the possible symmetry operations (in which the bulk is translated rigidly), the value of P_{cm} associated with one such translation can only differ from the comparable momentum of a second translation by the product of $\hbar$ and one of the wave-vectors within the First Brillouin Zone (defined by Born VonKarman boundary conditions [Ashcroft & Mermin 1976D] of the finite crystal). This result follows by considering the potential forms of interaction between the GS and possible, low-lying forms of excited states.

In particular, as a function of time t, for the lowest energy (GS) many-body wave function $\Psi_{GS}(r_1,.....,r_n,t)$ to have minimal coupling with outside processes, its overlap with any other many-body state $\Psi'(r_1,.....,r_n,t)$ must be minimized and remain constant. A requirement for this to occur is:

$$\frac{\partial < \Psi' | \Psi_{Gs} >}{\partial t} = \iiint d^3 r_1 ... d^3 r_n \frac{\partial (\Psi'^* \Psi_{GS})}{\partial t}$$

$$= -\int d^3 r \nabla \bullet < \Psi' | v(r) | \Psi_{GS} > + < \Psi' | \frac{V - V'}{i\hbar} | \Psi_{GS} >= 0, \quad (2)$$

where terms in the second equality are defined by the many-body Schroedinger equations of Ψ' and Ψ_{GS}. In general, the associated integrations are unrestricted. To minimize overlap in "bulk regions", unrestricted integrations over all of the coordinates in the multi-dimensional integral, term by term, can be restricted to regions in the bulk, based on the criteria that to find a possible GS, the associated overlap between this state and other states in the bulk region be minimized. In this limited context, by restricting states to have minimal overlap with Ψ_{GS}, additional restrictions are imposed on Ψ_{GS} (subject to the implicit assumption that, in general, at the boundaries of the bulk region, possible discontinuities in the gradient and vector potential, are allowed to take place). Then, the associated analysis proceeds by restricting the multi-dimensional integrations in Eq. 2, exclusively to the bulk region. Also, in Eq. 2, $\langle \Psi' | v(r) | \Psi_{GS} \rangle$ and is the matrix element associated with the (off-diagonal) contribution to the (many-body) particle velocity operator v, defined by its overlap with the states Ψ' and Ψ_{GS}:

$$< \Psi' | v(r) | \Psi_{GS} >= \sum_j \iiint d^3 r_1 .. d^3 r_n \delta^3 (r - r_j) \frac{1}{m_j} (\frac{\hbar}{2i} \left[\Psi'^* \nabla_{r_j} \Psi_{GS} - \nabla_{r_j} \Psi'^* \Psi_{GS} \right] - \frac{e_j}{c} \Psi'^* A_{eff}(r_j) \psi_{GS}), \quad (3)$$

where $A_{ef(}(r)=(A(r)+A'(r))/2$ is the arithmetic mean between the vector potential A'(r) associated with the state Ψ' and the comparable vector potential A(r), associated with the state Ψ_{GS}, and the final term in Eq. 2 is defined by the difference between the many-body potential energy associated with states Ψ' and $\tilde{\Psi}_{GS}$ In particular, this last term, is given by

$$< \Psi' | \frac{V - V'}{i\hbar} | \Psi_{GS} >=< \Psi' | \frac{V_{em} - V'_{em}}{i\hbar} | \Psi_{GS} > + < \Psi' | \frac{V_s - V'_s}{i\hbar} | \Psi_{GS} >, \quad (4)$$

where $< \Psi' | V_{em} - V'_{em} | \Psi_{GS} >$ is the difference in electromagnetic potentials associated with coupling between the vector potentials A'(r) and A(r),

$$< \Psi' | V_{em} - V'_{em} | \Psi_{GS} >= \int d^3 r \frac{(A(r) - A'(r))}{c} \bullet J(r), \quad (5)$$

defined by the associated current J(r),

$$< \Psi' | J(r) | \Psi_{GS} >= \sum_j \iiint d^3 r_1 .. d^3 r_n \delta^3 (r - r_j) \frac{e_j}{m_j} (\frac{\hbar}{2i} \left[\Psi'^* \nabla_{r_j} \Psi_{GS} - \nabla_{r_j} \Psi'^* \Psi_{GS} \right] - \frac{e_j}{c} \Psi'^* A_{eff}(r_j) \psi_{GS}),$$

and (in Eq. 4), the remaining contribution to the difference in potential energy is defined by any change in electrostatic or other (for example, inertial) contribution to the energy, associated with the transition from Ψ' (where the non-electro-dynamic portion of the potential energy is V_s') to Ψ_{GS} (which has a corresponding non-electro-dynamic potential energy V_s).

Eq. 2 vanishes identically whenever the energies associated with Ψ_{GS} and Ψ' are the same. When Ψ_{GS} has minimal coupling to the bulk, Eq. 2 holds identically, outside the bulk, provided all of the external forces vanish and the total internal flux of all particles into and away from the bulk region also vanishes. Thus, if the flux of particles, across all boundaries in the bulk vanishes, and the energies of the different states are the same within the bulk region, it follows from Eq. 2 that,

$$\int d^3 r \nabla \bullet < \Psi' | v(r) | \Psi_{GS} >= \int_{\partial V} dS \, \hat{n} \bullet < \Psi' | v(r) | \Psi_{GS} > = \frac{i}{\hbar} \iiint_V d^3 r_1 ... d^3 r_n \Psi'^* (V - V') \Psi_{GS} = 0 \quad (6)$$

where the integration in the final term extends over the bulk region, and the surface integral (associated with v(r)) extends over the boundary of the bulk region. In principle, although this

surface integral includes separate contributions from regions where v may become discontinuous (which are allowed to occur whenever V-V' becomes singular), for the purpose of identifying the GS, Ψ_{GS} and Ψ' can be selected in such a way that V-V' is never singular. Then, a necessary and sufficient condition to guarantee that the left-side (LS) of Eq. 2 vanishes within some volume, defined by a set of boundary planes, in which each point r on one boundary plane is related to a point r' on a second boundary plane, by one of the three vectors, is that

$$v(r+\vec{L}_\alpha)=v(r')=v(r). \qquad (7)$$

In the limit in which Ψ_{GS} and Ψ' are identically the same in the bulk region (but are allowed to be different outside the bulk), and A_{eff} equals a constant, Eq. 7 holds if and only if when for each coordinate r_i that is evaluated on a boundary at $r'=r_i+\vec{L}_\alpha$, then

$$|\Psi_{GS}(r_1,..,r_i+\vec{L}_\alpha..,r_n)|^2=|\Psi_{GS}(r_1,..,r_i..,r_n)|^2, \qquad (8)$$

and

$$\frac{\partial \ln\Psi_{GS}(r_1,..,r_i+\vec{L}_\alpha..,r_n)}{\partial r_i^m}=\frac{\partial \ln\Psi_{GS}(r_1,..,r_i..,r_n)}{\partial r_i^m}, \qquad (9)$$

where r_i^m is the x, y or z component (for m=1,2, or 3) of the coordinate $\mathbf{r_i}$. The general solution of Eqs. 8 and 9 is

$$\Psi_{GS}(r_1,..,r_i+\vec{L}_\alpha..,r_n)=\lambda_i\Psi_{GS}(r_1,..,r_i..,r_n),\ |\lambda_i|=1. \qquad (10)$$

Eq. 10 is a generalization of Bloch's theorem, for finite lattices that holds whenever it is possible to define boundaries through the three displacement vectors, $\vec{L}_\alpha$, for a GS that obeys Eq. 6. In particular, when Eq. 10 holds over distances that are smaller, it also holds when the smaller primitive vectors b_α are used. When $b_\alpha=\frac{\vec{L}_\alpha}{2N_\alpha}$ (where $2N_\alpha$ = number of unit cells between boundaries, defined by Eq. 9) , it follows from Eq. 10 that

$$\lambda_i(\vec{L}_\alpha)=\lambda_i(2N_\alpha b_\alpha)=\lambda_i(b_\alpha)^{2N_\alpha}. \qquad (11)$$

Since the right-side (RS) of Eq. 9 is independent of the initial displacement that appears on the LS, the LS must be stable with respect to additional variations in either b_α or $\vec{L}_\alpha$ (either through infinitesimal variations in the scale of either vector, or through a rigid translation of the lattice). In general, the RS of Eq. 5 does not vanish. But a rigid translation of the lattice occurs when Ψ' satisfies an alternative version of Eq. 10 associated with an alternative reference frame, in which l_i is replaced with a different eigenvalue λ_i' and the vector potential A is replaced with a different vector potential A' (where A and A' differ by a uniform constant, throughout the bulk). Because the associated transformation can be applied through an infinitesimally small displacement, it follows that $\nabla_{b_\alpha}\lambda(R_n)$ is independent of $\vec{b}_\alpha$. But, in order to have minimal overlap with the GS, the allowable states associated with alternative values A' of the vector potential must be selected so that the RS and LS of Eq. 5 vanish. This requirement leads to the constraint that A' be selected, relative to A, in such a way that

$$\ln\left(\frac{\lambda_i(b_\alpha)}{\lambda_i'(b_\alpha)}\right)=i\frac{\pi m}{N_\alpha}=ik\bullet b_\alpha, \qquad (12a)$$

where n is an integer, and k is one of the discrete vectors defined by the finite lattice. Here, for the different states (associated with the different values of $\lambda_i(b_\alpha)$ and $\lambda_i'(b_\alpha)$ in Eq. 12a) to be

orthogonal (which is necessary for minimal overlap between Ψ' and Ψ_{GS}), each possible value of $k \equiv \vec{k}_i$ on the far RS of the equation is required to be in the First Brillouin Zone, defined by

$$\vec{k}_i = \sum_{\alpha=1,3} \frac{i_\alpha \vec{g}_\alpha}{2N_\alpha} \quad ; -N_\alpha \le i_\alpha \le N_\alpha - 1,\ N = 8\, N_1\, N_2\, N_3, \qquad (12b)$$

where the three reciprocal lattice primitive vectors $\vec{g}_\alpha$ are constructed using,

$$\vec{g}_\alpha \bullet \vec{b}_{\alpha'} = 2\pi\delta_\alpha^{\alpha'}, \qquad (12c)$$

where $\delta_\alpha^{\alpha'} = 1$ when $\alpha = \alpha', \delta_\alpha^{\alpha'} = 0$ when $\alpha \neq \alpha'$. Eqs.12a-c have additional implications: Because $\lambda_i(b_\alpha)$ and $\lambda_i'(b_\alpha)$ in Eq. 12a are different but are related to each other through a uniform shift in the vector potential, associated with the requirement that the total flux, in Eq. 5 vanish, effectively, the equation establishes a preferential reference frame associated with the bulk GS and low-lying excited states (defined through Eqs. 10-11). In particular, in this frame, the zero of momentum of each state is selected so that the overlap between any two states possessing different wave-vectors vanishes (as a consequence of being orthogonal to each other). This requirement leads to the result that when each state is selected to be initially in the First Brillouin zone (which is appropriate when the GS is at rest, and the remaining states are related to each other and the GS through rigid, Galilean transformations), the difference in wave-vectors (as a result of preferentially picking the vector potential) always is required to be in the First Brillouin zone. The associated construction fixes the relative difference between the zeroes of momentum of the GS and the low-lying excited states, and zero of momentum of one low-lying excited state, relative to a second low-lying excited state.

The associated restriction on the relative differences in zeroes of momentum also restricts the implicit degeneracy associated with Umklapp processes in infinitely-repeating, periodic lattices. In particular, in infinitely-repeating periodic lattices, Born VonKarman boundary conditions are imposed, based on arbitrary (but large) values of $|\vec{L}_\alpha|$. But since these values are arbitrary, it is assumed that larger values can be employed. The arbitrariness in length-scale would imply that an integer multiple of $2N_\alpha$ could be arbitrarily added to n on the RS of the first equality of Eq. 12a. However, in a finite lattice, the displacement vectors, $\vec{L}_\alpha$, are determined unambiguously by the requirement of vanishing GS flux across a well-defined boundary (as in Eq. 7) and that states that are related to the GS by rigid translations of the bulk be orthogonal to the GS. In particular, when each $\vec{k}_i$ is in the First Brillouin Zone, many-body states associated with different sets of wave-vectors become orthogonal, provided the finite (discrete) Fourier transform, that is used to define the Bravais Lattice vectors R_n, involves the same, discrete set of integers (so that each of the possible integer values n_α that are used in forming the lattice vectors $R_n = n_1\vec{b}_1 + n_2\vec{b}_2 + n_3\vec{b}_3$ are constrained by the inequality, $-N_\alpha \le n_\alpha \le N_\alpha - 1$).

Since $|\lambda_i| = |\lambda_i'| = 1$ in Eq. 12, it follows that both Ψ_{GS} and Ψ' can be written using a common functional form Ψ, in which the dependence on changes in the phase associated with either eigenvalue (as in Eq. 12) occur through a plane-wave that changes as any of the coordinates is displaced by a Bravais vector R_n, and through a second function u that is periodic with respect to translations of any of its coordinates by R_n; i.e. for $\Psi = \Psi'$ or $\Psi = \Psi_{GS}$, Ψ can be written as

$$\Psi(r_1,....,r_n) = e^{i\sum_j k_j \bullet r_j}\, u(r_1,.....,r_n), \qquad (13)$$

where $u(r_1,.....,r_n) = u(r_1,..r_i + R_n...,r_n)$ for all coordinates $\mathbf{r_i}$. Because Ψ_{GS} or Ψ' can be written using Eq. 13, the gradient of $k_i \bullet r_i$ in the exponential factor simply alters the value of A or A' through a (trivial) gauge transformation (associated with changing the value of $\mathbf{p_o}$), for each particle in the many-body Schroedinger equation of the one state (associated with $V_s = V_s'$) that differs from the other only through a change in $\mathbf{p_o}$.

Thus, a large degree of symmetry exists, in which one, two,…n, Bravais translations, in principle could be performed, in which the energy is not changed, while the value of $\mathbf{p_o}$ associated with the coordinate of one (or more) particles is shifted relative to another. (This is the origin of the generalized, double Bloch symmetry that we have previously used [Chubb, T.A. 2005, Chubb & Chubb 2001].) In fact, outside forces constrain the lattice and break the associated degeneracy. As alluded to above, the lowest energy processes involve situations in which, in the bulk region, the state describes a configuration of particles that is neutral (on the average, in each unit cell), and in which all particles move with a common, velocity V_{cm}. In this limit, $\sum_i k_i \bullet r_i = \frac{V_{cm}}{\hbar}\sum_i m_i \bullet r_i = \frac{MV_{cm} \bullet R_{cm}}{\hbar}$, and the vector potential for each charged particle is measured relative to its constant zero of momentum.

In practice, determining $\mathbf{p_o}$ for the GS (and low-lying excited states) for each charged particle (in a charged many-body system) is formidable on a microscopic scale in finite crystals because as charge begins to accumulate, potentially large variations in electric field and charge density can occur. (Because of the greater control that, in principle, occurs in Optical Lattices (Denschlag et al 2002, Deutsch & Jessen 1998), the comparable problem is not as severe. Here, the limitations are defined by the degree of disorder that appears in the vicinity of the boundaries of the lattice, and by the degree of in-homogeneity associated with the externally applied Laser fields and outside sources of energy associated with rotations and gravity.)

In either case, in general, it is impossible to identify GS properties based on the kind of (simpler) rules that apply in bulk crystals, and calculations that include specific information about non-bulk regions (near surfaces or interfaces, in solids, and at the boundaries of the lattices in other cases) are required. In larger crystals, in solids, asymptotically, it is possible to understand, at least in an average sense, how by averaging many terms, a number of important approximate aspects of the associated coupling can occur in most crystals. The resulting perturbations break the degeneracy of the lowest energy states in the "bulk solid" by fixing the value of $\mathbf{p}_o$ associated with each particle of each state, relative to the comparable zero of momentum of every other particle, in every other state. This requirement, also fixes the value of the zero of energy ε as a function of $\mathbf{p}_o$; i.e. $\varepsilon = \varepsilon(\mathbf{p_o})$ for each particle and state relative to the electrostatic zero and physical vector potential that are present in the solid. The resulting values of $\varepsilon(\mathbf{p_o})$ define the lowest lying energy band states.

By requiring that $\langle \Psi_{GS} | \Psi_{GS} \rangle$ be constant and stable with respect to infinitesimal variations in each value of $\mathbf{p}_o$, it is possible to derive a generalization of the semi-classical dynamics and transport theory of charged (band state) particles (electrons and ions). Here, provided externally applied forces F and charge vary sufficiently slowly in the external regions, the gradient of each value of $\varepsilon(\mathbf{p_o})$ with respect to $\mathbf{p_o}$ **,** for a particular particle, identically equals the expectation value of its velocity operator v, averaged over the bulk and surface regions. Also, provided F varies sufficiently slowly, the associated changes in $\mathbf{p_o}$, obey $\Delta p_o = \int F\, dt$. Thus, a change in wave-vector $\Delta k = \frac{\Delta p}{\hbar}$, as a function of time, that is conventionally associated

with each band energy in the semi-classical theory (Ashcroft & Mermin 1976C), can rigorously be interpreted as a shift in the zero of momentum of each state. Details about this, and its implications on transport phenomena for the case of electrons and ions, are discussed in the next two sections of the paper. In the final section, a comparable generalization associated with neutral atoms is presented; in the final section, also, a number of additional important effects (associated with coherence and the onset of broken gauge symmetry) are presented that have bearing on an important practical problem, precision measurements of gravity, using ultra cold atoms, and possibly on a second important effect: the evolution of anomalous forms of heat that have been observed during the prolonged electrolytic loading of deuterium (D) into PdD lattices.

IV Semi-Classical Dynamics of Ion and Electron Band States in Finite Crystals

The semi-classical equations of motion that have been used to describe the dynamics of electrons in solids have never been formally justified. An important reason for this is that these equations do not hold in general. However, using the results of section III, it is possible to generalize these equations, formally, and explain how as a solid becomes sufficiently large, asymptotically, these equations can be required to be valid both for electrons and hydrogen ions, in the limit of vanishing T. The central physics involves appropriately incorporating external forces.

In larger crystals, the relevant dynamics approximately follows from averaging many terms, either on the RS or LS of Eq. 2. This is possible when Gauss's law applies. Then, characteristic changes in the electric field can, in principle, be used to identify trends associated with approximate effects involving charge distribution, which, in turn, can be used to determine asymptotic limits and average values of many of the terms in Eq.2. In particular, the idealized limit in which periodic order is disrupted only in directions normal to an interface (or surface) region can be used to illustrate how changes in a boundary can alter the conventional (bulk) picture (associated with energy bands, in an infinitely repeating, periodic solid) that can justify why (and when) the semi-classical equations of motion for describing the dynamics of bulk charges that occupy band states can be used to describe the conduction of charge (and other transport phenomena) in solids, in the presence of boundaries.

In particular, in this idealized limit, the generalized form of Bloch's theorem (Eq. 10) can apply in directions parallel to the crystal surface (or interface). But for this case, asymptotically, in directions normal to the surface, but sufficiently far away, both the electrostatic potential and electric field are required to exponentially decay (on the average). When the induced redistribution in charge associated with any applied field scales in a linear manner (which occurs universally in metals, when the applied field is uniform and constant), exponential decay in induced charge and its charge density also occur. The resulting coupling leads to finite overlap between states possessing different wave-vectors in the normal direction but preserves periodic symmetry in directions parallel to the surface. In practice, this means that in directions normal to the surface, the values of the momentum (and wave-vector) acquire an imaginary component. The associated perturbations break the degeneracy of the lowest energy states in the bulk solid by constraining the value of the local zero of momentum p_j associated with the local value of the vector potential $\boldsymbol{A}$ of a particular particle of a particular state, with respect to a particular coordinate r_j, relative to the average zero of momentum p_o. This requirement, as a consequence, fixes the value of any external vector potential $\boldsymbol{A}$, at all points in the solid, and the requirement can also define how each particle in the bulk region can interact with the electromagnetic field.

As a consequence, once the zero of momentum, p_o, of the solid (as a whole) is fixed, all states, associated with symmetries that are allowed in Eq. 10 can become possible (as opposed to a situation in which a more limited subset of states, associated with Eq. 1, are allowed). In particular, in the most general situation, $p_o = \sum_j p_j$, where p_j is the minimum value of momentum (which we will refer to as the local zero of momentum) associated with the dependence of Y_{GS} on the coordinate r_j, that asymptotically (as discussed below) can be related to a particular particle or (in situations involving correlation) a collection of particles. Each value of p_j, in turn, is fixed by the average variation in $A(r_j)$ that can result from its overlap with Ψ_{GS} with respect to this coordinate.

Consistent with the requirement that changes in p_j also preserve particle exchange symmetry, p_j is required to be the same for each indistinguishable particle of a particular kind. But different kinds of particles can (and usually will) have different values of p_j. In particular, extreme situations can occur, in which through particle exchange symmetry, counter-intuitive forms of coupling can occur (including Bose-Einstein Condensation) through energy minimization.

Classically, the lowest value of the energy (which is a convenient definition of the zero of energy) of a particle that possesses mass m and velocity v occurs, locally, when v=0 (so that $\frac{1}{2}mv^2 = 0$). Quantum Mechanically, the same definition can also be used within particular regions of space, but in the presence of boundaries, and when indistinguishable particles are present, non-local forms of coupling can occur. As a consequence, in general, every coordinate in Ψ_{GS} should be treated as having a separate zero of energy V_j. In practice, each value of V_j is defined (for example, using Eq. 3) through implicit matching conditions that require that changes in the zero of energy associated with the classical turning for a particular coordinate r_j (defined by $\frac{1}{2}mv(r_j)^2 = 0$) result in discontinuities in the logarithmic derivatives of Ψ_{GS} and/or Ψ_{GS}. Then, as a consequence of momentum conservation, at the boundaries of the bulk, the problem of determining V_j in the bulk is equivalent to the problem of solving an equivalent minimization problem (which is frequently expressed in terms of a well-defined Rayleigh-Ritz variational procedure) for each eigenvalue ε_j (which can be defined as a generalized form of band state energy) associated with the many-body Schroedinger equation. In particular, to determine the GS, it is possible (and consistent with energy minimization) to define each value of V_j, using, $V_j = \varepsilon_i$, and to require that $E_{GS} = \sum_j \varepsilon_j$.

The problem of solving the associated many-body Schroedinger Equation for each value of ε_j requires detailed information about the fluxes of particles at the boundaries of the bulk region as well as additional information (in situations in which correlation is present) associated with particle exchange symmetry, including effects involving the possible exchange of internal quantum numbers (such as magnetic spin). Because of the wide variability of boundary conditions that can be imposed, it is not possible, in general, to solve this particular problem uniquely without imposing particular restrictions on the behavior of Ψ_{GS} in non-bulk regions. But it is possible to use approximate boundary conditions associated with the relevant dynamics in order to understand a number of key features associated with the relevant effects.

In particular, considerable progress can be made by requiring that the functional form of the most general many-body wave function that is used to describe the GS (or in the comparable wave function that describes the low-lying excited states) asymptotically approach the functional

form that applies in the independent particle limit in non-bulk regions either at the boundaries of the bulk or (provided additional constraints are imposed) far from the boundaries of the bulk region. In particular, well-defined effects can be used to understand the behavior of the associated state in this asymptotic limit, immediately at the boundaries of the bulk region or far from the boundary (provided the wave function asymptotically approaches the associated functional form far from the boundaries and is non-vanishing and continuously differentiable between the boundary and the location far from the boundary where this functional form applies). When this limit applies, specifically, either at the boundary, asymptotically far from the boundaries of the bulk region, or at intermediate locations, in non-bulk regions, functional forms associated with Ψ_{GS} and more general functional forms that apply for wave functions Ψ (that describe low-lying excited states of the bulk) can be expressed using sums of products of single particle wave functions, describing fermions and bosons. Then, in these regions, each fermion (boson) wave function can be expressed using an anti-symmetrized (symmetrized) sum of products of single particle wave functions.

The significance of this limit is that when it applies, it is possible to identify and order the associated eigenvalues ε, based on the (conventional) nomenclature (associated with "occupied" and "unoccupied" states) of the independent, single particle picture, used in conventional band theory. As a consequence, values of ε involving "occupied states" (in Ψ_{GS}) can be distinguished from "unoccupied states" (that occur in the wave functions Ψ that describe the low-lying excited states of the bulk).

This point is significant because since any changes in p_j can alter potential forms of overlap involving a particular set of indistinguishable particles, counterintuitive relationships can occur (associated with energy minimization) in which changes in flux (in Eq. 3) can be enhanced or impeded by effects associated with fermion or boson occupation. These effects, which involve changes in $\mathbf{A(r_j)}$ that result from changes in $\mathbf{p_j}$, can lead to particular forms of coupling that are required to occur. As a consequence, the energy minimization procedure is constrained so that the total (ground state) flux of each particle (in Eq. 6) vanish when the integrations (in this equation) are extended throughout the solid and that this flux be stable with respect to any infinitesimal variation in $\mathbf{p_j}$ and the changes in the zero of energy associated with this form of variation. Because exchange symmetry does not alter the internal dynamics, it is possible to introduce the associated effects by selecting the "global" zero of energy in an appropriate way for each particle. This can be done either directly for bosons (specifically, deuterium nuclei, d's, or ultra cold bosonic atoms) or indirectly for fermions (including protons, p's, electrons, or ultra cold fermionic atoms). In particular, the value of the global zero can be equated with the lowest (for bosons) or highest (for fermions) value of the local zero of energy (i.e., the lowest or highest occupied band state eigenvalue ε), defined, asymptotically, by the non-bulk region (independent particle) wave function. Thus, in either (the fermion or boson) case, a single, independent, value of ε can be used to determine the behavior of the GS and lowest states of excitation, based on a relative state of motion, defined by the relative momentum between the bulk and non-bulk regions. In particular, in a reference frame that has momentum $\mathbf{p_j} \equiv \hbar k_j$, relative to a frame that is stationary, the local zero of energy (associated with a particular band state eigenvalue, ε) can be defined by the value of the local zero of the (highest or lowest occupied) energy of a single particle energy state ε ($=\varepsilon(\boldsymbol{k_j})$), associated with possible forms of interaction that can lead to excitations of the GS.

For this reason, in either case (for fermions or bosons), the average zero of energy can be defined relative to the lowest –lying states of excitation, using a single value of the energy

(which at T=0 can be equated with the chemical potential). By requiring that no changes occur in the bulk region, relative to non-bulk regions, all energies and changes in relative momentum between particles are fixed, with respect to the a reference frame in which the solid (as a whole), as in Eq. 1, is allowed to move rigidly. By imposing the effects of such rigid forms of motion on the associated dynamics, it is possible to identify the lowest energy forms of response, involving the bulk region, with respect to outside perturbations (and forces). For this reason, the identification of the zero of momentum and its evolution in response to external forces can be used to identify and introduce dynamical changes in the bulk region. In particular, as a consequence, because it is impossible to determine absolutely whether or not the bulk region as a whole, is in motion or at rest, with respect to non-bulk regions, each value of the local zero in wave vector $\boldsymbol{k_j}$ can be used to define the lowest lying excitations of the solid. For the same reason, the stability of the solid with respect to variations involving $\boldsymbol{k_j}$ can be used to define variations in the position and momentum of the bulk region (associated with displacements that do not alter the internal energy of the bulk) relative to non-bulk regions. As a consequence, relative to the local wave-vector $k_j \equiv \frac{p_i}{\hbar}$ (associated with the local zero of energy, defined by the band state, $\varepsilon = \varepsilon(k_i)$, in a particular frame), within the bulk region, to determine the GS it is required that: 1. The absolute zero (defined by $<\Psi_{GS}\ |E_{GS}\text{-}H|\ \Psi_{GS}>=0$) of the energy be independently stable with respect to variations of each eigenvalue, $\varepsilon = \varepsilon(k_i)$, and 2. The ground state flux in Eq. 6 (defined by $\Psi' = \Psi_{GS}$) vanish and be stable with respect to any infinitesimal change in any value of $\mathbf{k}_j$ (and shift in zero of energy $\varepsilon(k_i)$) associated with each coordinate in Ψ_{GS}, relative to its initial value. The first requirement (involving the stability of the absolute zero) is satisfied when

$$(E_{GS} - H)\frac{\partial \Psi_{GS}}{\partial \varepsilon(k_j)} = \Psi_{GS} \qquad (14)$$

(Here, $\frac{\partial \Psi_{GS}}{\partial \varepsilon(k_j)}$ is defined using perturbation theory, through an infinitesimal change in the effective zero of energy, $\varepsilon(k_j)$.) The second requirement is satisfied when

$$\iiint d^{3n}r\left(\frac{\partial \Psi_{GS}^{*}}{\partial \vec{k}_j}(E_{GS} - H)\Psi_{GS} + \Psi_{GS}^{*}(E_{GS} - H)\frac{\partial \Psi_{GS}}{\partial \vec{k}_j}\right) = 0, \qquad (15)$$

where $\frac{\partial \Psi_{GS}}{\partial \vec{k}_j}$ is the gradient of Ψ_{GS} with respect to the wave vector $\vec{k}_j = \frac{\vec{p}_j}{\hbar}$ associated with the coordinate r_j that is used to define the position of each particle. Here, the variation with respect to $\mathbf{k_j}$ includes the dependence of Ψ_{GS} on implicit effects that result from changes in the zero of energy, and on explicit changes that occur when the momentum $\mathbf{p_j}$ of each individual particle is separately varied. (In particular, by rigidly shifting the zero of this value of momentum, implicit forms of dependence occur, for example, in the plane-wave, phase factor that results from the Galilean transformation in Eq. 1 and related, alternative, approximately coherent, forms of motion.)

Specifically, here, the dependence on $\mathbf{k_j}$ is treated implicitly through the change in the zero of energy that is used to define the periodic function, u (in Eq. 13), and explicitly through the dependence on $\mathbf{k_j}$ that appears in the associated plane-wave factor (also in Eq. 13). In particular, in the periodic function u, each coordinate $\mathbf{r_j}$, by construction, has associated with it an implicit dependence on the zero of energy, through the eigenvalue $\varepsilon(\mathbf{k_i})$, that varies as the

wave-vector, $\mathbf{k}_j$, is changed. Although in a finite lattice, the spectrum of possible eigenvalues $\varepsilon(\mathbf{k}_j)$ is discrete, because these values are fixed by breaking a continuous symmetry (associated with allowing the lattice to rigidly shift over a continuum of possible momentum values), the gradient ($\frac{\partial \varepsilon(k_j)}{\partial \vec{k}_j}$) of each eigenvalue, with respect to changes in wave-vector $\mathbf{k}_j$ is well-defined. Also, in principle, the explicit dependence of Ψ on $\mathbf{k}_j$ (through the phase factor) can become quite complicated through direct and indirect forms of coupling to the electromagnetic (EM) field.

On the other hand, since the GS is required to have minimal coupling to outside processes, coupling between indistinguishable particles is distinctly different from the comparable coupling between particles that are distinguishable. Thus, it is possible to assign a preferential gauge (and zero of momentum) to each (indistinguishable) fermion or boson, subject to the requirement that Bose-Einstein (BE) or Fermi-Dirac (FD) statistics apply in an appropriate manner. In unusual circumstances, coupling to the EM field also can occur through effects associated with spin (and other internal states) that can alter the normal exchange properties (with respect to coordinates r_j associated with position) of fermions and bosons. (These effects, in particular, can become dominant in the asymptotic limit, involving vanishing T, without external forces.) For this reason, the manner in which variations in the zero of momentum are required to be consistent with BE or FD statistics is intimately related to the way the system is prepared.

But in most situations, the limit that applies at low T occurs when system momentum and energy are minimized and minimal (maximal) occupation of momentum states by fermions (bosons) takes place. In principle, as a consequence, it is possible that when exotic forms of interaction are present, situations can occur (involving fermions) in which a common value of $\mathbf{k}_j$ can appear as a pre-factor of many different coordinates ($\mathbf{r}_j$) in the phase factor in Eq. 13. But this kind of situation occurs infrequently. Thus, in most situations, when fermions are involved, it is possible to assign a single value of $\mathbf{k}_j$ to a single coordinate $\mathbf{r}_j$; while in the case of bosons (including situations that occur in superconductors, where even numbers of fermions become paired), because of particle exchange and coupling to internal quantum states, situations can occur involving many particles that can possess different coordinates $r_{i'}$, and a common wave-vector, $\mathbf{k}_j$. In general, to understand how potential coupling to a common wave-vector $\mathbf{k}_j$ can occur, for each set (or, potentially, subset) of indistinguishable particles, it is appropriate to identify a set {j'} of different coordinates ($\{r_{j'}\}$) and momenta ($\{p_{j'} = \hbar k_{j'}\}$) of indistinguishable particles that can have a common wave-vector $\mathbf{k}_j$.($= k_i, i \in \{j'\}$). Using this fact, it is possible to write the resulting variation in Ψ_{GS} with respect to changes $\mathbf{k}_j$ both implicitly (through $\frac{\partial \varepsilon(k_j)}{\partial \vec{k}_j}$) and explicitly (through the phase factor), using

$$\frac{\partial \Psi_{GS}}{\partial \vec{k}_j} = \sum_{\{j'\}} \frac{\partial \Psi_{GS}}{\partial \varepsilon_{j'}(k_j)} \frac{\partial \varepsilon_{j'}(k_j)}{\partial \vec{k}_j} + i \sum_{\{j'\}} r_{j'} \Psi_{GS}. \qquad (16)$$

Here, in the first term, a separate subscript (j') is used for each eigenvalue, $\varepsilon(k_j)$ ($\equiv \varepsilon_{j'}(k_j)$), in order to account for the possible change in the zero of energy ($\Delta\varepsilon_{j'}(k_j)$) that can occur in each coordinate ($r_{j'}$) of Ψ_{GS}, and the separate summations in both terms extend over values of j' associated with coordinates $r_{j'}$ in Ψ_{GS} where (within the phase factor in Eq. 13) a common wave-

vector k_j is used. Also, the number of independent wave-vector ($\mathbf{k}_{j'}$) values is $N = 8N_xN_yN_z$ (since $\mathbf{k_j}$ is in the First Brillouin Zone).

To identify either the GS or the lowest lying excitations of the GS, Eq. 16 must hold asymptotically for individual terms associated with different values of j'. This means that individual terms, associated with variations of Ψ_{GS} with respect to its dependence on a particular value of j' (through $\varepsilon_{j'}(k_j)$ and $r_{j'}$), can be treated as being independent from comparable variations involving a different value of j'. Then, for fermions, or for bosons, individual contributions for each band (associated with the index j') can be identified. As a consequence, using Eqs. 14-16, it follows that it is possible to relate the average value of the velocity of any of the (indistinguishable) particles associated with all coordinates r_j that possess wave-vector $\mathbf{k}_j$ to the variation in band energy using,

$$N_{F,B}(k_j)\frac{\partial \varepsilon_{j'}(k_j)}{\partial \vec{k}_j} = \frac{\frac{1}{m_j}\iiint d^{3n}r\left[\frac{\hbar}{2i}\left(\Psi_{GS}^{*}\frac{\partial \Psi_{GS}}{\partial r_{j'}} - \frac{\partial \Psi_{GS}^{*}}{\partial r_{j'}}\Psi_{GS}\right) - \frac{e_j \Psi_{GS}^{*} A(r_{j'})\Psi_{GS}}{c}\right]N_{F,B}(k_j)}{\iiint d^{3n}r \Psi_{GS}^{*}\Psi_{GS}}, \quad (17a)$$

where $N_{F,B}(k_j) \equiv n_{k_j}$ =0, 1 or 2 for fermions (depending on whether or not 0, 1 or 2 fermions with different spins occupy the band), and for bosons, $N_{F,B}(k_j)$=0, or N_b, where N_b= total number of bosons. In either case, since a common factor of $N_{F,B}(k_j)$ appears on both sides of Eq. 17a, in the independent particle limit (as in conventional band theory), in which Ψ_{GS} can be written in non-bulk regions, in terms of a sum of (suitably) symmetrized (or anti-symmetrized) products of individual wave functions $\phi_{\varepsilon(k)}$, it follows that

$$\frac{\partial \varepsilon_{j'}(k_j)}{\hbar \partial \vec{k}_j} \equiv \frac{1}{m_j}\iiint d^3 r_j \left[\frac{\hbar}{2i}\left(\phi^{*}_{\varepsilon_{j'}(k_j)}\frac{\partial \phi_{\varepsilon_{j'}(k_j)}}{\partial r_{j'}} - \frac{\partial \phi^{*}_{\varepsilon_{j'}(k_j)}}{\partial r_{j'}}\phi_{\varepsilon_{j'}(k_j)}\right) - \frac{e_j \phi^{*}_{\varepsilon_{j'}(k_j)} A(r_j)\phi_{\varepsilon_{j'}(k_j)}}{c}\right], \quad (17b)$$

where each single particle wave function has been normalized ($\iiint d^3 r_j \, |\phi_{\varepsilon_{j'}(k_j)}|^2 = 1$) to the region (of integration) that is used in the evaluation of the RS of Eq. 17b.

These results, which are exact for the GS at T=0, in the bulk, are the many-body generalization (for charged particles in finite crystals) of the expression that relates the gradient of the eigenvalue $\varepsilon(\mathbf{k_i})$ with respect to wave-vector $\mathbf{k_i}$ to the local velocity (and current) in the bulk region. This relationship, in turn, can be used in the semi-classical theory of conduction in solids (which is traditionally derived, using a heuristic approach based on "independent quasi-particles", associated with the semi-classical theory, in the limit of bands that are derived using infinitely-repeating periodically ordered lattices).

Eqs. 17a,b apply for ultra cold neutral atoms in optical lattices and, implicitly, in solids, for all charged particles (potentially, including p's, inside nuclei within the crystal), as in the conventional semi-classical theory. But, in solids, with the exception of ions of hydrogen and its isotopes, the average current from particular bands involving p's or d's and core electrons is entirely negligible. Also, no net contribution to the current occurs when the summation over coordinates $\mathbf{r}_i$ (on the LS of Eq. 13) and wave-vectors- $\mathbf{k}_i$ (on the RS) involves a filled band (which occurs when all values of $\mathbf{k}_i$ in the First Brillouin Zone are occupied in a particular band). As in conventional band theory, filled bands do not contribute to the current because $\varepsilon(\mathbf{k}_i)$ is a periodic function, with respect to translations by a reciprocal lattice vector.

In the semi-classical theory, as it applies to solids, the single particle relationship associated with Eq. 13 is used to derive particle fluxes, in which the perturbation V -V' is finite, on the RS of Eq. 6. Then, (implicitly) surface effects are accounted for through the minimization

procedure associated with Eqs. 14-16. This means the remaining terms (omitted from Eq. 6) in Eqs. 17(a,b), associated with extending the many-body state into surface regions, vanish. In a T=0 state, in the absence of an external Electric Field ($\vec{E}$), this can be justified using the asymptotic limit (alluded to above) in which both the charge and electrostatic field exponentially decay. In particular, provided the range over which any changes associated with this exponential decay can be appreciable is considerably larger than the characteristic length of any unit cell, the effect of the decay can be treated using a slowly-varying (envelope) function that can be held constant during the integration over any particular integration in a unit cell outside the bulk region. Then, it follows that (since each integrand is periodic) the dependence of this envelope function on the flux or normalization, globally, in the numerator and denominator of Eqs. 17(a,b), appears as a portion of a common pre-factor of a single (but distinct) integral (associated with the flux or normalization) from a single unit cell. As a consequence, in their most general form, Eqs. 17(a,b) hold, but how they apply requires that a particular form of coupling in the surface region be approximately valid. In situations, where the bulk region remains neutral, and in regions near the bulk, when the change in charge, on the average, decreases in a smoothly varying fashion, that occurs over many unit cells, within any particular cell, V-V' can effectively be viewed as not being altered by the presence of the surface. In this region of slowly-varying decay in charge and potential, from unit cell to unit cell, the net force that is applied at the boundaries of the solid can be averaged over many cells. Then, over the surface region, V-V' can be approximated using a classical force, multiplied by the distance where non-neutral forms of force apply. In this limit, the applied force merely shifts the zero of energy.

Thus, in this limit, to maintain charge neutrality, it is possible to have a net flux of charge across the boundaries of the solid, in which the flux imbalance is defined classically through the differences in $\vec{E}$ (associated with averaging the value of $\vec{E}$ over the entire solid) in regions (near surfaces and interfaces) where charge can accumulate. In particular, always, at sufficiently low T, net flux of all charged particles to and from the bulk region vanishes. This can occur when equal amounts of charge enter and leave the bulk, in which the zero of momentum of the many-body state is allowed to shift, uniformly, and the only net force acts on all of the particles uniformly. Then, effectively, a change in momentum at the boundary of the bulk leads to a perfectly rigid change in which all particles in the bulk move with a constant (fixed velocity) that is equivalent to a perfectly rigid form of interaction in which, effectively, all outside forces impart momentum directly to the CM of the solid. The associated shift is defined by the limit in which A and A' are different, non-uniform and non-periodic in the surface region but are required (on the average) to be uniformly constant in the bulk. This leads to a uniform (but time dependent) shift in the zero of momentum of the bulk, as defined by its instantaneous motion, relative to a particular initial time, and by the resulting coupling to the vector potential and static electromagnetic fields.

Since the bulk region is neutral, on the average, the value of its center-of-mass momentum is $P_{cm,o}=p_o=M_{bulk}V_{cm,o,}$, where M_{bulk} is the total mass of the bulk, and $V_{cm,o}$ is the absolute velocity of the bulk region. But since neither M_{bulk} or $V_{cm,o}$ can be measured (and neither quantity is conserved) without introducing external charge, it is only possible to relate $P_{cm,o}$, to the total CM momentum P_{cm} associated with both the bulk region ($P_{cm,o}$) and non-bulk region (=$P_{cm,nb}$) values of the momentum, using the relationship, $P_{cm}= P_{cm,o}+ P_{cm,nb}$, and to changes in the velocity V_{cm} of the CM of the solid. In particular, in the absence of external electromagnetic fields (and external vector potentials), near the GS, provided the solid is neutral,

on the average (with respect to individual unit cells), it follows that averaged over bulk and non-bulk regions, $P_{cm}=MV_{cm} = P_{cm,nb}+P_{cm,o} \equiv P_{cm,nb}+p_o$,where M=total mass of the solid.

But at the boundaries of the bulk, a net accumulation of charge can occur, which means that although it is not possible to measure $M_{bulk}V_{cm,o}$ directly, it is possible to impose the requirement that, instantaneously, as a function of time (as $T \rightarrow 0$), no net acceleration of the bulk relative to non-bulk region be allowed to take place. When this is true, $\frac{dMV_{cm}}{dt} = \frac{d(P_{cm,o} + p_o)}{dt} = 0$, which means that $\frac{dp_o}{dt} = -\frac{dP_{cm,nb}}{dt} = \frac{dP_{cm,o}}{dt}$.

Since there is no charge, on the average, in the bulk, it also follows that the requirement that $\frac{dMV_{cm}}{dt} = 0$ instantaneously, as T->0, also applies both for the sum of forces that act independently either on (all) negatively or positively charged particles. Also, because positive and negative charges respond to external fields by accelerating in opposite directions, the requirement that zero net flux of particles (or energy) occur at the boundaries of the bulk region implies that in the GS, the net currents from bulk and non-bulk regions, associated with positive and negative charges, separately vanish. Then it is possible to define an instantaneous rate of change $\frac{dp_o}{dt}$ of the zero of momentum, respectively, $\frac{dp_o}{dt} = \frac{dp_o^j}{dt}$, or $\frac{dp_o}{dt} = \frac{dp_o^{j'}}{dt}$ for positively or negatively charged particles in the bulk region. For this reason, although it is not possible to determine, unambiguously, the value of the CM velocity $V_{cm,o}$ of the bulk region, it is possible to relate changes in the flux of each kind of (positively or negatively charged) particle (and the associated currents) that result in response to changes in applied fields, based on the assumption that the bulk region remains in its ground state.

In particular, the resulting changes in flux occur through changes in M_{bulk} that result from the requirement that all changes in the bulk occur through rigid (Galilean) translations that only alter the many-body state of the GS by shifting the local zero of momentum of each coordinate (and total zero of momentum of the bulk). The changes in momentum (and mass) can be inferred, using Gauss's law (which is required to define the boundaries of the bulk region, and of the entire solid), and the following requirements: 1.For each rigid shift (through an effective Galilean transformation) of the bulk, separate values of $\Delta p_o = \Delta t \frac{dp_o}{dt} = \Delta t \frac{dp_o^{j''}}{dt}$ accompany the shift in momentum. (These values of Δp_o have opposite sign for situations associated with positively charged particles, which occur when j''=j, as opposed to situations associated with negatively charged particles, which occur when j''=j'.) 2. Each value of Δp_o ($\Delta p_o=\Delta p_o^j$ or $\Delta p_o=\Delta p_o^{j'}$, respectively for all positively or negatively charged particles) for each shift leads to a constant, uniform change of the vector potential in the bulk, and 3. The ground state, in bulk regions, is not altered by the sum of the two shifts, which means 4. The sum of externa1 forces F, associated with changes resulting from the two shifts, vanishes at the boundaries of the bulk region. To determine $\Delta P_{cm,o}^{j}$ and $\Delta P_{cm,o}^{j'}$, it follows that in the surface region $E = -\frac{\partial A}{c\partial t}$, and $\nabla \bullet A = 0$. Then, in the presence of a constant, spatially uniform, externally applied $\vec{E}$ field, and constant, spatially uniform B field, or both, the difference between an externally applied vector potential $A(x,t)$ and the (time independent) ground state vector potential $A_o(x)$ (that is used to define $P_{cm,nb}$) is defined by

$$A(x,t) - A_o(x) = (-\vec{E}ct + \frac{B \times x}{2}) \ . \qquad (18)$$

The fourth requirement is satisfied when with respect to the ground state, externally applied forces in non-bulk regions are balanced in the same regions by existing forces. As a consequence, formally,

$$\frac{dM^{j}V_{cm}^{j}}{dt} = \left(\frac{d\dfrac{<\Psi_{GS}{}^{j}\,|\,P_{cm,nb}^{j} - e^{j}/cA(x^{j})\,|\,\Psi_{GS}{}^{j}>}{<\Psi_{GS}\,|\,\Psi_{GS}>}}{dt}\right)$$

$$= \frac{<\Psi_{GS}{}^{j}\,|\,\dfrac{i[H_o, P_{cm,nb}^{j}]}{\hbar} + \dfrac{e^{j}\vec{E}}{\hbar} + e^{j}\dfrac{v(x_j)}{\hbar c}\times B]\,|\,\Psi_{GS}{}^{j}>}{<\Psi_{GS}\,|\,\Psi_{GS}>} \equiv 0, \qquad (19a)$$

where v(x_j) (=velocity of positively charged particles, as defined by Eq. 3), the only contributions to the integrations in the numerator occur from the non-bulk region (and its boundaries), H_o is the Hamiltonian, in the absence of outside perturbations, and the expectation value associated with the commutator, $<\Psi_{GS}|i[H_o,P_{cm}{}^{j}{}_{,nb}]|\ \Psi_{GS}>$, does not vanish because it involves an integration over a finite, limited volume (the non-bulk region). Also, here, and throughout, the notation $\Psi_{GS}{}^{j}$ in the numerator of Eq. 19a, and the associated short-hand, notation $P_{cm,o}^{j}$-$\frac{e_j}{c}A(x_j,t)$ in the first line, and subsequently, in the second line, refer to the portion of the expectation value of $P_{cm,nb}$-e/cA(x,t) in which the charge e_j and the vector potential A and momentum $P_{cm,nb}$ are restricted to coordinates x_j, that involve positively charged particles. In practice, this means that x_j refers to a location where e_j=|e|, and the dependence associated with changes in $P_{cm,nb}$ and changes in the electromagnetic fields, are included at locations where positively charged particles are allowed to couple to A, through overlap between Ψ_{GS} and $e_j A(x_j,t)$. Eq. 19(a), and remaining equations describing the evolution of the zero of momentum, as written above and below, apply for positively charged particles. They also can be used to determine the zero of momentum that applies when the coordinates r_j (associated with positively charged particles) are replaced with the comparable coordinates, r_j' (associated with negatively charged particles) and each positive charge e_j is replaced with a negative charge $e_j' = -e_j$.

Because relative changes in $\mathbf{P_{cm}}$ alter the wave function globally (as in Eq.1), in establishing the zero of momentum (and velocity), changes involving the CM momentum in the non-bulk regions can be used to define comparable changes in the bulk region. Specifically, when $\frac{dMV_{cm}^{j}}{dt} = 0$ (as in Eq. 19a), for the CM, it is possible to define a separate change in CM and force, associated with each positively or negatively charged particle (where j=j for positively charged particles, and j=j' for negatively charged particles). This means that $\frac{dP_{cm}{}^{j}}{dt} = \frac{dMV_{cm}^{j}}{dt} = \frac{dP_{cm,nb}^{j}}{dt} + \frac{dP_{cm,o}^{j}}{dt} = 0$, and $\frac{dP_{cm,nb}^{j}}{dt} = -\frac{dP_{cmo}^{j}}{dt} = 0$. But then since the integration in the numerator extends only over the non-bulk region, it follows from Eq. 19a that

$$-\frac{<\Psi_{GS}\,|\,\imath[H_o, P_{cm}^{j}]\,|\,\Psi_{GS}>|_{non-bulk}}{<\Psi_{GS}\,|\,\Psi_{GS}>} = -\frac{dP_{cm,nb}^{j}}{dt} = \frac{dP_{cm,o}^{j}}{dt} =$$

$$= + \frac{e^j \vec{E}}{\hbar} + e^j \frac{v(x_j)}{\hbar c} \times B. \quad (19b)$$

Also, from Eq.17a, it follows that for all particles, the average value of the total velocity v(x) (as in Eq. 19a) of a particular kind of particle can be expressed, using

$$\sum_j n_{k_j} \nabla_{k_j} \varepsilon(k) = \sum_j \iiint d^3 r_j v(x_j) \qquad .(19c)$$

This relationship holds either for positively or negatively charged particles, and the sum over j involves all possible occupied and unoccupied band state eigenvalues (for each kind of particle): It also follows from the definition of $P^j_{cm,o}$,

$$\frac{dP^j_{cm,o}}{dt} = \sum_{\{i\}} \frac{\hbar dk_i^j}{dt} \ . \qquad (19d)$$

But then when Eqs. 19d and 19c are substituted into Eq. 19b, separate summations involving k^j occur on both sides of the resulting expression. In particular, for each value of $\frac{\hbar dk_i^j}{dt}$ (from the summation on the RS of Eq. 19d) that appears on one-side of the resulting expression, a comparable term, of the form, $\nabla_{k_j} \varepsilon(k) = \iiint d^3 r_j v(x_j)$ (from the summation on the LS of Eq. 19c) appears on the opposite side of the expression. Because any value of momentum is possible, each summation can involve a limited (but the same) number of terms. Thus, for the equation to be valid, for arbitrary forms of occupation, it follows that the dependence on the local zero of momentum (through k) is systematically required to be balanced, term by term, on both sides of the equation. This means it is possible to assign a local, time-dependent change $\Delta k_i = \frac{\Delta t dk_i}{dt}$ for each component k_i of the wave-vector, independently, for positive or negative charges. Then, using Eqs. 19a-d, it follows that for each value of the local zero of the wave-vector k, and for each particle,

$$\frac{dk}{dt} = e_{j''} \vec{E} + e_{j''} \frac{\nabla_k \varepsilon(k)}{c} \times B. \qquad (20)$$

As a consequence, a separate (positive or negative) shift Δk of the local wave-vector zero occurs for each (positively or negatively charged) particle. In each case, the magnitude of the shift is the same for each kind of particle for each value of k. For the GS in bulk regions, no net change in charge occurs. Because some charge can leave the solid and because (in the presence of magnetic fields) the effects associated with the gradients of the band state eigenvalues are different for ions than electrons, for each value of k, Δk is very different for positively or negatively charged particles. Thus, effectively, ions and electrons can (and will) move with different velocities. In particular, as a function of time, Eq. 20 implies that all of the various wave-vectors are shifted by $\pm \frac{\Delta p(t)}{\hbar}$, based on Eq. 20, in bulk regions. (The positive value is used for positive charges, and the negative value is used otherwise.) Then, when charge is free to flow into and away from the bulk region, a quasi-steady state can evolve, that can be described, based on the interpretation that each "particle" moves (in the sense that its average

current is described by Eqs. 17(a,b)), while its wave-vector changes in time, from $k = k_o$ to $k = k_o \pm e\frac{(E + \nabla_k \varepsilon / c \times B)t}{\hbar}$.

The associated picture is a generalization of the semi-classical equations of motion (that are used in the associated theory of conductivity and transport). A requirement for its success is that the bulk region remain neutral and a quasi-equilibrium be established, in which charge in non-bulk regions redistributes itself sufficiently rapidly that the value of t not become so large that the value of k is forced to be comparable to a reciprocal lattice vector G_1. If this occurs, in fact, the zero of momentum of the bulk can become sufficiently large that each wave-vector is shifted by the same finite, amount. In the associated effect, which is the basis of Umklapp (or U-) processes, Zener tunneling and Bloch oscillations, all charged particles of a particular kind instantly acquire the same amount of momentum, and the bulk region, as a whole, recoils, relative to the surface.

In infinitely-repeating lattices, it has not been possible to rigorously identify bounds for the magnitude of momentum that can be transferred from the bulk to surface regions during such a form of rigid translation. Instead, a more approximate procedure, based on an approximate collision theory has been employed. In fact, as discussed in the next two sections, in finite lattices, it is possible to quantitatively establish precise bounds, associated with crystal size and the occupation of energy band states, for the magnitude of the potential transfer of momentum in Umklapp processes.

V Charge Transport at Finite T, in Finite Lattices

The semi-classical transport equations (Eqs. 17 and 20) apply only when the total force provided by non-bulk regions is approximately uniform over a sufficiently large (surface region) volume, where the charge exponentially decreases with increasing distance from the bulk region, and is balanced (through a shift in the zero of momentum) by an effective force provided by the bulk region. In general, the associated decay can occur at locations r where the effective, local kinetic energy, $(= \int d^{3n}r'(\Psi_{GS}^*(r'_1 .....r'_n)\sum_j \sum_k n_k \varepsilon_j(k) - V)\delta(r - r_j')\Psi_{GS}(r'_1 .....r'_n))$ is negative.

In practice, near the ground state configuration in a real solid, this decay increases monotonically, and exponentially with increasing distance z, above a plane defined by the classical turning point of the highest occupied, band state energy. As a consequence, in sufficiently large solids, these equations describe the time evolution of the zero of energy of any of the possible configurations of charge (in the bulk) in which the velocity flux of each type of charged particle (into and away from the region) vanishes. Also, they describe the rate of charge flow, in this context, only when the bulk region remains in its ground state.

Although at finite T, these equations do not apply, it is possible to derive more general, approximate transport equations (again in the limit of sufficiently large crystal size) that lead to a common rate of charge flow (for each kind of particle) at finite T. In particular, at finite T, since particle velocity flux is never rigorously conserved across all boundaries, the total energy and wave function normalization, within the bulk are not conserved. Despite this fact, beginning from a particular, many-body state configuration, within the bulk, it is possible, formally, to identify the dominant resonant processes, which asymptotically describe the average, temporal behavior of the bulk region over sufficiently long intervals of time, at low (but finite) T. Formally, in a finite solid, the associated transport equations can be derived either by introducing

complex values of the energy or time (or both) and by using perturbation theory, in a manner that is similar to the standard (R-matrix [Burke & Berrington 1993] and/or finite temperature, Dyson-Wick expansion theory [Bruus & Flensberg 2004, Lipavsky et al 1986]) many-body techniques that have been employed, previously, in infinitely-repeating lattices, and more recently in finite crystals (based on semi-empirical models [Burcin Unlu et al 2004]).

In particular, the same kinds of diagrammatic techniques and time ordering procedures (involving ordering of complex values of the time, along closed contours [Lipavsky et al 1986]) can be applied to each kind of particle, in order to derive approximate (Boltzmann-like) rate expressions based on the semi-classical limit of the Generalized Kadanoff Baym (GKB) equations (Lipavsky et al 1986, Langreth & Wilkins 1972). In the past, qualitatively, the impact of finite size effects has been assessed (Burcin Unlu et al 2004), based on the approximate picture that the underlying equations describe the time evolution of the quasi-particle states associated with the solid. In fact, a more rigorous picture applies: As opposed to describing the evolution of "quasi-particles", the semi-classical equations describe the possible evolution of any of the possible zeroes of energy and momentum that can be present (associated with a particular coordinate in the many-body wave function) that are initiated at low T in response to a Galilean transformation, defined by the shift in momentum of the bulk, as a result of externally applied forces.

From this, more precise picture, it is possible to include finite size effects more quantitatively. Also, although in general it is impossible to address many problems associated with the complete many-body problem, even in the long time limit, asymptotically, as a consequence of the implicit gauge symmetry (associated with translation symmetry of the bulk), formally, it is possible to identify a number of general features (that become dominant at low T) associated with fluctuations in the zeroes of energy and momentum of all or a portion of the particles in the many-body system. In particular, as a result of the associated, implicit symmetry, in the bulk, the ground state of the many-body system must be stable with respect to any variation of any of the possible zeroes of momentum, associated with a particular coordinate; while, for sufficiently large crystals, the lowest energy fluctuations occur through forms of rigid translations (Galilean transformations) that preserve particle-particle separations, in the bulk (which, as shown below, are Umklapp processes, in which the zeroes of momentum of all particles are uniformly shifted, by the same, constant amount).

These Umklapp-like processes are the dominant low-energy fluctuations because they preserve translation symmetry in the bulk. This fact can be justified formally, using the Lippman-Schwinger equation(LSE) (Levine 1999, Schwinger 1990), or, equivalently, from R-Matrix Theory (Burke & Berrington 1993). In particular, in general, if Ψ_o is the wave function that describes any of the initial, possible, low-lying, many-body states that are associated with either a particular region of space, or some finite portion of the energy (and momentum) spectrum, or both, through excitation and/or de-excitation of the initial state, an outside perturbation ΔV will induce overlap between Ψ_o and one or more states associated with a different ("forbidden") region of space or portion of the spectrum. It follows from the LSE (as well as R-Matrix theory) that the general rate of reaction

$$R = \lim_{t\to\infty} \frac{\partial \int d^{3n}r \left|\Psi_o^+(r_1,...,r_n,t) - \Psi_o^-(r_1,...,r_n,t)\right|^2}{\partial t}$$ (or, equivalently, lifetime $\tau \equiv \frac{1}{R}$), defined by the long time limit of the difference between the asymptotic form that Ψ_o approaches in the distant

future (Ψ_o^+) and past (Ψ_o^-) that results from excitation/de-excitation of the system, is given by (Schwinger 1990):

$$R \equiv \frac{1}{\tau} = \frac{2\pi}{\hbar} < \Psi_o \mid \Delta V \delta(E - H) \Delta V \mid \Psi_o >$$
$$\equiv \frac{2\pi}{\hbar} \sum_F \delta(E - E_{exact}(C_F)) \mid < \Psi_o \mid \Delta V \mid \Psi_{exact}(C_F) > \mid^2, \qquad (21)$$

where $\Psi_{exact}(C_F)$ is any many-body state, possessing a particular configuration (denoted by C_F) of particles that solves the Schroedinger equation of the exact Hamiltonian, H, associated with the exact potential V, and $E_{exact}(C_F)$ is its energy.

In the situation (associated with Umklapp-like processes) in which the perturbation preserves translation symmetry in the bulk region, ΔV vanishes except in non-bulk regions. For this case, the set of initial many-body states corresponds to the set of (degenerate) states associated with the bulk region, in the absence of overlap with non-bulk states, and the perturbation $\Delta V = V - V'$ induces the associated broken gauge symmtery that results from the overlap between these sets of states. But because of the energy-conserving delta function, in Eq. 21, in the associated summation over configurations, $\Psi_{exact}(C_F)$ and Ψ_o both have the same energy E. But because, formally, the inner product between states that have the same energy is independent of time, Eq. 21 can be re-written, using Eqs. 1-3. In particular, Eqs 1-3 imply that

$$i\hbar \int d^3 r \nabla \bullet < \Psi_o \mid v(r) \mid \Psi_{exact}(C_F) > = < \Psi_o \mid \Delta V \mid \Psi_{exact}(C_F) >$$
$$= i\hbar \sum_\alpha \int_{S_\alpha} d^2 r_\alpha < \Psi_o \mid v(r_\alpha) \mid \Psi_{exact}(C_F) >. \qquad (22)$$

Here, we have used Gauss's law and the definition of *v(r)* (given in Eq. 3) to convert the volume integral on the LS of the equation (in a formal sense) into a sum of surface integrals. The sum extends over the boundaries of all of the regions where the divergence on the LS, effectively, can become discontinuous. In particular, Eq. 21, in principle, can be applied to situations, in which, locally, violations in particle number and/or momentum conservation in the initial state are allowed to take place. This can occur as a result of discontinuities in momentum, vector potential or both, that can result from any broken gauge symmetry, over a region of any size. The summation on the RS extends over the boundaries of all of these "forbidden" regions.

In principle, each term in this summation can be viewed as an integral representation of a contribution to the matrix element of a particular scattering event. Substituting Eq. 22 into Eq. 21, we can relate the total reaction rate R to the square of a matrix element, derived exclusively from the total net flux of particles into and away from the "allowed" region (associated with any of the allowable states that have particular energies or momentum and/or are confined to a particular region):

$$R \equiv \frac{1}{\tau} = 2\pi\hbar \sum_F \delta(E - E_{exact}(C_F)) \mid \sum_\alpha \int_{S_\alpha} d^2 r_\alpha < \Psi_o \mid v(r_\alpha) \mid \Psi_{exact}(C_F) > \mid^2, \qquad (23)$$

In its most general form, the forbidden region boundaries can refer to locations where any "collision" (associated with the regions involving discontinuous changes in momentum) can occur.

Three key points associated with Eqs. 22 and 23 are: 1. Finite, but non-vanishing values of R occur when the overlap of $\Psi_{exact}(C_F)$ and Ψ_o with V-V' is finite but non-vanishing; 2. In

situations involving rigid (Mossbauer-like) translations, resulting from Umklapp-like processes that transfer momentum to the CM of the solid, this overlap vanishes in the bulk region, but because of the large degeneracy associated with the underlying gauge symmetry, many configurations are allowed (and are required, as a consequence of the energy-conserving delta function) to contribute to R; and 3. by construction, these translations alter the momentum only at the boundaries, can be infinitesimally small, and for sufficiently large crystals, are the lowest lying excitations.

Eq. 23 is a many-body version of a general set of equations that have been used either to describe scattering or to compute bound state eigenfunctions and eigenvalues of low energy electrons in solids. In particular, when the equation involves only a single particle, it reduces to the familiar rate expression that is used in multiple scattering theory (Gonis & Butler 2000). The generalization, associated with including more than one particle, which has been referred to as Generalized Multiple Scattering Theory (Chubb & Chubb 2000), in its most general form (as in Eq. 23), in principle, can be used to identify bounds for particular processes, provided it is possible to make plausible assumptions about the many-body wave function, its gradient, and the behavior of the vector potential, in various regions of space. In situations involving reduced values of R, associated with near ground state configurations, it is possible to use Eq. 23 to identify the impact of boundaries on potential forms of coherence (especially broken gauge symmetry).

In particular, beginning from Eq. 23, it is possible to identify the onset of new forms of broken gauge symmetry, associated with possible ionic conduction that can occur in situations involving high-loading (defined by the limit in which $x \rightarrow 1$ in PdH_x) of atomic hydrogen (H) and/or its isotopes into palladium (Pd), in finite size crystals (Chubb & Chubb 2000). The associated forms of coherent (resonant) interactions occur because of the large degeneracies associated with the energy conserving delta function when the energy E is small and/or the dominant scattering processes involve a small number of coherent interactions. In these kinds of situations, Eq. 23 can be used to identify and model the lowest forms of excitations. As discussed in the next section, beginning from Eq. 23, it is also possible to estimate critical values of fluxes of momentum, and temperature, associated with outside perturbations, in the presence of broken gauge symmetry, that can induce instabilities that can invalidate particular transport models.

At finite, but low T, these excitations provide the dominant forms of interaction. As a consequence, in principle, beginning from the Ground State, it is possible to describe the time evolution of the lowest energy fluctuations of the system, based on the GKB formalism, by generalizing an earlier procedure (Lipavsky et al 1986). Specifically, formally, based on the identity, $2\pi\delta(x) = i \lim_{\varepsilon \rightarrow 0}[\frac{1}{x+i\varepsilon} - \frac{1}{x-i\varepsilon}]$, it is always possible to re-write Eq. 23, in the form,

$$R \equiv \frac{1}{\tau} = \hbar \lim_{\varepsilon \rightarrow 0} \sum_{\alpha,\alpha' S_\alpha'} \int d^2 r_\alpha' \int_{S_\alpha} d^2 r_\alpha < \Psi_o \mid v(r_\alpha)(i) P_{\Psi(C_F)} [\frac{1}{E - H_{exact} + i\varepsilon} - \frac{1}{E - H_{exact} - i\varepsilon}] P_{\Psi(C_F)} v(r_\alpha') \mid \Psi_o >, \quad (24)$$

where, formally,

$$P_{\Psi(C_F)} = P_{\Psi(C_F)} P_{\Psi(C_F)} = \sum_F \left| \Psi_{exact}(C_F) \right\rangle \left\langle \Psi_{exact}(C_F) \right|, \quad (25)$$

represents the projection of the exact wave function onto the possible configurations that have appreciable overlap with the lowest-lying excited states, and $\frac{1}{E - H_{exact} + i\varepsilon}$ and $\frac{1}{E - H_{exact} - i\varepsilon}$,

respectively, are potential representations of the inverse of the (many-body) operators defined by the differences ($E - H_{exact} + i\varepsilon$ and $E - H_{exact} - i\varepsilon$) between the complex energies $E + i\varepsilon$ and $E - i\varepsilon$ and the exact, many-body Hamiltonian H_{exact} (in first quantized form) associated with the many-body Schroedinger equation.

As in applications of the single particle, quasi-particle, band theory picture to the many-body transport problem, involving infinitely-repeating lattices, in the more general situation, considered here, involving transport phenomena in finite lattices, it is convenient to adopt a second quantized picture, involving occupied and unoccupied states. This can be accomplished, beginning from the first quantized representation, associated with Eqs. 1-25, by introducing new coordinates into each wave function Ψ that asymptotically include the dependence in the various rate expressions, associated with non-vanishing contributions to the total flux, in which far from the bulk region, the associated contributions asymptotically (as in the case of the coordinates associated with particles in the bulk) approach the amounts that would be present, in a separable situation, in which single-particle (excited states) can be used to represent excitations of the many-body state from the ground state.

This is equivalent to allowing for the possibility that the dependence of the initial and final state many-body wave functions on some of the coordinates asymptotically (in the limit in which both states are nearly degenerate) include external sources of particles that have vanishing flux in the GS but can induce excitations in the bulk at particular rates, defined by Eq. 24. In practice, this can be accomplished by increasing the set of wave-vectors k_i and coordinates (associated initially with the N_T spatial coordinates r_i of the particles that have non-negligible flux at the boundaries of the bulk). In particular, the lowest energy fluctuations are defined by the possible rigid (Umklapp-like) translations, associated with situations in which each possible value of k_i is in the First Brillouin zone. As in conventional single particle band theory, the transport phenomena involving the coordinates associated with the hole-like states, which effectively involve negative charge relative to the charge associated with the coordinates that asymptotically approach occupied ("particle-like") single particle states, in the limit of near-degeneracy, is closely related to implicit symmetries (and coherence), that result from rigid translations (involving Umklapp-like processes).

Eq. 24 is rarely useful because of the large number of configurations and degrees of freedom that are required in the equation. In the band theory problem, on finite lattices, near T=0, the equation is useful for defining limits associated with the Umklapp-like processes that preserve periodic order (and the associated degeneracies) in the bulk region. At higher values of T, Eq. 24 can also be used to derive approximate (Boltzmann-like) transport equations, associated with the GKB formalism and to quantify limiting effects associated with particular time- and length- scales that restrict the validity of these kinds of equations in finite lattices.

In particular, near equilibrium, in the weak scattering limit, in infinitely-repeating, ordered lattices, historically, the microscopic theory (derived from the GKB formalism [Lipavsky et al 1986]) of transport phenomena (associated with heat and electrical conduction) involving electrons and holes has been developed, based on a perturbation expansion, in terms of retarded ($G_R(rt,r't') = \sum_k \int \frac{dw}{2\pi} \frac{\phi_k(r)\phi_k^*(r')}{w - \varepsilon(k) + i\delta} e^{-iw(t-t')}$) and advanced ($G_A(rt,r't') = \sum_k \int \frac{dw}{2\pi} \frac{\phi_k(r)\phi_k^*(r')}{w - \varepsilon(k) - i\delta} e^{-iw(t-t')}$) electron Greens functions of the unperturbed (mean field) Hamiltonian, an assumed functional form for the single electron (hole) density matrix,

$\rho^{<}(r,r',t)$ ($\rho^{>}(r,r',t)$), and an assumed model of the single-particle and many-body potential (also referred to as the effective scattering potential). In fact, in the weak scattering limit, in infinitely-repeating, periodic crystals, in principle, it is possible to derive the same transport equations, using Eqs. 24 and 25, directly, by formally expanding the effective inverses of the exact Hamiltonian (as they appear in Eq. 24) in terms of $G_A(rt,r't')$ and $G_R(rt,r't')$, to the desired order in the effective scattering potential and averaging over initial state energies.

Superficially, this alternative strategy for developing transport equations might seem to have little practical value because the same kinds of limiting approximations are necessary that are used in the existing strategy. In particular, in both situations, it is possible to derive transport equations by performing a Fourier transformation with respect to the difference variables r-r' and t-t'. But it is only possible to perform this form of transformation (which is referred to as a Weyl-Wigner transformation[Buot 1993; 1974]) by expanding the quantities (which are already part of a larger expansion) in terms of a second expansion, involving gradients (and higher order derivatives) of the various quantities associated with the initial expansion. In order for the associated expressions to converge rapidly, the effective scattering potential can only enter in a quasi-classical way, in which individual scattering events occur rapidly but are required to be separated by long intervals of time. For this reason, the limitations of transport equations, based on the GKB formalism, even in infinitely-repeating, periodic lattices, are not well-defined.

Starting from Eq. 24, the derivation of transport equations, from the associated perturbation procedure is equivalent to the GKB formalism because of inherent approximations involved in the perturbation expansions that are present when either approach is adopted. In fact, Eqs. 24 and 25, in principle, provide a complete solution to the many-body problem and (after suitable averaging is performed over the initial state) contain all of the information associated with any problem, involving transport phenomena. An important point is that to be useful, it is necessary to identify particular time-scales and regions of space in Eq. 24, where particular terms contribute with comparable magnitude to the total rate. The GKB formalism provides a particular, systematic procedure for identifying sets of terms that contribute in this way. (For this reason, it is possible to develop the associated GKB transport equations, beginning from Eq. 24.) However, this procedure has limited validity.

Because Eqs. 24 and 25 apply to more general, many-body situations, they can be especially useful in situations involving exact or approximate solutions to a particular problem. In particular, for example, when a solvable problem has an approximate solution in one region of space or as a function of energy and momentum, that asymptotically approaches an exact solution, as a result of variations of an externally applied, or internally-evolving potential, Eqs. 24 and 25 can be used to quantify the impact of changes in the potential on the rate (or lifetime) of a particular, many-body, resonant process. In the case of finite lattices, this feature can be especially useful since it can be used to quantify the impact of finite size on phenomena associated with transport, or with coherence, or both.

The ability to monitor the lifetime of particular resonant processes involving approximate solutions of a many-body problem can be especially useful for identifying critical time-scales associated with interactions between different kinds of particles. In particular, for example, in principle, collision rates, derived from Eq. 24, can be used to monitor the effects of over-lap and time-scale on the transition between adiabatic and non-adiabatic processes and forms of coupling involving vibrational (phonon) motion of the heavier, (nucleus + core electron) ionic cores (of atoms) and the lighter, conduction/valence electrons, in solids. In problems involving the behavior of ultra cold, neutral atoms, in optical lattices, critical length- and time- scales can be

identified for performing precision measurements of gravity, acceleration, and related quantities. In the next section, a related problem (the identification of critical length-scales for precision measurements of gravity gradient, through resonant, tunneling processes, in finite lattices), associated with applying Eq. 24 is addressed.

VI Onset of Broken Gauge Symmetry and Coherent Effects Involving Charged and Neutral Particles in Finite Lattices

In the limit of finite, but vanishingly small T, beginning with large (but finite) values of τ, as a result of gauge symmetry (and the onset of broken gauge symmetry), Eq. 24 also can be used to identify and isolate a hierarchy of coherent Umklapp-like processes, associated with rigid, Galilean transformations, in finite lattices. In particular, to understand the origin and significance of these kinds of processes, general features of the associated forms of overlap and coupling (through broken gauge symmetry) to non-bulk effects can be identified, without averaging Eq. 24 over initial state energies (as opposed to situations, associated with higher values of T, where this kind of averaging is required).

An important reason that this is possible is that broken gauge symmetry is initiated through processes that reduce the degeneracy of the system. In particular, the GS is required to have the lowest degeneracy and minimal overlap with other states that are related to it (in the absence of broken gauge symmetry) by rigid Galilean translations. Broken gauge symmetry reduces the overlap between the GS and these states (which are the lowest-lying excited states) through shifts in the zeroes of momentum of the various indistinguishable particles. Formally, in order to include the most general forms of processes that break gauge symmetry, it is necessary to include coupling between all (occupied and unoccupied) states (as opposed to only the occupied states), involving all energy eigenvalues, for all possible values of k_i that, in the absence of broken gauge symmetry, are required to be degenerate, as a consequence of the invariance of the bulk, with respect to rigid Galilean translation symmetry. For this reason, the many-body wave functions for the lowest-lying excited states and the GS are all required to include effects associated with the variation in the zeroes of all possible CM momenta, for all of the wave-vectors in the First Brillouin zone, in each filled band, and for all of the states in the highest (lowest) occupied fermion (boson) band. It is possible to include these additional dependences (which are implicit in the second quantized picture), by redefining N_T to be the number of coordinates associated with variations in the zeroes of momentum of all of the particles in the bulk and with fluxes that can remove or introduce particles into the bulk through finite overlap with the GS (in regions of the bulk solid) that can take place through rigid translations that preserve the degeneracy associated with rigid, translational symmetry.

In particular, to describe the lowest-lying excitations, it is necessary to relate the individual coordinates $(r_1,....,r_{N_T})$ of the various particles in the many-body wave function to the coordinate R_{cm} associated with the CM, the separation variables r_{ij} that describe the difference in the position of each particle from the remaining particles, and the total mass M of the collection of particles. The general relationship between the general coordinates $(r_1,....,r_{N_T})$ and R_{cm} and r_{ij} is:

$$r_{ij} = r_i - r_j = -r_{ji}; \quad R_{cm} = \frac{\sum_{i=1,N_T} m_i r_i}{M} \quad . \qquad (26)$$

It follows from Eq. 26 that

$$r_i = \sum_{j \neq i} \frac{m_j r_{ij}}{M} + R_{cm}; \qquad r_j = r_i - r_{ij} \quad (j \neq i), \tag{27}$$

and that

$$\nabla_{r_i} - \frac{m_i}{M} \nabla_{R_{cm}} = \sum_{j \neq i} \nabla_{r_{ij}} = \nabla_{r_i - R_{cm}}; \quad \nabla_{r_j} - \frac{m_j}{M} \nabla_{R_{cm}} = -\nabla_{r_{ij}}, \quad j \neq i, \tag{28}$$

where the summations in Eqs. 26-28, in principle, should be carried out over all N_T particles in the many-body system. In fact, the only contributions that are relevant in evaluating Eq. 24 occur from particles that have non-vanishing flux at the boundaries of the bulk region (and in what follows, N_T will be refer to the smaller number of particles that satisfy this constraint).

When the associated processes involve rigid translations (as in the potential overlap between the GS and/or the lowest energy excitations, associated with Umklapp-like processes), in the bulk region, the separation variables (r_{ij}) are held fixed. As a consequence, in the evaluation of the surface integrals, at the boundaries of the bulk,

$$\nabla_{r_i - R_{cm}} \Psi_{exact}(C_F)\,|_{boundary} = \nabla_{r_{ij}} \Psi_{exact}(C_F)\,|_{boundary} = \nabla_{r_i - R_{cm}} \Psi_o\,|_{boundary} = \nabla_{r_{ij}} \Psi_o\,|_{boundary} = 0, \tag{29a}$$

for each internal coordinate $r_i - R_{cm}$, associated with the position r_i of a particle, relative to the CM coordinate R_{cm} and each separation variable r_{ij}. It also follows (as a consequence of Eq. 28) that

$$\nabla_{r_i} \Psi_{exact}(C_F)\,|_{boundary} = \frac{m_i}{M} \nabla_{R_{cm}} \Psi_{exact}(C_F)\,|_{boundary}; \quad \nabla_{r_i} \Psi_o\,|_{boundary} = \frac{m_i}{M} \nabla_{R_{cm}} \Psi_o\,|_{boundary} \tag{29b}$$

Umklapp-like processes are dominant for sufficiently large lattices because: 1. In the absence of interaction (through fluxes of particles at the boundaries of the solid), it is never possible to determine if the bulk region is in motion or at rest; 2. Umklapp-like processes are equivalent to gauge transformations that preserve this symmetry, in the bulk. In particular, Eq. 1 is not valid in general (as a consequence of broken gauge symmetry). But it does hold (effectively) in the evaluation of contributions to the RS of Eq. 24, when the differences in velocity between each kind of indistinguishable particle associated with an initial and final state (GS or a low-lying excited state) preserve periodic order. This follows from the fact that by construction, when $\Psi_{exact}(C_F)$ and Ψ_o are low-lying excited states, both states obey the generalized form of Bloch's theorem (Eq. 10) and, as a consequence, are required to have a functional form, defined by Eq. 13. But because $u(r_1,.....,r_n) = u(r_1,..r_i + R_n ...,r_n)$ in Eq. 13, it follows that

$$\frac{\partial u(r_1,.....,r_n)}{\partial R_{cm}} = 0. \tag{30}$$

It also follows from from Eqs. 26 and 27, that the phase factor $\sum_i k_i \bullet r_i$ in Eq. 13 can be re-expressed, using the expression

$$\sum_i k_i \bullet r_i = \sum_{i=1,N_T-1} \sum_{j=i+1,N_T} \frac{k_{ij} \bullet r_{ij}}{M} + k_{cm} \bullet R_{cm} \quad , \tag{31}$$

where

$$k_{ij} = \frac{m_j k_i - m_i k_j}{M} \tag{32}$$

and

$$k_{cm} = \sum_{i=1,N_T} k_i. \tag{33}$$

Here, as in Eq. 13, each value of k_i is in the First Brillouin Zone. Eqs. 30 and 31 imply that any wave function $\Psi(r_1,.....,r_n)$ that has a functional form given by Eq, 13 obeys the equation,

$$\frac{\hbar}{i}\frac{\partial\Psi(r_1,.....,r_n)}{\partial R_{cm}} = \hbar k_{cm}\Psi(r_1,.....,r_n). \qquad (34a)$$

But when the transition involves a rigid translation of the bulk region, the only contributions that appear on the RS of Eq. 24, involve fluxes associated with $\nabla_{R_{cm}}\Psi_{exact}(C_F)$ and $\nabla_{R_{cm}}\Psi_o$. Then, because $\Psi_{exact}(C_F)$ and Ψ_o satisfy Eq. 13, Eq. 34a holds when $\Psi(r_1,.....,r_n) = \Psi_{exact}(C_F)$ or $\Psi(r_1,.....,r_n) = \Psi_o$. As consequence, the contribution to the flux that results from a rigid translation in Eq. 24 from each indistinguishable particle can be derived using the transformation associated with Eq. 1. In particular, by construction, if net particle flux is conserved (as in Eq. 7), in the neighborhood of the boundaries of the bulk, any momentum flux into and away from the bulk is balanced by a change in the vector potential, associated with a preferential choice of gauge (that establishes the fact that no net particle flux can take place).

By construction, as a consequence, the condition that no net flux be present allows us to always define the zero of momentum, associated with a particular value of the wave-vector, along a well-defined boundary, in such a way that different wave-vector states (as in Eq.12) be orthogonal. In a situation involving a rigid translation, however, a net flux can be present because only CM motion takes place, as a consequence of Eqs.29a-30, and it is no-longer possible to preferentially select the relative zeroes of momentum (associated with particular gauge transfomations) in this manner. But relative to the initial bulk region, in all sub-lattices, except those that include the boundary, it is still possible to require that different wave-vector states (defined by the different sub-lattices) remain orthogonal (since at the boundary of any of these sub-lattices, net vanishing particle flux holds). Also, no net flux of particles enters or leaves these regions since by construction, the lowest-lying excitations obey Bloch's theorem.

But in the regions that do include the boundary, states that have different sets of wave-vectors are no longer required to be orthogonal (since the boundary breaks translation symmetry). Also, since charge can accumulate in these regions, the precise location of the physical boundary is not well-defined, and it is possible for physical charge to accumulate. In general, the many-body wave function must remain continuous and single-valued, but the momentum (associated with any of the coordinates) can become discontinuous, without altering the particle flux, on both sides of each boundary. Asymptotically, the lowest energy excitations occur when the longest wave-length perturbations induce variations in a small number of separation variables r_{ij}. This occurs when effectively, after the initial bulk region is translated rigidly by a small integer multiple of primitive vectors $\vec{b}_\alpha$, within a larger lattice where a small variation in one or more of the separation variables r_{ij} is allowed to take place. In particular, initially, at all points within the bulk, for each of the coordinates, $(r_i, r_j, ...)$,

$\nabla_{r_{ij}}\Psi_o = 0 = \nabla_{r_{ij}}\Psi(C_F) = \sum_{i\neq j}\nabla_{r_{ij}}\Psi_o = \nabla_{r_i - R_{cm}}\Psi_o = \sum_{i\neq j}\nabla_{r_{ij}}\Psi(C_F) = \nabla_{r_i - R_{cm}}\Psi(C_F)$; while at the boundary, one or more derivatives ($\nabla_{r_{ij}}\Psi(C_F)$) of the excited state wave function $\Psi(C_F)$ becomes finite.

As in superfluids, in sufficiently large crystals, in principle, it is still possible to maintain a condition of vanishing particle flux across the boundary by introducing an effective gauge transformation; while in smaller crystals, particle flux can be minimized as a result of applying a similar transformation, but an exact cancellation is not guaranteed. In particular, the lowest energy configuration occurs when $\Psi(C_F) = \Psi_o$ everywhere in the bulk; while $\nabla_{r_{ij}}\Psi(C_F)$ takes on

a finite value for one value of r_{ij} at the boundary (which can only occur through a collision that leads to a discontinuity in $\nabla_{r_{ij}}\Psi(C_F)$). In the limit of finite *N*, each of these potential gauge transformations is constrained by the requirement that the possible discontinuity ΔA in vector potential be discretely quantized, according to:

$$\oint \frac{e_j}{c}\Delta A \bullet dl = 2\pi \mathrm{n}, \quad \mathrm{n} = \text{integer}, \tag{34b}$$

where the integration is along any closed loop that encloses the boundary, and n, in principle, is an arbitrary integer. In this limit, since the vector potentials outside and inside the initial bulk region are uniformly constant, ΔA is also a constant, and it follows that

$$N_\delta \frac{e_j}{c}\Delta A \bullet \vec{b}_\delta = \pi n_\delta, \; n_\delta = \text{integer}, \delta = 1,2,3; \delta \neq \alpha, \tag{34c}$$

where $\vec{b}_\delta$ ($\neq \vec{b}_\alpha$) is one of the two (remaining) primitive vectors that can be used to define each of lattice sites on the boundary of the lattice, and N_δ is defined by Eq. 12.

The lowest lying excitations occur when the absolute square of the flux (as in Eq. 24) becomes asymptotically small. Because the discontinuities ΔA are present in order to minimize differences between the true momentum and the CM momentum that result from variations in r_{ij}, that are allowed to take place outside the original bulk region, it follows that as these variations smoothly go to zero, ΔA also goes to zero. As a consequence of Eq. 12b, it follows that the lowest lying excitations are integer multiples of $\frac{e_j}{c}\Delta A = \frac{\hbar \vec{g}_\delta}{2N_\delta}$ and that they introduce small deviations in the average CM momentum

$$\begin{aligned}\int d^3r < \Psi_{exact}(C_F) | \nabla \bullet v(r) | \Psi_o > = \sum_j \iiint d^3r_1 .. d^3r_n \Big(\frac{\hbar}{2im_j} \Big[\Psi_{exact}(C_F) * \nabla^2_{r_j} \Psi_o - \nabla^2_{r_j} \Psi_{exact}(C_F) * \Psi_o \Big] - \\ - \frac{e_j}{c} \nabla \bullet (\Psi_{exact}(C_F) * A_{eff} \Psi_o) \Big) \\ = \int_{Lattice\ Boundary} d^2r \hat{n} \bullet \frac{1}{M} \Big(p_{cm} \pm \frac{\hbar \vec{g}_\delta}{2N_\delta} \Big) \langle \Psi_{exact}(C_F) | \rho(r) | \Psi_o \rangle \end{aligned} \tag{34d}$$

Here, $p_{cm} = \hbar k_{cm}$ is the total CM momentum of Ψ_o. (This is also the CM momentum of $\Psi_{exact}(C_F)$.) Also, $\rho(r) = \sum_j \delta^3(r - r_j)$ is the single particle density operator. The integration along the Lattice Boundary includes integrations over one region that has vanishing flux (defined by the initial bulk lattice boundary) and a second region where $\nabla_{r_{ij}}\Psi(C_F)$ is finite.

By construction, the particle flux in Eq. 34b provides the smallest contribution to the total rate (in Eq. 24). The associated rigid, Galilean transformation, technically, is an Umklapp process, but for an elongated lattice, in which the initial primitive vector $\vec{b}_\delta$ is replaced the vector $\vec{L}_\delta = 2N_\delta \bullet \vec{b}_\delta$ associated with the largest possible translations that are parallel to $\vec{b}_\delta$. This process has the smallest rate because, essentially, the broken symmetry occurs only once (when the bulk lattice is translated by a single primitive vector $\vec{b}_\delta$), through a single change in one derivative. In what follows, we will consider this type of broken gauge symmetry as a form of particle-hole excitation/de-excitation, as opposed to an alternative process (a pure Umklapp process), in which the CM momentum changes by a reciprocal lattice vector, defined by the original bulk lattice (as in Eq. 12c).

Symmetry can play an important role in pure Umklapp processes. In particular, when a common set of derivatives change in the same way, at many points, as a result of symmetry, pure

Umklapp processes can take place. In general, broken gauge symmetry occurs through loss of periodic order. The possible differences in flux that result from rigid translations are defined by the ranges of possible values that can result from the difference ($k_{cm} - k_{cm}'$) between the initial state (k_{cm}) and final state (k_{cm}') CM momenta. By construction, this difference identically equals a reciprocal lattice vector, or the sum of a reciprocal lattice vector and a wave-vector that falls within the First Brillouin Zone when a particular form of symmetry is present, in which within the sum, one or more contributions (from a particular wave-vector or wave-vectors) to $k_{cm} - k_{cm}'$ is repetitively added.

The symmetry associated with repetitively adding the same contribution can cause a large amount of momentum, effectively, to be transferred rigidly from all of the particles in the bulk through flux contributions at the boundaries of the bulk into excited state (hole-like) coordinates and into the motion of the CM, as a whole. The resulting effect is the basis of rigid, lattice recoil (as in the Mossbauer effect). As discussed below, it can also be used to explain electronic-Zener breakdown in finite lattices formed from insulators and semi-conductors. Potentially, as discussed below and elsewhere (Chubb, S.R. 2005B ; 2005C), the effect suggests a new, novel phenomenon, ionic-Zener breakdown, in which currents, involving hydrogen (H) and/or deuterium (D) ions (deuterons, d's), begin to flow, after a finite (crystal size dependent) period of time, through finite size crystals containing palladium (Pd) that has been loaded with H and/or D atoms .

In particular, whenever $k_{cm} - k_{cm}'$ falls within the First Brillouin zone, particle-hole excitation/de-excitation processes can take place in which one or more hole-like states become occupied (unoccupied) and/or one or more particle-like states become unoccupied (occupied). Momentum can be transferred from all particles in the bulk to the surface, in a partially coherent manner when $k_{cm} - k_{cm}'$ extends beyond the First Brillouin zone but is not identically equal to a reciprocal lattice vector. In this kind of situation, in addition to processes in which the dependences on coordinates associated with hole-like or particle-like single particle states are changed, an additional pure Umklapp process takes place. Coherent transfer of momentum can take place when $k_{cm} - k_{cm}'$ identically equals a reciprocal lattice vector. In this situation, a pure Umklapp process takes place, but no change occurs in the dependence on coordinates that are asymptotically associated with hole-like or particle-like states. The difference in CM wave-vectors $k_{cm} - k_{cm}'$ can equal a reciprocal lattice vector or the sum of a reciprocal lattice and a wave-vector in the first Brillouin zone when $k_{cm} - k_{cm}'$ is finite along particular directions parallel to one or more of the (three) reciprocal lattice vector generators $\vec{g}_\alpha$, but not in directions that are parallel to all three vectors. This is a consequence of Eqs. 12c and 33.

When the CM wave-vector is conserved along a single direction parallel to $\vec{g}_\alpha$, for each, non-vanishing value of $i_{\alpha,}$ or $i_{\delta,}$, at every value of $i_{\alpha,\delta}$ in the sum on the RS of Eq. 33, the same contribution, $\frac{i_\beta \vec{g}_\beta}{2N_\beta} + \frac{i_\delta \vec{g}_\delta}{2N_\delta}$ $(\beta \neq \alpha \neq \delta \neq \beta)$, appears.

$$(k_{cm} - k_{cm}')\,|_{i_\beta} = \sum_{i_\alpha = -N_\alpha, N_\alpha - 1} \frac{i_\beta \vec{g}_\beta}{2N_\beta} + \frac{i_\delta \vec{g}_\delta}{2N_\delta} = 2N_\alpha \left(\frac{i_\beta \vec{g}_\beta}{2N_\beta} + \frac{i_\delta \vec{g}_\delta}{2N_\delta}\right) \qquad (35)$$

A pure Umklapp process occurs whenever the expression on the far RS of Eq. 35 can be re-written as a sum of integer multiples of reciprocal lattice vectors. Since each primitive vector, $\vec{g}_\eta$ $(\eta = \alpha, \beta,$ or $\delta)$, is linearly independent from the remaining primitive vectors, for this last

condition to be satisfied, the coefficients of $\vec{g}_\beta$ and $\vec{g}_\delta$ must both be integers. As a consequence, a change in CM wave-vector, involving a pure Umklapp process (but no change in the coordinates associated with particle-hole excitation/de-excitation) takes place whenever $N_\alpha i_\beta$ is an integer multiple of N_β, and $N_\alpha i_\delta$ is an integer multiple of N_δ. A change in the coordinates associated with particle-hole excitation/de-excitation and a pure Umklapp process takes place, in the remaining situations (in which the CM wave-vector is conserved only along the direction parallel to $\vec{g}_\alpha$), provided $N_\alpha i_\beta \geq N_\beta$ or $N_\alpha i_\delta \geq N_\delta$. When $N_\alpha i_\beta < N_\beta$ and $N_\alpha i_\delta < N_\delta$, there is no Umklapp process, but a particle-hole excitation/de-excitation process takes place.

When the CM wave-vector is conserved along directions parallel to both $\vec{g}_\alpha$ and $\vec{g}_\alpha$, it follows from these equations that whenever all of the integers (i_α, and i_δ,) associated with contributions that are parallel to either of these directions vanish, and the contribution to the difference,

$$k_{cm} - k_{cm}' = \sum_{\{i_\eta \neq 0\}} \sum_{\eta=1,3} \frac{i_\eta \vec{g}_\eta}{2N_\eta}, \tag{36}$$

occurs only from values of $\frac{i_\eta \vec{g}_\eta}{2N_\eta} = \frac{i_\beta \vec{g}_\beta}{2N_\beta}$ that are parallel to $\vec{g}_\beta$. As a consequence, for each value of i_β, , at every value of i_α, and i_δ, in the sum on the RS of Eq. 33, a common contribution, $\frac{i_\beta \vec{g}_\beta}{2N_\beta}$ $(\beta \neq \alpha \neq \delta \neq \beta)$, appears. But this means that the total contribution, $(k_{cm} - k_{cm}')|_{i_\beta}$, for a given value of i_β, is given by

$$(k_{cm} - k_{cm}')|_{i_\beta} = \sum_{\substack{i_\alpha = -N_\alpha, N_\alpha - 1 \\ i_\delta = -N_\delta, N_\delta - 1}} \frac{i_\beta \vec{g}_\beta}{2N_\beta} = 4N_\alpha N_\delta \frac{i_\beta \vec{g}_\beta}{2N_\beta}. \tag{37}$$

Also, in principle, in Eq. 36, the sum over non-vanishing values of i_η (denoted by $\{i_\eta \neq 0\}$ in the equation), $i_\eta = i_\beta$ can take on any value between $-N_\beta$ and $N_\beta - 1$, and the total number of terms in this sum can vary between 1 and $2N_\beta$. Since any number of the values of i_β can be identical, it is convenient to designate each term in the associated set (from the set of non-vanishing values $\{i_\beta = i_\eta \neq 0\}$) with a separate index j; so that $i_\beta \equiv i_{\beta,j}$ is the jth element in the set. With these definitions, it follows that

$$(k_{cm} - k_{cm}') = \sum_j (k_{cm} - k_{cm}')|_{i_{\beta,j}} = 4N_\alpha N_\delta \frac{\vec{g}_\beta}{2N_\beta} \sum_j i_{\beta,j}. \tag{38}$$

A pure Umklapp process (without particle-hole excitation/de-excitation) occurs whenever the coefficient of $\vec{g}_\beta$ in Eq. 37 is an integer. This occurs identically when $N_\beta = i_\beta \times N_\alpha \times N_\delta$; $\beta \neq \alpha \neq \delta \neq \beta$ (for all, odd or even, integer values of i_β=integer, and N_β) . When the coefficient of $\vec{g}_\beta$ is greater than one but not equal to an integer, in addition to a pure Umklapp process, the change in CM momentum includes particle-hole excitation/de-excitation. This occurs when $1 < \frac{2 \times i_\beta \times N_\alpha \times N_\delta}{N_\delta} \neq$ integer; $\beta \neq \alpha \neq \delta \neq \beta$. When $1 > \frac{2 \times i_\beta \times N_\alpha \times N_\delta}{N_\delta} \neq$ integer, and $\beta \neq \alpha \neq \delta \neq \beta$, coordinates associated with particle-hole excitation/de-excitation are altered, without a pure Umklapp process taking place.

As mentioned above, pure Umklapp processes can cause a large amount of momentum, effectively, to be transferred rigidly from all of the particles in the bulk through flux contributions at the boundaries of the bulk into excited state (hole-like) coordinates and into the motion of the CM, as a whole. The largest amount of momentum that can be transferred in this manner occurs when (as in Eqs. 37 and 38) the CM momentum is conserved along the directions that are parallel to $\vec{g}_\alpha$ and $\vec{g}_\delta$, and along the third direction, the magnitude of $(k_{cm} - k_{cm}')|_{i_{\beta,j}}$ is maximized. For this case, the same, common value $i_{\beta,j} = 2N_\beta - 1$ appears in each term, in the sum in Eq.38, and none of the terms, associated with any of the $2N_\beta$ (particle or hole) coordinates in the band, vanish. For this case, the contribution to each term in the sum is $4N_\alpha N_\delta \frac{(2N_\beta - 1)\vec{g}_\beta}{2N_\beta}$. Since the sum extends over $2N_\beta$ values of $i_{\beta,j} = 2N_\beta - 1$, the magnitude of the total CM momentum $\Delta P_{CM}^{\max}$ is given by

$$|\Delta P_{CM}^{\max}| = \hbar(8N_\alpha N_\delta N_\beta - 4N_\alpha N_\delta)|\vec{g}_\beta| = (N - N_{2d}^{\alpha\delta})\hbar|\vec{g}_\beta|, \qquad (39)$$

where $N_{2d}^{\alpha,\delta} = 4N_\alpha N_\delta$ is the number of unit cells in the two dimensional lattice, defined by the primitive vectors $\vec{b}_\alpha$ and $\vec{b}_\delta$.

Eq. 39 illustrates that the maximum amount of momentum that can be transferred to the lattice from the Umklapp process is size dependent and, for sufficiently large lattices, scales linearly with the total number (N) of unit cells in the lattice. In principle, this kind of Umklapp process can take place in any sub-lattice, contained in the original lattice, in which Eq. 37 is valid, which leads to the constraint that $N_\alpha \geq 1, \quad N_\beta \geq 1, \quad N_\alpha \geq 1$. In fact, less stringent constraints apply in situations involving reduced symmetry: When a finite (even) number of unit cells are periodically ordered along one or more directions (parallel to one or more of the primitive vectors) a pure Umklapp process can take place in which some maximum amount of momentum can be transferred to the CM of the sub-lattice.

In particular, in 2-dimensional sub-lattices, defined by the two Bravais Lattice primitive vectors. $\vec{b}_\alpha$ and $\vec{b}_\delta$, an effective, maximal 2-dimensional change in CM momentum $\Delta P_{CM}^{\max,2d}$ can be obtained by restricting the values of k_i and k_i' (that appear in the difference $k_{cm} - k_{cm}' = \sum_i (k_i - k_i')$) to the 2-dimensional Brillouin Zone , defined (as in Eq.12b) by a sum $\frac{i_\alpha \vec{g}_\alpha}{2N_\alpha} + \frac{i_\delta \vec{g}_\delta}{2N_\delta}$ of integer (i_α) multiples of $\frac{\vec{g}_\alpha}{2N_\alpha}$ and integer (i_δ) multiples of $\frac{\vec{g}_\delta}{2N_\delta}$. When (as in Eq. 35) all values of k_{cm} are conserved along directions parallel to $\vec{g}_\alpha$,

$$\Delta P_{CM}^{\max,2d} = (N_{2d}^{\alpha,\delta} - N_{1d}^{\delta})\hbar|\vec{g}_\delta|, \qquad (40)$$

where $N_{1d}^{\delta} = 2N_\delta$ is the number of unit cells in the direction parallel to $\vec{b}_\delta$. When k_{cm} is not conserved along any direction, it follows that along any direction parallel to one of the three reciprocal lattice primitive vectors $\vec{g}_\alpha$, analogous to the 2-dimensional situation, an effective maximal, 1-dimensional change in CM momentum $\Delta P_{CM}^{\max,1d}$ occurs when the same (common), largest value of the difference in wave-vector, $k_{cm} - k_{cm}' = \sum_i (k_i - k_i')$ $k_{cm} - k_{cm}' = \sum_i (k_i - k_i')$ appears in each contribution. As in the 2- and 3- dimensional cases, the largest value occurs when the difference in wave-vector $k_i - k_i' = \frac{2N_\alpha - 1}{2N_\alpha}\vec{g}_\alpha$, and

$$\Delta P_{CM}^{\max,1d} = (N_{1d}^{\alpha} - 1)\hbar\,|\vec{g}_{\alpha}|. \qquad (41)$$

The maximal change in CM momentum (as in Eqs. 39-41) from a pure Umklapp process, in principle, can occur at any time. In the absence of excitation/de-excitation of the bulk, such a process does not change the zero of energy or momentum associated with any coordinate of the bulk many-body wave function. For this reason, Umklapp processes have special significance. In particular, when particle-hole excitation/de-excitation processes are stifled, large amounts of momentum can be transferred from the bulk in response to outside perturbing forces.

Because, in the presence of an applied field, the change in momentum that results from the semi-classical equations, increases linearly with time, and because Eq. 24 applies only in the limit of large values of τ, to adequately address situations involving the application of applied fields, for extended periods of time, based on the semi-classical equations, it is necessary to incorporate the possibility that charge can accumulate outside the bulk region through (potentially time-dependent) variations in the zeroes of energy and momentum. In principle, the associated, non-unitary coupling to additional, resonant processes, can be included through a dependence in each many-body state on additional unoccupied states associated with higher energy band eigenvalues (that result from scattering processes). In this case, however, in order to accommodate the potential loss of gauge symmetry and non-unitarity, and the possibility that charge can accumulate, the associated wave-vectors are no-longer required to be real, or to be restricted to the First Brillouin Zone, and the applicability of the formalism associated with low T processes (presented here), in general, need not apply. And a variant of the kind of heuristic approach (Burcin Unlu et al 2004)that has been employed, involving semi-empirical Hamiltonians, would be required. Possible implications of this higher T, long time limit will be explored at a later time (Chubb, S.R. 2005D).

In the presence of applied fields, however, a net flux of particles (associated with each matrix element in Eq. 23) at the boundary of the bulk region occurs. Such a flux results in a "rigid" translation of the bulk that is required to break the gauge symmetry and degeneracy (associated with a perfectly rigid Umklapp process) because of the loss of translation symmetry. For this reason, in most situations, the kind of pure Umklapp process that could result in the maximum amount of momentum being transferred to the CM (as in Eqs. 39-41), in general, will not take place. In particular, in situations involving unfilled bands and finite current, a competition between injected hole-like contributions (which lower the Fermi Energy by removing charge from the bulk region) and particle excitations occurs, in finite lattices, that eliminates the possibility of perfectly rigid Umklapp processeses, in which no excitation or de-excitation of the bulk takes place. (Here, excitation or de-excitation of the bulk refers to a process in which the zero of energy and zero of momentum involving a specific coordinate associated with a particle in the final state many-body wave function changes relative to the comparable zero of energy, involving the same coordinate and particle in the initial state.)

However, when the highest occupied fermion band is completely filled, and the highest (lowest) occupied fermion (boson) band has negligible dispersion, when external forces are applied for appreciable periods of time, the kinds of coherent, rigid, Umklapp processes, associated with Eqs. 39-41, can take place. In particular, provided the zero of energy and momentum associated with each hole-or particle- like coordinate remains fixed relative to the zero of energy and momentum of every other coordinate, no excitation or de-excitation of the bulk takes place. This can occur, rigorously, for all values of time t, provided that for all values of k,

$$\varepsilon(k) = \varepsilon(0) = \text{constant} \qquad . \text{(42a)}$$

This can also occur over finite, discrete intervals (integer multiples of the period of a Bloch oscillation [Bloch 1928]), defined by the condition that

$$\int_{t_o}^{t_o+T^{\alpha}{}_{Bloch}} dt \frac{dk}{dt} \bullet \nabla_k \varepsilon_j (\frac{dk^{\alpha}}{dt}(t-t_o)+k_o) = \varepsilon_j(\vec{g}_{\alpha}+k_o) - \varepsilon_j(k_o) = 0, \quad (42b)$$

where $T^{\alpha}{}_{Bloch} = \frac{|\vec{g}_{\alpha}|}{|\frac{dk^{\alpha}}{dt}|} = \hbar \frac{|\vec{g}_{\alpha}|}{|e_j \vec{E}|}$ is a particular, critical, interval of time (referred to as the Bloch oscillation period) that is associated with the potential breakdown of the single-band, semi-classical equations (as in Eq. 20).

In the complete picture (as presented here), the semi-classical equations only apply rigorously, in a perfect, finite lattice, to the GS and the lowest-lying excitations. (This is in contrast to the conventional quasi-particle picture where it is assumed they apply to states in higher energy bands, throughout an infinitely-repeating lattice.) There is an additional, implicit restriction that naturally occurs in the finite lattice situation, associated with Eq. 42b, that is not obvious in the quasi-particle picture (and, in fact, was a source of considerable confusion, for a number of years [Bouchard & Luban 1995]): Limitations of the semi-classical theory actually are required, associated with potential time-reversible phenomena (referred to as Bloch oscillations). In particular, since the semi-classical picture only applies rigorously to the band that has the lowest energy unoccupied states, the equations apply only approximately in situations in which excitations into higher energy bands take place. For this reason the potential breakdown of the single-band approximation in the conventional quasi-particle picture (for example, through Zener tunneling [Zener 1934]), in general, involves a complicated many-body problem.

In fact, in finite lattices, as discussed below, in the limit of finite, but vanishing-ly small T, Bloch oscillations are required in filled-band systems, in which the filled band has negligible dispersion. In other situations, changes in the relative proportion of occupied and unoccupied states either lead to collisions (as in Eq. 24) or involve a rigid band filling picture in which all of the occupied states are shifted uniformly (through a constant shift of the total zero of energy). These forms of excitation/de-excitation involve coupling between the GS and all states, which, in the absence of broken gauge symmetry, would be degenerate. By construction, in a lattice that remains fixed in size and structure, a limited, fixed, number of degenerate, many-body states are involved and (as a consequence of minimizing the overlap between these states) during the symmetry breaking process, each state is orthogonal to the others, within the volume, defined by the lattice.

At finite T, it is always possible that particular processes will result in a change in the total energy either from all of the (filled and partially filled) bands, or from the (partially filled) highest (lowest) occupied fermion (boson) band. But, relative to the absolute zero of energy, in the bulk, the lowest energy forms of symmetry- breaking processes asymptotically, at finite but vanishing-ly small T, conserve the total energy, relative to the zero of energy, by uniformly shifting all of the particle-like states (including those that are located in filled-bands) from every (occupied or unoccupied) band state since this is required by symmetry breaking processes (in order to minimize energy), and these processes always lower the energy of the lowest energy, many-body states.

But then, since the semi-classical equations apply rigorously only to the lowest energy forms of excitation, they apply only to the single band, that contains the zero of energy of the GS. Processes that involve inter-band transitions, or intra-band transitions (through particle-

hole excitation/de-excitation) that do not conserve the total energy (relative to the absolute zero of energy) or particle number associated with the bulk, by assumption, have finite rates (and lifetimes) that are defined by the collision terms that appear in Eq. 24. These processes do not occur, in the lowest energy forms of excitation.

In fact, Zener (1934) developed a phenomenological model that takes into account the possibility of inter-band transitions. In particular, Zener suggested that although Bloch's theory of conduction predicts that when a constant $\vec{E}$ field is applied to an insulator at room temperature, or to a semi-conductor (at low values of T), no current will flow, initially, after an interval of time that is greater than or equal to $T^{\alpha}{}_{Bloch}$, tunneling should be expected to take place from the valence band to higher bands, and that this would lead to a finite current.

He based this observation on a model in which the electrons should be viewed as quasi-particles that are free to oscillate (without producing current), in a manner that is consistent with the semi-classical equations. Within this context, he reasoned that whenever an oscillation takes place, a form of scattering is required, involving not only an effective reflection (associated with the oscillation) but also a form of transmission into a higher energy band state. In this way, beginning with a filled valence band in a 1-dimensional lattice, he reasoned that in electron systems, forms of electron "quasi-particle" tunneling from the highest occupied band to the lowest unoccupied band could take place, and that this would lead to a finite current. On the other hand, although Zener developed his tunneling arguments, based on the semi-classical equations, in doing so, implicitly, he introduced irreversible forms of scattering that are not rigorous. Ironically, he developed these ideas, based on observations by Bloch, that actually are more rigorous. In particular, (as discussed below) Bloch did identify the possibility of Bloch oscillations, but he dealt exclusively with the limit involving the single band that has the lowest unoccupied states, and, in doing so, he maintained time-reversal invariance.

Implicitly, the restriction that the semi-classical equations apply to a single band is equivalent to limiting the possible momentum ($\hbar\frac{dk}{dt}(t-t_o)$) that can be transferred by the constant external force $\hbar\frac{dk}{dt}$ over the interval of time $t-t_o$ to a particular set of indistinguishable particles, in the many body state. An approximate constraint that forces this to happen is that the particle-hole excitation/de-excitation process not involve coupling to phonons within the lattice. This constraint, in turn, can be imposed by requiring the magnitude of the change in energy between any two times, t_1 and t_2 , not exceed the minimal energy ($\hbar\Omega^{\min}_{phonon}$) that is required to excite phonons possessing a particular, minimal frequency ($\Omega^{\min}_{phonon}$), defined by the lattice:

$$|\int_{t_1}^{t_2} dt\frac{dk}{dt}\bullet\nabla_k\varepsilon_j|=|\varepsilon_j(k(t_2))-\varepsilon_j(k(t_1))|\leq\hbar\Omega^{\min}_{phonon} \qquad (43)$$

When Bloch (1928) developed the semi-classical equations, he recognized that in 1-dimension, the equations predict that, in the context of the heuristic "quasi-particle" picture that forms the basis of his theory of conduction, in the absence of collisions, in a perfect, infinite lattice, the effective electron momentum distribution function (defined by wave vectors in the First Brillouin Zone) could oscillate, as a function of time, indefinitely, with a period defined by $T^{\alpha}{}_{Bloch}$. Effectively, he also assumed that the theory would apply only to a single band.

In fact, the semi-classical equations do apply to a single band rigorously in finite but vanishing-ly small T, as a consequence of broken gauge symmetry. Bloch's use of the single band approximation is rigorous provided Eq. 43 is valid. However, he did not point out the

limitations associated with Eq. 43. In electron systems, this equation is never satisfied except in unusual situations. For this reason, the associated Bloch oscillation effect does not take place in any known, "naturally-occurring" solid. It's existence has been inferred from optically induced excitations in "artificial solids," consisting of multilayer heterostructures, involving very thin, alternating layers of GaAs and Al_xGa_{1-x} that were grown, using molecular beam epitaxial techniques (Feldmann et al 1992). Subsequently, beginning with measurements involving ultra cold, neutral atoms, in optical lattices, by Dahan et al (1996) and Wilkinson et al (1996) that were extended to situations involving BEC's in optical lattices, by Morsch et al (2001), and Denschlag et al (2002), the effect was observed in forms involving individual matter waves (neutral atoms) or coherent matter waves (neutral atoms in a BEC) in an optical lattice. An intuitive explanation for the fact that the effect is difficult to produce exists: Bloch oscillation periods are so long that collisions with phonons and lattice imperfections always take place before a single Bloch oscillation period has elapsed. In the work by Feldman et al, involving GaAs –AlGa supercells, by construction, the energy bands along a particular direction, can be forced to have negligible dispersion, and as a consequence, the inequality in Eq. 43 is satisfied.

An important reason that in the studies involving coherent matter waves in optical lattices (Morsch et al 2001 , Denschlag et al 2002) the effect could be observed directly is that the associated lattice and "quasi-particles" are formed with such a high degree of control that the effects of collisions can be eliminated, and the applied external force can be finely tuned. In particular, especially in the work involving BEC's: 1.The lattice, which is formed from counter-propagating laser beams, does not have phonons and imperfections (except for those associated with boundary and finite size limitations); 2. There is no long-range Coulomb interaction; 3. When the BEC density is sufficiently dilute, the quasi-particle oscillations are essentially collision-less, and with increasing density, the effects of collisions can be monitored and controlled; and 4. As opposed to creating the external force from an applied $\vec{E}$ field, which is subject to non-uniformity, especially near surfaces and interfaces, in this work (Morsch et al 2001 , Denschlag et al 2002), the electrostatic force ($e_j\vec{E}$) (that appears in the conduction of charged particles in solids) is replaced by an effective force (defined by the relative acceleration of the lattice with respect to the CM of the BEC), which is: 1. Independent of the charge; and 2. Can be precisely controlled. In particular, the velocity of the lattice can be changed arbitrarily by introducing an off-set in the frequency of one of the counter-propagating lasers. When the off-set is a constant, the lattice moves at constant velocity, relative to the CM of the BEC. When the off-set increases linearly with time, the lattice is uniformly accelerated, by a constant amount.

Since the energy bands are defined by externally applied (inertial or gravitational) forces, not by Coulomb interactions, and the manner in which the lattice is constructed (through the dipole potential) is provided by the external lasers, no coupling to phonons is required, and the upper limit in the inequality in Eq. 43, is defined either by the energy associated with the lifetime of the experiment, or by the energy band gap W (=the minimum difference in energy between the lowest energy band and the first excited state band), not by $\hbar\Omega_{phonon}^{\min}$. Because the force can be uniform, provided the BEC is loaded into the lattice, with an approximately uniform density (which can be accomplished using suitable Magneto-Optical-Trapping parameters [Denschlag et al 2002], and laser frequencies), except in the immediate vicinity of the boundaries of the lattice, in the rest frame of the BEC, the net, effective force that acts on the CM of the BEC (as in the situation associated with CM motion of the bulk, in Eqs. 19a,b) is directed opposite to and with the same magnitude as the force associated with the acceleration (provided by the lasers). As a consequence, provided the BEC occupies one of the states in the lowest energy band (so

that Eqs. 17a-c can be expected to apply), the semi-classical equations can be expected to rigorously apply, provided the time-scales associated with collisions are considerably longer than those associated with measurements, involving the behavior of the BEC in the lattice. In particular, this can be accomplished, for example, by adiabatically turning on the lattice potential (Denschlag et al 2002) and by preparing the BEC with a density that is sufficiently diffuse that the Thomas Fermi limit (Dalfovo et al 1999) applies and the time-scale $T_{TF} = \frac{\hbar}{\mu}$ (μ = chemical potential) , associated with collision-induced fluctuations of the BEC, is considerably longer than the lifetime of the experiment.

In fact, the intuitive quasi-particle picture has limitations. A more precise picture involves the onset of broken gauge symmetry in finite lattices and the manner in which this is introduced. In particular, Eq. 42a is the true limit that describes a perfect insulator, in a finite lattice. It also describes the limit associated with non-interacting atoms, as they are allowed to interact. In either limit, $\hbar \frac{dk}{dt} = e_j \vec{E}$ for a particular charge e_j in a solid, or $\hbar \frac{dk}{dt} = Ma$, M=mass of neutral atom, a=acceleration of atom, relative to an optical lattice. An important point that also should be emphasized is that in either limit, the physical transport of charge actually can occur through a rigid translation of the CM of the particular charged particles, as opposed to a form of tunneling. It is also possible that if the associated translation is stifled for a long enough period of time, either limit can provide a mechanism for large amounts of momentum to be transferred, effectively, in a coherent manner, to the CM through forms of coupling involving matrix elements that involve different CM momenta (as in Eqs. 39-41), associated with Umklapp processes.

Recently, it has been suggested (Chubb, S.R. 2005B ; 2005C) that precisely this alternative, coherent form of "Zener breakdown," may take place through a process, in which charge that is responsible for the insulator-to-conductor transition comes from (positively charged) ions of H (and its isotopes), as opposed to electrons. (When the coherent form of "Zener breakdown" involves D^+ ions, the transition is from an insulating to a superconducting state since d's are bosons.) In particular, in the limit in which a finite size crystal contains approximately one H or D atom per Pd atom, additional forcing of an H or D into the lattice can lead to these forms of ionic conduction in order to minimize energy (Chubb, S.R. 2005B ; 2005C). Such a form of conduction can be expected to take place in finite size crystals, provided the deviations from full-loading (x=1 in PdH_x or PdD) are sufficiently small because of the (4d-5s like, anti-bonding) orbital character and (delocalized, Pd-like) spatial distribution of the electronic states (Klein & Cohen 1992) immediately above and below the Fermi Energy. In infinitely-repeating lattices, the associated bonding characteristics are responsible for the strongly anharmonic behavior of the optical phonons (Klein & Cohen 1992).

An important distinction exists between cases involving finite, and infinitely-repeating, periodic PdH and/or PdD lattices. In finite PdH and/or PdD crystal lattices, in order to sustain high-loading ($x \rightarrow 1$ in PdH_x or PdD_x), externally applied electric (in the case of electrolysis) or pressure (in the case of gas-loading) fields are necessary, which means that even small variations in loading will induce variations in charge that extend throughout the crystal and into and away from the external regions that surround it (Chubb, S.R. 2005A ; 2005B). For this reason, in the case of finite-size crystals, these fluctuations can carry a small amount of ionic charge away from the crystal. When this happens, effectively, a finite size crystal, containing PdH or PdD, can conduct both electrons and p's or d's. This is not true in infinitely-repeating PdH or PdD

lattices, where the associated fluctuations are associated with coupling between Pd-like electrons and the dominant, low-energy, acoustical phonons.

The effect can occur in finite size crystals (but not in infinitely-repeating crystals) because the externally applied electric or pressure fields impart forces to the crystal. The effect can take place in PdH and PdD because (as a consequence of the electronic structure), provided the fluctuations in loading are small enough, the associated forces can be small enough that the associated many-body system can remain close to its GS. Effectively, this induces a shift in the zeroes of energy and momentum of the small ionic component associated with the fluctuation, relative to the comparable electronic component.

With increasing time, the amount of momentum increases. Each time the momentum exceeds a particular value associated with an Umklapp process, it becomes possible to alter the coordinates associated with holes and particles through an excitation of the system. But in the (effectively adiabatic) limit, in which the induced field (associated with the fluctuations) is sufficiently small, no excitation takes place, and effectively, the lattice is allowed to move rigidly. Eventually the momentum exceeds the maximal amount defined by the perfect, flat band limit, associated with Eq. (37). At this point, ion conduction takes place. In the limit of an infinitely-repeating, periodic solid, the lattice becomes infinitely large and the externally applied field becomes infinitesimal. But in this limit, the time that is required for the onset of ion conduction becomes infinite.

Realistic estimates (Chubb, S.R. 2005A; 2005B), for a situation involving electrolytic loading, suggest that in finite size PdD crystals, effectively, even small fluctuations in loading ($x = 1 \pm \delta$, $\delta \sim 3 \times 10^{-3}$, in PdH_x or PdD_x) can induce changes in momentum that may be large enough to account for some of the anomalies that have been observed in these systems (Arata & Zhang 1995 ; 1997A ; 1997B ; 1999 ; 2000A ; 2000B, Miles et al 2001). But whether or not this happens depends on the size of the crystal. In crystals that have characteristic dimensions of .01 millimeters, the oscillations can carry charge but only after a very long time (on the order of weeks). In crystals that have characteristic sizes of 10's of $\overset{o}{A}$, the applied electric fields can induce ion conduction in less than a hundredth of a second (Chubb, S.R. 2005C ; 2005D). The range of the possible Zener tunneling times (between fractions of a second and weeks), in these calculations, is consistent with the observed range of possible times associated with the onset of heat production, after the attainment of high-loading. This suggests that the observation that after high-loading, a variable “incubation”, or “triggering” time period is required to elapse before the onset of heat, may be related to the sizes of the crystals that are used in the experiments. The fact that the calculations suggest that the shortest times occur in smaller crystals may explain why the anomalous heat appears to be more reliably reproduced in systems that have crystals with characteristic dimensions that are on the scale of 10’s-100’s of nm (Arata & Zhang 1995 ; 1997A ; 1997B ; 1999 ; 2000A ; 2000B, Miles et al 2001). Arata and Zhang (2005), in particular, independently suggested a similar idea, based on evidence that they obtained in their experiments, involving Pd black.

An interesting and important result is that because, in principle, the Generalized Multiple Scattering formalism can be used to estimate rates associated with arbitrary forms of reactions, in finite regions of space, it can be used to estimate limiting time-scales, associated with finite-size effects. Implicitly, this fact has been used throughout this paper. In particular, using Eq. 23, it is possible to estimate the limiting time-scales associated with the impact of finite-size effects on dissipative processes involving collisions or with other effects associated with external forces that are not included in the measurements.

These estimates can be calculated when it is possible to model the many-body wave functions of both an initial (unperturbed) and a final (perturbed) Hamiltonian, in which the perturbation ΔV is associated with a particular process or effect. For example, in modeling the effects of collisions, ΔV could be equated with the non-linear terms in the Gross-Pitaevskii equation (Dalfovo et al 1999). Similarly, ΔV could be equated with the change in effective potential energy associated with corrections to the initial Hamiltonian that can result when the relative acceleration ($\vec{a}$) of the BEC, with respect to the lattice is non-uniform. For illustrative purposes, an estimate is given (immediately below) of the limiting time-scale associated with finite-size effects for a situation in which $\vec{a}$ is not uniformly constant over a particular region of the lattice. (The associated argument can also be applied to provide a comparable estimate of the limiting time-scale associated with finite size effects for a situation involving collisions. This case will be considered at a later time [Chubb, S.R. 2005D].)

When $\vec{a}$ is not uniformly constant over a particular region, but the BEC moves rigidly, to a first approximation, provided the associated non-uniformity in $\vec{a}$ varies slowly, the dependence of the many-body function $\Psi(r_1,...,r_{N_b})$ on the CM coordinates (r_{cm}) becomes separable from its dependence on each of the remaining, independent coordinates ($r_j - r_{cm}$, $j = 1, N_b$). (Here, as defined in section II, N_b refers to the total number of bosons.) But then, $\Psi(r_1,...,r_{N_b})$ can be re-expressed in the form,

$$\Psi(r_1,...,r_{N_b}) = \Phi(r_{cm})\Psi_{rel}(r_1 - r_{cm},....,r_{N_b} - r_{cm}), \qquad (44a)$$

where $\Phi(r_{cm})$ and $\Psi_{rel}(r_1 - r_{cm},....,r_{N_b} - r_{cm})$, respectively, describe the dependence of $\Psi(r_1,...,r_{N_b})$ on CM and the remaining (independent) coordinates. of the BEC. Also, in this limit, at a particular location r, $\vec{a} = \vec{a}(r)$ can be expressed in terms of its linear order Taylor Series expansion relative to its value at an initial position (r_o) of the CM of the BEC.

Again, for illustrative purposes, it is convenient to consider a particular (idealized) situation, in which the BEC is in free fall (along the z-axis), the local gravitational constant g only varies in the z-direction, the local gravitational acceleration is

$$-g\hat{z} \equiv -g(z)\hat{z} = -(g(z_{cm}) + (z - z_{cm})\frac{\partial g(z_{cm})}{\partial z_{cm}})\hat{z}, \qquad (44b)$$

and the lattice is also accelerated in the (negative) z-direction, uniformly, by an amount $|\vec{a}| = g(z_{cm})$. For this situation, in the frame of the lattice, the relative acceleration of the BEC is $\vec{a}_{latt}(z) = (-g(z) + g(z_{cm}))\hat{z}$, and the effective potential $V(z)$ that describes the CM motion is given by

$$V(z) = M_{BEC}\frac{(z - z_{cm})^2}{2}\frac{\partial g(z_{cm})}{\partial z_{cm}}. \qquad (45)$$

Through Eq. 23, it is possible to identify the minimum rate associated with the onset of finite size effects in measurements of $\left.\frac{\partial g(z_{cm})}{\partial z_{cm}}\right|_{z_{cm} = z_1} = g'(z_1)$ in a situation involving a particular value $z_{cm} = z_1$, relative to a comparable measurement of $\left.\frac{\partial g(z_{cm})}{\partial z_{cm}}\right|_{z_{cm} = z_2} = g'(z_2)$ that involves a different value of $z_{cm} = z_2$. By minimizing this rate, it is possible to identify critical values of the parameters (the number of lattice sites, *N*, and bosons, N_B) that are required to perform

measurements of $\frac{\partial g(z_{cm})}{\partial z_{cm}}$ with a specified level of accuracy. In addressing this last problem, we can require that $\frac{\partial g(z_{cm})}{\partial z_{cm}}$ be non-negative. (When $\frac{\partial g(z_{cm})}{\partial z_{cm}} < 0$, the net contributions at the boundaries of the lattice to the rate expression, in Eq. 23, asymptotically vanish since the associated solutions of the Schroedinger equation, which involve Hermite polynomials with imaginary arguments, are oscillatory. As a consequence, in the absence of additional perturbations, the time-scale associated with the onset of finite size effects, for this case, is non-physical since it is always infinite.)

For a particular, important application (involving gravity gradient measurements from airplanes [van Leeuwen 2001]), a measurement of $\frac{\partial g(z_{cm})}{\partial z_{cm}}$ is required to have an absolute error of 1 Eotvos (=E =10^{-9} m/(m-s) ~10^{-10} g/m). It is possible to use this value to obtain approximate bounds for critical values of various parameters associated with the lattice and BEC (that result from the onset of finite size effects) by minimizing the Reaction rate (from Eq. 23) that results from the overlap of an initial state BEC, which is in an eigenstate of a Hamiltonian H_o, associated with an initial potential $V_o(z) = M_{BEC}\frac{(z-z_1)^2}{2} g'(z_1)$, defined by the mass (=$M_{BEC}$) of the BEC and its gradient ($g'(z_1)$) at z=z_1 with an eigenstate of of a Hamiltoian H_F , which is identical to H_o, except that the Taylor series expansion is evaluated at the location z= z_2. The associated perturbation is

$$\Delta V(r) = V_F(r) - V_o(r) = M_{BEC}\left(\frac{(z-z_2)^2}{2} g'(z_2) - \frac{(z-z_1)^2}{2} g'(z_1)\right).$$

In a situation involving an infinite lattice, the initial and final states asymptotically approach the solutions of two, different, single-particle, harmonic oscillator Hamiltonians (that respectively have angular frequencies $\omega_1 = \sqrt{g'(z_1)}$ and $\omega_2 = \sqrt{g'(z_2)}$)). In the many-body situation, in a finite lattice, as a consequence of Eq. 6, minimal reaction rate occurs in the limit in which $\Psi_{rel}(r_1 - r_{cm},....,r_{N_b} - r_{cm})$ is the same in the initial and final states (so that the net flux from the relative coordinates vanishes), and the contribution from the CM coordinates, associated with the LS and RS of Eq. 6, is identically the same. This occurs when the CM portions of the initial and final state (which can both be assumed to be uniform and constant in directions perpendicular to the z-direction), respectively, can be described by wave functions $\Phi_o(r) = \frac{\phi_o(z)}{A^{1/2}}$and $\Phi_f(r) = \frac{\phi_f(z)}{A^{1/2}}$ that are given by the GS wave functions defined by the cross-sectional area *A* perpendicular to z, and the harmonic oscillator Hamiltonians, possessing frequencies ω_1 and ω_2:

$$\Phi_o(r) = \frac{1}{A^{1/2}}\left(\frac{M_{BEC}\omega_1}{\pi\hbar}\right)^{1/4} \exp(-\frac{M_{BEC}\omega_1 z^2}{2\hbar}), \qquad (46a)$$

and

$$\Phi_f(r) = \frac{1}{A^{1/2}}\left(\frac{M_{BEC}\omega_2}{\pi\hbar}\right)^{1/4} \exp(-\frac{M_{BEC}\omega_2 z^2}{2\hbar}). \qquad (46b)$$

It follows that when Eqs. 46a and 46b are substituted into Eq. 44a, $\Psi_o = \Phi_o(r_{cm})\Psi_{rel}$ and $\Psi_f = \Phi_f(r_{cm})\Psi_{rel}$, and these wave functions can be used to evaluate the flux, when they are

substituted into Eq. 6 (with $\Psi_f = \Psi'$, $\Psi_o = \Psi_{GS}$). Then, when $\Psi_{rel}(r_1 - r_{cm},....,r_{N_b} - r_{cm})$ is the same in the initial and final states (which is required for a minimal rate contribution from flux terms associated with the boundary), it follows that

$$\int d^3 r \nabla \bullet < \Psi' | v(r) | \Psi_{GS} > = \int_{\partial V} dS\, \hat{n} \bullet < \Psi' | v(r) | \Psi_{GS} > = i\phi_o(L)\phi_f(L) 2L(\omega_1 - \omega_2),$$

$$= i(\omega_1 - \omega_2) L e^{-\frac{(\omega_1+\omega_2)ML^2}{2\hbar}} (\omega_1\omega_2)^{1/4} \left(\frac{M_{BEC}}{\pi\hbar}\right)^{1/2} \qquad (47a)$$

where *2L* is the length of the lattice, and the factor of 2 (in the first line on the RS) is present because the contributions to the integral at each endpoint (defined by $r_{cm} = \pm L$) are equal. Also consistent with the assumption that the contributions (from finite size effects) to the rate expression be minimized (in Eq. 24), the final density of states can be derived using the expression that applies to a single-particle, harmonic oscillator (with final frequency ω_2):

$$\rho_{final}(E)\Big|_{E=\frac{\hbar\omega_1}{2}} = \sum_F \delta(E - E_{exact}(C_F)) = \sum_n \delta(\frac{\hbar\omega_1}{2} - (n+\frac{1}{2})\hbar\omega_2) = \frac{1}{\hbar\omega_1}. \qquad (47b)$$

It is possible to make an estimate of the minimal transition rate $R_{o\to f}$ (which can be used to infer critical values of the parameters associated with lattice site) between the initial and final states ($\Phi_o(r)$ and $\Phi_f(r)$) by substituting Eqs. 47a,b into Eq. 23:

$$R_{o\to f} = L^2(\omega_1\omega_2)^{1/2} \frac{M_{BEC}}{\hbar} \frac{(\omega_1 - \omega_2)^2}{\omega_1} e^{-(\frac{M_{BEC}(\omega_1+\omega_2)}{\hbar}L^2)}. \qquad (48)$$

As a function of L, the maximum value of $R_{o\to f}$ can be used to infer a critical values (L_{crit} and 2 L_{crit}). In particular, from the condition that $\frac{\partial R_{o\to f}}{\partial L}\Big|_{L=L_{crit}} = 0$, it follows that

$$L_{crit}^2 = \frac{\hbar}{M_{BEC}(\omega_1+\omega_2)}. \qquad (49)$$

Since at the surface of the earth (Snadden et al 1998) $g'(z_1) \cong 3.08\times10^{-6}\ (Htz)^2 = 3080\ E >> 1\ E = |g'(z_1) - g'(z_2)|$, with negligible error, the difference between ω_1 and ω_2 in the prefactor of $(\omega_1 - \omega_2)^2$ in Eq. 49 can be ignored. Then, it follows that the maximum value of $R_{o\to f}$ (= $R_{o\to f}(L_{crit}) \cong \frac{(\omega_1-\omega_2)^2}{\omega_1} e^{-1.0} \cong 2.010\times10^{-4}\ Htz$) does not depend on the value of $M_{BEC} = N_b M_{atom}$ and, thus, is independent of the number of bosons (N_b) and mass (M_{atom}) of an individual atom in the BEC. On the other hand, values of L_{crit}, lattice size (*=2* L_{crit} *=2*N_z $|b_z|$; $b_z = b_\alpha\big|_{\alpha=z} = \frac{\bar{L}_\alpha}{2N_\alpha}\Big|_{\alpha=z}$; $N_\alpha\big|_{\alpha=z} = N_z$), and N_z all depend on M_{BEC}. In the initial measurements (Anderson & Kasevich 1998) of g (based on optical lattices), the lattice spacing $|b_z|$=850nm, and (since in this experiment, vapors of ^{87}Rb were used) $M_{atom} \cong 144.04\times10^{-24}\ g$ (Chubb, S.R. 2000E). From these values, it follows that in this experiment, for N_b =1000000, the minimal, required vertical length $L_{\min} > 2l_{crit} \approx 912$ nm, and the minimal number of unit cells N_{min} >2; while for N_b =1000, $L_{\min} > 2l_{crit} \approx 28833$ nm, N_{min} >68, and for N_b =100, $L_{\min} > 2l_{crit} \approx 28833$ nm, N_{min} >214.

VII Conclusions

In this paper, a new formalism, Generalized Multiple Scattering, has been developed for estimating the rates of particular many-body processes, based on general properties of particular systems. This formalism is difficult to apply in many situations because it requires information about the fluxes of particles that enter and leave a particular region, where collisions are allowed to take place. The formalism is especially useful, however, for investigating the GS and lowest-energy excitations in situations involving broken gauge symmetry. In particular, in the presence of a gauge symmetry, the GS and lowest-energy excitations are degenerate. When the symmetry is broken, system energy is minimized when overlap with the GS is minimized.

In the case of ordered lattices, the relevant gauge symmetry involves the invariance of the many-body Hamiltonian with respect to Galilean transformations, in which the bulk region is translated rigidly without altering any of the particle-particle separations in the region. (Here, bulk region is defined to be portions of a solid or optical lattice, respectively, in which charge or the number of atoms is conserved.) Broken gauge symmetry occurs through effects that result from accumulation of charge (in solids) or changes in the potentials (in optical lattices) at the boundaries of the periodically ordered (bulk) region. The requirement that, in the presence of a broken gauge symmetry, minimal overlap occur between the GS and the lowest-lying excited states (associated with the initial gauge symmetry) imposes constraints on the form of the allowable states, in bulk regions. From this starting point, it is possible to prove a generalized form of Bloch's theorem and to generalize the associated semi-classical transport theory.

Because Bloch's theorem, by construction, occurs as a result of a broken gauge symmetry, implicitly, it is associated with a (potentially huge) set of degenerate states. These states are related to each other through coherent forms of rigid-body motion, associated with Umklapp processes. Again, by construction, since this broken gauge symmetry becomes dominant when collisions are reduced, the associated Umklapp processes become important either at low T or when collisions are stifled. Quantitative bounds for the amounts of momentum that can be transferred from a crystal lattice to a surface or interface (and vice-versa) through these kinds processes, traditionally, in models in which the lattice is infinitely-repeating and periodic, have been poorly defined. But in finite solids, at low, but finite temperature, precise, size-dependent bounds can be identified. In particular, although in larger crystals, collisions with phonons tend to reduce the magnitudes of the associated effects, in smaller crystals (or in optical lattices), this is not the case.

In a particular limit, in PdD and PdH crystals, a novel situation can occur in which H^+ and D^+ ions (in addition to electrons) can become charge carriers. At the transition between the ionic insulating- and conducting- state, a form of Zener/Ionic breakdown (similar to Zener/Electronic breakdown in insulators) in smaller PdD and PdH crystals can take place in which coherent Umklapp processes lead to effects that can be quite large. In the case of PdD, the associated effect can lead to a coherent form of interaction that mimics an insulator-superconductor transition. The ranges of time-scales (which vary between weeks and fractions of a second) for initiating this kind of effect appear to be consistent with the comparable ranges of incubation times that have been observed to be required before anomalous heat is produced during the prolonged electrolysis of D_2O by PdD. The fact that the shortest time-scales required for Zener/Ionic breakdown and the production of Excess Heat both occur in PdD crystals that have characteristic dimensions ~10's of nm suggests that Excess Heat is being triggered by Zener/Ionic breakdown.

Generalized Multiple Scattering Theory can be used to estimate the transition rate for a particular process, provided the process can be approximately represented, using known initial and final states. In the paper, a concrete example, involving the identification of critical length- and time- scales, associated with finite size, in the problem of measuring the gradient of the gravitational force, is used to illustrate this. The argument associated with this calculation illustrates that the critical length-scale of the lattice is inversely proportional to the square root of the number of ultra cold atoms that occupy a single coherent matter wave (Bose Einstein Condensate) state. The associated calculation provides quantitative information that will be useful in the problem of observing variations in gravitational force, using coherent atom waves, from airborne platforms.

Acknowledgements

I would like to acknowledge valuable discussions that took place more than a decade ago with Giuliano Preparata. These discussions, in particular, inspired me to examine the relationship between broken gauge symmetry and the theory of electron transport in finite solids. I also would like to thank Talbot Chubb and David Nagel for their help and encouragement. The specific calculation, related to gravity gradient measurements, was partially inspired by computations performed through the DoD High Performance Computing program. Financial support, for this research, was provided by the Office of Naval Research.

References

Anderson, B.P. & Kasevich, M.A. 1998 Macroscopic quantum interference from atomic tunnel arrays. *Science* **282**, 1686-1689.

Arata, Y. & Zhang, Y.-C. 1995 A new energy caused by "Spillover-deuterium." *Proc. Jpn. Acad.* **70B**, 106.

Arata, Y. & Zhang, Y.-C. 1997A Helium (4He, 3He) within deuterated Pd-black. *Proc. Jpn. Acad.*, **73B**, 1.

Arata, Y. & Zhang, Y.-C. 1997B Presence of helium (4/2He, 3/2He) confirmed in highly deuterated Pd-black by the new detecting methodology. *J. High Temp. Soc.* **23**, 110 (in Japanese)

Arata, Y. & Zhang, Y.-C. 1998 Anomalous difference between reaction energies generated within D_2O-Cell and H_2O-Cell. *Jpn. J. Appl. Phys.* **37**, L1274 -1276.

Arata, Y. & Zhang, Y.-C. 1999 Anomalous production of gaseous 4He at the inside of 'DS cathode' during D2O-electrolysis. *Proc. Jpn. Acad.*, **75B**, 281

Arata, Y. & Zhang, Y.-C. 2000A Definitive difference among [DS-D2O], [DS-H2O] and [Bulk-D2O] Cells in the deuterization and deuterium-reaction. *Proc. ICCF8*, 11-16.

Arata, Y. & Zhang, Y.-C. 2000B Deuterization and deuterium reactions in the electrolyses of D2O with the double structure cathode and the bulk cathode *Jpn. J. Appl. Phys.* **39**, 4198-202.

Arata, Y. & Zhang, Y.-C. 2005 Proc. ICCF10 London:World Scientific. In press.

Ashcroft, N. & Mermin, D. 1976A Solid State Physics. Forth Worth: Saunders College Publishing. Chap. 6, pp .96-104.

Ashcroft, N. & Mermin, D. 1976B Solid State Physics. Forth Worth: Saunders College Publishing. Chap. 26, pp. 526-528.

Ashcroft, N. & Mermin, D. 1976C Solid State Physics. Forth Worth: Saunders College Publishing. Chap 12, pp 214-241.

Ashcroft, N. & Mermin, D. 1976D Solid State Physics. Forth Worth: Saunders College Publishing. Chap. 8, p. 135.

Bloch, F. 1928 Quantum mechanics of electrons in crystal lattices. *Z. Phys.* **52**, 555-600.

Bouchard, A.M. & Luban, M. 1995 Bloch oscillations and other dynamical phenomena of electrons in semiconductor superlattices. *Phys. Rev. B* **52**, 5105–5123.

Bruus, H. & Flensberg,K. 2004 Many-Body Quantum Theory in Condensed Matter Physics, An Introduction. Oxford:Oxford University Press. pp. 184-225.

Buot, F.A. 1993 Mesoscopic physics and nanoelectronics: nanoscience and nanotechnology. *Physics Reports* **234**, 73-174.

Buot, F.A. 1974 Method for calculating $Tr(H^n)$ in solid state theory. *Phys. Rev. B* **10**, 3700-3705.

Burke, P.G. & Berrington, K.A. 1993 Atomic and molecular processes: an R-matrix approach. Bristol: IOP Publishing. 402 p.

Burcin Unlu, M.B., Rosen, B., Cui, H-L., Peiji, Z. 2004 Multi-band Wigner function formulation of quantum transport *Physics Letters A* **327**, 230-240.

Chubb, S.R. 2003 Importance of broken gauge symmetry in initiating LENR's. *Trans. Amer. Nuc. Soc.* **88** , 618-619.

Chubb, S.R. 2005A Nuts and Bolts of the Ion Band State Theory. *Proc ICCF10.* London:World Scientific, in press. Available on-line: http://www.lenr-canr.org/acrobat/ChubbSRnutsandbol.pdf

Chubb, S.R. 2005B Framework for understanding LENR processes, using conventional condensed matter physics," *Proc. ICCF11*, in press. Available on-line: http://www.lenr-canr.org/acrobat/ChubbSRframeworkf.pdf

Chubb, S.R. 2005C Coherent Zener breakdown and tunneling in finite lattices: *why nano-scale PdD crystals can turn-on faster*. *Trans. Amer. Nuc. Soc.*, in press.

Chubb, S.R. 2005D Conduction of charged particles at finite temperature in finite crystals. To be submitted to Physical Review B.

Chubb, S.R. 2005E The estimate in the text is based the value, one Atomic Unit=931.31 MeV/c^2=$1.6557\times10^{-24}g$

Chubb, S.R. & Chubb, T.A. 2000 Theoretical Framework for Anomalous Heat and ^{4}He in Transition Metal Systems. *Proc. ICCF8*, 385-396 (2000). Available on-line: http://www.lenr-canr.org/acrobat/ChubbSRtheoretica.pdf.

Chubb, T.A. 2005 *Proc ICCF10*. London:World Scientific. In press. Available on-line: http://www.lenr-canr.org/acrobat/ChubbTAtheddcoldf.pdf

Chubb , T.A. & Chubb, S.R. 2001 Deuteron Fluxing and the Ion Band State Theory. *Proc. ICCF8, ,* 391-396. Available on-line at: http://www.lenr- canr.org/acrobat/ChubbTAdeuteronfl.pdf

Dahan, M.B., Peik, E,, Reichel J., Castin, Y., & Salomon, C, 1996 Bloch oscillations of atoms in an optical potential. *Phys. Rev. Lett.* **76**, 4508-4511.

Denschlag, J.H., Simsarian, J.E., Haffner, H., McKenzie, C., Browaeys, A., Cho, D., Helmerson, K., Rolston, S.L. & Phillips, W.D. 2002 A Bose–Einstein condensate in an optical lattice. *J. Phys. B: At. Mol. Opt. Phys.* **35**, 3095–3110.

Deutsch, I.H. & Jessen, P.S. 1998 Quantum-state control in optical lattices *Phys Rev A*, **57**, 1972-1986.

Dalfovo, F., Giorgini S., Pitaevskii, L.P., & Stringari, S. 1999 Theory of Bose-Einstein condensation in trapped gases. *Rev. Mod. Phys.* **71**, 463.

Feldmann, J., Leo, K., Shah, J., Miller, D.A.B., Cunningham, J.E., Meier, T., von Plessen, G., Schulze, A., Thomas, P. & Schmitt-Rink, S. 1992 Optical investigation of Bloch oscillations in a semiconductor superlattice. *Phys. Rev. B* **46**, 7252.

Gonis, A. & Butler, W.H. 2000 Multiple Scattering in Solids. New York:Springer-Verlag. 285 p.

Klein, B.M. & Cohen, R.E. 1992 Anharmonicity and the inverse isotope effect in the palladium-hydrogen system. *Phys Rev B* **45**, 12405-12414.

Langreth, D.C. & Wilkins, J.W. 1972 Theory of spin resonance in dilute magnetic alloys. Phys. Rev. B 6, 3189-3227.

Levine, R.D. 1999 Quantum Mechanics of Molecular Rate Processes. NewYork: Dover. 348p.

Lipavsky, P., Spicka, V. & Velicky, B. 1986 Generalized Kadanoff-Baym ansatz for deriving quantum transport equations. *Phys. Rev. B* **34**, 6933-6942.

Miles, M.H., Fleischmann, M., & Imam, M.A. 2001 Calorimetric analysis of a Heavy Water Electrolysis Experiment Using a Pd-B alloy Cathode Washington, DC: Naval Research Laboratory Naval Research Laboratory memorandum report: NRL/MR/6320—01-8526, 155p.

Morsch, O., Muller, J.H., Cristiani, M., Ciampini, D. & Arimondo, E. 2001 Bloch oscillations and mean-field effects of Bose-Einstein condensates in 1D optical lattices *Phys. Rev. Lett.* **87**, 1040402/1-4.

Peierls, R. 1929 The kinetic theory of thermal conduction in crystals *Ann. Phys.* **3**, 1055

Schwinger, J. 1990 Nuclear energy in an atomic lattice. *Proc. ICCF1*, pp. 130-136.

Snadden, M.J., McGuirk, J.M., Bouyer, P., Haritos, K.G. & Kasevich, M.A. 1998 Measurement of the Earth's gravity gradient with an atom interferometer-based gravity gradiometer, Phys. Rev. Lett. 81, 971, 1998.

van Leeuwen, E.H. 2001 Airborne gravity gradiometry. Austral Tech Sci Eng (ATSE) Focus, 119, Nov/Dec 2001. Available on-line at: http://www.atse.org.au/index.php?sectionid=464

Wilkinson, S.R., Bharucha C.F., Madison, K.W., Niu, Q. & Raizen M. G. Observation of atomic Wannier-Stark ladders in an accelerating optical potential Phys. Rev. Lett. 76, 4512-4515 (1996).

Zener, C. 1934 A Theory of the Electrical Breakdown of Solid Dielectrics. *Proc. R. Soc.* A **145,** 523-529.